10th
INTERNATIONAL CONFERENCE ON GRAVITATION, ASTROPHYSICS & COSMOLOGY

ICGAC10

VIIth Rencontres du Vietnam

Quy Nhon, Vietnam – December 15 - 21, 2011

10th International Conference on Gravitation, Astrophysics and Cosmology

Sponsors

. Asia Pacific Center for Theoretical Physics (APCTP)

. Aix Marseille University (AMU)

ISBN
Thê Gioi Publishers
Printed in Vietnam

Proceedings of the Xth International conference on

Gravitation, Astrophysics and Cosmology (ICGAC10)

Quy Nhon, December 17-22, 2011

Gravitation, Astrophysics and Cosmology

edited by

Roland Triay, Aix-Marseille University

Jean Trân Thanh Vân, Rencontres du Vietnam

Ludwik M.Celnikier, Observatoire de Meudon

THE GIOI

PUBLISHERS

10th ICGAC

International Advisory Committee

Australia: David Blair;
Brazil : Mario Novello;
Canada: Valery P. Frolov, Don N. Page;
China: Rong-gen Cai, K. S. Cheng, Liao Liu, JunLuo, Wei-TouNi, Yong-jiu Wang;
France: Jean-Michel Alimi, Thibault Damour, Jean Tran Thanh Van, Roland Triay;
Germany: H. Dehnen, Claus Laemmerzahl;
Greece: Spiros Cotsakis;
India: Bala R. Lyer, Varun Sahni;
Japan: Yasunori Fujii, Seiji Kawamura, Masakatsu Kenmoku, Hideo Kodama, Kazuaki Kuroda, Misao Sasaki, Katsuhiko Sato;
Korea**:** Yong-Min Cho, Sang-Pyo Kim, Sung-Won Kim;
Russia: Gennadii S. Bisnovaty-Kogan, Dmitri V. Gal'tsov, Vladimi rN. Lukash, VitalyN.Melnikov, V. K. Milyukov, Igor D. Novikov, Valentin N. Rudenko, Alexei A. Starobinsky;
Taiwan: Chiang-Mei Chen, James M. Nester;
USA: Francis Everitt, Jong-Ping Hsu, H. J. Paik

International Program Committee

Gennadii S. Bisnovaty-Kogan (Russia),
Pierre Darriulat (Vietnam),
Yannick Giraud-Héraud (France),
Sang Pyo Kim (Korea),
Jun Luo (China),
Kei-ichi Maeda (Japan),
Vitaly Melnikov (Russia),
François Montanet (France),
Nguyen TrongHien (USA),
Carlo Rovelli (France),
Alexei Starobinsky (Russia),
Jean Tran Thanh Van (France),
Roland Triay (France) – Chair

Local Committee

Ludwik Celnikier (Observatoire de Meudon)
Dinh van Trung (Institute of Physics),
Do Hoang Son (University of Sciences of HoChiMinhCity),
Nguyen Dinh Huan (University of Vinh),
Nguyen Quynh Lan (Hanoi National University of Education),
Nguyen Thi Minh Phuong (Quy Nhon University),
Phan Bao Ngoc (Ho Chi Minh International University),
Roland Triay (Centre de Physique Théorique),
Jean Tran Thanh Van (Les Rencontres duVietnam),

Contents

†*Indicates an invited talk*

 †*Indicates an invited talk*

†*Indicates an invited talk*

 †*Indicates an invited talk*

†*Indicates an invited talk*

†*Indicates an invited talk*

Foreword

The Seventh Rencontres du Vietnam was held from the 15th to the 22nd of December 2011 in Quy Nhon, Vietnam. It hosted two international conferences:

- 14th EDS meeting, in the Blois Workshop series, entitled "Frontiers in QCD: Puzzles and Discoveries" 15-21 December 2011,

- **Tenth International Conference on Gravitation, Astrophysics and Cosmology (ICGAC10)**, 18-22 December 2011.

These conferences ran in parallel, with a common session for the presentation of results of mutual interest. More than 200 researchers from 29 different countries attended the Rencontres and most of them presented their ongoing research. "Twinning" the conferences in this was was particularly fruitful since researchers who are often unable to participate in events outside of their own speciality had an opportunity to meet, to exchange ideas and even to launch new cross-disciplinary activities.

The **ICGAC10** is the tenth in a series of biennial conferences (formerly ICGA) on Gravitation, Astrophysics and Cosmology, which take place in the Asia-Pacific region. The purpose of these meetings is to encourage cooperation among the member countries and within an international context, to promote high level studies on emergent topics, and to encourage young physicists to enter these fields. Professor Yong Min Cho, one of the founders of the Asia Pacific Center for Theoretical Physics, launched the first meeting. Previous meetings have been held in:

- Seoul, Korea (1993) at the Seoul National University,

- Hsinchu, Taiwan (1995) at the National Tsing Hua University,

- Tokyo, Japan (1997), at the Institute for Cosmic Ray Research at Tokyo University,

- Beijing, China (1999) at the Beijing Normal University,

- Moscow, Russia (2001) at the Institute of Gravitation and Cosmology, People's Friendship University of Russia

- Seoul, Korea (2003) at the Ewha Women's University,

- Jhongli, Taiwan (2005) at the National Central University

- Nara, Japan (2007) at the Nara Women's University,

- Wuhan, China (2009) at the Huazhong University of Science and Technology.

New insights emerged from the 36 key talks of the plenary sessions, as well as from the 35 parallel session talks. A notable feature of the 6 parallel sessions was the lively interaction and exchange among the 120 plus participants. Young scientists were encouraged to present posters, which enabled them to organize daily informal discussion sessions on their work. In addition to the usual themes, which comprised gravity, its experimental studies and theoretical developments, cosmology and astrophysics, this conference also covered astroparticle physics, a discipline in which Vietnamese scientists are particularly active.

Scientific Content

The conference began with a review of recent applications of the AdS/CFT correspondence in strongly coupled systems emphasizing hydrodynamic aspects in the physics of black holes. This was followed by a presentation of the mutual benefits of the ongoing research on cosmic ray air showers and LHC physics; these two talks were in common with the EDS meeting.

Important issues were addressed about the primordial era of the Universe, such as on the difficulties of avoiding an initial singularity and about the inflationary scenarios (the most general single-field inflationary models, the role of the Higgs boson field as source, on the evolution of linear cosmological perturbations when a Weyl term is added to the action in order to assess the role of ghosts,...). Modern cosmology began with the discovery of the Cosmic Microwave Background radiation (CMB). The photons which decoupled from the primordial plasma, with which they were in thermodynamic equilibrium, as shown by their spectral black body distribution, provide us with information on the initial conditions which led to large scale structure formation, and the properties of the foreground distribution of matter. The reasons why the measurements of the angular variations of CMB temperature are so important for cosmology were developed and some cosmological implications of the data analysis obtained by the WMAP satellite mission were discussed. These measurements will be enriched by ground based observations using the Atacama Cosmology Telescope project. Even though the Planck satellite HFI results (on for example polarization or non-gaussianity) will not be available before the beginning of 2013, some early results on blind detection of galaxy clusters and on the Cosmic Infrared Background were presented.

Concerning the dark energy issue, it was shown how local inhomogeneities affect the global expansion: this may explain the apparent acceleration of the cosmological expansion. Faced with the dark matter problem, some possible solutions were analyzed: these include a simple model for the relativistic extension of Modified Newtonian dynamics (MOND).

In order to explore a quantum theory of gravity, the unitarity, stability and renormalizability properties of the 3D higher derivative gravity models were presented. It was emphasized that the scaling index of the symmetry energy characterizes the universality classes of holographic QCD models. Some interesting cosmological implications of Horava-Lifshitz gravity solve the horizon problem and lead to scale-invariant cosmological perturbations even without inflation.

More generally, exact solutions in gravity and cosmology with extra dimensions were discussed. For example, one of the questions is whether particles undergoing transplanckian collisions in TeV-scale gravity can lose most of their energy via bremsstrahlung for impact parameters much larger than the gravitational radius of the presumably created black hole. Some features of the physics related to M2 and M5 branes were discussed, and Bubbles and Walls were revisited. It was pointed out that current observational data can already constrain the string theory landscape. Some developments of black holes in loop quantum gravity were reviewed.

A significant breakthrough on the origin of Gamma-Ray Bursts was proposed. The problem of the formation of a large-scale magnetic field in the accretion disks around black holes was discussed. In order to understand galactic radio jets, a theory of relativistic Poynting-flux jets based on the analogy between jets and transmission lines was presented. The new approach to vacuum polarization and the Hawking radiation of a Schwarzschild black hole, by analogy with the Heisenberg-Euler and Schwinger effective action in QED, was revisited. An analysis of cosmological perturbations in an expanding universe with a black hole was presented.

The contributions in astrophysics can have various objectives: they can be justified because they lead to a better understanding of the studied effect itself, but they can also be useful in specific disciplines. For example, gravitational lensing in plasma (useful in cosmology) turns out to be chromatic, according a review of the main properties of gravitational deflection in different media.

The main projects associated with astroparticle physics discussed at this meeting include: the Antares project for neutrino astronomy; the "Tianshan Radio Experiment for Neutrino Detection" (TREND) for the detection of high energy Extensive Air Showers (EAS), and (in the long term) for the detection of high energy tau neutrinos; the Telescope Array (TA) for ultra high energy cosmic rays, and the Large-scale cryogenic gravitational wave telescope (KAGRA), which has been under construction in the Kamioka mine in Japan since 2010.

Many recent results were presented, and in particular those from the Pierre Auger Observatory, on ultra-high energy cosmic rays (including measurements of the energy spectrum, mass composition, and the anisotropy in the arrival directions), as well as the analysis of cosmic rays observed with the AMIGA infill array. GeV and TeV gamma-ray astronomy using the Fermi Large Area Telescope LAT has entered a new productive phase, with highlights such as the hadronic generation mechanism of very high energy (800 GeV - 100 TeV) gamma-rays in Tycho's supernova remnant.

Crucial to our understanding of gravity are tests of the validity of the equivalence principle, of newtonian gravity and measurements of the gravitational constant G. A number of critical results were presented; no significant deviation from the inverse square law has been observed at a 95% confidence level, which establishes the most stringent constraint on non-Newtonian interactions in the range 0.7 mm to 5.0 mm. The results of the best world experiments on measurement of G and CODATA values were presented.

In summary, this multidisciplinary conference covered a very wide field, and these proceedings give a panoramic view of the excellent and dedicated work of the many participants.

Social Events

The welcome dinner at the Seagull Hotel was accompanied by a demonstration of traditional Vietnamese dances. Offered by the President of the Province of Binh Dinh, Mr. Le Huu Lôc, in honour of the participants, this memorable evening took place in the presence of Professor Nguyên Van Hiêu, former President of the Vietnamese Academy of Science and Technology, and Professor Phan Thanh Binh, President of the National University of Ho Chi Minh City. In his welcome speech at the ground breaking ceremony of the International Centre for Interdisciplinary Science and Education (ICISE) in Quy Nhon, President Le Huu Lôc emphasized that the development of science and technology is one of the major priorities of the province and reaffirmed his strong support for the creation and the development of the Centre. He invited all the participants to return to Quy Nhon in order to contribute to the scientific life of the Centre and cooperate with the University of Quy Nhon.

The Rencontres du Vietnam have always striven to bring science to general public; students and the general public were invited at the Palace of Culture of the Province to attend a talk given by Trinh Xuan Thuan, Professor at the University of Virginia (USA), entitled "The place of Man in the Universe: the Big Bang and its aftermath". Over 1500 inhabitants of Quy Nhon were present and their enthusiastic questions led to discussions for over an hour.

The VIIth Rencontres du Vietnam was followed with interest by the news media and the general public. More than 30 articles were published in various newspapers and magazines in Vietnam and Europe, in addition to the many reports relayed over the national television networks.

The various photographs in this volume give a taste of the of the convivial climate of the meeting, and in particular during the social events that we organized.

Acknowledgements

The funding agencies, which made this conference possible are:

- The Asia Pacific Center for Theoretical Physics (APCTP): the APCTP pursues the highest quality research in all areas of theoretical physics and promotes cooperation among scientists from its member countries in the Asia Pacific region,
- The Aix Marseille Université (AMU), formerly the Université de Provence; the AMU has an academic agreements with the Quy Nhon University and the Hanoi National University of Education.

We gratefully acknowledge the financial support, these grants were very welcome.

ICGAC10 was made possible thanks to the International Advisory Committee who maintains this biennual conference alive. The keen interest and enthusiasm were due mainly to the judicious choice of subjects and speakers made by the members of the International Program Committee. Finally, the session chairpersons ensured an orderly conference in which discussions and questions played a central and stimulating role. To all of them, we express our deep gratitude.

We gratefully acknowledge the enthusiastic support of Mr Nguyên van Thien, General Secretary, Mr Lê Huu Lôc, President of the Popular Committee, Mr Nguyên Tân and the staff of the International Relationship Department of the province of Binh Dinh, whose support contributed in no small measure in the success of these two international conferences. We would like to thank Professor Nguyên van Hiêu and Professor Phan Thanh Binh for their presence at the conferences and for their unfailing support. Many thanks are due to the Quy Nhon University and especially to Professor Nguyên Thi Minh Phuong who has participated actively in the organization of the conferences. We thank the staff of the Seagull Hotel and especially M. Nguyen van Phuc, General Director and Ms Tran Thi Hong Nhung, International Relationship Manager for their outstanding hospitality and care which were key elements in the success of the VIIIth Rencontres du Vietnam.

The talent and enthousiasm of Mr. Cu enabled these memorable events to be captured in beautiful photographs of which a sample can be found in this volume. We thank him warmly for his admirable work.

The Rencontres du Vietnam was responsible for the practical organization of the conferences. The relaxed atmosphere of the meeting was due to the dedicated work of:

- The conference secretariat: Isabelle Cossin, Maryvonne Joguet, Nicole Ribet, Mary-Ann Rotondo and Hady Schenten,
- The staff of the ICISE: Doan Minh Hoa, Nguyen Tân and Nguyen Thi Loi.

We thank them all warmly,
Jean Trân Thanh Vân and Roland Triay

The conference participants

Arrival: from left to right - Sang Pyo Kim, Angelo Tartaglia, Jean Trân Than Vân

Arrival: from left to right - James Nester, Jun Luo, Kei-ichi Maeda, Vera Yurievna and Vera Georgievna Sinitsyna

From left to right: General Secretary Nguyên van Thiên, President Lê Huu Lôc and Professor Jean Trân Than Vân at the welcome party

Ground breaking ceremony for the International Centre for Interdiscipllinary Science and Education (ICISE)

Participants visiting the Banh It towers

Astronomy & Relativistic Astrophysics

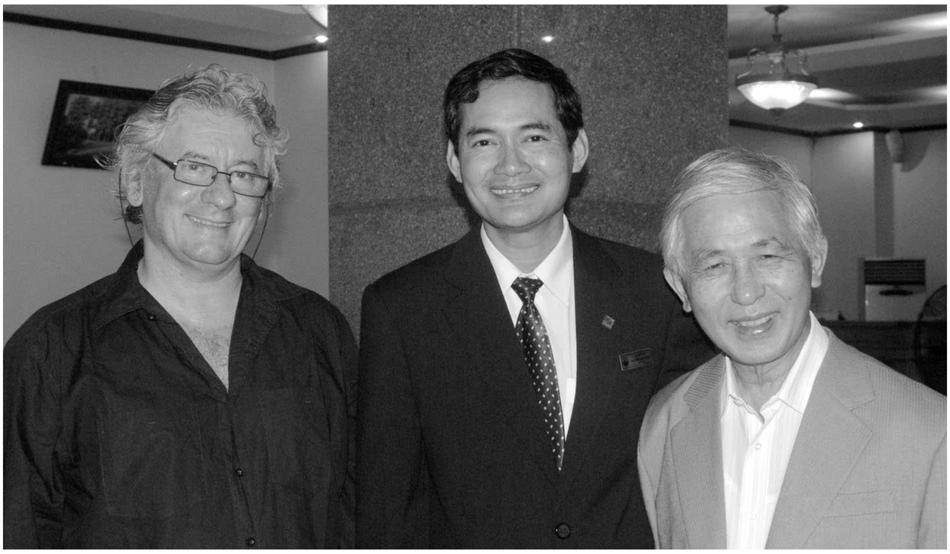

Roland Triay, M. Nguyên van Phuc (Director of Segull Hotel) and Jean Trân Thanh Van

Roland Triay and Truong Quy Nham (F & B manager of the Seagull Hotel)

Chromatic gravitational lensing

O.Yu. Tsupko[1,2], *G.S. Bisnovatyi-Kogan*[1,2]
[1]*Space Research Institute of Russian Academy of Sciences,*
Profsoyuznaya 84/32, Moscow 117997, Russia
[2] *National Research Nuclear University MEPhI,*
Kashirskoe Shosse 31, Moscow 115409, Russia
Email : tsupko@iki.rssi.ru

Abstract

We discuss gravitational lensing in plasma. We have shown that the gravitational deflection by point mass in the homogeneous plasma differs from the vacuum deflection and depends on the frequency of the photon. Therefore gravitational lensing in plasma is chromatic. We also discuss the photon deflection by point mass and mass distribution in non-homogeneous plasma. Our approach allows us consider two chromatic effects simultaneously: the gravitational deflection in plasma which differs from the vacuum case (new effect), and the non-relativistic effect (refraction) connected with the plasma inhomogeneity. We also discuss general properties of deflection of light ray in different media.

1 Introduction

Gravitational lensing is well developed theory which combines a wide range of phenomena connected with the deflection of light rays by gravity. Theory and observations of gravitational lensing include several big branches: strong lensing, weak lensing, microlensing. Now gravitational lensing is a powerful astrophysical tool for investigations of distant objects, a distribution of dark matter and large scale structure, the cosmic microwave background, discovery of planet and checking of the General Relativity [1], [2].

Theory of gravitational lensing is based on the Einstein deflection angle. The photon deflection angle in vacuum, in the Schwarzschild metric with a given mass M, is determined, for small deflection angles $\hat{\alpha} \ll 1$, by a formula

$$\hat{\alpha} = \frac{4GM}{c^2 b} = \frac{2R_S}{b}, \tag{1}$$

where b is the impact parameter, and $b \gg R_S$, $R_S = 2GM/c^2$ is the Schwarzschild radius. In the most astrophysical situations related with the gravitational lensing the approximation of the weak deflection is well satisfied.

Due to the gravitational deflection of light ray from source by the Einstein angle, the observed angular position of image of the distant source is changed. It is also possible that the multiple images of the same source are observed. The simplest situation of formation of multiple images is presented on Fig. 1. In general case, the flux from lensed image of source is different from the flux from source in absence of lensing. It is effect of magnification in the gravitational lensing. The gravitational lensing also changes an observed shape of source (effect of distortion).

Theory of gravitational lensing is developed for the light propagation in vacuum. The photon trajectories and deflection angles in vacuum don't depend on the photon frequency (or energy). Therefore gravitational lensing in vacuum is achromatic. For example, in Schwarzschild point-mass lens two images have complicated spectra, formed by the photons of different frequencies which undergo deflection by the same angle (Fig. 1).

It is interesting to consider the gravitational lensing in a plasma, because in space the light rays mostly propagate through this medium. When we work in the frame of geometrical optics what is usual for gravitational lensing, we can characterize properties of medium by using of the refractive index. In inhomogeneous medium (the refraction index depends on space coordinates) photon moves along curved trajectory, it is effect of refraction. The effect of the refractive deflection of light has no relation to gravity.

In medium the light rays move with the group velocity. For plasma with the index of refraction $n = 1 - \omega_e^2/\omega^2$ (ω_e^2 is the plasma electron frequency, ω is the frequency of the photon) we have the relations specific for plasma: the phase velocity is $v_{phase} = c/n$, the group velocity is $v_{group} = cn$, $v_{phase}v_{group} = c^2$.

Deflection of light rays due to action of both gravity and plasma is not new problem (see, for example [3]). This problem was considered in some works, in application to gravitational lensing it was discussed in details in [4] where gravitational lensing by gravitating body with surrounding spherically symmetric plasma distribution was considered. The consideration was usually done in a linear approximation, when the two effects: the vacuum deflection due to the gravitation (Einstein angle), and the deflection due to the non-homogeneity of the plasma, have been considered separately. The first effect is achromatic, the second one depends on the photon frequency because the plasma is dispersive medium, but equals to zero if the plasma is homogeneous.

A general theory of the geometrical optic in the curved space-time, in arbitrary medium, is presented in the book of Synge [5], see also [6], [7]. Similar to Synge approach for propagation of the light rays in presence both gravity and plasma was developed in the book of Perlick [8], and a general formulae for the light deflection in the Schwarzschild and Kerr metrics with the plasma are obtained in the form of an integral.

A rigorous treatment of the light bending in gravity and plasma requires an answer to the question: is the gravitational deflection of the light rays in the medium the same as in vacuum? For consideration of this problem we used a general theory of the geometrical optic in the curved space-time, in isotropic dispersive medium, developed by Synge [5]. We have shown that in the homogeneous plasma the gravitational deflection will differ from the vacuum case and will depend on the photon frequency [9], [10].

2 Gravitational bending of light rays in homogeneous plasma

We have considered static weak gravitational field and plasma with refractive index in this gravitational field

$$n^2 = 1 - \frac{\omega_e^2}{[\omega(r)]^2}\,, \quad \omega_e^2 = \frac{4\pi e^2 N(r)}{m} \equiv K_e N(r)\,. \tag{2}$$

Here $\omega(r)$ is the frequency of the photon, which depends on the space coordinate r due to the presence of the gravitational field (gravitational red shift). We denote $\omega(\infty) \equiv \omega$, e is the charge of the electron, m is the electron mass, ω_e is the electron plasma frequency, $N(r)$ is the electron concentration in inhomogeneous plasma.

We have shown for the first time that due to dispersive properties of plasma even in the homogeneous plasma the gravitational deflection differs from vacuum deflection angle, and gravitational deflection angle in plasma depends on frequency of the photon [9], [10]:

$$\hat{\alpha} = \frac{R_S}{b}\left(1 + \frac{1}{1 - (\omega_e^2/\omega^2)}\right). \tag{3}$$

This formula is valid under the condition of smallness of $\hat{\alpha}$. The presence of plasma increases the gravitational deflection angle. Formula is valid only for $\omega > \omega_e$, because the waves with $\omega < \omega_e$ do not propagate in the plasma. Under $\omega_e = 0$ (concentration $N(r) = 0$) or $\omega \to \infty$ this formula turns into the deflection angle for vacuum $2R_S/b$.

Gravitational deflection in homogeneous plasma is chromatic. In homogeneous plasma photons of smaller frequency, or larger wavelength, are deflected by a larger angle by the gravitating center. The effect of difference in the gravitational deflection angles is significant for longer wavelengths, when ω is approaching ω_e. That is possible only for the radio waves. Therefore, the gravitational lens in plasma acts as a radiospectrometer [9].

We should use formula (3) when we consider gravitational lensing of radiowaves by point or spherical body in presence of homogeneous plasma. This effect has a general relativistic nature, in combination with the dispersive properties of plasma. We should also emphasize that the plasma is considered here like the medium with given index of refraction, and this formula does not take into account gravitation of particles of plasma.

The observational effect of the frequency dependence may be represented on the example of the Schwarzschild point-mass lens. Instead of two concentrated images with complicated spectra, we will have two line 'rainbow' images, formed by the photons with different frequencies, which are deflected by different angles (Fig. 2).

Gravitational lensing also leads to magnification of source. This means that the flux of image is bigger or smaller than the flux of source, different images have different magnifications. In observations we don't know the intrinsic flux of source and its spectrum, but we can compare the fluxes of images in different frequencies. The ratios of the fluxes of images in different bands should be the same, if we consider lensing in vacuum, because gravitational deflection in vacuum is achromatic.

The magnification is determined by the deflection law [1]. In case of radio lensing in the plasma we have another formula for deflection instead Einstein angle, so formulae for magnification will be another. It leads to difference of magnigications of different images in different bands, when the light propagates in regions with different plasma density. By-turn it leads to difference of ratios of the fluxes of images in different bands (see details in [10]). It is another prediction of model of gravitational radiospectrometer for observation. We should mention that Thompson scattering and absorption during propagation of radiation through the plasma can significantly change the flux and complicate the investigation of the phenomena of lensing magnification.

3 Photon deflection in non-homogeneous plasma in presence of gravity

We have also derived the deflection angle for the photon moving in a weak gravitational field, in the Schwarzschild metric of point mass, in the arbitrary inhomogeneous plasma [10]:

$$\hat{\alpha}_b = \frac{R_S}{b} + \int_0^\infty \left(\frac{1}{1-(\omega_e^2/\omega^2)} \frac{R_S\, b}{r^3} + \frac{K_e}{\omega^2 - \omega_e^2} \frac{b}{r} \frac{dN(r)}{dr} \right) dz. \tag{4}$$

Approximation is that the whole deflection angle, from the combined plasma and gravity effects, remains small. Here ω_e depends on concentration $N(r)$, and integration can be performed by substitution of $N(r)$ and $r = \sqrt{b^2 + z^2}$, z is the axis of propagation of the unperturbed straight light ray with the impact parameter b .

To demonstrate the physical meaning of different terms in (4), we write this expression under condition $1 - n = \omega_e^2/\omega^2 \ll 1$. Carrying out the expansion of terms with the plasma frequency, we obtain:

$$\hat{\alpha}_b = \frac{2R_S}{b} + \frac{R_S\, b}{\omega^2} \int_0^\infty \frac{\omega_e^2}{r^3}\, dz + \frac{K_e b}{\omega^2} \int_0^\infty \frac{1}{r} \frac{dN(r)}{dr}\, dz + \frac{K_e b}{\omega^4} \int_0^\infty \frac{\omega_e^2}{r} \frac{dN(r)}{dr}\, dz. \tag{5}$$

The first term is a vacuum gravitational deflection. The second term is an additive correction to the gravitational deflection, due to the presence of the plasma. This term is present in the deflection angle both in the inhomogeneous and in the homogeneous plasma, and depends on the photon frequency. The third term is a non-relativistic deflection due to the plasma inhomogeneity (the refraction). This term depends on the frequency, but it is absent if the plasma is homogeneous. The forth term is a small additive correction to the third term.

In case of gravitational lensing by mass distribution we have the formula [10]:

$$\hat{\alpha}_b = \frac{4GM(b)}{c^2 b} + \frac{2GM(b)\, b}{c^2\omega^2} \int_0^\infty \frac{\omega_e^2\, dz}{r^3} + \frac{K_e b}{\omega^2} \int_0^\infty \frac{dN(r)}{dr} \frac{dz}{r} + \frac{K_e b}{\omega^4} \int_0^\infty \frac{dN(r)}{dr} \frac{\omega_e^2\, dz}{r}, \tag{6}$$

where $M(b)$ is the projected mass enclosed by the circle of the radius b. In another words it is the mass inside the cylinder with the radius b.

In case when the deflection angle in the Schwarzschild metric in presence of plasma is not small, the exact formula for light deflection angle in the Schwarzschild metric and plasma with spherically symmetric distribution of concentration in the form of integral can be used [8].

4 Discussion and Conclusions

We would like to formulate here the main properties of the gravitational deflection in different media:

(1) In vacuum the gravitational deflection is achromatic.

(2) If a medium is homogeneous (the refractive index n is constant, it does not depend on the space coordinates) and not dispersive (the refractive index does not depend on the photon frequency), the gravitational deflection angle is the same as in vacuum. A group velocity is smaller than light velocity in vacuum.

(3) If the medium is homogeneous but dispersive (the refractive index does not depend on the space coordinates but depends on the frequency), the gravitational deflection angle is different from the vacuum case and depends on the photon frequency. For example: plasma.

(4) If medium is non-homogeneous (the refractive index depends on the space coordinates), we will have also the refractive deflection. If medium is non-homogeneous and dispersive, the refractive deflection depends on the photon frequency.

Conclusions about the gravitational lensing in plasma are:

(i) In the homogeneous plasma gravitational deflection differs from vacuum (Einstein) deflection angle and depends on frequency of the photon. So gravitational lens in homogeneous plasma acts as a gravitational radiospectrometer. Gravitational lensing becomes chromatic on presence of plasma.

(ii) Plasma effects leads to changing of angular separation between images and ratios of fluxes, if we compare optical and radio waves. It leads to: in the observations the spectra of two images may be different in the long wave side due to different plasma properties along the trajectory of the images. It can give information about properties of plasma around lens.

(iii) We have carried out the calculations for models with the nonuniform plasma distribution: singular and nonsingular isothermal sphere; for hot gas inside the gravitational field of a black hole, and of a cluster of galaxies. For different gravitational lens models we compare the corrections to the vacuum lensing due to the gravity effect in plasma (second term in (6)), and due to the plasma inhomogeneity (third term in (6)). We have shown that the gravitational effect could be detected in the case of a hot gas in the gravitational field of a galaxy cluster [10].

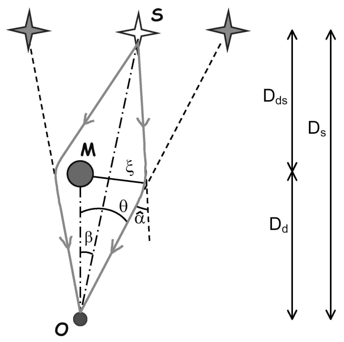

Figure 1: Lensing of the point source by the Schwarzschild point-mass lens in vacuum. Light rays from source S are deflected by angle $\hat{\alpha}$ by the point mass M. Observer O sees two images instead single real source S. Angular position of images θ_1 and θ_2 depends on angular position of source β, mass of lens M and distances between source, lens and observer D_s, D_d, D_{ds}, and can be calculated analytically [1].

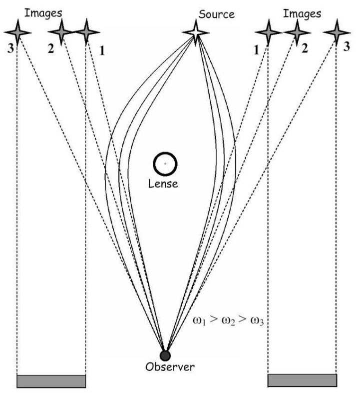

Figure 2: Lensing of the point source by the Schwarzschild point-mass lens in homogeneous plasma. Instead of two point images due to lensing in the vacuum we have two line images. The pairs of images, corresponding to the same photon frequency, are indicated by the same numbers. The photons of smaller frequency are deflected by a larger angle by the gravitating center. Two images with number 1 correspond to the vacuum lensing.

Acknowledgments

The work of OYuT and GSBK was partially supported by the Russian Foundation for Basic Research grant 11-02-00602, the RAN Program 'Origin, formation and evolution of objects of Universe' and the Russian Federation President Grant for Support of Leading Scientific Schools NSh-5440.2012.2.

The work of OYuT was also partially supported by the Russian Federation President Grant for Support of Young Scientists MK-8696.2010.2 and the Dynasty Foundation.

References

[1] P. Schneider, J. Ehlers and E. Falco, Gravitational lenses, Springer-Verlag, Berlin (1992).

[2] P. Schneider, C. S. Kochanek and J. Wambsganss, Gravitational Lensing: Strong, Weak and Micro, Swiss Society for Astrophysics and Astronomy Series: Saas-Fee Advanced Courses, Number 33, Springer, Berlin (2006).

[3] A. P. Lightman, W. H. Press, R. H. Price, S. A. Teukolsky, Problem Book in Relativity and Gravitation, Princeton University Press, Princeton, New Jersey, New York (1979).

[4] P. V. Bliokh and A. A. Minakov, Gravitational Lenses, Naukova Dumka, Kiev (1989) (in Russian).

[5] J. L. Synge, Relativity: the General Theory, North-Holland Publishing Company, Amsterdam (1960).

[6] J. Bičák and P. Hadrava, *General-relativistic Radiative Transfer Theory in Refractive and Dispersive Media*, Astron. and Astrophys 44 (1975) 389.

[7] S. Kichenassamy, R. A. Krikorian, *Relativistic radiation transport in dispersive media* , Physical Review D 32 (1985) 1866.

[8] V. Perlick, Ray Optics, Fermat's Principle, and Applications to General Relativity, Springer-Verlag, Berlin Heidelberg New York (2000).

[9] G. S. Bisnovatyi-Kogan and O. Yu. Tsupko, *Gravitational Radiospectrometer*, Gravitation and Cosmology 15 (2009) 20.

[10] G. S. Bisnovatyi-Kogan and O. Yu. Tsupko, *Gravitational lensing in a non-uniform plasma*, Mon. Not. R. Astron. Soc. 404 (2010) 1790.

Accretion into black holes, and relativistic jets

G.S. Bisnovatyi-Kogan[1], *A.S. Klepnev*[1], *R.V.E. Lovelace*[2]
[1] *Space Research Institute Rus. Acad. Sci., Moscow, Russia*
[2] *Cornell University, Ithaca, USA*
Email : gkogan@iki.rssi.ru

Abstract

We discuss the problem of the formation of a large-scale magnetic field in the accretion disks around black holes, taking into account the non-uniform vertical structure of the disk. The high electrical conductivity of the outer layers of the disk prevents the outward diffusion of the magnetic field. This implies a stationary state with a strong magnetic field in the inner parts of the accretion disk close to the black hole, and zero radial velocity at the surface of the disk. Structure of advective accretion disks is investigated, and conditions for formation of optically thin regions in central parts of the accretion disk are found. The problem of jet collimation by magneto-torsion oscillations is considered.

1 Introduction

Quasars and AGN contain supermassive black holes, about 10 HMXR contain stellar mass black holes - microquasars. Jets are observed in objects with black holes: collimated ejection from accretion disks.

Early work on disk accretion to a black hole argued that a large-scale magnetic field of, for example, the interstellar medium would be dragged inward and greatly compressed by the accreting plasma [10,11,13]. Subsequently, analytic models of the field advection and diffusion in a turbulent disk suggested, that the large-scale field diffuses outward rapidly [13,15], and prevents a significant amplification of the external poloidal field. This has led to the suggestion that special conditions (non-axisymmetry) are required for the field to be advected inward [19]. The question of the advection/diffusion of a large-scale magnetic field in a turbulent plasma accretion disk was reconsidered in [7], taking into account its non-uniform vertical structure. The high electrical conductivity of the surface layers of the disk, where the turbulence is suppressed by the radiation flux and the high magnetic field, prevents outward diffusion of the magnetic field. This leads to a strong magnetic field in the inner parts of accretion disks.

The standard model for accretion disks [18] is based on several simplifying assumptions. The disk must be geometrically thin and rotate at the Kepler angular velocity. These assumptions make it possible to neglect radial gradients and, to proceed from the differential to algebraic equations. For low accretion rates $\dot{M}$, this assumption is fully appropriate. However, for high accretion rates, the disk structure may differ from the standard model. To solve the more general problem, advection and a radial pressure gradient have been included in the analysis of the disk structure [17]. It was shown in [1], that for large accretion rates there are no local solutions that are continuous over the entire region of existence of the disk and undergo Kepler rotation. A self-consistent solution for an advective accretion disk with a continuous description of the entire region between the optically thin and optically thick regions had been obtained in [3,6].

2 The fully turbulent model

There are two limiting accretion disk models which have analytic solutions for a large-scale magnetic field structure. The first was constructed in [11] for a stationary non-rotating accretion disk. A stationary state in this disk (with a constant mass flux onto a black hole) is maintained by the balance between magnetic and gravitational forces, and thermal balance (local) is maintained by Ohmic heating and radiative heat conductivity for an optically thick conditions. The mass flux to the black hole in the accretion disk is determined by the finite electrical conductivity of the disk matter and the diffusion of matter across the large-scale magnetic field. It is widely accepted that the laminar disk is unstable to different hydrodynamic, magneto-hydrodynamic, and plasma instabilities which implies that the disk is turbulent. In X-ray binary systems the assumption about turbulent accretion disk is necessary for construction of a realistic models [18]. The turbulent accretion disks had been constructed for non-rotating models with a large-scale magnetic field. A formula for turbulent magnetic diffusivity was derived in [11], similar to the scaling of the shear α-viscosity in turbulent accretion disk in binaries [18], where the viscous stress tensor component $t_{r\phi} = \alpha P$, with $\alpha \leq 1$ a dimensionless constant, and P is the pressure in the disk midplane. Using this representation, the expression for the turbulent electrical conductivity σ_t is written as

$$\sigma_t = \frac{c^2}{\tilde{\alpha} 4\pi h \sqrt{P/\rho}}. \tag{1}$$

Here, $\tilde{\alpha} = \alpha_1 \alpha_2$. The characteristic turbulence scale is $\ell = \alpha_1 h$, where h is the half-thickness of the disk, the characteristic turbulent velocity is $v_t = \alpha_2 \sqrt{P/\rho}$. The large-scale magnetic field threading a turbulent Keplerian disk arises from external electrical currents and currents in the accretion disk. The magnetic field may become dynamically important, influencing the accretion disk structure, and leading to powerful jet formation, if it is strongly amplified during the radial inflow of the disk matter. It is possible only when the radial accretion speed of matter in the disk is larger than the outward diffusion speed of the poloidal magnetic field due to the turbulent diffusivity $\eta_t = c^2/(4\pi\sigma_t)$. Estimates in [15] have shown that for a turbulent conductivity (1), the outward diffusion speed is larger than the accretion speed. Thus it appears that there is no large-scale magnetic field amplification during Keplerian disk accretion. Numerical calculations in [15] are reproduced analytically for the standard accretion disk structure [7]. Far from the inner disk boundary the specific angular momentum is $j \gg j_{in}$. The characteristic time t_{visc} of the matter advection due to the shear viscosity is $t_{visc} = \frac{r}{v_r} = \frac{j}{\alpha v_s^2}$. The time of the magnetic field diffusion is $t_{diff} = \frac{r^2}{\eta} \frac{h}{r} \frac{B_z}{B_r}$, $\eta = \frac{c^2}{4\pi\sigma_t} = \tilde{\alpha} h v_s$. In the stationary state, the large-scale magnetic field in the accretion disk is determined by the equality $t_{vis} = t_{diff}$, what determines the ratio

$$\frac{B_r}{B_z} = \frac{\alpha}{\tilde{\alpha}} \frac{v_s}{v_K} = \frac{\alpha}{\tilde{\alpha}} \frac{h}{r} \ll 1 \, . \tag{2}$$

Here, $v_K = r\Omega_K$ and $j = r v_K$ for a Keplerian disk. In a turbulent disk a matter is penetrating through magnetic field lines, almost without a field amplification: the field induced by the azimuthal disk currents has $B_{zd} \sim B_{rd}$.

3 Turbulent disk with radiative outer zones

Near the surface of the disk, in the region of low optical depth, the turbulent motion is suppressed by the radiative flux, similar to the suppression of the convection over the photospheres of stars with outer convective zones. The presence of the outer radiative layer does not affect the estimate of the characteristic time t_{visc}

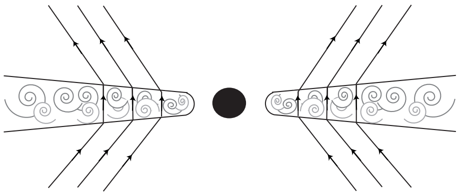

Figure 1: Sketch of the large-scale poloidal magnetic field threading a rotating turbulent accretion disk with a radiative outer boundary layer. The toroidal current flows mainly in the highly conductive radiative layers. The large-scale (average) field in the turbulent region is almost vertical.

of the matter advection in the accretion disk because it is determined by the main turbulent part of the disk. The time of the field diffusion, on the contrary, is significantly changed, because the electrical current is concentrated in the radiative highly conductive regions, which generate the main part of the magnetic field. The structure of the magnetic field with outer radiative layers is shown schematically in Fig.1.

Inside the turbulent disk the electrical current is negligibly small so that the magnetic field there is almost fully vertical, with $B_r \ll B_z$. In the outer radiative layer, the field diffusion is very small, so that matter advection is leading to strong magnetic field amplification. We suppose, that in the stationary state the magnetic forces could support the optically thin regions against gravity. When the magnetic force balances the gravitational force in the outer optically thin part of the disk of surface density Σ_{ph}, the following relation takes place [11]

$$\frac{GM\Sigma_{ph}}{r^2} \simeq \frac{B_z I_\phi}{2c} \simeq \frac{B_z^2}{4\pi} \,, \tag{3}$$

The surface density over the photosphere corresponds to a layer with effective optical depth close to 2/3 (e.g. [5]). We estimate the lower limit of the magnetic field strength, taking κ_{es} (instead of the effective opacity $\kappa_{eff} = \sqrt{\kappa_{es}\kappa_a}$). Writing $\kappa_{es}\Sigma_{ph} = 2/3$, we obtain $\Sigma_{ph} = 5/3$ (g/cm^2) for the opacity of the Thomson scattering, $\kappa_{es} = 0.4$ cm^2/g. The absorption opacity κ_a is much less than κ_{es} in the inner regions of a luminous accretion disk so we estimate the lower bound on the large-scale magnetic field in a Keplerian accretion disk as [7]

$$B_z = \sqrt{\frac{5\pi}{3}} \frac{c^2}{\sqrt{GM_\odot}} \frac{1}{x\sqrt{m}} \simeq 10^8 \mathrm{G} \frac{1}{x\sqrt{m}}, \quad x = \frac{r}{r_g}, \quad m = \frac{M}{M_\odot} \,. \tag{4}$$

The maximum magnetic field is reached when the outward magnetic force balances the gravitational force on the surface with a mass density Σ_{ph}. In equilibrium, $B_z \sim \sqrt{\Sigma_{ph}}$. We find that B_z in a Keplerian accretion disk is about 20 times less than its maximum possible value [11], for $x = 10$, $\alpha = 0.1$, and $\dot{m} = 10$.

4 Self-consistent numerical model

Self-consistent models of the rotating accretion disks with a large-scale magnetic field requires solution the equations of magneto-hydrodynamics. The solution with a small field will not be stationary, and a transition to the strong field solution will take place. Therefore the strong field solution is the only stable stationary solution for a rotating accretion disk. The vertical structure of the disk with a large scale poloidal magnetic field was calculated in [14], taking into account the turbulent viscosity and diffusivity, and the fact that the turbulence vanishes at the surface of the disk. Coefficients of the turbulent viscosity ν, and magnetic

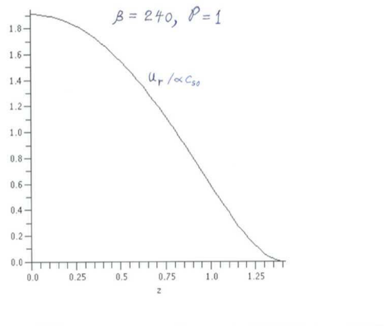

Figure 2: Distribution of the radial velocity over the thickness in the stationary accretion disk with a large scale poloidal magnetic field

diffusivity η are connected by the magnetic Prandtl number P ~1, $\nu = P\eta = \alpha\ \frac{c_{s0}^2}{\Omega_K}\ g(z)$, where α is a constant, determining the turbulent viscosity [18]; $\beta = c_{s0}^2/v_{A0}^2$, where $v_{A0} = B_0/(4\pi\rho_0)^{1/2}$ is the midplane Alfvn velocity. The function $g(z)$ accounts for the absence of turbulence in the surface layer of the disk [7]. In the body of the disk $g = 1$, whereas near the surface of the disk g tends over a short distance to a very small value, effectively zero. The smooth function with a similar behavior is taken [15] in the form $g(\zeta) = \left(1 - \frac{\zeta^2}{\zeta_S^2}\right)^\delta$, with $\delta \ll 1$. In the stationary state the boundary condition on the disk surface is $u_r = 0$, and only one free parameter - magnetic Prandtl number P remains in the problem. In a stationary disk vertical magnetic field has a unique value. The example of the radial velocity distribution for P =1 is shown in Fig.2 from [8].

5 Basic equations for accretion disk structure

We use equations describing a thin, steady-state accretion disk, averaged over its thickness [3,6]. These equations include advection and can be used for any value of the vertical optical thickness of the disk. We use a pseudo-newtonian approximation for the structure of the disk near the black hole, where the effects of the general theory of relativity are taken into account using the Paczynski-Wiita potential [16]

$$\Phi(r) = -\frac{GM}{r - 2r_g}. \tag{5}$$

Here M is the mass of the black hole, $2r_g = 2GM/c^2$ is the gravitational radius. The self-gravitation of the disk is neglected, the viscosity tensor $t_{r\phi} = -\alpha P$. The conservation of mass is expressed in the form $\dot{M} = 4\pi r h \rho v$, where $\dot{M}$ is the accretion rate, $\dot{M} > 0$, and h is the half thickness of the disk. The equilibrium in the vertical direction $\frac{dP}{dz} = -\rho z \Omega_K^2$ is replaced by the algebraic relation in the form $h = \frac{c_s}{\Omega_K}$, where $c_s = \sqrt{P/\rho}$ is the isothermal sound speed. The equations of motion in the radial and azimuthal directions are, respectively, written as

$$v\frac{dv}{dr} = -\frac{1}{\rho}\frac{dP}{dr} + (\Omega^2 - \Omega_K^2)r, \quad \frac{\dot{M}}{4\pi}\frac{d\ell}{dr} + \frac{d}{dr}(r^2 h t_{r\phi}) = 0, \tag{6}$$

where Ω_K is the Kepler angular velocity, given by $\Omega_K^2 = GM/r(r - 2r_g)^2$; $\ell = \Omega r^2$ is the specific angular momentum. Other components of the viscosity tensor are assumed negligibly small. The vertically averaged equation for the energy balance is $Q_{adv} = Q^+ - Q^-$, where

$$Q_{adv} = -\frac{\dot{M}}{4\pi r}\left[\frac{dE}{dr} + P\frac{d}{dr}\left(\frac{1}{\rho}\right)\right], Q^+ = -\frac{\dot{M}}{4\pi} r\Omega \frac{d\Omega}{dr}\left(1 - \frac{l_{in}}{l}\right), \quad (7)$$

$$Q^- = \frac{2aT^4c}{3(\tau_\alpha + \tau_0)h}\left[1 + \frac{4}{3(\tau_0 + \tau_\alpha)} + \frac{2}{3\tau_*^2}\right]^{-1}, \quad (8)$$

are the energy fluxes (erg/cm^2/s) associated with advection, viscous dissipation, and radiation from the surface, respectively, τ_0 is the Thomson optical depth, $\tau_0 = 0.4\rho h$ for the hydrogen composition. We have introduced the optical thickness for absorption, $\tau_\alpha \simeq 5.2 \cdot 10^{21} \frac{\rho^2 T^{1/2} h}{acT^4}$,and the effective optical thickness $\tau_* = [(\tau_0 + \tau_\alpha)\,\tau_\alpha]^{1/2}$. The equation of state is for a mixture of a matter and radiation $P_{\rm tot} = P_{\rm gas} + P_{\rm rad}$. The gas pressure is given by formula, $P_{\rm gas} = \rho RT$, R is the gas constant, and the radiation pressure is given by

$$P_{\rm rad} = \frac{aT^4}{3}\left[1 + \frac{4}{3(\tau_0 + \tau_\alpha)}\right]\left[1 + \frac{4}{3(\tau_0 + \tau_\alpha)} + \frac{2}{3\tau_*^2}\right]^{-1}. \quad (9)$$

The specific energy of the mixture of the matter and radiation is determined as $\rho E = \frac{3}{2}P_{\rm gas} + 3P_{\rm rad}$. Expressions for Q^- and P_{rad}, valid for any optical thickness, have been obtained in [1].

6 Method of solution and numerical results

The system of differential and algebraic equations can be reduced to two ordinary differential equations,

$$\frac{x}{v}\frac{dv}{dx} = \frac{N}{D}, \quad (10)$$

$$\frac{x}{v}\frac{dc_s}{dx} = 1 - (\frac{v^2}{c_s^2} - 1)\frac{N}{D} + \frac{x^2}{c_s^2}(\Omega^2 - \frac{1}{x(x-2)^2}) + \frac{3x-2}{2(x-2)}. \quad (11)$$

Here the numerator N and denominator D are algebraic expressions depending on x, v, c_s, and l_{in}, the equations are written in dimensionless form with $x = r/r_g$, $r_g = GM/c^2$. The velocities v and c_s have been scaled by the speed of light c, and the specific angular momentum l_{in} by the value c/r_g. This system of differential equations has two singular points, defined by the conditions $D = 0$, $\quad N = 0$. The inner singularity is situated near the last stable orbit with $r = 6r_g$. The outer singularity, lying at distances much greater than r_g, is an artifact arising from our use of the artificial parametrization $t_{r\phi} = -\alpha P$ of the viscosity tensor. The system of ordinary differential equations was solved by a finite difference method discussed in [2]. The method is based on reducing the system of differential equations to a system of nonlinear algebraic equations which are solved by an iterative Newton-Raphson scheme, with an expansion of the solution near the inner singularity and using of l_{in} as an independent variable in the iterative scheme [2]. The solution is almost independent of the outer boundary condition. The numerical solutions have been obtained for the structure of an accretion disk over a wide range of the parameters $\dot{m}$ ($\dot{m} = \frac{\dot{M}c^2}{L_{EDD}}$) and α. For low accretion rates, $\dot{m} < 0.1$, the solution for the advection model has $\tau_* \gg 1$, $v \ll c_s$, and an angular velocity is close to the Kepler velocity everywhere, except a very thin layer near the inner boundary of the disk. As the accretion rate increases, the situation changes significantly. The changes show up primarily in the inner region of the disk. Fig. 3 shows the radial dependences of the temperature of the accretion disk for the accretion rate $\dot{m} = 50$, and different values of the viscosity parameter $\alpha = 0.01, 0.1, 0.4$. Clearly, for large $\dot{m}$ and α the

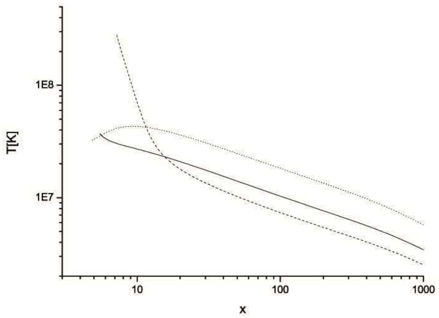

Figure 3: The radial dependence of the temperature of the accretion disk for an accretion rate $\dot{m} = 50$, and viscosity parameters $\alpha = 0.01$ (dotted curve), $\alpha = 0.1$ (smooth curve), and $\alpha = 0.4$ (dashed curve).

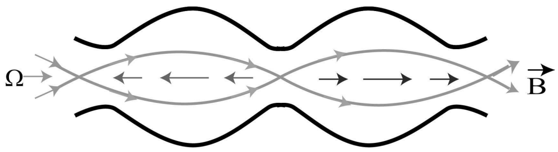

Figure 4: Qualitative picture of jet confinement by magneto-torsional oscillations.

inner part of the disk becomes optically thin. Because of this, a sharp increase in the temperature of the accretion disk is observed in this region.
Two distinct regions can be seen in the plot of the radial dependence of the temperature of the accretion disk. This is especially noticeable for a viscosity parameter $\alpha = 0.4$, where one can see the inner optically thin region with a dominant non-equilibrium radiation pressure P_{rad}, and an outer region which is optically thick with dominant equi- librium radiation pressure. Things are different when the viscosity parameter is small. Only a small (considerably smaller than for $\alpha = 0.4$) inner region becomes optically thin for accretion rates of $\dot{m} \approx 30 - 70$. Meantime, in the case of $\alpha = 0.01$, there are no optically thin regions at all.

7 Jet collimation by magneto-torsional oscillations.

Following [4], we consider the stabilization of a jet by a pure magneto-hydrodynamic mechanism associated with torsional oscillations. We suggest that the matter in the jet is rotating, and different parts of the jet rotate in different directions, see Fig.4. Such a distribution of the rotational velocity produces an azimuthal magnetic field, which prevents a disruption of the jet. The jet is representing a periodical, or quasi-periodical structure along the axis, and its radius oscillates with time all along the axis. The space and time periods of oscillations depend on the conditions at jet formation: the length-scale, the amplitude of the rotational velocity, and the strength of the magnetic field. The time period of oscillations can be obtained during the construction of the dynamical model, and the model should also show at what input parameters a long jet stabilized by torsional oscillations could exist.
Let us consider a long cylinder with a magnetic field directed along its axis. This cylinder will expand without limit under the action of pressure and magnetic forces. It is possible, however, that a limiting value of the radius of the cylinder could be reached in a dynamic state, in which the whole cylinder undergoes magneto-torsional oscillations. Such oscillations produce a toroidal field, which prevents radial expansion. There is therefore competition between the induced toroidal field, compressing the cylinder in the radial direction, and

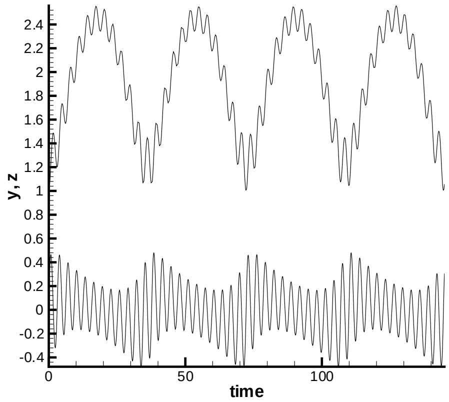

Figure 5: Time dependence of non-dimensional radius y (upper curve), and non-dimensional velocity z (lower curve), for $D = 2.1$, $y(0)$=1.

gas pressure, together with the field along the cylinder axis (poloidal), tending to increase its radius. During magneto-torsional oscillations there are phases when either the compression or expansion force prevails, and, depending on the input parameters, there are three possible kinds of behavior of such a cylinder that has a negligible self-gravity.

(1) The oscillation amplitude is low, so the cylinder suffers unlimited expansion (no confinement).

(2) The oscillation amplitude is high, so the pinch action of the toroidal field destroys the cylinder and leads to the formation of separated blobs.

(3) The oscillation amplitude is moderate, so the cylinder, in absence of any damping, survives for an unlimited time, and its parameters (radius, density, magnetic field etc.) change periodically, or quasi-periodically, in time.

After considerable simplifications, which details may be found in [4], the equation, describing the magneto-torsional oscillations of a long cylinder, takes the following form:

$$\frac{d^2\,y}{d\,\tau^2} = \frac{1 - D\,\sin^2\,\tau}{y}. \tag{12}$$

This equation describes approximately the time dependence of the outer radius of the cylinder $R(t)$ in the symmetry plane, where the rotational velocity remains zero. The dimensionless variables and the parameter D in (12) are defined as $\tau = \omega\,t$, $y = \frac{R}{R_0}$,with $R_0 = \frac{\sqrt{K}}{\omega}$, $D = \frac{1}{2\pi K C_m}\left(\frac{C_b\Omega_0}{z_0\omega}\right)^2$. The frequency of oscillations ω may be represented as $\omega = \alpha_n k V_A = \alpha_n \frac{B_{z,0}}{z_0}\sqrt{\frac{\pi}{\rho_0}}$, where k is the wave number, $k = 2\pi/z_0$, and V_A is the Alfven velocity, $V_A = B_{z,0}/\sqrt{4\pi\rho_0}$; $\alpha_n < 1$ is a coefficient determining the frequency of nonlinear Alfven oscillations, which are similar to the magneto-torsional oscillations under investigation. The example of the dynamically stabilized cylinder is given in Fig.5, from [4], y and z are non-dimensional radius, and radial velocity, respectively. Transition to stochastic regime in these oscillations was investigated in [9],

8 Discussion

The poloidal magnetic field is amplified during disk accretion, due to high conductivity in outer radiative layers. Stationary solution is obtained corresponding to $\beta = 240$, for Pr=1. Note, that the value of β is obtained using the density of the disk in the symmetry plane. The local value of β in the outer radiative regions is much lower, and approximately corresponds to equipartition between the pressure of a gas and magnetic field.

We have obtained a unique solution for the structure of an advection accretion disk surrounding a non-rotating black hole for different values of the viscosity parameter and accretion rate. This solution is global, trans-sonic, and, for high $\dot{m}$ and α, is characterized by a continuous transition of the disk from optically thick in the outer region to optically thin in the inner region. The model, with a correct accounting for the transition between the optically thick and optically thin regions reveals the existence of a temperature peak in the inner (optically thin) region. This peak might cause the appearance of a hard component in the spectrum, which could be observed.

A high temperature in the inner region of an accretion disk may lead to the formation of electron-positron pairs and change the emission spectrum of the disk at energies of 500 keV and above. Preliminary calculations have been done for a disk around a rapidly rotating black hole, with quasi-newtonian gravitational potential, approximating [20] the effects of the Kerr metric. We obtain that the temperature in the optically thin inner region substantially exceeds 500 keV, if the pair production is neglected. A consideration with a self-consistent account of pair creation is under way. In presence of a large scale magnetic field we may expect formation of relativistic jets with a high lepton excess.

We have shown that the existence and size of the optically thin region depend directly on the viscosity parameter α. When α= 0.5, a very substantial optically thin region is observed, when α= 0.1 we have a slight optically thin region, and when α= 0.01 no optically thin region is seen at all. This is because at very high $\dot{m}$ a large optical thickness is associated with a high density in the inner regions of the disk; at low $\dot{m}$ a large effective optical depth is connected with a high density because of a low temperature. Therefore, the effective optical depth has a minimum at intermediate values of $\dot{m}$, and for α= 0.01 this minimum turns out to be greater than unity. We obtain, that the geometric thickness of the disk in this model depends substantially on the accretion rate and more weakly, on the viscosity parameter α.

Acknowledgments

The work of GSBK, ASK was partially supported by the Russian Foundation for Basic Research grant 11-02-00602, the RAN Program 'Origin, formation and evolution of objects of Universe' and President Grant for Support of Leading Scientific Schools NSh-3458.2010.2. R.V.E.L was supported in part by NASA grants NNX08AH25G and NNX10AF63G and by NSF grant AST-0807129.

References

[1] Y.V. Artemova, G.S. Bisnovatyi-Kogan, G. Bjornsson, I.D. Novikov: 1996, *ApJ*, **456**, 119.

[2] Y.V. Artemova, G.S. Bisnovatyi-Kogan, I.V. Igumenshchev, I.D. Novikov: 2001, *ApJ*, **549**, p.1050.

[3] Y.V. Artemova, G.S. Bisnovatyi-Kogan, I.V. Igumenshchev, I.D. Novikov: 2006, *ApJ*, **637**, 968.

[4] G.S. Bisnovatyi-Kogan: 2007, *MNRAS*, **376**, 457.

[5] G.S. Bisnovatyi-Kogan 2001, *Stellar physics.* Vol.1,2. Berlin: Springer.

[6] G.S. Bisnovatyi-Kogan, A.S. Klepnev: 2010, *Astrophysics*, **53**, 409.

[7] G.S. Bisnovatyi-Kogan, R.V.E. Lovelace: 2007, *ApJL*, **45**, L167.

[8] G.S. Bisnovatyi-Kogan, R.V.E. Lovelace: 2010, *PoS* (Texas 2010) 008; arXiv:1104.4866.

[9] G.S. Bisnovatyi-Kogan, A.I. Neishtadt, Z.F. Seidov, et al.: 2011, *MNRAS*, **416**, 747.

[10] G.S. Bisnovatyi-Kogan, A.A. Ruzmaikin: 1974, *Ap&SS*, **28**, 45.

[11] G.S. Bisnovatyi-Kogan, A.A. Ruzmaikin: 1976, *Ap&SS*, **42**, 401.

[12] R.V.E. Lovelace: 1976, *Nature*, **262**, 649.

[13] R.V.E. Lovelace, M.M. Romanova, W.I. Newman: 1994, *ApJ*, **437**, 136.

[14] R.V.E. Lovelace, D.M. Rothstein, G.S. Bisnovatyi-Kogan: 2009, *ApJ*, **701**, 885.

[15] S.H. Lubow, J.C.B. Papaloizou, J.E. Pringle: 1994, *MNRAS*, **267**, 235.

[16] B. Paczynski, P.J. Wiita: 1980, *Astron. Ap.*, **88**, 23.

[17] B. Paczyoski, G.S. Bisnovatyi-Kogan: 1981, *Acta Astr.*, **31**, 283.

[18] N.I. Shakura, R.A. Sunyaev: 1973, *Astron. Ap.*, **24**, 337.

[19] H.C. Spruit, D.A. Uzdensky, 2005, *ApJ*, **629** 960.

[20] Y.V. Artemova, G. Bjornsson, I.D. Novikov, 1996, *ApJ*, **461**, 565.

Arrival of participants : Hoi-Lai Yu, Sang Pyo Kim, Vera Yurievna and Vera Georgievna Sinitsyna

Arrival of participants : Daniel Martin de Blas and Manu Paranjape

Evidence for non–standard Big Bang nucleosynthesis from the primordial abundance of ^{4}He

Trinh X. Thuan
University of Virginia, Astronomy Department
P.O. Box 400325, Charlottesville, VA 22904-4325, USA
txt@virginia.edu

Abstract

We present a new determination of the primordial helium mass fraction Y_p , based on ∼100 spectra of low-metallicity extragalactic H II regions. Using Monte Carlo methods to solve simultaneously for known systematic effects, we find the best value to be Y_p = 0.2565±0.0010 (statistical)±0.0050 (systematic). This value is higher at the 2σ level than the value given by standard big bang nucleosynthesis, implying deviations from it. The effective number of light neutrino species N_ν is equal to $3.68^{+0.80}_{-0.70}$ (2σ) and $3.80^{+0.80}_{-0.70}$ (2σ) for a neutron lifetime τ_n equal to 885.4±0.9 s and 878.5±0.8 s, respectively, larger than the experimental value of 2.993±0.011. This may be consistent with the existence of light sterile neutrinos suggested by neutrino oscillation experiments such as LSDN and MiniBooNE.

1 Introduction

The determination of the primordial ^{4}He (hereafter He) abundance and of some other light elements such as D, ^{3}He, and ^{7}Li, plays an important role in testing cosmological models. In the standard theory of big bang nucleosynthesis (SBBN), given the number of light neutrino species, the abundances of these light elements depend only on one cosmological parameter, the baryon-to-photon number ratio η. This means that accurate measurements of the primordial abundances of each of the four light elements can provide, in principle, a direct measurement of the baryonic density.

Because of the strong dependence of its abundance on η, deuterium has become the baryometer of choice. The D/H measurements in damped Lyα systems appear to converge to a mean primordial value, log D/H = 4.56±0.04, corresponding to a baryon mass fraction $\Omega_b h^2$ = 0.0213 0.001 [25]. This estimate of $\Omega_b h^2$ is in excellent agreement with the value of 0.02273±0.00062 obtained by [8] from analysis of five years of observations with the Wilkinson Microwave Anisotropy Probe (WMAP).

While a single good baryometer like D is sufficient to derive the baryonic mass density from BBN, accurate measurements of the primordial abundances of at least two different relic elements are required to check the consistency of SBBN. Among the remaining relic elements, ^{3}He can only be observed in the solar system and in the Galaxy, both of which have undergone significant chemical evolution, making it difficult to derive its primordial abundance [5]. The derivation of the primordial ^{7}Li abundance in metal-poor halo stars in the Galaxy is also beset by difficulties such as the uncertain stellar temperature scale and the temperature structures of the atmospheres of these very cool stars [7]. We are thus left with ^{4}He (hereafter He).

Although He is not a sensitive baryometer (the primordial helium mass fraction Y_p depends only logarithmically on the baryon density), its primordial abundance depends much more sensitively than that of D on the expansion rate of the universe, and on a possible lepton asymmetry in the early universe. This is for two reasons: 1) a faster expansion would leave less time for neutrons to convert into protons, and the resulting higher neutron abundance would result in a higher Y_p, and 2) Y_p depends sensitively on the neutron to proton ratio, which depends in turn on the numbers of electron neutrinos and anti-neutrinos. In that sense, He is both a good chronometer and/or a good leptometer, and is very sensitive to any small deviation from SBBN, and hence to new physics, much more so than the other three primordial light elements [29] [30]. Thus, accurate measurements of the primordial abundance of He are required to check the consistency of SBBN. However, to detect small deviations from SBBN and make cosmological inferences, Y_p has to be determined to a level of accuracy of less than a few percent.

2 Determination of the primordial He abundance from a large sample of low-metallicity HII regions

The primordial abundance of He can, in principle, be derived accurately from observations of the He and H emission lines from low-metallicity HII regions. While it is relatively straightforward to derive the helium abundance in an H II region with an accuracy of 10% if the spectrum is adequate, gaining one order of magnitude in the precision requires many conditions to be met. First, the observational data has to be of excellent quality. This has been the concern of our group [14] [15] [11] [12] [16]. We have spent the last two decades obtaining high signal-to-noise spectroscopic data of low-metallicity extragalactic H II regions, and our sample includes now a total of 86 H II regions in 77 galaxies. The sample is described in [16]. This constitutes by far the largest sample of high-quality data reduced in a homogeneous way to investigate the problem of the primordial helium abundance. To put things in perspective, the sample used in the pioneering work of [24] comprised only 5 objects, with considerably larger observational errors. Later, the sample of [23] included 36 objects and that of [22] 49 objects. With such a data set at hand, it is now generally believed that the accuracy of the determination of the primordial He abundance is limited presently, not so much by statistical uncertainties, but by our ability to account for systematic errors and biases. There are many known effects we need to correct for to transform the observed He I line intensities measured from a H II region emission-line spectrum into an He abundance. First, there are the effects which make the He and H lines deviate from their recombination values: (1) collisional excitation and (2) fluorescence excitation of the He I lines, (3) collisional and (4) fluorescent excitation of the H lines (effects (3) and (4) need to be considered because the He abundance is measured relative to that of H), (5) reddening, and (6) underlying stellar absorption in the He I lines. Finally, we need to consider (7) the temperature structure of the H II region, and (8) its ionization structure. All these corrections are at a level of a few percent except for effect (1), which can be much higher, exceeding 10% in the case of the He I λ5876 emission line in hot and dense H II regions. A detailed discussion of these various effects can be found in [16].

Izotov & Thuan [13] using the latest He I emissivities [26], equivalent widths of H I and He I absorption lines for different ages of single stellar populations and for a wide range of metallicities calculated from evolutionary stellar population synthesis [9], and estimates for collisional and fluorescence enhancements of hydrogen Balmer lines [19] [20], have recently presented a new determination of the primordial He mass fraction Y_p, based on the sample of 93 spectra of 86 low-metallicity extragalactic H II regions of [16]. Using Monte Carlo methods to solve simultaneously for all the above systematic effects as described in [16], they found from a linear regression of Y_p vs. oxygen abundance (Fig. 1) that the best value is $Y_p = 0.2565 \pm 0.0010$ (statistical)$\pm$0.0050 (systematic).

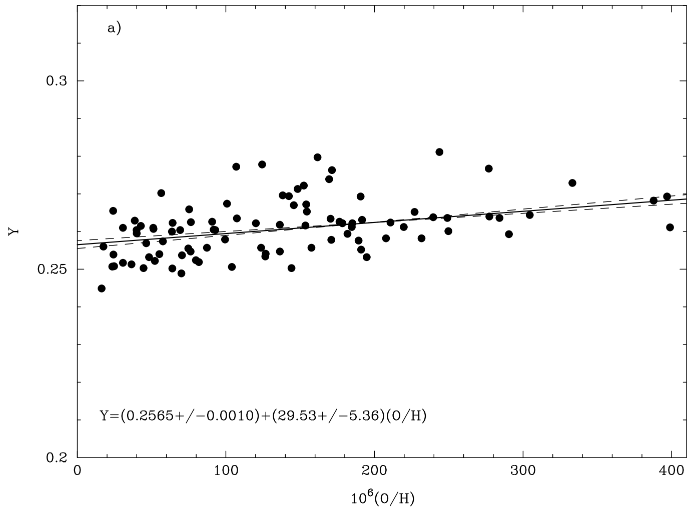

Figure 1: Linear regression of the helium mass fraction Y vs. oxygen abundance for a sample of $\sim$ 100 extragalactic H II regions. The Ys are derived with the He I emissivities from [26]. The electron temperature $T_e(\mathrm{He}^+)$ is varied in the range $(0.95 - 1)\times T_e$(O III). The oxygen abundance is derived adopting an electron temperature equal to $T_e(\mathrm{He}^+)$.

3 Deviations from SBBN

We use our derived value of the primordial He abundance along with the observed primordial abundances of other light elements to check the consistency of SBBN. Deviations from the standard rate of Hubble expansion in the early universe can be caused by an extra contribution to the total energy density, for example, by additional flavors of neutrinos. The total number of different species of weakly interacting light relativistic particles can be conveniently be parameterized by N_ν , the effective number of light neutrino species.

To determine N_ν, we use the statistical χ^2 technique, with the code described by [10] [18]. This code allows us to analyze the constraints that the measured He, D, and ^{7}Li abundances put on η and N_ν. For the primordial D abundance, we use the value obtained by [25]. As for ^{7}Li, its value derived from observations of low-metallicity halo stars [3] is $\sim$5 times lower than the one obtained from the five-year WMAP data analysis [8]. Because mechanisms that may lead to a reduction of the ^{7}Li primordial abundance, such as diffusion or rotationally induced mixing, are not well understood and we do not know how to correct for them, we have adopted the value of the primordial abundance of ^{7}Li abundance as derived from the WMAP data. The predicted primordial abundances of light elements depend on the adopted neutron lifetime τ_n . We have considered two values, the old one, τ_n = 885.4$\pm$0.9 s [4], and the new one, τ_n = 878.5$\pm$0.8 s [27] [28]. With the old value of τ_n and our best value of the primordial He abundance, Y_p = 0.2565$\pm$0.0010 (stat.)$\pm$0.0050 (syst.), the minimum χ_{min} (= 0.640524) is obtained when $\eta_{10} = 10^{10}\ \eta = 6.47$ and $N_\nu = 3.68$. This value of η_{10} is in agreement with η_{10} = 6.23$\pm$0.17 derived from the WMAP data [8]. If instead the new value of τ_n is adopted with the same value of Y_p, then the minimum χ_{min} (= 0.619816) is obtained when η_{10} = 6.51 and N_ν = 3.80. The values of η_{10} and N_ν depend only slightly on the value of the ^{7}Li abundance. They decrease by 3% and 2%, respectively, if the observed ^{7}Li abundance of [3] is adopted. The joint fit of η_{10} and N_ν is shown in Figure 2 for the two values of τ_n. The 1σ ($\chi^2 - \chi^2_{min}$ = 1.0) and 2σ ($\chi^2 - \chi^2_{min}$ = 2.71) deviations

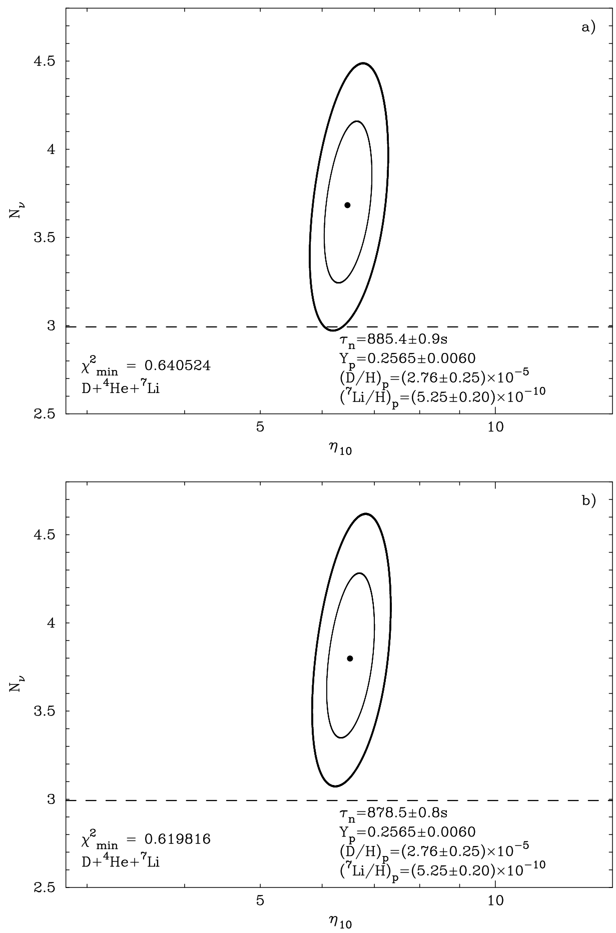

Figure 2: a) Joint fits to the baryon-to-photon number ratio, η_{10}, and the equivalent number of light neutrino species N_ν. A neutron lifetime $\tau_n = 885.4 \pm 0.9$s from [4] has been adopted. Thin and thick solid lines represent respectively 1σ and 2σ deviations. The experimental value $N_\nu = 2.993$ [6] is shown by the dashed line. b) The same as in (a), but with a neutron lifetime $\tau_n = 878.5 \pm 0.8$s [27] [28].

are shown respectively by the thin and thick solid lines. We find the equivalent number of light neutrino species to be in the range $N_\nu = 3.68^{+0.80}_{-0.70}$ (2σ) (Fig. 2a) in the first case, and $N_\nu = 3.80^{+0.80}_{-0.70}$ (2σ) (Fig. 2b) in the second case. Both of these values are only marginally consistent (at the 2σ level) with the experimental value of 2.993±0.011 [6] shown by the dashed line, implying deviations from SBBN. Note that, although both values are consistent with $N_\nu = 4.4\pm1.5$ derived from the analysis of five-year WMAP observations [17], the primordial helium abundance sets tighter constraints on the effective number of neutrino species than the cosmic microwave background (CMB) data, the error on N_ν being reduced by approximately half.

4 Summary and Discussion

We have derived the primordial helium mass fraction Y_p by linear regression of a sample of 93 spectra of 86 low-metallicity extragalactic H II regions. In this determination of Y_p, we have taken into account the latest developments concerning several known systematic effects. We have used Monte Carlo methods to solve simultaneously for the effects of collisional and fluorescent enhancements of He I recombination lines, of collisional and fluorescent excitation of hydrogen emission lines, of underlying stellar He I absorption, of possible temperature differences between the He^+ and [O III] zones, and of the ionization correction factor ICF (He^+ + He^{2+}).

Our best value is $Y_p = 0.2565\pm0.0010$ (stat.)±0.0050 (syst.), or 3.3% larger than the value derived from the microwave background radiation fluctuation measurements, assuming SBBN. In order to bring this high value of Y_p into agreement with the deuterium and five-year WMAP measurements, an equivalent number of neutrino flavors in the range 3.68–3.80, depending on the lifetime of the neutron, is required. This is higher than the canonical value of 3 and implies the existence of deviations from SBBN. It is interesting to note that recent neutrino oscillation experiments have raised the possibility of the existence of extra components of radiation. Thus the possibility of the presence of one or two species of light (with mass of order 1 eV) sterile neutrinos has been suggested by experiments such as the Liquid Scintillator Neutrino Detector (LSDN) experiment [1] and the Booster Neutrino Experiment (Mini-BooNE) [2]. Recent nuclear reactor experiments also favor additional neutrinos with mass in this range [21].

I thank Roland Triay and Jean Tran Thanh Van for having organized such a superb meeting in Quy Nhon, the site of the future International Science Center. I will also cherish the memory of my public lecture on “Man and the Cosmos”, the first such lecture in this Vietnamese coastal city, where 1500 people showed up!

References

[1] A.A. Aguilar-Arevalo et al. [LSND Collaboration], 2001, Phys. Rev. D. 64, 112007.

[2] A.A. Aguilar-Arevalo et al. [The MiniBooNE Collaboration], 2010, Phys. Rev. Lett. 105, 181801.

[3] M. Asplund, D.L. Lambert, P.E. Nissen, F. Primas, & V.V. Smith, 2006, ApJ, 644, 229.

[4] S. Arzumanov, et al. 2000, Phys. Lett. B, 483, 15.

[5] T.M. Bania, R. T. Rood, & D. S. Balser, 2002, Nature, 415, 54.

[6] C. Caso, et al. (Particle Data Group) 1998, Eur. J. Phys., C3, 1.

[7] C. Charbonnel, & F. Primas, A&A, 442, 961.

[8] J. Dunkley et al. 2009, ApJS, 180, 306.

[9] R.M. González Delgado, M. Cerviño, L.P. Martins, C. Leitherer, & P.H. Hauschildt, 2005, MNRAS, 357, 945.

[10] G. Fiorentini, E. Lisi, S. Sarkar, & F.L. Villante, 1998, Phys. Rev. D, 58, 063506.

[11] Y.I. Izotov, & T.X. Thuan, 1998, ApJ, 500, 188.

[12] Y.I. Izotov, & T.X. Thuan, 2004, ApJ, 602, 200.

[13] Y.I. Izotov, & T.X. Thuan, 2010, ApJ, 710, L67.

[14] Y.I. Izotov, T.X. Thuan, & V.A. Lipovetsky, 1994, ApJ, 435, 647.

[15] Y.I. Izotov, T.X. Thuan, & V.A. Lipovetsky, 1997, ApJS, 108, 1.

[16] Y.I. Izotov, T.X. Thuan, & G. Stasińska, 2007, ApJ, 662, 15.

[17] E. Komatsu, et al. 2009, ApJS, 180, 330.

[18] E. Lisi, S. Sarkar, & F.L. Villante, 1999, Phys. Rev. D, 59, 123520.

[19] V. Luridiana, 2009, Ap&SS, 324, 361.

[20] V. Luridiana, et al. 2009, ApJ, 691, 1712.

[21] G. Mention et al., 2011, Phys. Rev. D, 83, 073006.

[22] K.A. Olive, & Steigman, G., 1995, ApJS, 97, 49.

[23] B.E.J. Pagel, Simonson, E.A., Terlevich, R.J., & M.G. Edmunds, 1992, MNRAS, 255,325.

[24] M. Peimbert, & S. Torres-Peimbert, 1974, ApJ, 193, 327.

[25] M. Pettini, B.J. Zych, M.T. Murphy, A. Lewis, & C.C. Steidel, 2008, MNRAS, 391, 1499.

[26] R.L. Porter, R.P. Bauman, G.J. Ferland, & K. B. MacAdam, 2005, ApJ, 622, L73.

[27] A.P. Serebrov, et al. 2005, Phys. Lett.B, 605, 72.

[28] A.P. Serebrov, et al. 2008, Phys. Rev.C, 78, 035505.

[29] G. Steigman, 2006, Int.J.Mod.Phys.E, 15, 1.

[30] G. Steigman, 2007, Annu.Rev.Nucl.Part.Sci., 57, 463.

The Coldest Stars in the Universe

Ngoc Phan-Bao[1], *Cuong Dang-Duc*[1,2],
Thu Nguyen-Anh[1,2],
Duy Hoang-Ngoc[1], *Tuan Cao-Anh*[2]
[1]*Department of Physics,*
HCM International University - Vietnam National University, HCM, Vietnam.
[2]*Department of Physics, University of Education, HCM, Vietnam.*
Email : pbngoc@hcmiu.edu.vn

Abstract

Brown dwarfs are on the dividing line between planets and stars, and generally have masses between 13 and 75 Jupiters. As the theoretical minimum mass for a star to sustain hydrogen-burning fusion reactions is 75 Jupiters, therefore brown dwarfs are not massive enough to maintain stable fusion reactions during most of their lifetime. With such very low masses, brown dwarfs have estimated effective temperatures less than about 2700 K. The coolest known brown dwarfs have temperatures of about 300 K as cool as the human body. They are therefore the coldest stars in the universe. Due to their substellar mass and their extremely low temperature, the physical properties of brown dwarfs are quite different from those of low-mass stars (e.g., the Sun). Here we provide the basic physical properties of brown dwarfs such as temperature, mass, radius, spectral class with the most recent discoveries of coolest brown dwarfs using Wide-Field Infrared Survey Explorer. Based on our first detections of molecular outflows from young brown dwarfs in ρ Ophiuchi and Taurus, we then focus on the discussion of the brown dwarf origin that is the most important issue of the brown dwarf science.

1 Introduction

The existence of brown dwarfs was theoretically predicted in 1963 by Kumar [11], however until 1995 the first detections of brown dwarfs were claimed by Rebolo et al. [28] and by Nakajima et al. [21]. Up to now, large-scale surveys such as DEep Near Infrared Survey (DENIS), Two Micron All Sky Survey (2MASS) and Sloan Digital Sky Survey (SDSS) have discovered more than 1,000 nearby brown dwarfs.

In 1999, Martín et al. [18] and Kirkpatrick et al. [10] discovered dwarfs cooler than M stars, leading them to define a new class "L". Later in 2002, Burgasser et al. [4] discovered methane dwarfs, also leading them to define an additional class "T" for dwarfs even cooler than L dwarfs. These discoveries have extended the Harvard spectral class to be "O B A F G K M L T".

Recently completed and ongoing surveys, which are much deeper than the previous ones, such as UKIRT Infrared Deep Sky Surveys (UKIDSS), Wide-Field Infrared Survey Explorer (WISE) and Panoramic Survey Telescope and Rapid Response System (PANSTARS) have revealed the coolest brown dwarfs of spectral type Y. Using WISE data, Cushing et al. [8] have discovered the first six early-Y dwarf candidates. The estimated temperatures of these Y dwarf candidates are extremely low in the range from 300 K to 500 K and comparable to the humain body temperature. More even cooler dwarfs (i.e., later Y spectral types) are expected to be discovered by these surveys.

All these discoveries have greatly improved our understanding of the physical properties as well as the origin of brown dwarfs, bridging the gap between stars and planets.

We will provide the basic physical properties in Sec. 2, we present our discoveries of molecular outflows and discuss these findings in the context of brown dwarf formation in Sec. 3.

2 Basic Physical Properties of Brown Dwarfs

2.1 Mass

Mass is the most basic property of brown dwarfs, as it determines all other physical properties, such as temperature, radius and spectral class. Theoretical evolution models (e.g., Chabrier & Baraffe [5]) estimate brown dwarfs have masses between about 13 and 75 M_J (M_J: Jupiter mass). Direct mass measurements (e.g., Stassun et al. [32]) of brown dwarfs in eclipsing binary systems have generally agreed with the models. According to the theoretical models, stars with masses below about 0.3 solar masses are fully convective and thus these stars, not like the Sun, they do not have a radiative core. Since the mass of brown dwarfs is below this limit, therefore all brown dwarfs are fully convective. The lack of a radiative core in brown dwarfs significantly changes their magnetic field morphology (see Phan-Bao et al. [25] for more details).

One should note here that stars will burn lithium by the following reaction in at most 100 Myr [6], while brown dwarfs not massive enough to reach the core temperature required to do so:

$$^{7}Li + p \rightarrow 2^{4}He \tag{1}$$

The above reaction occurs at a lower temperature than is required for hydrogen-burning fusion. Theoretical models [5] estimate a lithium-burning minimum mass of ∼60 M_J. This provides the basis of the so-called "lithium test" [17, 27]. All brown dwarfs with masses in the range of 13-60 M_J will exhibit the 6708Å lithium absorption doublet, whereas more massive brown dwarfs (60-75 M_J) will destroy lithium at ages older than ∼100 Myr. The "lithium test" therefore is used to identify bona-fide brown dwarfs with masses below 60 M_J. However, there is strong age-dependence of the "lithium test" [6]: stars at ages younger than 100 Myr (depending on the mass) will also exhibit lithium. Therefore, the age of brown dwarfs must be taken into account when using this test to identify bona-fide brown dwarfs.

2.2 Temperature

The stellar temperature depends on both mass and age. Brown dwarfs have effective temperatures estimated from about 400 K to 2700 K (Leggett et al. [14]). Recently, using the WISE data Cushing et al. [8] have identified 6 early-Y dwarfs with temperature estimates down to ∼300 K even cooler than the human body temperature. These objects are the coolest brown dwarfs that have been revealed so far, reaching the boundary between brown dwarfs and giant planets.

2.3 Radius

All old brown dwarfs (∼1 Gyr) roughly have the same radius as Jupiter [6]. The radii of brown dwarfs vary by only ∼10% over their mass range. Young brown dwarfs may have larger radii, depending on their age. For example, brown dwarfs at an age of ∼1 Myr are about 500% larger than brown dwarfs at 1 Gyr [32]. Direct radius measurements of brown dwarfs by monitoring eclipsing binary systems have generally agreed with theoretical models. One should note that the brown dwarf radius can be affected by magnetic field effects, which may yield an increase of 10−15% in radius [7].

2.4 Spectral Class

Brown dwarfs may have spectral types of late-M (M7 or later), L, T and Y. In spectral class M, the optical spectrum of brown dwarfs is dominated by titanium oxide (TiO) and vanadium oxide (VO) molecules. In class L, metallic oxides (TiO and VO) quickly disappear and they are replaced by metallic hydrides (e.g., CrH and FeH), strong neutral atomic lines of alkali metals and sometimes Li I at 6708 Å. Whereas the near-infrared (NIR, $1-2.5$ μm) spectra of L dwarfs are similar to those of M dwarfs, dominated by absorption bands of water (H_2O) and carbon monoxide (CO), the NIR spectra of T dwarfs show strong absorption bands of methane (CH_4). These methane bands can be only found in the giant planets of the solar system and Titan. Class Y are expected to be even cooler than class T and their NIR spectra must show ammonia features (NH_3) significant enough to trigger a new spectral class ("Y"). Using NIR photometric data from WISE, Cushing et al. [8] have discovered the first six early-Y dwarf candidates. Their NIR spectra likely showing NH_3 absorption features. More cooler Y dwarfs are needed to be revealed to confirm these NH_3 features in the NIR spectra of Y dwarfs.

3 Molecular Outflows in Brown Dwarfs: New Constraints on Brown Dwarf Formation

Stars with a few solar masses can form by direct gravitational collapse mechanism [30]. The typical process of star formation starts with collapse, accretion and launching of material as a bipolar outflow [12]. For the case of very low mass objects at the bottom of the main sequence, brown dwarfs (BD) (13–75 $M_{\rm J}$) and very low-mass (VLM) stars (0.1–0.2 $M_{\odot}$) have masses significantly below the typical Jeans mass ($\sim$1 $\rm M_{\odot}$) in molecular clouds, and hence it is difficult to make a VLM stellar embyro by direct gravitational collapse but prevent subsequent accretion of material onto the central object once the VLM embryo formed. These VLM objects are therefore thought to form by different mechanisms (see [34] and references therein). Two major models have been proposed for their formation. In the standard formation model, they form like low-mass stars just in a scaled-down version, through gravitational collapse and turbulent fragmentation of low-mass cores (e.g., [23]). In the ejection scenario, the VLM objects are simply stellar embryos ejected from unstable multiple protostellar systems by dynamical interaction with the other embyros. These VLM embryos are ejected from their gas resevoir and then they become VLM stars and BDs (e.g., [29, 1, 2]).

Observations (see [15] and references therein) of the BD and VLM star properties in different star-forming regions such as their initial mass function, velocity and spatial distributions, multiplicity, accretion disks and jets have demonstrated that stars and BDs share similar properties. This strongly supports the scenario that BDs and VLM stars form as low-mass stars do. One should note that additional mechanisms (e.g., the ejection) are possible but they are not likely dominant in making VLM objects.

More observations are needed to understand how these VLM objects form, especially observations at very early stages provide us an insight into the formation mechanism of VLM objects. Therefore, we have searched for molecular outflows from young brown dwarfs at different classes in star-forming regions to characterize the outflow properties such as size, mass, mass-loss rate, velocity. These outflow properties not only provide strong observational constraints on theoretical models of brown dwarf formation (e.g., [16]) but also allow us to identify proto-brown dwarfs at different stages.

Here we report our observations of eight brown dwarfs and VLM stars in two star-forming regions ρ Ophiuchi and Taurus using the Submillimeter Array (SMA) and the Combined Array for Research in Millimeter-wave Astronomy (CARMA). Among these eight VLM objects, we have detected molecular outflows from three targets [24, 26]: (1) ISO-Oph 102, a brown dwarf with a mass of 60 $M_{\rm J}$ in ρ Ophiuchi; (2) MHO 5, a

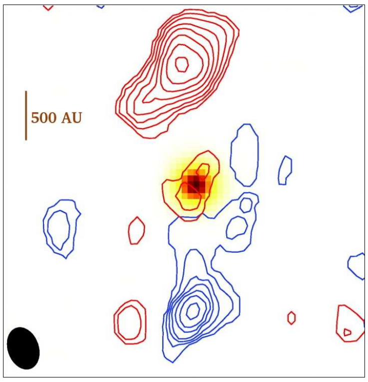

Figure 1: An overlay of the J-band (1.25 μm) near-infrared Two Micron All Sky Survey (2MASS) image of ISO-Oph 102 and the integrated intensity in the carbon monoxide (CO $J = 2-1$) line emission from 3.8 to 7.7 km s^{-1} line-of-sight velocities. The blue and red contours represent the blue-shifted (integrated over 3.8 and 5.9 km s^{-1}) and red-shifted (integrated over 5.9 and 7.7 km s^{-1}) emissions, respectively. The contours are 3,6,9,...times the rms of 0.15 Jy beam^{-1} km s^{-1}. The brown dwarf is visible in the J-band image. The position angle of the outflow is about 3°. The peaks of the blue- and red-shifted components are symmetric to the center of the brown dwarf with an offset of 10$''$. The synthesized beam is shown in the bottom left corner.

VLM star of 90 $M_{\rm J}$ in Taurus; (3) GM Tau, a brown dwarf of 75 $M_{\rm J}$ in Taurus. The outflow properties of these objects are similar to each other with outflow sizes of about 500-1000 AU, outflow masses of $10^{-4}M_\odot$, mass loss rates of $10^{-9}M_\odot$ yr^{-1}, and outflow velocities of 1-2 km s^{-1}. All these values are over 100 times smaller than those in low-mass stars.

Figure 1 shows an overlay of a near-infrared image and the integrated intensity in the carbon monoxide (CO $J = 2-1$) line emission at 230 GHz from ISO-Oph 102. Two spatially resolved blue- and red-shifted CO components are symmetrically displaced on opposite sides of the brown dwarf position, with the size of each lobe of about 8$''$ corresponding to 1000 AU in length. This is similar to the typical pattern of bipolar molecular outflows as seen in young stars [12].

The two outflow components (see Fig. 2) show a bow shock structure with a wide range of velocity, an effect of the interaction between the jet propagation and the ambient material, which appears very similar to the bow shock phenomena as seen in young stars [13]. Such a CO outflow morphology suggests that the jet-driven bow shock model (e.g., [19]) may be at work in ISO-Oph 102.

It is worthy to note that the IRS infrared (7.5-14.3 μm) [9] spectra of ISO-Oph 102, MHO 5, and GM Tau all show crystalline silicate features: enstatite ($MgSiO_3$) at 9.3 μm and very strong forsterite (Mg_2SiO_4) at 11.3 μm [24]. This provides a direct evidence of grain growth and dust settling, indicating the objects are in the transition phase between the class II and III (a class with an optically thin disk) and these VLM objects are reaching their final masses. As the outflow sweeps away the gas and dust in the vicinity of the young VLM objects, the coexistence of molecular outflow and crystallization therefore favors the rocky planet formation around these young brown dwarfs and VLM stars. We are currently modeling infrared spectra of young brown dwarfs to estimate the fraction of crystallization in the brown dwarf disk. The result of this modeling work may provide us some implications in finding planets forming around VLM stars and brown dwarfs.

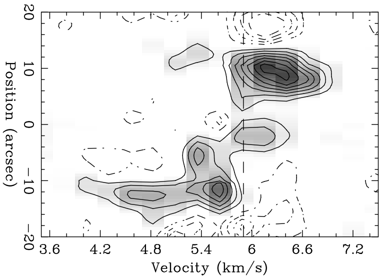

Figure 2: Position-Velocity (PV) cut diagram for CO $J = 2 \rightarrow 1$ emission from ISO-Oph 102 at a position angle of 3°. The contours are −12, −9, −6, −3, 3, 6, 9, 12,...times the rms of 0.2 Jy beam^{-1}. The systemic velocity of the brown dwarf, which is estimated by an average of the velocities of red- and blue-shifted components, is indicated by the dashed line. Our value of 5.9±0.27 km s^{-1} is consistent with the previously measured value [33] of 7±8 km s^{-1} within the error bar. Both blue- and red-shifted components shows a wide range of the velocity in their structure, which appears to be the bow-shock surfaces as observed in young stars [13]. These surfaces are formed at the head of the jet and accelerate the material in the bow-shock sideways (e.g., [19]).

Our detections clearly indicate that the bipolar molecular outflows in young brown dwarfs and very low-mass stars are very similar to outflows as seen in young stars but scaled down by three and two orders of magnitude for the outflow mass and the mass-loss rate, respectively. The detections also demonstrate that the molecular outflow process in VLM objects occurs in both low and high density environments (Taurus and ρ Ophiuchi) and thus support the idea that they likely share the same formation mechanism with low-mass stars. This suggests that the terminal stellar/brown dwarf (even planetary) mass is not due to different formation mechanisms but more likely due to the initial mass of the cloud core.

As optical jets are not observable due to the high extinction of a surrounding envelope in the very early stages of brown dwarf formation (e.g., class 0, class I), therefore molecular outflows offer us a unique tool to identify proto-brown dwarfs at the earliest stages. Figure 3 shows the total intensity map of CO emission of a proto-brown dwarf candidate in ρ Ophiuchi. Its position-velocity diagram reveals the blue and red-shifted outflow components. The central object is only visible at millimeter wavelengths (1.3 mm) with a flux density of 8±3 mJy, suggesting that this object is in a very early stage of star formation. The small-scale and low-velocity outflows (Fig. 4) are similar to those we observed in our young brown dwarfs and other proto-brown dwarfs (e.g., L1014-IRS, [3]), indicating that the source is very likely a proto-brown dwarf at class 0/I. Further observations are needed to confirm the source nature. The Atacama Large Millimeter/submillimeter Array (ALMA) with 10-100 times more sensitive and 10-100 times better angular resolution than the current mm/submm arrays is an excellent instrument for studying such these objects and searching proto-brown dwarfs/planetary mass objects at large-scales.

Acknowledgment This work has been supported by VietNam NAFOSTED grant 103.08-2010.17 (PI: N.P.-B.). The Submillimeter Array is a joint project between the Smithsonian Astrophysical Observatory and the Academia Sinica Institute of Astronomy and Astrophysics and is funded by the Smithsonian Institution and the Academia Sinica. Support for CARMA construction was derived from the Gordon and Betty Moore Foundation, the Kenneth T. and Eileen L. Norris Foundation, the James S. McDonnell Foundation, the Associates of the California Institute of Technology, the University of Chicago, the states of California, Illinois, and Maryland, and the National Science Foundation. Ongoing CARMA development and operations

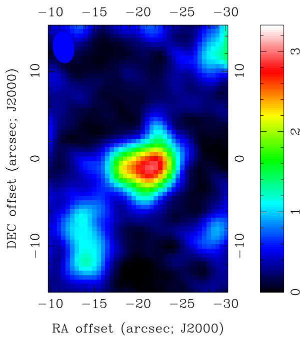

Figure 3: The integrated intensity in the carbon monoxide (CO $J = 2-1$) line emission from a proto-brown dwarf candidate over the line-of-sight velocity range from 3.5 to 6.4 km s^{-1}. The color bar indicates the intensity scale in Jy/beam. The synthesized beam is shown in the top left corner.

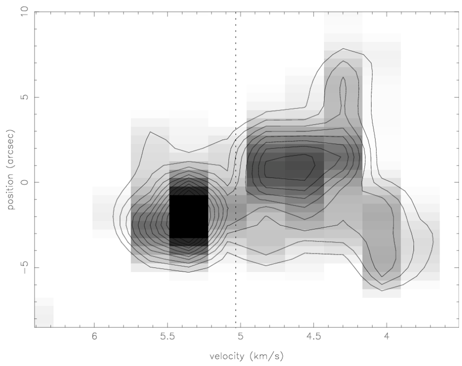

Figure 4: Position-Velocity (PV) cut diagram for CO $J = 2 \rightarrow 1$ emission from the proto-brown dwarf candidate at a position angle of 90°. The contours are 3, 6, 9, 12,...times the rms of 0.2 Jy beam^{-1}. The systemic velocity of $\sim 5.0 \pm 0.27$ km s^{-1} of the proto-brown dwarf candidate, which is estimated by an average of the velocities of red- and blue-shifted components, is indicated by the dashed line. Both blue- and red-shifted components show a small-scale and low-velocity outflows similar to those observed in ISO-Oph 102, MHO 5 and GM Tau.

are supported by the National Science Foundation under a cooperative agreement and by the CARMA partner universities. This work is based in part on observations made with the Spitzer Space Telescope, which is operated by the Jet Propulsion Laboratory, California Institute of Technology, under a contract with NASA.

References

[1] M.R. Bate, I.A. Bonnell, & V. Bromm, MNRAS, **332**, L65 (2002)

[2] M.R. Bate, & I.A. Bonnell, MNRAS, **356**, 1201 (2005)

[3] T.L. Bourke, A. Crapsi, P.C. Myers, et al., ApJ, **633**, L129 (2005)

[4] A. Burgasser et al., ApJ, **564**, 421 (2002)

[5] G. Chabrier, & I. Baraffe, A&A, **327**, 1039 (1997)

[6] G. Chabrier, & I. Baraffe, ARAA, **38**, 337 (2000)

[7] G. Chabrier, J. Gallardo, & I. Baraffe, A&A, **472**, L17 (2007)

[8] M. Cushing, et al., ApJ, **743**, 50 (2011)

[9] J.R. Houck, et al., ApJS, **154**, 18 (2004)

[10] D. Kirkpatrick, et al., ApJ, **519**, 802 (1999)

[11] S.S. Kumar, ApJ, **137**, 1121 (1963)

[12] C.J. Lada, ARA&A, **23**, 267 (1985)

[13] C.-F. Lee, L.G. Mundy, et al., ApJ, **542**, 925 (2000)

[14] S.K. Leggett, et al., ApJ, **667**, 537 (2007)

[15] K.L. Luhman, V. Joergens, C. Lada, J. Muzerolle, I. Pascucci, R. White, in *Protostars and Planets V*, edited by B. Reipurth, D. Jewitt, & K. Keil (Univ. Arizona Press, Tucson, 2007), p. 443

[16] M.N. Machida, et al., ApJ, **699**, 157 (2009)

[17] A. Magazzù, E.L. Martín, & R. Rebolo, A&A, **249**, 149 (1991)

[18] E.L. Martín, et al., AJ, **118**, 2466 (1999)

[19] C.R. Masson, L.M. Chernin, ApJ, **414**, 230 (1993)

[20] F. Motte, P. André, R. Neri, A&A, **336**, 150 (1998)

[21] T. Nakajima, et al., Nature, **378**, 463 (1995)

[22] A. Natta, L. Testi, J. Muzerolle, S. Randich, F. Comerón, P. Persi, A&A, **424**, 603 (2004)

[23] P. Padoan, & A. Nordlund, ApJ, **617**, 559 (2004)

[24] N. Phan-Bao, et al., ApJ, **689**, L141 (2008)

[25] N. Phan-Bao, et al., ApJ, **704**, 1721 (2009)

[26] N. Phan-Bao, et al., ApJ, **735**, 14 (2011)

[27] R. Rebolo, E.L. Martí, & A. Magazzù, ApJ, **389**, L83 (1992)

[28] R. Rebolo, M. R. Zapatero Osorio, & E. L. Martin, Nature, **377**, 129 (1995)

[29] B. Reipurth, & C. Clarke, AJ, **122**, 432 (2001)

[30] F.H. Shu, F.C. Adams, & S. Lizano, ARA&A, **25**, 23 (1987)

[31] F.H. Shu, et al., ApJ, **370**, L31 (1991)

[32] K. Stassun, et al., Nature, **440**, 16 (2006)

[33] E.T. Whelan, et al., Nature, **435**, 652 (2005)

[34] A. Whitworth, M.R. Bate, Å. Nordlund, B. Reipurth, H. Zinnecker, in *Protostars and Planets V*, edited by B. Reipurth, D. Jewitt, & K. Keil (Univ. Arizona Press, Tucson, 2007), p. 459

The Origin of Long, Short and Low-luminosity Gamma-Ray Bursts

Tsvi Piran[1], *Omer Bromberg*[1], *Ehud Nakar* [2] *& Re'em Sari*[1]
[1] *Racah Institute of Physics, The Hebrew University, Jerusalem 91904, Israel*
[2] *Raymond and Beverly Sackler School of Physics & Astronomy,*
Tel Aviv University, Tel Aviv 69978, Israel
Talk given by Tsvi Piran, email : tsvi.piran@mail.huji.ac.il

Abstract

The origin of Gamma-Ray Bursts is one of the most interesting puzzles in recent astronomy. During the last decade a consensus formed that long GRBs (LGRBs) arise from the collapse of massive stars and that short GRBs (SGRBs) have a different origin, most likely neutron star mergers. A key ingredient of the Collapsar model that explains how the collapse of massive stars produces a GRB is the emergence of a relativistic jet that penetrates the stellar envelope. The condition that the emerging jet penetrates the envelope poses strong constraints on the system [1]. Using these constraints we show that: (i) Low luminosity GRBs *ll*GRBs , a sub population of GRBs with a very low luminosities (and other peculiar properties: single peaked, smooth and soft) cannot be formed by Collapsars [2]. They have a different origin (most likely a shock breakout). (ii) On the other hand regular LGRBs must be formed by Collapsars [3]. (iii) While for BATSE the dividing duration between Collapsars and non-Collapsar is indeed at ~ 2 sec, the dividing duration is different for other GRBs detectors [4]. In particular most *Swift* bursts longer than 0.7 sec are of a Collapsar origin. This last results requires a revision of many conclusions concerning the origin of *Swift* SGRBs which were based on the classical 2 sec limit.

Gamma ray bursts (GRBs) are among the most amazing transients known. In a few second a GRB a comparable amount of energy than a star like our sun emits in its whole life time. Their origin has puzzled astronomers since their serendipitous discovery in the late sixties. After two decades in which it was believed that the GRBs are Galactic it was realized in the early nineties that they have a cosmological origin [5, 6, 7]. The distance scale have set immediately the energy scale to be $\gtrsim 10^{51}$ erg (including beaming corrections that were realized towards the end of the nineties [8, 9, 10]). Together with the short time scale this has led inevitably to the conclusion that the events involve the formation of a newborn compact object, most likely a black hole. This conclusion has left practically just two progenitors candidates: A collapsing massive star or the merger of two neutron stars (or a neutron star and a black hole).

The observations of a few (long) GRB afterglows in 1997 revealed that those bursts arose in star forming regions. Paczynski [11] who noticed that, quickly suggested that LGRBs are related to core collapse events. At roughly the same time MacFadyen & Woosley [12] suggested the Collapsar model. According to this model a GRB is produced by a relativistic jet that emerges from the center of a massive collapsing star and penetrates the stellar envelope. By now the name Collapsar is used with different variations[1]. We stress that here we use this original definition for a Collapsar: *A jet that penetrates the envelope of a Collapsing star.* Using numerical simulations MacFadyen & Woosley [12] demonstrated that a relativistic jet can indeed penetrate a stellar envelope. Again roughly at the same time Galama et al [13], discovered that GRB 980425

[1] In some cases it is used for any model that involve a collapsing star, regardless whether there is a jet or not. In other cases it is used to imply a situation in which the collapsing star has an accreting black hole as a central engine.

was associated with the powerful type Ic supernova: Sn 1998bw. However GRB 940425 was a strange GRB. It was very weak, with an energy a few orders of magnitude less than typical GRBs. Additionally it was single peaked and smooth and it had a very soft spectrum. It was not clear that this was a regular GRB and hence it was not enough to demonstrate a GRB-SNe connection. Shortly after that Bloom et al. [14] and others discovered red bumps on the afterglows of more distant and stronger GRBs . These red bumps were interpreted as the signatures of 98bw like supernovae supporting the GRB-SNe association. However the evidence for a GRB-SNe association was inconclusive until Sn 2003dh was discovered in association with the regular GRB 030329 [15, 16] . Since them a few other SN-GRb associations were discovered. Even though most of these GRB-Sn associations are with weak smooth single peaked GRBs[2] this is generally considered as a proof of the Collapsar model for LGRBs.

Kouveliotou et al., [17] discovered that the BATSE's GRBs' temporal distribution is divided to two groups short ($T_{90} < 2$ sec) and long ($T_{90} > 2$ sec.). Already in 1995 it was pointed out [18, 19] that the two groups have a different spatial distribution. The observed SGRBs are significantly nearer (and weaker). This suggested the possibility of different physical origin for the two populations. As it takes time (and energy) to cross the relatively large stellar envelope it was argued that SGRBs cannot be produced by a Collapsar [20]. While it is generally true that most Collapsar produce long bursts by now we know that some Collapsar can produce SGRBs (see §3 below). However a variant on this argument that we discuss here (in §2 and 3 below) shows that most SGRBs cannot be produced by Collapsars. Lack of detection of SGRB afterglow left the situation inconclusive until in 2005 *Swift* localized the first short bursts and the first afterglows of SGRBs were detected. It turned out that some SGRBs arise in elliptical galaxies and as such these are not associated with death of massive stars. The progenitors could be neutron star mergers (as suggested already in 1989 [21]). However as yet there is no conclusive proof of this origin [22].

We describe here new results concerning the nature of GRB progenitors. We briefly discuss in §1 some recent analytic results concerning relativistic jet penetration through the stellar envelope [1]. We then consider their implications on this picture. In §2 we demonstrate that low luminosity GRBs, those that appear in most GRB-SNe associations, cannot be produced by Collapsars [2]. While this might seems as a problem for the Collapsar model, we show in §3 that when combined with the GRBs' temporal distribution these consideration demonstrate that the long bursts originate from Collapsars [3]. Further inspection of the temporal distribution enables us [4] to estimate (in §4), for the first time, the fraction of Collapsars among SGRBs and to examine the implications of this conclusion.

1 Jet Propagation

A schematic picture of a relativistic jet propagating within a stellar envelope is depicted in Fig. 1. There are a few critical components. At the head of the jet there appears a double shock system [20]. While the jet is highly relativistic these shocks slow down the head and it typically propagates with a sub or mildly relativistic velocity. The hot material that streams sideways out of the jet's head produces a cocoon that engulfs the jet. While expanding sideways into the rest of the stellar envelope (this expansion will eventually blow out a fraction of the stellar envelope) it also squeezes the jet and produces an internal collimation shock within the jet [23].

As long as the jet is within the stellar atmosphere all its energy is dissipated at the jet's head. The total dissipated energy equals therefore the jet's luminosity times the time it takes to cross the envelope. Since the inner engine is much smaller than the envelope it is decoupled from the jet that crosses the envelope on a much larger scale and one can expect that the luminosity before and after the jet breaks out are comparable.

[2]Another association of a regular regular GRB and an SN - GRB 101219B and SN 2010ma, was discovered recently.

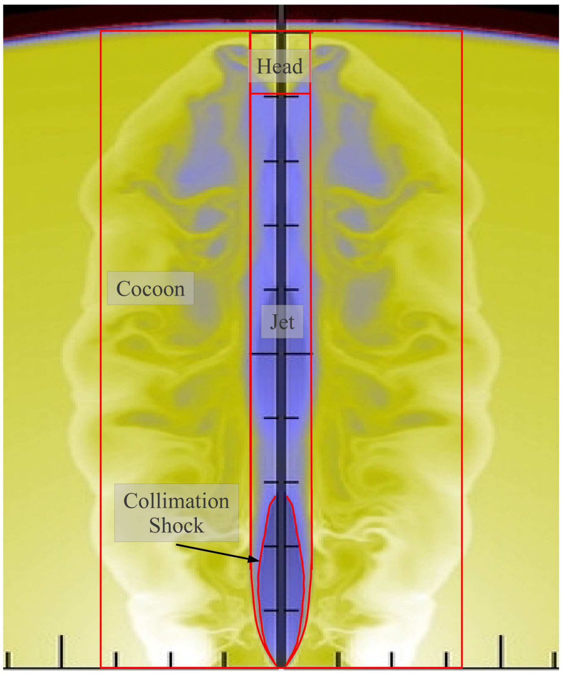

Figure 1: A schematic description of a jet propagating in a stellar atmosphere superimposed on a numerical jet simulation of [24].

Using the observed GRB luminosity to estimate the jet power before breakout we can estimate the duration of the dissipation phase as [1]:

$$t_B \simeq 15 \text{ sec} \cdot \left(\frac{L_{iso}}{10^{51} \text{ erg/sec}}\right)^{-1/3} \left(\frac{\theta}{10^\circ}\right)^{2/3} \left(\frac{R_*}{5R_\odot}\right)^{2/3} \left(\frac{M_*}{15M_\odot}\right)^{1/3}, \quad (1)$$

where L_{iso} is the isotropic equivalent jet luminosity, θ is the jet half opening angle and we have used typical values for a LGRB. R_* and M_* are the radius and the mass of the progenitor star, where we normalize their value according to the typical radius and mass inferred from observations of the few supernovae (SNe) associated with LGRBs. For the jet to break out the central engine must continue operating for a duration longer than t_B. If the inner engine stops before the jet's head crosses the envelope the jet will dissipate all its energy within the envelope and doesn't produce a regular GRB.

2 Low luminosity GRBs

We compare now the jet breakout time with the burst's duration. The duration of the prompt emission, approximated by T_{90}, is given simply by:

$$T_{90} = t_e - t_B, \tag{2}$$

where t_e is the total time that the engine powering the jet is active. Within the Collapsar model, without fine tuning only a small fractions of the bursts should have $T_{90}/t_B \ll 1$)see §3). Namely, it is unlikely that the engine operates just long enough to let the jet break out of the star and then stops right after breakout. This argument was used by Matzner /citeMatzner03 to argue that Collapsars cannot produce the majority of SGRBs, for which $T_{90}/t_B \ll 1$. This is indeed confirmed in Fig 2 in which the distribution of T_{90}/t_B is shown for both LGRBs and SGRBs. One can clearly see that these are two distinct populations.

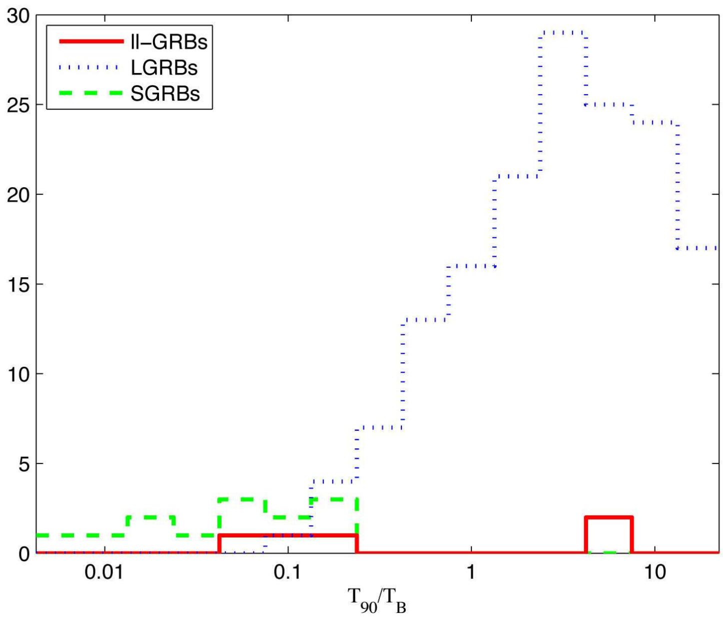

Figure 2: The distribution of T_{90}/t_B for LGRBs, *ll*GRBs and SGRBs (from [2]).

However, the same argument shows that another group of GRBs, low luminosity, *ll*GRBs , cannot be generated by Collapsars. Low luminosity GRBs are a group of six GRBs whose luminosities are around $10^{47} - 10^{49}$ ergs/sec, At least two orders of magnitude below the average luminosity of a typical GRBs. *ll*GRBs include GRB9890425 (the first GRB detected to accompany a Supernova - 1998bw) as well as a few other GRB-SN pairs: GRB 031203/SN2003lw; GRB060218/SN2006aj; GRB100316D/SN2010bh. GRB051109B which shows all the common properties of *ll*GRBs but lacks a reported SN. It is associated with a star forming region in a spiral galaxy at $z = 0.08$ [25]. Remarkably *ll*GRBs are not characterized just by their low luminosity. They are also single peaked, smooth and the peak energy of their photons is low. All these bursts are at low redshifts. With such a low luminosities they couldn't have been detected from further out. While only a few *ll*GRBs have been observed their actual rate is much higher than the rate of regular LGRBs [26]. In fact the rate of *ll*GRBs is so high that they cannot be significantly beamed as even with a modest beaming corrections their rate would exceed the rates of their associated SNe - broad lines type Ibc.

Like SGRBs, the observed distribution of *ll*GRBs is inconsistent with the predictions of the collapsar model. In particular a large fraction of *ll*GRBs have $T_{90}/t_B \ll 1$. The probability that the observed *ll*GRBs T_{90}/t_B distribution is consistent with the LGRBs distribution is smaller than 5% [2] implying that *ll*GRBs have a different origin. An interesting and likely possibility is that *ll*GRBs ' jets are weak and fail to breakout from their progenitors. A "failed jet" dissipates all its energy into the surrounding cocoon and drives its expansion. As the cocoon reaches the edge of the star its forward shock may become mildly or even ultra relativistic emitting the observed γ-rays when it breaks out. This idea that *ll*GRBs arise from shock breakouts was suggested shortly following the observations of GRB980425/SN1998bw [27, 28, 29]. It drew much more attention following the observation of additional *ll*GRBs with similar properties and especially with the observation of a thermal component in the spectrum of *ll*GRB 060218 [30, 31, 32]. Yet, it was hard to explain how shock breakout releases enough energy in the form of γ-rays. Katz, Budnik & Waxman [33] realized that the deviation of the breakout radiation from thermal equilibrium provides a natural explanation to the observed γ-rays. More recently, Nakar & Sari [34] calculated the emission from mildly and ultra-relativistic shock breakouts, including the post breakout dynamics and gas-radiation coupling. They find that the total energy, spectral peak and duration of all *ll*GRBs can be well explained by relativistic shock breakouts. Moreover, they find that such breakouts must satisfy a specific relation between the observed total energy, spectral peak and duration, and that all *ll*GRBs satisfy this relation. These results lend a strong support to the idea that *ll*GRBs are relativistic shock breakouts. From a historical point of view this understanding closes the loop with Colgate's [35] original idea, that preceded the detection of GRBs, that a SN shock b/reakout will produce a GRB.

As we discuss in the following section, the observed GRB duration distribution indicates the existence of many "failed jets" in which the enegine time is shorter than the breakout time. This is consistent with the observations that the rate of *ll*GRBs is much higher than the rate of regular LGRBs.

3 Long GRBs and Collapsars

As most of the GRBs associated with SNe are *ll*GRBs one might think at first that this new understanding rules out the Collapsar model for LGRBs. However, on the contrary, these arguments provide a new and unexpected direct observational proof for the Collapsar origin of LGRBs [3]. Consider again Eq. 2. Under very general conditions this equation results in a flat durations distribution for durations significantly shorter than the typical breakout time.

It follows from Eq. 2 that the distribution, $p_\gamma(T_{90})$ of the observed GRB durations is a convolution of the $p_e(t_e)$, the distribution of engine operating times, and $p_B(t_B)$ the distribution of jet breakout times. Under quite general conditions (more specifically unless p_e varies very rapidly around t_B, an unlikely situation) the following limits hold[3]:

$$p_\gamma(T_{90}) \approx \begin{cases} p_e(t_B) & T_{90} \lesssim t_B \\ p_e(T_{90}) & T_{90} \gg t_B \end{cases} . \tag{3}$$

Particularly interesting for our purpose here is the flat region, the plateau, that arises at short durations $T_{90} \lesssim t_B$. Remarkably such a plateau exists in all the observed GRB duration distributions (see Fig. 3). It wasn't observed so far because the "canonical" distribution plot [17] depicts $d\log(N)/d\log(T)$ instead of dN/dT. The longest durations of the plateau enables us to estimate t_B and from this to infer some the basic properties of the collapsing stars. We find, for example, that a typical progenitor size is $\sim 5R_\odot$. The plateau doesn't extend all the way to zero. At very short durations non-Collapsar SGRBs, that have a different origin, appear and dominate the distribution. As different detectors have different relative sensitivities to long (and soft) vs. short (and hard) GRBs the duration at which short non-Collapsars begin to dominate varies from one detector to another. To demonstrate this dependence on the detector's spectral window we artificially change BATSE's effectiveness for detection of hard SGRBs by considering only softer BATSE bursts (hardness ratio < 2.6). As expected, for this softer BATSE sample the non-Collapsars peak shrinks and the plateau extends down to shorter durations.

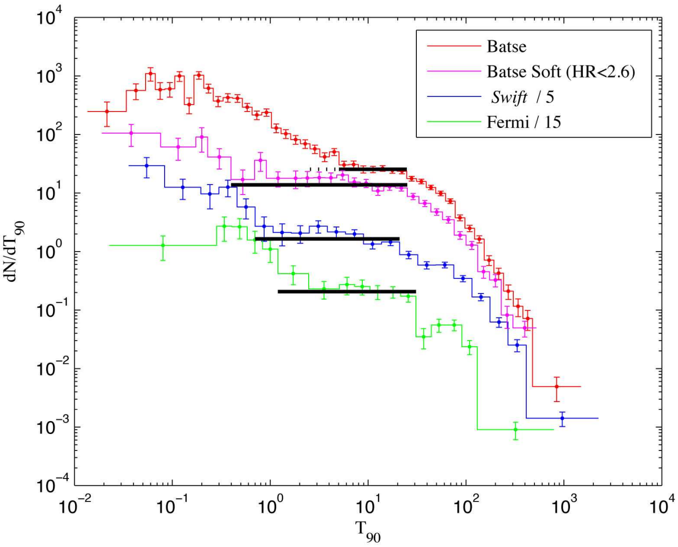

Figure 3: The duration distributions, dN/dT_{90}, of BATSE (red), *Swift* (blue) and Fermi GBM (green) GRBs. Also plotted is the distribution of the soft (hardness ratio < 2.6) BATSE bursts (magenta). For clarity the *Swift* values are divided by a factor of 5 and the Fermi GBM by 15. The dotted line that ranges down to ≈ 2 sec mark the duration range where Collapsars constitute more than 50% of the total number of BATSE GRBs. At shorter times the sample is dominated by non-Collapsars. Note that the quantity dN/dT is depicted and not $dN/d\log T$ as traditionally shown in such plots [17]. The black lines show the best fitted flat interval in each data set: $5-25$ sec (BATSE), $0.7-21$ sec (*Swift*), and $2.5-31$ sec (Fermi). The upper limits of this range indicate a typical breakout time of a few dozens seconds, in agreement with the prediction of the Collapsar model. The distribution at times $\gtrsim 100$ sec can be fitted as a power law with an index $-4 < \alpha < -3$ and it reflect the activity of the inner engine. . Soft BATSE bursts show a considerably longer plateau ($0.4-25$ sec), indicating that most of the soft short bursts are in fact Collapsars (from [3].)

The appearance of this plateau (and its dependence on the observed hardness) is the first direct observational proof of the Collapsar model. It demonstrates the existence of two independent time scales that determine the bursts' duration: the overall duration that the engine operates and the time it takes the jet to penetrate the stellar envelope.

Another interesting feature seen in Fig. 3 is the rapid decline at durations larger than t_B. At this regime according to Eq. 3 the distribution is dominated by $p_e(t_e)$, thus $p_e(T_{90}) \approx p_\gamma(T_{90})$. An extrapolation of this distribution to shorter engine operating times suggests that there are numerous cases in which $t_e < t_B$ and the jet fails to break out. This is in a very nice agreement with the very large event rate of *ll*GRB if these are interpreted as "failed jets".

4 Short non - Collapsar GRBs

Kouveliotou et al., [17] demonstrated that there are two populations of GRBs: long and short ones according to the observed duration larger or smaller than 2 sec. Shortly afterwards it became clear that these two populations have different origins[18, 19]. LGRBs arise from Collapsars and SGRBs from something else, most likely neutron star mergers. As we are still uncertain concerning the origin of SGRBs we denote them here as non-Collapsars. So far it was implicitly assumed that the division line between long and SGRB is sharp and at 2 sec regardless of the observing satellite. The existence of a plateau in the observed long (of Collapsar origin) GRBs enables us to determine, for the first time, the fractions of Collapsars vs. non-Collapsars as a function of the observed time for every specific detector. While we cannot determine if a specific bursts is Collapsar or not we can give now [4] a probabilistic estimate for a given duration and hardness.

The basic idea is very simple. For a given detector we determine the rate of detection of bursts within the plateau. This provides an estimate for the detection rate of short durations Collapsars by this detector. Now we can compare this rate to the rate of SGRBs at any given duration and obtain the Collapsar and non-Collapsar fractions as a function of duration. This estimates is performed for different detectors or even for different detection windows (hardness) for a specific detector.

Bromberg et al., [4] have fitted the different duration distributions with a plateau (representing Collapsars) and a lognormal distribution (for non-Collapsars). The fit is remarkably good and it enables us to estimate the fraction, f_{NC} of non-Collapsars from the total number of observed GRBs as a function of the observed duration, T_{90} (see Fig. 4). For Batse $T_{90} < 2$ sec is a reasonable threshold to identify non-Collapsars. This limit results in a probability $> 70\%$ for a correct classification for BATSE bursts. However, this condition is misleading for *Swift* bursts. At $t_{90} = 2$ sec a *Swift* burst has a $97^{+2}_{-23}\%$ to be a Collapsar! Clearly, for *Swift* a 2 sec division line results in a large number of misidentified Collapsars as non-Collapsars. We propose to draw the division line between collapsars and non-Collapsars at the duration where the probability that a GRB is a non-Collapsar is 50%. With this condition, a BATSE GRB can be classified as a non-Collapsar if its $T_{90} < 3.5$ ses. *Swift* bursts can be identified as non-collapsars only if their duration $T_{90} < 0.6$ sec, while the corresponding limit for GBM is $T_{90} = 1.7$ sec.

The results shown here can be expanded and improved when we consider the hardness of the bursts.

Using these results one can go back and examine various studies of short bursts that attempted to compare short (standing for non-Collapsars) with long (Collapsars) and check the samples used. A preliminary inspection of such studies [4] reveals that in some cases the short sample used was heavily contaminated by high probability potential Collapsars (with observed duration shorter than 2 sec) and it is possible and even likely that this have dominated the results of the study.

5 Conclusions

To conclude we summarize our basic findings. According to the Collapsar model a long GRB arises once a relativistic jet that emerges from the center of a collapsing massive star penetrates the stellar envelope. As long as the jet is within the stellar envelope all its energy is dissipated. The duration of this phase depends on the jet's luminosity, its opening angle and the size and density profile of the stellar envelope.

One can expect that the duration of a burst is typically comparable or longer than the jet breakout time. Indeed a comparison of the jet breakout time, of a typical LGRB shows that it is shorter than the duration of the burst. On the other hand the jet breakout time is much longer than the duration of a short burst. This provides the first indication that SGRBs are not produced by Collapsars. We have shown that a third group of bursts, *ll*GRBs also don't satisfy this condition. This implies that *ll*GRBs don't arise from Collapsars.

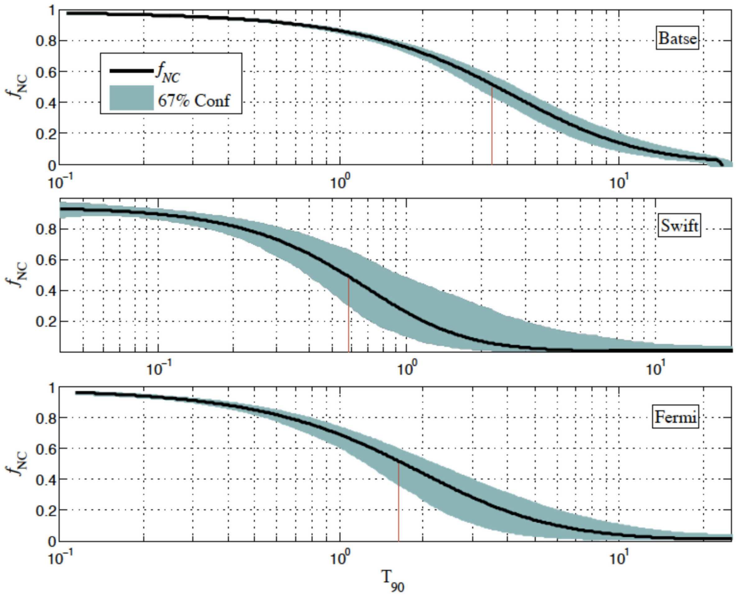

Figure 4: From top to bottom: BATSE, *Swift* and Fermi GBM fractions, f_{NC} of non-Collapsars from the total number of observed GRBs as a function of the observed duration, T_{90}. The shaded regions represent 67% confidence limits of f_{NC} . Also plotted in red are the T_{90} values for which $f_{NC} = 0.5$ (from [4]).

Within the Collapsar model the observed duration of a GRB is the difference between the time its central engine produces the jet, and the jet's breakout time. This directly implies that at short durations the rate of bursts produced by Collapsars should be independent of their duration. We have shown that such a behavior is observed in the duration distributions of all GRB satellites: BATSE, *Swift* and GBM. This provides the a direct proof of the Collapsar origin of LGRBs.

This last feature also enables us to determine the fraction of Collapsars within the observed SGRBs. This fraction depends on the characteristics of the detector. For BATSE the standard division between Collapsar and non-Collapsars is indeed at ~ 2 sec. However for the softer *Swift* many bursts shorter than 2 sec are of Collapsar origin. This might have led to some confusion in the past in interpreting observations of these short bursts as indications for properties of non-Collapsar GRBs.

This research was supported by an Advanced ERC grant and by the Israeli center for Excellent for High Energy AstroPhysics (TP), by an ERC starting grant and an ISF grant (EN) and by Packard, Guggenheim and Radcliffe fellowships (RS).

References

[1] Bromberg, O., Nakar, E., Piran, T., & Sari, R. 2011, Ap. J., 740, 100

[2] Bromberg, O., Nakar, E., & Piran, T. 2011, Ap. J. Lett., 739, L55

[3] Bromberg, O., Nakar, E., Piran, T., & Sari, R. 2012, Ap. J., 749, 110

[4] Bromberg, O., Nakar, E., Piran, T., & Sari, R. 2011, in preparation

[5] Meegan, C. A., Fishman, G. J., Wilson, R. B., et al. 1992, Nature, 355, 143

[6] Piran, T. 1992, Ap. J. Lett., 389, L45

[7] Mao, S., & Paczynski, B. 1992, Ap. J. Lett., 388, L45

[8] Rhoads, J. E. 1997, Ap. J. Lett., 487, L1

[9] Rhoads, J. E. 1999, Ap. J., 525, 737

[10] Sari, R., Piran, T., & Halpern, J. P. 1999, Ap. J. Lett., 519, L17

[11] Paczynski, B. 1998, Ap. J. Lett., 494, L45

[12] MacFadyen, A. I., & Woosley, S. E. 1999, Ap. J., 524, 262

[13] Galama, T. J., Vreeswijk, P. M., van Paradijs, J., et al. 1998, Nature, 395, 670

[14] Bloom, J. S., Kulkarni, S. R., Djorgovski, S. G., et al. 1999, Nature, 401, 453

[15] Hjorth, J., Sollerman, J., Møller, P., et al. 2003, Nature, 423, 847

[16] Stanek, K. Z., Matheson, T., Garnavich, P. M., et al. 2003, Ap. J. Lett., 591, L17

[17] Kouveliotou, C., Meegan, C. A., Fishman, G. J., et al. 1993, Ap. J. Lett., 413, L101

[18] Cohen, E., & Piran, T. 1995, Ap. J. Lett., 444, L25

[19] Piran, T. 1996, Compact Stars in Binaries, 165, 489

[20] Matzner, C. D. 2003, Mon. Not. RAS, 345, 575

[21] Eichler, D., Livio, M., Piran, T., & Schramm, D. N. 1989, Nature, 340, 126

[22] Nakar, E. 2007, Phys. Rep., 442, 166

[23] Bromberg, O., & Levinson, A. 2007, Ap. J., 671, 678

[24] Morsony, B. J., Lazzati, D., & Begelman, M. C. 2007, Ap. J., 665, 569

[25] Perley D. A., Foley R. J., Bloom J. S., Butler N. R., 2006, GCN, 5387, 1

[26] Soderberg A. M., et al., 2006a, Nature, 442,1014

[27] Kulkarni S. R., et al., 1998, Natur, 395, 663

[28] MacFadyen A. I., Woosley S. E., Heger A., 2001, ApJ, 550, 410

[29] Tan J. C., Matzner C. D., McKee C. F., 2001, ApJ, 551, 946

[30] Campana S., et al., 2006, Natur, 442, 1008

[31] Wang X.-Y., Li Z., Waxman E., Mészáros P., 2007, ApJ, 664, 1026

[32] Waxman E., Mészáros P., Campana S., 2007, ApJ, 667, 351

[33] Katz B., Budnik R., Waxman E., 2010,

[34] Nakar, E., & Sari, R. 2012, Ap. J., 747, 88

[35] Colgate, S. A. 1968, Canadian Journal of Physics, 46, 476

Relativistic Poynting-Flux Jets as Transmission Lines

R.V.E. Lovelace[1], *S. Dyda*[2], *& P.P. Kronberg*[3]

[1] *Department of Astronomy, Cornell University, Ithaca, NY 14853*

[2] *Department of Physics, Cornell University, Ithaca, NY 14853*

[3] *Theoretical Division, Los Alamos Nat. Lab, Los Alamos, NM 87545 and Department of Physics, University of Toronto, ON M5S 1A7, Canada*

email : lovelace@astro.cornell.edu

Abstract

Recent radio emission, polarization, and Faraday rotation maps of the radio jet of the galaxy 3C 303 have shown that one knot of this jet has a *galactic*-scale electric current of $\sim 3 \times 10^{18}$ Ampère flowing along the jet axis (Kronberg et al. 2011). We develop the theory of relativistic Poynting-flux jets by utilizing the analogy between the jets and transmission lines. The transmission line carries a current I_0, has a potential drop V_0, and a definite impedance $\mathcal{Z}_0 = \mathcal{O}(90)\ \Omega$. The electromagnetic energy flow in the transmission line or jet is $\mathcal{Z}_0 I_0^2$. Thus the observed current in 3C 303 can be used to calculate the electromagnetic energy flow in this magnetically dominated jet. Time-dependent but not necessarily small perturbations of a Poynting-flux jet - possibly triggered by a gas cloud penetrating the jet - are described by "telegrapher's equations, " which predict the propagation speed of disturbances and the effective wave impedance $\mathcal{Z}$. The disturbance of a Poynting jet by the cloud gives rise to localized dissipation in the jet which may explain the enhanced synchrotron radiation in the knots of the 3C 303 jet, and in the apparently stationary knot HST-1 in the jet from the nucleus of the galaxy M87 (Biretta et al. 1999).

Introduction: Radio emission, polarization, and Faraday rotation maps of the radio jet of the galaxy 3C303 (Kronberg et al. 2011) reveal that one longitudinal segment of this jet has a *galactic*-scale electric current owing along the jet axis. This current can be interpreted as a relativistic Poynting-flux jet. The formation of a Poynting-flux jet can be traced back to the dynamics of a large-scale magnetic field threading the accretion disk around a black hole. This magnetic field can arise from the dynamo processes in the disk possibly triggered by a star-disk collision. The field may be sufficiently strong that it suppresses the magneto-rotational instability with the result that the disk is non-turbulent and without viscosity. The disk will however continue to accrete owing to the angular momentum outflow in the Poynting-flux jet.

Here, we develop the theory of relativistic Poynting-flux jets by utilizing the analogy between the jets and transmission lines.

Theory: In cylindrical (r, ϕ, z) coordinates with axisymmetry assumed, the magnetic field has the form $\mathbf{B} = \mathbf{B}_p + B_\phi \hat{\boldsymbol{\phi}}$, with $\mathbf{B}_p = B_r \hat{\mathbf{r}} + B_z \hat{\mathbf{z}}$, and $B_r = -(1/r)(\partial\Psi/\partial z)$, and $B_z = (1/r)(\partial\Psi/\partial r)$. Here, $\Psi(r, z) \equiv r A_\phi(r, z)$ is the flux function. A simple form of this function is $\Psi(r, 0) = (1/2) r^2 B_0/[1 + 2(r/r_0)^3]$, where B_0 is the axial magnetic field strength in the center of the disk, and r_0 is the radius of the $O-$point of the magnetic field in the plane of the disk as indicated in Figure 1. This field could arise for $t \geq 0$ from dynamo processes in the disk triggered by a star-disk collision as discussed by Pariev, Colgate, & Finn (2007). The field may be sufficiently strong that it suppresses the magneto-rotational instability (MRI) so that the disk is non-turbulent and without viscosity. The disk will however continue to slowly accrete owing to the angular momentum outflow in the Poynting jet which gives a radial accretion speed much less than the

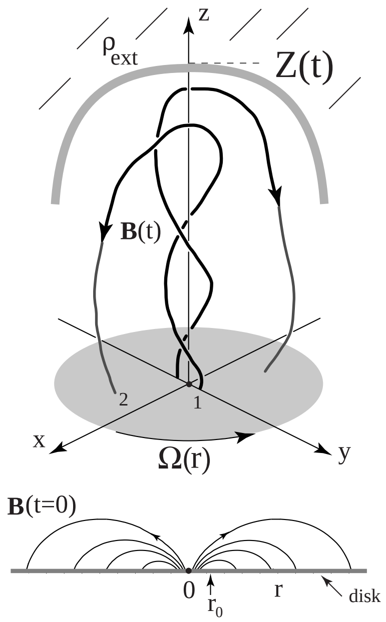

Figure 1: Sketch of the magnetic field configuration of a Poynting jet adapted from Lovelace and Romanova (2003). The bottom part of the figure shows the initial dipole-like magnetic field threading the disk which rotates at the angular rate $\Omega(r)$. The $O-$point of the initial field is at r_0. The top part of the figure shows the jet at some time later when the head of the jet is at a distance $Z(t)$. At the head of the jet there is force balance between electromagnetic stress of the jet and the ram pressure of the ambient medium of density $\rho_{\rm ext}$.

Keplerian velocity of the disk. This Ψ is taken to apply for $r \geq 0$ even though it is not valid near the horizon of the black hole. The contribution from the latter region is negligble for the considered conditions where $(r_g/r_0)^2 \ll 1$, where $r_g \equiv GM/c^2$. For a corotating disk around a Kerr black hole the disk's angular velocity viewed from a large distance is $\Omega = [c^3/(GM)]/[a_* + (r/r_g)^{3/2}]$, for $r > r_{\rm ms}$ where $r_{\rm ms}$ is the innermost stable circular orbit and a_* is the spin parameter of the black hole with $0 \leq a_* < 1$.

At large distances from the disk ($z \gg r_0$) the the flux function solution of the force-free Grad-Shafranov equation is found to be

$$\bar{\Psi} = \frac{\bar{r}^{4/3}}{[2\mathcal{R}\ (\Gamma^2-1)\ ]^{2/3}}\ , \tag{1}$$

(Lovelace & Romanova 2003), where Γ is the Lorentz factor of the jet, $\bar{r} \equiv r/r_0$, $\bar{\Psi} \equiv \Psi/\Psi_0$ with $\Psi_0 \equiv r_0^2 B_0/2$, and $\mathcal{R} \equiv r_0/r_g$. This dependence holds for $\bar{r}_1 \equiv [2(\Gamma^2-1)]^{1/2}/\mathcal{R} < \bar{r} < \bar{r}_2 = [2\mathcal{R}(\Gamma^2-1)]^{1/2}/3^{3/4}$. At the inner radius $\bar{r}_1$, $\bar{\Psi} = 1/\mathcal{R}^2$, which corresponds to the streamline which passes through the disk at a distance $r = r_g$. For $\bar{r} < \bar{r}_1$, we assume $\bar{\Psi} \propto \bar{r}^2$, which corresponds to $B_z = $ const. At the outer radius $\bar{r}_2$, $\bar{\Psi} = (\bar{\Psi})_{\rm max} = 1/3$ which corresponds to the streamline which goes through the disk near the $O-$point at $r = r_0$. Note that there is an appreciable range of radii if $\mathcal{R}^{3/2} \gg 1$.

For $\bar{r}_1 < r < \bar{r}_2$, the field components of the Poynting jet are

$$\bar{E}_r = -\sqrt{2}\ (\Gamma^2-1)^{1/2}\ \bar{B}_z\ ,\ \bar{B}_\phi = -\sqrt{2}\ \Gamma\ \bar{B}_z\ ,\ \bar{B}_z = \frac{2}{3}\frac{\bar{r}^{-2/3}}{[2\mathcal{R}(\Gamma^2-1)]^{2/3}}\ . \tag{2}$$

This electromagnetic field statisfies the radial force balance equation, $dB_z^2/dr+(1/r^2)d[r^2(B_\phi^2-E_r^2)]/dr=0$.

At the jet radius r_2, there is a boundary layer where the axial magnetic field changes from $B_z(r_2-\varepsilon)$ to zero at $r_2+\varepsilon$, where $\varepsilon \ll r_2$ is the half-width of this layer. The electric field changes from $E_r(r_2-\varepsilon)$ to zero at $r_2+\varepsilon$. The toroidal magnetic field changes from $B_\phi(r_2-\varepsilon)$ to $B_\phi(r_2+\varepsilon)$ where this change is fixed by the radial force balance. Thus for $r>r_2$, we have $E_r=0$, $B_z=0$, and $B_\phi=\sqrt{3}B_z(r_2-\varepsilon)(r_2/r)=\sqrt{(3/2)}\Gamma^{-1}B_\phi(r_2-\varepsilon)(r_2/r)$. Equivalently, $B_\phi(r_2+\varepsilon)/B_\phi((r_2-\varepsilon)=\sqrt{3/2}/\Gamma$.

The toroidal magnetic field for $r>r_2$ applies out to an 'outer radius' r_3 where the magnetic pressure of the jet's toroidal magnetic field, $B_\phi^2(r_3)/8\pi$, balances the external ram pressure $P_{\rm ex}=p_{\rm ex}+\rho_{\rm ex}(dr_3/dt)^2$, where $p_{\rm ex}=n_{\rm ex}k_{\rm B}T_{\rm ex}$ is the kinetic pressure of the external intergalactic plasma and $\rho_{\rm ex}$ is its density. The outward propagation of the jet will be accompanied by the non-relativistic expansion the outer radius, $dr_3/dt>0$.

We take as the 'jet current' the axial current I_0 flowing along the jet core $r\le r_2-\varepsilon$. From Ampère's law, $B_\phi(r_2)=-2I_0/(c\,r_2)$ or in convenient units, $B_\phi[{\rm G}]=-I_0[{\rm A}]/(5r[{\rm cm}])$. The net current carried by the jet ($r\le r_2+\varepsilon$) is $I_{\rm net}=\sqrt{3/2}\Gamma^{-1}I_0$.

Using equations (2), the energy flux carried by the Poynting jet can be expressed as

$$\dot{E}_J=\frac{c}{2}\int_0^{r_2} rdrE_rB_\phi=\mathcal{Z}_0I_0^2\ ,\ \text{where}\ \ \mathcal{Z}_0=\frac{3}{c}\beta\ [\text{cgs}]=90\beta\ \Omega\ [\text{MKS}]\ , \tag{3}$$

and $\beta=U_z/c=(1-\Gamma^{-2})^{1/2}$. Here, $\mathcal{Z}_0$ is the DC impedance of the Poynting jet. The conversion to MKS units is $c^{-1}\to(4\pi)^{-1}(\mu_0/\epsilon_0)^{1/2}=30\,\Omega$. Earlier, the impedance of a relativistic Poynting jet was estimated to be $\sim c^{-1}$ (Lovelace 1976).

For the observed axial current in the E3 knot in the jet of 3C 303, 3×10^{18} A (Kronberg et al. 2011), the electromagnetic energy flux is $\dot{E}_J\approx 8\times10^{45}\beta$ erg s^{-1}. This energy flux is much larger than the photon luminosity of the jet of 3.7×10^{41} erg s^{-1} integrated over 10^8 to 10^{17} Hz (Kronberg et al. 2011) assuming β is not much smaller than unity. For the E3 knot the jet radius is $r_2\approx0.5$ kpc so that $B_\phi(r_2)\approx0.4$ mG. The E3 knot is about 17.7 kpc from the galaxy nucleus.

Transmission Line Analogy: Here, we interpret the Poynting jet described by equations (6) - (8) in terms of a transmission line analogy as suggested by Lovelace & Ruchti (1983). The different physical quantities are measured in the 'laboratory' frame which is rest frame of the plasma outside of the jet at $r\ge r_2$. The effective potential drop across the transmission line is taken to be

$$V_0=-\frac{1}{2}r_0\int_0^{\bar{r}_2}d\bar{r}E_r(\bar{r})\ \ =\ \ \frac{r_0}{3^{1/4}}\frac{B_0}{\sqrt{\mathcal{R}}}\ , \tag{4}$$

where the factor of one-half accounts for the fact that the transmission line does not consist of two conduction surfaces.

The axial current flow of the jet is

$$I_0=-\frac{1}{2}cr_2B_\phi(r_2)=\frac{V_0}{\mathcal{Z}_0}\ , \tag{5}$$

with $\mathcal{Z}_0$ given by equation (3). The units of equations (4) and (5) are cgs. In MKS units note that a current $I_0=3\times10^{18}$ A gives a voltage $V_0=2.7\times10^{20}\beta$ V.

Electric and Magnetic Field Energies: The electric field energy per unit length of the jet in MKS units is

$$W_E=\frac{\epsilon_0}{2}2\pi\int_0^{r_2}rdrE_r^2\ =\ \frac{1}{2}CV_0^2\ ,\ \text{where}\ \ C=\frac{4\pi\epsilon_0}{3} \tag{6}$$

is the capacitance per unit length in Farads per meter and $\epsilon_0 = 8.854 \times 10^{-12}$ F/m.

The magnetic energy per unit length of the jet in MKS units is

$$W_B = \frac{\pi}{\mu_0}\int_0^{r_2} rdr(B_\phi^2 + B_z^2) + \frac{\pi}{\mu_0}\int_{r_2}^{r_3} rdr B_{\phi+}^2 \left(\frac{r_2}{r}\right)^2 \;=\; \frac{1}{2}LI_0^2 \;. \tag{7}$$

Here, $B_{\phi+}$ is the toroidal field at $r_2+\varepsilon$. Carrying out the integrals we find

$$L = \frac{3\mu_0}{4\pi}\left[1 + \frac{1}{2\Gamma^2} + \frac{1}{2\Gamma^2}\ln\left(\frac{r_3}{r_2}\right)\right] \;, \tag{8}$$

which is the inductance per unit length in Henries per meter with $\mu_0 = 4\pi \times 10^{-7}$ H/m.

Telegrapher's Equations: Time and space $(z-)$dependent but not necessarily small perturbations of a Poynting-flux jet are described by the Telegrapher's equations,

$$\frac{\partial \Delta V}{\partial t} = -\frac{1}{C}\frac{\partial \Delta I}{\partial z} \;, \qquad \frac{\partial \Delta I}{\partial t} = -\frac{1}{L}\frac{\partial \Delta V}{\partial z} \;, \tag{9}$$

where $(\Delta V,\ \Delta I)$ represent deviations from the equilibrium values $(V_0,\ I_0)$. The equations can be combined to give the wave equations

$$\left(\frac{\partial^2}{\partial t^2} - u_\varphi^2 \frac{\partial^2}{\partial z^2}\right)(\Delta V,\ \Delta I) = 0 \;, \tag{10}$$

where

$$u_\varphi = \frac{1}{\sqrt{LC}} \;=\; c\left[1 + \frac{1}{2\Gamma^2} + \frac{1}{2\Gamma^2}\ln\left(\frac{r_3}{r_2}\right)\right]^{-1/2} \;, \tag{11}$$

is the phase velocity of the perturbation. The general solution of equation (21) is

$$\begin{aligned} \Delta V &= \Delta V_+(z - u_\varphi t) + \Delta V_-(z + u_\varphi t) \;, \\ \Delta I &= \Delta I_+(z - u_\varphi t) + \Delta I_-(z + u_\varphi t) \;. \end{aligned} \tag{12}$$

It is readily shown that $\Delta V_+ = \mathcal{Z}\Delta I_+$ and $\Delta V_- = -\mathcal{Z}\Delta I_-$, where

$$\mathcal{Z} = \sqrt{\frac{L}{C}} = 90\left[1 + \frac{1}{2\Gamma^2} + \frac{1}{2\Gamma^2}\ln\left(\frac{r_3}{r_2}\right)\right]^{1/2} \Omega \text{ [MKS]}. \tag{13}$$

Irregularity in the Transmission Line: The transmission line may have an irregularity appear in it due for example to the intrusion of a plasma cloud at $t > 0$. The irregularity can be modeled as an extra impedance $\mathcal{Z}_\ell$ or 'load' across the transmission line at $z = 0$. This impedance is considered to go from $\mathcal{Z}_\ell(t < 0) = \infty$ to a constant value $\mathcal{Z}_\ell$ for $t > 0$. In general $\mathcal{Z}_\ell$ is complex with, for example, a positive imaginary part if it is dominantly capacitive. On either side of the discontinuity the line is assumed to have a real impedance $\mathcal{Z}$ given by equation (13). On the upstream side of $\mathcal{Z}_\ell$ $(z < 0)$, the line voltage is $V_0 + \Delta V_-$, where ΔV_- is the backward propagating wave. The current on this part of the line is $I_0 + \Delta I_-$. There is no forward propagating wave for the considered conditions. On the downstream side of $\mathcal{Z}_\ell$, the line voltage is $V_0 + \Delta V_t$ and the current is $I_0 + \Delta I_t$, where $(\Delta V_t,\ \Delta I_t = \Delta V_t/\mathcal{Z})$ represents the transmitted wave.

The standard conditions on the potential and current flow at $\mathcal{Z}_\ell$ $(z = 0)$ give $V_0 + \Delta V_- = V_0 + \Delta V_t$ and $I_0 + \Delta I_- = I_\ell + I_0 + \Delta I_t$, where $I_\ell = (V_0 + \Delta V_-)/\mathcal{Z}_\ell$ is the current flow through $\mathcal{Z}_\ell$. In this way we find

$$\Delta V_- = \frac{-\mathcal{Z}}{2\mathcal{Z}_\ell + \mathcal{Z}} V_0 \;=\; \Delta V_t \;. \tag{14}$$

Note that for $\mathcal{Z}_\ell \to \infty$, both ΔV_- and ΔV_t tend to zero.

The power loss rate in the load $\mathcal{Z}_\ell$ is

$$\dot{\mathcal{E}}_\ell = \frac{(V_0 + \Delta V_t)^2}{\mathcal{Z}_\ell} \;=\; \frac{4\mathcal{Z}_\ell}{(2\mathcal{Z}_\ell + \mathcal{Z})^2} V_0^2 \ . \tag{15}$$

We assume that this power goes into accelerating charged particles which in turn produce the observed synchrotron radiation. This power could account for the emission of the E3 knot of 3C 303 (Kronberg et al. 2011) and the emission of the HST-1 knot in the M87 jet (Biretta 1999).

Acknowledgments: RVEL thanks Van Thanh Tran, Roland Triay, Hady Schenten, and others for organizing this superb meeting. He also thanks Gena Bisnovatyi-Kogan and Marina Romanova for valuable discussions. RVEL was supported in part by NASA grants NNX10AF-63G and NNX11AF33G and by NSF grant AST-1008636. PPK was supported by NSERC (Canada) grant A5713.

References

[1] Biretta J.A., Sparks W.B., & Macchetto F. 1999, ApJ, 520, 621

[2] Kronberg P.P., Lovelace R.V.E., Lapenta; G. & Colgat, S.A. 2011, ApJ, 741, L15

[3] Li H., Lovelace R.V.E., J. M. Finn J.M., & Colgate S.A. 2001, ApJ, 561, 915

[4] Lovelace R.V.E. 1976, Nature, 262, 649

[5] Lovelace, R.V.E., & Ruchti C.B. 1983, in *Positron-electron pairs in astrophysics; Proc. of Workshop*, AIP, , p. 314

[6] Lovelace, R.V.E., Li H., Koldoba A.V. , Ustyugova, G.V., & Romanova M.M. 2002, ApJ, 572, 445

[7] Lovelace R.V.E., & Romanova M.M. 2003, ApJ, 596, L162

[8] Ustyugova, G.V., Lovelace, R.V.E., Romanova M.M., Li H., & Colgate, S.A. 2000, ApJ, 541, L21

[9] Pariev V.I., Colgate, S.A., & Finn J.M. 2007, ApJ, 658, 129

Impact of nuclear input parameters for r-process nucleosynthesis studies

Ilka Petermann

University of Malaya, Department of Physics, Kuala Lumpur, Malaysia

Email : *ilka@um.edu.my*

Abstract

The determination of the age of the oldest objects in the universe, giving a lower limit of the age of the universe itself, is of great interest in astrophysics and cosmology. With the detection of the long-lived isotopes of Th and U in a single star, their application as cosmochronometers has become possible. Performing network calculations, the production of Th and U can be studied for different input of the underlying massmodel and the astrophysical environment. A comparison with the abundance pattern of very metal-poor stars can serve as a reference to check the validity of the assumptions and to better understand their influences on the final outcomes of the calculations. Once the initial amount of Th and U are known, age estimations of stellar objects can be accomplished.

1 Methods

It is known that heavy neutronrich nuclei are produced in the r-process. The r-process is a series of $r$apid neutron capture reactions and successive β-decays in explosive scenarios with extremely high neutron densities. Although its astrophysical site has not been unambiguously identified, supernovae of type II are commonly accepted as a very promising site. As the environmental conditions do not allow a description via a nuclear statistical equilibrium, a system of network equations has to be solved to describe the evolution of the abundances for each isotope with time. In addition to the standard nuclear physics input (neutron captures, β-decays) the most relevant fission rates (neutron-induced, β-delayed and spontaneous fission) were added to an existent database. We have implemented these rates in a fully implicit network, (see also [1]) that includes approximately 7000 nuclei up to ^{300}Ds. The set of differential equations is linearized and solved using the Newton-Raphson method. The largest fraction of nuclei relevant for the r-process are located far on the neutron-rich region. They are not yet accessible by experiment, hence theoretical descriptions have to be applied to determine the relevant quantities. The masses, as the basic ingredient, were taken in this work from the Extended Thomas-Fermi plus Strutinsky-Integral (ETFSI, [2]) , Finite-Range Droplet model (FRDM, [3]) and Hartree-Fock-Bogolyubov approach (HFB, [4]).

2 Cosmochronometry

In general, an initial amount of the cosmochronometers Th and U was theoretically calculated and by assuming a purely exponential decay of the nuclei the age of the stellar object could be determined. With the network calculations of this work it is now possible to calculate the abundances till the latest times (Fig. 1) and perform a direct comparison with observational data (Fig. 2). It is seen, that a broader range of nuclei than previously assumed is responsible for the built-up of Th and U. The direct comparison of calculated abundance ratios with data from observation leads to discrepancies that are assumed to be

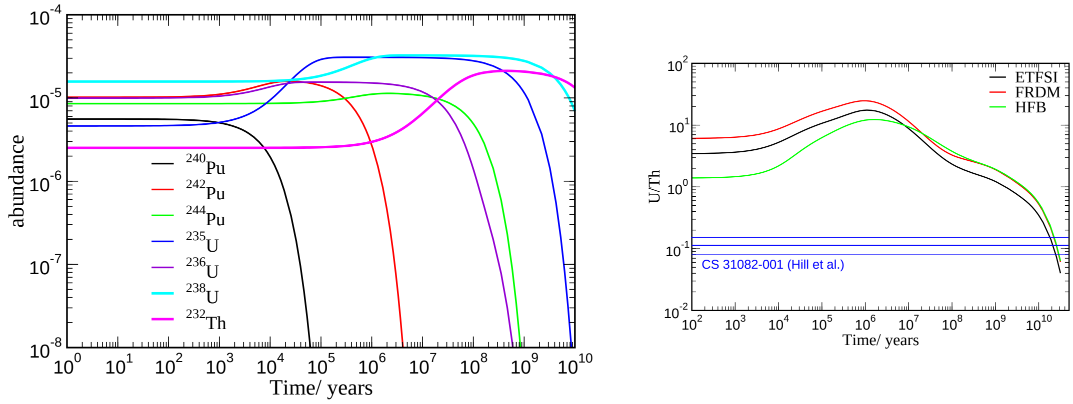

Figure 1: Left: Evolution with time of the longlived isotopes of Th, U and progenitors, here for the case using FRDM. Right: Comparison of the calculated abundance ratio U/Th with observational data for the extremely metal-poor star CS 31082-001 [5].

due to the properties of the underlying massmodel, thus further investigations in that directions remain necessary.

References

[1] R. Hix and F.-K. Thielemann, *Computational methods for nucleosynthesis and nuclear energy generation.*, Journal of Computational and Applied Mathematics 109 (1999)

[2] J.M. Pearson and S. Goriely, *Nuclear mass formulas for astrophysics*, Nuclear Physics A 777 (2006)

[3] P. Moeller et al., *Nuclear Ground-State Masses and Deformations*, Atomic Data and Nuclear Data Tables 59 (1995)

[4] S. Goriely et al., *A Hartree-Fock Nuclear Mass Table*, Atomic Data and Nuclear Data Tables 77 (2001)

[5] V. Hill et al., *First stars. I. The extreme r-element rich, iron-poor halo giant CS 31082-001. Implications for the r-process site(s) and radioactive cosmochronology*, Astronomy & Astrophysics 387 (2002)

Differentially rotating neutron stars

D. Gondek-Rosinska[1], *M.Kucaba*[1], *A. Snopek*[1],
M. Szkudlarek[1],
L. Villain[2] *& M. Ansorg*[3]
[1]*Institute of Astronomy, University of Zielona Góra,*
ul. Lubuska 2, 65-265 Zielona Góra, Poland}
[2]*LMPT, Univ. F. Rabelais, 37200 Tours, France*
[3] *Theoretisch-Physikalisches Institut, Friedrich-Schiller-Universität Jena,Germany*
Email : dorota@astro.ia.uz.zgora.pl

Abstract

An understanding of differentially rotating relativistic stars is key to many areas of astrophysics, in particular to the emission of gravitational waves. A newly born, proto-neutron star or a compact remnant of neutron stars binary merger are expected to rotate differentially and to be important sources of gravitational radiation. We summarize studies of properties of differentially rotating neutron stars and strange stars, mainly focusing on their maximal masses.

1 Calculations and results

The study of differentially rotating neutron stars (NSs) is a complicated task, involving the solution of Einstein's equations in a dynamical regime while, at the same time, many microphysical phenomena need to be taken into account. Therefore, one of the first steps in their modelling is the analysis of axisymmetric and stationary configurations that can mimic both a quasi-stationary evolution of a newly born NS (e.g. Villain et al. 2004) or a state reached after the merging of two NSs (e.g. Baumgarte et al. 2000). Such configurations of differentially rotating relativistic stars have already been the subject of numerous works (e.g. Stergioulas 2003 for review), where the simple rotation law introduced by Komatsu et al.. (1989) was adopted.

The maximum allowed mass of NSs provides a method of observationally distinguishing neutron stars from black holes. The maximum mass of differentially rotating NSs is not uniquely defined. For given equation of state (EOS) it depends on rotation law and degree of differential rotation.

The effect of the degree of differential rotation and an equation of state of dense matter on the maximum mass of differentially rotating NSs was studied recently by many authors. It was found (Lyford et al. 2003, Morrison et al. 2004) that differential rotation can significantly increase the maximum allowed mass (by more than 60%) of NSs and temporarily stabilize a hyper-massive NS. The calculations were done for broad ranges of maximum mass densities and degrees of differential rotation, for both polytropic and realistic EOS. The highest increase was obtained for moderately stiff EOS.

Recently Ansorg et al. (2009) have calculated differentially rotating NSs using a highly accurate relativistic code based on a multi-domain spectral method. They found various types of configurations (called A,B, C and D). Two of them (type B and D) were not considered in previous works, mainly due to numerical limitations. The maximum allowed mass for the new types of configurations and moderate degree of differential rotation can be even 2-4 times higher then the maximum mass of non-rotating NSs with the same EOS (Gondek-Rosinska et al. 2012, Snopek et al. 2012).

Strange stars (SSs) are considered as a possible alternative to NSs as compact objects. Fully relativistic calculations of differentially rotating SSs (Szkudlarek et al., 2012) have shown much larger mass increases for strange stars described by MIT bag model than for NSs for the same degree of differential rotation.

All results suggest that differential rotation can play an important role in e.g. the dynamical stability of the remnant formed in the coalescence of binary NS. Depending on the degree of differential rotation, the masses of merging NSs and the stiffness of EOS the merger remnant can collapse to a black hole or be temporarily supported by rotation against collapse (NS or SS).Gravitational wave observations of coalescing binary NSs may permit one to distinguish these outcomes and constrain the nuclear equation of state.

Acknowledgments: This work was supported by the FOCUS 4/2007 Program of Foundation for Polish Science, the Polish grants NN 203 511 238 and DPN/N176/VIRGO/2009, by CompStar a Research Networking Programme of the European Science Foundation and by the Associated European Laboratory "Astrophysics Poland-France"

References

[1] Ansorg M., Gondek-Rosinska D., Villain L., *MNRAS*,**396**,2359,(2009)

[2] Baumgarte T.W., Shapiro S.L., Shibata M., *ApJL*, **528**,L29, (2000).

[3] Gondek-Rosinska D., Kowalska I., Villain, L., Ansorg, M., in preparation

[4] Komatsu H., Eriguchi, Y., & Hachisu, I.,*MNRAS*,**237**,355,(1989)

[5] Lyford *et al*, *ApJ*,**583**,410, (2003).

[6] Morrison, I. A., Baumgarte, T.W., Shapiro, S.L., *ApJ*, **610**, 941, (2004)

[7] Snopek A., Kucaba M., Gondek-Rosinska D. et al., in preparation (2012)

[8] Stergioulas N., *Living Rev. Relativity*, 6, (2003)

[9] Szkudlarek M., Gondek-Rosinska D. et al., in preparation (2012)

Hidden markov model (HMM) and stochastic differential equation (SDE) of solar radiation sequences

Ly Van Tran, Richard Emilion, Romain Abraham

Mathématiques et Applications, Physique Mathématique d'Orléans (MAPMO), Université d'Orléans, Bâtiment de Mathématiques, 45067 Orléans Cedex 2, France

Email : tranvanly@math.cnrs.fr

Abstract

Analyzing the time sequence of classes of solar days leads us to think that the solar radiation days would be governed by a Hidden Markov Chain with some underlying unobservable mechanism of solar radiation. Under this consideration, we have first established HMM (X_t, Y_t) for solar radiation sequences. The Markov chain X_t is homogeneous and is not observed directly, instead we observe the scalar process Y_t. Then, the problem of estimating the parameters for HMM is discussed. New exact filters for obtaining Maximum Likelihood parameter estimates are derived from the Expectation Maximization (EM) algorithm.

1 HMM and SDE of Solar Radiation Day

The HMM (X_t, Y_t) where X_t is a stationary Markov step process with a finite number of states $\mathbf{S} = \{a_1, a_2, ..., a_n\}$. We denote its transition probabilities by

$$P_{ij}(\varepsilon) = P(X_{t+\varepsilon} = a_j | X_t = a_i) = \begin{cases} 1 - \lambda_i \varepsilon + o(\varepsilon), & j = i, \quad \varepsilon \to 0 \\ \lambda_{ij}\varepsilon + o(\varepsilon), & j \neq i, \quad \varepsilon \to 0 \end{cases}$$

with $\lambda_i = \lambda_{ii} = \sum_{j \neq i} \lambda_{ij}$. The observation process (solar radiation) Y_t is given by SDE

$$dY_t = [\langle X_t, g \rangle I_t - Y_t]\, dt + dB_t, \quad g = (g_1, g_2, ..., g_n)$$

where B_t is a standard Brownian motion independent of X_t and I_t is the direct beam radiation.

2 Parameter estimation

Using the EM algorithm, new estimates $\widehat{\lambda}_{ij}$, $\widehat{g}_j$ of parameters λ_{ij}, g_j in HMM (X_t, Y_t) are given by

$$\widehat{\lambda}_{ij} = \frac{\langle \sigma(\mathcal{J}_t^{ij} X_t), \underline{1} \rangle}{\langle \sigma(\mathcal{O}_t^i X_t), \underline{1} \rangle}, \qquad \widehat{g}_j = \frac{\langle \sigma(\mathcal{T}_t^i X_t), \underline{1} \; + \langle \sigma(\mathcal{M}_t^i X_t), \underline{1} \rangle}{\langle \sigma(\mathcal{N}_t^i X_t), \underline{1} \rangle}$$

where :

- $p_t = \pi_0 + \int_0^t A p_s ds + \int_0^t C_s p_s dY_s$
- $\sigma(\mathcal{J}_t^{ij} X_t) = \int_0^t \langle p_s, e_i \rangle \lambda_{ji} e_i ds + \int_0^t A \sigma(\mathcal{J}_s^{ij} X_s) ds + \int_0^t C_s \sigma(\mathcal{J}_s^{ij} X_s) dY_s$

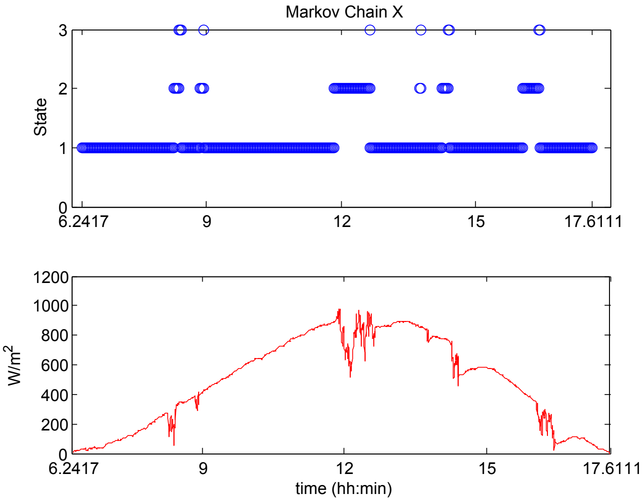

Figure 1: Simulation of the Hidden Markov Model of solar radiation day

- $\sigma(\mathcal{O}_t^i X_t) = \int_0^t \langle p_s, e_i \rangle e_i ds + \int_0^t A\sigma(\mathcal{O}_s^i X_s) ds + \int_0^t C_s \sigma(\mathcal{O}_s^i X_s) dY_s$
- $\sigma(\mathcal{T}_t^i X_t) = \int_0^t I_s(g_i I_s - Y_s) \langle p_s, e_i \rangle e_i ds + \int_0^t A\sigma(\mathcal{T}_s^i X_s) ds$
- $\sigma(\mathcal{M}_t^i X_t) = \int_0^t I_s Y_s \langle p_s, e_i \rangle e_i ds + \int_0^t A\sigma(\mathcal{M}_s^i X_s) ds + \int_0^t C_s \sigma(\mathcal{M}_s^i X_s) dY_s$
- $\sigma(\mathcal{N}_t^i X_t) = \int_0^t I_s^2 \langle p_s, e_i \rangle e_i ds + \int_0^t A\sigma(\mathcal{N}_s^i X_s) ds + \int_0^t C_s \sigma(\mathcal{N}_s^i X_s) dY_s$

References

[1] J. R. Elliott, L. Aggoun and J. B. Moore, *Hidden Markov Models : Estimation and control*, Springer (2010).

[2] A. Dembo and O. Zeitouni, *Parameter estimation of partially observed continuous time stochastic processes via the EM algorithm*. Vol. 23: Stochastic Processes and their Applications.1986), pg. 91-113.

[3] T. Soubdhan, R. Emilion and R. Calif, *Classification of daily solar radiation distributions using a mixture of Dirichlet distributions*, Solar Energy (2009).

Yannick Giraud-Héraud and Nguyen Thi Minh Phuong

Le Kim Ngoc and Jean Trân Thanh Van, Yannick Giraud-Héraud, Cyrille Rosset and Isabelle Cossin

Astroparticle Physics

At the registration desk : Luc Blanchet and Kei-ichi Maeda

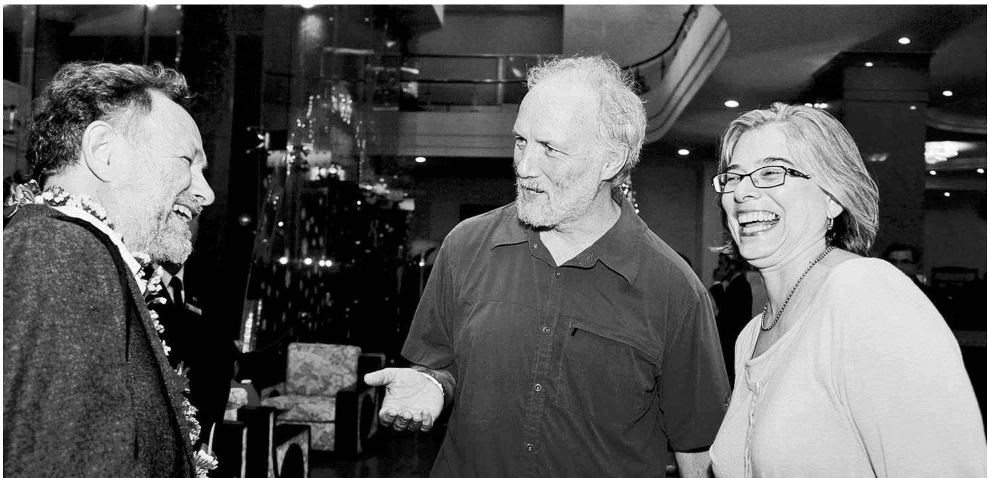

Yannick Giraud-Héraud, Mark Halpern and Michelle Alman

KAGRA Design Status

Shinji Miyoki[1], *KAGRA Collaborators*[2]
[1]*Institute for Cosmic Ray Research, the University of Tokyo,*
5-1-5 Kashiwanoha, Kashiwa, Chiba 277-8582 Japan.
[2]*http://gwcenter.icrr.u-tokyo.ac.jp/en/plan/organization,*
Email : miyoki@icrr.u-tokyo.ac.jp

Abstract

Large-scale cryogenic gravitational wave telescope (named KAGRA) is under construction in the Kamioka mine in Japan since 2010. At least one gravitational wave events from a binary neutron star coalescence per year is expected with the targeted strain sensitivity of 3×10^{-24} $[1/\sqrt{\mathrm{Hz}}]$. KAGRA is also desired to be one of members of the international gravitational wave detection network formed by LIGO, VIRGO and GEO. Different with other present gravitational wave detectors, KAGRA is constructed underground to obtain low seismic noise environment, and utilizes cryogenic sapphire mirrors and suspensions to reduce thermal noise that is the final barrier to reach the quantum noise limiting sensitivity.

1 Introduction

Large-scale cryogenic gravitational-wave telescope (named KAGRA) is currently under construction in the Kamioka mine in Japan. Direct detection of at least one gravitational wave (GW) event per year within 240 Mpc is expected by KAGRA. The direct detection of GW is highly desired to verify the general relativity theory, to obtain unique information about compact stars and supernovae and to be a new window to observe the Universe. Kilometer-scale GW detectors such as advanced LIGO[1] in USA, advanced Virgo[2] and GEO-HF[3] in Europe are now being upgraded to obtain the same or higher sensitivity after their first astrophysical coincident observation for GW events within $\sim$15 Mpc range with some astrophysical results except no remarkable GW detection. Although the commissioning schedule of KAGRA (2017 or 2018) is behind that of adv.LIGO and adv.VIRGO (2014 or 2015), KAGRA is regarded as one of an important base of the international gravitational wave detection network because KAGRA's position and the detector directionality can effectively cover dead angles of the other GW detectors and enhance the positioning accuracy of GW events.

KAGRA has two unique features in its detector configuration. One is that it will be constructed underground, especially in hard rocks of Hida gneiss with a few faults. Stable detector operation and few up-converted excess noise are expected due to low seismic motion not only in the observation band (10Hz$\sim$1kHz) but also in the lower frequency range below the observation band. The other special feature is to utilize cryogenic mirrors and suspensions for reduction of mirror and suspension thermal noises. Owing to cryogenic mirrors, thermal lensing effect that is one of obstacles for adv.LIGO and adv.VIRGO is expected to be negligible[4].

For the first feasibility check of an underground and cryogenic laser interferometer for KAGRA, a 20-meter Fabry-Perot type laser interferometer(named LISM) was moved from a city area to a site 1000 meter underground in the same Kamioka mine. LISM stable operation was successfully demonstrated[5], and drastic displacement noise enhancement[6] over the difference of seismic noise between the city area and the

Kamioka mine was also verified. For the final investigation, a Cryogenic Laser Interferometer Observatory (CLIO) with 100-meter baseline was newly built near LISM[7]. We introduced sapphire mirrors cooled around 15 K, cryostat systems cooling the sapphire mirrors, ultra-stable pulse-tube type refrigerators[8] cooling the cryostats and a laser frequency(wave length) stabilization system for the precise length measurement to CLIO. Finally, the suspension thermal noise reduction according to its temperature and thermo-elastic noise reduction of sapphire mirrors were demonstrated for the first time[9]. Owing to these results, KAGRA project was approved in 2010. In this paper, we will present the main part design of KAGRA.

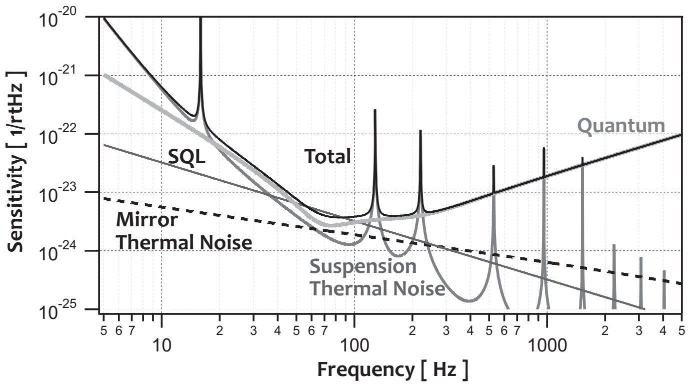

Figure 1: KAGRA sensitivity curve and noise components.

2 KAGRA Interferometer Design

2.1 Targeted Sensitivity

Figure.1 shows the most promising KAGRA sensitivity curve designed to be dominated by quantum noise, such as radiation pressure noise and shot noise. 23kg sapphire mirror mass and 50 W laser power just before a power recycling mirror(PRM) are assumed. The sensitivity reaches the standard quantum limit(SQL) around 100Hz, where we expect to observe macroscopic quantum effect of kg-scale mirrors[10]. The mirror suspension thermal noise is close to the radiation pressure noise, and some mechanical resonances of sapphire suspension fibers appear around the most sweet observation band. These resonances are resulted from the sapphire suspension fiber's thickness that is required to ensure 2W heat transfer through them for cooling a sapphire mirror. On the other hand, the mirror thermal noise due to coating is well below the targeted sensitivity, except for around 100Hz. The resulting neutron star inspiral range becomes 240 Mpc, so at least one GW event per year can be detected by KAGRA.

2.2 Underground Facility

KAGRA will be constructed underground. At least 200 meter ground coverage is ensured to obtain same level low seismic noise environment with deep underground like CLIO. The seismic noise level is 1/100$\sim$1/1000 smaller than city area except $\sim$0.3 Hz peak known as a micro-seismic noise due to ocean waves. The perpendicular arm is rotated in a counterclockwise direction by 30 degrees from the north. There are two access tunnels towards the corner station and the perpendicular arm end station, respectively. The tunnel floor has a tilt of 1/300 for water drainage. The diameter of the arm tunnels is about 4 meter, the height in each station is 10 meter at most. At four cryostats positions, there are second floors to keep the stability as a base for the mirror suspension point.

2.3 Optical Configuration

Figure.2 shows the optical configuration of KAGRA. 180W laser source will be prepared as a light source. After passing through a pre-mode cleaner for pre-frequency stabilization, higher transverse mode rejection and intensity noise reduction at the modulation frequencies for the interferometer control, it is injected into a 30 meter length triangle shape mode cleaner again for the same purposes. After passing through an isolator and bouncing on two mode-matching mirrors, the pre-stabilized beam is injected in to the main interferometer part. The main interferometer is a Power Recycled Fabry-Perot Michelson Interferometer(PR-FPMI) with the Resonant Sideband Extraction(RSE) technique[11]. Compared with a Michelson Interferometer, the Fabry-Perot cavity contributes amplification of GW effects mainly for sensitivity enhancement for the lower frequency range, the power recycling technique to reduction of shot noise with trade off radiation pressure noise enhancement, and RSE to retainment of observation bandwidth for sensitivity enhancement mainly for the higher frequency range. The finesse of the arm cavity is set 1550. The power recycling gain is 10. So, the expected storage power in one FP cavity is over 500($\sim$800 at most) kW. For the better mirror alignment signal extraction, the folded power and signal recycling cavities are introduced. An output mode cleaner in front of the GW signal detection port is prepared to reject stray and higher transverse light. KAGRA will be operated as FPMI using the silica input and output test masses at 300K ahead of the PR-FPMI configuration with RSE using the sapphire input and output test masses at cryogenic temperature as shown in Figure.2. The substrate of four main mirrors that compose arm FP cavities is crystal sapphire. The required absorption loss is less than 20($\sim$50 at present) ppm/cm. The size of mirrors is 22cm($\sim$25 is targeted) cm in diameter and 15cm in thickness. The expected mechanical loss of the sapphire mirror is 10^{-8} at 20 K. Optical coating films on mirrors are multilayered of SiO_2/Ta_2O_5. The allowed loss of coating is less than 45 ppm. The other mirrors substrate are silica, including a beam splitter.

2.4 Vibration Isolation of Mirrors

Figure.3 shows three types of mirror suspension for seismic noise isolation and expected isolated seismic noise by type-A suspension[12]. Type-A and type-B are seven(six) and five(four) stage pendulums for horizontal (vertical) motion, respectively, while type-C are combination of a stack and a double pendulum. Type-A system is applied to arm cavity sapphire mirrors, while type-B to the beam splitter, the power recycling cavity mirrors and the signal recycling cavity mirrors. Type-C system is applied for the mode cleaner cavity mirrors, four arm cavity silica mirrors and a photo detector, as shown in Figure.2

2.5 Cryogenic System

One of singular situation for KAGRA cryogenic system is that the sapphire mirrors are inevitably exposed to 300K area to form a Fabry-Perot cavity. The other is that heat absorbed inside the sapphire mirrors should be extracted only by the thermal conduction of a series connection of suspension sapphire fibers between sapphire mirrors and their upper masses and heat link pure aluminum wires between several upper masses to some cold anchors without any excess seismic noise introduction through these heat link wires. Figure.4 shows the cryostat and radiation duct shield design for cooling the sapphire mirror and its suspension system inside. The cryostat has three layers structure that are an outside vacuum tank, an outer radiation shield cooled around 80 K and an inner radiation shield cooled around 8K. These radiation shields are covered

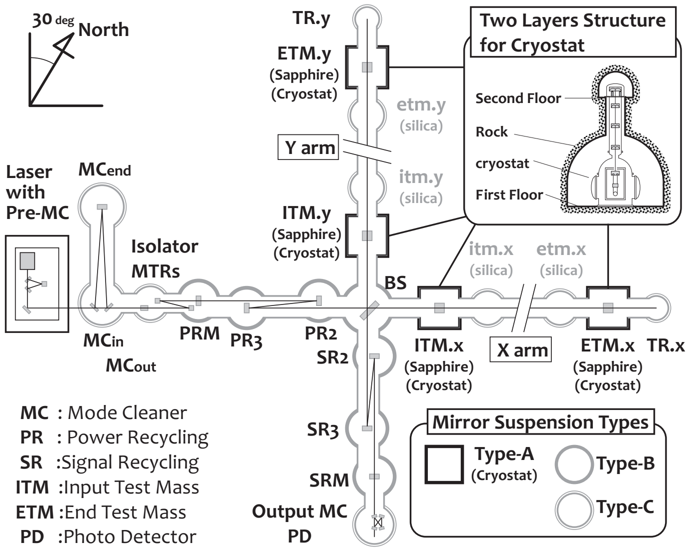

Figure 2: KAGRA optical configuration.

by multi-layered films to minimize the heat introduction from the outer area, and are cooled by at most four two-stage pulse tube type refrigerators with vibration reduction function manufactured by SUMITOMO Heavy industry Inc. A heat anchor point that is directly connected with the refrigerator second stage($\sim$ 4K head) is prepared to reject inner shield vibration. Each cryostat has two $\sim$17m radiation shield ducts equipped with baffles to reduce heat injection from 300K area. The diameter of the heat radiation shield duct is 90cm and five baffles position and the baffles' hole diameter size are optimized[13]. The estimated heat road at the sapphire mirror position is well below 2W due to laser power absorption.

References

[1] G. Harry for the LIGO Scientific Collaboration, "Advanced LIGO: the next generation of gravitational wave detectors", Class. Quantum Grav., **27** (2010) 084006.

[2] "Advanced Virgo Baseline Design", The Virgo Collaboration, VIR-0027A-09 (2009); available from https://pub3.ego-gw.it/itf/tds/ .

[3] B. Willke *et al.*, "The GEO-HF project", Class. Quantum Grav., **23** (2006) S207-S214.

[4] T.Tomaru *et al.*, "Thermal lensing in cryogenic sapphire substrates", Class. Quantum Grav., **19** (2002) pp.2045-2049.

[5] S.Sato *et al.*, "Ultra-stable performance of an underground-based laser interferometer observatory for gravitational waves", Phys. Rev. D, **69** (2004) 102005.

[6] M.Ohashi *et al.*, "Design and construction status of CLIO", Class. Quantum Grav., **20** (2003) pp.599-607.

[7] S.Miyoki *et al.*, "Status of the CLIO project ", Class. Quantum Grav., **21** (2004) S1173-1182.

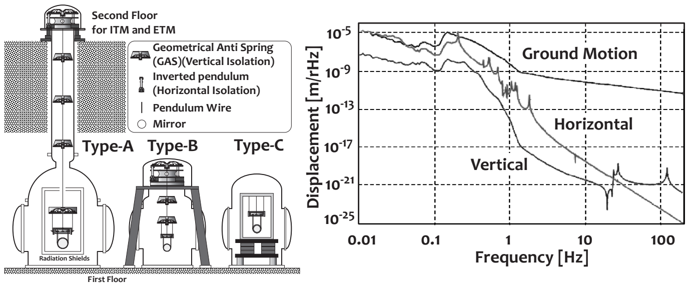

Figure 3: Mirror suspension for seismic noise isolation and expected seismic noise isolation by type-A[12].

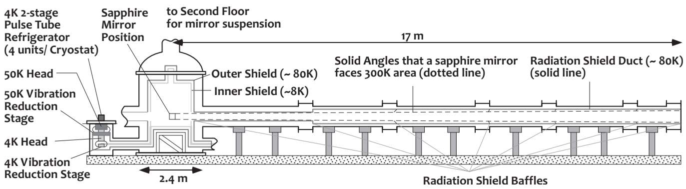

Figure 4: KAGRA cryostat and radiation shield duct system[13].

[8] R.Li *et al.*, "Vibration-Free Pulse Tube Cryocooler System for Gravitational Wave Detectors II — Colling Performance and Vibration —", Proceedings of the 13th International Cryocooler Conference (ICC13) Mar.29-Apr.1 2004 New Orleans USA (Cryocoolers **13** (2005) pp.703-710).

[9] T.Uchiyama *et al.*, "Reduction of thermal fluctuations in a cryogenic laser interferometric gravitational wave detector", Physical Review Letters, accepted in February 2012.

[10] B.Abbott *et al.*, "Observation of a kilogram-scale oscillator near quantum ground state", New J. Phys., **11** (2009) 073032.

[11] J. Mizuno *et al.*, "Resonant sideband extraction: a new configuration for interferometric gravitational wave detectors", Phys. Lett. A, **175** (1993) pp.273-276.

[12] Master thesis of T.Sekiguchi, the School of Science, the University of Tokyo.

[13] Y.Sakakibara *et al.*, "Reflectivity Measurements of Metals for LCGT Thermal Radiation Shields at Cryogenic Temperature and Wavelength of 10 μm", Journal of Cryogenic and Superconductivity Society of Japan, **46** (2011) pp.434-440.

Jean Tran Thanh Van at the Ground Breaking ceremony for the ICISE

Recent results from the Pierre Auger Observatory on ultra-high energy cosmic rays

P.T. Nhung[1], *for the Pierre Auger Collaboration*[2]
[1] *VATLY/INST, 179 Hoang Quoc Viet, Cau Giay, Hanoi, Vietnam*
[2] *Observatorio Pierre Auger, Av. San Martín Norte 304, 5613 Malargüe, Argentina*
(Full author list at http://www.auger.org/archive/authors_2011_12.html)
Email : ptnhung@mail.vaec.gov.vn

Abstract

The Pierre Auger Observatory is the largest observatory ever built to study ultra-high energy cosmic rays. Its hybrid detector system covers 3000 km^2 in the Argentinean pampas and consists of 24 fluorescence telescopes and of a ground array of 1660 water Cherenkov detectors. The construction of the Observatory was completed in 2008 but it has been taking data since January 2004 and accumulated the world's largest data set of ultra-high energy cosmic rays. Recent results, including measurements of the energy spectrum, mass composition, and the anisotropy in the arrival directions are presented.

1 Introduction

Cosmic rays are charged particles with energies up to 10^{20} eV, nearly two orders of magnitude higher than the nominal energy in the centre of mass system of the Large Hadron Collider (LHC) at CERN. Although cosmic rays were discovered one century ago, they are still today extensively studied in all energy ranges. At energies in excess of 10^{18} eV, ultra-high energy cosmic rays (UHECR) are the subject of extensive studies including measurements of the energy spectrum, of the nature of the primaries and the identification of possible sources.

UHECRs are studied from their interaction with the Earth atmosphere, which produces cascades of secondary particles called extensive air showers. These may be detected using two different techniques. One consists in sampling the particle density on ground, the other in detecting the fluorescence light emitted by nitrogen molecules excited by the shower. The two techniques are complementary and are affected by very different sources of systematic uncertainties. The UHECR flux is extremely low, requiring very large exposure to reach sufficient statistics. The Pierre Auger Observatory is the largest hybrid observatory combining the strengths of both detection techniques [1]. Its construction was completed in 2008. It has been taking data since 2004 and has accumulated the world's largest UHECR data set with unprecedented accuracy. It is located in the Argentinean pampas. Its surface detector (SD) consists of 1660 water Cherenkov detectors, located on a triangular grid covering 3000 km^2 with 1.5 km mesh size. Each SD detector contains a cylindrical volume of ultra pure water, 1.2 m in height and 3.6 m in diameter. The Cherenkov light produced in the water volume is observed using three $9''$ spherical photomultiplier tubes. Signals are digitized in 25 ns bins, time-stamped using a local GPS receiver, and transferred by radio to the central data acquisition system. The telescopes of the fluorescence detector (FD) are grouped in four stations of six telescopes each, located at the edges of the SD array [2]. Each telescope has a field of view of 30^o in azimuth and 28.6^o in elevation. The fluorescence light is UV filtered and reflected by a 11 m^2 spherical mirror onto an array of 440 hexagonal

PMT pixels. Signals are digitized with 100 ns resolution. The FD operates during clear, moonless nights exclusively, limiting its duty cycle to 10-15%. On the contrary, the SD operates with nearly 100% duty cycle and provides a large statistics data sample with an easily calculable aperture. The FD provides a measurement of the shower longitudinal profile, and therefore a calorimetric measurement of the primary energy together with a direct observation of the shower maximum depth, X_{max}, a quantity sensitive to the primary mass composition. Hybrid events, detected by both the SD and FD, provide a calibration of the energy scale. They also allow for important cross-checks, in particular of the measurements of the shower arrival direction and of the triggering efficiency.

The Pierre Auger Observatory is addressing the main issues of UHECR physics, including energy spectrum, anisotropies in the arrival direction distribution and mass composition of the primaries.

2 Energy spectrum

The UHECR energy spectrum has been measured [3] from 10^{18} eV up to above 10^{20} eV where the highest energy showers have been observed. The higher energies are more easily accessible to the SD that has the larger exposure, 2.09 10^4 km^2 sr yr, while the lower energies are only accessible to the FD. In practice, two independent energy distributions have been measured, one using SD data and the other using hybrid data, namely showers detected simultaneously by the FD and by at least one SD detector. SD data cover the period from January 2004 to December 2010 and hybrid data from November 2005 to September 2010. Both distributions are found to be mutually consistent in the region where they overlap (from $\sim 3\ 10^{18}$ eV to $\sim 7\ 10^{19}$ eV) and are combined in a single spectrum that is displayed in Figure 1 after multiplication by the cube of the measured energy, E^3. As SD energies are calibrated using hybrid showers [4], both distributions share a common systematic uncertainty of 22% in the energy scale. However, the normalization uncertainties are independent, 6% for the SD data and between 6% and 10% for the hybrid data. Note that a small change in energy scale shifts data diagonally in Figure 1 and, within systematic uncertainties, the data are consistent with the most recent HiRes data [5], which have much lower statistics but a systematic energy uncertainty of 17%.

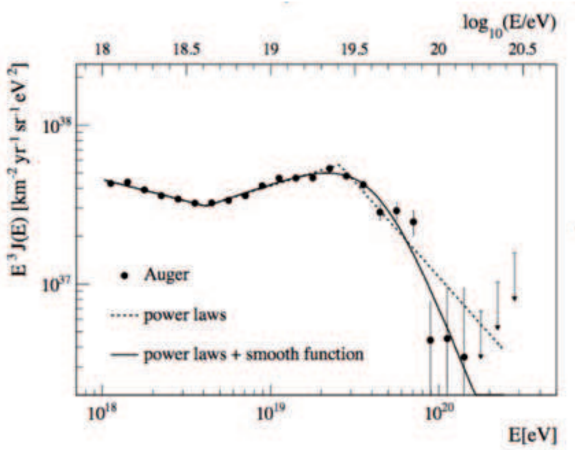

Figure 1: The Pierre Auger Observatory energy spectrum combining SD and hybrid data [3].

The extension to lower energies, made possible by the inclusion of hybrid events, is based on a detailed calculation of the energy-dependent exposure taking proper account of measured atmospheric and detector conditions and using severe selection criteria meant to minimize the influence of the mass composition and energy uncertainty.

The main feature of the measured spectrum is the evidence, with unprecedented significance, for a high energy suppression that is consistent with the early calculation made by Greisen, Zatsepin and Kuzmin (GZK) [6] of the effect of the interaction with the Cosmic Microwave Background (CMB). Extension of such calculations to primary nuclei and to other processes [7] indicates that proton and iron nuclei have a much smaller probability of being dissociated before reaching Earth than intermediate nuclei have. Moreover, the flux suppressions associated with proton and iron nuclei occur at nearby energies, preventing significant information on the mass composition to be obtained from the shape of the energy spectrum. Finally, it must be noted that the interpretation of the flux suppression in terms of interactions with the CMB does not exclude additional contributions related to the acceleration mechanism.

The lower energy range [3] is dominated by a break occurring at an energy of $10^{18.61\pm0.01}$ eV, referred to as the ankle and usually associated with the transition from galactic to extra-galactic sources. Power law fits give indices of respectively 3.27 ± 0.02 and 2.68 ± 0.01 below and above the break.

3 Anisotropies of the highest energy events

The GZK effect limits the horizon from which UHECR can be observed well below 100 Mpc. Within the GZK horizon, matter is distributed very anisotropically, dominated by the Centaurus-Hydra-Virgo-Pavo supercluster and including major voids [8]. The excellent pointing accuracy of the Pierre Auger Observatory, better than 1^{o}, makes it possible to search for sources in the directions where UHECR showers are pointing back. The main obstacle to such a search is the presence of magnetic fields on the way from extragalactic sources to the Earth, the most harmful being the closest to Earth, namely those contained in the disk of the Milky Way. Such searches have been made using Pierre Auger Observatory data [9] and have given evidence for a positive correlation within an angle of 3.1^{o} between the arrival directions of showers having energies in excess of 55 EeV and the positions of nearby ($<$ 75 Mpc) Active Galactic Nuclei (AGN) from the VCV catalogue [10]. The fraction of correlating events is 0.38 compared with 0.21 for an isotropic distribution of the sources. As illustrated in Figure 2, it was originally measured at a much higher level, 0.69, corresponding to a statistical fluctuation of about three standard deviations. This has triggered extensive searches for instrumental effects and analysis biases, none of which has revealed any dysfunction.

Indications of positive correlations are also obtained using normal galaxy catalogues or X-ray galaxy catalogues, showing that they are essentially associated with the anisotropic distribution of matter within the GZK horizon. In particular, a concentration of events in the Centaurus region suggests a possible association with Cen A, the closest AGN to Earth, only 4 Mpc away. However, the measured correlations are much less sharp than expected for protons in this high energy range, suggesting that the images might be blurred by magnetic deflections significantly larger than expected for proton primaries. If this were the case, one would expect showers having their origins in a same source but having different energies to point back to a line in the sky, the farther away from the source the lower the energy. A search for such multiplets [11] has been performed using showers having energies in excess of 20 EeV. The largest multiplet found is a 12-plet with source galactic coordinates ($l = -46.7^{o}$, $b = 13.2^{o}$) but the probability that it occurs by chance from an isotropic distribution is 6%, too large to claim any evidence for a positive effect. Two decuplets are observed in the Cen A region, again insufficiently significant. The search for UHECR sources remains therefore largely inconclusive. Progress requires, among others, a precise determination of the primary mass composition as the magnetic deflection experienced by iron nuclei would make it extremely difficult to reveal possible correlations.

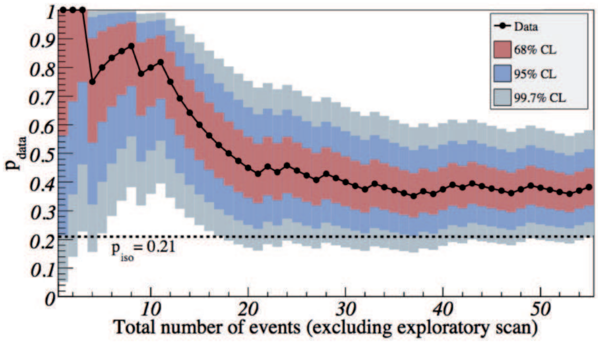

Figure 2: Most likely degree of correlation, $p_{data} = k/N$ as a function of the total number of time ordered events, N. k is the number of correlating events. The 68%, 95% and 99.7% confidence level intervals are shown. The horizontal dashed line shows the isotropic expectation of 0.21 [9].

4 Mass Composition

The main difference between showers induced by a proton and an iron nucleus of the same energy (we have seen that other nuclei are unlikely to survive the journey to Earth) is that the latter interact higher in the upper atmosphere than the former do. The average depth $\langle X_{max} \rangle$, measured in g/cm^2, at which shower development reaches maximum is, therefore, smaller by about 100 g/cm^2. This estimate, obtained from models of the shower development, is quite robust: in spite of the lack of relevant accelerator data, the constraints imposed by energy-momentum conservation and by the known properties of the strong QCD interaction, leave little freedom to depart significantly from this value. Similarly, the fluctuation of X_{max} around the mean, $Rms(X_{max})$, is lower for iron than for proton by about 40 g/cm^2 in the UHECR region. The dependence on energy of these quantities is predicted to be linear in the logarithm of the energy and the so-called elongation rates, the derivatives $\partial/\partial \lg(E)$, are rather reliably predicted. This is illustrated in Figure 3 where model predictions of X_{max} and $Rms(X_{max})$ are displayed as a function of energy for protons and iron nuclei separately. The FD measurements of these quantities are shown on the same figure [12].

For both quantities, the measured elongation rates [12] are significantly smaller than predicted, suggesting an evolution from lighter to more massive nuclei. However, data from other observatories [13] do not show such a trend as clearly as the Pierre Auger Observatory data do. A recent exhaustive review [14] of the experimental situation shows that the issue is not yet settled. Extreme care has been taken to ascertain the validity of the Pierre Auger Observatory measurement, in particular the absence of bias in the event selection. Possible biases might result from the limited elevation range of the FD field of view (FOV). Showers landing close to an FD station tend to have X_{max} near the high elevation limit of the FOV, thereby introducing a bias favouring larger X_{max} values. On the contrary, nearly vertical showers tend to have X_{max} near ground, thereby introducing a bias favouring smaller X_{max} values. To avoid such biases, fiducial volume cuts are applied to the data, depending on shower geometry and on energy. A minimal range of visible atmospheric depths is required, such that X_{max} can be detected and measured with good resolution independent of the nature of the primary particle. Simulations of the detection and reconstruction processes have provided independent checks of the bias-free nature of the results. The typical X_{max} measurement uncertainty is estimated using simulations and independently validated using showers that are seen by two or more fluorescence telescopes; comparing the corresponding X_{max} values gives a resolution of 20±2 g/cm^2 at

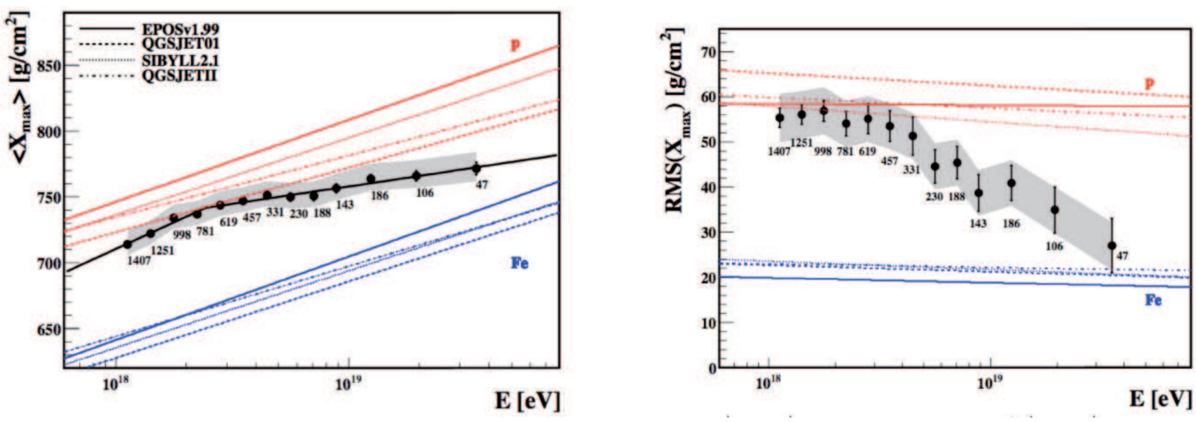

Figure 3: Mean and RMS values of the X_{max} distribution as a function of energy [12]. Data are compared with expectations for proton and iron primaries from four representative hadronic interaction models.

10^{19} eV, in excellent agreement with the simulation prediction, providing additional confidence in the validity of the analysis.

Another estimator of the primary mass composition is the muon density on ground. As iron nuclei interact higher in the upper atmosphere than protons do, the muon density on ground is predicted to be larger, typically by 30-40%. Here again, the value of this ratio is quite robust but the absolute value of the muon density is more model dependent. Indeed the density measured at the Pierre Auger Observatory using the SD [15] is outside the predicted proton-iron window, significantly higher than the predicted iron value, precluding useful information on the primary mass composition and raising questions on the validity of the description of the muon component in conventional shower development models. In summary, for the issue to be settled, a detailed description of the respective evolutions of the proton and iron components is necessary but still lacking.

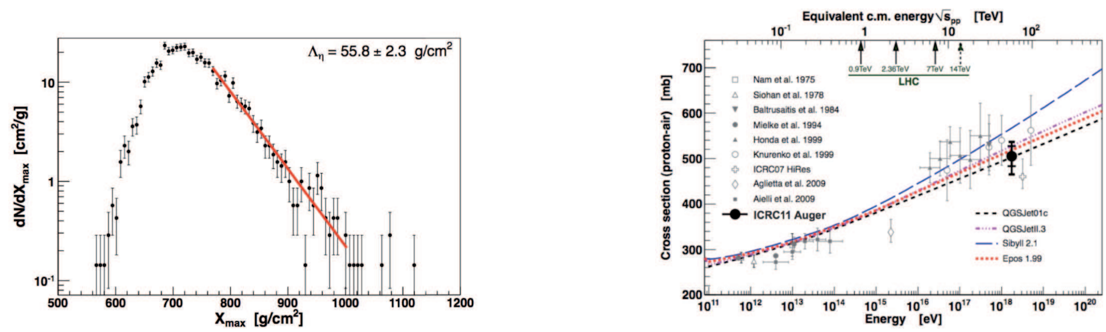

Figure 4: Pierre Auger Observatory measurements of the proton-air cross-section. Left panel: Fit of the interaction length to the tail of the X_{max} distribution. Right panel: Pierre Auger Observatory result compared with other measurements and model predictions. The inner error bars are statistical only, while the outer include all systematic uncertainties for a helium fraction of 25% and 10 mb photon systematics.

The tail of the X_{max} distribution toward higher values provides a measure of the proton-air cross-section, its rate of decrease being governed by the interaction length. Hybrid Pierre Auger Observatory data collected in the energy interval from 10^{18} to $10^{18.5}$ eV, where a large fraction of protons is still present, have been used to estimate the proton-air cross-section at a centre-of-mass energy of 57 TeV [16]. The result, displayed in Figure 4, favours a relatively low cross-section, in qualitative agreement with early LHC measurements at lower energy [17].

5 Conclusion

The Pierre Auger Observatory has contributed major advances to UHECR physics. While the presence of a high-energy flux suppression in the GZK energy range, expected from interactions with the CMB, is now clearly established, several issues remain unsettled. Up to now, it has not been possible to identify individual sources from the measured arrival directions of UHECRs. This could be related to magnetic deflections, resulting either from higher primary charges or from larger magnetic fields than commonly expected. A detailed understanding of the evolution with energy of the primary mass composition has become essential: the currently observed trend toward higher masses between the ankle and the GZK suppression raises a number of issues, including possible changes in hadronic interactions at these energies, which have become central to UHECR physics.

The continued collection by the Pierre Auger Observatory of UHECR data at a rate of 7000 km^2 sr per year will double the presented statistics in three years from now. Upgrades of the detector are being implemented, including the doubling of the elevation range of the field of view of three telescopes of one of the FD stations and the construction of a small infill array that locally increases the density of the SD detectors and includes underground muon detectors. In addition, radio detection techniques are currently being explored.

References

[1] The Pierre Auger Collaboration, Nucl. Instrum. Methods A523 (2003) 50.

[2] The Pierre Auger Collaboration, Nucl. Instrum. Methods A613 (2010) 29.

[3] The Pierre Auger Collaboration, Phys. Lett. B 685 (2010) 239;
F. Salamida for the Pierre Auger Collaboration, *Update on the measurement of the CR energy spectrum above 10^{18} eV made using the Pierre Auger Observatory*, Proc. 32$^{\mathrm{nd}}$ ICRC, Beijing, 2011, arXiv:1107.4809v1 [astro-ph.HE].

[4] R. Pesce for the Pierre Auger Collaboration, *Energy calibration of data recorded with the Surface Detectors of the Pierre Auger Observatory: an update*, Proc. 32$^{\mathrm{nd}}$ ICRC, Beijing, 2011, arXiv:1107.4809v1 [astro-ph.HE].

[5] R. U. Abbasi et al., Astropart. Phys. 32 (2009) 53.

[6] K. Greisen, Phys. Rev. Lett. 16 (1966) 748;
G.T. Zatsepin and V.A. Kuzmin, Pisma Zh.Eksp. Teor. Fiz 4 (1966) 114.

[7] D. Allard, Proc. Rencontres de Moriond 2009, arXiv:0906.3156;
D. Allard et al., J. Cosm. Astrop. Phys. 10 (2008) 33;
D. Harari, S. Mollerach and E. Roulet, J. Cosm. Astropart. Phys. 11 (2006) 12.

[8] A.P. Fairall and W.R. Paverd, *Large scale structures in three dimensions*, in Clustering in the Universe, XXXth Rencontres de Moriond, Les Arcs, March 11-18 1995, p.67, Ed. Frontières.

[9] The Pierre Auger Collaboration, Science 318 (2007) 938;
The Pierre Auger Collaboration, Astropart. Phys. 29 (2008) 188;
The Pierre Auger Collaboration, Astropart. Phys. 34 (2010) 314.

[10] M. P. Véron-Cetty and P. Véron, Astron. & Astrophys. 455 (2006) 773.

[11] G. Golup for the Pierre Auger Collaboration, *Search for energy-position correlated multiplets in Pierre Auger Observatory data*, Proc. 32nd ICRC, Beijing, 2011, arXiv:1107.4805v1 [astro-ph.HE];
The Pierre Auger Collaboration, *Search for signatures of magnetically-induced alignments in the arrival directions measured by the Pierre Auger Observatory*, Astropart. Phys., in press (2011), arXiv:1111.2472v1 [astro-ph.HE].

[12] P. Facal San Luis for the Pierre Auger Collaboration, *The distribution of shower maxima of UHECR air showers*, Proc. 32nd ICRC, Beijing, 2011, arXiv:1107.4804v1 [astro-ph.HE];
M. Unger [Pierre Auger Coll.], Nucl. Phys. B 190 (2009) 240;
The Pierre Auger Collaboration, Phys. Rev. Lett. 104 (2010) 091101;
D. Garcia-Gamez for the Pierre Auger Collaboration, *Measurement of atmospheric production depths of muons with the Pierre Auger Observatory*, Proc. 32nd ICRC, Beijing, 2011, arXiv:1107.4804v1 [astro-ph.HE];
D. Garcia-Pinto for the Pierre Auger Collaboration, *Measurements of the longitudinal development of air showers with the Pierre Auger Observatory*, Proc. 32nd ICRC, Beijing, 2011, arXiv:1107.4804v1 [astro-ph.HE].

[13] S. Knurenko and A. Sabourov [Yakutsk Coll.], Nucl. Phys. B (Proc. Suppl.) 212-213 (2011) 241;
R. Abbasi et al. [HiRes Coll.], Phys. Rev. Lett. 104 (2010) 161101;
C. Jui et al. [Telescope Array Coll.], Proc. APS DPF Meeting (2011), arXiv:1110.0133v1 [astro-ph.IM].

[14] K. H. Kampert and M. Unger, *Measurements of the cosmic ray composition with air shower experiments*, Astropart. Phys., in press (2012), arXiv:1201.0018v2 [astro-ph.HE].

[15] A. Castellina for the Pierre Auger Collaboration, Proc. 31st ICRC, Łódź, Poland, 2009, arXiv:0906.2319v1[astro-ph.CO];
J. Allen for the Pierre Auger Collaboration, *Interpretation of the signals produced by showers from cosmic rays of $10^{19}\,eV$ observed in the surface detectors of the Pierre Auger Observatory*, Proc. 32nd ICRC, Beijing, 2011, arXiv:1107.4804v1 [astro-ph.HE].

[16] R. Ulrich for the Pierre Auger Collaboration, *Estimate of the proton-air cross-section with the Pierre Auger Observatory*, Proc. 32nd ICRC, Beijing, 2011, arXiv:1107.4804v1 [astro-ph.HE].

[17] G. Aad et al., ATLAS Collaboration, 2011, arXiv:1104.0326 [hep-ex];
CMS Collaboration, presentation at DIS workshop, Brookhaven, 2011.

Arriving of the participants at the Ground Breaking ceremony for the ICISE

The Rencontres du Vietnam secretarial staff: Hady Schenten, Maryvonne Joguet, Nguyên Thi Loi, Isabelle Cossin and Nicole Ribet

Ultra-High Energy Hadronic Interaction Models and LHC Data

T. Pierog
Karlsruhe Institute of Technology (KIT), IKP, D-76021 Karlsruhe, Germany
Email : Tanguy.Pierog@kit.edu

Abstract

Currently the uncertainty in the prediction of shower observables for different primary particles and energies is dominated by differences between hadronic interaction models. The LHC data on minimum bias measurements can be used to test Monte Carlo generators and these new constrains will help to reduce the uncertainties in air shower predictions. In this article, after a short introduction on air showers we will show the results of the comparison between the updated version of high energy hadronic interaction models with LHC data. Results for air shower simulations and their consequence for and from Astrophysics will be discussed.

1 Introduction

Most of the Astronomy and Astrophysics is done using electromagnetic signals from radio to gamma rays. It gives precious informations on the various objects observed in the Universe and their history. In fact a part of these signals is produced by elementary charged particles like electrons or nuclei which can escape the source and reach the Earth after a long propagation through the (extra)galactic medium. Eventually these charged particles may cross the path of the Earth and enter our field of view: they are cosmic rays. Due to the steeply falling energy spectrum of cosmic rays, direct detection by satellite- or balloon-borne instruments is only possible up to about $\sim 10^{14}$ eV. Fortunately, at such high energies, the cascades of secondary particles produced by cosmic rays reach the ground and can be detected in coincidence experiments. The cascades are called extensive air showers (EAS) and are routinely used to make indirect measurements of high energy cosmic rays. The upper limit of the detectable energy is given by the area and exposure time of the detector. For instance, the Pierre Auger Observatory (PAO) [1], which is currently taking data in Argentina, is designed to detect particles of $\sim 10^{20}$ eV for which the flux is less than one particle per km^2 and century.

Air showers can be observed using different detection techniques. The most frequently employed technique is the measurement of secondary particles reaching ground. Using an array of particle detectors (for example, sensitive to $e^{\pm}$ and $\mu^{\pm}$), the arrival direction and information on mass and energy of the primary cosmic ray can be reconstructed. The main observables are the number and the lateral (Fig. 2 left-hand side) and temporal distributions of the different secondary particles. At energies above $\sim 10^{17}$ eV, the longitudinal development of a shower can be directly observed by measuring the fluorescence light induced by the charged particles traversing the atmosphere. Two main observables can be extracted from the longitudinal shower profile: the energy deposit or the number of particles, $N_{\max}$, at the shower maximum and $\mathrm{X}_{\max}$, the atmospheric depth of the maximum (see Fig. 2 right-hand side). Again, these quantities can be used to estimate the energy and mass of the primary particles. Shower-to-shower fluctuations of all observables also provide very useful composition information.

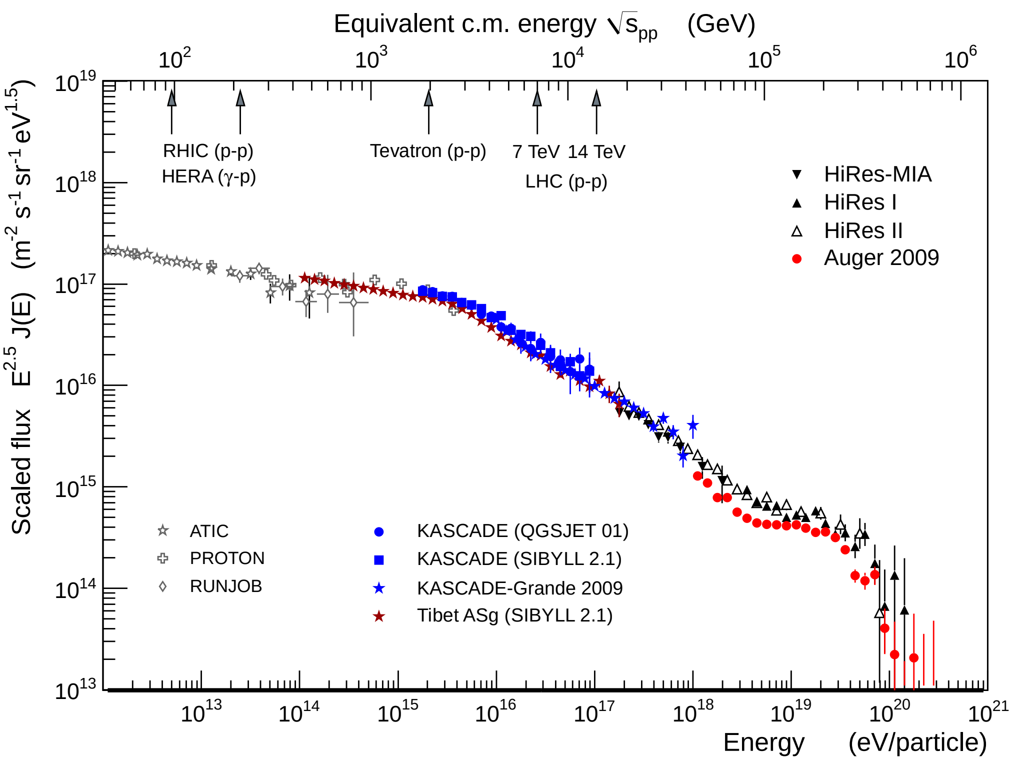

Figure 1: Flux of cosmic ray arriving at Earth rescaled by the energy to the power 2.5. Data references are given in [2].

As a consequence of the indirect character of the measurement, detailed simulations of air showers are needed to extract information on the primary particle from shower observables. Indeed the cascade is initiated by a first hadronic interaction between the initial charged primary cosmic ray and one nucleus from the atmosphere. After their propagation limited by their cross section, the secondary hadronic particles will interact again forming the hadronic cascade which is the skeleton of the EAS. At each hadronic interaction about one third of the energy goes into the π^0 which immediately decay into two photons feeding the electromagnetic cascade. After few hadronic generations, more the 90% of the energy of the primary particle is carried by the electromagnetic component of the EAS. Whereas electromagnetic interactions are well understood within perturbative QED, hadronic multi-particle production cannot be calculated within QCD from first principles. Differences in modelling hadronic interactions, which cannot be resolved by current accelerator data, are the main source of uncertainty of air shower predictions [3, 4].

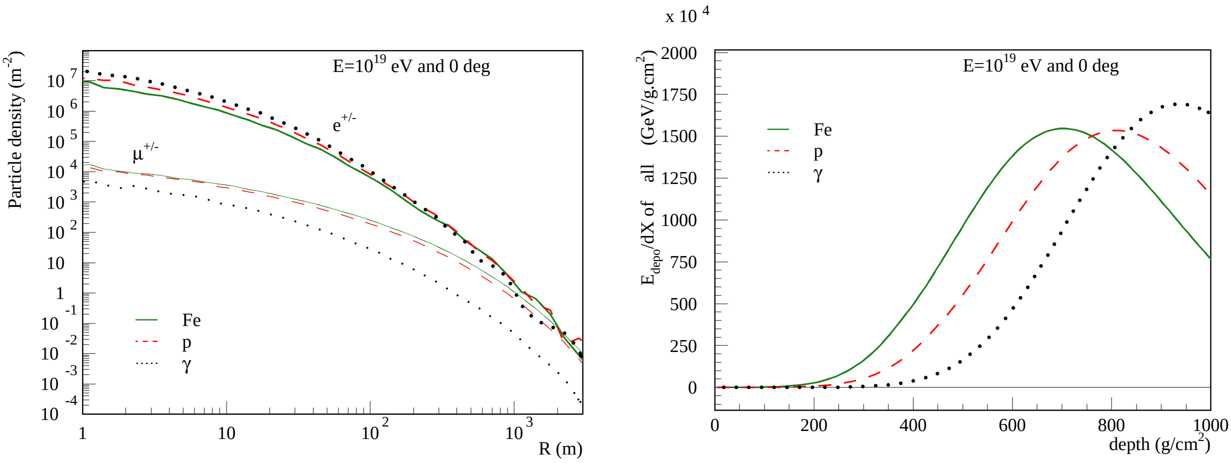

Figure 2: Left-hand side: Lateral distribution functions for electrons (and positrons) (thick lines) and muons (thin lines) at ground for a mean vertical EAS at 10^{19} eV induced by different primaries (full for iron, dashed for proton and dotted for gamma). Right-hand side: longitudinal energy deposit distribution.

In this article, we will discuss changes in the hadronic model predictions after LHC data and their consequences on air shower observables. In the first section, we will compare the results of the hadronic interaction models with LHC data. Then, using detailed Monte Carlo simulations done with CONEX [5], the new predictions for X_{max} will be presented and the astrophysical consequences will be discussed.

2 Hadronic Interaction Models and LHC data

To qualitatively describe the dependence of shower development on some basic parameters of particle interaction, decay and production, a very simple toy model can be used. Although initially developed for electromagnetic (EM) showers [6] it can also be applied to hadronic showers [7].

It is clear that such a model is only giving a very much over-simplified account of air shower physics.

However, the model allows us to qualitatively understand the dependence of many air shower observables on the characteristics of hadronic particle production. According to [7], the parameters of hadron production being most important for air shower development are the cross section (or mean free path), the multiplicity of secondary particles of high energy, and the production ratio of neutral to charged particles. Until the start of LHC, these parameters were not well constrained by particle production measurements at accelerators. As a consequence, depending on the assumptions of how to extrapolate existing accelerator data, the predictions of hadronic interaction models differ considerably.

There are several hadronic interaction models commonly used to simulate air showers. Here we will focus on the two high energy models which were updated to take into account LHC data at 7 TeV: QGSJETII-03 [10, 11] changed into QGSJETII-04 [15] and EPOS 1.99 [8, 9] replaced by EPOS LHC. There is no major change in these models but in addition to some technical improvements, some parameters were changed to reproduce TOTEM [16] cross sections. Both are based on Gribov-Regge multiple scattering, perturbative QCD and string fragmentation. The former versions reproduce accelerator data and even first LHC data reasonably well [13] but predict different extrapolations above $E_{\rm cms}$ ~1.8 TeV ($E_{\rm lab} \sim 10^{15}$ eV) that lead to very different results at high energy [4, 14] which can be improved using LHC data.

2.1 Cross section

As described in [7], the cross section is very important for the development of air showers and in particular for the depth of shower maximum. As a consequence, the number of electromagnetic particles at ground is strongly correlated to this observable (if the shower maximum is closer to ground, the number of particles is higher).

The proton-proton scattering total cross section is usually used as an input to fix basic parameters in all hadronic interaction models. Therefore it is very well described by all the models at low energy, where data exist [17]. And then it diverges above 2 TeV center-of-mass (cms) energy because of different model assumptions. As shown on Fig. 3 the new point measured by the TOTEM experiment at 7 TeV reduces the difference between the models by a factor of 5 (50 to 10 mb). In all the figures EPOS LHC is represented by a full (blue) line, QGSJETII-04 by a dotted (red) line, EPOS 1.99 by a dashed (black) line and QGSJETII-03 by a dashed-dotted (green) line.

2.2 Multiplicity

According to [7], the multiplicity plays a similar kind of role as the cross section, but with a weaker dependence (log). On the other hand, the predictions from the models had much larger differences. As shown Fig. 4 left-hand side, the particle density at mid-rapidity is well reproduced by all the models up to 2 TeV where Tevatron data [19] constrain the results, but at the highest energies in π-air, the difference can be as high as a factor of 10 (Fig. 4 right-hand side). After re-tuning until 7 TeV to be compatible with CMS data [20], the difference even at high energy in π-air is less than a factor of 2.

So for both cross section and multiplicity, when the models are constrained by LHC data up to 7 TeV, the extrapolation to the highest energy is not so different any more. This will have a strong impact on uncertainty in air shower simulations.

3 EAS Simulations

Using the air shower simulation package CONEX and the new versions of the high-energy hadronic interaction models, we can get an estimate of the resulting uncertainties.

In the following EAS simulation results using EPOS LHC and QGSJETII-04 are presented and compared to former results using QGSJETII-03 and EPOS 1.99.

As shown in Fig. 5, the mean depth of shower maximum, X_{max}, for proton and iron induced showers simulated with CONEX is still different for EPOS LHC and QGSJETII-04. But now the elongation rate (the slope of the mean X_{max} as function of the primary energy) is the same in both cases while EPOS 1.99 had an elongation rate larger than QGSJETII-03. The difference between the 2 models is a constant shift of about $20g/cm^2$ (close to the experimental systematic error in PAO) while before the difference were increasing up to $50g/cm^2$ at the highest energies

This is very important to study the primary cosmic ray composition. If the models converge to a similar elongation rate, it will allow us to have a more precise idea on possible changes in composition at the “ankle” for instance where the PAO measured a break in the elongation rate of the data.

4 Summary

Using a simple cascade model, it is possible to find the main parameters of hadronic interactions that influence air shower predictions. For the mean depth of shower maximum, $\langle X_{max} \rangle$, these parameters are the inelastic cross sections, the secondary particle multiplicity, and the inelasticity (not studied here). Using recent LHC data at 7 TeV it is possible to reduce the uncertainty in the extrapolation of the hadronic interaction models used for EAS simulations. Using pre- and post-LHC versions of the QGSJETII and EPOS models, it has been showed that the difference between these models has been reduced by a factor of 5 at the highest energy, resulting in a very similar elongation rate. There is still a systematic shift in X_{max} of about $20g/cm^2$ due to remaining differences in the multiplicity (and elasticity) of the models. This uncertainty is comparable to the experimental uncertainty in the measurement of X_{max}. As a consequence the interpretation of the data using post-LHC data will be more reliable especially concerning the possible change in mass composition with energy as summarized in [23]. On the one hand, if some change in the nature of the primary cosmic rays can be associated to some spectral feature such as the “ankle”, the astrophysical origin of the cosmic ray may be solved. On the other hand if we could fix the mass of the primary cosmic rays from some astrophysical measurement, it would give very strong constrain on the physics of the hadronic interactions.

5 Acknowledgment

We would like to thank R. Engel and D. Heck for their help and fruitful discussion and S. Ostapchenko for providing the code of QGSJETII-04.

References

[1] J. Abraham, et al. [Pierre Auger Observatory], *Nucl. Instrum. Meth.* **A523**, 50–95 (2004).

[2] R. Engel, D. Heck and T. Pierog, Ann. Rev. Nucl. Part. Sci. **61** (2011) 467.

[3] J. Knapp, D. Heck, and G. Schatz, Wissenschaftliche Berichte FZKA 5828, Forschungszentrum Karlsruhe (1996).

[4] J. Knapp, D. Heck, S. J. Sciutto, M. T. Dova, and M. Risse, *Astropart. Phys.* **19**, 77–99 (2003), [astro-ph/0206414].

[5] T. Bergmann, et al., *Astropart. Phys.* **26**, 420–432 (2007), [astro-ph/0606564].

[6] W. Heitler, *Quantum Theory of Radiation*, Oxford University Press, Oxford, 1944, 2nd edition.

[7] J. Matthews, *Astropart. Phys.* **22**, 387–397 (2005).

[8] K. Werner, F.-M. Liu, and T. Pierog, *Phys. Rev.* **C74**, 044902 (2006), [hep-ph/0506232].

[9] T. Pierog, and K. Werner, *Nucl. Phys. Proc. Suppl.* **196**, 102–105 (2009), [arXiv:0905.1198 [hep-ph]].

[10] S. Ostapchenko, *Phys. Rev.* **D74**, 014026 (2006), [hep-ph/0505259].

[11] S. Ostapchenko, *Phys. Lett.* **B636**, 40–45 (2006), [hep-ph/0602139].

[12] S. Ostapchenko, *Czech. J. Phys.* **56**, A149–A159 (2006), [hep-ph/0601230].

[13] D. d'Enterria, R. Engel, T. Pierog, S. Ostapchenko and K. Werner, Astropart. Phys. **35** (2011) 98 [arXiv:1101.5596 [astro-ph.HE]].

[14] R. Engel, and H. Rebel, *Acta Phys. Polon.* **B35**, 321–330 (2004).

[15] S. Ostapchenko, Phys. Rev. D **83** (2011) 014018 [arXiv:1010.1869 [hep-ph]].

[16] T. Csörgö *et al.* [TOTEM Collaboration], [arXiv:1204.5689 [hep-ex]].

[17] H. Jung, et al. (2009), [arXiv:0903.3861 [hep-ph]].

[18] C. Caso, et al., *Eur. Phys. J.* **C3**, 1 (1998).

[19] F. Abe, et al., *Phys. Rev.* **D41**, 2330 (1990).

[20] V. Khachatryan, et al. [CMS Collaboration], *Phys. Rev. Lett.* **105**, 022002 (2010), [arXiv:1005.3299 [hep-ex]].

[21] J. Blümer, R. Engel, and J. R. Hörandel, *Prog. Part. Nucl. Phys.* **63**, 293–338 (2009), [arXiv:0904.0725 [astro-ph.HE]].

[22] J. Abraham, et al. [Pierre Auger Observatory], *Phys. Rev. Lett.* **104**, 091101 (2010), [arXiv:1002.0699 [astro-ph.HE]].

[23] K.-H. Kampert and M. Unger, Astropart. Phys. **35** (2012) 660 [arXiv:1201.0018 [astro-ph.HE]].

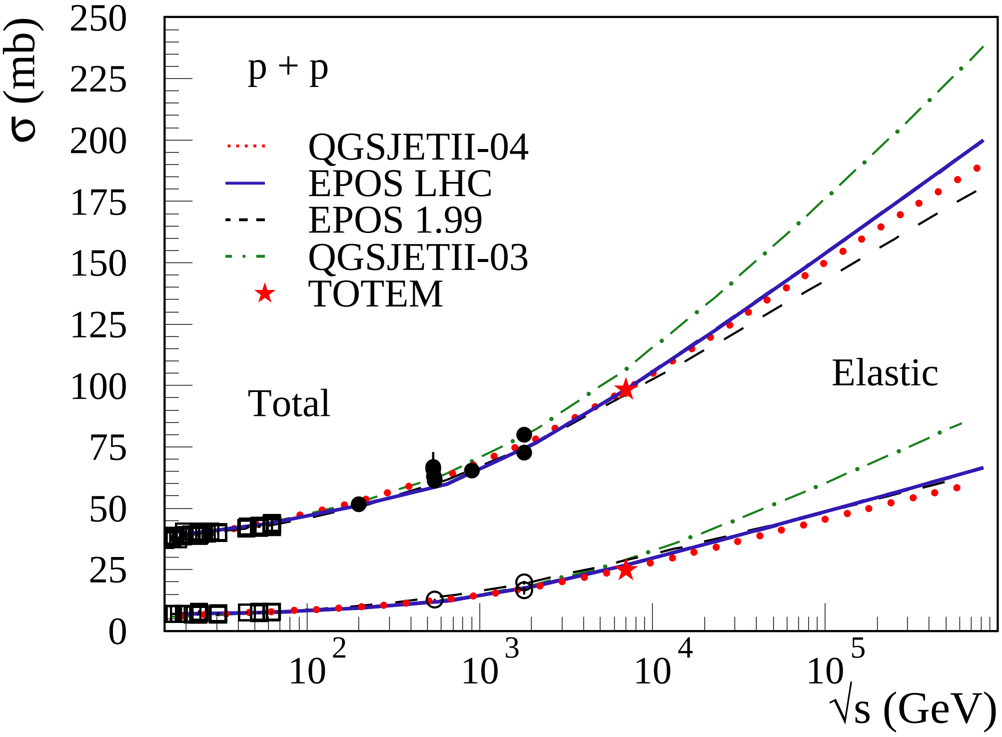

Figure 3: Total and elastic p-p cross section as calculated with EPOS LHC (full line), QGSJETII-04 (dotted line), EPOS 1.99 (dashed line) and QGSJETII-03 (dashed-dotted line). Points are data from [18] and the star is the LHC measurement by the TOTEM experiment [16].

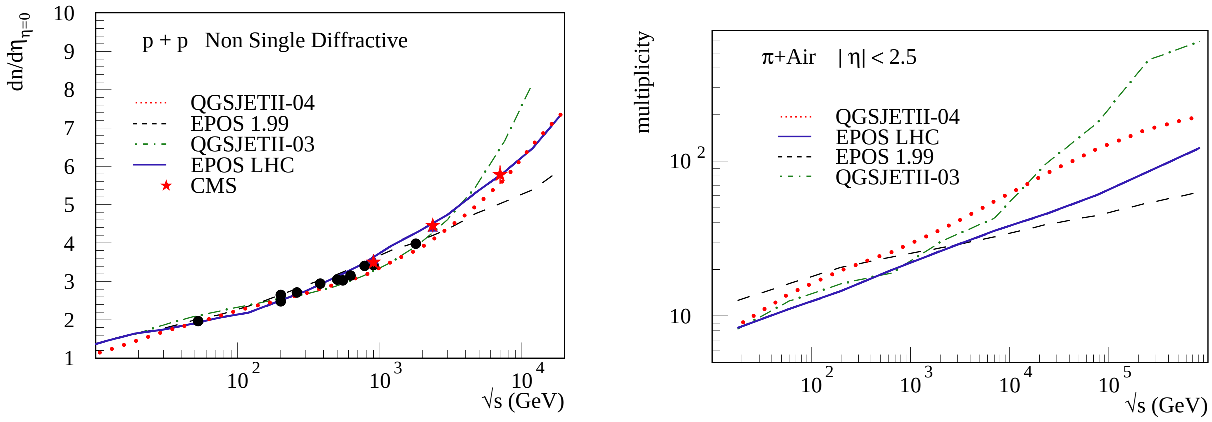

Figure 4: Particle density at $\eta = 0$ for non single diffractive events (NSD) (left-hand side) and multiplicity for $|\eta| < 2.5$ of π-air collisions (right-hand side) as a function of center of mass energy. Simulations with EPOS 1.99 (full line), QGSJETII-04 (dotted line), EPOS 1.99 (dashed line) and QGSJETII-03 (dashed-dotted line). Points are data and red stars are from CMS experiment [20].

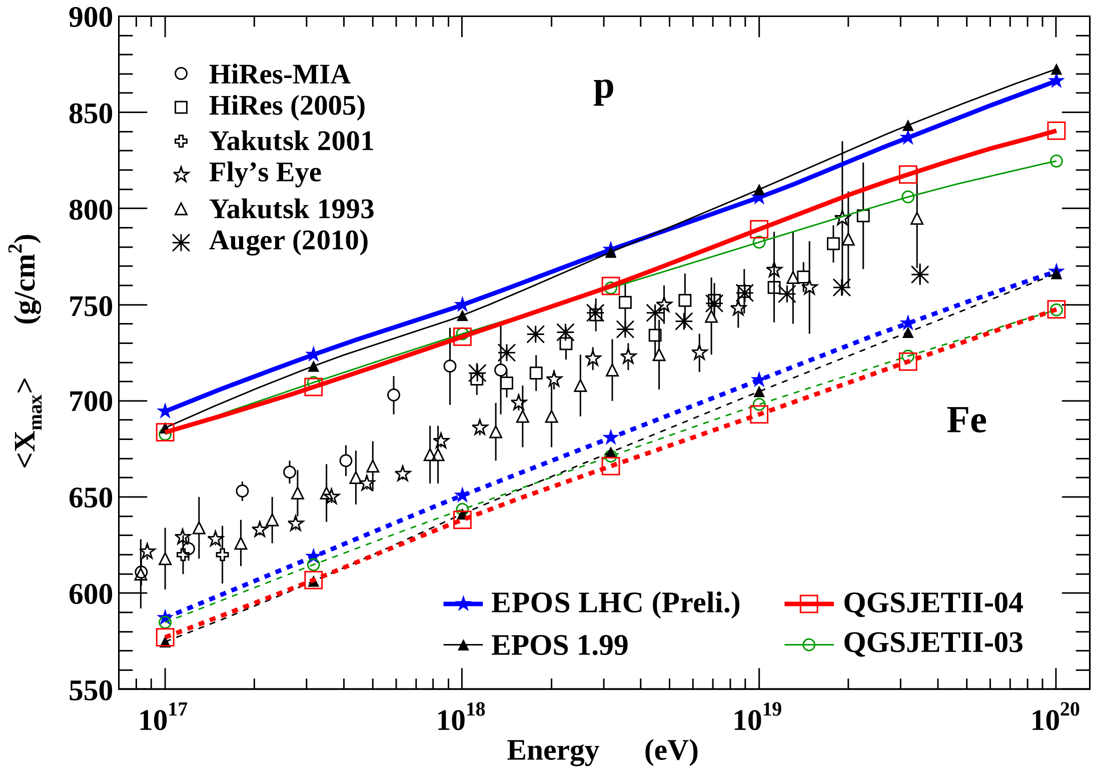

Figure 5: Mean X_{max} for proton and iron induced showers as a function of the primary energy. Predictions of different high-energy hadronic interaction models, full lines for proton and dashed lines for iron with full triangles for EPOS 1.99, open squares for QGSJETII-04, open circles for QGSJETII-04, and full stars for EPOS LHC, are compared to data. Refs. to the data can be found in [21] and [22].

ANTARES and the status of high-energy neutrino astronomy

Véronique Van Elewyck, for the ANTARES Collaboration
APC, Univ. Paris Diderot, CNRS/IN2P3, CEA/Irfu, Obs. de Paris, France
Email : elewyck@apc.univ-paris7.fr

Abstract

Neutrinos have long been proposed as an alternative to cosmic rays and photons to explore the high-energy sky, as they can emerge from dense media and travel across cosmological distances without being deflected nor absorbed. Besides tracing the existence of hadronic processes inside astrophysical sources, they could also reveal new types of sources, yet unobserved with photons or cosmic rays. This contribution presents the current status and results of the ANTARES neutrino telescope, recently deployed in the Mediterranean Sea, in the general context of high-energy neutrino astronomy[1].

1 The ANTARES neutrino telescope

The ANTARES detector [2] is the first undersea neutrino telescope; its deployment at a depth of 2475m in the Mediterranean Sea near Toulon was completed in May 2008. It consists in a 3D array of 884 optical modules distributed on 12 lines anchored to the sea bed and connected to the shore through an electro-optical cable. Two other neutrino telescopes are currently operating worldwide; the most advanced one, IceCube [3], is located at the South Pole. It has recently achieved its final configuration with 86 strings, instrumenting one km^3 of ice at a depth between 1450m and 2450m. Another detector has been operating for some years in Lake Baikal [4] in a smaller configuration.

ANTARES detects the Cherenkov radiation emitted by charged leptons (mainly muons, but also electrons and taus *via* the associated showers) induced by cosmic neutrino interactions with matter inside or near the instrumented volume. The knowledge of the timing and amplitude of the light pulses recorded by the optical modules allows to reconstruct the trajectory of the muon and to infer the arrival direction of the incident neutrino. The design of ANTARES is optimized for the detection of up-going muons produced by neutrinos which have traversed the Earth, in order to limit the background from down-going atmospheric muons. Its field of view is $\sim 2\pi\,\mathrm{sr}$ for neutrino energies 100 GeV $\lesssim E_\nu \lesssim$ 100 TeV. Its location in the Northern hemisphere makes it especially suited for the observation of Galactic sources.

2 Searches for high-energy cosmic sources

High-energy neutrinos are expected to be emitted as a byproduct of the interactions of accelerated protons (and possibly heavier nuclei) with ambient matter and radiation in (extra-)galactic astrophysical sources. As a result of neutrino oscillations, the expected ratio of neutrino flavours at Earth is ν_e:ν_μ:ν_τ = 1:1:1.

Cosmic sources of neutrinos can be searched for in different ways:
- **Diffuse flux searches** look for an all-sky excess of high-energy events above the irreducible background of atmospheric neutrinos. Such methods are especially suited to reveal the bulk of extragalactic sources (such

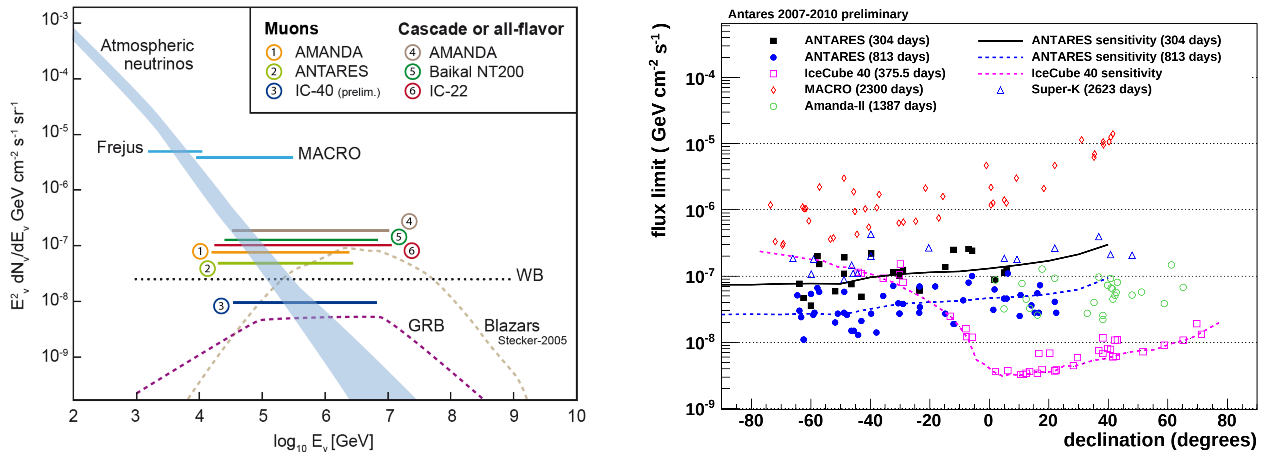

Figure 1: **Left:** 90% C.L. integral upper limits on the diffuse flux of extraterrestrial neutrinos (normalized to one flavour), as taken from Katz & Spiering [1] where all references can be found. The coloured band indicates the measured flux of atmospheric neutrinos. **Right:** 90% C.L. upper limits for a neutrino flux with an E^{-2} spectrum for candidates sources (points) and the corresponding sensitivities (lines) in function of declination. The figure also shows the results of the MACRO and Super-Kamiokande experiments, which were not principally devoted to neutrino astronomy. Taken from [5] (see references therein).

as active galactic nuclei or gamma-ray bursts) which are too faint to be detected individually. They rely on energy estimators which are typically related to the total number and multiplicity of photon hits in the PMTs. No significant excess over atmospheric neutrinos has been observed so far. An overview of the limits set in the TeV-PeV range by ANTARES, IceCube and their predecessors, using both muon tracks (induced by ν_μ only) and contained showers (induced by all flavors of neutrinos) are presented in Fig.1 (left panel).
- **Point source searches** aim at detecting significant excesses of events from one particular spots (or regions) of the sky. They can be performed either blindly over the full sky, or in the direction of a-priori selected candidate source locations that correspond e.g. to known gamma-ray emitters. Such searches are well-suited to look for steady, point-like sources, in particular in the Galaxy. They rely on a good angular resolution, which above 10 TeV is essentially determined by the scattering length of light in the medium, yielding a median error angle on the neutrino direction of about 0.5° for IceCube and 0.4° for ANTARES (note that one can expect 0.1° resolution for a km^3 deep-sea detector). The latest results of point sources searches by ANTARES and IceCube (in its 40-string configuration) are presented in Fig.1 (right panel), showing the nice complementarity in their field of view and the large improvement in sensitivity gained over the past 15 years by the development of dedicated instruments for neutrino astronomy.
- Multimessenger searches develop specific strategies to look for neutrinos with timing and/or directional correlations with potential sources of gamma-rays (in connection with the GCN alerts), ultra-high energy cosmic rays (such as CenA) and gravitational waves. The limited space-time search window allows a drastic reduction of the atmospheric background, therefore enhancing the sensitivity to faint signals that would have remained undetected otherwise. The capabilities of the ANTARES data acquisition system make it well suited for the search for transient astrophysical sources such as AGN flares and GRBs. Similar searches are performed by the IceCube detector; in the case of GRBs, upper limits have begun to constrain models in which UHECRs are predominantly protons in the framework of the standard fireball paradigm. Conversely, the occurrence of a special event in a neutrino telescope (such as the near-simultaneous arrival of two or more neutrinos from the same direction) could indicate that a highly energetic burst has occurred and may

be used as a trigger for optical, x-ray, and gamma-ray follow-ups. Both IceCube and ANTARES currently have alert programs established or in development with e.g. fast optical telescope networks like ROTSE and TAROT, and gamma-ray telescopes such as Swift, Fermi, MAGIC, and VERITAS.

3 Summary

Neutrino astronomy has entered an exciting time with the successful operation of the first undersea neutrino telescope (ANTARES) and the completion of the first km^3-scale neutrino telescope at the South Pole (IceCube), approaching the sensitivity levels required to test at least part of the flux predictions from astrophysical sources. For an in-depth overview of the results discussed hereabove, we refer the reader to [5] for ANTARES and [6] for IceCube, where all references to published papers can be found.

References

[1] for recent reviews on the subject, see e.g. J. K. Becker, Phys. Rept. **458** (2008), 173-246; B. Baret and V. Van Elewyck, Rept. Prog. Phys. **74** (2011) 046902 ; U. F. Katz and C. Spiering, arXiv:1111.0507 .

[2] M. Ageron *et al.* [ANTARES Coll.] , NIM **A 656** (2011) 11-38.

[3] F. Halzen and S. R. Klein, Rev. Sci. Instrum. **81** (2010) 081101.

[4] A. Avrorin *et al.* [Baikal Coll.], NIM A **626-627** (2011) S13.

[5] S. Adrian-Martinez *et al.* [ANTARES Coll.], arXiv:1112.0478.

[6] R. Abbasi *et al.* [IceCube Coll.], arXiv:1111.2736 and arXiv:1111.2741.

Searching for gravitational wave signals from rotating neutron stars

Andrzej Królak
for the LIGO Scientific Collaboration and the Virgo Collaboration
Institute of Mathematics, Polish Academy of Sciences,
Śniadeckich 8, 00-956 Warsaw, Poland

Abstract

We review mechanisms of gravitational wave radiation from rotating neutron stars. We describe data analysis methods to search for gravitational wave signals from rotating neutron stars in the data of ground-based detectors. We present status of the searches for these signals in the data of the LIGO and Virgo kilometer-scale laser interferometric detectors.

1 Mechanisms of gravitational wave radiation from rotating neutron stars

The basic gravitational-wave emission from a rotating neutron star is expected to be due to non-axisymmetric distortions of the star with the dimensionless amplitude h_o of the signal observable at the Earth given by

$$h_o = 4 \times 10^{-25} \left(\frac{\epsilon}{10^{-6}}\right) \left(\frac{I}{10^{38}\ \mathrm{kg\ m}^2}\right) \left(\frac{100\ \mathrm{pc}}{d}\right) \left(\frac{\nu}{100\ \mathrm{Hz}}\right)^2, \tag{1}$$

where ϵ is a relative measure of non-axisymmetry of the star, I is the moment of inertia with respect to the rotation axis, d is the distance to the star, and ν is the spin frequency [1]. The non-axisymmetry can arise due to deformations of the crust of the neutron star that could be acquired during birth in a supernova, strong magnetic fields present in neutron stars [2], or differential heating from accreted matter leading to differential density gradients [3]. Other possible emission mechanisms are the instability of the r-modes of the star driven by gravitational radiation [4] and a free precession due to misaligned rotation and symmetry axes [5].

As the estimates of the amplitude h_o of the signal are very uncertain, it is important to have an upper limit on h_o. One such limit can be obtained by assuming that all energy emitted by a rotating neutron star is radiated in gravitational waves. This can be estimated for known pulsars, where the first derivative $\dot{\nu}$ of the spin frequency is measured. The spin down limit amplitude h_{sd} is then given by

$$h_{sd} = 8 \times 10^{-24} \sqrt{\left(\frac{I}{10^{38}\ \mathrm{kg\ m}^2}\right) \left(\frac{100\ \mathrm{Hz}}{\nu}\right) \left(\frac{|\dot{\nu}|}{10^{-10}\ \mathrm{Hz/s}}\right)} \left(\frac{100\ \mathrm{pc}}{d}\right) . \tag{2}$$

Sometimes the spin frequency of the star is unknown, but its characteristic age τ can be estimated. Using the age estimate $\tau = \nu/(4|\dot{\nu}|)$, which also assumes that the star is losing all its energy through gravitational radiation, we have an *indirect spin down limit* amplitude h_{isd} called *age-based limit*:

$$h_{isd} = 2 \times 10^{-23} \sqrt{\left(\frac{I}{10^{38}\ \mathrm{kg\ m}^2}\right) \left(\frac{1000\ \mathrm{yr}}{\tau}\right)} \left(\frac{100\ \mathrm{pc}}{d}\right) . \tag{3}$$

An interesting indirect upper limit on the amplitude of the GW signal called torque balance limit can be obtained using the observation that the spin frequencies of the neutron stars in low mass X-ray binary systems seem to cluster in a narrow range around 300 Hz which is lower than the theoretical maximum spin frequency of around 1400 Hz. Thus, one may suppose that an equilibrium develops between the angular momentum gained by accretion with that lost through gravitational radiation. This gives an amplitude h_{isdX}

$$h_{isdX} = 5 \times 10^{-27} \sqrt{\left(\frac{300\ \mathrm{Hz}}{\nu}\right)\left(\frac{F_X}{10^{-8}\mathrm{erg\ cm}^{-2}\mathrm{s}^{-1}}\right)}\,, \tag{4}$$

where F_X is the observed X-ray energy flux on Earth.

2 Data analysis methods

The estimates of the previous section show that the gravitational wave signal from a rotating neutron star is expected to be very weak and therefore very long data stretches need to be analyzed. The data analysis method that gives the highest detection probability is the *coherent matched-filtering* method. Using the *maximum likelihood estimation method*, one can reduce the dimensionality of the parameter space of the coherent search by using the so called $\mathcal{F}$-statistic [6]. Application of the $\mathcal{F}$-statistic to very long data stretches is computationally prohibitive; therefore less computationally demanding semi-coherent methods were developed. These are *StackSlide*, *Hough*, and *PowerFlux* methods (see [9] for a more detailed description). To search for GW signals from known pulsars, a very efficient method was developed using a Bayesian method [8]. With this method one obtains distributions of the unknown parameters conditional on the data by marginalizing over the unknown parameters like phase and polarization angles and variance of the noise using their reasonable *a priori* distributions.

3 Recent results of searches in the LIGO and Virgo data

Searches for continuous GW signals can be divided into three classes: *targeted searches* - searches for gravitational waves from known pulsars, where frequency, sky position and sometimes polarization are known, *directed searches* - position in the sky is known, and *wide-parameter* searches - unknown sky position, frequency, distance, and polarization. All these types of searches were performed in LIGO and Virgo data. Here we summarize some of the recent results.

3.1 Targeted searches

Targeted search using LIGO S5 data. The search involved 116 known millisecond and young pulsars and used Bayesian analysis [10]. The pulsars included the Crab pulsar for which a sensitivity was reached below the spin down limit (see eq. (2)) and the limit placed on the power radiated by gravitational waves was less than 2% of the available spin down power. Also the spin down limit was reached for the X-ray pulsar J0537-6910 under the assumption that any gravitational wave signal from it stayed phase locked to the X-ray pulses over timing glitches.

Targeted search using VIRGO VSR2 data for the Vela pulsar. This analysis [11] involved three independent methods: the Bayesian method used in LIGO S5 search [8] and two matched-filtering methods. The first matched-filtering method used the $\mathcal{F}$ and $\mathcal{G}$ [7] statistics and the second matched-filtering method involved matched-filtering on the signal Fourier components [12]. All three methods produced consistent results. The spin down limit was beaten, and the observational upper limit of the power radiated by gravitational waves is less than about 40% of the available spin down power. This was possible because of the better sensitivity of the Virgo detector at low frequencies.

3.2 Directed searches

A search was performed for continuous gravitational radiation from the neutron star in the supernova remnant Cassiopeia A [13]. The search coherently analyzed 12 days of S5 data using the $\mathcal{F}$-statistic. A band of frequencies from 100 to 300 Hz was searched and a wide range of first and second frequency derivatives appropriate for the age of the remnant and for different spin-down mechanisms. Confidence limits (95%) of $0.7 - 1.2 \times 10^{-24}$ on amplitude h_o were imposed (see Fig. 3 of [13]). Also, limits were imposed on the amplitude of the r-modes of the neutron stars.

3.3 Wide-parameter searches

Einstein@Home search. The Einstein@Home [14] project carries out wide-parameter searches for periodic gravitational signals using the $\mathcal{F}$-statistic to perform a coherent analysis of around a day of data followed by a post-processing procedure to find significant candidate signals. The most recently completed analysis [15] involved a search of 840 hours of data from 66 days of the S5 LIGO run. The data were divided into 30 h long stretches that were analyzed coherently. The full sky was searched with a bandwidth from 50Hz to 1500Hz and the frequency derivative $\dot{f}$ range was $-f/\tau < \dot{f} < 0.1f/\tau$, for a minimum spin-down age τ of 1000 years below 400Hz and 8000 years above 400 Hz. The post-processing procedure involved coincidences among candidates found in 28 segments analyzed. The search did not reveal statistically significant signals. The estimated sensitivity (Figure 4 of [15]) shows that in the 125 Hz to 225 Hz band, more than 90% of sources with dimensionless gravitational wave strain tensor amplitude greater than 3×10^{-24} would have been detected.
Power Flux search. A search of the whole S5 data set using the PowerFlux method has recently been completed [16]. An all sky search was performed with this method in the frequency band from 50Hz to 800Hz and with the frequency time derivative in the range from -6×10^{-9} Hz/s to 0. The 95% confidence upper limits (see Figure 1 of [16]) on h_o for the most favorable circular polarization ranged from 4×10^{-25} to 2×10^{-23}.

The upper limits obtained with searches for periodic gravitational waves begin to be astrophysically interesting by imposing non-trivial constraints on the structure and evolution of the neutron stars.

Acknowledgments

The authors gratefully acknowledge the support of the United States National Science Foundation for the construction and operation of the LIGO Laboratory, the Science and Technology Facilities Council of the United Kingdom, the Max-Planck-Society, and the State of Niedersachsen/Germany for support of the construction and operation of the GEO600 detector, and the Italian Istituto Nazionale di Fisica Nucleare and the French Centre National de la Recherche Scientifique for the construction and operation of the Virgo detector. The authors also gratefully acknowledge the support of the research by these agencies and by the Australian Research Council, the International Science Linkages program of the Commonwealth of Australia, the Council of Scientific and Industrial Research of India, the Istituto Nazionale di Fisica Nucleare of Italy, the Spanish Ministerio de Educación y Ciencia, the Conselleria d'Economia Hisenda i Innovació of the Govern de les Illes Balears, the Foundation for Fundamental Research on Matter supported by the Netherlands Organisation for Scientific Research, the Polish Ministry of Science and Higher Education, the FOCUS Programme of Foundation for Polish Science, the Royal Society, the Scottish Funding Council, the Scottish Universities Physics Alliance, The National Aeronautics and Space Administration, the Carnegie Trust, the Leverhulme Trust, the David and Lucile Packard Foundation, the Research Corporation, and the Alfred P. Sloan Foundation.

AK acknowledges support of the MNiSzW grant no. N N203 387237.

References

[1] J.L. Zdunik, M. Bejger, and P. Haensel 2008 *Astronomy and Astrophysics* **491** 489

[2] A. Melatos and D.J.B. Payne 2005 *Astrophys. J* **623** 1044

[3] L. Bildsten 1998 *Astrophys. J* **501** L89

[4] B. Owen et al 1998 *Phys. Rev.* D **58** 084020

[5] D. I. Jones 2012 *MNRAS* **420** 2325

[6] P. Jaranowski, A. Królak and B.F. Schutz 1998 *Phys. Rev.* D **58** 063001

[7] P. Jaranowski and A. Królak 2010 *Class. Quant. Grav.* **27** 194015

[8] R. Depuis R and G. Woan 2005 *Phys. Rev.* D **72** 102002

[9] B.P. Abbott et al 2008 *Phys. Rev.* D **77** 022001

[10] B.P. Abbott et al 2010 *Astrophys. J* **713** 671

[11] J. Abadie et al 2011 *Astrophys. J* **737** 93

[12] P. Astone et al 2010 *Class. Quant. Grav.* **27** 194016

[13] J. Abadie et al 2010 *Astrophys. J* **722** 1504

[14] http://einstein.phys.uwm.edu

[15] B.P. Abbott et al 2009 *Phys. Rev.* D **80** 044003

[16] B.P. Abbott et al 2012 *Phys. Rev.* D **85** 022001

Status of the TREND project

Olivier Martineau-Huynh for the TREND collaboration
Laboratoire de Physique Nucléaire et des Hautes Energies,
CNRS/IN2P3 and Université Pierre et Marie Curie, Paris, France,
Institute of High Energy Physics, Chinese Academy of Sciences, Beijing, China, and
National Astronomical Observatories of China,
Chinese Academy of Sciences, Beijing, China
Email : omartino@in2p3.fr

Abstract

The Tianshan Radio Experiment for Neutrino Detection (TREND) is a sino-french collaboration (CNRS/IN2P3 and Chinese Academy of Science) developing an autonomous antenna array for the detection of high energy Extensive Air Showers (EAS) on the site of the 21CMA radio observatory. The array is composed of 50 antennas covering a total area of $\approx$1.2 km^2. The autonomous detection and identification of EAS was achieved by TREND on a prototype array in 2009. This result was confirmed soon after when EAS radio-candidates could be tagged as cosmic ray events by an array of particle detectors running in parallel at the same location. This result is an important milestone for TREND, and more generally, for the maturation of the EAS radio-detection technique. In a long term perspective, TREND is intended to search for high energy tau neutrinos. Here we only report on the results achieved so far by TREND.

1 Introduction

Charged particles created during the development of an extensive air shower (EAS) generate a coherent emission detectable at radio frequencies ($<$ 200 MHz). The radio-detection technique shows interesting potentialities for the detection of cosmic rays with energies above 10^{17} eV (low cost, easiness of deployment and stability of the response of the antennas,...) and pioneering experiments [1],[2] obtained very encouraging results on the radio-detection of EAS. Still, the radio technique is not yet mature: more data is necessary to better understand the mechanism of shower generation, and self-triggering of the radio array is a necessary technical improvement. Among several other projects [3], TREND aims at tackling these two issues. We briefly report on this effort here.

2 The TREND setup

The TREND setup was developed on the site of the 21cm Array radio telescope [4], in the Tianshan mountain range (Xinjiang autonomous province, China). It benefits from the infrastructure of the 21CMA and its exceptional radio environment. A 6-antennas array could be promptly deployed in 2009 by adapting elements of the 21CMA setup. This prototype was used to test the principle of EAS autonomous radio-detection. The array was then extended to 15 antennas, while a setup of 3 particle detectors was also installed at the same location. An offline analysis of 29 live days of hybrid data showed that 13 EAS candidates selected from the radio data were coincident with cosmic ray events identified with the particle detectors setup. This validates

our principle of radio-identification of EAS. These results are detailed in [5].
The TREND array was then extended to 50 antennas, for a total area of ≈1.2 km^2. The system has been running in stable condition since March 2011. The good performance of the array could be checked through the reconstruction of plane trajectories in the sky (see figure 1), with an angular resolution of ≈ 1^o and an amplitude resolution of 15%.

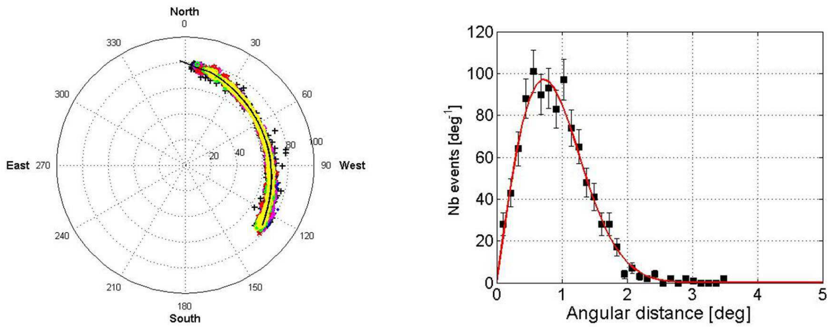

Figure 1: *Left: skyplot of a plane trajectory reconstructed by TREND. Right: histogram of the angular distance between the estimated and reconstructed plane positions for the events shown in the left panel.*

3 EAS radio-identification with TREND

EAS radio candidates are supposed to exhibit features distinct from background electromagnetic events. Prompt (<300 ns) electromagnetic transients are expected, as well as plane wavefronts. Well-focused patterns on ground, with a rapid drop in amplitude when moving away from the shower axis, is another characteristics of EAS radio signals. The search for such signatures is implemented in the algorithm we developed for the selection of EAS radio-candidates. This algorithm is presently being refined to be applied to the full 50-antennas array data, but EAS radio-candidates could already be identified (figure 2).

4 Conclusion

The TREND project has been able to identify EAS candidates through their radio signatures only. We are confident that the 50-antennas array will allow to collect large statistics of EAS radio-events. This should prove helpful to better understand and control this promising technique.

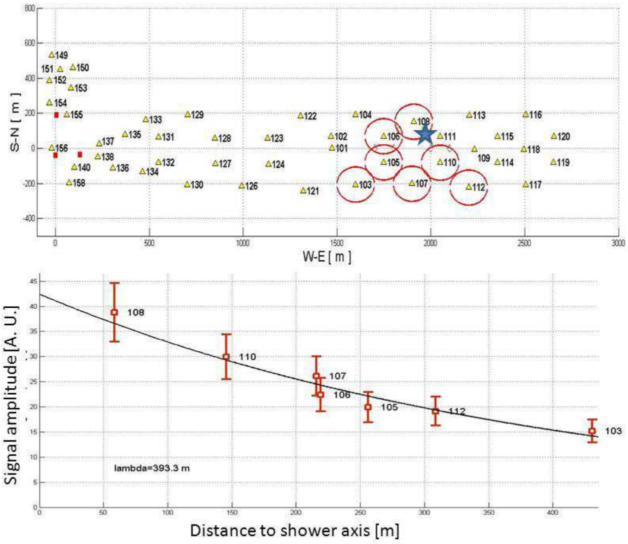

Figure 2: Top: TREND 50-antennas array. Triangles are antennas, squares are particle detectors. Also shown with circles is the pattern at ground of an EAS radio-candidate. The incoming wave is reconstructed as a plane with $\theta = 50.5^o$ and $\phi = 4.2^o$. The reconstructed core position is shown as a blue star. Bottom: antennas signal amplitudes as a function of the distance to the reconstructed shower axis, and exponential fit ($\lambda = 393$ m).

References

[1] D. Ardouin et al., Nucl. Instrum. Meth. A 555, 148 (2005).

[2] H. Falcke et al., Nature 435, 313 (2005) [astro-ph/0505383].

[3] B. Revenu for the Pierre Auger Collaboration, 4th International Workshop on Acoustic and Radio Neutrino Activities, Nantes, 2010.

[4] The 21 cm Array, http://21cma.bao.ac.cn.

[5] D. Ardouin et al., Astropart. Phys. 34, 717 (2011) [astro-ph/1007.4359].

The Telescope Array

J.N. Matthews for the Telescope Array Collaboration
University of Utah, Department of Physics and Astronomy,
High Energy Astrophysics Institute, Salt Lake City, UT 84112 USA
Email : jnm@physics.uitah.edu

Abstract

The Telescope Array (TA) Project is the largest ultra high energy cosmic ray experiment in the northern hemisphere. The observatory has been collecting data since 2008 using a hybrid of fluorescence telescopes and scintillator surface detectors. The first results from the experiment including the monocular spectrum from the Middle Drum fluorescence site and the spectrum from the scintillator array are in excellent agreement with the spectrum from the High Resolution Fly's Eye. In addition, a first pass at a composition measurement has been made and indicates a predominantly light composition in the 10^{19}eV region. Finally, some of the ongoing work of the group is presented including a novel technique for an end to end calibration of the telescopes involving a 40 MeV linear accelerator.

The Telescope Array Collaboration was forged by members of the High Resolution Fly's Eye (HiRes) and the Akeno Giant Air Shower Array (AGASA) to study Ultra High Energy Cosmic Rays. The purpose of Telescope Array is to a) understand the differences between the results of HiRes and AGASA, b) to study the spectrum, composition, and anisotropy of ultra high energy cosmic rays, and c) to study the galactic to extra-galactic transition of cosmic rays. Over time, the collaboration has grown to include groups from the US, Japan, South Korea, Russia, and Belgium.

The Telescope Array Observatory is located about 2.5 hours south of Salt Lake City, Utah in the USA, just west of the town of Delta. The high energy component (Phase-I) of the Telescope Array consists of 38 fluorescence telescopes (9728 PMTs) located in three batteries at the corners of a triangle which is approximately 30 km on each leg. The telescopes overlook an array of 507 scintillator surface detectors in the space between. The Telescope Array is complete and has been operational since about 1/2008. More details can be found in [1] and [2].

It is natural to begin by comparing the the spectrum from the northern fluorescence telescope site with that of the High Resolution Fly's Eye (HiRes) experiment since the equipment is the same. They have simply been refurbished. Using the same average atmosphere (VAOD = 0.04), same cuts and (almost) the same analysis programs. A few changes do need to be made. The telescopes are now pointing in different directions. In particular, they observe over a broader range of elevation angles, making longer tracks in the cameras. Another difference is that the night sky in Delta is darker than that in Dugway, resulting in thresholds which are about 20% lower. The first three years of Telescope Array data from the northern site shows excellent agreement with the spectrum measured by HiRes. Likewise the spectrum measured by the TA scintillator surface array is in excellent agreement. [1] The spectrum presented by the Auger collaboration at the ICRC2011 in Beijing is 20% lower in normalization. However, if one increases the energy of the Auger spectrum by 20%, the agreement with the TA and HiRes measurements is good. [3]

Most TA events are observed by multiple detector systems. We have examined some of the stereo data from the two southern fluorescence sites. The analysis must take into account the acceptance bias and reconstruction bias when comparing the data to the Monte Carlo. Many reconstructed parameters (such as track length. zenith angle, azimuthal angle, and impact parameter) of the data are all well modeled by

QGSjet-II protons or QGSjet-II iron. However, when the Xmax distribution of the data (for a series of energy slices) is compared to that of protons or iron for various models including QGSjet-I, QGSjet-II, and SIBYLL there is a sharp difference. In all cases, the data looks much more like protons than iron. [4]

The best fit is to QGSjet-I protons. Looking at the evolution of the mean depth of shower maximum with energy, the data is a good match to QGSjet-II or QGSjet-I protons. It is farther from SIBYLL protons. We do a KS test to quantify these statements. The data is completely compatible with QGSjet-I, QGSjet-II or SIBYLL protons at all energies between $10^{18.3}$ eV and $10^{19.9}$ eV. However, the data is incompatible with the iron simulation of any of these models between $10^{18.3}$ eV and $10^{19.3}$ eV. For energies greater than $10^{19.3}$ eV, the amount of data is not sufficient for TA to distinguish and it is compatible with both protons and iron simulations. [4]

We have also looked for anisotropy in a variety of ways. We have looked for auto-correlation, correlation with large scale structure and correlation with AGNs using the Auger claim from their 2010 Astroparticle Physics paper. No sign of anisotropy was found.

Other activities are underway at the Telescope Array. One of these is the installation of a small linear accelerator. The 40 MeV accelerator excites the nitrogen in the atmosphere just like an air shower. Thus, the accelerator provides an end-to-end calibration of the telescopes and of the technique. The accelerator fired its first pulses of electrons into the Utah sky in September 2010. [6] In addition, the group is trying to observe cosmic rays via radar reflection from the extensive air shower plasma using a 54 MHz television transmitter. [7]

In conclusion, the Telescope Array has picked up where HiRes left off. It is the largest ultra high energy cosmic ray observatory in the northern hemisphere and is actively collecting data. The preliminary results are in excellent agreement with those of HiRes. Data collection and analysis will continue for the next several years.

1 Acknowledgments

The Telescope Array experiment is supported by the Ministry of Education, Culture, Sports, Science and Technology-Japan through Kakenhi grants on priority area (431) "Highest Energy Cosmic Rays", basic research awards 18204020(A), 18403004(B) and 20340057(B); by the U.S. National Science Foundation awards PHY-0307098, PHY-0601915, PHY-0703893, PHY-0758342, and PHY-0848320 (Utah) and PHY-0649681 (Rutgers); by the Korea Research Foundation (KRF-2007-341-C00020); by the Korean Science and Engineering Foundation (KOSEF, R01-2007-000-21088-0); A Korean WCU grant (R32-2008-000-10130-0) from MEST and the National Research Foundation of Korea(NRF), by the Russian Academy of Sciences, RFBR grants 07-02-00820a and 09-07-00388a (INR), the FNRS contract 1.5.335.08, IISN and Belgian Science Policy under IUAP VI/11 (ULB). The foundations of Dr. Ezekiel R. and Edna Wattis Dumke, Willard L. Eccles and the George S. and Dolores Dore Eccles all helped with generous donations. The State of Utah supported the project through its Economic Development Board, and the University of Utah through the Office of the Vice President for Research. The experimental site became available through the cooperation of the Utah School and Institutional Trust Lands Administration (SITLA), U.S. Bureau of Land Management and the U.S. Air Force. We also wish to thank the people and the officials of Millard County, Utah, for their steadfast and warm support. We gratefully acknowledge the contributions from the technical staffs of our home institutions.

References

[1] J.N. Matthews *et al.*, Proceedings ICRC2011, Beijing, China, H.E.1.3, Vol 2, #1306, (2011) p273.
[2] H. Tokuno *et al.*, NIM-A v676 (2012) p54-65. arXiv:1201.0002v1
[3] D. Ivanov *et al.*, Proceedings ICRC2011, Beijing, China, H.E.1.3, Vol 2, #1297, (2011) p258.
[4] Y. Tameda *et al.*, Proceedings ICRC2011, Beijing, China, H.E.1.3, Vol 2, #1268, (2011) p246.
[5] P. Tinyakov *et al.*, Proceedings ICRC2011, Beijing, China, H.E.1.3, Vol 2, #1317, (2011) p293.
[6] T. Shibata *et al.*, Proceedings ICRC2011, Beijing, China, H.E.1.4, Vol 3, #1252, (2011) p305.
[7] J. Belz *et al.*, Proceedings ICRC2011, Beijing, China, H.E.1.4, Vol 3, #1314, (2011) p336.

Very high energy cosmic ray production in Historical Supernova Remnants

V.G. Sinitsyna and V.Yu. Sinitsyna
P.N.Lebedev Physical Institute, Russian Academy of Science
Email : sinits@sci.lebedev.ru

Abstract
We present the results of observations of two types of Galactic supernova remnants with the SHALON mirror Cherenkov telescope of Tien-Shan high-mountain Observatory: the plerion Crab Nebula and the shell-type supernova remnants Cas A and Tycho. The experimental data have confirmed the prediction of the theory about the hadronic generation mechanism of very high energy (800 GeV - 100 TeV) γ-rays in Tycho's supernova remnant. The data obtained suggest that the very high energy γ-ray emission in the objects being discussed is different in origin.

Introduction

The hypothesis that supernova remnants (SNRs) are unique candidates for cosmic-ray sources [1, 2] has been prevalent from the very outset of cosmic-ray physics. Recent observations of several SNRs in X-rays and TeV γ-rays will help in solving the problem of the origin of cosmic rays and are key to understanding the mechanism of particle acceleration at a propagating shock wave.

Crab Nebula (SN 1054)

The Crab Nebula, most famous SNR, plays an important role in the modern astrophysics. Since the first detection with ground based telescope the Crab has been observed by the number of independent groups using different methods of registration of γ-initiated showers [3 - 6]. Perhaps the most important fact is that this source with a stable flux can be used to calibrate Cherenkov telescopes in both Northern and Southern Hemispheres. However, quite recently, the AGILE [7] and Fermi LAT [8] satellite experiments have reported on a flare exceeding the nominal flux from the Crab in the energy range from 100 MeV to 2 - 5 GeV by a factor of 4, which was assumed to be absolutely stable and, consequently, was used as a "standard candle". No flux increase was detected in the observations of the MAGIC [9] and VERITAS [10] ground-based telescopes in the same period.

The spectrum of γ-rays from the Crab has been measured in the energy range 0.8 TeV to 30 TeV at the SHALON telescope [3 - 6] with a statistical significance [11] of 36.1σ. The integral energy spectrum is well described by the single power law $I(>E_\gamma) \propto E_\gamma^{-1.40\pm0.07}$(Fig. 1 left). To made a description of the intensity and spectral shape in the TeV region, the model of Inverse Compton (IC) scattering of the ambient photons in the nebula in the Ref. [6] is used. Additionally, we need the assuming about magnetic field strength in the region of TeV emission (Fig. 1, right). The average magnetic field in the region of TeV γ-ray emission is extracted from the comparison of $0.8 - 30$ TeV (SHALON data) and X-ray (Chandra data [12]) emission regions (Figs. 1); and it ranges from 62 nT up to 153 nT with the average value 67 ± 7 nT. The γ-ray emission regions observed by SHALON in the Crab correlate well with the emission regions of synchrotron photons in the energy range 0.4 - 2.1 keV.

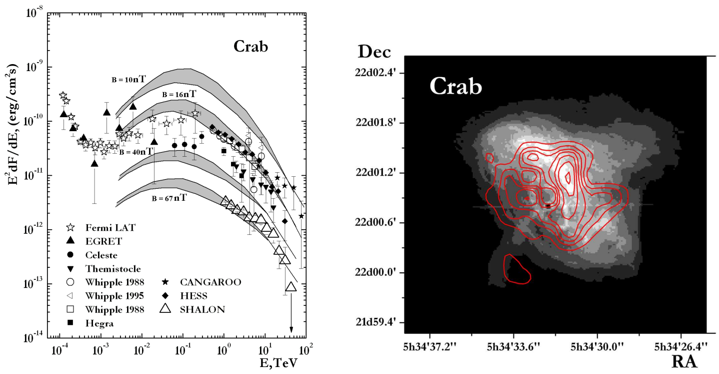

Figure 1: **left** – The Crab spectral energy distribution by SHALON [3 - 6] in comparison with other experiments [5]; **right** – A Chandra X-ray image of Crab [12]. The central part 200" × 200" of Crab PWN in the energy range 0.2-4 keV. The contour lines show the TeV - structure by SHALON observations.

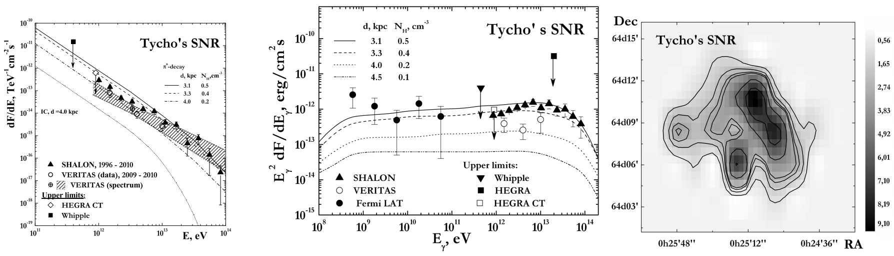

Figure 2: The Tycho's SNR characteristics **from left to right:** The differential spectrum of Tycho's SNR; Spectral energy distribution of the γ-ray emission from Tycho's SNR; The Tycho's SNR image in TeV γ-rays by SHALON.

Finally, the TeV γ-ray spectrum of Crab by SHALON is generated via IC scattering of soft, mainly optical, photons which are produced by relativistic electrons and positrons, in the nebula region around 1.5'(Fig. 1) from the pulsar with specific average magnetic field of about 67 ± 7 nT.

Tycho's SNR (SN 1572)

Tycho supernova remnant has been observed by SHALON telescope since 1996. This object has long been considered as a candidate to cosmic ray hadrons source in Northern Hemisphere. Tycho's SNR has been detected by SHALON at TeV energies [3 - 5] (in observations of 1996 - 2010 years) with a statistical significance [11] of 17σ. The integral γ-ray flux above 0.8 TeV was estimated as $(0.52 \pm 0.05) \times 10^{-12} cm^{-2} s^{-1}$. The energy spectrum of γ-rays in the observed energy region from 0.8 TeV is well described by the power law with exponential cutoff, $I(> E_\gamma/1TeV) = (0.42 \pm 0.04) \times 10^{-12} \times (E_\gamma/1TeV)^{-0.93\pm0.09} exp(-E_\gamma/35TeV)$ (Fig. 2). Recently, Tycho's SNR was also confirmed with VERITAS [13] in observations of 2008 - 2010 years. The high energy γ-ray emission from Tycho'SNR was detected with Fermi LAT [14] in the range 400 MeV - 100 GeV (Fig. 2).

A nonlinear kinetic model of cosmic ray acceleration in supernova remnants is used in [15, 16] to describe the properties of Tycho's SNR. The expected flux of γ-quanta from π°-decay, $F_\gamma \propto E_\gamma^{-1}$, extends up to ~ 30 TeV, while the flux of γ-rays originated from the IC scattering has a sharp cutoff above the few TeV, so the detection of γ-rays with energies up to 80 TeV by SHALON (Fig. 2) is an evidence of their hadronic origin [15 - 17]. The additional information about parameters of Tycho's SNR can be predicted in frame of nonlinear kinetic model if the TeV γ- quantum spectrum of SHALON telescope is taken into account: a source distance 3.1 - 3.3 kpc and an ambient density N_H $0.5 - 0.4$ cm^{-3} and the expected π°-decay γ-ray energy spectrum extends up to about 100 TeV.

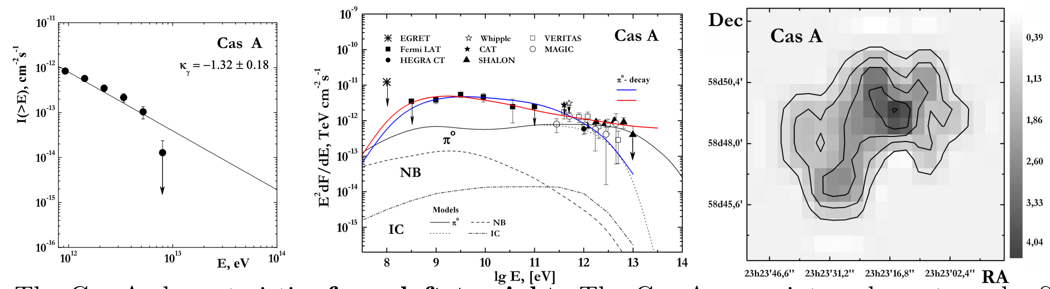

Figure 3: The Cas A characteristics **from left to right:** The Cas A γ-ray integral spectrum by SHALON experiment; Spectral energy distribution of the γ-ray emission from Cas A; The Cas A image in TeV γ-rays by SHALON

Cassiopeia A (SN 1680)

Cassiopeia A (Cas A) is the youngest of historical supernova remnant in our Galaxy. Its overall brightness across the electromagnetic spectrum makes it a unique object for studying high-energy phenomena in SNRs. Cas A was detected in TeV γ rays, first by HEGRA [18] and later confirmed by MAGIC [19] and VERITAS [20]. The high energy γ-ray emission from Cas A was detected with Fermi LAT [21] in the range 500 MeV - 50 GeV.

Cas A was observed with SHALON telescope during the 27 hours of autumn 2010 [5]. The γ-ray source associated with the SNR Cas A was detected above 800 GeV with a statistical significance [11] of 7.1σ with a γ-quantum flux above 0.8 TeV of $I_{CasA}(>0.8TeV) = (0.68 \pm 0.13) \times 10^{-12} cm^{-2} s^{-1}$ (Fig. 3, left).

The favored scenarios (both, hadronic and leptonic) in which the γ-rays of 500 MeV - 10 TeV energies are emitted in the shell of the SNR like Cas A are considered in [21, 22]. Figure 3 presents spectral energy distribution of the γ-ray emission from Cas A by SHALON in comparison with other experiment data (see Fig. 3 and [5]) and with theoretical predictions [21, 22]. The detection of γ-ray emission at 5 - 10 TeV and the hard spectrum below 1 TeV would favor the π°-decay origin of the γ-rays in Cas A SNR.

References

[1] E. G. Berezhko and G. F. Krymskii, Usp. Fiz. Nauk 154(1) (1988) 49.

[2] S. P. Reynolds, Ann. Rev. Astron. Astrophys. 46 (2008) 89.

[3] V. G. Sinitsyna, AIP (Conf. Proc.) 515 (2000) 205; 293.

[4] V. G. Sinitsyna et al., Nucl. Phys. B (Proc.Suppl.) 196 (2009) 437; *ibid.*,175-176 (2008) 455; *ibid.*, 151 (2006) 112; *ibid.*, 122 (2003) 247, 409; *ibid.*, 97 (2001) 215, 219; *ibid.* 75A (1999) 352.

[5] V. G. Sinitsyna and V. Yu. Sinitsyna, Astronomy Letters, 37(9) (2011) 621.

[6] A. M. Hillas, et al., ApJ, 1998, **503**: 744.

[7] M. Tavani et al., Science 331 (2010) 736.

[8] A. A. Abdo, et al., Science 331(6018) (2010) 739.

[9] M. Mariotti, *Astron. Telegramm* No. 2967 (2010).

[10] R. Ong, *Astron. Telegramm* No. 2968 (2010).
[11] T.-P. Li and Y.-Q. Ma, ApJ. 272 (1983) 317.
[12] F. D. Seward, W. H. Tucker and R. A. Fesen, ApJ. 652 (2006) 1277.
[13] V. A. Acciari et al., *arXiv:astro-ph/ 1102.3871v1.*
[14] F. Giordano, et al., *arXiv:astro-ph/ 1108.0265v.*
[15] H. J. Völk, et al., *in Proc. 27th ICRC, Hamburg*, 2 (2001) 2469.
[16] E. G. Berezhko et al., Astrophys. Space Sci. 309 (2007) 385.
[17] H. J. Völk, E. G. Berezhko, L. T. Ksenofontov, A&A 483(2) (2008) 529.
[18] F. Aharonian, et al., A&A 370 (2001) 112.
[19] J. Albert et al., A&A 474 (2007) 937.
[20] V. A. Acciari, et al., ApJ 714 (2010) 163.
[21] A.A. Abdo, et al., ApJ 710 (2010) L92.
[22] E. G. Berezhko, G. Pühlhofer, H. J. Völk, A&A 400 (2003) 971.

Extragalactic Background Light expected from observations of TeV extragalactic sources at distances from $z = 0.018$ to $z = 1.375$

V.Yu. Sinitsyna and V.G. Sinitsyna
P.N.Lebedev Physical Institute, Russian Academy of Science
Email : sinits@sci.lebedev.ru

Abstract

Extragalactic background radiation blocks the propagation of TeV γ-ray over large distances by producing e^+e^- pairs. As a result, primary spectrum of γ-source is changed, depending on spectrum of background light. So, a hard spectra of Active Galactic Nuclei with high red shifts allow the determination of a EBL spectrum. The redshifts of SHALON TeV γ-ray sources range from 0.018 to 1.375 those spectra are resolved at the energies from 800GeV to 30 TeV. Spectral energy distribution of EBL constrained from observations of Mkn421, Mkn501, OJ287, 3c454.3 and 1739+522 together with models and measurements are presented.

Introduction

The γ-astronomical researches are carrying out with SHALON [1] mirror Cherenkov telescope since 1992. During the period 1992 - 2011 SHALON has been used for observations of extragalactic sources of different type (see Table 1) and [2 - 7]. Our method of the data processing is described in [1 - 4]. Some representative results on fluxes, spectra are shown in Table 1 and also in [2 - 7]. and Figures in these proceedings.

Table 1: The catalogue of metagalactic γ-ray sources observed by SHALON

Sources	Observable flux[a]	k_γ [b]	Distance [c]	z	Type
NGC 1275	(0.78 ± 0.13)	-2.25 ± 0.10	71	0.018	Seyfert
SN2006 gy	(3.71 ± 0.65)	-3.13 ± 0.27	83	0.019	SN
Mkn 421	(0.63 ± 0.14)	-1.87 ± 0.11	124	0.031	BL Lac
Mkn 501	(0.86 ± 0.13)	-1.85 ± 0.11	135	0.034	BL Lac
Mkn 180	(0.65 ± 0.23)	-2.16 ± 0.15	182	0.046	BL Lac
OJ 287	(0.26 ± 0.07)	-1.43 ± 0.18	1070	0.306	BL Lac
3c4543	(0.43 ± 0.13)	-0.85 ± 0.07	5489	0.859	FSRQ
1739+522	(0.53 ± 0.10)	-0.93 ± 0.09	9913	1.375	FSRQ

[a] Integral flux at energy $> 800 GeV$ in units of $10^{-12} cm^{-2} s^{-1}$
[b] Power index in case of power fit of observable data
[c] Distance in Mpc

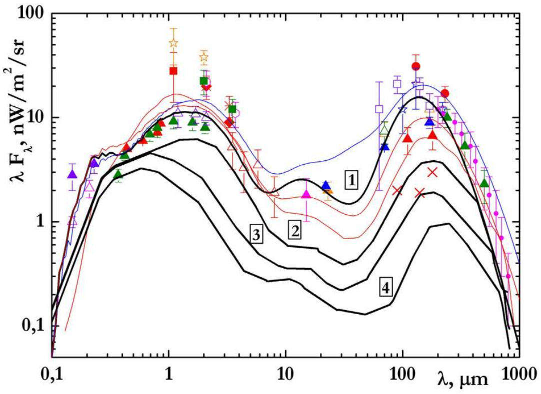

Figure 1: Spectral energy distribution of EBL: measurements [8] and models [9, 10] and EBL shape constrained from observations of the extragalactic sources by SHALON: 1 - Mkn 421 (z=0.031), Mkn 501 (z=0.034); 2 - OJ287 (z=0.306); 3 - 3c454.3(z=0.859); 4 - 1739+522 (z=1.375)

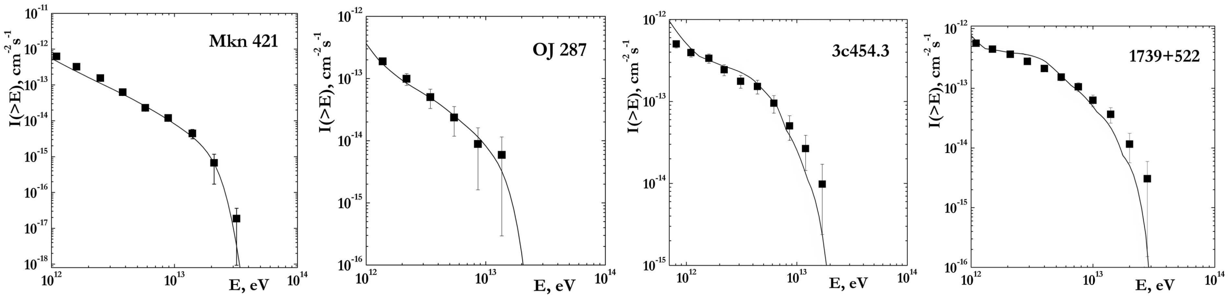

Figure 2: The measured spectra for Mkn 421, OJ287, 3c454.4 and 1739+522 (black squares) together with spectra attenuated by EBL (lines, see text)

Extragalactic Background Light

As the TeV γ-rays can be absorbed due to interaction of low-energy photons of Extragalactic Background Light (EBL), the primary spectrum of γ-source is changed, depending on spectrum of background light. So, a hard spectra of AGNi with high red shifts of 0.03 - 1.8 allow the determination an absorption by EBL and thus its spectrum. The redshifts of SHALON very high energy gamma-ray sources range from z=0.018 to z=1.375. Among them bright enough AGNi Mkn421, Mkn 501 and 3c454.3, 1739+522 (4c+51.37) those spectra are resolved in the TeV energy band from 800 GeV to ~20-30 TeV. The fit of a simple power law function to the observational data presented in Table 1. Also, the measured spectra can be fitted by a power law with an exponential cutoff: $F(>E) \propto E^{-\gamma} \times exp(-E/E_{cutoff})$ with hard power indices of about $\gamma \sim 1.55$ for Mkn 421 and Mkn 501 and $\gamma \sim 0.6$ for 3c454.3 and 1739+522. The value of E_{cutoff} ranges from 11 ± 2 TeV for Mkn421, Mkn 501 and to 7 ± 2 TeV for distant sources.

It has mentioned that the observed spectra are modified by γ-ray attenuation, i.e. $F_{observed}(E) = F_{intrinsic}(E) \times exp(-\tau(E,z))$ where $\tau(E,z)$ is optical depth for pair creation for a source at redshift z, and at an observed energy E. According to the definition of the optical opacity the medium influences on the primary source spectrum at $\tau \geq 1$, but for $\tau < 1$ the medium is transparent, so the measuring of source spectrum in the both range of τ can give the intrinsic spectrum of the source to constrain the EBL density. The optical depth for sources at redshifts from 0.031 to 1.375 was calculated with assumption of EBL shapes shown in Fig. 1. We used the EBL shape from Best-fit model and Low-SFR model [10] (see Fig. 1 thick black line 1 corresponds to Low-SFR model) to calculate the attenuated spectrum of Mkn 421 and Mkn 501 in assumption of simple power low intrinsic spectrum of the source with spectrum index of $\gamma = 1.5$, taken from the range of $\tau < 1$. The result is shown at Fig. 2 with line; the black squares are observational data for Mkn 421. The shapes of EBL density constrained from the spectra of the high redshift sources OJ287 (z=0.306), 3c454.3 (z=0.859) and 1739+522 (1.375) are shown in Fig. 1 with curves 2, 3 and 4, respectively. For these sources the slope of intrinsic spectrum is taken $\gamma = 0.9 - 1.2$. The attenuated spectra for OJ287, 3c454.3 and 1739+522 are also presented at Fig. 2 (thin lines) together with observational data. Observations of distant metagalactic sources have shown that the Universe is more transparent to very high-energy γ-rays than previously believed.

References

[1] S. I. Nikolsky and V. G. Sinitsyna, *in Proc. Int. Workshop on VHE γ-ray Astronomy*, Crimea, ed. A. A. Stepanian *et al.*, (1989) 11.

[2] V. G. Sinitsyna *et al.,* Int. J. Mod. Phys. A no. 29, (2005) 7029, 7023.

[3] V. G. Sinitsyna *et al.,* Nucl. Phys. B (Proc. Suppl.) 196 (2009) 251, 442; *ibid.* 175-176 (2008) 463; 151 (2006) 108; *ibid.* 122 (2003) 247, 409; *ibid.* 97 (2001) 215, 219; *ibid.*75A (1999) 352.

[4] S. I. Nikolsky and V. G. Sinitsyna, Phys. Atom. Nucl. 67 (2004) 1900.

[5] V. G. Sinitsyna, AIP (Conf. Proc.) 515 (2000) 205, 293.

[6] V. G. Sinitsyna,*et al.,* Izv. Ross. Akad. Nauk Ser. Fiz. 75(3) (2011) 437; *ibid.* 73(5) (2009) 657; *ibid.* 71(7) (2007) 94; *ibid.* 69(3) (2005) 422; *ibid.*, 66(11) (2002) 1667, 1660; *ibid.* 63(3) (1999) 608; *ibid.* 61(3) (1997) 603.

[7] V. G. Sinitsyna, *et al.,* J. Phys. Soc. Jpn., Suppl. A 78 (2009) 192, 92.

[8] R. C. Gilmore, *et al.*, *ArXiv:1104.0671*

[9] T. M. Kneiske, *et al.* A&A 386 (2002) 1; A&A 413 (2004) 807.

[10] F.W. Stecker, M.A. Malkan & S.T. Scully ApJ. 648 (2006) 774;

Superluminal neutrinos in the light of extradimension approach

Vo Van Thuan
Institute for Nuclear Science and Technology (INST)
179 Hoang Quoc Viet Street, Nghiado, Hanoi, Vietnam
Email: vvthuan@vaec.gov.vn

Abstract

Based on the space-time symmetry with two time-like extradimensions we have proposed a generalized superluminal transformation (GSLT) and introduced its application to the lepton sector. In this model, neutrinos can be adopted as superluminal partners of massive charged leptons.

1 Introduction

The tachyon problem had been discussed intensively for two decades since 1960 [1]. Parker proposed a formal two-dimension superluminal special Lorentz transformation (2D-SSLT) which converts the roles of time and space and transmutes an electric charged particle into a superluminal magnetic monopole [2]. Performing the scheme of 4D-SSLT for Minkowski space-time, Recami made a step toward to the realistic tachyon theory based on space-time symmetry [3, 4]. The experiments showed that the real mass terms of neutrinos are small and their imaginary mass terms are negligible. Indeed, we had no direct evidence of tachyon until the recent claim of observation of faster-than-light neutrinos by the OPERA [5], which causes a deep concern and needs independent experiments for verification. In this work we show that the specific behavior of neutrinos can be understood and correctly described by an extension of 4D-SSLT which is called the generalized superluminal transformation (GSLT) and has been reported in our previous studies [6, 7, 8].

2 GSLT model

Following the concept of space-time symmetry developed by Parker and Recami [2, 3] we construct [6, 7] an ideal 6D flat symmetrical extended $\{3, 3\}$ time-space $\{t_1, t_2, t_3 | x_1, x_2, x_3\}$ in which Minkowski 4D space-time is embedding. The 6D quadratic equation reads:

$$dt_i{}^2 = dx_j{}^2; \quad i, j = 1, 2, 3 \tag{1}$$

Where t_i and x_j are general coordinates, describing all kinds of motion, translation as well as acceleration. Any extra-fluctuations in this extended space-time can be expressed by 6D plane waves transmitting in this time-space:

$$\frac{\partial^2 f}{\partial t_i^2} - \frac{\partial^2 f}{\partial x_j^2} = 0; \tag{2}$$

This is the equation of a massless scalar field where $f(t_i, x_j)$ is a harmonic function. Here the natural units are used throughout ($c = \hbar = 1$). The two time-like transverse extra-dimensions $\{t_1, t_2\}$ added to form the

6D space-time are then implied to be hidden from the subluminal observers. It was shown in [7] that from (2) after compacting time-like extradimensions, we can naturally derive the quantum mechanic equations of motion in our Minkowski 4D space-time and the time-like transverse axes $\{t_1, t_2\}$ are hidden under the two well-known parameters: the quantum wave function ψ and the proper time t_0. In general, space and/or time are not flat. A transformation from 6D space-time to a subluminal 4D space-time (or to a superluminal 4D time-space) is performed by adding curvature elements of the general relativity ds_0 (or ds_n) to (1) by oscillation (or rotation) along axes t_0 (or x_n) orthogonal to the linear coordinates $t_3 \in \{t_k\}$ (or $x_3 \in \{x_l\}$). Those curvatures may be caused by quantum fluctuations in an averaged physical vacuum potential [7]. From (1) we obtain:

$$dt_k{}^2 + (dt_0{}^2 - ds_0{}^2) = dx_l{}^2 + (dx_n{}^2 - ds_n{}^2); \quad k, l = 1, 2, 3 \tag{3}$$

Where t_k and x_l describe strictly linear translational motion. The 6D space-time geometry (3) can be now reformulated into 4D-quadratic forms. For the subluminal 4D space-time like Minkowski 4D-geometry, it reads:

$$[dt_3{}^2 + dt_0(t_1, t_2)^2] - dx_l{}^2 = dt^2 - dx_l{}^2 = ds_0{}^2; \tag{4}$$

And for the superluminal 4D time-space, the 6D geometry (3) turns to:

$$[dx_3{}^2 + dx_n(x_1, x_2)^2] - dt_k{}^2 = dz^2 - dt_k{}^2 = ds_n{}^2; \tag{5}$$

Where t in (4) and z in (5) are getting curved temporal and spatial axes, correspondingly. The 4D observers synchronizing with the curvature along t (or z) can not identify this curved evolution rather to accept t (or z) as a linear axis. When ds_0 or ds_n is invariant, in each of both 4D-frames (4) and (5) we can postulate an independent Lorentz invariance, separately. When $ds_0 = ds_n = ds > 0$, both 4D-frames are getting in an absolute space-time symmetry and Lorentz invariance is extended for 4D-SSLT. Considering a material particle in a 4D superluminal frame $K'\{x', y', z, t_3\}$ moving with a relative speed $\beta' > 1$ along the longitudinal linear axis x_3 in a 4D subluminal frame $K\{x, y, x_3, t\}$, based on the traditional Lorentz transformation, we proposed in [6] the following 4D-SSLT between K and K':

$$dt = \gamma(dz - \beta dt_3);\ dx_3 = \gamma(dt_3 - \beta dz);\ \ dx = i.dx' = dv;\ dy = i.dy' = dw; \tag{6}$$

In according to Recami formalism [3] 4D-SSLT (6) includes two actions: the first is to replace β' by a converted $\beta = 1/\beta' < 1$, equivalent to turn temporal axes to spatial ones; then $\gamma = (1-\beta^2)^{-1/2}$; the second is to convert all imaginary variables into real ones to meet the physical reality. In addition, we replaced the original imaginary spatial axes $\{x', y'\}$ (in according to [3]) by two real transverse time-like plane axes $\{v, w\}$. In the superluminal geometry (5) a tachyon is to travel along a single spatial curved axis z, while being able to "evolve" freely in Euclidean 3D-time $\{v, w, t_3\}$. For the space-time symmetry, the absolute value of tachyonic imaginary mass is assumed equal exactly the proper mass of its subluminal partner. Moreover, instead of electric charge the tachyon has an additive magnetic monopole [2, 4], i.e. leptonic tachyons are electrically neutral. Indeed, we proved in [8] that along with 4D-SSLT (6), Dirac equation for electron should be treated simultaneously by a Majorana-like representation to be covariant, i.e. being converted into an equation for massive Majorana neutrino. There we assumed also that the sign of magnetic charge correlates strictly with neutrino helicity.

In reality, however, neutrinos are almost massless and have no additive charge. Therefore, the SSLT should not conserve the spatial interval ds_n explicitly. The modification of 4D-SSLT (6) is performed by a linear factorization of the curved axis z through the intermediate 6D extra-geometry (3):

$$dz = \gamma_3 dx_3 + \gamma_4 ds_n; \tag{7}$$

Where γ_3, γ_4 are anti-commutative parameters like covariant Dirac matrices. The combination (6) and (7) formulates 6D-GSLT, which almost compensates ds_n by $dx_n = \phi(x_1, x_2)$ and converts the superluminal geometry (5) into:

$$dx_3{}^2 - dt_k{}^2 = \delta s(x_n)^2; \tag{8}$$

Where $\delta s(x_n)$ is a tiny dynamic parameter governed by rotating variation of $\{x_1, x_2\} \in \{x_j\}$ in (1). When $\delta s \to 0$ the quadratic equation (8) characterizes 4D time-space geometry of a time-like luxon, rather of tachyon. In GSLT, explicitly, the conventional 4D-Lorentz invariance is no more conserved for time-like objects! From the view of a subluminal observer, the spatial curvature of tachyon is identified as an intrinsic angular momentum (spin) in Euclidean 3D-space $\{x, y, x_3\}$, rather than its imaginary mass term. Therefore, the motion of tachyon in appearance is now described like a translation along the linear axis x_3 of an almost massless neutrino with a fixed spin, i.e. helicity.

3 Experimental constraints

Based on the formalism of 6D-GSLT (6) and (7) in [6, 7, 8] we formulated from Eq. (2) realistic Dirac-like equations for both massive leptons and neutrinos. We proposed a simplified model in according to the geometry (8) that the main terms of imaginary mass and magnetic charge of neutrino are hidden, while due to parity non-conservation (PNC) in the weak interaction, there is still revealed a small term $\delta s(x_n)$ proportional to Fermi constant G_F. In the result, only tiny residues δm_s of transcendent mass and δg_T of magnetic charge can be observed. In [6] the measurable values estimated by this GSLT model are compared in a qualitative consistency with the data of PNC experiments, neutrino oscillations and SN1987A observation. We also proposed in [6] experiments searching for collective effects of magnetic fluxes induced by intense neutrino beams from the Sun or from nuclear reactors.

Another situation is found in the recent claim of faster-than-light neutrino effect [5]: a speed-up time difference of $\Delta t = 57 \pm 10$ nsec on the distance of $L = 731$ km has been reported at averaged neutrino energy $E_\nu = 17$ GeV. Applying a simple equation from the superluminal time-space symmetrical theory: $\Delta t = (L/2c)[m(eV)/p_\nu(eV)]^2$, we found an absolute value of very large imaginary mass $m \approx 116$ MeV for those faster-than-light muon neutrinos, which is surprisingly close to the rest mass of muons $m_0 = 105$ MeV. The latter seems to meet well the 4D-SSLT with a symmetrical geometry (5). However, on the other hand, there was no energetic dependence observed. Generally, this puzzle is considered like a systematic effect and should be clarified by independent experiments, in particular, by T2K or MINOS.

For conclusion, we emphasize that the variation between the symmetrical geometries (5) and (8) in the frame of the reported GSLT, as a model of the general relativity, should not violate the classical Lorentz invariance of the special relativity for bradyon objects in 4D-Minkowski subluminal world.

Acknowledgement: The author thanks deeply his colleagues of the Institute for Nuclear Science and Technology (INST, Hanoi) and the Rencontres du Vietnam (Orsay) for longterm support. The study has been partly funded by the National Council for Basic Science and the Cooperative Research Project No. 760/2008/HD-NDT (MOST, Vietnam) for the period 2006-2011.

References

[1] O.M.P. Bilaniuk, V.K. Deshpande and E.C.G. Sudarshan, Am.J.Phys. 30(1962)718. *See also:* Tachyon, monopoles and relative topics. Ed. E. Recami. North-Holland, Amsterdam, 1978 *and reference there.*

[2] L. Parker, Phys.Rev. 188(1969)2287.

[3] E. Recami and R. Mignani, Lett.Nuov.Cim. 4(1972)44.
[4] E. Recami and R. Mignani, Phys.Lett. B62(1976)41.
[5] T. Adam et al., OPERA Collaboration, hep-ph/1109.4897v2 (2011).
[6] Vo Van Thuan, Proc. Osaka Forum on Frontiers of Basic Science, Hanoi, 27-29 Sept. 2005. Ed. H.Takabe et al., Osaka Univ. Press (2006)98.
[7] Vo Van Thuan, IJMPA 24(2009)3545.
[8] Vo Van Thuan, Communications in Physics 19(2009)59.

Nguyên van Hiêu and Jean Trân Thanh Van

Chung-I Tan (co-chair of EDS meeting)

Black Holes, Worm Holes

Ground Breaking

Handshake. . . showing the support of AMU at the creation of the ICISE

Regular black holes and the stability problem

K.A. Bronnikov

Center for Gravitation and Fundamental Metrology, VNIIMS,

46 Ozyornaya St., Moscow 119361, Russia, and

Institute of Gravitation and Cosmology, PFUR,

6 Miklukho-Maklaya St., Moscow 117198, Russia

Email *: kb20@yandex.ru*

Abstract

We compare different types of regular static, spherically symmetric black holes and discuss their particular type, black universes, which contain an expanding, asymptotically de Sitter T-region, able to model the observed Universe; such models exist in the presence of phantom matter. Next, we consider the stability of static self-gravitating scalar fields with different potentials $V(\phi)$ in general relativity. Their general feature is that the effective potential for perturbations is singular at a throat (if any) but generically admits regularization, which in turn leads to regular perturbations of the scalar field and the metric. As examples, we consider some particular black-universe models and find a stable family among them.

1 Regular black holes

In black hole (BH) physics, and gravitation theory as a whole, one of the long-standing problems is the existence of curvature singularities beyond the event horizon in BH solutions obtained under the simplest and the most natural physical conditions (the Schwarzschild, Reissner–Nordström, Kerr and Kerr-Newman solutions of general relativity (GR) and their counterparts in many alternative theories of gravity). Singularities are places where a classical theory of gravity does not work. Therefore, a full understanding of BH physics requires avoidance of singularities or/and modification of the corresponding classical theory and addressing quantum effects. Of great interest are the opportunities of singularity avoidance in the framework of classical gravity.

Let us discuss the possible geometry of classical nonsingular BHs, restricting ourselves to asymptotically flat static, spherically symmetric configurations. We begin with the general static, spherically symmetric metric

$$ds^2 = A(u)dt^2 - \frac{du^2}{A(u)} - r^2(u)d\Omega^2, \qquad (1)$$

written in terms of the quasiglobal coordinate u, convenient for dealing with BH horizons. A flat asymptotic ($u \to \infty$) corresponds to $A(u) \to 1$ and $r(u) \approx u$. A centre $u = u_c$ (if any) corresponds to $r = 0$ in a static region; horizons (if any) are described by regular zeros of the function $A(u)$, and their number, order and disposition determine the global causal structure of space-time.

Four simplest types of regular 4D asymptotically flat, static, spherically symmetric BHs known in the literature can be presented as follows (see Fig. 1).

1. BHs with a regular centre ($r \to 0,\ A \to A_c > 0$), which can only be located in an R-region ($A > 0$). These BHs have either two simple horizons or one double horizon, and their causal structures are the same as those of Reissner–Nordström space-times (diagrams 1b and 1c in Fig. 1).

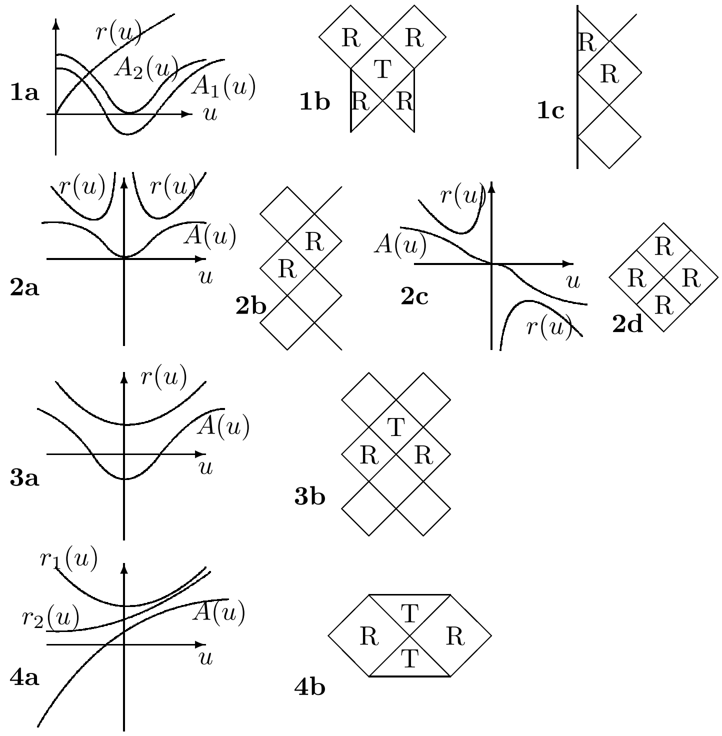

Figure 1: Plots showing the qualitative behaviour of the metric functions and Carter-Penrose diagrams for four types of regular BHs. Diagrams 1b and 1d refer to curves A_1 and A_2 in plot 1a, respectively. Diagram 2b refers to plot 2a, diagram 2d to plot 2c, 3b to 3a and 4b to 4a. The R and T letters in the diagrams designate the R and T space-time regions. Diagrams 1b, 1c, 2b and 3b are infinitely extendible upward and downward. In all diagrams, all inner slanting lines depict horizons while all boundaries correspond to $r = \infty$, except for verticals in diagrams 1b and 1d describing a regular centre, $r = 0$, and horizontal lines in diagram 4b corresponding to $r = \infty$ or to $r = r_0 > 0$, according to the curves $r_1(u)$ or $r_2(u)$ at large negative u.

There are numerous examples ([1, 2, 3] and others) of such BH solutions where $r \equiv u$ and the stress-energy tensor (SET) of matter obeys the condition $T^0_0 \equiv T^1_1$. This condition is invariant under radial boosts, making it possible to ascribe the source to vacuum matter [1]. Such solutions have been obtained, e.g., in GR coupled to nonlinear electrodynamics with the Lagrangian $L(F)$, $F := F_{\mu\nu}F^{\mu\nu}$ ($F_{\mu\nu}$ is the Maxwell tensor) [3] and in some versions of quantum gravity in a semiclassical approximation [4, 5, 6]; see also references therein.

2. BHs without a centre, having second-order horizons of infinite area (so-called cold BHs because their Hawking temperature is always zero) [7, 8, 9]. Their possible causal structures are shown in diagrams 2b and 2d in Fig. 1. Such BHs have been obtained in the Brans-Dicke scalar-tensor theory with the coupling constant $\omega < -3/2$, for which the scalar is of phantom nature. These solutions form some special families and have singular counterparts in GR with a minimally coupled phantom scalar field ("anti-Fisher cold BHs" [10].

3. BHs with a causal structure of a non-extreme Kerr BH without a singular ring [11, 12] (diagram 3b). They were found as solutions to the effective equations [13] describing 4D gravity in an RS2 type brane world.

It should be stressed, however, that these 4D equations do not form a closed set, and to study the full 5D geometry of the bulk one should solve the corresponding 5D equations; there are only tentative results in this direction [14].

4. BHs with a Schwarzschild-like causal structure [15] (diagram 4b) but cosmological expansion instead of a singularity, termed *black universes* [16]. They were obtained [15] as generic solutions of GR minimally coupled to phantom scalar fields with proper potentials. Such fields have recently become popular in the cosmological context since they provide the pressure to density ratio $p/\varepsilon = w < -1$. This kind of equation of state is probably required for describing the Dark Energy responsible for the accelerated expansion of our Universe.

The above list is certainly incomplete: thus, one can easily imagine structures with a larger number of horizons (e.g., add a smooth peak twice crossing the u axis in any plot of $A(u)$).

For a minimally coupled scalar field ϕ in GR, with the Lagrangian

$$L = [R - \varepsilon(\partial\phi)^2 - 2V(\phi)]/(16\pi) \tag{2}$$

($\varepsilon = +1$ for a normal scalar and $\varepsilon = -1$ for a phantom one), an example of a black-universe solution for $\varepsilon = -1$ is [15]

$$r = (u^2 + b^2)^{1/2}, \qquad b = \text{const} > 0. \tag{3}$$

$$B(u) := \frac{A(u)}{r^2(u)} = \frac{c}{b^2} + \frac{1}{r^2} + \frac{3m}{b^3}\left(\frac{bu}{r^2} + \tan^{-1}\frac{u}{b}\right), \tag{4}$$

$$\phi = \pm\sqrt{2}\tan^{-1}(u/b) + \phi_0, \tag{5}$$

$$V = -\frac{c}{b^2}\frac{r^2+2u^2}{r^2} - \frac{3m}{b^3}\left(\frac{3bu}{r^2} + \frac{r^2+2u^2}{r^2}\tan^{-1}\frac{u}{b}\right). \tag{6}$$

The solution behaviour is controlled by two integration constants: c that moves the plot of $B(u) \equiv A/r^2$ up and down, and m determining the maximum of $B(u)$. Asymptotic flatness at $u = +\infty$ implies $2bc = -3\pi m$, where m is the Schwarzschild mass defined in the usual way.

Under this asymptotic flatness assumption, at $m = 0$ we obtain the simplest configuration, the Ellis wormhole [17]: $A \equiv 1$, $V \equiv 0$. At $m < 0$, there is a wormhole with an AdS metric at the far end, corresponding to the effective cosmological constant $\Lambda = V(-\infty) < 0$.

At $m > 0$, it is a black universe, a regular BH with de Sitter expansion far beyond the horizon, corresponding to $\Lambda = V(-\infty) > 0$. The horizon radius cannot be smaller than $b = r(0) = r_{\min}$. Since $A(0) = 1 + c$, the throat $u = 0$ is situated in the R-region if $c > -1$, precisely at the horizon if $c = -1$ and in the T-region beyond the horizon if $c < -1$. Black universes combine the properties of wormholes (absence of a centre, a regular minimum of $r(u)$) and BHs (a horizon separating R and T regions).

Quite naturally, such unusual objects require unusual matter for their existence. We saw how they can be obtained using a phantom scalar field. As shown in [16], such solutions also exist in much more general frameworks for the description of phantom matter, such as scalar-tensor theories and k-essence.

An example of a black-universe solution without phantoms has been obtained [18] within a brane-world scenario of RS2 type, where exotic matter is replaced by a “tidal” contribution to the effective SET coming from the bulk geometry [13]. Another example [19] uses the notion of a “trapped ghost” [20], i.e., a scalar field which has phantom properties only in a strong-field region, while away from it all standard energy conditions are observed. This can explain why ghosts, or phantoms, are not observed under usual physical conditions but certainly does not remove the well-known basic shortcomings of phantom fields.

A structure similar to a black universe was obtained in a semiclassical limit of loop quantum gravity [21, 22], with a minimum radius $r_{\min}$ of the order of Planck's length (while in our model it is arbitrary) and without isotropization at late times.

2 The stability problem

Let us now briefly discuss the stability problem for static, spherically symmetric configurations obtained in the theory (2). To begin with, due to the scalar field, a multipole expansion of the perturbations contains the monopole (spherically symmetric) degree of freedom. More than that, monopole perturbations are the most "dangerous" in the sense of instability. The point is that in many important cases linear perturbation equations can be reduced to Schrödinger-like equations with certain effective potentials with respect to some "wave function", while the role of an energy level is played by a frequency squared. Negative energy levels correspond to imaginary frequencies, hence a possible exponential growth of the perturbations, i.e., instability. Higher multipoles generally lead to positive contributions into the effective potentials, like centrifugal barriers in quantum mechanics. Therefore if a system under study is unstable, this instability will most probably manifest itself under monopole perturbations.

Therefore we here discuss only monopole perturbations. The only dynamic degree of freedom is then connected with scalar perturbations $\delta\phi = \phi(u,t) - \phi(u)$, where $\phi(u)$ belongs to the background static solution to the field equations due to (2). Linear perturbations of the metric functions can be excluded using the linearly perturbed Einstein equations, which leads to the wave equation for the gauge-invariant perturbation $\psi = r\delta\phi - (r/r')\delta r$ (see [24] and references therein):

$$\begin{aligned}
&\ddot\psi - \psi_{xx} + V_{\rm eff}(x)\psi = 0,\\
&V_{\rm eff}(x) = A(u)\biggl[\varepsilon(r^2V-1)\frac{\phi'^2}{r'^2} + \frac{2r\phi'}{r'}V_\phi + \varepsilon V_{\phi\phi} + \frac{Ar''+A'r'}{r}\biggr].
\end{aligned} \tag{7}$$

Here, x is the so-called tortoise coordinate defined by $dx = du/A(u)$; the prime stands, as before, for d/du, the index x for $\partial/\partial x$, the index ϕ for $d/d\phi$, and the dot for $\partial/\partial t$; all quantities involved in the effective potential $V_{\rm eff}(x)$ are taken from the static solution. Gauge invariance means physically the freedom of choosing the reference frame in perturbed space-time; using gauge-invariant quantities gurantees that the perturbations under study are not a pure coordinate effect but correspond to real disturbances of the system.

The further substitution $\psi(x,t) = y(x)\,{\rm e}^{i\omega t}$, $\omega = {\rm const}$, which is possible since the background is static, leads to the Schrödinger-like equation

$$y_{xx} + [\omega^2 - V_{\rm eff}(x)]y = 0. \tag{8}$$

If there is a nontrivial solution to (8) with ${\rm Im}\,\omega < 0$, satisfying physically reasonable conditions at the ends of the range of u (in particular, the absence of ingoing waves. which forbids energy pumping to the system from outside), then the static system is unstable since $\delta\phi$ can exponentially grow with t. Otherwise it is stable in the linear approximation. Thus, as usual in such studies, the stability problem is reduced to a boundary-value problem for Eq. (8).

The main difficulty with this study for systems with phantom fields is the existence of throats where $V_{\rm eff}$ has a singularity due to $r' = 0$. In the generic case $r^2V < 1$, the potential $V_{\rm eff}$ has there a wall of infinite height. As a result, perturbations are actually independent at different sides of the throat and necessarily turn to zero at the throat itself, and we lose information on possible modes perturbing the throat radius. As shown in [24], the potential $V_{\rm eff}$ can be regularized on the throat by means of the so-called S-deformation method:

one should find such a function $S(x)$ that $V_{\rm eff} = S^2 + S_x$, then the new unknown function $\chi = (-\partial_x + S)\psi$ satisfies the equation

$$\ddot\chi - \chi_{xx} + W_{\rm reg}(x)\chi = 0, \tag{9}$$

with the new effective potential

$$W_{\rm reg}(x) = -S_x + S^2 = -V_{\rm eff}(x) + 2S^2. \tag{10}$$

For this procedure to work, it should hold $S \approx -1/x$ and $V_{\rm eff} \approx 2/x^2$ at small x if $x = 0$ is the throat. It has been shown [24] that, for a generic solution the potential $V_{\rm eff}$ for spherically symmetric perturbations satisfies this necessary condition for regularization. Moreover, if a solution $\chi(x)$ to Eq. (9) is known, it generically creates regular perturbations of the scalar ϕ and the metric.

This method has been used in [23] where the instability was found for a family of solutions with $\varepsilon = -1$, $V(\phi) = 0$, the so-called anti-Fisher wormholes. In [24], a similar instability was found for other branches of the solution for $\varepsilon = -1$, $V(\phi) = 0$, which include many singular configurations and anti-Fisher cold BHs. However, for configuration with nonzero $V(\phi)$, including the black universes described above, it is hard to find the proper function $S(x)$, therefore their stablity in the cases where the throat is located outside the horizon has not been studied by now. There are only some tentative results for black universes where the minimum of r is located outside the static region [25], that is, $c \le -1$. As usual in BH stability studies, we actually discuss the stability of the static region, imposing the proper boundary conditions at the horizon and at infinity. It turns out that the black universe (3)–(6) is stable under radial perturbations in the case $c = -1$, but it is unstable for all $c < -1$. In other words, the only stable branch of our black-universe solutions corresponds to the case where the minimum of r is located precisely at the horizon.

3 Conclusion

Among different regular BH models, black universes seem to be of particular interest since their late-time asymptotic can in principle describe our accelerating Universe; moreover, they are a particular realization of the Null Big Bang idea [26, 27], according to which the expansion of our Universe began from a horizon rather than from a singularity, and then followed a rapid isotropization connected with particle creration. However, a stability study of a simple black-universe, given by solution (3)–(6), has revealed only a special family of stable solutions, namely those with a horizon located at the minimum radius $r = b$. There remain a lot of questions yet to be unswered: Can there be stable models with wormhole-like throats located outside the horizon? How general is the instability result for models with a minimum radius inside the horizon? Will the inclusion of electric or magnetic fields stabilize such black universes? And so on. There is a hope to answer at least some of them in the near future.

The work was supported in part by the Russian Foundation for Basic Research Grant No. 09-02-00677a, by NPK MU grant at PFUR, and by FTsP “Nauchnye i nauchno-pedagogicheskie kadry innovatsionnoy Rossii” for the years 2009-2013.

References

[1] I. Dymnikova, Gen. Rel. Grav. **24**, 235 (1992).

[2] E. Ayon-Beato and A. Garcia, Regular black hole in general relativity coupled to nonlinear electrodynamics. Phys. Rev. Lett. **80**, 5056 (1998); gr-qc/9911046.

[3] K.A. Bronnikov, Regular magnetic black holes and monopoles from nonlinear electrodynamics. Phys. Rev. D **63**, 044005 (2001); gr-qc/0006014.

[4] Leonardo Modesto, John W. Moffat, and Piero Nicolini, Black holes in an ultraviolet complete quantum gravity. Phys. Lett. B **695**, 397 (2011); arXiv: 1010.0680.

[5] I. Arraut, D. Batic, and M. Nowakowski, Maximal extension of the Schwarzschild spacetime inspired by noncommutative geometry, arXiv: 1001.2226

[6] Euro Spallucci and Stefano Ansoldi, Regular black holes in UV self-complete quantum gravity. Phys. Lett. B **701**, 471 (2011); arXiv: 1101.2760.

[7] M. Campanelli and C.O. Lousto, Are black holes in Brans-Dicke theory precisely the same as in general relativity? Int. J. Mod. Phys. D **2**, 451 (1993); gr-qc/9301013.

[8] K.A. Bronnikov, G. Clément, C.P. Constantindis and J.C. Fabris, Cold scalar-tensor black holes: causal structure, geodesics, stability. Grav. Cosmol. **4**, 128 (1998); Phys. Lett. A **243**, 121 (1998).

[9] K.A. Bronnikov, C.P. Constantinidis, R.L. Evangelista and J.C. Fabris, Electrically charged cold black holes in scalar-tensor theories. Int. J. Mod. Phys. D **8**, 481 (1999); gr-qc/9902050.

[10] K.A. Bronnikov, M.S. Chernakova, J.C. Fabris, N. Pinto-Neto, and M.E. Rodrigues, Cold black holes and conformal continuations. Int. J. Mod. Phys. D **17**, 25 (2008); gr-qc/0609084.

[11] R. Casadio, A. Fabbri and L. Mazzacurati, New black holes in the brane-world? Phys. Rev. D **65**, 084040 (2002); gr-qc/0111072.

[12] K.A. Bronnikov, H. Dehnen and V.N. Melnikov, General class of black holes in a brane world. Phys. Rev. D **68**, 024025 (2003); gr-qc/0304068.

[13] T. Shiromizu, K. Maeda and M. Sasaki, The Einstein Equations on the 3-Brane World, Phys. Rev. D **62**, 024012 (2000); gr-qc/9910076.

[14] R. Casadio and L. Mazzacurati, Bulk shape of brane-world black holes. Mod. Phys. Lett. **A 18**, 651 (2003); gr-qc/0205129.

[15] K.A. Bronnikov and J.C. Fabris, Regular phantom black holes. Phys. Rev. Lett. **96**, 251101 (2006); gr-qc/0511109.

[16] K.A. Bronnikov, H. Dehnen and V.N. Melnikov, Regular black holes and black universes. Gen. Rel. Grav. **39**, 973 (2007); gr-qc/0611022.

[17] H. Ellis, Ether flow through a drainhole: A particle model in general relativity. J. Math. Phys. **14**, 104 (1973).

[18] K.A. Bronnikov and E.V. Donskoy, Possible black universes in a brane world. Grav. Cosmol. **16**, 42 (2010); arxiv: 0910.4930.

[19] K.A. Bronnikov and E.V. Donskoy, Black universes with trapped ghosts. Grav. Cosmol. **17**, 31 (2011); arxiv: 1110.6030.

[20] K.A. Bronnikov and S.V. Sushkov, Trapped ghosts: a new class of wormholes. Class. Quantum Grav. **27**, 095022 (2010); arxiv: 1001.3511.

[21] A. Peltola and G. Kunstatter, Complete, single-horizon quantum corrected black hole spacetime. Phys. Rev. D **79**, 061501 (2009); arXiv: 0811.3240.

[22] L. Modesto, Space-time structure of loop quantum black hole, arXiv: 0811.2196.

[23] J.A. González, F.S. Guzmán and O. Sarbach, Instability of wormholes supported by a ghost scalar field. I. Linear stability analysis. Class. Quantum Grav. **26**, 015010 (2009); arxiv: 0806.0608.

[24] K.A. Bronnikov, J.C. Fabris, and A. Zhidenko, On the stability of scalar-vacuum space-times. Eur. Phys. J. C **71**, 1791 (2011); arxiv: 1109.6576.

[25] K.A. Bronnikov, R.A. Konoplya, and A. Zhidenko, in preparation.

[26] K.A. Bronnikov and I.G. Dymnikova, Regular homogeneous T-models with vacuum dark fluid, Class. Quantum Grav. **24**, 5803 (2007); Arxiv: 0705.2368.

[27] K.A. Bronnikov and O.B. Zaslavskii, Matter sources for a Null Big Bang, Class. Quantum Grav. **25**, 105015 (2008); Arxiv: 0710.5618.

Wei-Tou Ni and Vitaly Melnikov

Andrey Doroshkevich, Gennady Bisnovatyi-Kogan and Vitaly Melnikov

Lessons from Schwinger Effective Action for Black Holes

Sang Pyo Kim

Department of Physics, Kunsan National University, Kunsan 573-701, Korea

Email : sangkim@kunsan.ac.kr

Abstract

We revisit the Hawking radiation by comparing the effective actions in the in-out formalism, and advance an interpretation of the vacuum polarization and the Hawking radiation. The equivalence exists between the spinor QED effective action in a constant electric field and the nonperturbative effective action of a massless boson on the horizon of a Schwarzschild black hole.

1 Introduction

Pair production in strong background fields has been one of the most important issues in theoretical physics since the computation of the one-loop effective action in a constant electromagnetic field by Heisenberg and Euler [1] and Schwinger [2] and the discovery of the black hole radiation by Hawking [3]. The virtual pairs from vacuum fluctuations are separated into real pairs by the strong electric field in the Schwinger mechanism and by the causal horizon of the black hole in the Hawking radiation, as summarized in Table 1.

The pair production is accompanied by the vacuum polarization, that is, the real part of the nonperturbative effective action. In quantum electrodynamics (QED), for instance, the mean number of pairs or the vacuum persistence (twice the imaginary part of the effective action) is closed related to the pole structure of the vacuum polarization. In the in-out formalism based on the Schwinger variational principle, the effective action is the scattering matrix amplitude between the in- and the out-vacua, which can be manifestly realized by the Bogoliubov transformation method [4].

In this talk, we revisit the new approach to the vacuum polarization and the Hawking radiation of a Schwarzschild black hole in analogy with the Heisenberg-Euler and Schwinger effective action in QED [5]. Though it results from quantum field theory at one-loop, not from quantum gravity, the nonperturbative effective action, however, may still shed light on quantum aspects of black holes.

Table 1: Strong Field Physics: Analogy between QED and Black Hole

	Strong QED	**Black Hole**
External agent	Electric field	Event horizon
Pair production	Schwinger mechanism	Hawking radiation
Nonperturbative action	Vacuum polarization	Stress tensor

2 Schwinger Mechanism and Effective Action

The vacuum polarization and the pair production have been systematically studied in spinor QED by Heisenberg and Euler and in scalar as well as spinor QED by Schwinger. The vacuum polarization may be written as [2]

$$\mathcal{L}_{\rm eff} = (-1)^{2\sigma} \frac{(1+2\sigma)}{2} \frac{qE}{2\pi} \int \frac{d^2\mathbf{k}_\perp}{(2\pi)^2} \mathcal{P} \int_0^\infty \frac{ds}{s} \exp\Bigl(-\frac{m^2+\mathbf{k}_\perp^2}{2qE} s\Bigr) \times \Bigl[\frac{\cos^{2\sigma}(s/2)}{\sin(s/2)} - \frac{2}{s} + (-1)^{2\sigma}\frac{1-\sigma}{6} s\Bigr], \qquad (1)$$

where $\sigma = 0$ for scalar QED and $\sigma = 1/2$ for spinor QED. The vacuum persistence, twice the sum of residues at simple poles of the vacuum polarization, is given by

$$2{\rm Im}\mathcal{L}_{\rm eff} = (-1)^{2\sigma} \frac{(1+2\sigma)(qE)}{2\pi} \int \frac{d^2\mathbf{k}_\perp}{(2\pi)^2} \ln\Bigl(1 + (-1)^{2\sigma}\mathcal{N}_{\mathbf{k}}\Bigr), \qquad (2)$$

where the mean number of produced pairs and the inverse temperature from the Unruh effect [6] are

$$\mathcal{N}_{\mathbf{k}} = e^{-\beta(\frac{\mathbf{k}_\perp^2}{2m} + \frac{m}{2})}, \quad \beta = \frac{2\pi}{(qE/m)}. \qquad (3)$$

The inversion of spin-statistics has been argued in the vacuum polarization [7, 8] and in the vacuum persistence [6], but its physical origin and meaning has not been understood yet. The Schwinger limit is the critical strength for e^-e^+ pair production, $E_c = m^2/|e| = 1.3 \times 10^{16}$ V/cm.

In the in-out formalism the Schwinger variational principle leads to the effective action [4]

$$e^{iW} = e^{i\int d^Dx\sqrt{-g}\mathcal{L}_{\rm eff}} = \langle 0, {\rm out}|0, {\rm in}\rangle. \qquad (4)$$

The effective action (4) is equivalent to summing the Feynman diagrams in Figure 1. The pair production necessarily makes the effective action complex since $|0,{\rm out}\rangle \neq |0,{\rm in}\rangle$. Further, the vacuum persistence and the mean number of produced pairs are related through

$$e^{-2{\rm Im}W} = |\langle 0,{\rm out}|0,{\rm in}\rangle|^2, \quad 2{\rm Im}W = (-1)^{2\sigma} VT \sum_{\mathbf{k}} \ln[1 + (-1)^{2\sigma}\mathcal{N}_{\mathbf{k}}]. \qquad (5)$$

In the above $2{\rm Im}W/(VT) = 2{\rm Im}\mathcal{L}_{\rm eff}$ is the decay-rate of the in-vacuum per unit volume and per unit time and for a small pair-production rate, $2{\rm Im}\mathcal{L}_{\rm eff} \simeq \sum_{\mathbf{k}} \mathcal{N}_{\mathbf{k}}$.

Recently Kim, Lee and Yoon have further developed the in-out formalism and introduced the gamma-function regularization (Γ-regularization) [9, 10, 11]. The zero-temperature effective action for bosons and fermions is given by

$$\frac{W}{VT} = \mathcal{L}_{\rm eff} = (-1)^{2\sigma} \sum_{\mathbf{k}} \ln \alpha^*_{\mathbf{k}}. \qquad (6)$$

Here $\alpha_{\mathbf{k}}$ is the Bogoliubov coefficient between the out- and the in-vacua for each quantum number $\mathbf{k}$

$$\hat{a}_{{\rm out},\mathbf{k}} = \alpha_{\mathbf{k}} \hat{a}_{{\rm in},\mathbf{k}} + \beta_{\mathbf{k}} \hat{a}^\dagger_{{\rm in},\mathbf{k}}, \qquad (7)$$

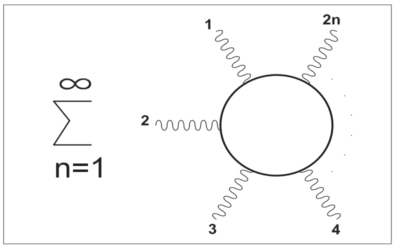

Figure 1: One-loop diagrams: the internal loop denotes a charged particle and the external legs (wave lines) denote the background photons and/or gravitons.

and the coefficients satisfy the relation from the spin-statistics theorem

$$|\alpha_{\mathbf{k}}|^2 + (-1)^{2\sigma}|\beta_{\mathbf{k}}|^2 = 1. \tag{8}$$

The mean number of produced pairs in (5) is given by $\mathcal{N}_{\mathbf{k}} = |\beta_{\mathbf{k}}|^2$. In a constant electric field, the Bogoliubov coefficient may be found from the spin-diagonal component of the Dirac or the Klein-Gordon equation

$$\alpha_{\mathbf{k}} = \frac{\sqrt{2\pi}}{\Gamma(-p)} e^{-i(p\pm1)\frac{\pi}{2}}, \quad p = -\frac{1}{2} \mp \frac{i}{2\pi}\mathcal{S}_{\mathbf{k}}, \tag{9}$$

where the upper (lower) sign is from the time-dependent (Coulomb) gauge and $\mathcal{S}_{\mathbf{k}} = (m^2 + \mathbf{k}_\perp^2 - 2i\sigma qE)/(2qE)$ is the instanton action [10].

Table 2 summarizes the background fields in which the pair production and/or the effective actions have been known. The in-out formalism has proved a consistent and computationally powerful method for the effective action and/or the pair production for an electromagnetic field in a curved spacetime such as de Sitter (dS) space or anti-de Sitter (AdS) space. Since the Bogoliubov coefficients can be derived from the exact solution of the field equation, it is expected that the effective action may be found when the background field and/or the spacetime have certain symmetry, leading to the exact solution. For instance, the Dirac or the Klein-Gordon equation in a constant electric field has the spectrum generating algebra $SU(1,1)$ and dS and AdS spaces have the maximal symmetry of the given dimensions.

3 Vacuum Polarization and Hawking Radiation

The Hawking radiation of bosons and fermions from a charged rotating black hole is given by [17]

$$N_J(\omega) = \frac{1 - |R_J|^2}{e^{\beta(\omega - m\Omega_H - q\Phi_H)} + (-1)^{2\sigma}}, \quad \beta = \frac{1}{k_{\mathrm{B}}T_{\mathrm{H}}}, \quad T_{\mathrm{H}} = \frac{\kappa}{2\pi}. \tag{10}$$

Here R_J is the amplification factor, Ω_H the angular momentum of the hole, Φ_H the electric potential and κ the surface gravity on the event horizon. In the case of the zero amplification factor, the vacuum persistence is

$$2\mathrm{Im}W = -(-1)^{2\sigma} \sum_J \ln(1 - (-1)^{2\sigma} e^{-\beta(\omega - m\Omega_H - q\Phi_H)}). \tag{11}$$

Table 2: Exact Effective Action and/or Pair Production

Background Fields	**EA** and **PP**	**Reference**
Constant EM-field	EA and PP	Heisenberg-Euler [1]
		Schwinger [2]
Sauter-type E-field	PP	Nikishov [12]
Sauter-type E-field	EA and PP	Dunne-Hall [13]
		Kim-Lee-Yoon [9, 10]
E-field in dS and AdS space	PP	Kim-Page [14]
		Kim-Hwang-Wang [15]
dS space	EA and PP	Kim [16]
EA: effective action	PP: pair production	

Note the change of sign in contrary to the QED case.

A four-dimensional Schwarzschild black hole with mass M has the inverse temperature $\beta = 8\pi M$. Denoting $J = \{\omega, l, m, p\}$, with the spherical harmonics l, m and the polarization p and the energy ω, the Bogoliubov coefficients for a massless boson field are found [4]

$$\alpha_J = A_J e^{2\pi M\omega}\Gamma(1+i4M\omega), \quad \beta_J = -A_J e^{-2\pi M\omega}\Gamma(1+i4M\omega). \tag{12}$$

Now the effective action (6) takes the form

$$W = i(8\pi M)\sum_l (2l+1)(2p+1)\int \frac{d\omega}{2\pi}\ln\Gamma(1-i4M\omega). \tag{13}$$

Employing the Γ-regularization, we find the effective action per unit horizon area [5]

$$\mathcal{L}_{\rm eff} = -\frac{1}{16\pi M}\sum_l (2l+1)(2p+1)\int \frac{d\omega}{2\pi}\mathcal{P}\int_0^\infty \frac{ds}{s}e^{-4M\omega s}\Big[\frac{\cos(s/2)}{\sin(s/2)} - \frac{2}{s}\Big]. \tag{14}$$

It is remarkable that the effective action (14) and the vacuum persistence (11) have the form (1) and (2) of spinor QED in a constant electric field.

The vacuum persistence quantifies the decay rate of the vacuum due to the Schwinger mechanism or the Hawking radiation. Further, it is known that the trace anomalies explain the vacuum persistence, that is, the Schwinger mechanism and the Hawking radiation. In fact, the vacuum persistence for bosons per unit horizon area [5]

$$2{\rm Im}\mathcal{L}_{\rm eff} = \sum_l (2l+1)(2p+1)\frac{\pi}{12}\frac{1}{\beta^2}, \tag{15}$$

is equal to the total flux from the gravitational anomalies [18].

4 Conclusion

We have presented the one-loop effective action for QED in a constant electric field and the Hawking radiation of a Schwarzschild black hole in the in-out formalism. It consists of the vacuum polarization and the vacuum persistence responsible for pair production. The prominent feature of the nonperturbative effective action for a Schwarzschild black hole is that it shares many features in common with spinor QED effective action in a constant electric field.

There remain a few questions to be further pursued: firstly, to find the local effective action outside the horizon, secondly, to investigate the amplification (grey body) factor, and thirdly, to find the effective action at two-loop and higher loops. Still another interesting question is the Schwinger effect in a Reissner-Nörstrom black hole. Finally, the origin of spin-statistics inversion of QED differently from gravity challenges a further study [5, 6, 7, 8].

5 Acknowledgements

The author would like to thank W-Y. Pauchy Hwang, Hyun Kyu Lee and Yongsung Yoon for early collaborations and Eun Ju Kang for drawing the figure. The participation of ICGAC10 was supported by Basic Science Research Program through the National Research Foundation of Korea (NRF) funded by the Ministry of Education, Science and Technology (2011-0002-520). The work of this paper was supported in part by National Science Council Grant (NSC 100-2811-M-002-012), Taiwan.

References

[1] W. Heisenberg and H. Euler, *Folgerungen aus der Diracschen Theorie des Positrons*, Z. Phys. 98 (1936) 714.

[2] J. Schwinger, *On gauge invariance and vacuum polarization*, Phys. Rev. 82 (1951) 664.

[3] S. W. Hawking, *Particle creation by black holes*, Commun. Math. Phys. 43 (1975) 199.

[4] B. S. DeWitt, *Quantum Field Theory in Curved Spacetime*, Phys. Rept. 19 (1975) 295.

[5] S. P. Kim and W-Y. P. Hwang, *Vacuum Polarization and Persistence on the Black Hole Horizon* [arXiv:1103.5264].

[6] W-Y. P. Hwang and S. P. Kim, *Vacuum persistence and inversion of spin statistics in strong QED*, Phys. Rev. D 80 (2009) 065004.

[7] B. Müller, W. Greiner and J. Rafelski, *Interpretation of external fields as temperature*, Phys. Lett. A 63 (1977) 181.

[8] L. Labun and J. Rafelski, *Acceleration and Vacuum Temperature*, [arXiv:1203.6148].

[9] S. P. Kim, H. K. Lee and Y. Yoon, *Effective Action of Scalar QED in Electric Field Backgrounds*, Phys. Rev. D 78 (2008) 105013.

[10] S. P. Kim, H. K. Lee and Y. Yoon, *Action of QED in Electric Field Backgrounds II. Spatially Localized Fields*, Phys. Rev. D 82 (2010) 025015.

[11] S. P. Kim, *Probing the Vacuum Structure of Spacetime* [arXiv:1102.4154].

[12] A. I. Nikishov, *Barrier scattering in field theory removal of Klein paradox*, Nucl. Phys. B 21 (1970) 346.

[13] G. V. Dunne and T. M. Hall, *QED effective action in time dependent electric backgrounds*, Phys. Rev. D 58 (1998) 105022.

[14] S. P. Kim and D. N. Page, *Schwinger pair production in dS_2 and AdS_2*, Phys. Rev. D 78 (2008) 103517.

[15] S. P. Kim, W-Y. Pauchy Hwang and T-C. Wang, *Schwinger mechanism in dS_2 and AdS_2 revisited* [arXiv:1112.0885].

[16] S. P. Kim, *Vacuum Structure of de Sitter Space* [arXiv:1008.0577].

[17] D. N. Page, *Hawking radiation and black hole thermodynamics*, New J. Phys. 7 (2005) 203.

[18] S. P. Robinson and F. Wilczek, *Relationship between Hawking Radiation and Gravitational Anomalies*, Phys. Rev. Lett. 95 (2005) 011303.

Viscosity and Black Holes

Dam Thanh Son
Institute for Nuclear Theory, University of Washington, Seattle, WA 98195-1550, USA
Email : dtson@uw.edu

Abstract

We review recent applications of the AdS/CFT correspondence in strongly coupled systems, in particular the quark gluon plasma.

1 Introduction

The discovery of Hawking radiation[1] confirmed that black holes are endowed with thermodynamic properties such as entropy and temperature, as first suggested by Bekenstein[2] based on the analogy between black hole physics and equilibrium thermodynamics. For black branes, i.e., black holes with translationally invariant horizons, thermodynamics can be extended to *hydrodynamics*—the theory that describes long-wavelength deviations from thermal equilibrium. Thus, black branes possess hydrodynamic properties of continuous fluids and can be characterized by kinetic coefficients such as viscosity, diffusion constants, etc. From the perspective of the holographic principle[3, 4], the hydrodynamic behavior of a black-brane horizon is identified with the hydrodynamic behavior of the dual theory.

In this talk, we argue that in theories with gravity duals, the ratio of the shear viscosity to the volume density of entropy is equal to a universal value of $\hbar/4\pi$. A lot of attention has been given to this fact due to the discovery of a perfect liquid behavior at RHIC. We will also review recent attempts to extend AdS/CFT correspondence to nonrelativistic systems.

2 Dimension of η/s

The standard textbook definition of the shear viscosity is as follows. Take two large parallel plates separated by a distance d. The space between the two plates is filled with a fluid. Let one plate moves relative to the other with a velocity v. Then the drag force acting on a unit area of the plate is

$$\frac{F}{A} = \eta \frac{v}{d} \tag{1}$$

which defines the viscosity η. It is measured in kg m^{-1} s^{-1}. In d spatial dimensions, shear viscosity η is measured in kg m^{2-d} s^{-1}. The volume density of entropy s is measured in m^{-d} (in units where the Boltzmann constant k_B is set to one). The ratio η/s thus has the dimension of kg m^2 s^{-1}, i.e., the same as the Planck constant $\hbar$. This observation is more than merely a curiosity, as we shall see shortly.

3 Viscosity from dual gravity description

Consider a field theory dual to a black-brane metric. One can have in mind, as an example, the $\mathcal{N} = 4$ supersymmetric Yang-Mills theory dual to the the near-extremal D3 brane in type IIB supergravity,

$$ds^2 = \frac{r^2}{R^2}(-f dt^2 + dx^2 + dy^2 + dz^2) + \frac{R^2}{r^2 f}dr^2, \qquad f = 1 - \frac{r_0^4}{r^4}\,, \tag{2}$$

but our discussion is not tied to any specific form of the metric. All black branes have an event horizon ($r = r_0$ for the metric (2)), which is extended along several spatial dimensions ($x,\ y,\ z$ in the case of (2)). The dual field theory is at a finite temperature, equal to the Hawking temperature of the black brane.

The entropy of the dual field theory is equal to the entropy of the black brane, which is proportional to the area of its event horizon,

$$S = \frac{A}{4G}\,, \tag{3}$$

where G is the Newton constant (we set $\hbar = c = 1$). For black branes A contains a trivial infinite factor V equal to the spatial volume along directions parallel to the horizon. The entropy density s is equal to $a/(4G)$, where $a = A/V$.

The shear viscosity of the dual theory can be computed from gravity in a number of approaches[5, 6, 7]. Here we use Kubo's formula, which relates viscosity to equilibrium correlation functions. In a rotationally invariant field theory,

$$\eta = \lim_{\omega\to 0} \frac{1}{2\omega} \int dt\, d\vec{x}\, e^{i\omega t}\, \langle [T_{xy}(t,\vec{x}),\, T_{xy}(0,\mathbf{0})]\rangle\,. \tag{4}$$

Here T_{xy} is the xy component of the stress-energy tensor (one can replace T_{xy} by any component of the traceless part of the stress tensor). We shall now relate the right hand side of (4) to the absorption cross section of low-energy gravitons.

According to the AdS/CFT correspondence[8], the stress-energy tensor $T_{\mu\nu}$ couples to metric perturbations at the boundary. Following Klebanov[9], let us consider a graviton of frequency ω, polarized in the xy direction, and propagating perpendicularly to the brane. In the field theory picture, the absorption cross section of the graviton by the brane measures the imaginary part of the retarded Greens function of the operator coupled to h_{xy}, i.e., T_{xy},

$$\sigma_{\rm abs}(\omega) = -\frac{2\kappa^2}{\omega}\,{\rm Im}\,G^{\rm R}(\omega) = \frac{\kappa^2}{\omega}\int dt\, d\vec{x}\, e^{i\omega t}\, \langle [T_{xy}(t,\vec{x}),\, T_{xy}(0,\mathbf{0})]\rangle\,, \tag{5}$$

where $\kappa = \sqrt{8\pi G}$ appears due the normalization of the graviton's action. Comparing (4) and (5), one finds

$$\eta = \frac{\sigma_{\rm abs}(0)}{2\kappa^2} = \frac{\sigma_{\rm abs}(0)}{16\pi G}\,. \tag{6}$$

The absorption cross section $\sigma_{\rm abs}$, on the other hand, is calculable classically by solving the linearized wave equation for h^x_y. It can be shown (see Appendix) that under rather general assumptions the equation for h^x_y is the same as that of a minimally coupled scalar. The absorption cross section for the scalar is constrained by a theorem[10, 11], which states that in the low-frequency limit $\omega \to 0$ this cross section is equal to the area of the horizon, $\sigma_{\rm abs} = a$. Since $s = a/4G$, one immediately finds that

$$\frac{\eta}{s} = \frac{\hbar}{4\pi}\,, \tag{7}$$

where $\hbar$ is now restored. This shows that the ratio η/s does not depend on the concrete form of the metric within the assumptions of[10, 11].

Indeed, explicit calculations of the viscosity using the AdS/CFT correspondence or the "membrane paradigm" technique show that the ratio η/s is the $1/(4\pi)$ for Dp[5, 7], M2 and M5[12] branes and $\mathcal{N}=2^*$ deformations of the D3 metric[7, 13].

Dual gravity description of gauge theories is valid in the regime of infinitely strong coupling. As Eq. (7) shows, in this regime the ratio η/s appears to be universal (independent of the coupling constant and other microscopic details of the theory). Let us now argue that the ratio η/s approaches infinity in the limit of vanishing coupling.

The entropy density s of a weakly coupled system is proportional to the number density of quasiparticles n,

$$s \sim n\,. \tag{8}$$

The shear viscosity is proportional to the product of the energy density and the mean free time (time between collisions) τ

$$\eta \sim n\epsilon\tau\,, \tag{9}$$

where ϵ is the average energy per particle (which is of the order of the temperature T). Therefore

$$\frac{\eta}{s} \sim \epsilon\tau\,. \tag{10}$$

Now, in order for the quasiparticle picture to be valid, the width of the quasiparticles must be small compared to their energies, i.e., one should have

$$\frac{\hbar}{\tau} \ll \epsilon \tag{11}$$

which means that

$$\frac{\eta}{s} \gg \hbar\,. \tag{12}$$

The observation that η/s is a constant in strongly coupled theories with gravity dual and is large in weakly coupled theories prompts us to formulate the "viscosity bound" conjecture: in any finite-temperature field theory, the ratio of shear viscosity to entropy density cannot be smaller than the value of this ratio in theories with gravity duals:

$$\frac{\eta}{s} \geqslant \frac{\hbar}{4\pi}\,. \tag{13}$$

As we have seen, the bound (13) can be understood as a consequence of the uncertainty principle: the product of the energy and the mean free time of a quasiparticle cannot be smaller than $\hbar$. The precise numerical coefficient $1/(4\pi)$ cannot, however, be obtained from the uncertainty principle alone.

It turns out that the viscosity bound is can be violated by corrections proportional to $1/N_c$, where N_c is the number of colors [14, 15]. It still seems that there is a lower bound on η/s. In one particular model, causality is violated when one tries to make η/s smaller than 64% of $1/4\pi$ [16].

4 Nonrelativistic holography

The nonrelativistic equivalence of $\mathcal{N}=4$ SYM theory is the Fermi gas at unitarity. The symmetry of the system is the Schrödinger symmetry. Recently, a metric has been found that realizes this symmetry [17, 18]:

$$ds^2 = -2\frac{dx^+}{z^4} + \frac{-2dx^+dx^- + d\vec{x}^2 + dz^2}{z^2} \tag{14}$$

Furthermore, it has been found that this metric can be realized in string theory [19, 20, 21]. The shear viscosity satisifies $\eta/s = 1/4\pi$. The thermal conductivity has also been calculated; its value corresponds to the Prandtl number equal to 1 [22].

References

[1] S. W. Hawking, Commun. Math. Phys. **43**, 199 (1975).

[2] J. D. Bekenstein, Phys. Rev. **D7**, 2333 (1973).

[3] G. 't Hooft, gr-qc/9310026.

[4] L. Susskind, J. Math. Phys. **36**, 6377 (1995).

[5] G. Policastro, D. T. Son and A. O. Starinets, Phys. Rev. Lett. **87**, 081601 (2001).

[6] G. Policastro, D. T. Son and A. O. Starinets, J. High Energy Phys. **0209**, 043 (2002).

[7] P. Kovtun, D. T. Son and A. O. Starinets, J. High Energy Phys. **0310**, 064 (2003).

[8] For review, see: O. Aharony, S. S. Gubser, J. M. Maldacena, H. Ooguri and Y. Oz, Phys. Rep. **323**, 183 (2000).

[9] I. R. Klebanov, Nucl. Phys. **B496**, 231 (1997).

[10] S. R. Das, G. W. Gibbons and S. D. Mathur, Phys. Rev. Lett. **78**, 417 (1997).

[11] R. Emparan, Nucl. Phys. **B516**, 297 (1998).

[12] C. P. Herzog, J. High Energy Phys. **0212**, 026 (2002).

[13] A. Buchel and J. T. Liu, Phys. Rev. Lett. **93**, 090602 (2004).

[14] Y. Kats and P. Petrov, JHEP **0901**, 044 (2009).

[15] A. Buchel, R. C. Myers and A. Sinha, arXiv:0812.2521 [hep-th].

[16] M. Brigante, H. Liu, R. C. Myers, S. Shenker and S. Yaida, Phys. Rev. Lett. **100**, 191601 (2008).

[17] D. T. Son, Phys. Rev. D **78**, 046003 (2008).

[18] K. Balasubramanian and J. McGreevy, Phys. Rev. Lett. **101**, 061601 (2008).

[19] C. P. Herzog, M. Rangamani and S. F. Ross, JHEP **0811**, 080 (2008).

[20] J. Maldacena, D. Martelli and Y. Tachikawa, JHEP **0810**, 072 (2008).

[21] A. Adams, K. Balasubramanian and J. McGreevy, JHEP **0811**, 059 (2008).

[22] M. Rangamani, S. F. Ross, D. T. Son and E. G. Thompson, JHEP **0901**, 075 (2009).

Computation of black hole entropy from Ashtekar-Wheeler-DeWitt field theory

Chopin Soo
National Cheng Kung University, Tainan, Taiwan
Email : cpsoo@mail.ncku.edu.tw

Abstract

Canonical quantization of spherically-symmetric Ashtekar-Wheeler-DeWitt midisuperspace theory is performed. Semiclassical states, with integration constant identified with the mass parameter of black holes, are solved exactly from the Hamilton-Jacobi equation. These states can be matched to Schwarzschild spacetimes in usual standard spherically-symmetric form and also in Painleve-Gullstrand form. The Hamilton function remains well-defined at the classical singularity; and it has an imaginary contribution (independent of the Immirzi parameter in Ashtekar-Barbero theory) which can be interpreted as yielding the correct Bekenstein-Hawking entropy-area relation.

1 Introduction

Black holes are spherically symmetric classical solutions of Einstein's equations. It is reasonable to expect many of their properties can be understood and derived from semiclassical states of Einstein's theory in the spherically-symmetric sector. In particular, it makes sense to seek a simple and clean derivation of the Bekenstein-Hawking area-entropy relation, and an understanding of its origin by solving for the exact semiclassical Hamilton-Jacobi function in spherically symmetric quantum gravity[1].

1.1 Constraints in the spherically-symetric sector

For the spherically-symmetric sector, the Killing vectors are just the usual orbital angular momentum operators. Since the theory in the Ashtekar formulation[2] has local internal gauge symmetry, we require the Lie derivatives of the basic variables with respect to the Killing vectors to vanish only modulo local $SO(3)$ (with generators denoted by $T_{1,2,3}$) gauge transformations. Labeling spatial coordinates by (x, θ, φ), the generic spherically-symmetric connection, and the conjugate densitized triads are then[3]

$$\begin{aligned} A &= a_3 T_3 dx + [a_1 \tau_1 + a_2 T_2]\, d\theta + [-a_1 T_2 + a_2 T_1] \sin\theta d\varphi + T_3 \cos\theta d\varphi, \\ \tilde{E} &= z T_3 \sin\theta \partial_x + [r\cos\Theta T_1 + r\sin\Theta T_2] \sin\theta \partial_\theta + [r\cos\Theta T_2 - r\sin\Theta T_1]\, \partial_\varphi; \end{aligned} \tag{1}$$

and the spatial three-metric is $ds^2 = \frac{r^2(x)}{z(x)} dx^2 + z(x)\, d\Omega^2$. The dynamical variables (r, z, Θ) and their conjugate momenta are functions only of x but independent of θ and φ.

In the spherically-symmetric sector, the quantum Gauss Law constraint in the Ashtrekar formulation:

$$\hat{\tilde{G}}(x)\Phi[r, z, \Theta] = \left[z' - 2i\gamma\ell_p^2 \frac{\delta}{\delta\Theta} \right] \Phi[r, z, \Theta] = 0 \tag{2}$$

has the exact solution:

$$\Phi[r, z, \Theta] = Q\Psi[r, z] \tag{3}$$

wherein $Q = e^{\frac{iF[\tilde{E}]}{\kappa\gamma\hbar}}$ with $F[\tilde{E}] \equiv \int_\Sigma d^3x\, \Gamma^i_a \tilde{E}^a_i = 4\pi \int dx\, \Theta' z$ being precisely the generating function of the canonical transformation between Ashtekar variables with densitized triad and gauge connection $(\tilde{E}^{ai}, A_{ai} = \gamma K_{ai} + \frac{\delta F}{\delta \tilde{E}^{ai}} = \frac{\gamma\kappa\hbar}{i} Q^{-1} \frac{\delta}{\delta \tilde{\mathcal{E}}^{ai}} Q)$ and ADM variables with densitized triad and extrinsic curvature $(\tilde{\mathcal{E}}^{ai} = \tilde{E}^{ai}, K_{ai})$. Therefore, while $\Phi[r, z, \Theta]$ is the wave function for the Ashtekar theory, $\Psi[r, z] = Q^{-1}\Phi[r, z, \Theta]$ can be identified with the Wheeler-DeWitt wave function[4].

The quantum diffeomorphism constraint (modulo Gauss Law) and Hamiltonian constraint operate on $\Psi[r, z] = Q^{-1}\Phi[r, z, \Theta]$. For semiclassical states $\Psi[r, z] = e^{iS[r,z]/\hbar}$, the consequent restrictions are

$$z' \frac{\delta S}{\delta z} - r \frac{d}{dx} \frac{\delta S}{\delta r} = 0, \quad [\frac{1}{4} r^2 (\frac{\delta S}{\delta r})^2 + z\, r \frac{\delta S}{\delta z} \frac{\delta S}{\delta r}] + \frac{r^2 z\, ({}^3R - 2\Lambda)}{8G^2} = 0; \tag{4}$$

and the solution for the Hamilton-Jacobi function $S[r, z]$ is

$$S_m[r, z] = -\frac{1}{G} \int dx \left[\frac{r}{z^{1/4}} \sqrt{2m - W} \right] + \frac{z'}{2} \ln \left(\frac{z^{1/4} z'}{2r} - \sqrt{2m - W} \right) \Bigg], \tag{5}$$

with $W(x) := \sqrt{z}\left(1 - \frac{z'^2}{4r^2}\right)$. These states can be matched to Schwarzschild spacetimes in usual standard spherically-symmetric form and also in Painleve-Gullstrand form by comparing the semiclassical phase space variables $(r, z; p_r, p_z)$ with the spatial metic and extrinsic curvatures of the corresponding Schwarzschild metrics yielding, in particular, the correspondence $\sqrt{z} = R$, the radial coordinate of the black hole.

1.2 Semiclassical states, black hole entropy and Bekenstein-Hawking relation

Remarkably, due to the particular form of the exact semiclassical wave function, whenever $1 - \frac{2m}{\sqrt{z}} < 0$, the logarithm in the integrand of S_m acquires an $i\pi$ factor, and the imaginary contribution to the Hamilton-Jacobi function is

$$\mathrm{Im}(S_m) = G^{-1} \int dx\, \frac{z'}{2}\, \pi = \frac{\pi}{2G} \int_0^{z_H} dz = \frac{\pi z_H}{2G}; \tag{6}$$

wherein $z_H : 1 - \frac{2m}{\sqrt{z_H}} = 0$. This yields $\sqrt{z_H} = 2m$, the Schwarzschild radius. Thus $\mathrm{Im}(S) = \frac{\pi z_H}{2G} = \frac{A_H}{8G}$ wherein $A_H = 4\pi(2m)^2$ is precisely the area of the classical black hole event horizon!

For each semiclassical physical state S_m corresponding to a classical black hole solution of mass m, the wave function has the form $\langle r, z|\Psi_m\rangle = e^{-\frac{A_H}{8\hbar G} + \frac{i}{\hbar}\mathrm{Re}[S_m]}$ with norm $\langle \Psi_m|\Psi_m\rangle = \exp(-\frac{A_H}{4l_p^2})(\int drdz)$. Superpositions of semiclassical states do not solve the Hamilton-Jacobi equation which is non-linear in the momenta. The *total* normalized density matrix describing semiclassical distribution with different masses is mixed,

$$\rho = \frac{1}{\int dm' \langle \Psi_{m'}|\Psi_{m'}\rangle} \int dm\, |\Psi_m\rangle\langle\Psi_m| = \frac{1}{\int dm'\, \omega_{m'}} \int dm\, \omega_m |\Psi'_m\rangle\langle\Psi'_m|; \tag{7}$$

wherein $\omega_m = e^{-\frac{A_H}{4\hbar G}}$, and $\int_0^\infty dm\, \omega_m = \frac{l_p}{4}$. This yields the interpretation that the semiclassical entropy of *each* black hole configuration of mass m is $S^m_{\mathrm{bh}} = -\kappa_{\mathrm{B}} \ln \omega_m = \frac{\kappa_{\mathrm{B}} A_H}{4l_p^2}$, which is exactly the Bekenstein-Hawking entropy-area relation *independent of the Immirzi parameter* γ. Each semiclassical state with integration constant m can be matched to a classical black hole solution, and each semiclassical state comes with an exponential factor depending only on m which can be interpreted as the probability for the configuration with semiclassical state $|\Psi'_m\rangle$ in a total mixed semiclassical density matrix which permits all values of m to appear.

The "problem of time" in the normalization of the wavefunction can be addressed: suppose a certain combination $f(r,z)$ is adopted as the internal clock; then the requirement of normalization at a particular time $f(r,z) = T$ merely changes the normalization condition discussed above to $\langle\Psi_m|\Psi_m\rangle|_T = e^{-\frac{A_H}{4\hbar G}}(\int \delta(f(r,z) - T)drdz)$. This only entails the replacement of $(\int drdz)$ by $(\int \delta(f(r,z) - T)drdz)$ without altering the conclusions.

Acknowledgements: This work has been supported in part by the Nat. Science Council of Taiwan under Grant Nos. NSC 98-2112- M-006-006-MY3 and 99-2811-M-006-015, and by the Nat. Center for Theoretical Sciences, Taiwan.

References

[1] C. H. Chou, C. Soo and H. L. Yu, *Black holes and Rindler superspace: classical singularity and quantum unitarity* Phys. Rev. D76 (2007) 084004-1.

[2] A. Ashtekar, *New variables for classical and quantum gravity*, Phys. Rev. Lett. 57 (1986) 2244; *New hamiltonian formulation of general relativity* Phys. Rev. D36 (1987) 1587.

[3] P. Forgacs and N. S. Manton *Space-Time Symmetries in Gauge Theories* Commun. Math. Phys. 72 (1980) 15.

[4] Bryce S. DeWitt, *Quantum Theory of Gravity. I. The Canonical Theory* Phys. Rev. **160**, 1113 (1967); J. A. Wheeler, *Superspace and the nature of quantum geometrodynamics*, Battelle Rencontres, edited by C. M. DeWitt and J. A. Wheeler, W. A. Benjamin, New York (1968).

Some Interesting Properties of A White Hole in The Vector Model for Gravitational Field

Vo Van On

University of Thu Dau Mot, S.R Vietnam

Email : onvv@tdmu.edu.vn

Abstract

There is a strange macro object existing in the vector model for gravitational field, which we called white hole. In this paper we show some its interesting properties as the surface vibration, very high gravitational red shift and blue shift. We consider also the radial motion of a particle into the white hole.

1 White holes in the vector model for gravitational field

In the vector model for gravitational field, we assume that gravitational field is a vector field, its source is the gravitational mass of matter. Along with the energy-momentum tensor of matter, this vector field contributes to warp the space - time by the following equation([1])

$$R_{\mu\nu} - \frac{1}{2}g_{\mu\nu}R - g_{\mu\nu}\Lambda = -\frac{8G\pi}{c^4}(T_{Mg.\mu\nu} + \omega' T_{g.\mu\nu}) \tag{1}$$

where $T_{Mg,\mu\nu}$ is the energy - momentum tensor of matter. $T_{g,\mu\nu}$ is the energy-momentum tensor of the gravitational field. From this equation, we have obtained a metric of space - time outside a non rotating, non charged spherically symmetric object as follows([2], [3])

$$ds^2 = c^2(1 - 2\frac{GM_g}{c^2 r} - \omega'\frac{G^2M_g^2}{c^4r^2})dt^2 - (1 - 2\frac{GM_g}{c^2r} - \omega'\frac{G^2M_g^2}{c^4r^2})^{-1}dr^2 - r^2(d\theta^2 + \sin^2\theta d\varphi^2) \tag{2}$$

Where M_g is the gravitational mass of the object.
From experimental data in the Solar system, we have found that $/\omega'/ \approx 0.06$.([2]) The graph of $e^\nu = 1 - 2\frac{GM_g}{c^2r} - \omega'\frac{G^2M_g^2}{c^4r^2}$ is showed in fig.1.

We calculate radii r_1,r_2 for the Sun with mass M_S and an any object with mass M when $\omega' \approx -0.06$

- with $M_S = 2\times 10^{30}kg$: $r_1 \approx 0.045km$, $r_2 \approx 2.9543km$, $r_S \approx 3km$
- with M: $r_1 \approx \frac{M}{M_S}\times 0.045km$, $r_2 \approx \frac{M}{M_S}\times 2.9543km$.

Thus, due to the gravitational collapse, firstly from the radius r_2 the body becomes a black hole but then to the radius r_1 it becomes visible. Therefore, this model predicts the existence of a new universal body after a black hole disappeared, we call it to be the white- black hole in the vector model for gravitational field.

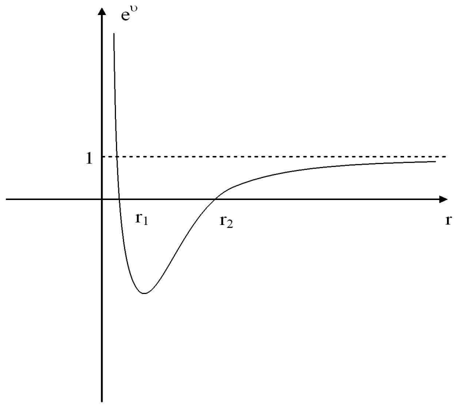

Figure 1: *Black hole starts from* $r_2 \rightarrow r_1$ *, white hole starts from* $r_1 \rightarrow 0$

2 Properties of a white hole

2.1 Surface vibrations of a white hole

In this section, we consider only first- order approximation of the surface vibration of a white hole with gravitational mass M_g , a better approximation will be considered in an other paper. Because this is a period after the black hole was formed, so the attractive force and repulsive force from the center are very greater than the pressure within the object, so we ignore the pressure. From the metric (2) we have

$$g_{00} = (1 - 2\frac{GM_g}{c^2 r} + 0.03\frac{G^2 M_g^2}{c^4 r^2}) = (1 - 2\frac{\varphi_g}{c^2}) \tag{3}$$

therefore the motion of a material element m_i at the surface of the object M_g is described by the equation

$$r'' = (-\frac{GM_g}{r^2} + 0.03\frac{G^2 M_g^2}{c^2 r^3}) \tag{4}$$

We can set

$$r = r_1 + \delta r \tag{5}$$

Retaining only the first degree of small parameter, we have the following equation

$$\delta r'' = -\omega^2 \delta r \tag{6}$$

with $a = GM_g; b = 0.03\frac{G^2 M_g^2}{c^2}$ and $\omega^2 = r_1^{-3}(\frac{3b}{r_1} - 2a)$. From equation(6), we see that the surface of the sphere r_1 takes a quasi-harmonic oscillation.

2.2 The red shift and the blue shift of a white hole

A special property of white holes in the model is the gravitational red and blue shift. In this model, the formula of the gravitational shift Z is

$$Z = (1 - \frac{r_S}{r} + 0.015\frac{r_S^2}{r^2})^{-1/2} - 1 \tag{7}$$

From the formula(7),the red and blue shift Z is follows: a/the region I (normal object), $r : \infty \to r_2$ with red shift $Z : 0 \to +\infty$; b/the region II (black hole), $r : r_2 \to r_1$; c/the region III (white hole), $r : r_1 \to r_0$ with red shift $Z : +\infty \to 0$; d/ the region IV (a white hole) $r : r_0 \to 0$ with blue shift $Z : 0 \to -1$
The graph of Z as a function of r is shown in the fig.2 and fig.3.

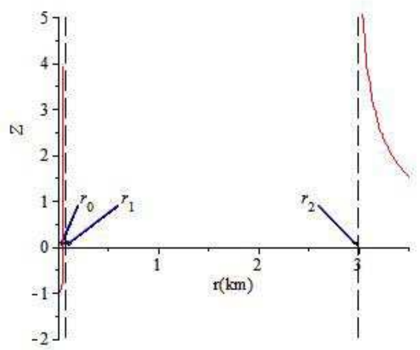

Figure 2: *A white-black hole with mass M_{Sun} has the radii as follows:* $r_0 = 0.045km; r_1 = 0.04596km; r_2 = 2.9543km$

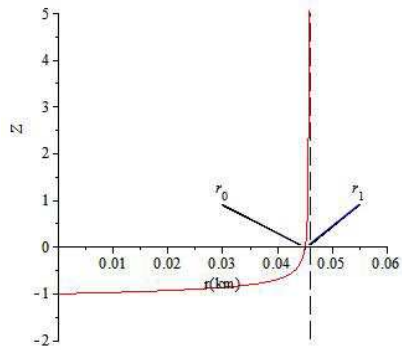

Figure 3: *A white hole with mass M_{Sun} has the radii as follows:* $r_0 = 0.045km; r_1 = 0.04596km$

3 Radial motion of a particle into a white hole

We consider a particle falling radially into the central body, the motion can be described by the geodesic equation

$$\frac{dv^\mu}{ds} + \Gamma^\mu_{\nu\sigma} v^\nu v^\sigma = 0 \tag{8}$$

The result is the particle takes an infinite time to reach to the radius $r_2 = 0.985r_S$

$$t = -1.0467r_2 \ln(r - r_2) + C \tag{9}$$

When the particle falling into the white hole, the regions III and IV ,the particle takes also a finite time to reach to the radius zero and an infinite time to reach to the radius $r_1 = 0.1532r_S$

$$t = -0.0513r_1 \ln(r_1 - r) + C \tag{10}$$

4 Discussions

With the strange properties of the white holes in the vector model for gravitational field as above discussion, what can the candidates of white holes be ? In our opinion, the candidates of white holes can be quasars! Quasars have the properties as follows([4]): - Quasars have the high red shift, - Quasars have the sizes are small by observed data, - Quasars have the variation of the brightness in the optical domain and the x-ray domain. - Have not observed quasars blue shift yet. A more detailed research of the problem shall do in the future.

References

[1] Vo Van On,*Einstein's equation in the vector model for gravitational field*, Science and Technology Development Journal **10**,n.6(2007),pp.15-25.

[2] Vo Van On,*Absence of singularity in Schwarzschild metric in the vector model for gravitational field*, Communications in Physics,**18**(2008) pp.175-184

[3] Vo Van On,*A vector model for gravitational field in curvature space-time*, KMITL Science Journal,**8**(2008),pp. 1-11.

[4] F.D. Kahn and H.P. Palmer, Quasars: Their Importance in Astronomy and Physics, The University of the Manchester at the university Press(1967),pp.12-47

Chopin Soo, Eyo Ita, Hoi-Lai Yu and Hai-Yang Cheng

A view of the audience; the site of the ICISE can be glimpsed through the scaffolding

Cosmology

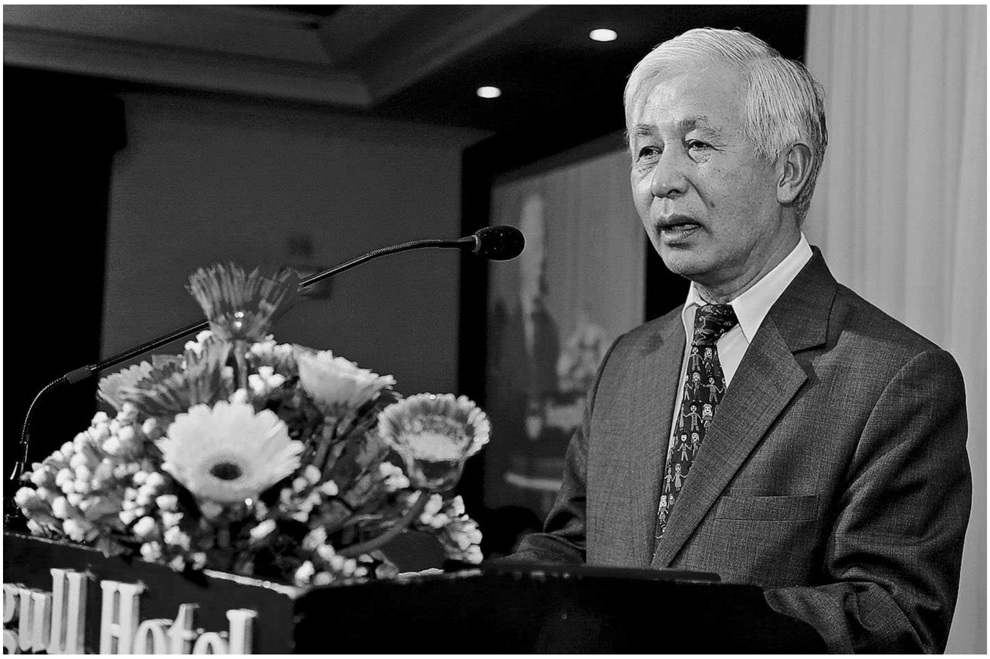

Jean Trân Thanh Van at the welcome party

The president Lê Huu Lôc at the welcome party

Recent results on measurements and interpretation of CMB fluctuations

A. Doroshkevich
Astro Space Center FIRAN, Moscow, Russia
dorr@asc.rssi.ru

Abstract

In this presentation we shortly consider the progress achieved in investigations of the cosmic microwave background (CMB) radiation and discuss some of possible cosmological implications of these investigations.

1 Introduction

During last ten years high progress had been achieved in investigations of the cosmic microwave background (CMB) radiation and its fluctuations. First of all this is the 7 years observations of the WMAP mission [1], [2], [3]. These observations were performed for multipoles $2 \leq \ell \leq 900$ at frequencies 23, 30, 40, 60, and 90 GHz. However further on this information was significantly extended by the ground observations, such as, [4] at frequencies 95, 150 and 220 GHz, [5] at frequencies 100 and 150 GHz, and [6] at frequencies 148, 218 and

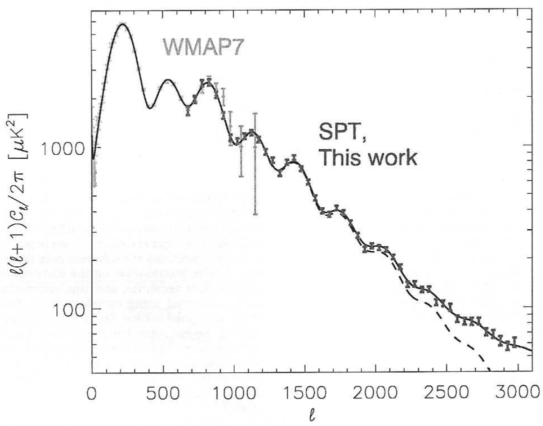

Figure 1: Power spectrum of the CMB fluctuations [4]

227 GHz. Thus now we observe the power spectrum of the CMB fluctuations up to the multipole number $\ell \sim 3000$. For larger ℓ the CMB fluctuations are masked by radiation of the aromatic dust concentrated within galaxies at redshifts $z \sim 2$. It is important also that together with observations of temperature fluctuations their polarization was also measured.

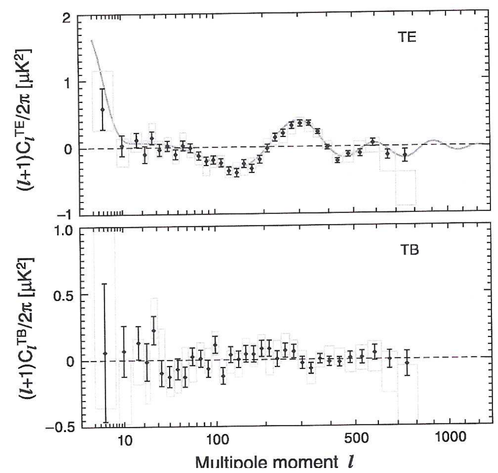

Figure 2: E and H modes of the polarization of the CMB fluctuations [3]

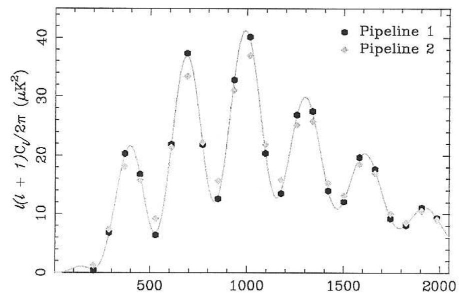

Figure 3: E modes of the polarization of the CMB fluctuations for larger multipoles [5]

2 Main results of the CMB measurements

Main results of the CMB measurements are presented in Figs. 1, 2 and 3.

Comparison of the positions and shapes of observed peaks with expectations of linear theory allows to formulate valuably the standard ΛCDM cosmological model with the domination of the dark energy at small redshifts, to measure accurately the density of the dark matter and baryonic component. Now we can approximately estimate the period of secondary ionization of the Universe z_{reio} and find with a reasonable precision the shape and amplitude of the primeval power spectrum. Moreover the high difference between amplitudes of E and H modes polarizations presented in Fig. 2 significantly restricts some popular versions of the inflationary models.

Table 1: Main parameters of the standard ΛCDM cosmological model [3]

parameter	7year	5year
Ω_Λ	0.734 ± 0.03	0.742 ± 0.030
$\Omega_{DM}h^2$	0.111 ± 0.006	0.110 ± 0.006
$10\Omega_b h^2$	0.226 ± 0.006	0.227 ± 0.006
n_s	0.963 ± 0.014	0.963 ± 0.014
τ	0.088 ± 0.015	0.087 ± 0.017
H_0	$71 \pm 2.5 km/s$	$72 \pm 2.7 km/s$
σ_8	0.801 ± 0.03	0.796 ± 0.036
z_{reio}	10.5 ± 1.2	11.0 ± 1.4

Here Ω_Λ, Ω_{DM} and Ω_b are the dimensionless density of the dark energy, dark matter and baryonic component correspondingly, H_0 is the Hubble const. and $h = H_0/70km/s$ is the dimensionless Hubble const., n_s is the power index of the large scale power spectrum and σ_8 measures the amplitude of perturbations. τ and z_{reio} are the reionization optical depth and redshift.

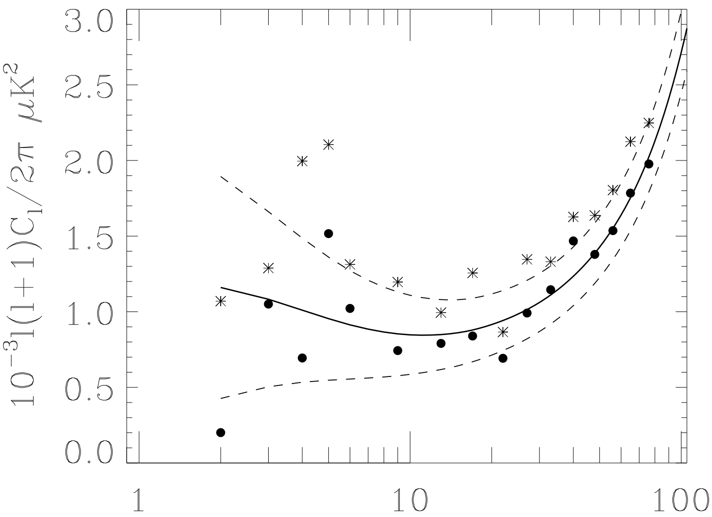

Figure 4: The $10^{-3}\Delta T^2$ for the WMAP data (points) and obtained according to the QV method (stars). Solid and dashed lines show the theoretically expected values and their scatter [8].

3 Some anomalies of the WMAP results

As is well known the discrimination between the CMB signal and various foregrounds (both galactical and extragalactical) is the typical *incorrect* problem because even for multi frequencies observations the number of unknown variables is larger then number of measurements. Various methods for solution such problems are well developed and one of them – namely the Internal Linear Combination (ILC) method – is described in details in [7].

Results obtained with the ILC method are quite reasonable. But more detailed analysis reveals four anomalies of the WMAP results. These are the small amplitude of the quadrupole ($\delta T^2 \approx 249K^2$ instead of the expected $\delta T^2 \approx 1250K^2$), the noticeable correlation between orientation of quadrupole and octopole (axis of evil), some asymmetry between temperatures fluctuations in north and south hemispheres, and existence of four deep valleys of cooler temperature at south hemisphere. In paper [2] these anomalies are explained as random statistical fluctuations.

Table 2: For Q and V bands of the WMAP-7 data, amplitudes of the quadrupole, a_{2m}, and the octopole a_{3m}, are listed in μK [8].

	WMAP		QV method	
m	$\ell = 2$	$\ell = 3$	$\ell = 2$	$\ell = 3$
0	11.77	-6.48	-65.21	1.59
1	-0.77	-12.19	-13.86	-21.50
-1	6.21	2.03	8.97	-0.32
2	-14.12	21.99	-17.34	19.80
-2	-17.94	0.59	-10.98	4.03
3	–	-11.71	–	-7.90
-3	–	33.55	–	36.40

However more detailed analysis of the problem separation of the CMB signal and foregrounds demonstrates ([8]) that the ILC method is instable in respect to some variations of the procedure of the CMB separation and final estimates of the CMB amplitudes can strongly vary. Non the less the analysis of simulations in [8] shows that there is at least one approach which provides reasonable precision $-\sim 10\%-$ for reconstruction of the angular power spectrum. It is interesting that the application of this approach for the WMAP observations (Q and V channels) –QV results–eliminates three first anomalies noted above.

4 Some applications of the WMAP results

Main results of the CMB analysis were discussed above. However, the measured amplitude of the quadrupole component of the CMB fluctuations allows us restrict also some speculations in respect the general properties of the Universe. As is well known there are only nine Bianki models of homogeneous but anisotropic Universe. In these models the anisotropy is linked with four factors, namely, the anisotropy of cosmological expansion, anisotropy of the curvature of the Universe, the matter rotation or an existence of the anisotropic matter distribution (for example, homogeneous magnetic field or a large scale stream of unknown particles). This cosmological anisotropy inevitably generates the quadrupole fluctuations of the CMB. Therefore the measured amplitude of the quadrupole component strongly restricts the integrated action of these four factors. As was shown in [9] the admissible amplitudes of these factors are negligible and cannot be now registered by direct observations. This means that many attempts to give cosmological interpretatio for the anisotropy in properties of quasars or in orientation of galactic rotations are incorrect and all tlese effects can be caused by various local effects.

Further progress of the CMB analysis can be associated manly with detailed measurements and discrimination between the thermal and kinetik Sunyaev– Zeldóvich effect what allows to estimate directly the peculiar velocity of clusters of galaxies.

References

[1] E. Komatsu et al., *Seven year wilkinson microwave anisotropy probe observations: cosmological interpretation*, 2011, ApJS.,192, 18.

[2] C. Bennett et al., *Seven year wilkinson microwave anisotropy probe observations: are there cosmic mirowave background anomalies*, 2011, ApJS., 192, 17

[3] D. Larson et al, *Seven year wilkinson microwave anisotropy probe observations: power spectra and wmap-derived parameters*, 2011, ApJS., 192, 16

[4] R. Keisler et al., *a measurement of the damping tail of the cosmic microwave background power spectrum with the south pole telescope*, 2011, ApJ, 743, 28

[5] M.Broun et al., *improved measurements of the temperature and polarization of the CMB from QUAD*, 2009, ApJ, 705, 978

[6] J.Fowler et al., *The ATACAMA cosmology telescope: a measurement of the* $600 \leq \ell \leq 8000$ *cosmic microwave background power spectrum at 148 GHz*, 2010, ApJ, 722, 1148.

[7] G. Hinshaw et al., *Three year wilkinson microwave anisotropy probe observations: temperature analysis*, 2007, ApJS., 170, 288

[8] A. Doroshkevich, O. Verkhodanov, CMB component separation in the pixel domain, 2011, PhysRev D, 83d3002D

[9] M. Demiański, A. Doroshkevich, Extensions of the standard cosmological model: Anisotropy, rotation, and the magnetic field, 2007, PhysRev D, 75, 123517

Cultural theatre performance

Flower bouquets for the actors

Higgs boson as the main character in the early Universe

Dmitry Gorbunov
Institute for Nuclear Research of the Russian Academy of Sciences,
60-th October Anniversary pr. 7a, Moscow 117312, Russia
Email : gorby@ms2.inr.ac.ru

Abstract

The SM Higgs boson field H can be responsible for the inflationary stage in the early Universe [1], if it is nonminimally coupled to gravity, $\xi R H^\dagger H$. The usual normalization of the scalar perturbations amplitude to $\delta\rho/\rho \sim 10^{-4}$ requires large coupling constant $\xi \sim 10^4$, which naturally limits [2, 3] the region of applicability of the perturbative description of the model. At strong coupling scale, which depends on the value of the Higgs boson field [4], nonrenormalizable interactions may appear. As we show, they can be responsible for the neutrino oscillations at low energies and give rise to successful leptogenesis at preheating stage in the early Universe [5].

1 Introduction

The Higgs sector of the Standard Model of particle physics (SM) still remains hidden: neither the Higgs boson, nor its self-coupling or couplings to other SM particles have been observed. Meanwhile it plays a crucial role in the Model, being responsible for the spontaneous breaking of the electroweak symmetry, emerging of fermion and vector boson masses and restoration of the unitarity in scatterings with massive vector bosons in a final state.

The Higgs boson is the only fundamental scalar in the SM. Quite remarkably, the scalars are believed to play an important role in the very early Universe providing the inflationary expansion [6, 7, 8] before the Hot Big Bang stage. It is tempting to adopt the Higgs boson to do the inflaton's job. This idea was realized with non-minimal Higgs coupling to gravity [1] and called as *the Higgs inflation.* However, the analysis of theories with non-minimal coupling of the Higgs field to gravity revealed that they enter into a strong coupling regime above certain Higgs-dependent cutoff, which may be considerably below the Planck scale [2, 3, 4].

Assuming that the effective theory, complementing the Standard Model (or its minimal extension with stable particles to be dark matter) contains a set of higher dimensional operators suppressed by the Higgs-dependent cutoff, we analyze the reheating of the Universe after the Higgs inflation. We found that extra terms do not spoil the Higgs inflation, but can lead to baryogenesis and dark matter production at the reheating stage of the Universe expansion. Likewise they can also result in neutrino mass generation and favor the proton decay at the rate to be probed by the upcoming experiments. Hence, in the suggested setup the Higgs field can be the main character in the play "the youth of the Universe", which details are obscured at present by ten billion years of cosmological expansion. The main three phenomenological problems of the SM — neutrino oscillations, baryon asymmetry of the Universe and dark matter — may spring from the strong dynamics in the Higgs-gravity sector.

2 The Higgs inflation

The model is described by the action

$$S = \int d^4x\sqrt{-g}\left(-\frac{M_P^2}{2}R - \xi H^\dagger H R + \mathcal{L}_{SM}\right)$$

where $\mathcal{L}_{SM}$ stands for the SM lagrangian and R is the scalar curvature. In a unitary gauge $H^T = \big(0\,,(h+v)/\sqrt{2}\big)$ (and neglecting $v = 246$ GeV) one has

$$S = \int d^4x\sqrt{-g}\left(-\frac{M_P^2+\xi\,h^2}{2}R + \frac{(\partial_\mu h)^2}{2} - \frac{\lambda\,h^4}{4}\right).$$

The slow roll behavior, usually needed for the inflationary stage (see e.g. [11]), and sufficiently flat potential, required to produce scalar perturbations with a scale-invariant spectrum of 10^{-5}-amplitude, are achieved due to modified kinetic term even for $\lambda \sim 1$. Normalization of the scalar perturbation amplitude to the WMAP measurement of CMB anisotropy gives [1]

$$\xi \approx 47000 \times \sqrt{\lambda}\,. \tag{1}$$

It is convenient to work further in the Einstein frame, where $(M_P^2 + \xi\,h^2)\,R \to M_P^2\,\tilde{R}$ and which is related to the previous (Jordan frame) via conformal transformation

$$g_{\mu\nu} = \Omega^{-2}\tilde{g}_{\mu\nu}\,, \qquad \Omega^2 = 1 + \frac{\xi\,h^2}{M_P^2}\,.$$

For canonically normalized field χ

$$\frac{d\chi}{dh} = \frac{M_P\sqrt{M_P^2 + (6\xi+1)\xi\,h^2}}{M_P^2+\xi\,h^2}\,,\;\; U(\chi) = \frac{\lambda M_P^4\,h^4(\chi)}{4(M_P^2+\xi\,h^2(\chi))^2}\,,$$

we have a flat potential at large fields: $U(\chi) \to \text{const}$ at $h \gg M_P/\sqrt{\xi}$, see Fig.1.

At inflationary stage the scalar potential coincides with that in the R^2-inflation [6],

$$U(\chi) = \frac{\lambda M_P^4}{4\xi^2}\left(1 - \exp\left(-\frac{\sqrt{2}\,\chi}{\sqrt{3}M_P}\right)\right)^2$$

and the flatness is protected against the higher order operators and quantum corrections by approximate shift symmetry $\chi \to \chi + \text{const}$. After inflation the Universe enters the matter dominated stage with energy confined in the inflaton field with effective lagrangian

$$\mathcal{L} = \frac{1}{2}\partial_\mu\chi\partial^\mu\chi - \frac{\lambda}{6}\frac{M_P^2}{\xi^2}\,\chi^2\,.$$

The higgs-inflaton couples to the SM fields which eventually (see details in [10]) reheats the Universe. The maximal temperature in the SM plasma T_r is estimated to be [10]

$$3.4\times10^{13}\,\text{GeV} < T_r < 1.1\times10^{14}\left(\frac{\lambda}{0.25}\right)^{1/4}\text{GeV}\,,$$

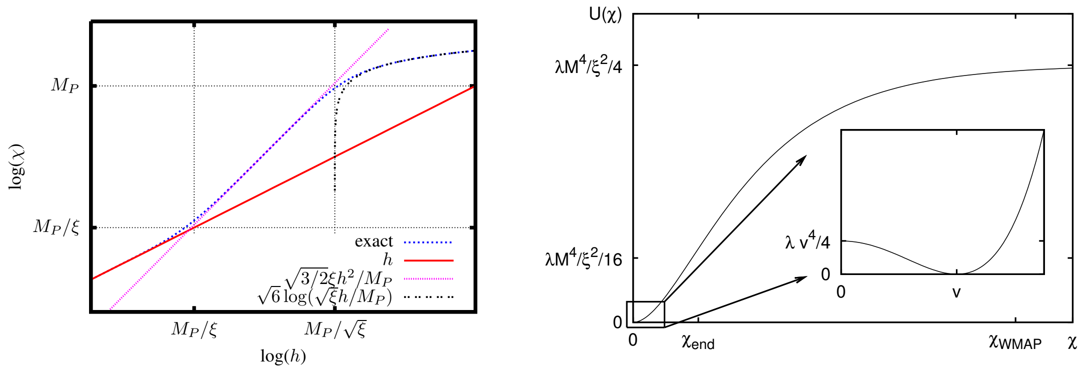

Figure 1: Relation between the Higgs field h and canonically normalized inflaton field χ (left panel [10]) with inflaton potential $U(\chi)$ (right panel [1]).

that fixes the number of required inflationary e-foldings (see [11]) to [9] $N_e = 57$. This temperature is much lower than that in the R^2-inflation [12], which allows to distinguish the two models with accurate measurements of the amplitudes and tilts of the scalar and tensor perturbations spectra[9]. In particular, for the Higgs inflation we have for the scalar tilt n_s and tensor-to-scalar amplitudes ratio r (see definitions in [11])

$$n_s = 0.967\,, \quad r = 0.0032\,.$$

Large value of parameter ξ (1) gives rise to the strong coupling problem in the model [2, 3]. The energy scale Λ of the strong coupling depends on the value of the Higgs field [4] and differs in different sectors of the model. In the Jordan frame the effective gravity scale is $\Lambda^2_{\text{Planck}} \simeq M_P^2 + \xi h^2$, it determines the scale of strong coupling in graviton scatterings, see Fig. 2. Similarly, for the higgs-gravity interactions and for gauge

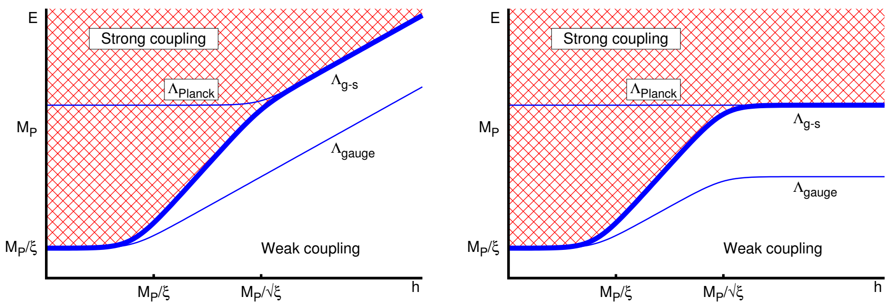

Figure 2: Regions of the strong coupling in the Jordan frame (left panel) and in the Einstein frame (right panel) for tensor (Planck), scalar (g-s) and vector (gauge) sectors of the model [5].

interactions the strong coupling scales are (see Fig. 2)

$$\Lambda_{g-s}(h) \simeq \begin{cases} \frac{M_P}{\xi}\,, & \text{for } h < \frac{M_P}{\xi}\,, \\ \frac{\xi h^2}{M_P}\,, & \text{for } \frac{M_P}{\xi} < h < \frac{M_P}{\sqrt{\xi}}\,, \\ \sqrt{\xi} h\,, & \text{for } h > \frac{M_P}{\sqrt{\xi}}\,. \end{cases} \qquad \Lambda_{\rm gauge}(h) \simeq \begin{cases} \frac{M_P}{\xi}\,, & \text{for } h < \frac{M_P}{\xi}\,, \\ h\,, & \text{for } \frac{M_P}{\xi} < h\,. \end{cases}$$

The theory has to be UV-completed above the strong coupling scales.

3 The role of nonrenormalizable interactions

One can expect various nonrenormalizable operators originated from the UV-completing theory and suppressed by the strong coupling scales,

$$\delta\mathcal{L}_{\rm NR} = \qquad -\frac{a_6}{\Lambda^2}(H^\dagger H)^3 + \dots \tag{2}$$

$$+\frac{\beta_L}{4\Lambda}F_{\alpha\beta}\bar{L}_\alpha \tilde{H} H^\dagger L^c_\beta + \frac{\beta_B}{\Lambda^2} O_{\text{baryon violating}} + \dots + \text{h.c.} \tag{3}$$

$$+\frac{\beta_N}{2\Lambda}H^\dagger H \bar{N}^c N + \frac{b_{L\alpha}}{\Lambda}\bar{L}_\alpha(\hat{D}N)^c\tilde{H} + \dots \tag{4}$$

Here L_α are SM leptonic doublets, $\alpha = 1, 2, 3$, N stands for right handed sterile fermions (neutrinos) potentially present in the model, $\tilde{H}_a = \epsilon_{ab}H^*_b$, $a, b = 1, 2$, and

$$\Lambda = \Lambda\left(h\right) = \left\{\Lambda_{g-s}\left(h\right)\,,\ \Lambda_{\rm gauge}\left(h\right)\,,\ \Lambda_{\rm Planck}\left(h\right)\right\}\,.$$

Note that couplings can differ significantly in different regions of h: presently $h < M_P/\xi$, while at preheating $M_P/\xi < h < M_P/\sqrt{\xi}$.

Let us start with discussion of possible role of the nonrenormalizable operators in low energy physics, where the Higgs field takes electroweak vacuum expectation value v and the strong coupling scale is $\Lambda = M_P/\xi \simeq 0.6 \times 10^{14}$ GeV. Operators (3) violate lepton and baryon numbers and with $\beta_L = 0.2$ can explain the active neutrino masses required for neutrino oscillations,

$$\Lambda \sim 0.6 \times 10^{14}\,\text{GeV} \times \frac{\beta_L}{0.2} \times \left(\frac{3\times10^{-3}\,\text{eV}^2}{\Delta m^2_{\rm atm}}\right)^{1/2}\,.$$

Dimension-6 baryon number violating operator $\frac{\beta_B}{\Lambda^2}QQQL$ makes proton unstable. Nonobservation of the proton decay puts a limit

$$\Lambda > \sqrt{\beta_B}\times 10^{16}\,\text{GeV}\,\times\left(\frac{\tau_{p\to\pi^0 e^+}}{1.6\times10^{33}\,\text{years}}\right)^{1/4}$$

which for $\Lambda = M_P/\xi \simeq 0.6 \times 10^{14}$ GeV implies a strong upper bound on the coupling constant

$$\beta_B < 0.4 \times 10^{-4}\,.$$

One concludes that either baryon B and lepton numbers L_α are significantly different or we will observe proton decay in the next generation experiment.

We proceed with study of leptogenesis driven by the same lepton number violating dimension-5 operator together with the SM Yukawa couplings

$$\mathcal{L}_Y = -Y_\alpha \bar{L}_\alpha H E_\alpha + \text{h.c.}\,, \qquad \mathcal{L}^{(5)}_{\nu\nu} = \frac{\beta_L}{4\Lambda}F_{\alpha\beta}\bar{L}_\alpha\tilde{H}H^\dagger L^c_\beta + \text{h.c.}$$

For the lepton charge operator $\hat{Q}_L$ one finds

$$i\,\frac{d}{dt}\,\hat{Q}_L = \left[\hat{H}_{\rm int}, \hat{Q}_L\right]\;,\quad \Delta n_L \equiv n_L - n_{\bar{L}} = \langle Q_L \rangle$$

and the lepton asymmetry Δn_L evolves as

$$\frac{d\Delta n_L}{dt} \propto {\rm Im}\left(\beta_L^4\,{\rm Tr}\big(FF^\dagger FYYF^\dagger YY\big)\right) \propto \beta_L^4 y_\tau^4 \cdot {\rm Im}\left(F_{3\beta}F^*_{\alpha\beta}F_{\alpha 3}F^*_{33}\right)\;.$$

Putting all numbers in the formula above one obtains for the gauge cutoff $\Lambda = h$

$$\beta_L^4\left(\frac{y_\tau}{0.01}\right)^4\left(\frac{0.25}{\lambda}\right)^{5/4}\times 10^{-10} < \Delta_L < \beta_L^4\left(\frac{y_\tau}{0.01}\right)^4\left(\frac{0.25}{\lambda}\right)\times 10^{-9}\;,$$

and for gravity-scalar cutoff $\Lambda = \xi\, h^2/M_P$

$$\beta_L^4\left(\frac{y_\tau}{0.01}\right)^4\left(\frac{0.25}{\lambda}\right)^{13/4}\times 6.3\times 10^{-13} < \Delta_L < \beta_L^4\left(\frac{y_\tau}{0.01}\right)^4\left(\frac{0.25}{\lambda}\right)^2\times 2.4\times 10^{-10}\,.$$

The lepton asymmetry further transfers to the baryon asymmetry Δ_B via sphaleron processes. Hence, one can hope obtain the required amount of baryon asymmetry of the Universe $\Delta_B \approx \Delta_L/3 \sim 10^{-10}$ with help of the nonrenormalizable operators.

Actually, in both cases the asymmetry can be significantly increased with presence of the following operators

$$\delta\mathcal{L}^\tau = y_\tau L_\tau H E_\tau + \beta_y L_\tau H E_\tau \frac{H^\dagger H}{\Lambda^2} + \ldots$$

Then one can fancy the hierarchy

$$1 \sim \beta_y \gg y_\tau \sim 10^{-2}\;,$$

which gives an enhancement factor up to 10^8 in front of β_L^4 in the formulas above! Thus, the nonrenormalizable operators certainly can explain the baryon asymmetry of the Universe.

With sterile fermions (neutrinos) introduced to the theory, the higher order terms (4) contribute to their production in the early Universe both at preheating and at hot stage. These fermions may form the dark matter component [5].

References

[1] F. L. Bezrukov and M. Shaposhnikov, *The Standard Model Higgs boson as the inflaton,* Phys. Lett. B 659 (2008) 703 [arXiv:0710.3755 [hep-th]].

[2] C. P. Burgess, H. M. Lee and M. Trott, *"Power-counting and the Validity of the Classical Approximation During Inflation,* JHEP 0909 (2009) 103 [arXiv:0902.4465 [hep-ph]].

[3] J. L. F. Barbon and J. R. Espinosa, *On the Naturalness of Higgs Inflation,* Phys. Rev. D 79 (2009) 081302 [arXiv:0903.0355 [hep-ph]].

[4] F. Bezrukov, A. Magnin, M. Shaposhnikov and S. Sibiryakov, *Higgs inflation: consistency and generalisations,* JHEP 1101 (2011) 016 [arXiv:1008.5157 [hep-ph]].

[5] F. Bezrukov, D. Gorbunov and M. Shaposhnikov, *Late and early time phenomenology of Higgs-dependent cutoff,* JCAP 1110 (2011) 001 [arXiv:1106.5019 [hep-ph]].

[6] A. A. Starobinsky, *A New Type of Isotropic Cosmological Models Without Singularity,* Phys. Lett. B 91 (1980) 99.

[7] A. H. Guth, *The Inflationary Universe: A Possible Solution to the Horizon and Flatness Problems,* Phys. Rev. D 23 (1981) 347.

[8] A. D. Linde, *A New Inflationary Universe Scenario: A Possible Solution of the Horizon, Flatness, Homogeneity, Isotropy and Primordial Monopole Problems,* Phys. Lett. B 108 (1982) 389.

[9] F. Bezrukov and D. Gorbunov, *Distinguishing between R^2-inflation and Higgs-inflation,* arXiv:1111.4397 [hep-ph].

[10] F. Bezrukov, D. Gorbunov and M. Shaposhnikov, *On initial conditions for the Hot Big Bang,* JCAP 0906 (2009) 029 [arXiv:0812.3622 [hep-ph]].

[11] D. S. Gorbunov and V. A. Rubakov, Introduction to the theory of the early universe: Cosmological perturbations and inflationary theory, World Scientific, Singapore (2011), 489 p.

[12] D. S. Gorbunov and A. G. Panin, *Scalaron the mighty: producing dark matter and baryon asymmetry at reheating,* Phys. Lett. B 700, 157 (2011) [arXiv:1009.2448 [hep-ph]].

Cosmological Perturbation of Universe with Black Hole

Sung-Won Kim
Ewha Womans University, Seoul 120-750, Korea
Email : sungwon@ewha.ac.kr

Abstract

In this paper, the cosmological perturbation is studied for the expanding universe with a black hole. The scalar perturbation and conformal-Newton gauge are adopted for this study. There are the accretion processes of dark energy onto the black hole in these models. The perturbations of black hole mass change rate are derived in terms of mass and heat flows for four cases according to the models.

1 Introduction

Recently there is a successful model for dark energy accretion onto a black hole.[1] The model shows the black hole mass change rate due to the accretion. In the model the mass change rate was derived in terms of the equation of state parameter. If there is the interaction between the dark energy and dark matter, the multi component accretion model is more useful. By observation, inhomogeneous dark matter and inhomogeneous dark energy require the perturbed cosmological model.[2] There are some questions on the perturbed model. How do the equations of motion for perturbed terms evolve? Will the perturbed terms change the mass rate of black hole? Are there any differences in perturbed conserved equations? To answer these questions, the cosmological perturbation is studied for the expanding universe with a black hole.

2 Accretion onto a black hole in the universe

Among the several solutions, we adopt the Faraoni-Jacques (F-J) solution[3] for a black hole in the expanding universe. It is a strongly gravitating object in a FRWL (Friedmann-Robertson-Walker-Lemaitre) background. The spacetime metric is given by

$$ds^2 = \frac{B^2(t,r)}{A^2(t,r)}dt^2 - a^2(t)A^4(t,r)(dr^2 + r^2 d\Omega^2), \tag{1}$$

where $A = 1 + \frac{m(t)}{2r}, B = 1 - \frac{m(t)}{2r}$. It is the generalization of McVittie solution[4] in a background of an imperfect fluid with a radial heat flux and, possibly, a radial mass flow simulating accretion onto a black hole embedded in a generic FRWL universe. For the mass flow, the term ${G_0}^1$ is very important which is calculated by

$${G_0}^1 = \frac{2m}{r^2 a^2 A^5 B}\left(\frac{\dot{m}}{m} + \frac{\dot{a}}{a}\right) = \frac{2m}{r^2 a^2 A^5 B}\frac{\dot{m_{\rm H}}}{m_{\rm H}} \neq 0 \tag{2}$$

with the Hartle-Hawking quasi-local mass $m_{\rm H} \equiv m(t)a(t)$. We can study this model in three cases according to the existences of the heat and mass flows. The first case is the perfect fluid model with radial flow u. The mass change rate of the black hole is

$$\dot{m}_{\rm H} = -GB^2au(P+\rho)\mathcal{A}\sqrt{1+a^2A^4u^2}. \tag{3}$$

Here $\mathcal{A} = \int\int d\theta d\phi\sqrt{g_\Sigma} = 4\pi a^2A^4r^2$ is the area of the spherically symmetric sphere of radius r. This case satisfy de Sitter $(P=-\rho)$ model only and thus $\dot{m}_{\rm H} = 0$, no accretion. The second case is the imperfect fluid model without the radial mass flow $(u=0, q\neq 0)$. The mass change rate of the black hole is

$$\dot{m}_{\rm H} = -GaB^2\mathcal{A}q \tag{4}$$

which is determined by heat flow q. The third case is imperfect fluid and radial mass flow $(u\neq 0, q\neq 0)$. The four velocity and heat current are defined as follows,

$$u^\mu = \left(\frac{A}{B}\sqrt{1+a^2A^4u^2}, u, 0, 0\right),\ q^\nu = (0, q, 0, 0),\ u_\mu q^\mu \neq 0. \tag{5}$$

The conservation law in this case is

$$q = -(P+\rho)\frac{u}{2}, \tag{6}$$

which means that the ingoing radial flow of mass is approximately outgoing radial heat current. The mass change rate of the black hole is

$$\begin{aligned} \dot{m}_{\rm H} &= -GaB^2\mathcal{A}\sqrt{1+a^2A^4u^2}[(P+\rho)u+q], & (7)\\ &= -\frac{G}{2}aB^2\mathcal{A}\sqrt{1+a^2A^4u^2}(P+\rho)u, \qquad u<0. & (8)\end{aligned}$$

For negative u (accretion), in all cases the mass change rates are positive. However, in the exotic matter accretion case, such as phantom energy with $P+\rho<0$, the mass change rate is negative and the black hole mass will decrease.

3 Accretion onto a black hole in perturbed universe

For the cosmological perturbation problem, only the scalar linear perturbation is considered here. In conformal-Newton gauge, the perturbed model is given by

$$ds^2 = a^2(\eta)[(1+2\Psi)d\eta^2 + (1+2\Phi)\delta_{ij}]. \tag{9}$$

If proper anisotropy of medium equals zero, then we can set $\Psi = -\Phi$ such as dust matter and scalar field. The Bardeen's potentials Ψ and Φ are gauge-invariant perturbations of metric.[5] If we perturb the F-J metric[3] as

$$ds^2 = \frac{B^2}{A^2}(1+2\Phi)dt^2 - A^4a^2(1-2\Phi)(dr^2+r^2d\Omega^2), \tag{10}$$

the terms relating to the mass flow are

$$
\begin{aligned}
-R_{01} &= \frac{2m}{r^2AB}\left(\frac{\dot{m}}{m}+\frac{\dot{a}}{a}\right)+\left(\frac{2A'}{A}-\frac{2B'}{B}\right)\dot{\Phi}+2\left(\frac{2\dot{A}}{A}+\frac{\dot{a}}{a}\right)\Phi'+2\dot{\Phi}' \\
&= \frac{2m}{r^2AB}\frac{\dot{m}_{\mathrm{H}}}{m_{\mathrm{H}}}+2\left(\ln\frac{A}{B}\right)'\dot{\Phi}+2(\ln A^2a)^{\cdot}\Phi'+2\dot{\Phi}', \qquad (11)\\
R &= \big[6B^3(A'(2+4\Phi-r\Phi')+r(1+2\Phi)A'') \\
&\quad +2AB^2[B'(2+4\Phi+r\Phi')+rB''(1+2\Phi)-B(2\Phi'+r\Phi'')] \\
&\quad -48ra^2A^5B(1-2\Phi)\dot{A}^2+6raA^6(1-2\Phi)\Big(2a\dot{A}\dot{B}+B\{-9\dot{a}\dot{A} \\
&\quad -2a\ddot{A}+11a\dot{A}\dot{\Phi}\}\Big)+6rA^7(1-2\Phi)\Big(\dot{B}a\dot{a}-a^2\dot{B}\dot{\Phi}-B\dot{a}^2 \\
&\quad +5a\dot{a}B\dot{\Phi}-a\ddot{a}B+a^2B\ddot{\Phi}\Big)\Big]\Big/[ra^2A^5B^3]. \qquad (12)
\end{aligned}
$$

For the accretion case, there is a radial flow as $u^\mu=(u^0,u,0,0)$. In unperturbed case, the equation for the velocity is $u^\mu u_\mu = u^0 g_{00}u^0+ug_{rr}u=1$ or

$$u^0=\frac{1}{\sqrt{g_{00}}}\sqrt{1-g_{rr}u^2}. \qquad (13)$$

The velocity equation for the perturbed metric

$$g_{00}\ \rightarrow\ g_{00}(1+2\Phi),\ g_{11}\ \rightarrow\ g_{11}(1-2\Phi) \qquad (14)$$

is

$$(u^0+\delta u^0)g_{00}(1+2\Phi)(u^0+\delta u^0)+(u+\delta u)g_{11}(1-2\Phi)(u+\delta u)=1. \qquad (15)$$

The first-order constraint is

$$g_{00}u^0(\delta u^0+u^0\Phi)+g_{11}u(\delta u-u\Phi)=0. \qquad (16)$$

The perturbed energy-momentum tensor components for the perfect fluid model are

$$
\begin{aligned}
\delta T^0{}_0 &= (\delta\rho+\delta P)u^0u_0-\delta P+2(\rho+P)u^0u_0\Phi, & (17)\\
\delta T^1{}_1 &= (\delta\rho+\delta P)u^1u_1-\delta P-2(\rho+P)u^1u_1\Phi, & (18)\\
\delta T^2{}_2 &= -\delta P, & (19)\\
\delta T^3{}_3 &= -\delta P, & (20)\\
\delta T^1{}_0 &= (\delta\rho+\delta P)u_0u^1+2(\rho+P)u^1u_0\Phi+(\rho+P)u_0\delta u^1. & (21)
\end{aligned}
$$

If we consider the quintessence dark energy perturbation as

$$\phi(t,r)=\phi_0(t)+\delta\phi(r,t), \qquad (22)$$

the energy-momentum tensor and Lagrangian density are

$$T^\mu{}_\nu=\partial^\mu\phi\partial_\nu\phi-\mathcal{L}_\phi\delta^\mu_\nu,\quad \mathcal{L}_\phi=\frac{1}{2}\partial^\mu\phi\partial_\mu\phi-V(\phi). \qquad (23)$$

The perturbed energy-momentum tensor components in quintessence dark energy model are

$$\delta T^0{}_0 = \dot\phi_0\dot{\delta\phi} - 2\Phi\frac{A^2}{B^2}\dot\phi_0^2 + V'(\phi_0)\delta\phi, \tag{24}$$

$$\delta T^0{}_1 = \frac{A^2}{B^2}\dot\phi_0\delta\phi_{,1}, \tag{25}$$

$$\delta T^1{}_1 = -\left[\dot\phi_0\dot{\delta\phi} - 2\Phi\frac{A^2}{B^2}\dot\phi_0^2 - V'(\phi_0)\delta\phi\right]. \tag{26}$$

The conservation law of energy-momentum tensor can be rewritten as

$$\begin{aligned}&\dot{\delta\rho} + (\rho+P)\frac{B}{A}\delta u' - 3(\rho+P)\dot\Phi + 3(\delta\rho - \delta P)\left(\frac{2\dot A}{A} + \frac{\dot a}{a}\right)\\ &+(\rho+P)\frac{B}{A}\left(\frac{B'}{B} + \frac{2A'}{A} + \frac{1}{r}\right)\delta u = 0,\end{aligned} \tag{27}$$

$$\begin{aligned}&\frac{A^5a^2}{2B}(\rho+P)\dot{\delta u} + \delta P' + \frac{A^5a^2}{2B}(\dot\rho + \dot P)\delta u + (\rho+P)\Phi'\\ &+\frac{5A^5a^2}{2B}(\rho+P)\delta u\left(\frac{2\dot A}{A} + \frac{\dot a}{a}\right) + (\delta\rho + \delta P)\left(\frac{B'}{B} - \frac{A'}{A}\right) = 0,\end{aligned} \tag{28}$$

The mass term is

$$T_0{}^1 = \frac{B}{A}(q+\delta q) \quad \text{or} \quad q = 0, \delta q = \frac{1}{2}(\rho+P)\delta u. \tag{29}$$

From the Einstein's equation,

$$\frac{2m}{r^2AB}\frac{\dot m_{\rm H}}{m_{\rm H}} + 2\left(\ln\frac{A}{B}\right)'\dot\Phi + 2(\ln A^2a)^{\cdot}\Phi' + 2\dot\Phi' = 4\pi G T_0{}^1. \tag{30}$$

Here we calculate the mass change rate for the four cases. The first case is the perfect fluid without the radial flow with nonzero δu. $(q = 0, \delta q = 0, u = 0, \delta u \neq 0)$. In perturbed case, the radial flow is $u^\mu = \left(\frac{A}{B}(1-\Phi), \delta u, 0, 0\right)$ or $u_\mu = \left(\frac{B}{A}(1+\Phi), g_{11}\delta u, 0, 0\right)$. The perturbed energy-momentum tensor components are

$$\delta T^0{}_0 = \delta\rho, \tag{31}$$

$$\delta T^1{}_1 = -\delta P, \tag{32}$$

$$\delta T^1{}_0 = (\rho+P)u_0\delta u. \tag{33}$$

If perfect fluid property is changed by perturbation for nonzero δq

$$\delta T^1{}_0 = (\rho+P)u_0\delta u + u_0\delta q, \tag{34}$$

the Einstein's equation becomes

$$\frac{2m}{r^2AB}\frac{\dot m_{\rm H}}{m_{\rm H}} + 2\left(\ln\frac{A}{B}\right)'\dot\Phi + 2(\ln A^2a)^{\cdot}\Phi' + 2\dot\Phi' = 4\pi G(\rho+P)\delta u. \tag{35}$$

In this case $\dot{m}_{\rm H}=0$ or Eq. (35) becomes

$$2\left(\ln\frac{A}{B}\right)'\dot{\Phi}+2(\ln A^2a)^{\cdot}\Phi'+2\dot{\Phi}'=4\pi G(\rho+P)\delta u. \tag{36}$$

Here if we perturb the terms $m_{\rm H}$ and $\dot{m}_{\rm H}$,

$$\delta m_{\rm H}=m\delta a=-ma\Phi=-m_{\rm H}\Phi, \tag{37}$$

$$\delta\dot{m}_{\rm H}=-(\dot{m}_{\rm H}\Phi+m_{\rm H}\dot{\Phi})=-m_{\rm H}\dot{\Phi}. \tag{38}$$

If $\Phi'=0$, the Einstein's equation becomes

$$\frac{2m}{r^2AB}\frac{\delta\dot{m}_{\rm H}}{m_{\rm H}}=4\pi G(\rho+P)\delta u=4\pi G(1+\omega)\rho\delta u. \tag{39}$$

Thus $\delta\dot{m}_{\rm H}$ is determined by $\omega,\delta u$.

In the second case of the perfect fluid with the radial flow ($u\neq 0, q=0$),

$$T^1{}_0=(\rho+P)u_0u. \tag{40}$$

By Einstein's equations, only $(\rho+P)=0$ is accepted. The perturbed matter is

$$\delta T^1{}_0=u_0u(\delta\rho+\delta P). \tag{41}$$

If perfect fluid property is changed by perturbation ($\delta q\neq 0$), then

$$\delta T^1{}_0=u_0u(\delta\rho+\delta P)+u_0\delta q. \tag{42}$$

Since $\dot{m}_{\rm H}=0$,

$$\frac{2m}{r^2AB}\frac{\delta\dot{m}_{\rm H}}{m_{\rm H}}=4\pi G[(\delta\rho+\delta P)\delta u+\delta q]=4\pi G[(1+c_S^2)\delta\rho\delta u+\delta q]. \tag{43}$$

Here $\delta\dot{m}_{\rm H}$ is determined by $c_S,\delta\rho,\delta u$, and δq. The sound speed is defined as $c_S^2=\frac{\partial P}{\partial\rho}$.

In the third case of the imperfect fluid without the radial flow ($u=0, q\neq 0$),

$$T^1{}_0=u_0q=\frac{B}{A}q,\quad G^1{}_0=-8\pi\frac{B}{A}q, \tag{44}$$

$$q=\frac{-\dot{m}_{\rm H}}{4\pi r^2a^3A^6}\neq 0. \tag{45}$$

Because $\delta u^0=-u^0\Phi$, the perturbed energy-momentum tensor is

$$\delta T^1{}_0=u_0(q\Phi+\delta q). \tag{46}$$

If we accept $\delta u\neq 0$, then

$$\delta T^1{}_0=u_0(q\Phi+\delta q)+(\rho+P)u_0\delta u. \tag{47}$$

Since $\dot{\Phi}=-\frac{\delta\dot{m}_{\rm H}}{m_{\rm H}}-\frac{\dot{m}_{\rm H}}{m_{\rm H}}\Phi$,

$$\frac{2m}{r^2AB}\left(\frac{\delta\dot{m}_{\rm H}}{m_{\rm H}}+\frac{\dot{m}_{\rm H}}{m_{\rm H}}\Phi\right)=4\pi G[u_0(q\Phi+\delta q)+(1+\omega)\rho u_0\delta u]. \tag{48}$$

In the fourth case of the imperfect fluid with radial flow ($u \neq 0, q \neq 0$), the background energy-momentum tensor is

$$T^1{}_0 = u_0 u(\rho + P) + u_0 q = \frac{1}{2} u_0 u(\rho + P), \tag{49}$$

since $q = -\frac{1}{2}(\rho + P)u$. The perturbed energy-momentum tensor is

$$\delta T^1{}_0 = \frac{1}{2} u_0 u(\delta\rho + \delta P) + \frac{1}{2}\delta(u_0 u)(\rho + P). \tag{50}$$

$$\frac{2m}{r^2 AB}\left(\frac{\delta \dot{m}_{\mathrm{H}}}{m_{\mathrm{H}}} + \frac{\dot{m}_{\mathrm{H}}}{m_{\mathrm{H}}}\Phi\right) = 4\pi G\left[\frac{1}{2} u_0 u(1 + c_S^2)\delta\rho + \frac{1}{2}\delta(u_0 u)(1 + \omega)\rho\right]. \tag{51}$$

4 Summary and Discussion

We studied the dark energy accretion onto black hole in the perturbed expanding universe. The black hole mass change rates are obtained for the different models of heat and mass flows. In perturbed case, perturbed mass rate will be given by Bardeen potential, perturbed radial flow, and sound speed. We will try to calculate the detail form of potential in next study. With the general case of geometry and matter, including black hole perturbation.

References

[1] E. Babichev, V. Dokuchaev, Yu. Eroshenko, Phys.Rev.Lett. 93 (2004) 021102.
[2] For recent review, see C. Uggla and J. Wainwright, Class. Quantum Grav. 28 (2011) 175017.
[3] V. Faraoni and A. Jacques, Phys. Rev. D76 (2007) 063510.
[4] G.C. McVittie, Mon. Not. R. Astr. Soc. 93 (1933) 325.
[5] J. M. Bardeen, Phys. Rev. D22 (1980) 1882.

G-inflation

Masahide Yamaguchi[1], *Tsutomu Kobayashi*[2], *Jun'ichi Yokoyama*[3]
[1] *Department of Physics, Tokyo Institute of Technology, Tokyo 152-8551, Japan*
[2] *Hakubi Center, Kyoto University, Kyoto 606-8302, Japan and*
Department of Physics, Kyoto University, Kyoto 606-8502, Japan
[3] *RESCEU, Graduate School of Science, The University of Tokyo, Tokyo 113-0033, Japan and*
IPMU, The University of Tokyo, Kashiwa, Chiba, 277-8568, Japan
Email : gucci@phys.titech.ac.jp

Abstract

In this talk, we have discussed generalized Galileons as a framework to develop the most general single-field inflation models ever, (Generalized) G-inflation, containing previous examples such as k-inflation, extended inflation, and new Higgs inflation as special cases. We have also investigated the background and perturbation evolution in this model, calculating the most general quadratic actions for tensor and scalar perturbations to give the stability criteria and the power spectra of primordial fluctuations.

1 Introduction

Scalar fields play important roles in cosmology. On the one hand, inflation in the early Universe is now becoming a part of standard cosmology that is driven by a scalar field called the inflaton [1, 2]. The conventional inflaton action consists of a canonical kinetic term and a sufficiently flat potential [2]. [See Ref. [3] for the latest review.] Non-canonical kinetic terms [4] also arise naturally in some particle physics models of inflation. On the other hand, it is strongly suggested that the present Universe is dominated by mysterious dark energy. In the decoupling limit of the Dvali-Gabadadze-Porrati brane model [5], the scalar field has a non-linear derivative self-interaction [6], which was later generalized to Galileons [7] with applications to inflation [8]. Thus, in recent years, there have been growing interests in scalar field theories beyond the canonical one.

The most attractive feature of higher derivative theories possessing the Galilean invariance $\partial_\mu\phi \to \partial_\mu\phi + b_\mu$ is that field equations derived from such a theory contain derivatives only up to second order [7], so that it can avoid ghosts. Unfortunately, however, this desired feature ceases to exist for the curved background spacetime [9]. To preserve the second-order nature of field equations, the "covariantization" of the Galileon has been proposed by Deffayet et al. [9, 10], where the theory is no longer Galilean invariant. In Ref. [11], it is pointed out that the equivalent theory has already been proposed by Horndeski [12]. The equivalence of both theories is explicitly shown in Ref. [13].

The purpose of this talk is to provide a comprehensive and thorough study of the most general non-canonical and non-minimally coupled single-field inflation models (named (Generalized) G-inflation) yielding second-order field equations making use of Ref. [10], which is the most general extension of the Galileons but is no longer based on a symmetry argument.

In this talk based on Ref. [13], we have clarified the generic behavior of the inflationary background and investigated the nature of primordial tensor and scalar perturbations at linear order. Given a specific model, our formulas are helpful to determine the evolution of cosmological perturbations and its observational consequences.

2 Generalized Higher-order Galileons and Kinetic Gravity Braiding

Galileons [7] and their covariant extension [9] have been further generalized to yield the most general scalar field theories with second-order field equations [10],

$$\begin{aligned}
\mathcal{L}_2 &= K(\phi, X), && (1)\\
\mathcal{L}_3 &= -G_3(\phi, X)\Box\phi, && (2)\\
\mathcal{L}_4 &= G_4(\phi, X)R + G_{4X}\left[(\Box\phi)^2 - (\nabla_\mu\nabla_\nu\phi)^2\right], && (3)\\
\mathcal{L}_5 &= G_5(\phi, X)G_{\mu\nu}\nabla^\mu\nabla^\nu\phi - \frac{G_{5X}}{6}\left[(\Box\phi)^3 - 3\,(\Box\phi)\,(\nabla_\mu\nabla_\nu\phi)^2 + 2\,(\nabla_\mu\nabla_\nu\phi)^3\right], && (4)
\end{aligned}$$

where $X := -\partial_\mu\phi\partial^\mu\phi/2$, R is the Ricci tensor, $G_{\mu\nu}$ is the Einstein tensor, $(\nabla_\mu\nabla_\nu\phi)^2 = \nabla_\mu\nabla_\nu\phi\nabla^\mu\nabla^\nu\phi$, $(\nabla_\mu\nabla_\nu\phi)^3 = \nabla_\mu\nabla_\nu\phi\nabla^\nu\nabla^\lambda\phi\nabla_\lambda\nabla^\mu\phi$, and $G_{iX} = \partial G_i/\partial X$. Setting $G_3 = X$, $G_4 = X^2$, and $G_5 = X^2$, the above Lagrangians reproduce the covariant Galileons introduced in Ref. [9]. The non-minimal couplings to gravity in $\mathcal{L}_4$ and $\mathcal{L}_5$ are necessary to eliminate higher derivatives that would otherwise appear in the field equations. Note that we do not need a separate gravitational Lagrangian other than $\mathcal{L}_4$; for $G_4 = M_{\rm Pl}^2/2$, $\mathcal{L}_4$ reduces to the Einstein-Hilbert term. We obtain a non-minimal coupling of the form $f(\phi)R$ from $\mathcal{L}_4$ by taking $G_4 = f(\phi)$. The non-standard kinetic term $G^{\mu\nu}\partial_\mu\phi\partial_\nu\phi$ as considered in Ref. [14] turns out to be a special case $G_5 \propto \phi$ of $\mathcal{L}_5$ after integration by parts. Equation (24) of Ref. [15], which is obtained from a Kaluza-Klein compactification of higher-dimensional Lovelock gravity, turns out to be equivalent to $\mathcal{L}_5$ with $G_5 = -3X/2$.

We thus consider a gravity + scalar system described by the action

$$S = \sum_{i=2}^{5}\int d^4x\sqrt{-g}\mathcal{L}_i, \qquad (5)$$

which is the most general single scalar theory resulting in equations of motion containing derivatives up to second order.

3 Background equations

Let us derive the equations of motion describing the background evolution from (5). The easiest way is to substitute $\phi = \phi(t)$ and the metric $ds^2 = -N^2(t)dt^2 + a^2(t)d\mathbf{x}^2$ to the action. Variation with respect to $N(t)$ gives the constraint equation, $\sum_{i=2}^{5}\mathcal{E}_i = 0$, where

$$\begin{aligned}
\mathcal{E}_2 &= 2XK_X - K, && (6)\\
\mathcal{E}_3 &= 6X\dot\phi HG_{3X} - 2XG_{3\phi}, && (7)\\
\mathcal{E}_4 &= -6H^2G_4 + 24H^2X(G_{4X} + XG_{4XX}) - 12HX\dot\phi G_{4\phi X} - 6H\dot\phi G_{4\phi}, && (8)\\
\mathcal{E}_5 &= 2H^3X\dot\phi\,(5G_{5X} + 2XG_{5XX}) - 6H^2X\,(3G_{5\phi} + 2XG_{5\phi X})\,. && (9)
\end{aligned}$$

Variation with respect to $a(t)$ yields the evolution equation, $\sum_{i=2}^{5}\mathcal{P}_i = 0$, where

$$\mathcal{P}_2 = K, \tag{10}$$

$$\mathcal{P}_3 = -2X\left(G_{3\phi}+\ddot{\phi}G_{3X}\right), \tag{11}$$

$$\begin{aligned}\mathcal{P}_4 &= 2\left(3H^2+2\dot{H}\right)G_4 - 12H^2XG_{4X} - 4H\dot{X}G_{4X} - 8\dot{H}XG_{4X} - 8HX\dot{X}G_{4XX}\\ &\quad +2\left(\ddot{\phi}+2H\dot{\phi}\right)G_{4\phi} + 4XG_{4\phi\phi} + 4X\left(\ddot{\phi}-2H\dot{\phi}\right)G_{4\phi X},\end{aligned} \tag{12}$$

$$\begin{aligned}\mathcal{P}_5 &= -2X\left(2H^3\dot{\phi}+2H\dot{H}\dot{\phi}+3H^2\ddot{\phi}\right)G_{5X} - 4H^2X^2\ddot{\phi}G_{5XX}\\ &\quad +4HX\left(\dot{X}-HX\right)G_{5\phi X} + 2\left[2\left(HX\right)^{\cdot}+3H^2X\right]G_{5\phi} + 4HX\dot{\phi}G_{5\phi\phi}.\end{aligned} \tag{13}$$

The background quantities $\mathcal{E}_i$ and $\mathcal{P}_i$ are defined in an analogous way in which the energy density and the isotropic pressure of a usual scalar field are defined.

Variation with respect to $\phi(t)$ gives the scalar-field equation of motion,

$$\frac{1}{a^3}\frac{\mathrm{d}}{\mathrm{d}t}\left(a^3J\right) = P_\phi, \tag{14}$$

where

$$\begin{aligned}J &= \dot{\phi}K_X + 6HXG_{3X} - 2\dot{\phi}G_{3\phi} + 6H^2\dot{\phi}\left(G_{4X}+2XG_{4XX}\right) - 12HXG_{4\phi X}\\ &\quad +2H^3X\left(3G_{5X}+2XG_{5XX}\right) - 6H^2\dot{\phi}\left(G_{5\phi}+XG_{5\phi X}\right),\end{aligned} \tag{15}$$

$$\begin{aligned}P_\phi &= K_\phi - 2X\left(G_{3\phi\phi}+\ddot{\phi}G_{3\phi X}\right) + 6\left(2H^2+\dot{H}\right)G_{4\phi} + 6H\left(\dot{X}+2HX\right)G_{4\phi X}\\ &\quad -6H^2XG_{5\phi\phi} + 2H^3X\dot{\phi}G_{5\phi X}.\end{aligned} \tag{16}$$

4 Quadratic actions for tensor and scalar perturbations

In this section, our goal is to compute quadratic actions for tensor and scalar cosmological perturbations in Generalized G-inflation. We use the unitary gauge in which $\phi = \phi(t)$ and begin with writing the perturbed metric as

$$\mathrm{d}s^2 = -N^2\mathrm{d}t^2 + \gamma_{ij}\left(\mathrm{d}x^i + N^i\mathrm{d}t\right)\left(\mathrm{d}x^j + N^j\mathrm{d}t\right), \tag{17}$$

where

$$N = 1+\alpha, \quad N_i = \partial_i\beta, \quad \gamma_{ij} = a^2(t)e^{2\zeta}\left(\delta_{ij}+h_{ij}+\frac{1}{2}h_{ik}h_{kj}\right). \tag{18}$$

Here, α, β, and ζ are scalar perturbations and h_{ij} is a tensor perturbation satisfying $h_{ii} = 0 = h_{ij,j}$.

4.1 Tensor perturbations

The quadratic action for the tensor perturbations is found to be

$$S_T^{(2)} = \frac{1}{8}\int \mathrm{d}t\mathrm{d}^3x\, a^3\left[\mathcal{G}_T\dot{h}_{ij}^2 - \frac{\mathcal{F}_T}{a^2}(\vec{\nabla}h_{ij})^2\right], \tag{19}$$

where

$$\mathcal{F}_T := 2\left[G_4 - X\left(\ddot{\phi}G_{5X} + G_{5\phi}\right)\right], \tag{20}$$

$$\mathcal{G}_T := 2\left[G_4 - 2XG_{4X} - X\left(H\dot{\phi}G_{5X} - G_{5\phi}\right)\right]. \tag{21}$$

The squared sound speed is given by $c_T^2 = \mathcal{F}_T/\mathcal{G}_T$. One sees from the action (19) that ghost and gradient instabilities are avoided as long as $\mathcal{F}_T > 0, \quad \mathcal{G}_T > 0$. Note that c_T^2 is not necessarily unity in general, contrary to the standard cases.

To evaluate the primordial power spectrum, let us assume that $\epsilon := -\dot{H}/H^2 \simeq$ const, $f_T := \dot{\mathcal{F}}_T/(H\mathcal{F}_T) \simeq$ const, and $g_T := \dot{\mathcal{G}}_T/(H\mathcal{G}_T) \simeq$ const. Then, we find the power spectrum of the primordial tensor perturbation:

$$\mathcal{P}_T = 8\gamma_T \left.\frac{\mathcal{G}_T^{1/2}}{\mathcal{F}_T^{3/2}}\frac{H^2}{4\pi^2}\right|_{\text{at sound horizon exit}}, \tag{22}$$

where $\gamma_T = 2^{2\nu_T-3}|\Gamma(\nu_T)/\Gamma(3/2)|^2(1-\epsilon-f_T/2+g_T/2)$ and $\nu_T := (3-\epsilon+g_T)/(2-2\epsilon-f_T+g_T)$. The tensor spectral tilt is given by $n_T = 3-2\nu_T$. Contrary to the predictions of the conventional inflation models, the blue spectrum $n_T > 0$ can be obtained for $4\epsilon + 3f_T - g_T < 0$.

4.2 Scalar perturbations

The quadratic action for scalar perturbations is given by

$$S_S^{(2)} = \int \mathrm{d}t\mathrm{d}^3x\, a^3\left[\mathcal{G}_S\dot{\zeta}^2 - \frac{\mathcal{F}_S}{a^2}(\vec{\nabla}\zeta)^2\right], \tag{23}$$

where

$$\mathcal{F}_S := \frac{1}{a}\frac{\mathrm{d}}{\mathrm{d}t}\left(\frac{a}{\Theta}\mathcal{G}_T^2\right) - \mathcal{F}_T, \qquad \mathcal{G}_S := \frac{\Sigma}{\Theta^2}\mathcal{G}_T^2 + 3\mathcal{G}_T, \tag{24}$$

$$\Sigma = X\sum_{i=2}^{5}\frac{\partial\mathcal{E}_i}{\partial X} + \frac{1}{2}H\sum_{i=2}^{5}\frac{\partial\mathcal{E}_i}{\partial H}, \qquad \Theta = -\frac{1}{6}\sum_{i=2}^{5}\frac{\partial\mathcal{E}_i}{\partial H}. \tag{25}$$

The squared sound speed is given by $c_S^2 = \mathcal{F}_S/\mathcal{G}_S$, and ghost and gradient instabilities are avoided as long as $\mathcal{F}_S > 0 \quad \mathcal{G}_S > 0$.

To evaluate the power spectrum of the curvature perturbation, we assume that $\epsilon \simeq$ const, $f_S := \dot{\mathcal{F}}_S/(H\mathcal{F}_S) \simeq$ const, $g_S := \dot{\mathcal{G}}_S/(H\mathcal{G}_S) \simeq$ const, and define $\nu_S := (3-\epsilon+g_S)/(2-2\epsilon-f_S+g_S)$. The power spectrum is given by

$$\mathcal{P}_\zeta = \frac{\gamma_S}{2}\left.\frac{\mathcal{G}_S^{1/2}}{\mathcal{F}_S^{3/2}}\frac{H^2}{4\pi^2}\right|_{\text{at sound horizon exit}}, \tag{26}$$

where $\gamma_S = 2^{2\nu_S-3}|\Gamma(\nu_S)/\Gamma(3/2)|^2(1-\epsilon-f_S/2+g_S/2)$. The spectral index is $n_s - 1 = 3 - 2\nu_S$. An exact scale-invariance is obtained if $\epsilon + \frac{3}{4}f_S - \frac{1}{4}g_S = 0$. Here again, ϵ, f_S, and g_S are not necessarily very small (as long as $n_s - 1 \simeq 0$). Taking now the limit $\epsilon, f_T, g_T, f_S, g_S \ll 1$, the tensor-to-scalar ratio is given by

$$r = 16\left(\frac{\mathcal{F}_S}{\mathcal{F}_T}\right)^{3/2}\left(\frac{\mathcal{G}_S}{\mathcal{G}_T}\right)^{-1/2} = 16\frac{\mathcal{F}_S}{\mathcal{F}_T}\frac{c_S}{c_T}. \tag{27}$$

5 Summary

In this talk, generic inflation models named (Generalized) G-inflation, driven by a single scalar field, have been studied. Our gravity + scalar-field system is described by the generalized Galileons, which do not have higher derivatives in the field equations despite the non-minimal coupling. This class of inflation models is the most general ever proposed in the context of single-field inflation. We have determined the most generic quadratic actions for tensor and scalar perturbations. Using them, we have presented the stability criteria for both types of perturbations. The primordial power spectra have also been computed.

Acknowledgments

This work was supported in part by JSPS Grant-in-Aid for Research Activity Start-up No. 22840011 (T.K.), for Scientific Research Nos. 23340058 (J.Y.) and 21740187 (M.Y.), and for Innovative Areas No. 21111006 (J.Y.).

References

[1] A. A. Starobinsky, JETP Lett. **30**, 682 (1979) [Pisma Zh. Eksp. Teor. Fiz. **30**, 719 (1979)]; A. H. Guth, Phys. Rev. D **23**, 347 (1981); K. Sato, Mon. Not. Roy. Astron. Soc. **195**, 467 (1981).

[2] A. D. Linde, Phys. Lett. B **108**, 389 (1982); A. Albrecht and P. J. Steinhardt, Phys. Rev. Lett. **48**, 1220 (1982); A. D. Linde, Phys. Lett. B **129**, 177 (1983).

[3] M. Yamaguchi, Class. Quant. Grav. **28**, 103001 (2011) [arXiv:1101.2488 [astro-ph.CO]].

[4] C. Armendariz-Picon, T. Damour and V. F. Mukhanov, Phys. Lett. B **458**, 209 (1999) [arXiv:hep-th/9904075].

[5] G. R. Dvali, G. Gabadadze and M. Porrati, Phys. Lett. B **485**, 208 (2000) [arXiv:hep-th/0005016].

[6] M. A. Luty, M. Porrati and R. Rattazzi, JHEP **0309**, 029 (2003) [arXiv:hep-th/0303116]; A. Nicolis and R. Rattazzi, JHEP **0406**, 059 (2004) [arXiv:hep-th/0404159].

[7] A. Nicolis, R. Rattazzi, E. Trincherini, Phys. Rev. **D79**, 064036 (2009). [arXiv:0811.2197 [hep-th]].

[8] T. Kobayashi, M. Yamaguchi, J. Yokoyama, Phys. Rev. Lett. **105**, 231302 (2010). [arXiv:1008.0603 [hep-th]]. C. Burrage, C. de Rham, D. Seery, A. J. Tolley, JCAP **1101**, 014 (2011). [arXiv:1009.2497 [hep-th]]; K. Kamada, T. Kobayashi, M. Yamaguchi, J. Yokoyama, Phys. Rev. **D83**, 083515 (2011) [arXiv:1012.4238 [astro-ph.CO]]; T. Kobayashi, M. Yamaguchi and J. Yokoyama, Phys. Rev. D **83**, 103524 (2011) [arXiv:1103.1740 [hep-th]]; X. Gao, JCAP **1110**, 021 (2011) [arXiv:1106.0292 [astro-ph.CO]]; X. Gao, T. Kobayashi, M. Yamaguchi and J. Yokoyama, Phys. Rev. Lett. **107**, 211301 (2011) [arXiv:1108.3513 [astro-ph.CO]];

[9] C. Deffayet, G. Esposito-Farese, A. Vikman, Phys. Rev. **D79**, 084003 (2009). [arXiv:0901.1314 [hep-th]].

[10] C. Deffayet, X. Gao, D. A. Steer and G. Zahariade, Phys. Rev. D **84**, 064039 (2011) [arXiv:1103.3260 [hep-th]].

[11] C. Charmousis, E. J. Copeland, A. Padilla, P. M. Saffin, [arXiv:1106.2000 [hep-th]].

[12] G. W. Horndeski, Int. J. Theor. Phys. 10 (1974) 363-384.

[13] T. Kobayashi, M. Yamaguchi and J. Yokoyama, Prog. Theor. Phys. **126**, 511 (2011) [arXiv:1105.5723 [hep-th]]. See also references in this paper.

[14] C. Germani, A. Kehagias, Phys. Rev. Lett. **105**, 011302 (2010). [arXiv:1003.2635 [hep-ph]].

[15] K. Van Acoleyen, J. Van Doorsselaere, Phys. Rev. **D83**, 084025 (2011). [arXiv:1102.0487 [gr-qc]].

Dam Thanh Son, Le Kim Ngoc, Nguyên van Hiêu and Nguyên van Thiêu

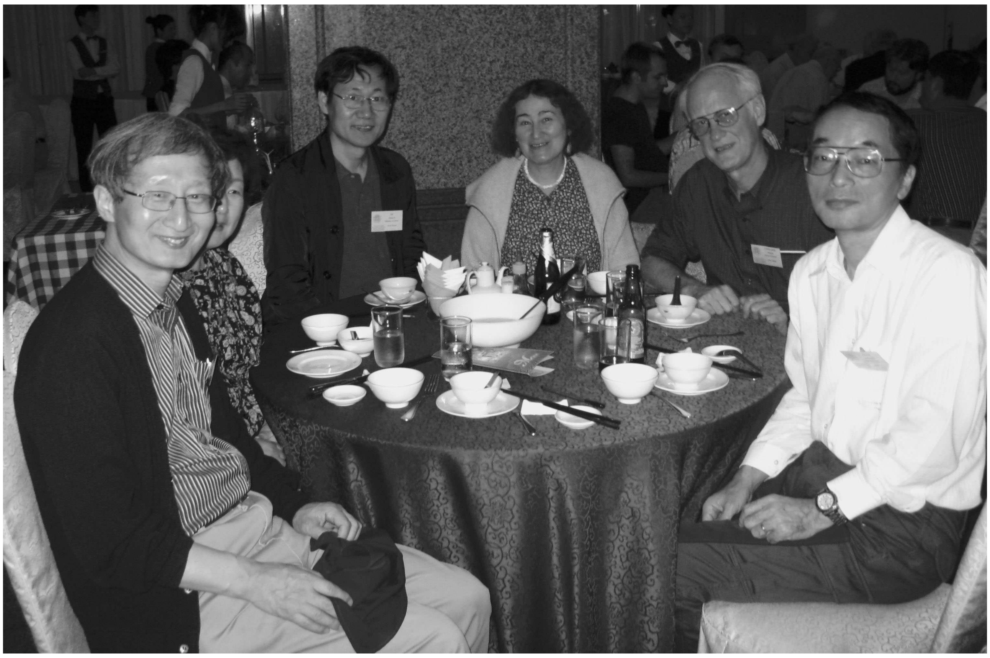

Bum-Hoon Lee, Mrs. Lee, Sang-Jin Sin, Marina Romanova, Richard Lovelace and Nobuyoshi Ohta

Did the universe have a beginning?

Audrey Mithani and Alexander Vilenkin
Institute of Cosmology, Department of Physics and Astronomy,
Tufts University, Medford, MA 02155, USA
Email : vilenkin@cosmos.phy.tufts.edu

Abstract

We discuss three candidate scenarios which seem to allow the possibility that the universe could have existed forever with no initial singularity: eternal inflation, cyclic evolution, and the emergent universe. The first two of these scenarios are geodesically incomplete to the past, and thus cannot describe a universe without a beginning. The third, although it is stable with respect to classical perturbations, can collapse quantum mechanically, and therefore cannot have an eternal past.

1 Introduction

One of the most basic questions in cosmology is whether the universe had a beginning or has simply existed forever. It was addressed in the singularity theorems of Penrose and Hawking [1], with the conclusion that the initial singularity is not avoidable. These theorems rely on the strong energy condition and on certain assumptions about the global structure of spacetime.

There are, however, three popular scenarios which circumvent these theorems: eternal inflation, a cyclic universe, and an "emergent" universe which exists for eternity as a static seed before expanding. Here we shall argue that none of these scenarios can actually be past-eternal.

Inflation violates the strong energy condition, so the singularity theorems of Penrose and Hawking do not apply. Indeed, quantum fluctuations during inflation violate even the weak energy condition, so that singularity theorems assuming only the weak energy condition [2] do not apply either. A more general incompleteness theorem was proved recently [3] that does not rely on energy conditions or Einstein's equations. Instead, it states simply that past geodesics are incomplete provided that the expansion rate averaged along the geodesic is positive: $H_{av} > 0$. This is a much weaker condition, and should certainly apply to the past of any inflating region of spacetime. Therefore, although inflation may be eternal in the future, it cannot be extended indefinitely to the past.

Another possibility could be a universe which cycles through an infinite series of big bang followed by expansion, contraction into a crunch that transitions into the next big bang [4]. A potential problem with such a cyclic universe is that the entropy must continue to increase through each cycle, leading to a "thermal death" of the universe. This can be avoided if the volume of the universe increases through each cycle as well, allowing the ratio S/V to remain finite [5]. But if the volume continues to increase over each cycle, $H_{av} > 0$, meaning that the universe is past-incomplete.

We now turn to the emergent universe scenario, which will be our main focus in this paper.

2 Emergent universe scenario

In the emergent universe model, the universe is closed and static in the asymptotic past (recent work includes [6, 7, 8, 9, 10]; for early work on oscillating models see [11]). Then $H_{av} = 0$ and the incompleteness theorem

[3] does not apply. This universe can be thought of as a "cosmic egg" that exists forever until it breaks open to produce an expanding universe. In order for the model to be successful, two key features are necessary. First, the universe should be stable, so that quantum fluctuations will not push it to expansion or contraction. In addition, it should contain some mechanism to exit the stationary regime and begin inflation. One possible mechanism involves a massless scalar field ϕ in a potential $V(\phi)$ which is flat as $\phi \to -\infty$ but increases towards positive values of ϕ. In the stationary regime the field "rolls" from $-\infty$ at a constant speed, $\dot{\phi} = const$, but as it reaches the non-flat region of the potential, inflation begins [12].

Graham et al. [10] recently proposed a simple emergent model featuring a closed universe ($k = +1$) with a negative cosmological constant ($\Lambda < 0$) and a matter source which obeys $P = w\rho$, where $-1 < w < -1/3$. Graham et al. point out that the matter source should not be a perfect fluid, since this would lead to instability from short-wavelength perturbations [10]. One such material that fulfills this requirement is a network of domain walls, which has $w = -2/3$. Then the energy density is

$$\rho(a) = \Lambda + \rho_0 a^{-1} \tag{1}$$

and the Friedmann equation for the scale factor a has solutions of the form of a simple harmonic oscillator:

$$a = \omega^{-1}(\gamma - \sqrt{\gamma^2 - 1}\cos(\omega t)), \tag{2}$$

where

$$\omega = \sqrt{\frac{8\pi}{3} G|\Lambda|} \tag{3}$$

and

$$\gamma = \sqrt{\frac{2\pi G \rho_0^2}{3|\Lambda|}}. \tag{4}$$

In the special case where $\gamma = 1$, the universe is static. Although this model is stable with respect to classical perturbations, we will see that there is a quantum instability [13, 14].

2.1 Quantum mechanical collapse

We consider the quantum theory for this system in the minisuperspace where the wave function of the universe ψ depends only on the scale factor a. In the classical theory, the Hamiltonian is given by

$$\mathcal{H} = -\frac{G}{3\pi a}\left(p_a^2 + U(a)\right), \tag{5}$$

where

$$p_a = -\frac{3\pi}{2G} a\dot{a} \tag{6}$$

is the momentum conjugate to a and the potential $U(a)$ is given by

$$U(a) = \left(\frac{3\pi}{2G}\right)^2 a^2 \left(1 - \frac{8\pi G}{3} a^2 \rho(a)\right). \tag{7}$$

With the Hamiltonian constraint $\mathcal{H} = 0$, enforcing zero total energy of the universe, we recover the oscillating universe solutions discussed in [10].

We quantize the theory by letting the momentum become the differential operator $p_a \to -i\frac{d}{da}$ and replacing the Hamiltonian constraint with the Wheeler-DeWitt equation [15]

$$\mathcal{H}\psi = 0. \tag{8}$$

From the Hamiltonian in Eq. (5), the WDW equation becomes

$$\left(-\frac{d^2}{da^2} + U(a)\right)\psi(a) = 0, \tag{9}$$

with the potential from Eqs. (1) and (7). Note that in quantum theory the form of the potential (see Fig. 1) is no longer that of a harmonic oscillator. Instead, there is an oscillating region between the classical turning

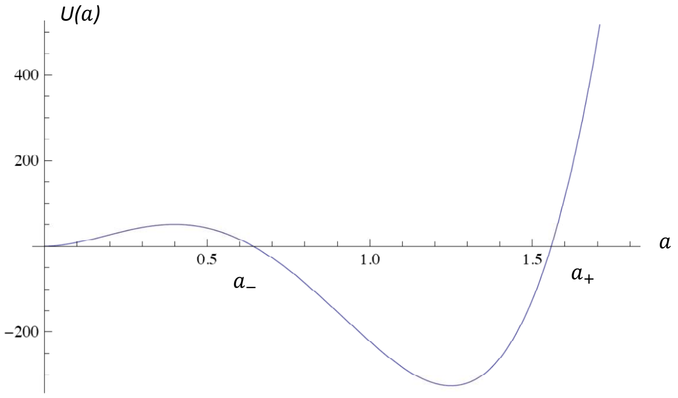

Figure 1: The potential $U(a)$ with turning points a_+ and a_-

points a_+ and a_-, which are given by

$$a_\pm = \omega^{-1}\left(\gamma \pm \sqrt{\gamma^2 - 1}\right), \tag{10}$$

and the universe may tunnel through the classically forbidden region from a_- to $a = 0$. The semiclassical tunneling probability as the universe bounces at a_- can be determined from[1]

$$\mathcal{P} \sim e^{-2S_{WKB}} \tag{11}$$

where the tunneling action is

$$S_{WKB} = \int_0^{a_-} \sqrt{U(a)}da = \frac{9M_P^4}{16|\Lambda|}\left[\frac{\gamma^2}{2} + \frac{\gamma}{4}\left(\gamma^2 - 1\right)\ln\left(\frac{\gamma - 1}{\gamma + 1}\right) - \frac{1}{3}\right]. \tag{12}$$

For a static universe, $\gamma = 1$ and $a_- = a_+ = \omega^{-1}$,

$$S_{WKB} = \frac{3M_P^4}{32|\Lambda|}. \tag{13}$$

Since the tunneling probability is nonzero, the simple harmonic universe cannot last forever.

[1]Semiclassical tunneling in oscillating universe models has been studied in the early work by Dabrowski and Larsen [13].

2.2 Solving the WDW equation

First let us examine the well-known quantum harmonic oscillator. In that case, the wave function is a solution to the Schrodinger equation

$$\frac{1}{2}\left(-\frac{d^2}{dx^2}+\omega^2x^2\right)\psi(x)=E\psi(x). \tag{14}$$

After imposing the boundary conditions $\psi(\pm\infty)\to 0$, the solutions represent a discrete set of eigenfunctions, each having energy eigenvalue $E_n=\left(n+\frac{1}{2}\right)\omega$. However, in the case of the simple harmonic universe the wave function is a solution to the WDW equation (9), which has a fixed energy eigenvalue $E=0$ from the Hamiltonian constraint. From the form of the potential in Fig. 1, it seems that we must choose $\psi(\infty)\to 0$, so that the wave function is bounded at $a\to\infty$. We are then not free to impose any additional condition at $a=0$, or the system will be overdetermined. The wave function in the under-barrier region $0<a<a_-$ is generally a superposition of growing and decaying solutions, and we can expect that the solution that grows towards $a=0$ will dominate (unless the parameters of the model are fine-tuned; see [14] for more details).

A numerical solution to the WDW equation is illustrated in Fig. 2. It exhibits an oscillatory behavior between the classical turning points and grows by magnitude towards $a=0$. This indicates a nonzero probability of collapse. Similar behavior is found for the case of $\gamma=1$, corresponding to a classically static universe.

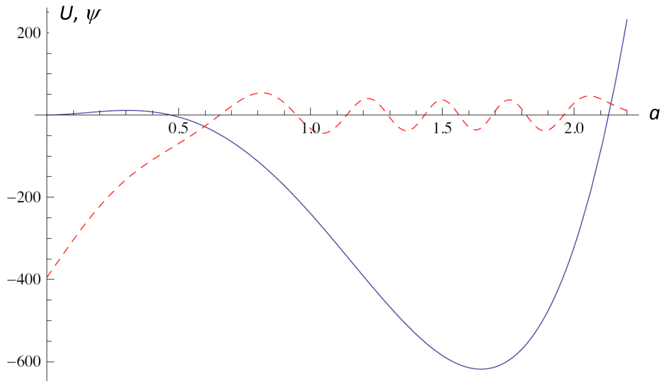

Figure 2: Solution of the WDW equation with $|\Lambda|/M_P^4=.028$ and $\gamma=1.3$ (dashed line). The WDW potential is also shown (solid line).

One can consider a more general class of models including strings, domain walls, dust, radiation, etc.,

$$\rho(a)=\Lambda+\frac{C_1}{a}+\frac{C_2}{a^2}+\frac{C_2}{a^3}+\frac{C_4}{a^4}+\ldots. \tag{15}$$

For positive values of C_n, the effect of this is that the potential develops another classically allowed region at small a. So the tunneling will now be to that other region, but the qualitative conclusion about the quantum instability remains unchanged. Altering this conclusion would require rather drastic measures. For example, one could add a matter component $\rho_n(a)=C_n/a^n$ with $n\geq 6$ and $C_n<0$. Then the height of the barrier becomes infinite at $a\to 0$ and the tunneling action is divergent. Note, however, that such a negative-energy matter component is likely to introduce quantum instabilities of its own.

3 Did the universe have a beginning?

At this point, it seems that the answer to this question is probably yes.[2] Here we have addressed three scenarios which seemed to offer a way to avoid a beginning, and have found that none of them can actually be eternal in the past. Both eternal inflation and cyclic universe scenarios have $H_{av} > 0$, which means that they must be past-geodesically incomplete. We have also examined a simple emergent universe model, and concluded that it cannot escape quantum collapse. Even considering more general emergent universe models, there do not seem to be any matter sources that admit solutions that are immune to collapse.

References

[1] S. W. Hawking and G. F. R. Ellis, The Large Scale Structure of Spacetime (Cambridge University Press, Cambridge, England, 1973).

[2] A. Borde and A. Vilenkin, *Eternal inflation and the initial singularity*, Phys. Rev. Lett. 72, 3305 (1994) [gr-qc/9312022].

[3] A. Borde, A.H. Guth and A. Vilenkin, *Inflationary Spacetimes Are Incomplete in Past Directions*, Phys. Rev. Lett. 90, 151301 (2003) [gr-qc/0110012].

[4] P. J. Steinhardt and N. Turok, *A cyclic model of the universe*, Science 296, 1436 (2002) [hep-th/0111030].

[5] R.C. Tolman, Relativity, Thermodynamics and Cosmology. Oxford University Press (1934).

[6] G.F.R. Ellis and R. Maartens, *The emergent universe: inflationary cosmology with no singularity*, Class. Quantum Grav. 21, 223 (2004) [gr-qc/0211082v4].

[7] J.D. Barrow, G.F.R. Ellis, R. Maartens, and C.G. Tsagas, *On the stability of the Einstein static universe*, Class. Quant. Grav. 20, L155 (2003) [gr-qc/0302094].

[8] S. del Campo, E. Guendelman, A.B. Kaganovich, R. Herrera and P. Labrana, *Emergent universe from scale invariant two measures theory*, Phys. Lett. B 699, 211 (2011), [arXiv:1105.0651].

[9] P. Wu and H. Yu, *Emergent universe from the Hořava-Lifshitz gravity*, Phys. Rev. D81, 103522 (2010) [arXiv:0909.2821].

[10] P.W. Graham, B. Horn, S. Kachru, S. Rajendran, and G. Torroba, *A Simple Harmonic Universe*, [arXiv:1109.0282].

[11] M. P. Dabrowski, *Oscillating Friedmann cosmology*, Ann. Phys. 248, 199 (1996) [gr-qc/9503017].

[12] D.J. Mulryne, R. Tavakol, J.E. Lidsey and G.F.R. Ellis, *An emergent universe from a loop*, Phys. Rev. D71, 123512 (2005) [astro-ph/0502589].

[13] M. P. Dabrowski and A. L. Larsen, *Quantum tunneling effect in oscillating Friedmann cosmology*, Phys. Rev. D52, 3424 (1995) [gr-qc/9504025].

[14] A.T. Mithani and A. Vilenkin, *Collapse of simple harmonic universe*, JCAP 01 (2012) 028 [arXiv:1110.4096v4].

[15] B.S. DeWitt, *Quantum Theory of Gravity. 1. The Canonical Theory*, Phys. Rev. 160, 1113 (1967).

[2]Note that we use the term “beginning” as being synonimous to past incompleteness.

An Ermakov Invariant and Temperature Fluctuations in the Early Universe

Debashis Gangopadhyay

S.N.Bose National Centre for Basic Sciences, JD-Block, Sector-III,

Salt Lake, Kolkata-700098, India

Email : debashis@rkmvu.ac.in,khokag@gmail.com

Abstract

A k-essence scalar field model has lagrangian $\mathcal{L} = -V(\phi)F(X)$, with $X = \nabla_\mu\phi\nabla^\mu\phi$ and V the potential. In an epoch,when the scale factor was very small compared to the present epoch but very large compared to the inflationary epoch (so that one is already in an expanding and flat universe) L takes the form of a time-dependent oscillator. The Ermakov invariant then leads to an invariant quadratic form involving the Hubble parameter and the logarithm of the scale factor. One can also estimate fluctuations of temperature of the background radiation in these early stages of the universe.

1 Introduction

A $k-$essence lagrangian is taken as $\mathcal{L} = -V(\phi)F(X)$. The energy density is $\rho = V(\phi)[F(X) - 2XF_X]$ with $F_X \equiv \frac{dF}{dX}$ and $XF_X^2 = Ca^{-6}$ and a is the scale factor. Taking the Robertson-Walker metric, using the scaling law and the zero-zero component of Einstein's field equations and a homogeneous and isotropic spacetime with curvature constant $k = 0$ [1]

$$\mathcal{L} = -c_1\dot{q}^2 - c_2\dot{\phi}e^{-3q} \tag{1}$$

$q(t) = ln\ a(t)$, $c_1 = 3(8\pi G)^{-1}$, $c_2 = 2V\sqrt{C}$. $q(t), \phi(t)$ are generalised coordinates. We work in natural units, V is in suitable dimensionless units, $\sqrt{C}$ is a dimensionless constant and the ϕ is a scalar function. All time variables are $t \equiv t/t_0$. So $q, \dot{q}$ etc. are dimensionless. In 4 dimensions Newton's constant G has dimension $[M]^{-1}[L]^3[T]^{-2}$. So $\frac{1}{G} \equiv \frac{1}{m_P^2 G}$ is dimensionless. We restrict to the domain i.e. $-1 < q < 0$. Here a is small when q is small and $|a| < 1$ for $|q| < 1$. Also ,$V(\phi) \equiv V_0 = const.$. As $\phi(t)$ does not have a kinetic term and hence no dynamics, relegate it to a time dependent parameter (*not a field*) by writing $g(t) = 2\sqrt{C}V_0\dot{\phi}$. This theory is different from (1) as now there is only one generalised coordinate q. Expanding the exponential in (1) upto $O(q^2)$: $\mathcal{L} = -\frac{M}{2}[\dot{q}^2 + 12\pi m_P^2 Gg(t)q^2] - (\frac{1}{2})g(t)$. $M = \frac{3}{4\pi m_P^2 G}$, $c = 1$.Put $12\pi m_P^2 Gg(t) = -\Omega^2(t)$. This means $\phi(t) = -\frac{1}{24\pi m_P^2 G\sqrt{C}V_0}\int dt\Omega^2(t)$. Thus $\mathcal{L} = -\frac{M}{2}[\dot{q}^2 - \Omega^2(t)q^2] - (\frac{1}{2})g(t)$. The term $\frac{1}{2}g(t)$ is a total time derivative and hence ignorable. Then (1) becomes [2]

$$\mathcal{L} = -\frac{M}{2}[\dot{q}^2 - \Omega^2(t)q^2] \tag{2}$$

In contradistinction to (1) , (2) is a theory with only one degree of freedom q. Varying ϕ for a constant potential is disallowed as it leads to the absurdity $a(t) = constant$. Ignoring the overall negative sign we have a time dependent oscillator for $q(t) = ln\ a(t)$.

2 The Ermakov Invariant

The Hamiltonian $\mathcal{H}$ corresponding to (2) is

$$\mathcal{H} = \frac{M}{2}[p^2 + \Omega^2(t)q^2] = \frac{M}{2}[H^2 + \Omega^2(t)q^2] \tag{3}$$

where $p = \dot{q} = \frac{\dot{a}}{a} = H$, H is the Hubble parameter. The Ermakov invariant is [3] $I = \frac{1}{2}[\rho^{-2}q^2 + \left(\rho H - \frac{1}{M}\dot{\rho}q\right)^2]$, where $\rho(t)$ satisfies Ermakov's equation $\frac{1}{M^2}\ddot{\rho} + \Omega^2\rho - \rho^{-3} = 0$. Putting in the values of M and simplifying,

$$I = \mathcal{A}(t)(ln\ a(t))^2 - \mathcal{B}(t)(ln\ a(t))H(t) + \mathcal{C}(t)H^2 \tag{4}$$

with $\mathcal{A}(t) = \frac{\rho^{-2}(t)}{2} + \frac{32\pi^2G^2}{9}(\dot{\rho}(t))^2$; $\mathcal{B}(t) = \frac{8\pi G\rho(t)\dot{\rho}(t)}{3}$; and $\mathcal{C}(t) = \frac{\rho^2(t)}{2}$. I is an invariant for the Hamiltonian $\mathcal{H}$ in the sense: $\frac{dI}{dt} = \frac{\partial I}{\partial t} + [I, \mathcal{H}]_{Poisson\ bracket} = 0$. Thus,the early universe admits an invariant quadratic form in H and a with time dependent coefficients. These are functions of the solutions of the Ermakov equation.

3 Temperature fluctuations

Write $q(t) = q_{cl}(t) + x(t)$ where $x(t)$ is the fluctuation from the classical value $q_{\rm cl}$ and $0 \leq x(t) \leq \infty$. Then the quantum mechanical amplitude for $loga(t)$ to evolve from the value q_a at time t_a to q_b at time t_b is given by [2] $\langle q_b, t_b | q_a, t_a\rangle = \langle lna(t_b), t_b | lna(t_a), t_a\rangle = F(t_b, t_a)e^{\frac{i}{\hbar}S_{\rm cl}}$. $S_{\rm cl} = \int_{t_a}^{t_b} L_{\rm cl}dt = \int_{t_a}^{t_b} dt[\frac{M}{2}\dot{q}_{cl}^2 - \frac{1}{2}\Omega^2(t)q_{cl}^2]$. $\Omega(t)$ has been re-labelled as $\Omega(t) \rightarrow \sqrt{M}\Omega(t)$. (Factors of $\hbar$ and c will be put equal to unity at the end). The fluctuations $x(t)$ satisfy $\ddot{x} + \Omega^2(t)x = 0$. Ω is real, so we have quasi-periodic solutions. Consider two solutions: $x_1(t) = \psi(t)sin\zeta(t, t_a)$; $x_2(t) = \psi(t)sin\zeta(t_b, t)$ satisfying the boundary conditions $x_1(t_a) \equiv x_{1a} = 0$; $x_2(t_b) \equiv x_{2b} = 0$ with $\psi(t)$ satisfying the Ermakov-Pinney equation $\ddot{\psi} + \Omega^2(t)\psi - \psi^{-3} = 0$. $\zeta(t,s) = \nu(t) - \nu(s) = \int_s^t dt\psi^{-2}(t)$. $\psi(t)$ and $\nu(t)$ can be interpreted as the amplitude and phase of the time dependent oscillator. Then the fluctation factor $F(t_b, t_a) = \left(\frac{M\sqrt{(\dot{\nu}_b\dot{\nu}_a)}}{2\pi i\hbar sin\zeta(t_b,t_a)}\right)^{\frac{1}{2}}$. Classical solutions satisfying relevant boundary conditions are found , i.e. $q(t = t_a) = q_a, q(t = t_b) = q_b$ and then $\langle q_b, t_b|q_a, t_a\rangle = \left(\frac{M\sqrt{(\dot{\nu}_b\dot{\nu}_a)}}{2\pi i\hbar sin\zeta(t_b,t_a)}\right)^{\frac{1}{2}}\left(exp(\frac{iS_{cl}^+}{\hbar}) - exp(\frac{iS_{cl}^-}{\hbar})\right)$. Here $S_{\rm cl}^{\pm} = \left(\frac{\dot{\psi}_b q_b^2}{\psi_b} - \frac{\dot{\psi}_a q_a^2}{\psi_a}\right) + \frac{1}{sin\zeta(t_b,t_a)}\left((\dot{\nu}_b q_b^2 + \dot{\nu}_a q_a^2)cos\zeta(t_b, t_a) \mp 2\sqrt{(\dot{\nu}_b\dot{\nu}_a)}q_b q_a\right)$ Now assume $\dot{\nu} << 1$ .Note that the temperature of the background radiation in a homogeneous universe is inversely proportional to the scale factor i.e. $T(t_a) \equiv T_a = \frac{1}{a(t_a)}$ (in appropriate dimensionless units). For $\psi(t) = e^{\gamma t}, 0 < \gamma < 1$ and for $\dot{\nu} << 1$ the probability for the logarithm of inverse temperature evolution is [2]

$$P(b,a) = |\langle ln\ (\frac{1}{T_b}), t_b|ln\ (\frac{1}{T_a}), t_a\rangle|^2 \approx \left(\frac{3m_{\rm Pl}^2}{\pi^2}\right)\frac{(ln\ T_a)^2(ln\ T_b)^2\left(1 - 3\gamma(t_a + t_b)\right)}{(t_b - t_a)^3} \tag{5}$$

where $\hbar = c = 1$. $\phi(t)$ can be determined from the Ermakov equation for the given choice of $\psi(t)$ [2]. The time evolution of ϕ has been shown to be consistent with that obtained from Supernova Ia data [4]. So we now have a new formalism to describe fluctuations of the background temperature. $\dot{\nu}(t_a), \dot{\nu}(t_b), \zeta(t_b, t_a)$ are related to solutions of the Ermakov-Pinney equation. The bounds on these functions may be estimated from phenomenological observations of satellite data if the fluctuations of the background temperature can ever be accurately determined.

I thank the organisers of ICGAC10 for a wonderful conference.

References

[1] D.Gangopadhyay and S.Mukherjee,*Logarithm of the scale factor as a generalised coordinate in a lagrangian for dark matter and dark energy*, Phys.Lett. B665 (2008) 121 [arXive:0710.5366]. .

[2] D.Gangopadhyay,*Estimating temperature fluctuations in the early universe*, Grav. and Cosmol. 16 (2010) 231 [arXive:0903.3806].

[3] D.Gangopadhyay and S.Mukherjee,*On a cosmological invariant as an observational probe in the early universe*, Grav. and Cosmol. 17 (2011) 231 [arXive:1010.3806].

[4] A. Bandyopadhyay, D.Gangopadhyay and A.Moulik,*The k-essence scalar field in the context of Supernova Ia observations*, Euro.Phys.Jour. C72 (2012) 1943 [arXive:1102.3554].

Gravitational Galaxy Clustering in an Expanding Universe

Manzoor A. Malik

Department of Physics, University of Kashmir, Srinagar-190006, India

Email : mmalik@kashmiruniversity.ac.in

Abstract

Statistical mechanical approach is shown to provide an elegant description of various aspects of gravitational galaxy clustering. The galaxy distribution function derived from statistical mechanical considerations shows excellent agreement with observations and N-body simulation results. Applicability of statistical mechanics to gravitating systems, motivation for pursuing it further and a roadmap for future is presented.

1 Introduction

Statistical mechanical description of gravitational galaxy clustering owes its origin to the Gravitational Quasi-Equilibrium Distribution [1, 2], a relatively older but useful thermodynamic description of gravitating systems. The new and improved statistical mechanical description of gravitating systems [3, 4, 5, 6, 7, 8] not only provides a more fundamental basis for its thermodynamic predecessor but also provides insights into many new aspects of galaxy clustering.

The fundamental question that can be asked at the very outset is whether a statistical mechanical description is possible for a gravitating system. At the face of it the answer appears to be in negative for there cannot be a rigorous equilibrium statistical mechanical description for infinite gravitating systems that are basically unstable. Further, a statistical mechanical description would require the evaluation of the system's partition function which may not be so straight forward for a many-body gravitating system. Another difficulty is infinite range of the gravitational force and that it cannot be shielded.

The basic idea that makes a statistical mechanical (or thermodynamical) description possible is the assumption of quasi-equilibrium, according to which galaxy clustering evolves through a sequence of equilibrium states. The quasi-equilibrium evolution of galaxy clustering is based on the physical grounds that the local dynamical timescale in an overdense region is faster than the global gravitational timescale so that local equilibria can arise faster than the cosmic expansion can disrupt them. Then, the usual thermodynamic quantities such as density, pressure, temperature, chemical potential, and correlation energy are well defined and relax locally at a faster rate than they change globally due to the expansion of the universe. This (quasi-equilibrium) approximation works well and its validity has been debated at length in the literature [1, 9, 10]. N-body simulations of galaxy clustering [11, 12] support the idea of quasi-equilibrium evolution, although the detailed conditions under which it can hold are still unclear.

The other difficulty of evaluation of the partition function, that requires the evaluation of configuration integral incorporating the many-body gravitational potential, is overcome by invoking that the infinite range gravitational force has a finite effective range. The justification comes from the observation that the expansion of the universe cancels the effect of the long range gravitational field for distances greater than a certian finite distance [9].

The above considerations facilitate evaluation of the partition function and once it is known, all the thermodynamic quantities (being derivatives of free energy) can be obtained from which the distribution function follows easily.

2 Clustering Parameter

The clustering parameter b, which infact is a measure of gravitational attraction and hence clustering, was a guess in the original thermodynamic description [2], dictated by the condition that b takes the values 0 to 1 for homogeinity and complete clustering respectively. The beauty of the statistical mechanical approach is that the physical form of the clustering parameter follows here directly from the calculations and is exactly of the same form as the Saslaw-Hamilton guess [2]. Further, it now covers a whole range of features that (directly or indirectly) determine clustering. For example, the features like i) extended nature of galaxies [3] ii) contribution of higher order terms [4] iii) multi-component nature of the system [5, 6, 8] are inherently contained in the clustering parameter itself.

The most general form of the clustering parameter that incorporates the features of a three-component system besides the extended nature of galaxies [8] is:

$$b_3 = \frac{b_\epsilon}{\left(1 + \frac{N_2}{N_1} + \frac{N_3}{N_1}\right)} \left[1 + \frac{\left(\frac{N_2}{N_1}\right)\left(\frac{m_2}{m_1}\right)^3}{1 - b_\epsilon + \left(\frac{m_2}{m_1}\right)^3 b_\epsilon} + \frac{\left(\frac{N_3}{N_1}\right)\left(\frac{m_3}{m_1}\right)^3}{1 - b_\epsilon + \left(\frac{m_3}{m_1}\right)^3 b_\epsilon} \right], \tag{1}$$

where N_1, N_2 and N_3 are the number of particles of mass m_1, m_2 and m_3 respectively, such that $N = N_1 + N_2 + N_3$ is the total number of particles in the system.

From equation (1), it follows easily that for $m_1 = m_2 = m_3$ (i.e. all galaxies having the same mass), $b_3 = b_\epsilon$ which is defined by [3]

$$b_\epsilon = \frac{\beta \bar{n} T^{-3} \alpha(\epsilon/R_1)}{1 + \beta \bar{n} T^{-3} \alpha(\epsilon/R_1)} \tag{2}$$

since $\beta \bar{n} T^{-3} = b/(1-b)$; b_ϵ is related to b by

$$b_\epsilon = \frac{b\alpha(\epsilon/R_1)}{1 + b\left\{\alpha(\epsilon/R_1) - 1\right\}} \tag{3}$$

It simply follows that for the point-mass approximation ($\epsilon = 0, \alpha = 1$), b_ϵ reduces to its original point-mass form deduced from thermodynamic considerations [1].

The advantage of equation (1) is that it incorporates the extended nature of galaxies as well as the multi-component nature of the system besides having a rigorous mathematical basis.

3 Distribution Function

The fundamental requirement for a statistical mechanical description is the evaluation of gravitational many-body partition function. This had been done in [3, 4] for a single-component system, [5, 6, 8] for a multi-component system (adding new features all the time), by invoking some physically motivated assumptions. Once the partition function is known, all thermodynamic quantities can be evaluated as these are just first or second order derivatives of free energy which is related to the partition function $Z_N(T, V)$ by $F =$

$-T \ln Z_N(T,V)$. The most important of these results is, of course, the spatial galaxy distribution function $f(N)$, which can be derived from its general realtion to the grand canonical partition function Z_G, the chemical potential μ and the sum over energy states Z_N. In the quest for completeness, many new features have been incorporated in the distribution function from time to time [3, 4, 5, 6, 8], each time explaining an important property of the system.

We start here with the three-component distribution function because all other previous results [3, 5, 6] except [4] are just special cases of it. It is worth mentioning here that in reference [4], effect of the inclusion of higher order terms is taken into account and it is shown that the effect on the distribution function is negligible for high N. Thus, for all practical purposes, we may treat the following distribution function as the most general one:

$$\begin{aligned} f(N,\epsilon) = \frac{\bar{N}(1-b_\epsilon)}{N!}\left[\bar{N}(1-b_\epsilon)+Nb_\epsilon\right]^{N_1-1} \times \frac{\left[\bar{N}(1-b_\epsilon)+\left(\frac{m_2}{m_1}\right)^3 Nb_\epsilon\right]^{N_2}}{\left[(1-b_\epsilon)+\left(\frac{m_2}{m_1}\right)^3 b_\epsilon\right]^{N_2}} \\ \times \frac{\left[\bar{N}(1-b_\epsilon)+\left(\frac{m_3}{m_1}\right)^3 Nb_\epsilon\right]^{N_3}}{\left[(1-b_\epsilon)+\left(\frac{m_3}{m_1}\right)^3 b_\epsilon\right]^{N_3}} \times e^{-Nb_3-\bar{N}(1-b_3)}, \end{aligned} \tag{4}$$

If we choose the mass of any one component to be the same as any of the other two (say $m_2 = m_3$), the above relation faithfully reduces to the earlier results [5] for a two-component system. It is easy to see that the original result [3],

$$f(N,\epsilon) = \frac{\bar{N}(1-b_\epsilon)}{N!}\left[\bar{N}(1-b_\epsilon)+Nb\right]^{N-1} e^{-\bar{N}(1-b_\epsilon)-Nb_\epsilon}, \tag{5}$$

is retrieved if $m_1 = m_2 = m_3$. The result of Saslaw and Hamilton [2] is just the special case of above equation for $\epsilon = 0$.

While various manifestations of the spatial galaxy distribution function obtained from statistical mechanical considerations have been discussed in the literature [3, 4, 5, 6, 8], a few points are worth a mention. For instance, since the extended nature of galaxies is a reality, an objective theory has to take into account the effect of this extended nature. Though the extended nature of galaxies is shown to have a negligible effect on the distribution function, it has been systematically explored from these considerations. Again, it is known that galaxies constituting a cluster have diverse mass profiles. The statistical mechanical description makes it possible to successfully account for those diverse mass profiles of galaxies. Also, the theory has a rigorous mathematical background and lends a more fundamental basis to results obtained earlier from thermodynamic considerations.

4 Discussion

Although, distribution functions had been proposed during the times of Herschel [13] who simply counted the numbers of galaxies in cells of a given size and shape on the sky, a more informative description which could be related to the underlying gravitational physics was proposed by Saslaw and vastly improved by his collaborators Hamilton, Fang, Aarseth, Itoh, Inagaki, Yang and others. The theory known as the Gravitational Quasi-equilibrium Distribution (GQED), reviewed in [1], showed excellent agreement with N-body simulation results and observations.

A more fundamental basis to the results of GQED is provided by the statistical mechanical description. The advantages of a statistical mechanical description are manifold. Firstly, this description settles the issue of the physical form of the clustering parameter which had been introduced as an ansatz in the original GQED theory. Secondly, it takes care of the extended nature of galaxies in the form of the softening parameter ϵ which is a representative of an isothermal halo surrounding each galaxy. Softening the potential has also the advantage of removing the divergences when two galaxies approach each other arbitrary closely. Third, it brings in the feature of the multi-component nature of the system by being able to account for the different mass profiles of the galaxies. Earlier models used to consider galaxies as point masses with each galaxy having the same mass. However, since in reality galaxies are neither point structures nor have the same masses, bringing in this feature is important in its own right.

There, however, are some issues for which we have either only incomplete answers or no answers. For example; while as the quasi-equilibrium approximation is quite useful, the detailed conditions under which it can hold are not known. Further, we assume an initial Poisson distribution while the CMB observations suggest that the initial fluctuations might not have been Poisson. The distribution function can account for only a small fraction of the Dark Matter which may reside in the galaxy halos. What amount (and nature) of Dark Matter can destroy agreement with the theory is yet to be investigated.

Of course, the ultimate test of a theory is its agreement with experiment. Our experiments are the computer N-body simulation results and the observations. The theory shows remarkably good agreement with both and hence motivates us to pursue it further.

References

[1] Saslaw W. C. (2000), *The Distribution of the Galaxies: Gravitational Clustering in Cosmology*, (New York: Cambridge University Press).

[2] Saslaw W. C. and Hamilton A. J. S, (1984), *ApJ*, **276**, 13

[3] Ahmad F., Saslaw W. C. and Bhat N. I., (2002), *ApJ* **571**, 576.

[4] Ahmad F., Saslaw W. C. and Malik M. A., (2006), *ApJ*, **645**, 940.

[5] Ahmad F., Malik M. A. and Masood S., (2006), *Int. J. Mod. Phys. D*, **15**, 8, 1267.

[6] Malik M. A., Ahmad F., Shakeel Ahmad and Sajad Masood, (2009), *Int. J. Mod. Phys. D*, 18, 6, 1.

[7] Saslaw W. C. and Ahmad F., (2010), *ApJ*, **720**, 1246

[8] Malik M. A., Ali R. N. and Ahmad F., (2011), *Astro. Sp. Sc.* (Early online)

[9] Saslaw W. C. and Fang F. (1996), *ApJ.* **460**, 16.

[10] Saslaw W.C., Chitre S.M., Itoh M. and Inagaki S., 1990, ApJ, 365, 419

[11] Itoh M., (1990), *PASJ*, **42**, 481

[12] Itoh M., Inagaki S. and Saslaw W.C., (1988), *ApJ.* **331**, 45

[13] Herschel, W. (1784), *Phil. Trans.*, LXXIV, 437

The background field method applied to cosmological phase transition

Phan Hong Lien
Le Quy Don University of Technology, 100 Hoang Quoc Viet, Hanoi, Vietnam
Email : phlien.mta@gmail.com

1 One loop free energy density at $T \neq 0$

Phase transition is a complicated physical process whose nature is non pertubative phenomenon. There has been considerable interest in the symmetry in both hot scalar field theories and hot gauge theories for cosmology. It is shown that the phase transition in the early Universe could be described by non-Abelian gauge theories at high temperature. Our main aim is to apply the background gauge field method at high temperature to investigate cosmological phase transition.

We start from the Lagrangian density

$$\begin{aligned} L_0 = &- \frac{1}{4} F^a_{\mu\nu} F^{a\mu\nu} + \bar{\mathbf{\Psi}}(i\gamma^\mu D_\mu - G_i \Phi_i)\mathbf{\Psi} \\ &+ \left[(D_\mu - i\mu\delta_{\mu 0})\Phi_i\right]^+ \left[(D^\mu - i\mu\delta^{\mu 0})\Phi_i\right] - m^2 \Phi_i^+ \Phi_i - \lambda(\Phi_i^+ \Phi_i)^2 \\ &- \frac{1}{2\xi}\left(\partial^\mu A^a_\mu\right)^2 - \partial_\mu \omega_a^* \partial^\mu \omega_a + f_{abc}(\partial_\mu \omega_a^*) A^b_\mu \omega^c. \end{aligned} \tag{1}$$

where μ is chemical potential, G_i and λ are coupling constants, $\lambda > 0$.

The one loop thermal effective potential reads

$$\begin{aligned} V_\beta = &- \frac{1}{2}(\mu^2 - m^2)\phi^2 + \frac{\lambda}{4}\phi^4 - \frac{1}{2}\delta_{ab} M^2_{ab} A^2_{0\mu} - \frac{\pi^2 T^4}{90}\left(N_B + \frac{7}{8}N_F\right) \\ &+ \frac{T^2}{24}\left\{(\mu^2 - m^2 - \frac{\lambda}{2}\phi^2) + 3TrM^2_{ab} + \frac{1}{2}Tr\left[\gamma_0(M + \mu\gamma_0)\gamma_0(M + \mu\gamma_0)\right]\right\} \\ &- \frac{T}{12\pi}\left(\mathfrak{M}^3 + \delta_{ab} M^3_{ab}\right) - \frac{g^2 T^3}{48 \times 4\pi}\left(\mathfrak{M} + \delta_{ab} M_{ab} + 2M\right) \\ &+ \frac{g^2}{(4\pi)^2}\left(\frac{11}{12}N - \frac{1}{6}N_F + \frac{1}{12}N_B\right)\left(\frac{1}{\epsilon} - 2ln\frac{\bar{\eta}}{4\pi T} + 2\gamma_E\right)\int dx F^a_{\mu\nu} F^{a\mu\nu}. \end{aligned} \tag{2}$$

Hence, the scalar thermal mass is

$$\mathfrak{M}^2 = (\mu^2 - m^2) + \frac{\lambda}{24}T^2 - \frac{\lambda}{2}\phi^2. \tag{3}$$

2 Some numerical results

In the case of $\mu \leq m$, the free energy density is minimum at $\Phi_0 = 0$ at any temperature T, i.e the symmetry is not broken.

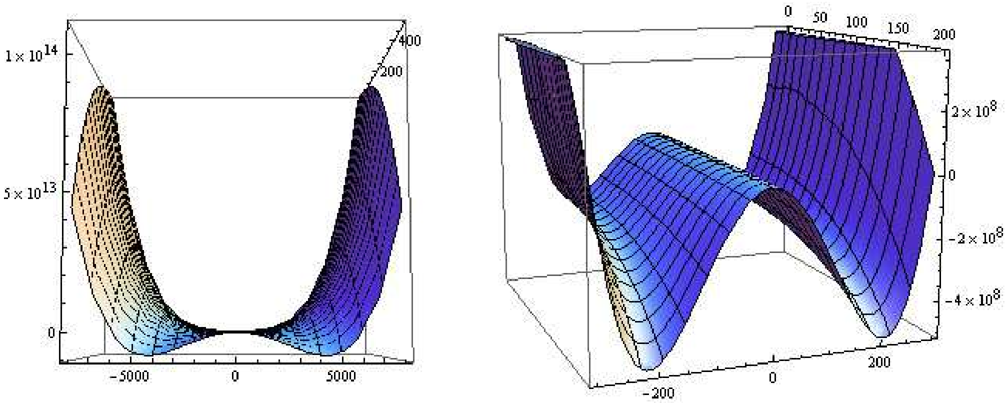

Fig. 1. The effective potential with $g = 10GeV, \lambda = 0.1, T = 0 \div 200MeV$.

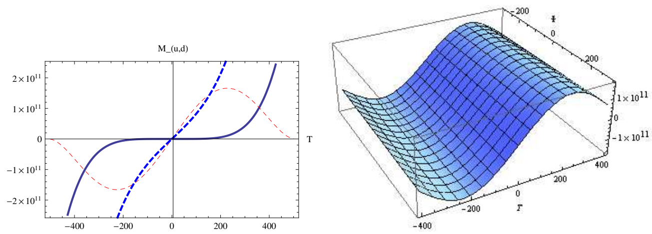

Fig. 2. The squared scalar mass $\mathfrak{M}^2$ as a function of temperature T.

In Fig. 2, we can see that the effective squared scalar mass is changed from negative to positive value when the temperature is high enough. These are just phenomena of symmetric breaking, when the cosmological phase transition is manifested. It is the first order phase transition.

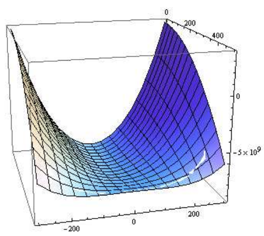

Fig. 3. The effective mass as a function of chemical potential.

In Fig. 3, the free energy has a discontinuity when $\mu \geq m$. It is shown by the discontinuous buffer between the symmetry and its breaking part. This is just the cosmological phase transition. Furthermore, the restoration of symmetry does appear, that means after symmetry was spontaneously broken, the Universe is asymmetry.

We have studied the free energy as a function of temperature and non-zero chemical potential by background gauge field method in frame of Abelian theories. Hence the mechanism of cosmological phase transition is investigated. The graphic solutions have shown that in the early Universe it is first order phase transition. Furthermore, after the symmetry is spontaneously broken, non-restoration of symmetry in hot gauge field theories for Cosmology.

Characterizing the average properties of an inhomogeneous universe

Masaaki Morita
Okinawa National College of Technology, 905 Henoko, Nago, Okinawa 905-2192, Japan
Email : morita@okinawa-ct.ac.jp

Abstract

In standard cosmology, the global dynamics of the universe is assumed to be described by a homogeneous and isotropic FLRW universe model, but a realistic universe model should include local inhomogeneities, and the physical properties of such a realistic model averaged over a sufficiently large scale do not necessarily coincide with those of the FLRW universe. In this article, we give an overview of works studying how local inhomogeneities affect the global expansion. We also point out that a natural measure of inhomogeneity is derived, which is identical to the *relative information entropy*, and discuss its temporal behaviour.

successfully described by a homogeneous and isotropic Friedmann-Lemaître-Robertson-Walker (FLRW) universe model on large scales. In spite of its simplicity, the validity of this hypothesis is highly non-trivial because a realistic universe model should include local inhomogeneities, and the physical properties of such a realistic model averaged over a sufficiently large scale do not necessarily coincide with those of the FLRW universe. This fact is now widely noticed in the context of dark energy cosmology, because the effect of inhomogeneities may be an alternative to introducing an exotic matter for the cosmic acceleration. (See, e.g. Ref. [1] for a comprehensive review.)

In this article, we give an overview of recent works which have formulated averaging of an inhomogeneous universe to explore how local inhomogeneities affect the global expansion, and discuss the possibility of inhomogeneities as 'effective dark energy'. We also point out that, within the formulation of averaging, a measure of inhomogeneity naturally arises, which is identical to the *relative information entropy*, and discuss its temporal behaviour in connection with the cosmic acceleration.

1 Averaging inhomogeneous universes

Let us begin with the basic equations that govern the dynamics of a spatially averaged inhomogeneous universe, along the formulation developed by Buchert [2]. We restrict our consideration to an irrotational pressureless fluid with energy density ϱ and four-velocity u^μ, and work in a time-orthogonal foliation with the line element

$$\mathrm{d}s^2 = -\mathrm{d}t^2 + g_{ij}\mathrm{d}X^i\mathrm{d}X^j \,, \tag{1}$$

where X^i are coordinates in the $t =$ const. hypersurfaces (with three-metric g_{ij}) that are comoving with the fluid so that the four-velocity $u^\mu = (1, \mathbf{0})$. We introduce the expansion tensor $\Theta_{ij} := (1/2)\dot{g}_{ij}$, where an overdot ($\dot{}$) denotes time derivative, and its trace $\theta := g^{ij}\Theta_{ij}$ (the local expansion rate), and the traceless part $\sigma_{ij} := \Theta_{ij} - (1/3)\theta g_{ij}$ (the shear tensor). Using these quantities as dynamical variables, the continuity equation and the Raychaudhuri equation are written as

$$\dot{\varrho} + \varrho\theta = 0 \,, \tag{2}$$

$$\dot{\theta} = -4\pi G\varrho - \frac{1}{3}\theta^2 - 2\sigma^2\,, \tag{3}$$

where $\sigma^2 := (1/2)\sigma^i{}_j\sigma^j{}_i$ is the rate of shear squared.

We define averaging of a scalar quantity $A(t, X^i)$ by the Riemannian volume average over a compact spatial domain $\mathcal{D}$:

$$\langle A(t,X^i)\rangle_{\mathcal{D}} := \frac{1}{V_{\mathcal{D}}}\int_{\mathcal{D}} A(t,X^i)\sqrt{\det(g_{ij})}\,\mathrm{d}^3X\ ; \qquad V_{\mathcal{D}}(t) := \int_{\mathcal{D}}\sqrt{\det(g_{ij})}\,\mathrm{d}^3X\,. \tag{4}$$

We also introduce an effective scale factor via the volume (normalized by the volume of the initial domain $V_{\mathcal{D}_\mathrm{i}}$), $a_{\mathcal{D}}(t) := (V_{\mathcal{D}}(t)/V_{\mathcal{D}_\mathrm{i}})^{1/3}$. Then the averaged expansion rate is expressed as $\langle\theta\rangle_{\mathcal{D}} = \partial_t V_{\mathcal{D}}/V_{\mathcal{D}} = 3\,\partial_t a_{\mathcal{D}}/a_{\mathcal{D}}$. The key concept in the averaging formalism is *non-commutativity* of two operations, spatial average and time evolution. This is expressed by a *commutation rule* for the averaging of a scalar field A [2]:

$$\frac{\partial}{\partial t}\langle A\rangle_{\mathcal{D}} - \left\langle\frac{\partial A}{\partial t}\right\rangle_{\mathcal{D}} = \langle A\theta\rangle_{\mathcal{D}} - \langle A\rangle_{\mathcal{D}}\langle\theta\rangle_{\mathcal{D}} = \langle\delta A\,\delta\theta\rangle_{\mathcal{D}}\,, \tag{5}$$

where $\delta A := A - \langle A\rangle_{\mathcal{D}}$ and $\delta\theta := \theta - \langle\theta\rangle_{\mathcal{D}}$. Averaging Eqs. (2) and (3) with the help of Eq. (5) yields

$$\frac{\partial}{\partial t}\langle\varrho\rangle_{\mathcal{D}} + \langle\varrho\rangle_{\mathcal{D}}\langle\theta\rangle_{\mathcal{D}} = 0\,, \tag{6}$$

$$3\frac{\ddot{a}_{\mathcal{D}}}{a_{\mathcal{D}}} + 4\pi G\langle\varrho\rangle_{\mathcal{D}} = Q_{\mathcal{D}}\ ; \qquad Q_{\mathcal{D}} := \frac{2}{3}\left(\langle\theta^2\rangle_{\mathcal{D}} - \langle\theta\rangle_{\mathcal{D}}^2\right) - 2\langle\sigma^2\rangle_{\mathcal{D}}\,, \tag{7}$$

where $Q_{\mathcal{D}}$ is the 'kinematical backreaction term', which appears due to inhomogeneities of cosmic matter distribution and leads the effective cosmic expansion given by $a_{\mathcal{D}}$ to deviate from the Friedmannian one. Equation (7) tells us that the kinematical backreaction term consists of the fluctuation of the expansion rate and the averaged shear rate; the former plays the role of 'effective dark energy', and the latter can be regarded as additional matter density. The backreaction $Q_{\mathcal{D}}$ has been estimated with linear perturbations of a spatially flat FLRW universe model in Ref. [3].

2 Relative information entropy

In order to introduce a quantity that measures how the universe is inhomogeneous within the formulation, we pay particular attention to the commutation rule for the matter density field:

$$\frac{\partial}{\partial t}\langle\varrho\rangle_{\mathcal{D}} - \left\langle\frac{\partial\varrho}{\partial t}\right\rangle_{\mathcal{D}} = \langle\varrho\theta\rangle_{\mathcal{D}} - \langle\varrho\rangle_{\mathcal{D}}\langle\theta\rangle_{\mathcal{D}} = \langle\delta\varrho\,\delta\theta\rangle_{\mathcal{D}}\,. \tag{8}$$

This means that the time evolution of the averaged density field does not coincide with the average of the density field evolved locally. We consider that the difference between $\langle\varrho\rangle\dot{}_{\mathcal{D}}$ and $\langle\dot{\varrho}\rangle_{\mathcal{D}}$ leads to the entropy production for the matter density field. This idea brings us to write

$$\frac{\partial}{\partial t}\langle\varrho\rangle_{\mathcal{D}} - \left\langle\frac{\partial\varrho}{\partial t}\right\rangle_{\mathcal{D}} = -\frac{\dot{\mathcal{S}}}{V_{\mathcal{D}}}\,, \tag{9}$$

where $\mathcal{S}$ is an entropy associated with the density field. Looking for a functional of the matter density field that satisfies Eq. (9), we find that the answer is [4]:

$$\mathcal{S}\{\varrho\,\|\,\langle\varrho\rangle_{\mathcal{D}}\} := \int_{\mathcal{D}}\varrho\ln\frac{\varrho}{\langle\varrho\rangle_{\mathcal{D}}}\sqrt{\det(g_{ij})}\,\mathrm{d}^3X\,, \tag{10}$$

which is identical to the *Kullback-Leibler relative information entropy.* Note that, for strictly positive density, $\varrho > 0$, the entropy $\mathcal{S}$ is positive definite if $\varrho \neq \langle\varrho\rangle_{\mathcal{D}}$, and $\mathcal{S} = 0$ if and only if $\varrho = \langle\varrho\rangle_{\mathcal{D}}$.

Let us explore the temporal behaviour of the entropy $\mathcal{S}$ to verify whether the $\mathcal{S}$ possesses the time-increasing nature. From Eqs. (8) and (9), the time derivative of the entropy is immediately found to give

$$\frac{\partial}{\partial t}\mathcal{S}\{\varrho \parallel \langle\varrho\rangle_{\mathcal{D}}\} = -\int_{\mathcal{D}} \delta\varrho\,\delta\theta\sqrt{\det(g_{ij})}\,\mathrm{d}^3X = -V_{\mathcal{D}}\langle\delta\varrho\,\delta\theta\rangle_{\mathcal{D}}\,. \tag{11}$$

We expect from Eq. (11) that the time derivative of $\mathcal{S}$ will generally be positive in view of cosmological structure formation, because, on average, an overdense region ($\delta\varrho > 0$) tends to contract ($\delta\theta < 0$) to form a cluster, and an underdense region ($\delta\varrho < 0$) tends to expand ($\delta\theta > 0$) to form a void. To be more precise, however, how inhomogeneities evolve depends on initial conditions, particularly at an early stage of the evolution. At a sufficiently late stage, the effect of initial conditions will get weaker and inhomogeneities will evolve according to the intuitive manner as we mentioned above, leading to the positivity of the time derivative of the entropy. This idea implies the importance of examining whether the second time derivative of the entropy is positive, i.e. the *time-convexity* of the entropy. Differentiation of Eq. (11), together with Eqs. (3) and (5), yields

$$\frac{\ddot{\mathcal{S}}}{V_{\mathcal{D}}} = 4\pi G\langle(\delta\varrho)^2\rangle_{\mathcal{D}} + \frac{1}{3}\langle\varrho(\delta\theta)^2\rangle_{\mathcal{D}} + 2\langle\varrho\sigma^2\rangle_{\mathcal{D}} + \langle\varrho\rangle_{\mathcal{D}}Q_{\mathcal{D}} - \frac{2}{3}\langle\theta\rangle_{\mathcal{D}}\frac{\dot{\mathcal{S}}}{V_{\mathcal{D}}}\,. \tag{12}$$

In order to clarify the conditions under which the positivity of $\dot{\mathcal{S}}$ holds, the sign of $\ddot{\mathcal{S}}$ is crucial, in particular at the instant $t = t_{\mathrm{c}}$ when $\dot{\mathcal{S}} = 0$. If $\ddot{\mathcal{S}}(t = t_{\mathrm{c}})$ is shown to be positive, we can conclude that $\dot{\mathcal{S}}$ is always positive thereafter. Note that, from Eq. (12), this applies to the case when the backreaction term $Q_{\mathcal{D}}$ is positive at $t = t_{\mathrm{c}}$. Therefore, if the presence of inhomogeneities is responsible for the effectively accelerated cosmic expansion, the entropy production $\dot{\mathcal{S}}$ becomes positive after a sufficient time.

The positivity of $\dot{\mathcal{S}}$ has been explored using linear perturbations of a spatially flat FLRW universe model, and a spherically symmetric Lemaître-Tolman-Bondi solution in Ref. [5].

3 Summary and conclusion

We have presented the formulation of averaging an inhomogeneous universe, which yields a Friedmann-like equation with the 'kinematical backreaction term'. That equation tells us that the effective cosmic expansion is led to deviate from a Friedmannian one due to the effect of the backreaction. We also have proposed a natural measure of inhomogeneity within the averaging formulation, and have discussed the temporal behaviour of the measure. The measure is identical to the *relative information entropy* for cosmic matter distribution. It is of interest that the temporal increase of the entropy is somehow linked to the signature of the backreaction.

References

[1] T. Buchert, Gen. Relativ. Gravit. 40 (2008) 467 [arXiv:0707.2153v3].
[2] T. Buchert, Gen. Relativ. Gravit. 32 (2000) 105 [arXiv:gr-qc/9906015v2].
[3] N. Li and D. J. Schwarz, Phys. Rev. D 76 (2007) 083011 [arXiv:gr-qc/0702043v3].
[4] A. Hosoya, T. Buchert, and M. Morita, Phys. Rev. Lett. 92 (2004) 141302 [arXiv:gr-qc/0402076v1].
[5] M. Morita, T. Buchert, A. Hosoya, and N. Li, AIP Conf. Proc. 1241 (2010) 1074 [arXiv:1011.5604v1].

Observational constraints to the decaying dark matter model by using Markov Chain Monte Carlo Approach

N.V.Khanh, N.Q.Lan, N.A.Vinh
Hanoi National University of Education, 136 Xuan Thuy, Cau Giay, Hanoi
G. J. Mathews
Center for Astrophysics, Department of Physics,
University of Notre Dame, Notre Dame, IN 46556, U.S.A.

Abstract

We discuss a cosmology in which cold dark-matter begins to decay into relativistic particles at a recent epoch ($z < 1$). We show that the large entropy production and associated bulk viscosity from such decays leads to a recently accelerating cosmology consistent with observations. We investigate the effects of decaying cold dark matter in a $\Lambda = 0$, flat, initially matter dominated cosmology. We perform a constraint on the decaying dark matter model with bulk viscosity, by using the Markov Chain Monte Carlo (MCMC) method and the combined observational data from the type Ia supernovae, and cosmic microwave background.

1 Introduction

Modern cosmology is now faces the dilemma that most of the mass-energy in the universe is attributed to material of which we know almost nothing about. In particular, we wish to understand the nature and origin of both the dark energy responsible for the present apparent acceleration [1] and the cold dark matter [2] responsible for most of the gravitational mass of galaxies and clusters. The simple coincidence that both of these unknown entities currently contribute comparable mass energy toward the closure of the universe begs the question as to whether they could be different manifestations of the same physical phenomenon. Indeed, suggestions along this line have been made by many [See [3] for a review].

In our previous work [4, 5] we have proposed that the unity of dark matter and dark energy could be explained if the dark energy could be produced from a delayed decaying dark-matter particle. That previous work demonstrated dark-matter particles that begin to decay to relativistic particles near the present epoch will produce a cosmology consistent with the observed cosmic acceleration deduced from the type Ia supernova distance-redshift relation without the need for a cosmological constant. Hence, this paradigm has the possibility to account for the apparent dark energy without the well known the fine tuning and smallness problems [3] associated with a cosmological constant. Also in this model, the apparent acceleration is a temporary phenomenon. This avoids some of the the difficulties in accommodating a cosmological constant in string theory. This model thus shifts the dilemma in modern cosmology from that of explaining dark energy to one of explaining how an otherwise stable heavy particle might begin to decay at a late epoch.

That previous work, however, was limited in that it only dealt with the supernova-redshift constraint and the difference between the current content of dark matter content compared to that in the past. Previous work did not consider the broader cosmological constraints available from simultaneous fits to the cosmic microwave background (CMB) and its effect on the early formation of large scale structure (LSS). Although our decaying dark matter scenario does not occur during the photon decoupling epoch and the early structure formation epoch, it does affect the CMB fits and LSS due to differences in the look back time from the changing dark matter/dark energy content at photon decoupling relative to the present epoch. Hence, in this work we consider a simultaneous fit to the CMB as a means to constrain this paradigm to unify dark matter and dark energy. We deduce constraints on the parameters of decaying the dark matter cosmology by using the Markov Chain Monte Carlo method applied to the 7 year CMB data from WMAP7 [6].

This paper is organized as follows: In section II, we derive the background dynamic equation for the evolution of a universe with decaying dark matter. In section III, we describe the method and to fit the CMB data. In the last section, we summarize the fitting results and conclusions.

2 Cosmological model

Possible candidates for decaying dark matter and delayed decaying dark matter have been discussed in detail elsewhere [4, 7, 8, 9, 10] and need not be repeated here. The time evolution of an homogeneous and isotropic expanding universe follows the Friedmann equation:

$$H^2 = \frac{\dot{a}^2}{a^2} = \frac{8\pi G}{3}(\rho_{DM} + \rho_b + \rho_r + \rho_\Lambda + \rho_M + \rho_D) \tag{1}$$

where $\rho_{DM}, \rho_b, \rho_r, \rho_\Lambda$ are the densities of stable dark matter, baryon, stable relativistic particles, dark energy respectively. ρ_M denotes the energy density of heavy decaying dark matter particles, ρ_D denotes the energy density of light relativistic particles specifically produced by decaying dark matter. ρ_M and ρ_D are given by [5]

$$\rho_M = \rho_h(t_d)a^{-3}e^{-\lambda(t-t_d)} \quad , \tag{2}$$

$$\rho_D = a^{-4}[\rho_r + 9\int_{t_d}^{t} H^2 a(t')^4 \xi(t')dt'] \quad , \tag{3}$$

where we have denoted t_d as the time at which decays begin, and the integral term gives the effective dissipated energy density in light relativistic species due to the cosmic bulk viscosity

The continuity equation for the matter and the total energy density ρ are given by

$$\dot{\rho_m} = -3\frac{\dot{a}}{a}(\rho_m + \frac{\rho_r}{3} - 3\xi_m\frac{\dot{a}}{a}) \ ; \ \ \dot{\rho} = -3\frac{\dot{a}}{a}(\rho + p - 3\xi\frac{\dot{a}}{a}) \quad , \tag{4}$$

where the matter pressure is taken as negligible $p_m \approx 0$. Here ξ and ξ_m are the bulk viscosity for the total density and matter respectively, so the evolution behavior of radiation is remains $\rho_r = a^{-4}$.

The effect of the bulk viscosity is to replace the fluid pressure with an effective pressure. The first law of thermodynamics in an adiabatic expanding universe then gives [4]

$$p_{eff} = p - \xi 3\frac{\dot{a}}{a} \quad . \tag{5}$$

3 Statistical Analysis With the Observational Data

We use the Markov Chain Monte Carlo (MCMC) method [11] to fit the cosmological parameters in the decaying dark matter model. We have modified the publicly available CosmoMC package [11] to satisfy this decaying dark matter model. We determine the best value of parameter in the decaying dark matter,using the maximum likelihood method and we take the total likelihood function $\chi^2 = -2logL$ as the product of the separate likelihood functions of each data set. Thus, we get

$$\chi^2 = \chi^2_{SN} + \chi^2_{CMB} \quad . \tag{6}$$

Then, one can obtain the best fitting values of parameters by minimizing χ^2

Type supernovae data and constraint: The brightness of the type Ia supernovae standard candle with redshift is given by a simple relation for a flat $\Lambda = 0$ cosmology. The luminosity distance relation becomes,

$$D_L = \frac{c(1+z)}{H_0}\int_0^z [\Omega_m(z') + \Omega_r(z') + \Omega_\lambda(z')]^{-1/2} dz' \quad , \tag{7}$$

where H_0 is the present value of the Hubble constant. The contribution to the closure density from the energy density of the decaying cold dark matter particles is $\Omega_m(z) = (8\pi G\rho_{m0}/3H_0^2)e^{-\lambda t}(1+z)^3$, the relativistic particles initially present contribute $\Omega_r = (8\pi G\rho_{m0}/3H_0^2)(1+z)^4$, the relativistic particles from decaying dark matter contribute $\Omega_\lambda = (8\pi G\rho_{m0}/3H_0^2)(1+z)^4$.
On other hand, the apparent magnitude of the supernovae is related to the luminosity distance by

$$\triangle m(z) = m(z) - M = 5log_{10}[d_L(z)/Mpc] + 25, \tag{8}$$

where $\triangle m(z)$ is the distance modulus and M is the absolute magnitude which is assumed to be constant for type Ia supernovae standard candles. The χ^2 for the supernovae Ia is given by [14]

$$\chi^2_{SN} = \Sigma^N_{i,j=1}[\triangle m(z_i)^{obs} - \triangle m(z_i)^{th})](C^{-1}_{SN})_{ij}[\triangle m(z_i)^{obs} - \triangle m(z_i)^{th}] \tag{9}$$

Here C_{SN} is the covariance matrix with systematic errors.

CMB constraint: The characteristic angular scale θ_A of the peaks of the angular power spectrum in CMB anisotropies is defined as [13]

$$\theta_A = \frac{r_s(z_*)}{r(z_*)} = \frac{\pi}{l_A} \ , \tag{10}$$

where l_A is the acoustic scale, z_* is the redshift at decoupling, and $r(z_*)$ is the comoving distance at decoupling

$$r(z) = \frac{c}{H_0}\int_0^z \frac{dz'}{H(z)} \ . \tag{11}$$

The Hubble parameter H(z) is

$$H(z) = H_0[(1+z)^3\Omega_{dm} + (1+z)^4\Omega_r + (1+z)^{1-3\omega}\Omega_\lambda]^{1/2} \quad , \tag{12}$$

and $r_s(z_*)$ is the comoving sound horizon distance at decoupling defined by

$$r_s(z_*) = \int_0^{z^*} \frac{(1+z)^2 R(z)}{H(z)} dz \ , \tag{13}$$

where the sound speed distance R(z) is given by [12]

$$R(z) = [1 + \frac{3\Omega_{b0}}{4\Omega_{\gamma 0}}(1+z)^{-1}]^{-1/2} \quad , \tag{14}$$

and the scale factor is

$$R = \sqrt{\Omega_{m0}} \int_0^{z_*} \frac{dz'}{H(z')} \quad . \tag{15}$$

We use the fitting function for the redshift at decoupling z_* proposed by Hu and Sugiyama [15]

$$z_* = 1048[1 + 0.00124(\Omega_{b0}h^2) - 0.738][1 + g_1(\Omega_{m0}h^2)^{g2}] \quad , \tag{16}$$

where

$$g_1 = \frac{0.0783(\Omega_{b0}h^2)^{-0.238}}{1 + 39.5(\Omega_{b0}h^2)^{0.763}}, g_2 = \frac{0.56}{1 + 21.1(\Omega_{b0}h^2)^1.81} \quad . \tag{17}$$

The χ^2 of the cosmic microwave background fit is constructed as $\chi^2_{CMB} = -2lnL = \Sigma X^T (C^{-1})_{ij} X$ [6], where

$$X^T = (l_A - l_A^{WMAP}, R - R_A^{WMAP}, z_* - z_*^{WMAP}), l_A^{WMAP} = 302.09, R_A^{WMAP} = 1.725, z_*^{WMAP} = 1091.3 \quad . \tag{18}$$

Table 1 shows the the inverse covariance matrix used in our analysis.

Table 1: inverse covariance matrix given by [6]

case	l_A	R	z_*
l_A	2.305	29.698	-1.333
R	29.698	6825.27	-113.18
z_*	-1.333	-113.18	3.414

Table 2: fitting results of the parameters with 1σ is actually the 68.84 % contour , 2σ is actually the 95.17 % contour regions in DDM model with 20377 samples in total.

parameter	
Ω_D	0.112 ± 0.01
Ω_b	0.0225 ± 0.002
Ω_m	0.235 ± 0.01
n_s	0.0968 ± 0.001
h	0.71 ± 0.01

4 Result and Conclusion

As a first step we performed a MCMC analysis in the parameter space of $(\Omega_b h^2, \Omega_m h^2, \Omega_D h^2, h)$ for a cosmology in which all dark matter is allowed to start decay at $t_d = 3$ Gyr. All other parameters fixed at values from the WMAP7 analysis. Table 2 summarizes the deduced cosmological parameters from this work.

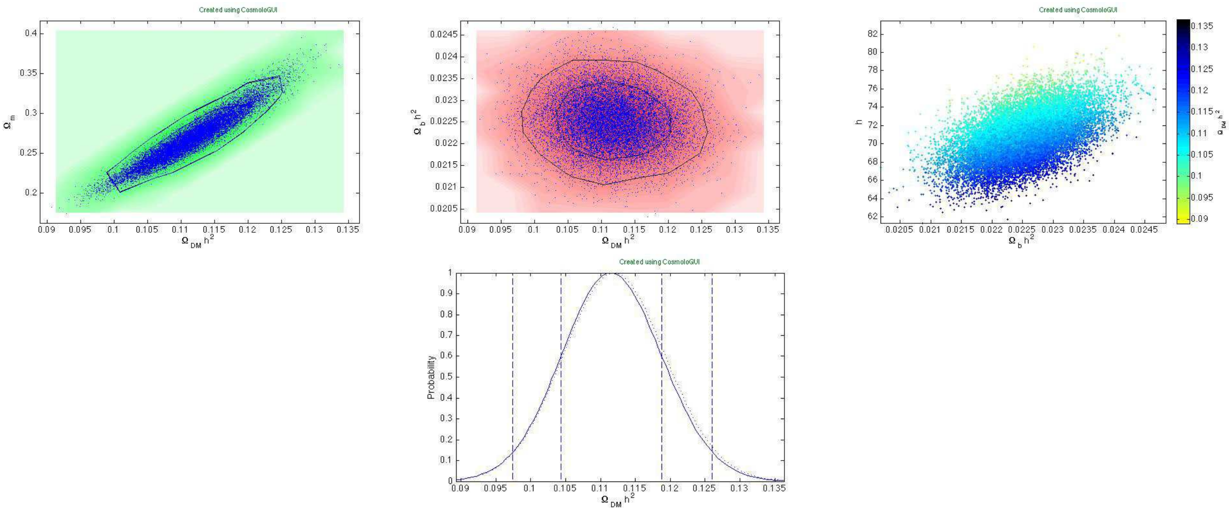

Figure 1: The constraints of the parameters $(\Omega_b h^2, \Omega_m h^2, \Omega_D h^2, h)$. The data we used are SN+CMB, the dotted curves are the mean likelihood of the samples, the solid curves are the probability for parameters

The associated likelihood contours are summarized in figures 1a-d. We find that this cosmology produces an equivalent fit to that of the standard ΛCDM model, but without a cosmological constant. Most parameters obtain values consistent with the WMAP7 analysis.

An important test of this cosmology, therefore could be a detection of an excess cosmic background in relativistic neutrinos.

In summary, we have studied the evolution of the delayed decaying dark matter model with bulk viscosity by using a MCMC analysis to fit the SNIa and CMB data. We have shown that comparable fits to that of the ΛCDM cosmology can be obtained, but at the price of introducing a background in hidden relativistic particles.

This work was supported in part by the National Foundation for Science and Technology Development (NAFOSTED) under grant No: 103.02.112.09. Work at the University of Notre Dame supported by the U.S. Department of Energy under Nuclear Theory Grant No. DE-FG02-95-ER40934 and in part (NQL) by the NSF through the Joint Institute for Nuclear Astrophysics (JINA). We wish to also acknowledge support from Rencontres du Vietnam for attending the ICGAC10 conference.

References

[1] A.G. Riess, AJ, 115, 1009, 1998; S. Perlmutter, et al. Nature, **391**, 51 (1998).

[2] J. L. Feng, J. Phys. **G32** 1391 (2006).

[3] R. Bean, S. Carroll, and M. Trodden, astro-ph/0510059.

[4] J.R.Wilson, G.J.Mathews, and G.M.Fuller, Phys. Rev.D75 043521 (2007)

[5] G. J. Mathews, N. Q. Lan and C. Kolda, Physical Review D 78, 043525 (2008).

[6] E. Komatsu et al. [WMAP Collaboration], Astrophys. J. Suppl. 192, 18 (2011)

[7] M. S. Turner, G. Steigman and L. M. Krauss, Phys. Rev. lett., **52**, 2090 (1984).

[8] A. G. Doroshkevich and M. Yu. Khlopov, Mon. Not. Roy. Astr. Soc. **211** 279 (1984); A.G.Doroshkevich, M.Yu.Khlopov and A.A.Klypin Mon. Not. Roy. Astr. Soc. **239** 923 (1989); M.Yu.Khlopov, *Cosmoparticle physics*, (World Scientific, Singapore) 1999.

[9] M. Lattanzi, J.W.F. Valle Phys. Rev. Lett. **99**, 121301 (2007).

[10] K. Abazajian, G. M. Fuller, and M. Patel, Phys. Rev., **D64**, 023501 (2001).

[11] A. Lewis and S. Bridle, Phys. Rev. D 66, 103511 (2002)

[12] G. Mangano, G. Miele, S. Pastor and M. Peloso, Phys. Lett. B 534, 8 (2002).

[13] L. Page et al. , The Astrophysical Journal Supplement Series, 148:233241, 2003

[14] R. Amanullah, C. Lidman, D. Rubin, G. Aldering, P. Astier, K. Barbary, M. S. Burns and A. Conley et al., Astrophys. J. 716, 712 (2010).

[15] W. Hu and N. Sugiyama, Astrophys. J. 471, 542 (1996)

[16] S. Weinberg, *Gravitation and Cosmology: Principles and Applications of the General Theory of Relativity*, (John Wiley & Sons, Inc. New York) (1972); Astrophys. J., 168, 175 (1971).

Dark Energy As Bulk Viscosity From Decaying Dark Matter

N.Q.Lan[1], *N.V.Khanh*[1], *G. J. Mathews*[2], *and I. S-Suh*[2]

[1] *Hanoi National University of Education, 136 Xuan Thuy, Cau Giay, Hanoi*

[2] *Center for Astrophysics, Department of Physics,*

University of Notre Dame, Notre Dame, IN 46556, U.S.A.

Abstract

We discuss a cosmology in which cold dark-matter begins to decay into relativistic particles at a recent epoch ($z < 1$). We show that the large entropy production and associated bulk viscosity from such decays leads to a recently accelerating cosmology consistent with observations. We investigate the effects of decaying cold dark matter in a $\Lambda = 0$, flat, initially matter dominated cosmology. We show that this model satisfies the cosmological constraint from Type Ia supernovae at high redshift and CMB power spectrum.

The simple coincidence that dark matter and dark energy currently contribute comparable mass energy toward the closure of the universe begs the question as to whether they could be different manifestations of the same physical phenomenon (unified dark-matter). The possibility of particular interest in this work [1] is that of a bulk viscosity within the cosmic fluid. Such a term resists the cosmic expansion and therefore acts as a negative pressure. Indeed, it has been shown [3] that for the right viscosity coefficient, an accelerating cosmology can be achieved without the need for a cosmological constant.

We have proposed [1, 2] a simple mechanism for the formation of such bulk viscosity by the decay of a dark matter particle into relativistic products. Such decays heat the cosmic fluid and cause it to fall out of pressure and temperature equilibrium and can therefore be represented by a bulk viscosity. We have computed the magnitude-redshift relation for Type Ia supernovae in this cosmology and have shown that a single decay does not reproduce these data unless decays are delayed, e.g. by a cascade of particle decays, or a late decaying particle.

The physical origin of bulk viscosity in a system can be traced to deviations from local thermodynamic equilibrium. The bulk viscosity, therefore, is a measure of the pressure required to restore equilibrium to a compressed or expanding system [4, 5]. It is natural for such a term to exist in the cosmologically expanding universe anytime the fluid is out of equilibrium. For the cosmology proposed here, the attainment of equilibrium as the universe expands is delayed by the gradual decay of one or more species to another which occurs over $\sim 10^{10}$ yrs. This leads to nontrivial dependence of pressure on density as the universe expands, and therefore a bulk viscosity.

The existence of such dissipation leads[1] to a modification of the perfect-fluid energy-momentum tenor. The effect of bulk viscosity is to replace the fluid pressure with an effective pressure given by, $p_{eff} = p - \zeta 3(\dot{a}/a)$. Thus, for large ζ it is possible for the negative pressure term to dominate and an accelerating cosmology to ensue. Although such a pressure term is absent from the Friedmann equation, the bulk viscosity does appear in the conservation condition $T^{\mu\nu}{}_{;\nu} = 0$. The total density for the Friedmann equation will then include not only terms from heavy and light dark matter, but a dissipated energy density in bulk viscosity.

Bulk viscosity can be thought of [6, 4] as a relaxation phenomenon. It derives from the fact that the fluid requires time to restore its equilibrium pressure from a departure which occurs during expansion. The viscosity coefficient ζ depends upon the difference between the pressure $\tilde{p}$ of a fluid being compressed or expanded and the pressure p of a constant volume system in equilibrium. Of the several formulations [4] the basic non-equilibrium method [7] is most consistent with p_{eff} as defined above. Following the derivation in [6], we have inferred [1] the following ansatz for the bulk viscosity of the cosmic fluid due to particle decay,

$$\zeta = \rho_{\rm h}\tau_{\rm e}\left[1 - \frac{\rho_{\rm l} + \rho_\gamma}{\rho}\right]^2 \quad , \tag{1}$$

where the square of the term in brackets comes from inserting our derivation into the linearized relativistic transport equation of [8], and τ_e is an effective decay rate defined in [1].

To avoid observational constraints the decay products must have very little energy in photons or charged particles. Neutrinos are thus a natural candidate for such a background which might arise from decaying heavy sterile neutrinos [9] or SUSY dark matter. For supersymmetric dark matter candidates, the initially produced dark matter relic might be a superWIMP to produce the correct relic density. Later, this superWIMP decays to a lighter stable dark matter particle, or the light supersymmetric particle itself might be unstable to decay. One might imagine an R-parity violating decay in which a particle might decay by coupling to right-handed neutrinos which then decay to normal neutrinos. Another possibility could be gauge-mediated supersymmetry breaking involving the decay of a supersymmetric sneutrino into a gravitino plus a light neutrino.

We have compared various cosmological models with some of the recent combined data from the High-Z Supernova Search Team and the Supernova Cosmology Project [10]. We found [1] that, although the bulk viscosity indeed provides a negative pressure, a flat $\Lambda = 0$ cosmology with bulk viscosity from decay of a single dark-matter species does not do better than a ΛCDM in reproducing the supernova distance-red shift relation. In fact it is much worse than the usual ΛCDM cosmology and is even worse than a pure matter dominated cosmology. The reason for this is that, although the bulk viscosity is substantial, it scales with the decaying dark matter which falls off faster with time than a^{-3} because of the decay. An accelerating cosmology requires a nearly constant value of ρ_{tot} with time.

We have shown[2], however, that if the emergence of the bulk viscosity can be delayed by invoking a late-decaying dark matter particle then an excellent fit can be obtained to the SNIa luminosity-redshift relation. This can be achieved if the dark matter particle becomes unstable only at late times due to a time dependent mass crossing or a cosmic phase transition.

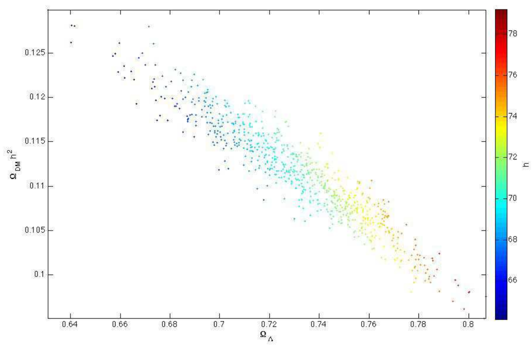

Figure 1: Decaying Dark Matter model, CMB data is used The points show pairs of values of the DM density,$\Omega_{DM}h^2$, and the DE density,Ω_Λ implied by the WMAP data alone, colour-coded according to their value of the Hubble parameter

We study of the effects of dark matter decay and self-interacting dark matter on the formation and evolution of cosmic structures, and a quantitative analysis of the magnitude of relativistic corrections to an inhomogeneous distribution of matter is being made [2]. We also discuss the late decaying dark matter scerenio

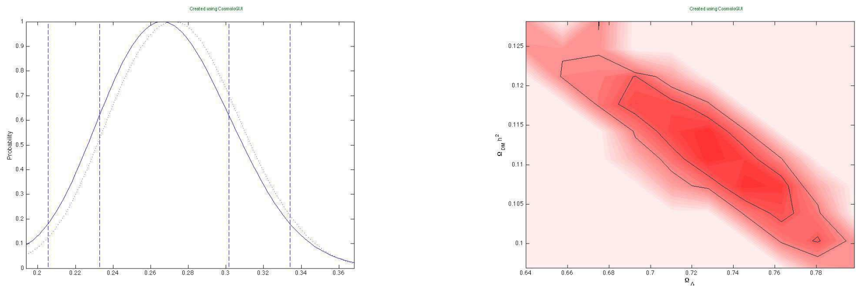

Figure 2: **Left:** Probability plot for a flat Dark matter model. All datasets are used. Ω_m results from chain; $0.232 < \Omega_m < 0.301$ at 68.0 percent confidence and $0.205 < \Omega_m < 0.334$ at 95.0 percent confidence best fit:$\Omega_m = 0.27$. **Right:** Confidence contours for a Decaying Dark Matter model. All datasets are used.

using a Monte Carlo Markov Chain Analysis of Cosmic Microwave Background Radiation(COSMOMC). Figure 1 shows the values of the DM density,$\Omega_{DM}h^2$, and the DE density,Ω_Λ implied by the WMAP data alone for various values of the Hubble parameter. Figure 2 (left)shows the probability plot for a flat dark matter model, while Figure 2 (right) shows the contours of 1 and 2σ confidence limit for a decaying dark matter model.

This work was supported in part by the National Foundation for Science and Technology Development (NAFOSTED) under grant No: 103.02.112.09.

References

[1] J.R.Wilson, G.J.Mathews, and G.M.Fuller, Phys. Rev.D75 043521 (2007)

[2] G. J. Mathews, N. Q. Lan and C. Kolda, Physical Review D 78, 043525 (2008).

[3] R. F. Sawyer, Phys. Rev. D74, 043527 (2006), J.C. Fabris, S.V.B.Goncalves, and R. de Sa Ribeiro, astro-ph/0503362.

[4] H. Okumura and F. Yonezawa, Physics A, 321, 207 (2003).

[5] C. Xinzhong and E. A. Spiegel, Mon. Not. T. Astron. Soc., **323**, 865 (2001).

[6] S. Weinberg, *Gravitation and Cosmology: Principles and Applications of the General Theory of Relativity*, (John Wiley & Sons, Inc. New York) (1972); Astrophys. J., 168, 175 (1971).

[7] W. G. Hoover, A. J. Ladd, R. B. Hickman, B. L. Holian, Phys. Rev. **A21**, 1756 (1980); W. G. Hoover, D. J. Evans, R. B. Hickman, A. J. Ladd, W. T. Ashurst, B. Moran, Phys. Rev. **A22**, 1690 (1980)

[8] L. H. Thomas, Quart. J. Math. (Oxford), 1, 239 (1930).

[9] K. Abazajian, G. M. Fuller, and M. Patel, Phys. Rev., **D64**, 023501 (2001).

[10] P.Garnavich, et al., Astrophys. J.,509, 74; S.Perlmutter, et al. Nature, 391, 51(1998); A.Riess, et al., Astrophys. J.607,(2004)

The Planck Early Results and Perspective

Cyrille Rosset
APC, CNRS, Université Paris Diderot
10 rue Alice Domon et Léonie Duquet 75205 Paris Cedex 13
Email : cyrille.rosset@apc.univ-paris-diderot.fr

Abstract

Launched in May 2009, Planck is the third-generation satellite dedicated to the measurements of the cosmic microwave background (CMB) anisotropies. This ESA mission yielded its first results early 2011. Although centered on non-CMB aspects, they show the excellent quality of the data acquired so far. We show highlights of some early results and in particular the harvest of nearly 200 clusters of galaxies detected via the Sunyaev-Zel'dovich effect. Other studies include the galactic dust emission and the Cosmic Infrared Background anisotropies, two components among the main foregrounds to be removed before the CMB analysis can start.

1 Introduction

The Planck mission is the third generation of satellite dedicated to the measurement of the Cosmic Microwave Background (CMB) anisotropies, after COBE (1989) and WMAP (2001). The mission is lead by ESA, with major contributuion from french and italian spatial agency and NASA. It was launched successfully on 14 May 2009, and has been surveying stably and continuously the sky in millimetric and submillimetric wavelengths in intensity and polarization until 15 January 2012.

The main scientific goal of the mission is to measure the CMB temperature and polarization anisotropies. The sensitivity of its instruments, LFI (Low Frequency Instrument) and HFI (High Frequency Instrument) will allow to measure the CMB power spectrum up to $\ell \sim 2400$ with precision limited by cosmic variance.

The first Planck data products and analyses, concerning the first 14 months of data, were released in January 2011. In section 2, we will describe the satellite and its instruments, and their in-flight performance. We will also describe the data analysis of the HFI. In section 3, we will highlight two important results obtained by Planck, on the Sunyaev-Zeldovich effect and on the cosmic infrared background.

2 The Planck mission, in-flight performance and data analysis

The Planck satellite consists of a 1.5 m primary mirror telescope with two instruments at its focal plane : the Low Frequency Instrument (LFI) with 22 detectors at three frequencies (30, 44 and 70 GHz), and the High Frequency Instrument (HFI) with 52 detectors at six frequencies (ranging from 100 to 857 GHz). The resolution ranges from ~ 30 to ~ 4 arcmin (from low to high frequencies). The two instruments are based upon different technologies : the LFI uses antenna coupled with High Electron Mobility Transistor amplifiers, working at 20 K, while HFI is based on bolometers cooled at 100 mK using a He^3-He^4 dilution refrigerator. Finally, the detectors at frequencies between 30 GHz and 353 GHz are sensitive to polarization.

The satellite has been launched successfully on 14 May 2009, and reached its nominal thermal state on 3 July 2009. Except for one incident on 6 August 2009, the HFI remained cooled for the whole mission, until He^3 was exhausted on mid-January 2012. The sensitivity of the instrument, which was expected to be ten times better than WMAP, is confirmed by the mesured noise level of the detectors which is below the requirement for most of the detectors. The expected final sensitivity to CMB, taking into account the full 30 months of the mission is 0.33 μK$\cdot$deg, to be compared with the sensitivity of 3.4 μK$\cdot$deg for 9-year WMAP maps.

The main difficulty in data analysis was due to the rate of cosmic ray higher than expected (typically one per second instead of one per minute). The glitches in raw signal could be detected and removed thanks to the high redundancy of data : Planck spins at 1 rpm and each detector scans between 40 and 70 times the same circle on the sky. A few regular families of glitches have been discovered in the data, and using templates, it was possible to subtract the long tail of glitches (time constant of ~ 1 s), allowing to discard only 10% of the data.

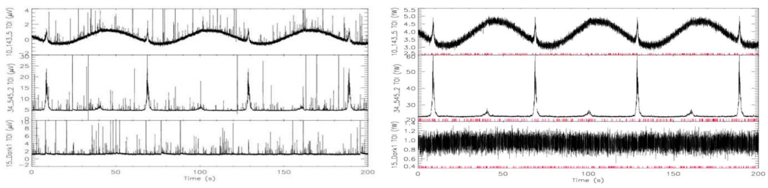

Figure 1: Three minutes of raw data for three detectors (143 GHz, 545 GHz and blind detector) including cosmic rays *(top)* and the same data after deglitching algorithm *(bottom)*.

The deglitched data are then calibrated and projected on a map, taking into accound the low frequency noise. Details on the treatments performed can be found in [1]. The final products released in January 2011 include nine maps for the nine Planck frequencies, but with CMB removed, and a catalogue of compact sources. From these data, 25 papers were published, mainly on galaxy clusters, galaxies and Milky Way (see [2] and reference therein).

3 Some early results

The frequency coverage of Planck has allowed blind detection of clusters of galaxies through the Sunyaev-Zeldovich effect. The clusters are detected as point sources, cold at 143 GHz and hot at 353 GHz, while the signal drops to zero at 217 GHz. This typical signature made it possible to detect 169 already known clusters and discover 20 new clusters, of which 12 have been confirmed by X-ray observations. These observations permitted to measure the scaling relation between the SZ signal and the X-ray luminosity which was found in excellent agreement over the explored luminosity range with X-ray based predictions.

Another important study concerned the Cosmic Infrared Background (CIB). This signal arises from the emission of early galaxies during their formation. The galaxies are barely resolved individually, and thus, when removing foreground (Galactic dust) and background (CMB) emissions, the surveys reveal a web structure characteristic of CIB. CIB anisotropies are a new tool for structure formation and evolution study. Planck has measured the CIB from 857 GHz down to 217 GHz in 6 independent regions. The sepctral energy densities were found to be identical for both CIB mean and anisotropies, reflecting the fact that both are produced by the same sources, as expected. Moreover, the anisotropy power spectrum excluded a simple model where galaxies trace the linear theory matter power spectrum with scale-independent bias.

The understanding of the CIB is important for CMB studies as it is one of the foregrounds which may have consequences on the CMB analysis.

4 Conclusion

Planck HFI has finished taking data in January 2012, as expected, due to depletion of Helium 3. The mission was a success and provided data for four full-sky surveys. The redundancy of data will allow to control systematic, which will be of high importance for CMB analysis, such as polarization or non-gaussianity studies, for which the signal is expected to be very low. First cosmology results are expected to be published in begining of 2013.

References

[1] Planck HFI Core Team, *Planck Early Results VI. The High Frequency Instrument processing*, A&A, 536 (2011) [arXiv:1101.2048].

[2] Planck Collaboration, *Planck Early Results I. The Planck mission*, A&A, 536 (2011) [arXiv:1101.2022].

Isocurvature perturbations in extra radiation

Toyokakzu Sekiguchi[1], *Etsuko Kawakami*[2], *Masahiro Kawasaki*[2], *Koich Miyamoto*[2], *Kazunori Nakayama*[3]

[1] *Department of Physics and Astrophysics, Nagoya University, Nagoya 464-8602, Japan*

[2] *Institute for Cosmic Ray Research, University of Tokyo, Kashiwa 277-8582, Japan*

[3] *Department of Physics, University of Tokyo, Bunkyo-ku, Tokyo 113-0033, Japan*

Email :sekiguti@nagoya-u.jp

Abstract

Recent cosmological observations, including measurements of the CMB anisotropy and the primordial helium abundance, indicate the existence of an extra radiation component in the Universe beyond the standard three neutrino species. In this talk, we explore the possibility that the extra radiation has isocurvature fluctuation and its observational signatures.

1 Primordial perturbations

We mostly follow formalism in Ref. [1]. Various primordial perturbations, including the curvature perturbations ζ and isocurvature perturbations in dark radiation $S_{\rm DR}$, can be generated from fluctuations in scalar fields,

$$
\begin{aligned}
\zeta &= N_{\phi_i}\delta\phi_i + \dots, &(1)\\
S_{\rm DR} &= S_{\phi_i}\delta\phi_i + \dots. &(2)
\end{aligned}
$$

Here, $\delta\phi_i$ is quantum fluctuation of a scalar field ϕ_i, We consider a scenario where the inflaton ϕ and a spectator scalar field σ, contribute to both the adiabatic and isocurvature perturbations. Using the δN formalism [2]the expansion coefficients up to leading order can be given as

$$
\begin{aligned}
N_\phi &= \frac{1}{M_{\rm P}^2}\frac{V}{V_\phi}, &(3)\\
N_\sigma &= \frac{3+R}{6\sigma_i}\left(\frac{\hat{R}_r R_r^{(\sigma)}}{R_r} + \frac{\hat{R}_X R_X^{(\sigma)}}{R_X}\right), &(4)\\
S_\sigma &= -\frac{3+R}{2\sigma_i}\frac{\hat{R}_r\hat{R}_X}{\hat{R}_{\rm DR}}\left(\frac{R_r^{(\sigma)}}{R_r} - \frac{R_X^{(\sigma)}}{R_X}\right)(1-\hat{c}_\nu), &(5)\\
S_\phi &= 0. &(6)
\end{aligned}
$$

The meanings of the symbols are as follows: M_P is the reduced Planck mass. V is the potential of ϕ. V_ϕ and $V_{\phi\phi}$ are the first and second derivatives of V, respectively. R_i is the ratio of the energy density of a fluid i to the total energy density at the decay of σ, and $\hat{R}_i$ is that at the electron-positron annihilation. The subscripts r, X and DR mean the relativistic particles in the Standard Model, the extra radiation and

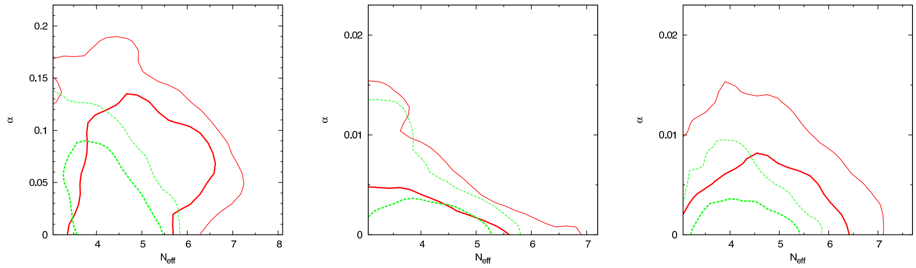

Figure 1: 68 % and 95 % CL constraints in $N_{\rm eff}$-α plane from the CMB (red solid) and ALL (green dashed) datasets. From left to right, shown are the constraints for the uncorrelated, totally correlated, and totally anti-correlated cases.

the dark radiation, respectively. $R_i^{(\sigma)}$ is the ratio of energy density of the fluid i generated by σ decay at that time, and $R \equiv 3R_\sigma/(4-R_\sigma)$, where R_σ is the ratio of energy density of σ to the total energy density at its decay. σ_i is the amplitude of the oscillation of σ when it starts to oscillate. $\hat{c}_\nu \simeq 0.405$ is the ratio of the energy density of neutrino to that of standard model relativistic particles (photons and neutrinos) after the electron-positron annihilation. Using these quantities, we obtain the auto and cross power spectra of initial perturbations

$$P^{\zeta\zeta}(k) \quad = \quad [N_\phi^2 + N_\sigma^2]P_{\delta\phi}(k), \tag{7}$$
$$P^{\zeta S_{\rm DR}}(k) \quad = \quad N_\sigma S_\sigma P_{\delta\phi}(k), \tag{8}$$
$$P^{S_{\rm DR}S_{\rm DR}}(k) \quad = \quad S_\sigma^2 P_{\delta\phi}(k), \tag{9}$$

where $P_{\delta\phi}(k)$ is the power spectrum of the fluctuations of the scalar fields. Here, we assumed that ϕ and σ have the same power spectrum for the sake of clarity. In addition, the effective number of neutrinos can be given as

$$\Delta N_{\rm eff} = \frac{3\hat{R}_X}{\hat{c}_\nu \hat{R}_r}. \tag{10}$$

2 Constraints from observation

We adopt CMB data of WMAP 7-year result [3]and ACT [4], data from the baryon acoustic oscillation (BAO) [5] and the direct measurement of the Hubble constant (H0) [6]. Hereafter, we will refer to sets of combined datasets of WMAP+ACT and WMAP+ACT+BAO+H0 as “CMB” and “ALL”, respectively. Assuming that the primordial perturbation spectra can be represented by power-law with the same spectral indices, they can be parametrized as follows,

$$\begin{pmatrix} P^{\zeta\zeta} & P^{\zeta S_{\rm DR}} \\ P^{S_{\rm DR}\zeta} & P^{S_{\rm DR}S_{\rm DR}} \end{pmatrix} = \frac{2\pi^2}{k^3} A_s \left(\frac{k}{k_0}\right)^{n_s-1} \begin{pmatrix} 1-\alpha & \gamma\sqrt{\alpha(1-\alpha)} \\ \gamma\sqrt{\alpha(1-\alpha)} & \alpha \end{pmatrix}. \tag{11}$$

Constraints on $N_{\rm eff}$ and α for uncorrelated ($\gamma = 0$), totally correlated ($\gamma = 1$) and totally anti-correlated ($\gamma = -1$) cases are shown in Fig. 1, where we assumed $N_{\rm eff} \geq 3$ as a prior. We do not find evidence for nonzero isocurvature perturbations and current data is consistent with purely adiabatic initial perturbations.

We would like to comment on the possible non-Gaussianity generated in our model. Multiple scalar fields contribute to the primordial perturbations in our model and local-type non-Gaussianity can be generated, which often occurs in multi-field models. Since the extra radiation isocurvature perturbation are best constrained from CMB, we can constrain such the non-Gaussianity from the future CMB surveys including Planck. For details, see Ref. [7].

References

[1] M. Kawasaki, K. Miyamoto, K. Nakayama and T. Sekiguchi, JCAP **1202**, 022 (2012) [arXiv:1107.4962 [astro-ph.CO]].

[2] M. Sasaki, E. D. Stewart, Prog. Theor. Phys. **95**, 71-78 (1996). [astro-ph/9507001]. D. H. Lyth, K. A. Malik, M. Sasaki, JCAP **0505**, 004 (2005). [astro-ph/0411220].

[3] D. Larson *et al.*, Astrophys. J. Suppl. **192**, 16 (2011) [arXiv:1001.4635 [astro-ph.CO]]. N. Jarosik *et al.*, Astrophys. J. Suppl. **192**, 14 (2011) [arXiv:1001.4744 [astro-ph.CO]].

[4] S. Das *et al.*, Astrophys. J. **729**, 62 (2011) [arXiv:1009.0847 [astro-ph.CO]].

[5] B. A. Reid *et al.* [SDSS Collaboration], Mon. Not. Roy. Astron. Soc. **401**, 2148 (2010) [arXiv:0907.1660 [astro-ph.CO]].

[6] A. G. Riess *et al.*, Astrophys. J. **699**, 539 (2009) [arXiv:0905.0695 [astro-ph.CO]].

[7] E. Kawakami, M. Kawasaki, K. Miyamoto, K. Nakayama and T. Sekiguchi, arXiv:1202.4890 [astro-ph.CO].

Energy spectrum estimation of axion radiation from topological defects

Toyokakzu Sekiguchi[1], *Takashi Hiramatsu*[2], *Masahiro Kawasaki*[3], *Kenichi Saikawa*[3], *Masahide Yamaguchi*[4], *Jun'ichi Yokoyama*[5]

[1] *Department of Physics and Astrophysics, Nagoya University, Nagoya 464-8602, Japan*

[2] *Yukawa Institute for Theoretical Physics, Kyoto University, Kyoto 606-8502, Japan*

[3] *Institute for Cosmic Ray Research, The University of Tokyo, Kashiwa 277-8582, Japan*

[4] *Department of Physics, Tokyo Institute of Technology, Tokyo 152-8551, Japan*

[5] *Research Center for the Early Universe, Graduate School of Science, The University of Tokyo, Tokyo 113-0033, Japan*

Email :sekiguti@nagoya-u.jp

Abstract

We present results of our simulation of axionic strings and domain walls generated in the early Universe. We developed new method for identification of strings and energy spectrum estimation. By estimating the abundance of axions radiated from the strings and domain walls, we present a constraint on the axion decay constant.

We simulate dynamics of a complex Peccei-Quinn (PQ) scalar field $\Phi(\vec{x}, t)$, whose equation of motion is given by

$$\left[\frac{\partial^2}{\partial t^2} + 3H(t)\frac{\partial}{\partial t} - \frac{1}{R(t)^2}\nabla^2\right]\Phi(\vec{x}, t) = \frac{\partial V_{\rm eff}}{\partial \Phi^*}, \tag{1}$$

where an effective potential at finite temperature T is

$$V_{\rm eff}[\Phi; T] = \frac{\lambda}{2}(|\Phi|^2 - \eta^2) + \frac{\lambda}{3}T^2|\Phi|^2. \tag{2}$$

Here, $R(t)$ is the scale factor, $H(t) = \frac{dR}{dt}/R$ is the Hubble parameter, $\eta = f_a$ is the energy scale of PQ symmetry and λ is the self-coupling constant. The PQ phase transition occurs at the critical temperature $T_{\rm crit} \equiv \sqrt{3}\eta$. We simulate the evolution of $\Phi(\vec{x}, t)$ from the initial time $t_{\rm ini} = 0.25 t_{\rm crit}$ to the end time $t_{\rm end} = 25 t_{\rm crit}$, where $t_{\rm crit}$ is the time of the PQ phase transition transition. Our lattice simulation has the number of grids $N_{\rm grid} = 512^3$.

We developed two new techniques in the analysis [1]. One is the new method for identification of strings based on the minimum phase difference. Our method is invariant under the global phase rotation of complex scalar fields, which is essential in identification of global strings. Another is the estimation of energy spectrum of axion radiation based on pseudo power spectrum estimator. This allows us to remove the contamination from string cores and unbiased estimation.

Figure 1 shows the energy spectrum of axions radiated from axion between $t_1 = 12.25 t_{\rm crit}$ and $t_2 = 25 t_{\rm crit}$. We observe that the spectrum is sharply peaked at around the horizon, which corresponds to $k = 3.6\tau_{\rm crit}^{-1}$ at $t = t_1$ ($k = 2.5\tau_{\rm crit}^{-1}$ at $t = t_2$), and its amplitude is exponentially suppressed toward higher k, which is consistent with Ref. [2].

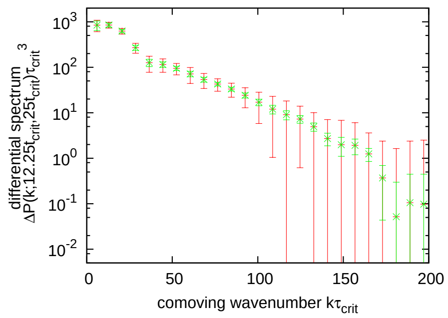

Figure 1: Differential energy spectrum of radiated axions. Green (red) bars correspond to statistical errors alone (statistical and systematic errors).

Based on the scaling property of string networks, we can estimate the number density of axions radiated from the strings. Using result from our simulation, the density parameter of axion $\Omega_{\rm axion}$ can be estimated as

$$\Omega_{\rm axion}h^2 = (1.66 \pm 0.25)\left(\frac{f_a}{10^{12}{\rm GeV}}\right)^{1.19}, \tag{3}$$

which gives an upper bound on the axion decay constant $f_a \leq 1.3 \times 10^{11}$ GeV. Furthermore, by including the contribution from the string-wall system formed at the QCD phase transition [3], the constraint becomes $f_a \leq (1.2 - 2.3) \times 10^{11}$ GeV.

References

[1] T. Hiramatsu, M. Kawasaki, T. Sekiguchi, M. Yamaguchi and J. Yokoyama, Phys. Rev. D **83**, 123531 (2011) [arXiv:1012.5502 [hep-ph]].

[2] M. Yamaguchi, M. Kawasaki and J. Yokoyama, Phys. Rev. Lett. **82**, 4578 (1999) [arXiv:hep-ph/9811311].

[3] T. Hiramatsu, M. Kawasaki, K. Saikawa and T. Sekiguchi, arXiv:1202.5851 [hep-ph].

Dark Universe or Twisted Universe?

André Tilquin[1], *Thomas Schücker*[2]
[1] *Centre de Physique des Particules de Marseille.* [2] *Centre de Physique Théorique*
CNRS–Luminy, Case 907 F-13288 Marseille Cedex 9
Email : tilquin@cppm.in2p3.fr

Abstract

We confront Einstein-Cartan's theory with the Hubble diagram. Using today's supernovae Ia data we find that torsion can contribute to a certain amount of cold dark matter. On the contrary torsion can't replace dark energy.

1 Introduction

We propose to use Einstein-Cartan's theory [1] as model of cosmology. Space-time torsion is allowed without however modifying the Einstein-Hilbert action. Consequently energy-momentum is still the source of space-time curvature and the source of torsion is half-integer spin with the same coupling constant.

2 Einstein-Cartan equations

The reader can find details of the calculation in references [2] [3]. In presence of torsion, there are 2 general equations. Einstein's equation is obtained by varying the total action with respect to the orthogonal frame $e^a =: e^a{}_\mu \, \mathrm{d}x^\mu$:

$$R^c{}_{acb} - \tfrac{1}{2} R^{cd}{}_{cd}\,\eta_{ab} - \Lambda\eta_{ab} = 8\pi G\tau_{ab}, \tag{1}$$

with τ_{ab} the energy-momentum tensor. Cartan's equation is obtained by varying the total action with respect to the connection:

$$T^c e^d \epsilon_{abcd} = -8\pi G S_{ab}, \tag{2}$$

with T^c the torsion 2-form and S_{ab} the spin tensor.

The most general $SO(3) \ltimes \mathbb{R}^3$-invariant energy-momentum tensor contains two functions of time, the energy density $\rho(t)$ and the pressure $p(t)$ and one usually assumes an equation of state $p(t) =: w\,\rho(t)$. Likewise the most general spin density has two functions of time $s(t)$ and $\tilde{s}(t)$ in the two irreducible components: $S_{0jk} =: -s(t)\,\delta_{jk}$ and $S_{ijk} =: -\tilde{s}(t)\,\epsilon_{ijk}$ and we assume two equations of state: $s(t) =: w_s\,\rho(t)$ and $\tilde{s}(t) =: w_{\tilde{s}}\,\rho(t)$. Then the generalised Friedmann equations read:

$$3\,\frac{b^2 - f^2}{a^2} = \Lambda + 8\pi G\rho \quad ; \qquad 2\,\frac{b'}{a} + \frac{b^2 - f^2}{a^2} = \Lambda - 8\pi G p, \tag{3}$$

$$3\,\frac{a' - b}{a} = 8\pi G w_s \rho \quad ; \qquad 2\,\frac{f}{a} = 8\pi G w_{\tilde{s}} \rho. \tag{4}$$

with two additional functions $b(t)$ and $f(t)$. The first is parity even, the second is parity odd. Putting the pressure to zero, we have four equations for four unknown functions: a, b, f and ρ. The Friedmann like closure relation for a flat Universe reads:

$$1 = \Omega_{m0} + \Omega_{\Lambda 0} + 2\Omega_{s0} - \Omega_{s0}^2 + \frac{9}{4}\,\Omega_{\tilde{s}0}^2, \tag{5}$$

$$\Omega_m := \frac{8\pi G\rho}{3H^2}\,, \quad \Omega_\Lambda := \frac{\Lambda}{3H^2}\,, \quad \Omega_s := w_s H\,\frac{8\pi G\rho}{3H^2}\,, \quad \Omega_{\tilde{s}} := w_{\tilde{s}} H\,\frac{8\pi G\rho}{3H^2}\,. \tag{6}$$

3 Data analysis

The type 1a supernovae Hubble diagram is constructed using the Union 2 sample [4].The magnitude of supernovae is written as $M(z) = m_s + 2.5\log\ell(z)$ where m_s is a normalization parameter and $\ell(z)$ the apparent luminosity at maximum. The Einstein-Cartan cosmology fit is performed using 3 or 4 free parameters (m_s, Ω_m, $\Omega_s\,\Omega_{\tilde{s}}$) while Ω_Λ is derived from equation (5).

Table 1 presents the results of the fit. Minimum χ^2 for all theories are statistically equivalent. If in the parity even case the preferred value for Ω_m is compatible with baryon matter density, in the odd-parity case, the preferred value of Ω_m is in agreement with the usual total matter density of 0.27. In all cases, the cosmological constant energy density is only slightly changed.

	Ω_m	Ω_Λ	Ω_s	$\Omega_{\tilde{s}}$	χ^2_{min}
Einstein	$0.35^{+0.10}_{-0.11}$	$0.88^{+0.19}_{-0.11}$	0.	0.	530.0
even-parity torsion	$0.09^{+0.30}_{-0.07}$	$0.83^{+0.10}_{-0.16}$	$0.04^{+0.01}_{-0.07}$	0.	530.4
odd-parity torsion	$0.27^{+0.03}_{-0.02}$	$0.73^{+0.04}_{-0.11}$	0.	$0.^{+0.22}_{-0.22}$	530.4
odd-even parity	$0.08^{+0.27}_{-0.07}$	$0.85^{+0.10}_{-0.15}$	$0.04^{+0.02}_{-0.06}$	$0.^{+0.01}_{-0.01}$	530.0

Table 1: Fit results (1 σ errors) for Einstein and Einstein-Cartan theories. No flatness constraint is imposed in pure Einstein's theory.

In figures 3 the result of the Hubble diagram fit with even and odd Einstein-Cartan theory is shown (upper curve). The agreement between fitted curve and data points is excellent. The lower curve shows the fit resulting from putting $\Omega_\Lambda = 0$ and suggests that the cosmological constant can not be replaced by torsion.

We test this hypothesis by using the log likelihood ratio technique. We perform the analysis using simultaneously even and odd parity torsion. The χ^2 of the fit is higher than 560 in both cases leading to a 5.4σ significance. The cosmological constant can not be replaced by torsion.

4 Conclusion

We find that a fit of Einstein-Cartan's theory to the Hubble diagram is compatible with no dark matter in case of even parity torsion, while on the contrary is incompatible at 5 σ level with the replacement of the cosmological constant by torsion, parity preserving or not.

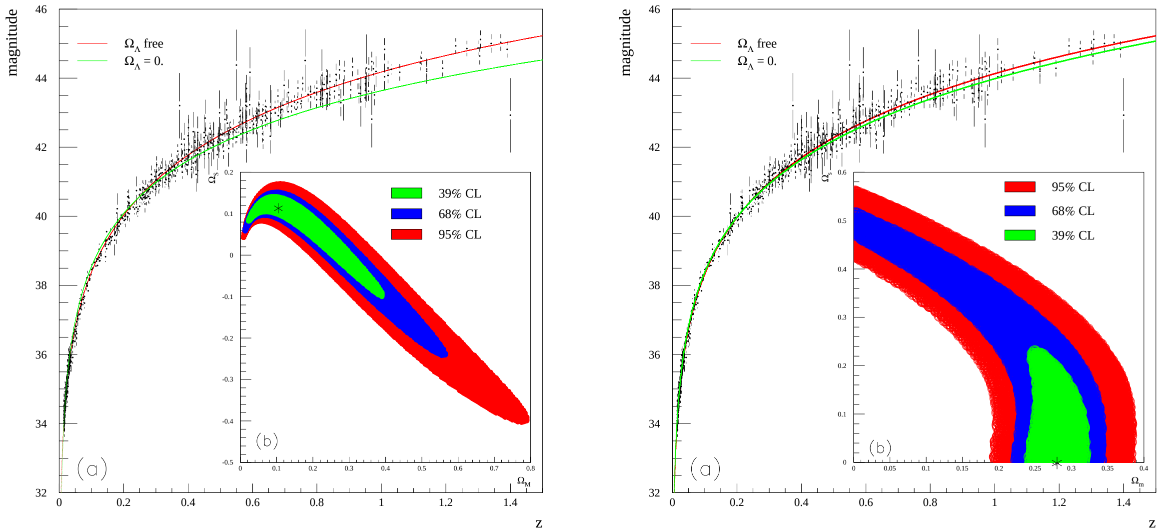

Figure 1: (a) Fit results using the Union 2 Supernovae sample. The red curve (upper) corresponds to the Einstein-Cartan 3-fit (m_s, Ω_m, Ω_s left hand side and $m_s, \Omega_m, \Omega_{\tilde{s}}$ right hand side) while the green (lower) curve represents the 2-fit assuming $\Omega_\Lambda = 0$. (b) $39\%, 68\%$ and 95% confidence level contour in the (Ω_m, Ω_s) and $(\Omega_m, \Omega_{\tilde{s}})$ plane.

References

[1] É. Cartan, *Sur les variétés à connexion affine et la théorie de la rélativité généralisée (première partie),* Ann. Éc. Norm. Sup. **40** (1923) 325.

[2] A. Tilquin and T. Schücker, *Torsion, an alternative to dark matter?,* arXiv:1104.0160 [astro-ph.CO], Gen. Rel. Grav. in press.

[3] T. Schücker and A. Tilquin , *Torsion, an alternative to the cosmological constant?,* arXiv:1109.4568 [astro-ph.CO].

[4] R. Amanullah, et al., *Spectra and HST Light Curves of Six Type IA Supernovae at 0.511 < z < 1.12 and the Union2 Compilation*; ApJ: April 9, 2010

Evolution of the equation of state parameters of cosmological tachyonic field components through mutual interaction

Murli Manohar Verma[1], *Shankar Dayal Pathak*[2]
Department of Physics, Lucknow University, Lucknow 226 007, India
Email : [1]*sunilmmv@yahoo.com,* [2]*prince.pathak19@gmail.com*

Abstract
We study the perturbed equation of state (EOS) parameters of the cosmological tachyonic scalar field components and their mutual time-dependent interaction. It is shown that the discrete temperature-dependent pattern of the EOS emerges from an initial continuum along the evolution of the universe. This leads to two major components in form of dark energy and dark matter, and also suggests a solution to the cosmological constant problem and the coincidence problem.

1 Introduction

In the backdrop of the work done in the standard cosmological model for quintessence dark energy and dark matter [1], we propose the evolutionary history of the universe with interacting dark energy— in form of a part of the string-inspired tachyonic scalar field [2]. The other component mimics the cosmological constant of inflation era. However, each component undergoes a perturbation and so changes flavours. The mutual interaction makes the cosmological constant drop from a very high value to the very small one, and thus leads to a possible solution of the cosmological constant problem [3]. The EOS of the field depends on temperature, condensing into a discrete characteristic pattern from a continuum as the universe expands and cools. It is, therefore, reasonably expected that this condensation must grow faster with the ongoing acceleration of the universe. These aspects can be constrained with the current observations of the Hubble parameter at various redshifts.

2 Perturbed equation of state parameters

A small perturbation $\varepsilon(t)$ in the EOS of the first component of the tachyon field—the cosmological constant— now called shifted cosmological parameter(SCP), is introduced with the new EOS as $w'_\lambda = -1+\varepsilon(t)$. The energy density and pressure of SCP respectively are $\rho'_\lambda = V(\phi)\sqrt{1-\partial^i\phi\partial_i\phi}$ and $P'_\lambda = -V(\phi)\sqrt{1-\partial^i\phi\partial_i\phi}+\varepsilon V(\phi)\sqrt{1-\partial^i\phi\partial_i\phi}$. As the second component, shifted dust matter (SDM) has pressure $P'_m = -\varepsilon V(\phi)\sqrt{1-\partial^i\phi\partial_i\phi}$ with EOS $w'_m = -\frac{\varepsilon}{\partial^i\phi\partial_i\phi}+\varepsilon$, while the EOS of the over-all tachyonic scalar field is $w_{total} = (\partial^i\phi\partial_i\phi - 1)$.

Considering the time-dependent interaction strength among the field components, $Q = \gamma\dot{\rho}'_m$ and $\dot{\phi}^2 << V(\phi)$, we have SDM energy density scaling as

$$\rho'_m = \rho'^0_m \left(\frac{a}{a_0}\right)^{-\frac{3}{1-\gamma}(1+\varepsilon-\varepsilon/\dot{\phi}^2)}. \tag{1}$$

It is found that $w'_m + w'_\lambda = -1 - \varepsilon/\dot{\phi}^2 + 2\varepsilon$, that is, $w'_m + w'_\lambda \neq w_{total}$ while $w'_m + w'_\lambda = w_{total} + w'$ where $w' = -\varepsilon/\dot{\phi}^2 - \dot{\phi}^2 + 2\varepsilon$. For SCP

$$\rho'_\lambda = \rho'^0_\lambda x^{3\varepsilon} - \frac{\gamma\rho'^0_m(1-\varepsilon/\dot{\phi}^2+\varepsilon)}{1-\varepsilon/\dot{\phi}^2+\gamma\varepsilon}\left[x^{\frac{3}{1-\gamma}(1-\varepsilon/\dot{\phi}^2+\varepsilon)} - x^{3\varepsilon}\right] \tag{2}$$

where $x = a_0/a = 1+z$, and in the absence of perturbation ($\varepsilon \to 0$) we have $\rho'_\lambda \to \rho'^0_\lambda - \gamma\rho'^0_m\left[(\frac{a_0}{a})^{3/1-\gamma} - 1\right]$.

The Friedmann equation for spatially flat universe ($k = 0$) now becomes

$$H^2(x) = H_0^2\left[\Omega'^0_m x^\alpha + \Omega'^0_\lambda x^{3\varepsilon} + \frac{\Omega'^0_m\gamma(1+\varepsilon-\varepsilon/\dot{\phi}^2)}{(1+\gamma\varepsilon-\varepsilon/\dot{\phi}^2)}\left(x^{3\varepsilon} - x^\alpha\right)\right]. \tag{3}$$

We can also determine the epoch of equality (z_{eq}) at which $\rho'_m = \rho'_\lambda$ by solving

$$(1+z_{eq})^{\alpha-3\varepsilon} + \frac{\gamma(1-\varepsilon/\dot{\phi}^2+\varepsilon)}{(1-\varepsilon/\dot{\phi}^2+\gamma\varepsilon)}\left[(1+z_{eq})^{\alpha-3\varepsilon} - 1\right] = \frac{\Omega'^0_\lambda}{\Omega'^0_m} \tag{4}$$

where $\alpha = \frac{3}{1-\gamma}(1+\varepsilon-\varepsilon/\dot{\phi}^2)$ and Ω'^0_λ and Ω'^0_m are the present values of density parameter of the cosmological constant and matter respectively. Taking $\Omega'^0_\lambda = 0.73$ and $\Omega'^0_m = 0.27$ we have $\Omega'^0_\lambda/\Omega'^0_m \approx 2.70$. The values of γ and ε can be inferred from observations. In the absence of perturbation and interaction $z_{eq} \simeq 0.3932$. At specific $z = z'$ when the values of $\dot{\rho'_\lambda}$ and $\dot{\rho'_m}$ are equal, we get

$$\frac{\rho'_m}{\rho'_\lambda} = \frac{\varepsilon(1-\gamma)}{(1+\gamma)(1-\varepsilon/\dot{\phi}^2+\varepsilon)}. \tag{5}$$

Clearly, from (5) we see that in the absence of perturbation ($\varepsilon \to 0$) the ratio $\rho'_m/\rho'_\lambda \to 0$, which is un-physical.

3 Temperature-dependence of the EOS

The tachyonic field EOS $w_\phi = \dot{\phi}^2 - 1$ crucially hinges on the kinetic energy term which is naturally expected to be function of temperature. With the effective EOS as $\tilde{w}(T) = \dot{\phi}^2/2$, the field energy density evolves as

$$\rho_\phi = \rho^0_\phi\left(\frac{a}{a_0}\right)^{-6\tilde{w}(T)}. \tag{6}$$

Consequent to the temperature variation $T \propto a^{-1}$, the EOS of cosmic tachyonic scalar field changes accordingly ($\tilde{w}(T) = 0$, $1/2$ or $2/3$ correspond to the cosmological constant, pressureless matter or radiation respectively). The break-up of the continuum of EOS into a discrete temperature-dependent pattern manifesting in distinct forms of components resembles the symmetry breaking phenomena in the early universe. Although the present observations do not unambiguously constrain the exact form of kinetic energy of the tachyonic field as a function of temperature, we study two forms, *viz.*, $\dot{\phi}^2(T) = \alpha T^n exp(\beta T^m)$ and $\dot{\phi}^2(T) = AT^n + Bexp(\beta T^m)$ where α, β and A, B are constants.

4 Conclusion

We have shown that the interaction strength among tachyonic field components with perturbed EOS ascertains their respective evolution. The interaction strength itself can be constrained by the Hubble parameter observations at different redshifts. The interaction also alleviates the cosmological constant problem. The EOS of the field evolves and condenses, as the universe cools, from a continuum to discrete pattern representing the forms— dark energy and dark matter— which we mostly observe in the universe at present. The break-up of these compatible forms at a specific epoch indicates a possible explanation of the coincidence problem.

5 Acknowledgement

The authors acknowledge the financial support F. No. 37-431/2009 (SR) received from UGC, New Delhi for pursuance of this work.

References

[1] L. Amendola, *Coupled quintessence*, Phys. Rev. D 62 (2000) 043511 [astro-ph/9908023].

[2] A. Sen, *Rolling tachyon*, JHEP 0204 (2002) 048 [hep-th/0203211].

[3] M. M. Verma, *Dark energy as a manifestation of the non-constant cosmological constant*, Astrophys. Space Sci. 330 (2010) 101.

Experimental Gravity

Sung-Won Kim, Sean Hayward and Sang Pyo Kim

Misao Sasaki and Dmitry Gal'tsov

Experimental test of the Gravitational Inverse-Square Law at short-ranges

*Shan-Qing Yang, Bi-Fu Zhan, Wen-Hai Tan, Qing-Lan Wang, Cheng-Gang Shao, Liang-Cheng Tu & Jun Luo**

Key Laboratory of Fundamental Physical Quantities Measurement Ministry of Education,

School of Physics, Huazhong University of Science and Technology,

Wuhan 430074,People's Republic of China

**Email : junluo@mail.hust.edu.cn*

Abstract

Motivated by a variety of theories that predict new phenomena of gravitation, we test the gravitational $1/r^2$ law at millimeter ranges by using a dual-modulation torsion pendulum. The non-Newtonian force between two macroscopic tungsten plates is measured at separations ranging down to 0.4 mm. We find no deviations from Newtonian $1/r^2$ law with 95% confidence level, and this work establishes the most stringent constraints on non-Newtonian interaction in the ranges from 0.7 mm to 5.0 mm. Some of the work we report here has already appeared in Letter form [Phys. Rev. Lett. 108, 081101 (2012)], and this paper just includes a brief introduction of the experiment approach for testing the $1/r^2$ law at millimeter ranges and our next plans.

1 Introduction

Generally, it was widely assumed that the Newtonian $1/r^2$ Law should be valid with the scales from infinity to roughly the Planck length $R_P = \sqrt{G\hbar/c^3} = 1.6 \times 10^{-35}$ m. Recently, the gravitation interaction at length scales down to several micrometers has aroused considerable interest due to the two so-called hierarchy problems of gravity: the gauge hierarchy problem of 10^{16} times discrepancy between the Planck mass ($M_P = \sqrt{\hbar c/G} = 1.2 \times 10^{16}\mathrm{TeV/c^2}$) and natural mass scale of the standard model of particles physics ($M_{SM} \approx 1\mathrm{TeV/c^2}$) [1, 2]; the cosmological constant problem of at least 10^{60} times smaller than the predicted zero-point energy density [3, 4, 5, 6, 7]. Driven by these gravity problems, various theoretical speculations [8, 9, 10, 11, 12], motivated in large part by string-theory consideration, hence predicted the deviation of the Newtonian $1/r^2$ law at short range of below 1 mm. Therefore, any experiment effort devoted to validating the expectation will help to understand the fundamental nature of gravity. The Yukawa-type potential due to new interactions is typically taken to modify the gravitational inverse-square law:

$$V(r) = -G\frac{m_1 m_2}{r}(1 + \alpha e^{-r/\lambda}), \tag{1}$$

where α and λ are the strength and length scale of a new interaction, G is Newtonian gravitational constant, m_1 and m_2 are the two point masses separated by distance r. A large amount of experimental works [9, 10, 11, 12, 13, 14, 15, 16, 17] and on-going searches [18] for possible violation of Newtonian $1/r^2$ law over short scales had been performed. However, the current bounds for $0.7 \text{ mm} \leq \lambda \leq 5.0$ mm are not as strong as in other regions, which motivates us to perform the further test of Newtonian $1/r^2$ law at this region.

2 Principle and design

A schematic drawing of the apparatus is shown in Fig. 1. An I-shaped symmetric torsion pendulum, suspended by a 600-mm-long and 25-μm-diameter pure tungsten fiber, was assembled face to face with an I-shaped symmetric attractor in a vacuum chamber. The non-Newtonian force between two macroscopic tungsten plates with dimensions of $15.994 \times 15.986 \times 1.787$ mm^3 (W1) and $20.804 \times 20.778 \times 1.787$ mm^3 (W3), attached on the pendulum and the attractor,respectively, is directly measured for separations ranging from 0.4 mm to 1.0 mm. The net torque change of the Newtonian force was counteracted by two tungsten counterweight masses (W2 and W4). Because the separations between the compensation blocks is larger than that between the test mass and the source mass, the expected non-Newtonian effect (between W1 and

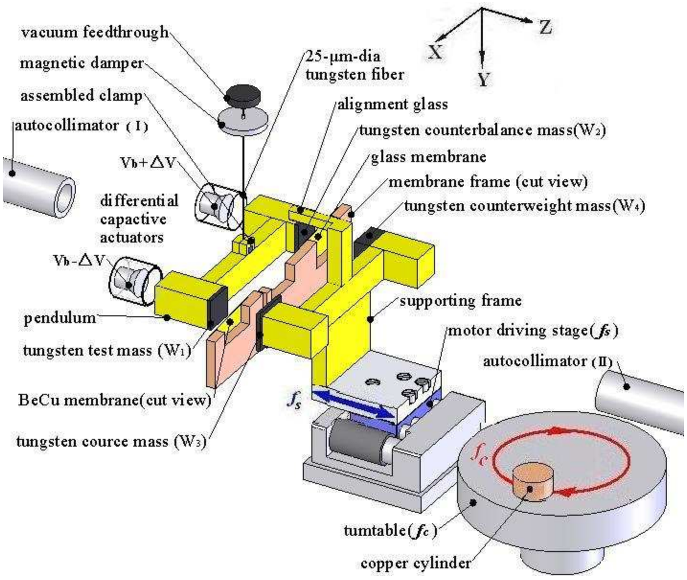

Figure 1: (color online) Schematic drawing of experimental setup (not to scale).

W3) should not be suppressed. Therefore, the test is a null experiment with respect to the net Newtonian torque on the balance.

To eliminate the electrostatic force, a stiff thin shielding membrane was inserted between the test mass and the source mass. The twist angle of the pendulum was monitored by an autocollimator, and then controlled by using a feedback controlling system. In this case, the tungsten fiber was always untwisted during the measurement and the feedback voltage ΔV reflected the changes of all effective torques experienced by the pendulum. The quasistatic pendulum allowed us to achieve a small separation (263 ± 1 μm) between the test mass and the shielding membrane. A motor translation stage was then operated continuously with a frequency f_s (=0.20 mHz) to move the source mass backwards and forwards in a ranges from 0.4 to 1.0 mm. Meanwhile, a copper cylinder for gravitational calibration, mounted on a turntable fixed outside of the vacuum chamber, was rotated continuously at another frequency f_c (=0.25 mHz). Each set of experimental data was recorded continuously with approximately 1 day. By extracting the expected signal at the frequency f_s, we can get some information about the gravity.

3 Signal extraction and results

Each data run was broken into separate "cuts" containing exactly the lowest common multiple of the dual modulation periods 2000 s. For each "cut", the feedback voltage ΔV at frequency $f(f = f_s, f_c)$ was fitted with

$$\begin{aligned}\Delta V(t) &= a_c \cos(2\pi f_c t) + b_c \sin(2\pi f_c t) \\ &+ a_s \cos(2\pi f_s t) + b_s \sin(2\pi f_s t) + \sum_{n=1}^{2} c_m P_m,\end{aligned} \tag{2}$$

where the c_m coefficients of the Legendre polynomials P_m accounted for a continuous creeping of the tungsten fiber, subscripts c, s denote the calibrating signal and the expected non-Newtonian one, and the a, b are the cosine component and the sine one, respectively. Then the voltage signals were converted to torque signals by incorporating the transfer function of the closed-loop performance. For 11 data sets (~ 430 cuts) with the gap ranging from 0.4 to 1.0 mm, the mean amplitude of the expected torque at $f = f_s$ was yielded as

$$\Delta\tau_s = (0.4 \pm 0.9_{stat} \pm 0.9_{syst}) \times 10^{-16} \text{ Nm}, \tag{3}$$

where the first uncertainty is statistic, and the second is systematic uncertainty, which was determined by taking the errors of all actual measurements of the dimensions and positions of the apparatus into account. Some systematic errors induced from the electromagnet effects of the driving stage, the temperature variation and the magnetic effect were studied and corrected correspondingly.

4 The non-null experiment

In order to check the validity of the null experiment design, the non-null experiment was performed by extending the separation between the test mass and the source mass, where the obvious net Newtonian torque allows precision measurements with the same procedure. By varying the gap at $0.8 - 1.4$ mm, $1.1 - 1.7$ mm $\cdots 3.7 - 4.3$ mm, respectively, some non-null test were done. The total experiment results show a perfect consistent with the theoretical calculations of the change of the Newtonian torque (shown in Fig. 2), which provide an additional check to the total experimental system, and hence further enhance the null experiment's confidence.

5 Conclusion

The total uncertainty of the torque noise is computed to be $\Delta\tau_s \leq 1.3 \times 10^{-16}$ Nm, and we used $2\Delta\tau_s$ to set constraints on the additional Yukawa interaction according to Eq.(1). We establish the new best constraints on non-Newtonian interaction in the ranges from 0.7 mm to 5.0 mm under 95% confidence level, shown in Fig. 3. At the length scale of several millimeters, we improve the previous bounds by up to a factor of 8, and find no deviations from the Newtonian $1/r^2$ law.

6 Some progress

Aiming to explore some new phenomena of gravitation at an even shorter range, we are preparing an improved experiment at attractor to pendulum separations down to about 120 μm. Up to now, the new apparatus

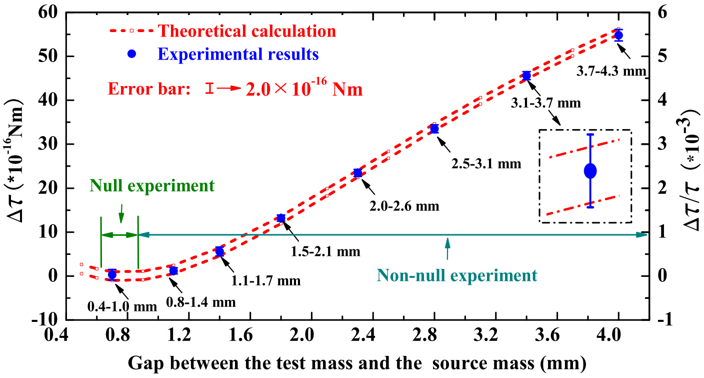

Figure 2: (color online) Comparison of the change of the Newtonian torque ($\Delta\tau$) between the theoretical calculations (dash) and the experimental results (dot) in each $0.6-$mm$-$range experiment. The gap between the two dashes shows an uncertainty of less than 2×10^{-16} Nm, yielded by the dimension errors of the apparatus. The τ ($\sim 1 \times 10^{-12}$ Nm), accounting for the net Newtonian torque between the pendulum and the source mass platform, is a constant on the lever of 3% in the total experimental region ($0.4 - 4.3$ mm), and a perfect cancellation of it was designed at the gap of 0.7 mm. The inset is a magnified view of the result obtained in $3.1 - 3.7$ mm.

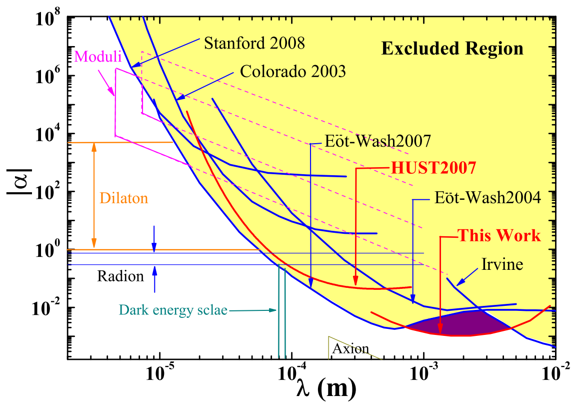

Figure 3: (color online) caption(color online) Upper limits on Yukawa violations of Newtonian $1/r^2$ law. The shaded region is excluded with 95% confidence level. The heavy lines labeled Stanford 2008 [12], Colorado 2003 [13], Eöt-wash 2004 and 2007 [14], HUST 2007 [15], This work [19], and Irvine [16] show the experimental constraints, respectively. Lighter lines showed various theoretical predictions summarized in [7].

for this experiment has been assembled. The sensitivity of the close-loop pendulum with the pendulum-membrane gap being 70 μm was measured to be $\sim 1 \times 10^{-14}$Nm/$\sqrt{\text{Hz}}$ at several mHz frequency range, which is enough for testing the non-Newtonian signal at sub-millimeter ranges. Now, we are researching the electromagnetic effect of the translation motor (used to move the source masses), and looking forward to getting some new results in the near future.

7 Acknowledgement

We are very appreciated to Riley Newman, Ho Jung Paik and Vadim Milyukov for helpful suggestion and discussion. This work was supported by the National Basic Research Program of China under Grant No.2010CB832802.

References

[1] N. Arkani-Hamed, S. Dimopoulos, and G. Dvali, Phys.Lett. B **429**, 263 (1998); Phys. Rev. D **59**, 086004 (1999).

[2] N. Arkani-Hamed, S. Dimopoulos, G. Dvali, and N. Kaloper, Phys. Rev. Lett. **84**, 586(2000).

[3] S. Dimopoulos and G. F. Giudice, Phys. Lett. B **379**, 105 (1996).

[4] R. Sundrum, J. High Energy Phys. **9907**, 001 (1999); Phys. Rev. D **69**, 044014 (2004).

[5] L. Randall and R. Sundrum, Phys. Rev. Lett. **83**, 4690 (1999).

[6] D. B. Kaplan and M. B. Wise, J. High Energy Phys. **0008**, 037 (2000).

[7] E. G. Adelberger, B. R. Heckel, and A. E. Nelson, Annu. Rev. Nucl. Part. Sci. **53**, 77 (2003).

[8] E. G. Adelberger *et al.*, Phys. Rev. Lett. **98**, 131104 (2007).

[9] R. S.Decca *et al.*, Phys. Rev. Lett. **94**, 240401 (2005);

[10] M. Masuda and M.Sasaki, Phys. Rev. Lett. **102**, 171101 (2009).

[11] S. K. Lamoreaux, Phys. Rev. Lett. **78**, 5 (1997); A. O. Sushkov, W. J. Kim, D. A. R. Dalvit and S. K. Lamoreaux, *ibid* **107**, 171101 (2011).

[12] J. Chiaverini *et al.*,Phys. Rev. Lett. **90**, 151101 (2003); A. A. Geraci *et al.*, Phys. Rev. D **78**,022002 (2008).

[13] J. C. Long *et al.*, Nature(London) **421**, 922 (2003).

[14] C.D. Hoyle et al., Phys. Rev. D **70**, 042004 (2004); D. J. Kapner *et al.*, Phys. Rev. Lett. **98**, 021101 (2007).

[15] L. C. Tu *et al.*, Phys. Rev. Lett. **98**, 201101 (2007).

[16] J. K. Hoskins, R. D. Newman, R. Spero, and J. Schultz, Phys. Rev. D **32**, 3084 (1985).

[17] M. V. Moody and H. J. Paik, Phys. Rev. Lett. **70**, 1195 (1993).

[18] R. D. Newman, E. C. Berg, and P. E. Boynton, Space Sci. Rev. **146**, 175 (2009).

[19] S. Q. Yang *et al.*, Phys. Rev. Lett. **108**, 081101 (2012).

Vietnamese Cham dance performance

Vietnamese Cham dance performance

The Newtonian Gravitation Constant: Results of Measurements and CODATA Values.

Vadim Milyukov
Lomonosow Moscow State University, Sternberg Astronomical Institute,
Universitetskii pr. 13, Moscow, 119234, Russia
Email : milyukov@sai.msu.ru

Abstract

Measurement of the Newtonian constant of gravitation in a laboratory experiment has more, than two hundred year's history. Although the accuracy of the best modern experimental measurements of the Newtonian gravitational constant reaches 15–40 ppm, the scattering of G absolute values is large enough. The results of the G measurements which were used for CODATA adjustments, as well as CODATA values are considered in the paper.

Introduction

The Newtonian gravitational constant G together with Planck's constant $\hbar$ and the speed of light c are the fundamental constants of nature. If absolute values of fundamental constants such as c and $\hbar$ are known with high accuracy, a situation with the gravitational constant G absolutely by others. Due to the weakness and nonshieldability of gravitational interaction accuracy of experimental determination of G is essential below accuracy of other fundamental constants.

The first device for measurement of a mutual gravitational attraction of small laboratory bodies – the horizontal torsion balance – has been made at the end of XVIII century by Henry Cavendish, outstanding English scientist. Hundred years later after Newton's discovering the law of gravitation, the Cavendish experiment, done in 1797-98, was the first experiment to measure the force of gravity between masses in the laboratory, and the first to give accurate values for the gravitational constant, $G = (6.67 \pm 0.07) \times 10^{-11}\ m^3 kg^{-1} s^{-2}$, with a relative uncertainty of 10^4 ppm [1] (a relative uncertainty is expressed in units of part per million, i.e. $10^4 \times 10^{-6}$). Cavendish also has determined the mass and the mean density of the Earth. Consequently, the history of the experimental measurements of G is more than two hundred years.

The modern experimental installations for measurement of gravitational constant are complicated devises, performed on the high technology level, but the main part of the majority of them is also the horizontal torsion balance. After 2000 several new results on the measurement of G with a relative error, less than 50 ppm have been published. Table 1 summarizes the various results of the G measurements which were used for CODATA adjustments, as well as CODATA values. The results after 2000 are also compared graphically in Fig. 1.

CODATA values of the gravitational constant

The Task Group on Fundamental Constants of the Committee on Data for Science and Technology (CODATA) was established in 1969 to periodically provide the scientific and technological communities with a self-consistent set of internationally recommended values of the basic constants and conversion factors of physics and chemistry based on all the relevant data available at a given point in time.

Table 1: The best world experiments on the measurement of G and CODATA

Authors, year of publication		$G \times 10^{-11}$ $m^3kg^{-1}s^{-2}$	STD $\times 10^{-11}$ $m^3kg^{-1}s^{-2}$	ppm
1. Heil and Chrzanowski, 1942	[2]	6.6720	0.0041	615
CODATA 1973	[3]	**6.6720**	**0.0041**	**615**
2. Rose, Beams, et al., 1969	[5]	6.6740	0.0030	450
3. Ponticis, 1972	[6]	6.6714	0.0006	90
4. Sagitov, Milyukov, et al., 1979	[7]	6.6745	0.0008	120
5. Luther and Towler, 1982	[8]	6.6726	0.0005	75
CODATA 1986	[4]	**6.67259**	**0.00085**	**128**
6. Michaelis, et al., 1995	[9]	6.7154	0.0006	90
7. Karagioz, Izmailov, 1996	[10]	6.6729	0.0005	75
8. Bagley and Luther, 1997	[11]	6.6740	0.0007	105
CODATA 1998	[14]	**6.673**	**0.010**	**1500**
9. Jun Luo, et al., 1999	[12]	6.6699	0.0007	105
10. Fitzgerald and Armstrong, 1999	[13]	6.6742	0.0007	105
11. Gundlach and Merkowich, 2000	[15]	6.674215	0.000092	14
12. Quinn, Speake et all., 2001	[16]	6.67559	0.00027	41
13. Schlamminger et all., 2002	[17]	6.67407	0.00022	33
14. Kleinevoß, 2002	[18]	6.67422	0.00098	150
15. Armstrong and Fitzgerald, 2003	[19]	6.67387	0.00027	41
CODATA 2002	[20]	**6.6742**	**0.0010**	**150**
16. Hu, Guo, and Luo, 2005	[21]	6.6723	0.0009	130
17. Schlamminger et all., 2006	[22]	6.67425	0.00010	16
CODATA 2006	[23]	**6.67428**	**0.00067**	**100**
18. Jun Luo, et al., 2009	[24]	6.67349	0.00018	26
19. Parks and J. E. Faller, 2010	[25]	6.67234	0.00014	21
CODATA 2010	[26]	**6.67384**	**0.00080**	**120**

The first set of recommended values of the constants provided by CODATA was published in 1973 [3]. The recommended value of the Newtonian gravitation constant $G = (6.6720 \pm 0.0041) \times 10^{-11}$ $m^3kg^{-1}s^{-2}$ (615 ppm) was mainly based on the Heil and Chrzanowski results, obtained in 1942 [2]. The next CODATA adjustment of the fundamental physical constants was made in 1986 [4]. By this time several new results of measurements of G have been reported [5, 6, 7, 8]. Due to some reasons the CODATA recommended value of the gravitational constant was based on the Luther and Towler result [8], but with the arbitrarily doubled uncertainty, what reflects the fact, that, historically, measurements of G have been difficult to carry out: $G = (6.67259 \pm 0.00043) \times 10^{-11}$ $m^3kg^{-1}s^{-2}$ (128 ppm).

Within 90th years of the last century large enough numbers of laboratory experiments on the measurement of the Newtonian Gravitation constant were done with relative accuracy about of 100 ppm and less [9, 10, 11, 12, 13]. Nevertheless, the discrepancies between the values of the gravitational constant obtained in these experiments remained large enough. In particular, the value $G = 6.7146$ obtained in *Physikalish Technische Bundesanstalt* (Germany) [9], was more than on 40 standard deviations (i.e. more than 5000 ppm) above the G value recommended CODATA in 1986. As a result of such scattering of G values, CODATA should increase significantly an uncertainty and recommended in 1998 value $G = (6.673 \pm 0.010) \times 10^{-11}\ m^3 kg^{-1} s^{-2}$ [14], with a relative error of 1500 ppm. I.e. "uncertainty of knowledge" of G has increased almost in 10 times!

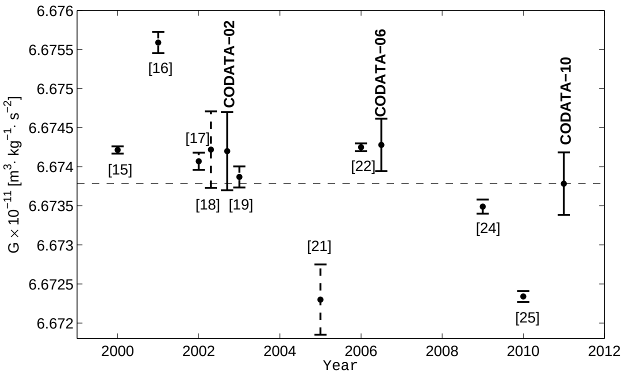

Figure 1: The results of the best world experiments on measurement of G and CODATA values. The dash line is the CODATA-2010 value.

During following years (2000–2002) five new results, four of them with relative errors less than 50 ppm, have been published. These are the experiment of *University of Washington* (USA) with a relative error of 14 ppm [15], the experiment of *University of Bermingam* (Great Britain) with a relative error of 41 ppm [16], the experiment of *University of Zurich* (Switzerland) with a relative error of 33 ppm [17], the experiment of *University of Wuppertal* (Germany) with relative error of 150 ppm [18] and the experiment of *the Measurement Standards Laboratory* (New Zealand) with uncertainty of 40 ppm (the final result was reported in 2003 [19]). Although the situation with G has improved considerably since 1998 adjustment, these new results are not in complete agreement, as can be seen from the Table 1 and Fig. 1. These new G values are not crossed inside of confidential intervals. Based on weighted means of results after 1998, all of which round to $G = 6.6742 \times 10^{-11}\ m^3 kg^{-1} s^{-2}$, as well as their uncertainties, the relatively poor agreement of the data, and the historic and apparently continuing difficulty of assigning an uncertainty to a measured value of G that adequately reflects its true reliability, CODATA has taken as the 2002 recommended value $G = (6.6742 \pm 0.0010) \times 10^{-11}\ m^3 kg^{-1} s^{-2}$ with relative error of 150 ppm [20].

During next 4 years no new competitive independent result for G has become available, only two revisions of the existing results have been made by researchers involved in the original work. One of the two results that have changed is from *the Huazhong University of Science and Technology* [21] and the other is from *the University of Zurich* [22]. The basement for the 2006 adjustment was the same as in 2002 with the exception of these two revised results. The overall agreement of the eight values of G in Table 1 (items 7, 8, 11, 12, 14, 15, 16, 17) has improved somewhat since the 2002 adjustment, but the situation is still far from satisfactory.

Based on the fact that all pointed eight values of G in Table 1 are credible, and that the two results with the smallest uncertainties, *University of Washington* – 2000 and *University of Zurich* – 2006, are highly consistent with one another, the value of the Newtonian gravitational constant, recommended by CODATA in 2006 is equal $G = (6.67428 \pm 0.00067) \times 10^{-11}\ m^3 kg^{-1} s^{-2}$ with relative error of 100 ppm [23].

It seemed that the situation with the absolute value of G has been finally stabilized and we got the "true value" of G. But that value is being challenged by the results of two different experiments, which have been realized in *Huazhong University of Science and Technology* (China) and in *Sandia National Laboratories* (USA). The Chinese researchers led by academician Jun Luo used as usually the torsion balance to measure the gravitation forces between it and probe masses. They obtained a value of $G = 6.67349 \times 10^{-11}\ m^3 kg^{-1} s^{-2}$, with an uncertainty of 26 ppm, about three standard deviations below CODATA-2006 value. James Faller and Harold Parks at *Sandia National Laboratories* used a laser interferometer to measure the displacement of pendulum bobs by various masses. Their result ($6.67234 \times 10^{-11}\ m^3 kg^{-1} s^{-2}$, with an uncertainty of 21ppm) is an enormous 10 standard deviations lower than CODATA-2006 value.

In June of 2011 CODATA introduced the new value of G based on the whiting mean of all data available at the end of 2010: $G = (6.67384 \pm 0.00080) \times 10^{-11}\ m^3 kg^{-1} s^{-2}$ with relative error of 120 ppm [26]. The new results pulled down the value of G compared to 2006 and the final uncertainty has become larger.

Conclusion

Since the first laboratory measurement of Cavendish over 200 years ago, the reduction in uncertainty in G has been only two order of magnitude. Progress in the measurement of G occurs slowly enough: the error value decreases approximately 10 times per century, and the knowledge of the absolute value of G is still rather poor. Moreover, since 1986, i.e. during 25 years, the uncertainty of the CODATA recommended value practically has not changed. Measurement of the gravitational constant is connected with absolute measurements of three physical values - time, mass and length. Of course, such experiments are not free from systematic errors, that is why it is so important to measure G in a variety of ways. “Big G is the Mt. Everest of precision measurement science, and it should be climbed” (James Faller).

References

[1] H. Cavendish, *Experiments to determine the density of the Earth*, Philos. Trans. R. Soc. London 88, (1798) 469.

[2] P. Heil, P. Chrzanovski, *A new determination of the constant of gravitation, Journ. of research National Bureau of Standards*, USA 29 (1) (1942) 1.

[3] E. R. Cohen and B. N. Taylor, *The 1973 least-squares adjustment of the fundamental constants*, J. Phys. Ref. Data 2 (1973) 663.

[4] E. R. Cohen and B. N. Taylor, *The 1986 adjustment of the fundamental physical constants*, Rev. Mod. Phys. 59 (1987) 1121.

[5] R. D. Rose, et al., *Determination of the Gravitational Constant G*, Phys. Rev. Lett. 23 (1969) 655.

[6] C. Ponticis, *Determination de la constante de gravitation par la metode de resonance*, Comptes Rendus Acad. Sci. Paris. 274 ser. B (1972) 437.

[7] M. U. Sagitov, V. K. Milyukov, et al., *New determination of the Cavendish gravitational constant*, Dok. Acad. Nauk SSSR 245 (1979) 567 [Sov. Phys. Dokl. 245 (1981) 20].

[8] G.G. Luther and W.R Towler, *Redetermination of the Newtonian Gravitational Constant G*, Phys. Rev. Lett. 48 (1982) 121.

[9] W. Michaelis et al., *A new precise determination of Newton's gravitational constant*, Metrologia, 32 (1995/96) 267.

[10] O.V. Karagioz and V. P. Izmailov, *Measurement of the gravitational constant with a torsion balance*, Izmeritelnaya Tekhnika 39, 3 (1996) [Measurement Techniques 39, 979 (1996)].

[11] C.H. Bagley and G.G. Luther, *Preliminary Results of a Determination of the Newtonian Constant of Gravitation: a Test of the Kuroda Hypothesis*, Phys. Rev. Lett. 78 (1997) 3047.

[12] Jun Luo, et al., *Determination of the Newtonian gravitational constant G with a nonlinear fitting method*, Phys. Rev. D. 59 (1999) 042001.

[13] M.P. Fitzgerald and T.R. Armstrong, *The measurement of G using the MSL torsion balance*, Meas. Sci. Technol., 10 (1999) 439.

[14] P. J. Mohr and B. N. Taylor, *CODATA recommended values of the fundamental physical constants: 1998*, Rev. Mod. Phys. 72 (2000) 351.

[15] J.H. Gundlach and S. M. Merkowich, *Measurement of Newton's Constant Using a Torsion Balance with Angular Acceleration Feedback*, Phys. Rev. Lett. 85 (2000) 2869.

[16] T.J. Quinn, C.C. Speake, S.J, Richmann, et al., *A New Determination of G Using Two Methods*, Phys. Rev. Lett. 87 (2001) 111101.

[17] St. Schlamminger, E. Holzschuh, W. Kundig, *Determination of the Gravitational Constant with a Beam Balance*, Phys. Rev. Lett. 89 (2002) 161102.

[18] U. Kleinevoß, Bestimmung der Newtonschen Gravitationskonstanten G, Ph.D. thesis (University of Wuppertal) 2002.

[19] T. R. Armstrong and M. P. Fitzgerald, *New Measurements of G Using the Measurement Standards Laboratory Torsion Balance*, Phys. Rev. Lett. 91 (2003) 201101.

[20] P. J. Mohr and B. N. Taylor, *CODATA recommended values of the fundamental physical constants: 2002*, Rev. Mod. Phys. 77 (2005) 1.

[21] Z.-K. Hu, J.-Q. Guo, and J. Luo, *Correction of source mass effects in the HUST-99 measurement of G*, Phys. Rev. D 71 (2005) 127505.

[22] St. Schlamminger, et al., *Measurement of Newton's gravitational constant*, Phys. Rev. D 74 (2006) 082001.

[23] P. J. Mohr, B. N. Taylor, and D. B. Newell, *CODATA recommended values of the fundamental physical constants: 2006*, Rev. Mod. Phys. 80 (2008) 633.

[24] Jun Luo, et al., *Determination of the Newtonian Gravitational Constant G with Time-of-Swing Method*, Phys. Rev. Lett. 102 (2009) 240801.

[25] H. V. Parks and J. E. Faller, *Simple Pendulum Determination of the Gravitational Constant*, Phys. Rev. Lett. 105 (2010) 110801.

[26] Official website of CODATA (http://www.codata.org/).

Nguyen Anh Vinh, Nguyen Quynh Lan, Phan Van Dong and Nguyen Van Khanh

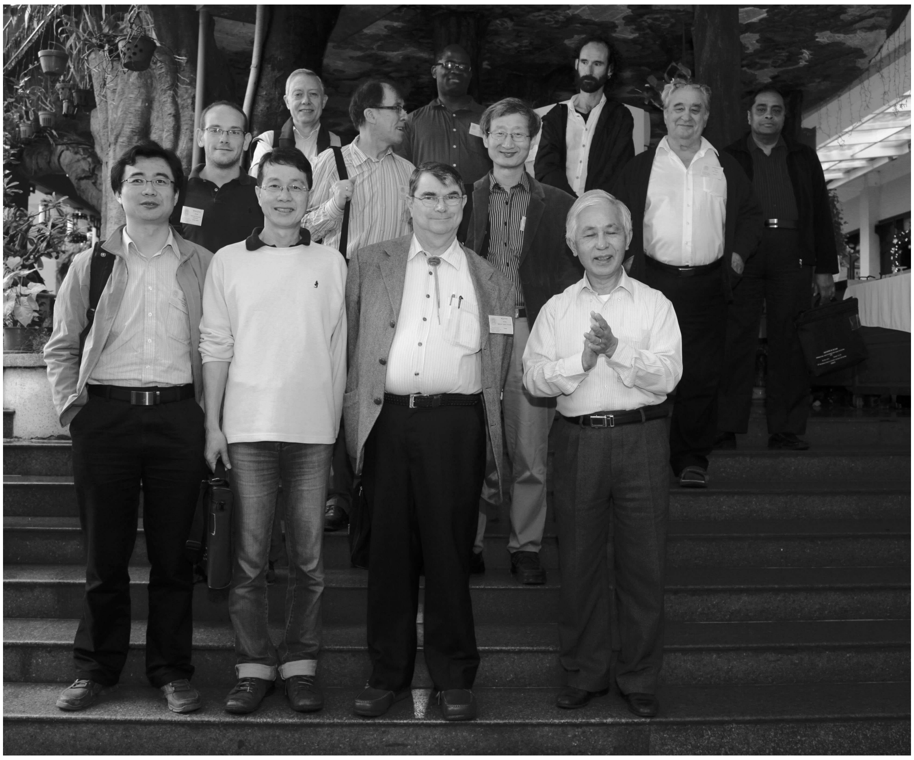

(from left to right, from the front to the back) Zhong Kun Hu, Hoi-Lai Yu, James Nester, Jean Trân Thanh Van; Olivier Minazzoli, Andrzej Krolak, Bum-Hoon Lee, Pierre Darriulat; Angelo Tartaglia, Eyo Ita, Martin O'Loughlin and Manu Paranjape

Equivalence Principles, Lense-Thirring Effects, and Solar-System Tests of Cosmological Models

Wei-Tou Ni[1,2]

[1] *Center for Gravitation and Cosmology (CGC), Department of Physics*
National Tsing Hua University, Hsinchu, Taiwan, 30013 Republic of China
[2] *Shanghai United Center for Astrophysics (SUCA)*
Shanghai Normal University, Shanghai, 20234 China
Email : weitou@gmail.com

Abstract

In this talk, we review the empirical status for modern gravitational theories with emphases on (i) Equivalence Principles; (ii) Lense-Thirring effects and the implications of Gravity Probe B experiment; (iii) Solar-System Tests of Cosmological Models.

This contribution can be found at URL arXiv:1204.1859

Determination of the Gravity Anomaly Sources in the Mekong Delta using Wavelet Transform with the Optimal Resolution

Duong Hieu Dau[1], *Tran Thanh Phuc*[1], *Dang Van Liet*[2]
[1] *College of Natural Science, Cantho University*
[2] *The University of HCM City*
Email : dhdau@ctu.edu.vn

Abstract

The invert potential field problem for determination of the gravity anomaly boundaries (3D) in the Mekong delta was carried out by continuous wavelet transform (CWT). The data filters with parameters chosen appropriately have improved the resolution for the proposal method of analysis. The relative shape and size of the gravity source were estimated from contour lines of the wavelet transform modulus maxima. The analytic results by Multiscale edge detection method (MED) using experimental data of the Mekong delta show that there were 19 gravity anomaly sources of different sizes in this region. The result of the location, depth and size of these source is consistency to the traditional methods before but the level of detail for this technique is much higher.

1 Introduction

Recently, the combination of Continuous wavelet transform and Multiscale edge detection method was used frequently to quick localize and characterize of the gravity and magnetic source for the invert potential field problems (P. Sailhac, A. Galdeano, D. Gibert, F. Moreau, C. Delor; 2000). However, this technique is actually effective in determining the anomaly boundary if a filter with the appropriate parameters were chosen in accordance to the wavelet function applied for MED method (D. V. Liet, D.H. Dau and L.P.Toan; 2009). In this study, the line-weight function (LWF) filtering was hold (A.Fiorentini and L. Mazzatini; 1966) in the gravity data of the Mekong delta to enhance the resolution of the result for boundary plotting of gravity sources at different depths.

2 Theory

2.1 Wavelet transform

The continuous wavelet transform for one-dimension signal $f(x)$ is given by:

$$W(s,b) = \frac{1}{\sqrt{s}} \int_{-\infty}^{+\infty} f(x)\overline{\psi}(\frac{b-x}{s})dx = \frac{1}{\sqrt{s}}(f^{*}\overline{\psi}) \tag{1}$$

where $s \in R^{+}$ is the scale parameter, and $b \in R$ is the phase parameter (displacement), $\psi(x)$ is a selected wavelet function. The continuous wavelet transform has the advantage for using various wavelet functions correlating to the type of information of analyzing.

2.2 Med method

The MED technique is related to the determination of the maximum magnitude of the continuous wavelet transform at different scale on the experimental data (A.Grossmann, M. Holschneider, R. Martinet and J. Morlet; 1987). Poisson-Hardy wavelet function was constructed from the second derivative of transition function that allows the transfer characteristic of the invert potential field problem. This complex wavelet function has the type as follow:

$$\psi^{(PH)}(x) = \psi^{(P)}(x) + i\psi^{(H)}(x) \tag{2}$$

$$\psi^{(P)}(x) = -\frac{2}{\pi} \times \frac{1-3x^2}{(1+x^2)^3} \tag{3}$$

$$\psi^{(H)}(x) = Hilbert(\psi^{(P)}(x)) = \frac{2}{\pi} \times \frac{-3x+x^3}{(1+x^2)^3} \tag{4}$$

2.3 Line-weight function

For digital image processing technique, Gaussian filter shows the effectiveness of the low-pass filter for removing noise at high frequency and the information hidden in the high parts as well. A. Fiorentini, L.Mazzatini, (1966) introduced a LWF filter to remove noise but enhancing the contrast for image resolution. LWF can be written in the combinations of

$$\mathrm{h_0(x/\sigma)} \quad \text{and} \quad \mathrm{h_2(x/\sigma) : L(x/\sigma) = c_0h_0(x/\sigma) + c_2h_2(x/\sigma)} \tag{5}$$

where Gaussian function $h_0(x/\sigma)$ can be written as:

$$\mathrm{h_0(x/\sigma)} = \frac{1}{\sigma\sqrt{\pi}}\exp(-\frac{\mathrm{x}^2}{2\sigma^2}) \tag{6}$$

and $\mathrm{h_2(x/\sigma)}$ is the second derivative of Gaussian function:

$$\mathrm{h_2(x/\sigma)} = \frac{1}{\sqrt{8\pi\sigma^2}}\left(-\exp[-\frac{\mathrm{x}^2}{2\sigma^2}] + \frac{\mathrm{x}^2}{\sigma^2}\exp[-\frac{\mathrm{x}^2}{2\sigma^2}]\right) \tag{7}$$

Based on the analysis of D.V. Liet and L.P. Toan (2009), LWF could be used for enhancing the resolution of CWT on the gravity data to detect the properties of geophysics sources using MED method. The parameters of LWF were selected from the test results on the gravity model having values (c_0 = 0.07 and c_2 = - 0.1).

2.4 Proceduce for source boudary estimation

The process for boundary determination at different scale using CWT and MED method would be done by 7 steps as follow:

1- Filtering data by LWF function
2- Fitting signal length with the cut off data technique
3- Taking CWT on processing gravity signal by function named Poisson - Hardy

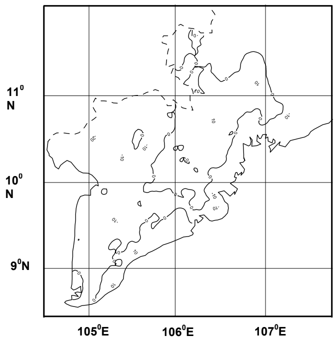

Figure 1: The contour lines of the gravity anomaly of the Mekong delta (data was provided by the South Vietnam Geological Mapping Division).

4- Changing the scale s of the CWT on processing gravity signal

5- Drawing the contours of the maximum magnitude of the CWT in the geographical maps of the Mekong delta.

6- Detecting of the properties for the gravity anomalies source in different depths

3 Research region

In this paper, the gravity sources from the southern land part of Vietnam were detected. The research area located at the Mekong Delta, from Ca mau (latitude 83^0 North) to Long An (latitude 11^0) and from Ha Tien (longitude $104^0 80$ East) to Go Cong (longitude $105^0 50$). The topography of this region is quite flat, average height above sea level is about 4m. Hills and mountains were distributed in the An Giang Province (Cam mountain is situated on the altitude of 716 m). The most important river in the Mekong delta is Cuu Long. The real data of gravity anomaly was provided by the South Vietnam Geological Mapping Division (200 Ly Chinh Thang, Ward 9, District 3, Ho Chi Minh City). Experiment was measured by gravitimeter (Tensodynamomelt) placed on the helicopter flying at an altitude of 50 m above the ground.
The profile was organized on the 267 lines along the equator. Each line has same latitude and its longitude changed from 104.5630 to 109.4080 East. Measurement step is 0.018 degrees (equivalent to 2 km).

4 Result

The result of analyzing gravity sources in the Mekong region using CWT and MED method based on the gravity anomaly data show that there was about 19 gravity anomaly sources different in size, shape and depth. They were mostly distributed at the major fault system of the South. Figure 2 is the map of distribution for gravity anomaly sources using the source boundary plotting technique after analyzing the maximum modulus of wavelet transform coefficient (at a scale s = 1, corresponding to a depth of 1.8 km).

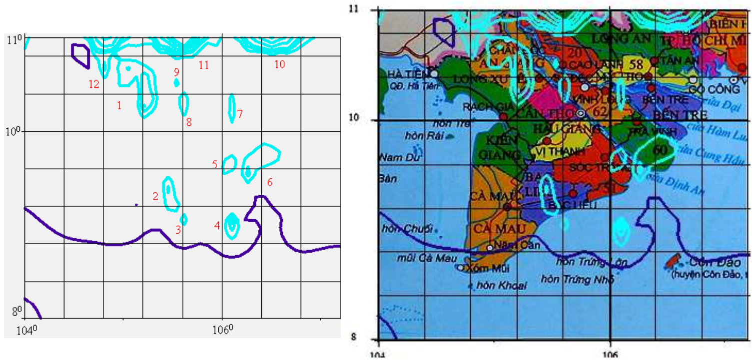

Figure 2: Gravity anomaly source boundaries using wavelet transform and MED method (s = 1)

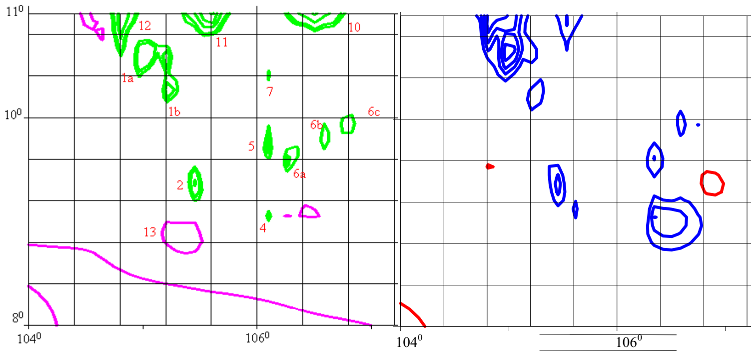

Figure 3: Gravity anomaly source boundaries using wavelet transform and MED method with s = 3(a), and s = 5 (b) corresponding to different depths of 4.8 km and 8.4 km.

5 Conclusion

Taking advantage of CWT and MED method combined with LWF filtering algorithm, the resolution for boundary detection of the gravity anomaly source was enhanced by drawing the boundary layers at different depths from 1.8 km to 8.4 km (corresponding to the scale from 1 to 8). In the Mekong delta region, 19 gravity anomaly sources of different sizes were discovered. Some of these sources were distributed at the major fault system of the South. The estimation for the localization, depth and size of the gravity anomaly source is consistency to the traditional methods before, but the resolution for the boundary layer plotting technique is much higher. Many applications from this research can be used for other geophysics analysis.

Table 1: The data structure of gravity anomaly, after filtering with LWF and wavelet analyzing with the wavelet function named Poisson-Hardy (Scale changes from 1 to 8).

Longitude (Degree)	Latitude (Degree)	$\triangle$g (mgal)	$\triangle$g(mgal) after filter	wavelet modulus S=1	wavelet modulus S=2	wavelet modulus S=3	wavelet modulus S =...	wavelet modulus S=8
107.4226	13.96751	-99	89	1.5423	1.5141	1.4296		1.371
107.4408	13.96751	-94	58	0.111	-0.6456	-1.3365		-1.5145
107.4590	13.96751	-90	51	1.4849	0.5369	-1.3735		-1.2892
107.4772	13.96751	-90	49	-0.7491	0.2882	1.4098		-1.05
107.4954	13.96751	-87	-133	0.0286	1.0131	-1.4423		-0.727
107.5137	13.96751	-252	40	1.4101	-1.2572	-0.8475		-0.3226
107.5319	13.96751	-432	-54	-0.6276	-0.2774	-0.098		0.1643
107.5501	13.96751	-111	-108	1.1145	0.7968	0.6746		0.6588
107.5683	13.96751	-19	-206	-0.83	-1.3963	1.3838		1.1238
...	...	...	...	...	...	...	...	...
...	...	...	...	...	...	...	...	...

References

[1] A. Fiorentine and L, Mazzantini, (1966), Neuron inhibition in the human fovea: A study of interaction between two line stimuli, Atti Fond G Ronchi, Vol.21, pp.738-747.

[2] A. Grossmann, M. Holschneider, R. Martinet, and J. Morlet, (1987) Detection of abrupt changes in sound signals with the help of wavelet transforms In verse Problems, An Interdisciplinary Study (Adv. Electron. Electron. Phys. 19), San Diego, CA: Academic, pp. 298-306.

[3] D. V. Liet, D. H. Dau and L.P. Toan (2009), Using the line-weight function to enhance the resolution of interpretation of gravity and magnetic data by wavelet transform; National Conference of Vietnamese Geophysics, Dec-2009.

[4] D. Marr, E.C. Hildreth, (1980), Theory of edge detection, Proc. R. Soc. London, B. 207, pp.187-217

[5] P. Sailhac, A. Galdeano, D. Gibert, F. Moreau, C. Delor, (2000), Identification of sources of potential fields with the continuous wavelet transform: Complex wavelets and applications to magnetic profiles in French Guiana, Journal of Geophysical Research, Vol. 105, pp. 19455-19475.

A simple proposal to measure the speed of gravity

M. B. Paranjape

Groupe de physique des particules, Département de physique, Université de Montréal,

C.P. 6128, succ. Centre-ville, Montréal, Québec, Canada H3C 3J7

Email : paranj@lps.umontreal.ca

Abstract

We propose an experiment to directly detect the speed of gravity in the laboratory. If one is able to detect the static gravitational field of a massive body in the laboratory, then moving that body induces changes in the gravitational field that propagate to the detector with a finite time delay, equal to the distance between the body and the detector divided by the speed of gravity. When moving two bodies, changes to the gravitational field will contribute constructively or destructively, which allows for the measurement of the speed of gravity

1 Introduction

At the present time, great efforts are being made to detect gravitational waves, fundamental predictions of Einstein's theory of general relativity [1]. However any moving mass creates gravitational disturbances. For typical terrestrial periodic motion with frequencies generally less than 10000 Hertz, the wavelength of the gravitational waves is of the order of 10^4 metres, and hence the wave zone approximation is not possible. However, these disturbances propagate from the mass at the speed of gravity. It would be an important confirmation of Einsteinian relativity to measure the speed of propagation of these gravitational disturbances.

2 Static forces

Consider a configuration of two masses m_1 and m_2 a distance r_1 and r_2 respectively on opposite sides of a detector of gravitational force, which has an effective mass m. Aligning all the masses along the x axis, we find the gravitational force on the detector is

$$F = Gm\left(\frac{m_1}{r_1^2} - \frac{m_2}{r_2^2}\right) \tag{1}$$

along the x direction. We can choose the masses m_i and the distances r_i so that the force exactly cancels, say $m_i/r_i^2 \equiv M/R^2$, so that $F = 0$.

Now suppose we move the masses so that $r_i \to r_i + \delta_i$. With $\epsilon_i = \delta_i/r_i$, then the force is to first order in ϵ_i

$$F = Gm\left(\frac{m_1}{(r_1+\delta_1)^2} - \frac{m_2}{(r_2+\delta_2)^2}\right) \approx \frac{2GmM}{R^2}\left(\epsilon_2 - \epsilon_1\right). \tag{2}$$

It is clear that we can choose the displacements so that $\epsilon_1 = \epsilon_2 = \epsilon$ and $F = 0$.

3 Time dependent forces

Now suppose the ϵ_i becomes time dependent, $\epsilon \to \epsilon \sin(\omega t)$. Then is the static analysis still valid? The answer is no. The force at time t at the detector corresponds to Newton's law for each mass m_i however at a position corresponding to the retarded time t_{ri}, respectively. The retarded time is simply $t_{ri} = t - \Delta_i t$ where $\Delta_i t = r_i/v_g$ is the distance to the detector divided by the speed of gravity, v_g. Thus the force is

$$F = \frac{2GmM}{R^2}\epsilon\left(\sin\omega t - \sin\omega(t-\Delta t)\right). \tag{3}$$

where $\Delta t = \Delta_1 t - \Delta_2 t = (r_1 - r_2)/v_g$, appropriately translating the zero of time. The point-like approximation for the masses and the use of the retarded Newton force law can be justified if the linear dimensions of the masses are small in comparison to the distances r_i, this will be spelled out in detail elsewhere. Then using the simply trigonometric identity $\sin A - \sin B = 2\sin\frac{(A-B)}{2}\cos\frac{(A+B)}{2}$ we get

$$F \approx \frac{2GmM\epsilon\omega}{R^2}\frac{(r_1 - r_2)}{v_g}\epsilon\left(\cos\omega(t+\Delta t/2)\right). \tag{4}$$

aproximating the sin by its argument. Thus we see that there is a net force on the detector that is periodically varying and with a coefficient that is a function of v_g. Using unremarkable values for the masses and distances involved, say 1 kilogram and 1 metre gives us a force of 6.67×10^{-11} newtons. Forces of this magnitude, plus or minus several orders of magnitude are easily measurable in the laboratory. Then for an ω of 1000 $\sim$ 10,000 hertz and ϵ of say a tenth, and $r_1 - r_2 \sim 1$ metre, we get a diminution of the force by a factor of

$$\epsilon\omega(r_1 - r_2)/v_g = 10^{-6} \sim 10^{-7} \tag{5}$$

where the equality is valid assuming v_g is the speed of light. Thus observing this force and the corresponding amplitude in the detector would allow for the determination of the speed of gravity. Evidently the Q value of the detector will be decisive in whether or not the effect can be observed. Happily, Q values for gravity detectors are quite high.

4 Possibilities for measurement

There are two types of detectors of gravity which could in principle be used to detect this effect and measure the speed of gravity. Detectors of gravitational force are torsion balances [2], micro-cantilevers [3] and similar devices. It is however important that the motion intrinsic to the detector be small in comparison to the motion of the masses. Torsion balances are notorious for large intrinsic motion [4] and thus can even be unsuitable for our purposes. Micro-cantilevers do not suffer this problem, their displacement is in the range of microns and thus their motion can in principle be neglected. The Q values of these detectors is in the range of $10^4 \sim 10^5$ which is just a little smaller than desirable.

The other possibility are detectors of gravitational potential seem to have Q values that are incredibly high, $Q \sim 10^{10}$ is easily attainable [5]. Hence it seems that such detectors would easily have the sensitivity to detect our effect. However, the gravitational potential is negative definite, the potential from the two masses does not cancel. How to overcome this difficulty will be explained in a future publication.

5 Acknowledgements

We thank NSERC of Canada for financial support and Richard MacKenzie and Viktor Zacek for useful discussions.

References

[1] Ligo Collaboration, Nuclear Instruments and Methods in Physics Research Section A: Accelerators, Spectrometers, Detectors and Associated Equipment Volume 517, Issues 13, 21 January 2004.

[2] C. D. Hoyle, D. J. Kapner, B. R. Heckel, E. G. Adelberger, J. H. Gundlach, U. Schmidt, and H. E. Swanson, Phys. Rev. D 70, 042004 (2004); E.G. Adelberger, J.H. Gundlach, B.R. Heckel, S. Hoedl and S. Schlamminger, Part. Nucl. Phys. 62, 102 (2009).

[3] Joshua C. Long, Hilton W. Chan, Allison B. Churnside, Eric A. Gulbis, Michael C. M. Varney, John C. Price, Nature 421, 922-925 (2003); S. J. Smullin, A. A. Geraci, D. M. Weld, J. Chiaverini, S. Holmes, and A. Kapitulnik, Phys. Rev. D 72, 122001 (2005).

[4] We thank the members of the audience at the Xth International Conference on Gravitation, Astrophysics and Cosmology, Quy Nhon, Vietnam, December, 2011 for bringing this to our attention.

[5] Atom Interferometry, Paul R. Berman, Academic Press, 1996.

MEASUREMENT OF G BY USING A HIGH-Q SILICA FIBER WITH TIME-OF-SWING METHOD

Qing Li, Cheng-Gang Shao, Shan-Qing Yang & Jun Luo

Key Laboratory of Fundamental Physical Quantities Measurement of Ministry of Education,

School of Physics, Huazhong University of Science and Technology

Wuhan 430074, People's Republic of China

Email : qlllp45@163.com

Abstract

We will measure the Newtonian gravitational constant G by using a high-Q silica fiber with time-of-swing. The fiber will be coated with a thin Bi layer on a Ge layer. The prospective uncertainty of the G value will be determined <20 ppm.

1 Introduction

In our latest G measurement with time-of-swing method by using a tungsten fiber [1, 2], the largest uncertainty is contributed by the fiber's anelastic effect which brings in a correction of -211.80(18.69) ppm [3]. According to the hypothesis of $1/\pi Q$ [4], it is known that a direct approach to reduce anelasticity is using a high-Q fiber to replace the tungsten fiber. Fused silica (synthetic fused silicon dioxide) is known to have an inherent loss that about 2 orders of magnitude lower than that of metals [5]. Compared to metal, fused silica is an insulator and it should be coated with metal to avoid the potential electrostatic effect. In next G measurement with time-of-swing method, we will use the coated silica fiber with a high-Q of $> 5 \times 10^4$ and the anelasticity is expected to only bring in a correction of $\sim$6 ppm. Besides, we will use the angular acceleration feedback method [6] which is insensitive with the anelastic effect to measure G in the same laboratory synchronously. The prospective uncertainties of the G values by the two different methods will be both <20 ppm and their systematic errors will be studied and compared in detail.

2 Study of Silica Fiber

The fused silica fibers are pulled from Heraeus [7] Suprasil-311 rods using oxygen-hydrogen flame by hand. The Q's of silica fibers with diameters of $\sim$37 μm and lengths of $\sim$18 cm are measured at a high vacuum of $\sim 10^{-5}$ Pa. Fig. 1 shows the measured loss angle ϕ varying with the ratio of the coating thickness to the fiber's diameter. It is obviously that the loss angle of Ge and Bi layers (signed with B) are less than that of Au layer (signed with A). Under coating condition of a 7-nm-thicker Bi layer on a 3-nm-thicker Ge layer, a Q of $\sim$68000 is achieved. Under this level of Q, the anelastic effect will only bring in a correction of $\sim$5 ppm in next G measurement with time-of-swing method.

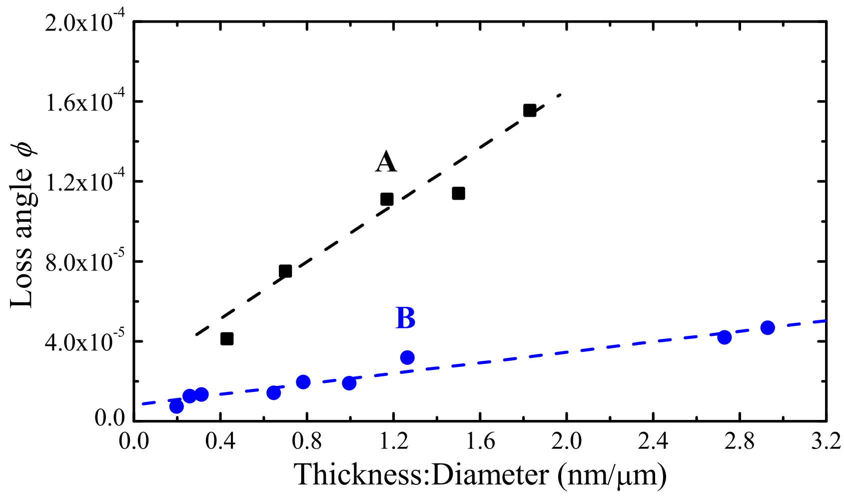

Figure 1: (color online). The measured loss angle ϕ varying with the ratio of the coating thickness to the fiber's diameter. A: coated with Au, B: coated with Bi on Ge. The dashed line represents the least-square fit.

References

[1] J. Luo, Q. Liu, L. C. Tu, C. G. Shao, L. X. Liu, S. Q. Yang, Q. Li and Y. T. Zhang, Physical Review Letters, 102 (2009) 240801.

[2] L. C. Tu, Q. Li, Q. L. Wang, C. G. Shao, S. Q. Yang, L. X. Liu, Q. Liu and J. Luo, Physical Review D, 82 (2010) 022001.

[3] S. Q. Yang, L. C. Tu, C. G. Shao, Q. Li, Q. L. Wang, Z. B. Zhou and Jun Luo, Physical Review D, 80 (2009) 122005.

[4] K. Kuroda, Physical Review Letters, 75 (1995) 2796.

[5] S. Rowan, R. Hutchins, A. McLaren, N. A. Robertson, S. M. Twyford and J. Hough, Physics. Letters. A. 227 (1997) 153.

[6] J. H. Gundlach and S. M. Merkowitz, Physical Review Letters, 85 (2000) 2869.

[7] Heraeus-Amersil Corporation, 3473 Satellite Boulevard, Duluth, GA 30136-5821.

Scheme for test of the equivalence principle with rotating cold molecules

Zhong-Kun Hu, Yi Ke, Jun Luo

School of Physics, Huazhong University of Science and Technology,

Wuhan 430074, People's Republic of China

Email : zkhu@mail.hust.edu.cn

Abstract

We present here a novel scheme for testing the equivalence principle with rotating cold molecules whose rotational states are different. The proposed experiment may open a new way for testing the equivalence principle and the possible coupling between rotation and gravity.

1 Introduction

In 2001, Zhang *et al.* developed a phenomenological model for the spin-spin interaction between rotating extended bodies [1]. Based on this theoretical model, a dimensionless parameter representing the strength of violation of the equivalence principle can be defined as follows:

$$\eta_s = \frac{\Delta g}{g} = \kappa \left(\frac{\boldsymbol{S}_1 \cdot \boldsymbol{S}_e}{G m_1 M_e R_1} - \frac{\boldsymbol{S}_2 \cdot \boldsymbol{S}_e}{G m_2 M_e R_2} \right), \tag{1}$$

where G is the Newtonian gravitational constant, m_1 , m_2 , and M_e are the masses of the two rotating bodies and the Earth, respectively, and $\boldsymbol{S}_1$, $\boldsymbol{S}_2$,and $\boldsymbol{S}_e$ are their spin angular momenta correspondingly, R_1 and R_2 are the distances between the centers of the two gyroscopes and the Earth, respectively, and the parameter κ represents the universal coupling factor for the spin-spin interaction.

We now propose a novel scheme for testing the equivalence principle using rotating cold molecules, whose angular momenta will be polarized vertically up or down. The rotating speed of molecules can been made 8 orders of magnitude higher than that of mechanical gyroscopes. In addition, molecules have a smaller dimension, which is helpful to testing the equivalence principle in a small spatial dimension.

2 Cooling of molecules

There are many techniques to slow and cold molecules, such as photoassociation or Feschbach resonances, buffer-gas cooling, electrostatic Stark deceleration, and optical Stark deceleration. Among these methods, we prefer to use the technique of electrostatic Stark deceleration [2], which takes advantage of the molecular DC Stark effect to decelerate and cool down molecules and thus is a general method. This method can apply to many types of molecules as long as they have a large electric dipole moment. The temperature of molecules after deceleration can reach the mK range.

3 Control of molecular rotation

Rotating molecules using laser has been demonstrated in experiment [3], where molecules are rotated by a pair of left and right circularly polarized nonresonant laser pulses with opposite chirps, using femtosecond laser technology. The combination of the two fields form a linearly polarized laser field to rotate molecules due to their induced dipole moment.

Using a microwave field to rotate molecules has also been mentioned [4]. Molecules are initially prepared in a particular rotational state, e.g. the ground rotational state. With the help of quantum optimal control theory, a specially tailored microwave field can be designed to transfer molecules to a given final state, e.g. an angular momentum oriented state.

We also can select out molecules in particular rotational states from thermal equilibrium distribution using the hexapole state-selection technique [5]. In the inhomogeneous field produced by the hexapole, molecules in different rotational states in general have different Stark shifts and thus different trajectories. So with an appropriately adjustment of the voltage on the hexapole rods, molecules in a given rotational state can be focused at the exit of the hexapole system.

4 Measurement of g of molecules

The free fall acceleration g of molecules can be measured by taking advantage of the Doppler effect. During the free fall of molecules, they have an overall Doppler shift relative to the laser which propagates vertically. Measuring the Doppler shifts $\Delta\omega_1$ and $\Delta\omega_2$ at times t_1 and t_2 can get the g value:

$$g = \left| \frac{\Delta\omega_2 - \Delta\omega_1}{k(t_2 - t_1)} \right|, \tag{2}$$

where k is the wave vector of the laser.

If we can further cool down the molecules to the μK level, the phenomenon of the Bloch oscillations can be used to measure g. Considering molecules trapped in a one-dimensional vertical optical lattice created by two interfering laser beams in gravity field, they will execute Bloch oscillations with a frequency ν_B given by

$$\nu_B = \frac{mg\lambda_L}{2h}, \tag{3}$$

where λ_L is the wavelength of the laser, and m is the molecular mass. The experiment applying Bloch oscillations of cold atoms to gravity measurement has been reported with a relative precision of 10^{-7} [6]. The high measurement precision with atoms indicates that the measurement of gravitational acceleration using cold molecules trapped in a vertical optical lattice is a promising method.

Raman type matter-wave interferometer is an analogue of optical interferometer and can be used to gravity measurement [7]. In a typical atom interferometry gravimeter, atoms free fall and interact with Raman lasers. The acceleration g can be extracted from the following expression:

$$\phi_g = k_{eff} g T^2, \tag{4}$$

where ϕ_g is interferometer phase, k_{eff} is the effective wavevector of the Raman lasers, and T is the time interval of the Raman pulses. If the idea of atom interferometry gravimeter can be extended to molecules, the measurement precision of the gravitational acceleration of molecules has a potential to reach the level of $10^{-9}g$.

5 Conclusions

We have proposed a novel scheme for testing the equivalence principle with rotating cold molecules with different rotational states.

We are grateful to Professor Y. Z. Zhang in Institute of Theoretical Physics for helpful discussions. This work is supported by the National Basic Research Program of China (Grant No. 2010CB832806) and the National Natural Science Foundation of China (Grant Nos. 10875045 and 41127002).

References

[1] Y. Z. Zhang, J. Luo, and Y. X. Nie, *Gravitational effects of rotating bodies*, Mod. Phys. Lett. A 16 (2001) 789.

[2] H. L. Bethlem, G. Berden, and G. Meijer, *Decelerating neutral dipolar molecules*, Phys. Rev. Lett. 83 (1999) 1558.

[3] D. M. Villeneuve *et al.*, *Forced molecular rotation in an optical centrifuge*, Phys. Rev. Lett. 85 (2000) 542.

[4] R. S. Judson, K. K. Lehmann, H. Rabitz, and W. S. Warren, *Optimal design of external fields for controlling molecular motion: application to rotation*, J. Mol. Struct. 223 (1990) 425.

[5] K. H. Kramer and R. B. Bernstein, *Focusing and orientation of symmetric-top molecules with the electric six-pole field*, J. Chern. Phys. 42 (1965) 767.

[6] N. Poli *et al.*, *Precision measurement of gravity with cold atoms in an optical lattice and comparison with a classical gravimeter*, Phys. Rev. Lett. 106 (2011) 038501.

[7] A. Peters, K. Y. Chung, and S, Chu, *Measurement of gravitational acceleration by dropping atoms*, Nature (London) 400 (1999) 849.

G-Gran Sasso: an experiment for the terrestrial measurement of the Lense-Thirring effect by means of ring-lasers

Angelo Tartaglia
Politecnico di Torino, Corso Duca degli Abruzzi 24, 10129 Torino, Italy and INFN
Email : angelo.tartaglia@polito.it

Abstract

The talk presents a proposal for a new experiment aimed to the detection of the gravito-magnetic Lense-Thirring effect at the surface of the Earth. The proposed technique uses a three-dimensional set of gyrolasers and exploits the anisotropic propagation of light in the gravitational field of a rotating mass. The experiment is planned to be built in the Gran Sasso National Laboratories in Italy and is based on an international collaboration among various Italian groups, the Technische Universität München and the Canterbury University in Christchurch (NZ).

1 Introduction

Until now the General Relativistic drag of the inertial frames in the field of a rotating mass (Lense-Thirring effect [1] [2]) has been experimentally verified only twice: by Ciufolini and collaborators [3] and by the Gravity Probe B (GP-B) experiment led by Francis Everitt [5]. In the former case the attained accuracy has been 10%; in the latter the accuracy has been 19%. In both cases the measurements were based on the material precession of angular momenta. The only ongoing further experiment is LARES, launched on February 13 2012 [4], whose objective is the measurement of the Lense-Thirring (LT) effect with the accuracy of a few %, possibly 1%.

Here I am presenting the recently proposed G-GranSasso experiment to test the terrestrial LT effect; the Principal Investigator is Angela Di Virgilio of the Pisa section of the Italian INFN. The proposal is presented by a collaboration among five universities in Italy plus the INFN and the Technische Universität München; a permanent consultancy exists with the Canterbury University in Christchurch (NZ). G-GranSasso will use light as a probe and will exploit the anisotropic propagation of light in the gravitational field of a rotating mass. A three-dimensional array of ring-lasers located in an underground terrestrial laboratory will measure the asymmetry evidencing various relativistic effects, including LT with the expected accuracy of 1%. The present sensitivity of the best existing ring laser [1] is approximately one order of magnitude above the threshold to be trespassed in order to measure LT; it is then reasonable to expect the right sensitivity to be attainable in a specially designed new instrument adopting the best technologies of the moment. The details of our proposal may be found in [6].

2 Light in axially symmetric space-times

A steadily rotating mass is surrounded by a space-time endowed with an axial symmetry around a time-like axis. Choosing a reference frame centered on the body and polar space coordinates the general line element

[1] It is G, located in Wettzell, Germany.

of such a space-time is:

$$ds^2 = g_{00}dt^2 + g_{rr}dr^2 + g_{\theta\theta}d\theta^2 + g_{\phi\phi}d\phi^2 + 2g_{0\phi}dtd\phi. \tag{1}$$

In a terrestrial (then non-inertial) laboratory and up to the first Post Newtonian (PN) approximation keeping the angular momentum of the earth it is [6]:

$$\begin{aligned} g_{0\phi} &\simeq (2\tfrac{j}{r} - r^2\tfrac{\omega}{c} - 2\mu r\tfrac{\Omega_\oplus}{c})\sin^2\theta \\ g_{00} &\simeq 1 - 2\tfrac{\mu}{r} - \tfrac{\omega^2 r^2}{c^2}\sin^2\theta \end{aligned} \tag{2}$$

In (2) a couple of shorthand symbols have been used:

$$\begin{aligned} \mu &= G\tfrac{M_\oplus}{c^2} \approx 4.4 \times 10^{-3}\ m \\ j &= G\tfrac{J_\oplus}{c^3} = G\tfrac{\Omega_\oplus I_\oplus}{c^3} \approx 1.75 \times 10^{-2}\ m^2 \end{aligned} \tag{3}$$

G is Newton's gravitational constant; $\mathbf{J}_\oplus$ is the angular momentum of the earth and $I_\oplus$ is its moment of inertia; $\Omega_\oplus$ is the angular velocity of the planet and ω is the absolute angular velocity of the apparatus (in practice it will coincide with $\Omega_\oplus$).

Let us consider a ring laser made of an active cavity from which two light beams emerge in opposite directions. A number of mirrors (≥ 3) give rise to a closed loop in space, along which the two counter-propagating light beams move. It turns out that light takes different times to go round in clock or counter-clock sense; in a ring-laser the anisotropy shows up in the form of a beat frequency of standing waves [6]. The final frequency difference (the expected signal) is [6]:

$$\begin{aligned} \delta f &= 4\tfrac{A}{\lambda P}[\mathbf{\Omega}_\oplus - 2\tfrac{\mu}{R}\Omega_\oplus \sin\theta \hat{\mathbf{u}}_\theta + \tfrac{GJ_\oplus}{c^2R^3}(2\cos\theta\hat{\mathbf{u}}_R + \sin\theta\hat{\mathbf{u}}_\theta)]\cdot\hat{\mathbf{u}}_n \\ &= 4\tfrac{A}{\lambda P}[\mathbf{\Omega}_\oplus + \mathbf{\Omega}_g + \mathbf{\Omega}_B]\cdot\hat{\mathbf{u}}_n \end{aligned} \tag{4}$$

The ring laser has been assumed to be contained in a plane; A is the area contoured by the light beams; P is the length of the loop; λ is the wavelength of the light of the laser; θ is the colatitude of the site; $\hat{\mathbf{u}}_n$ is the unit vector along the normal to the plane of the ring; $\hat{\mathbf{u}}_R$ is the radial unit vector; $\hat{\mathbf{u}}_\theta$ is the unit vector along the local meridian (towards increasing colatitudes); R is the radius of the earth or, to say better, the radial distance of the laboratory from the center of the earth.

Considering the orders of magnitude we see that $\Omega_\oplus \simeq 7.2 \times 10^{-5}\ s^{-1}$ and $\Omega_G \sim \Omega_B \approx 10^{-9} \times \Omega_\oplus \approx 10^{-13}\ s^{-1}$. These numbers set the goal to be attained in order to measure the properly general relativistic effects, i.e. the $\mathbf{\Omega}_G$ and $\mathbf{\Omega}_B$ "precession rates".

3 G-GranSasso

The proposal named G-GranSasso is to build a set of square ring lasers (not less than three) in a three-dimensional array, with a high enough sensitivity to reveal the general relativistic contributions and especially the LT effect. Two possible configurations are under analysis: a cubic concrete monument carrying six lasers on its faces; an octahedron made of three square loops. In the former case we would have a redundancy factor 2; the octahedral configuration instead lends the possibility to better control the geometry using resonating cavities (Fabry-Pérot interferometers) along the main diagonals.

In any case the side of the square loops would be 6 m long, giving a scale factor $S = 4A/\lambda P$ 50% higher than for G; the power of the laser should be 200 nW; the quality factor of the resonating cavities would be $Q = 3 \times 10^{12}$. The whole instrument would be located deeply under ground in the Gran Sasso National Laboratories in Italy; the reason of the underground laboratory choice is the screening from the surface mechanical noise. The objective is to measure the general relativistic "precessions" with an accuracy of the order of $\sim 1\%$.

First analyses and evaluations show that the LT effect could be revealed with the desired accuracy after a several months long integration time [6].

References

[1] J. Lense, H. Thirring, *Phys. Z.* **19**, 156-163 (1918)

[2] H. Thirring, *Phys. Z.* **19**, 33 (1918)

[3] I. Ciufolini, E. Pavlis, *Nature* **431**, 958 (2004); I. Ciufolini et al., *Space Sci Rev* **148**, 71-104 (2009).

[4] I. Ciufolini, *Class. Quantum Grav.* **17**, 2369 (2000).

[5] C.W.F. Everitt *et al.*, *Phys. Rev. Lett.* **106**, 221101 (2011).

[6] F. Bosi *et al.*, *Phys. Rev. D* **84**, 122002 (2011).

Some experimental evidences of long-range gravitational-like interaction in a neutral cold gas

D. Wilkowski[1,2,3], *J. Barré*[4], *M. Chalony* [1], *B. Marcos*[4] *and A. Olivetti*[4]

[1] *Institut Non Linéaire de Nice, Université de Nice Sophia-Antipolis, CNRS, 06560 Valbonne, France.*

[2] *Centre for Quantum Technologies, National University of Singapore, 117543 Singapore, Singapore.*

[3] *PAP, School of Physical and Mathematical Sciences, Nanyang Technological University, 637371 Singapore, Singapore.*

[4] *Laboratoire J.-A. Dieudonné, Université de Nice Sophia-Antipolis, CNRS, 06109 Nice, France.*

Email : David.Wilkowski@ntu.edu.sg

Abstract

We show that a quasi one dimensional cold gas of atoms coupled with quasi-resonant laser beams can exhibited long range gravitational-like interaction.

1 Introduction

When the interactions between the microscopic components of a system act on a length scale comparable to the size of the system, one may call them "long range". For instance, the inverse-square law of the gravitational force between two point masses is one of the best known and oldest law in Physics, since it was published in 1687 by Sir Isaac Newton in his famous book Principia. In the many particles world, this law is responsible for dramatic collective effects such as the collapse of a gravothermal catastrophe or the clustering at the origin of the structures of galaxies in the present universe. The statistical equilibrium of gravitational systems is theoretically well established (see for example [1]). At fixed temperature, we know for example that the stability of the extended phase, dominated by the long range interaction, or the collapsed phase, dominated by the short range repulsive interaction, depend on the dimension of the system. In 1D system, only the extended phase is stable where as in 2D we expected a phase transition for a critical temperature. Finally in 3D, only the collapsed phase is stable and the extended one is metastable. On the experimental side: We have recently show some experimental evidences of a gravitational-like interaction on an 1D test system consisting in a cold gas of neutral Strontium atoms in interaction with two counter-propagating quasi-resonant lasers [2]. To our knowledged no such controllable experimental system was reported before. We briefly review the important result in this proceeding. In section 2 we will discuss the experimental apparatus. One signature of the gravitational-like interaction is given in section 3. We finally give our conclusion and perspectives in section 4.

2 Experimental apparatus

As described in [3], our ^{88}Sr cold atomic sample is produced as follow; after a loading and a precooling stage on the broad $^1S_0 \rightarrow {}^1P_1$ dipole-allowed transition ($\Gamma/2\pi = 32$ MHz, $\omega_{\rm r}/2\pi = 10.6$ kHz), the atoms are transferred to a MOT operating on the narrow $^1S_0 \rightarrow {}^3P_1$ intercombination transition at 689 nm ($\Gamma/2\pi = 7.5$ kHz, $\omega_{\rm r}/2\pi = 4.7$ kHz). This final cooling stage lasts for 130 ms and leads to a cold gas containing about 2×10^7 atoms at a temperature of $T = 2\,\mu$K. A few tens of milliseconds before switching off the MOT, a far-off resonant dipole trap, centered on the atomic gas, is turned on. About 1% of the initial atoms are transfered in the dipole trap. It consists of a single focused laser beam at 780 nm. The laser power is 120 mW for a beam waist of $23(2)\,\mu$m, corresponding to a potential depth of $T_0 \simeq 20\,\mu$K. 50 ms after the MOT stage, a counter-propagating pair of beams, aligned with the long axis of the dipole trap and red-detuned with respect to the $^1S_0 \rightarrow {}^3P_1$ transition is turned on for 450 ms. These beams are at the origin of the gravitational-like interaction [2].

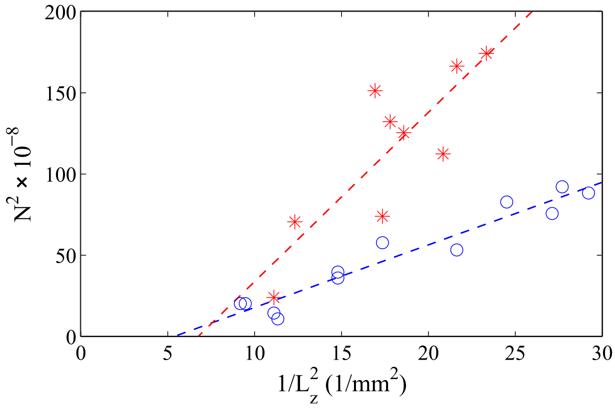

Figure 1: Dependency of the longitudinal size of the cloud with the number of atoms for $\delta = 5.7(5)\Gamma$ and $I = 0.6\ \mu$Wcm^{-2}. The blue circle (red star) data points correspond to temperature $1.5(2)\,\mu$K ($2.1(2)\,\mu$K). The optical depth is in the range of 0.6-0.2 according to atoms number variations. The blue and the red dashed lines are linear fits.

3 Signature of the gravitational-like interaction

One has to note that the counter-propagating laser beams are red-detuned with respect to the atomic resonance considered here. Thus, laser cooling is at play and the temperature T of the cold atomic cloud is fixed [5]. The mean kinetic energy is then $\langle E_c \rangle \propto NT$, where N is the atoms number. In the 1D gravitational potential, the mean potential energy is $\langle U \rangle \propto \int \mathrm{d}z\mathrm{d}z'\ n(z)n(z') \mid z - z' \mid$, where $n(z)$ is the one body density. Using a Gaussian ansatz for the density and the virial theorem to link $\langle E_c \rangle$ and $\langle U \rangle$, we find that:

$$L_z \propto \frac{T}{N}. \tag{1}$$

Fig. 1 shows that the cloud's size L_z is in agreement with this prediction for two temperature ranges: $1.5(2)\,\mu$K (blue circle) and $2.1(2)\,\mu$K (red star). Linear fits correspond to the blue dashed line for $1.5(2)\,\mu$K and the red dashed line for $2.1(2)\,\mu$K. The fitting expression is $N^2 = a_1/L_z^2 + a_2$, where a_1 and a_2 are free parameters. The presence of the holding trap is revealed when N goes to zero by the finite.

Further experimental evidences were found analyzing the density distribution and the out-of-equilibrium evolution of the cold cloud [2].

4 conclusion and perspectives

Long range gravitational-like interaction is revealed using an laser cooled strontium cloud coupled to a counter-propagating quasi-resonant laser beams. We found a $1/N$ dependency of L_z which is a clear signature of the long range nature of the interaction. In future, we will focus on the 2D case where phase transition from the extended phase to the collapse is expected.

References

[1] A. Campa, T. Dauxois, and S. Ruffo, Phys. Rep. **480**, 57 (2009).

[2] M. Chalony, J. Barré, B. Marcos, A. Olivetti and D. Wilkowski, Submitted to Phys. Rev. Lett. (2012) [atom-ph 1202.1258].

[3] T. Chaneliere, L. He, R. Kaiser and D. Wilkowski, Eur. Phys. J. D **46**, 507 (2008).

[4] M. Chalony, A. Kastberg, B. Klappauf and D. Wilkowski, Phys. Rev. Lett.**107**, 243002 (2011).

[5] H. Metcalf and P. van der, Phys. Rep. **244**, 203 (1994).

General Relativity

Visiting the site of the Cham Towers : Angelo Tartaglia, Viatcheslav Mukhanov and Alexander Vilenkin

Nobuyoshi Ohta, Kei-ichi Maeda and Keiji Igi

Weyl Cosmology

N. Deruelle[1], *M. Sasaki*[2], *Y. Sendouda*[3] *and A. Youssef*[4]
[1] *APC, UMR 7164 du CNRS, Université Paris 7, 75205 Paris Cedex 13, France*
[2] *Yukawa Institute for Theoretical Physics, Kyoto University, Kyoto 606-8502, Japan*
[3] *Graduate School of Science and Technology, Hirosaki University, Hirosaki 036-8561, Japan*
[4] *Institut für Physik, Humboldt-Universität zu Berlin, Rudower Chaussee 25, 12489 Berlin*

Abstract

In order to assess the role of ghosts in cosmology, we study the evolution of linear cosmological perturbations during inflation when a Weyl term is added to the action. We find that vector perturbations can no longer be ignored and that scalar modes diverge in the newtonian gauge but remain bounded in the comoving slicing. The square of the Weyl tensor, which is gauge invariant, remains bounded however.

We then show that the ghost degrees of freedom of Weyl gravity can be eliminated by a simple mechanism based on local Lorentz symmetry breaking. We demonstrate how the mechanism works in a cosmological setting and compute the modified CMB power-spectrum predicted by our theory.

1 Introduction

The description general relativity (GR) gives of the present accelerated expansion of the universe as well as its early history is usually seen as lacunar or unnatural. This state of affairs led to different attempts to generalize GR, the most natural of which consists in adding diffeomorphism-invariant operators, i.e scalars constructed from the Riemann tensor, to the Hilbert-Einstein action. The relevant operators depend on the stage of the universe investigated: the operator R^2 is expected to be important in the early universe and negligible today. The opposite being true for the operator $1/R$.

As shown in [1], these theories generically possess ghosts when linearized around Minkowski spacetime, that is, the Hamiltonian contains negative kinetic terms and, as a consequence, the energy spectrum of the metric perturbations is not bounded from below (just as in the toy model with lagrangian $(\Box\phi)^2$ studied earlier by Pais and Uhlenbeck, [2]). In fact most "higher derivative theories", that is, yielding equations of motion of differential order higher than two, are thought to possess ghosts (to the notable exception of $f(R)$ theories of gravity, see [3] for a review). Classically, when interactions are turned on, the system can develop singularities in a finite time. Quantum mechanically, a Hamiltonian unbounded from below indicates that either the system is unstable for it has no ground state, ot it possesses negative norm states [4]. The literature abounds with studies on the viability of these theories, with no clear consensus in the community (see in particular [5, 6]).

2 Ghosts at work

The afore-mentioned uncertainties about the viability of higher-derivative theories with ghosts, led us to investigate the concrete cosmological implications of such a theory in [7]. Indeed the study of the evolution of linear cosmological perturbations of higher-derivative theories during inflation is certainly a privileged setup to make testable predictions in this area.

Consider the action

$$\begin{aligned} S =& \frac{1}{2\kappa}\int d^4x\,\sqrt{-g}\,R - \frac{1}{2}\int d^4x\,\sqrt{-g}\,\left(\partial_\mu\phi\,\partial^\mu\phi + 2V(\phi)\right) \\ &- \frac{\gamma}{4\kappa}\int d^4x\,\sqrt{-g}\,C_{\mu\nu\rho\sigma}\,C^{\mu\nu\rho\sigma}\,, \end{aligned} \tag{1}$$

where g is the determinant of the metric $g_{\mu\nu}$, R is the scalar curvature and $C_{\mu\nu\rho\sigma}$ is the Weyl tensor.[1] The two first terms describe Einstein's gravity minimally coupled to a scalar field ϕ with potential $V(\phi)$. The last term was first introduced by Weyl (see [8] for a review). The resulting equations of motion (eom) are:

$$G_{\mu\nu} - \gamma\,B_{\mu\nu} = \kappa\,T_{\mu\nu} \quad \text{with} \quad \begin{cases} T_{\mu\nu} = \partial_\mu\phi\,\partial_\nu\phi - g_{\mu\nu}\left(\frac{1}{2}\partial_\rho\phi\,\partial^\rho\phi + V(\phi)\right)\,, \\ B_{\mu\nu} = 2D^\rho D^\sigma C_{\mu\rho\nu\sigma} + G^{\rho\sigma}\,C_{\mu\rho\nu\sigma}\,, \end{cases} \tag{2}$$

where $G_{\mu\nu}$ is the Einstein tensor and $B_{\mu\nu}$ is the Bach tensor [9]. Equations (2) are fourth order differential equations for the metric components. They therefore possess extra, "run-away", solutions compared to the Einstein, $\gamma = 0$, ones, which can drastically modify the predictions, even in the small γ limit.

Although the presence of these ghost degrees of freedom is harmless at linear level around Minkowski spacetime on which all modes propagate independently of each other, it may however happen that the malignancy of ghosts shows up already at linear level, if the background is richer than Minkowski spacetime. Here we aim at assessing the role of the Weyl term on the evolution of linear cosmological perturbations when the Friedmann-Lemaître background is that of single-field inflation.

When the metric is that of a conformally flat Friedmann-Lemaître spacetime, $ds^2 = a(\eta)^2\,(-d\eta^2 + d\vec{x}^2)$, the Weyl term does not contribute and the eom (2) for the scale factor $a(\eta)$ and the background inflaton $\phi = \varphi(\eta)$ are:

$$\frac{\kappa}{2}\varphi'^2 = \mathcal{H}^2 - \mathcal{H}'\,, \quad \kappa\,a^2\,V = 2\mathcal{H}^2 + \mathcal{H}'\,,$$

where a prime denotes differentiation with respect to conformal time η and where $\mathcal{H} \equiv a'/a$. In terms of the six gauge invariant quantities[2] (see [10]):

$$\Psi_\mathrm{n} = A + \mathcal{H}\,(B - E') + (B - E')'\,, \quad \Phi_\mathrm{n} = C + \mathcal{H}\,(B - E')\,, \quad \bar\Psi_i = \bar B_i - \bar E_i'\,, \quad \bar h_{ij}$$

the perturbed metric and scalar field reduce to:

$$ds^2 = a(\eta)^2\,\{-(1 + 2\Psi_\mathrm{n})\,d\eta^2 + 2\bar\Psi_i\,d\eta\,dx^i + [(1 + 2\Phi_\mathrm{n})\,\delta_{ij} + \bar h_{ij}]\,dx^i\,dx^j\}\,, \quad \delta\phi = \chi_\mathrm{n}.$$

The eom for these perturbations are:

$$\Box\bar h_{ij} - 2\mathcal{H}\,\bar h_{ij}' = \frac{\gamma}{a^2}\Box\Box\bar h_{ij}\,, \tag{3}$$

$$\bar\Psi_i = \frac{\gamma}{a^2}\Box\bar\Psi_i\,, \tag{4}$$

[1] See [7] for notations and conventions.

[2] We choose to work in the coordinate system $B = E = 0, \bar E_i = 0$ ("newtonian" or "longitudinal" gauge, hence the subscript n appended to the gauge invariant scalar perturbations).

and

$$
\begin{cases}
6\mathcal{H}\,\Phi_{\rm n} - 2\triangle\Phi_{\rm n} - \kappa\left(\varphi'\,\chi_{\rm n}' + 2a^2\,V\,\Psi_{\rm n} + a^2\,V_{,\varphi}\,\chi_{\rm n}\right) = \dfrac{2\gamma}{3a^2}\triangle\triangle W\,, \\
\mathcal{H}\,\Psi_{\rm n} - \Phi_{\rm n}' - \dfrac{\kappa\,\varphi'\,\chi_{\rm n}}{2} = \dfrac{\gamma}{3a^2}\triangle W'\,, \\
-(\Phi_{\rm n} + \Psi_{\rm n}) = \dfrac{\gamma}{a^2}\left(W'' - \dfrac{1}{3}\triangle W\right)\,,
\end{cases}
\tag{5}
$$

where $W \equiv \Psi_{\rm n} - \Phi_{\rm n}$, $\Box \equiv \eta^{\mu\nu}\,\partial_{\mu\nu}$ and $\triangle \equiv \delta^{ij}\,\partial_{ij}$.

We now study the evolution of the perturbations. We shall work in Fourier space and, to simplify notations, we shall omit the index $\vec{k}$ on the Fourier components.

Vector: Vector modes, once constrained to vanish in GR, obey now the equation

$$\bar{\Psi}_i'' + \left(k^2 + \frac{a^2}{\gamma}\right)\bar{\Psi}_i = 0$$

whose zero-mode solutions are given in the WKB approximation by

$$\bar{\Psi}_i \propto \frac{1}{\sqrt{a}}\, e^{\pm it/\sqrt{\gamma}}.$$

Tensor: Equation (3) for the two tensor perturbations $\bar{h}_{ij}$ is a fourth order differential equation which hence describes no longer two, as in standard inflation, but four degrees of freedom. In the WKB approximation, we find that the four independent tensorial zero-modes behave as

$$\bar{h}_{ij} \propto \left\{1\,,\quad \int^t \frac{dt}{a^3}\,,\quad a^{-3/2}\,e^{it/\sqrt{\gamma}}\,,\quad a^{-3/2}\,e^{-it/\sqrt{\gamma}}\right\}$$

hence confirming that as inflation progresses a generic linear combination of the four modes will tend to a constant.

Scalar: The analysis of the three Eq. (5) for the scalar perturbations is slightly more involved. However one can extract from them a master equation for W (see [7]). These equations are fourth order and therefore describe two degrees of freedom, and not only one as in standard inflation. To have a grip of their behaviour we assume power-law inflation: $a(t) \propto t^p$ with $p > 1$. Using the WKB approximation, the four independent zero-modes have the following late time behaviour

$$W \propto \{1\,,\quad t^{-(1+p)}\,,\quad t^{\frac{p}{2}}\,e^{it/\sqrt{\gamma}}\,,\quad t^{\frac{p}{2}}\,e^{-it/\sqrt{\gamma}}\}\,. \tag{6}$$

These behaviours are in striking contrast to those of the tensor modes which are dominated by the constant, Einstein-mode. Here both Einstein modes are subdominant. The evolution of a typical Fourier component of W is given in Fig. 1.

As one can see, not only does the Fourier component W never "freeze out" but its amplitude *increases* as inflation proceeds instead of tending to a constant as in standard inflation when $\gamma = 0$.

Knowing W, we can compute the behaviour of all cosmological perturbations of the model. We find that scalar modes diverge in the newtonian gauge but remain bounded in the comoving slicing.

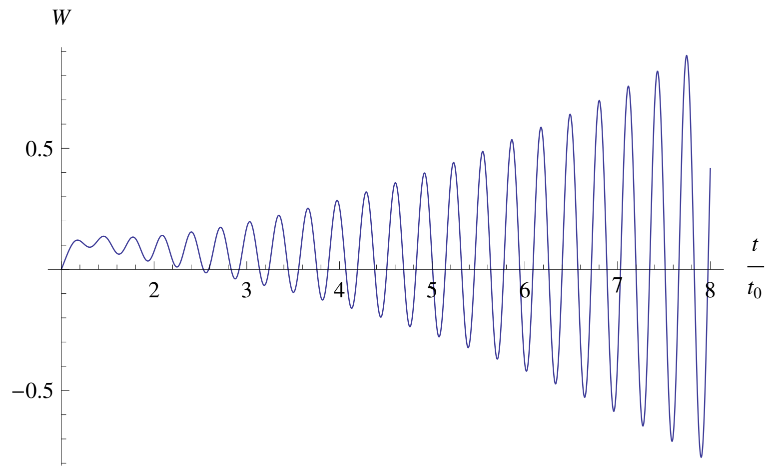

Figure 1: Evolution in cosmic time of a Fourier component of the scalar mode W in power-law inflation.

Because of this strong dependence on the coordinate system, we also examine the evolution of the gauge-invariant quantity:

$$W_2 = C^{\mu}{}_{\nu\rho\sigma}C_{\mu}{}^{\nu\rho\sigma} = C^{\mu}{}_{\nu\rho\sigma}C_{\mu}{}^{\nu\rho\sigma}\Big|_{\text{Minkowski}} a^{-4}.$$

Using (6), the leading behaviour of $|W_2|$ is found to be (see appendix A of [7]): $\left|\frac{k^4}{a^4}W_2\right| \sim k^4 t^{-3p}$: $|W_2|$ decays with time, whatever the gauge. Hence the fact that the scalar modes diverge in the newtonian gauge does not necessarily imply a ghost instability.[3]

In fact, a complete study of the role of Weyl's ghosts in inflation requires an analysis of observables, such as the CMB temperature fluctuations. This is left to future work.

3 Ghosts exorcism via Lorentz breaking

In this section we present a modification of the Weyl gravity action that is free of ghosts around cosmological backgrounds. Our model is specified by the action:

$$S[g_{\mu\nu},\chi] = \frac{1}{2\kappa}\int d^4x\sqrt{-g}\,\left(R + 2\gamma\, C_{\mu\nu\rho\sigma}\, C_{\alpha\beta\gamma\delta}\,\gamma^{\mu\alpha}\,\gamma^{\nu\beta}\,\gamma^{\rho\gamma}\,u^{\sigma}\,u^{\delta}\right) + S_{\chi}[g_{\mu\nu},\chi] \tag{7}$$

where

$$u_{\alpha} \equiv \frac{\partial_{\alpha}\chi}{\sqrt{-\partial_{\alpha}\chi\,\partial^{\alpha}\chi}} \quad \text{and} \quad \gamma_{\alpha\beta} \equiv g_{\alpha\beta} + u_{\alpha}\,u_{\beta}\,,$$

where $S_{\chi}[g_{ab},\chi]$ is only requested to yield solutions in which $\partial_a\chi$ is everywhere timelike and future-directed. The vector field u^a then determines a preferred time direction and that necessarily implies that the theory breaks local Lorentz covariance.

The eom read

$$G_{\alpha\beta} - \gamma\, B_{\alpha\beta} = \kappa T^{\chi}_{\alpha\beta}\,, \tag{8}$$

[3] We thank V. Mukhanov for having discussed this point with us.

where $T_\chi^{\alpha\beta} \equiv 2\,(-g)^{-1/2}\,\delta S_\chi/\delta g_{\alpha\beta}$ is the energy-momentum tensor of χ. The eom for χ , on the other hand, is

$$\frac{1}{\sqrt{-g}}\,\frac{\delta S_\chi}{\delta\chi} - \nabla_\alpha\Gamma^\alpha = 0\,, \tag{9}$$

where $\nabla_\alpha\Gamma^\alpha$ is the variational derivative with respect to χ of the Weyl part of the action. As one can see from the expression of $B_{\alpha\beta}$ in [11], the Einstein equation (8) contains the derivatives of the metric up to fourth order. However, as a closer examination shows, $B_{\alpha\beta}$ contains only time derivatives up to second order only if u^α is timelike. Note that our Weyl action does not give rise either to timelike derivatives higher than second in the scalar field eom (9) because the divergence term only contains spacelike derivative of the spacelike vector Γ_α .

Expanding the action around cosmological backgrounds to quadratic order in the gauge-invariant perturbations as in section (2), we find that (i) the latter is independent on the scalar variables and (ii) vector perturbations are constrained to vanish just as in pure Einstein gravity. The total action for the remaining, tensor, perturbations is (in Fourier space):

$$S_{\rm T}[\{h^\lambda_{\vec k}\}] = \frac{1}{8\kappa}\sum_{\lambda=1,2}\int d\eta\, d^3k\,\left[(a^2+4\gamma k^2)|h'^\lambda_{\vec k}|^2 - a^2k^2\,|h^\lambda_{\vec k}|^2\right]\,, \tag{10}$$

where $k=|\vec k|$ and λ denotes the two graviton polarizations. Since γ must be positive (otherwise the graviton modes would be tachyonic on Minkowski spacetime), $(a^2+4\gamma k^2)$ is always positive, so that the kinetic terms $|h'^\lambda_{\vec k}|^2$ in (10) are always positive, and the graviton never becomes a ghost on a FLRW background.

By studying the early-time, large k limit, we are able to find the adequate vacuum-state and to carry out the quantization of these tensor degrees of freedom on a de Sitter background.[4] After horizon crossing, that is in the limit $\eta\to 0$, we have $h_k \propto k^{-3/2}$. As a consequence, the power spectrum is scale invariant just like the one of ordinary gravitational waves in Einstein theory on a de Sitter background. However its amplitude depends on γ through the constant Ξ the explicit expression of which can be found in [11]:

$$\mathcal{P}(k;\eta\to 0) \equiv \frac{2\kappa\,H^2}{\pi^2}\,\Xi\,.$$

Our calculations should be viewed as a first step towards potentially testable predictions of higher-derivative gravity and Lorentz violations in the early universe.

References

[1] K.S. Stelle, Gen. Rel. Grav. **9**, 353 (1978).

[2] A. Pais and G.E. Uhlenbeck, Phys. Rev. **79**, 145 (1950).

[3] A. De Felice and S. Tsujikawa, Living Rev. Rel. **13**, 3 (2010).

[4] D.G. Boulware and D. Gross, Nucl. Phys. B **233**, 1 (1984).

[5] S.W. Hawking and T. Hertog, Phys. Rev. D **65**, 103515 (2002); C.M. Bender and P.D. Mannheim, Phys. Rev. Lett. **100**, 110402 (2008);
I. Antoniadis, E. Dudas and D.M. Ghilencea, Nucl. Phys. B **767**, 29 (2007);
A.V. Smilga, Phys. Lett. B **632**, 433 (2006).

[4] Quantization will make sense only when $0<\gamma H^2<1$, (see [11]).

[6] A.V. Smilga, Nucl. Phys. B **706**, 598 (2005); SIGMA **5**, 017 (2009).

[7] N. Deruelle, M. Sasaki, Y. Sendouda and A. Youssef, JCAP **03**, 040 (2011).

[8] H.-J. Schmidt, `arXiv:gr-qc/0602017`.

[9] R. Bach, Math. Zeitschr. **9**, 110 (1921).

[10] J.M. Bardeen, Phys. Rev. D **22**, 1882 (1980).

[11] N. Deruelle, M. Sasaki, Y. Sendouda and A. Youssef, arXiv:1202.3131v1.

Relativistic MOND theory based on the Khronon scalar field

Luc Blanchet and Sylvain Marsat
Institut d'Astrophysique de Paris — UMR 7095 du CNRS,
Université Pierre & Marie Curie, 98[bis] *boulevard Arago, 75014 Paris, France*
Email : blanchet@iap.fr, marsat@iap.fr

Abstract

We investigate a model of modified gravity recovering the modified Newtonian dynamics (MOND) in the non-relativistic limit, based on the introduction of a preferred time foliation violating Lorentz invariance in the weak-field regime. Lorentz-invariance violation has been studied in the framework of Einstein-æther theory, the generalization of which, known as non-canonical Einstein-æther theory, having been proposed as a relativistic formulation of MOND. Our model can be seen as a minimal specialization to the hypersurface orthogonal case, which allows a different interpretation in terms of the preferred time : it can be either treated as a dynamical scalar field in a 4D formulation, or chosen as the time coordinate in a 3+1 formulation. We discuss the equivalence of the two points of view and the non-relativistic limit of the model.

1 Motivation

As an alternative to the standard Λ-CDM model, performing well in cosmology and on large scales but leaving open questions at galactic scales, the Modified Newtonian Dynamics (MOND) [12] intends to answer the missing mass problem by a phenomenological modification of gravity in the weak-field, large distances regime. It has proven successfull concerning galactic observations, while needing some extension at the scale of clusters of galaxies and for cosmology (for reviews, see [14, 6]). We will adopt for MOND its modified Poisson-equation version [2]:

$$\boldsymbol{\nabla} \cdot \left[\mu \left(\frac{|\boldsymbol{g}|}{a_0} \right) \boldsymbol{\nabla} \phi \right] = 4\pi G \rho \, , \tag{1}$$

where ρ is the ordinary matter density, ϕ is the Newtonian potential, $\boldsymbol{g} = \boldsymbol{\nabla}\phi$ is the gravitational field, $a_0 = 1.2\,10^{-10}\,\mathrm{m\,s^{-2}}$ is a universal constant acceleration scale, and μ is an interpolation fonction of the ratio $x = |\boldsymbol{g}|/a_0$, with asymptotic behaviour : $\mu(x) \to 1$ $[x \to +\infty]$ and $\mu(x) \sim x$ $[x \to 0]$.

This modified Poisson equation is a purely non-relativistic formula, while a relativistic theory is needed to address issues concerning cosmology and gravitational lensing. Several relativistic extensions for MOND have been proposed in the past, including a tensor-vector-scalar theory (TeVeS) [1, 16], a bimetric theory [13], non-canonical Einstein-Æther theories [18, 8], and a modified dark matter theory [3].

With a completely different motivation, the Hořava-Lifshitz approach [9] introduced a Lorentz invariance breaking preferred foliation of spacetime to build a power-counting renormalizable theory of gravity in the strong-field regime. This approach has been improved and extended in [5].

In this contribution, which is a summary of our recent paper [4] (see also [15]) to which we refer for more details, we investigate a specific relativistic extension of MOND, that can be either understood as a Lorentz-invariance breaking theory using a preferred time foliation, or as a hypersurface-orthogonal restriction of non-canonical Einstein-Æther theories.

2 Non-canonical Einstein-Æther theories

Einstein-Æther theories have been introduced as a phenomenological approach to Lorentz-invariance violation [11]. A preferred direction of time is described by a dynamical, timelike unit vector n^μ. The corresponding Lagrangian density is usually written as:[1]

$$\mathcal{L}_{Æ} = \frac{\sqrt{-g}}{16\pi}\Big[R + \mathcal{K} + \lambda(n^\mu n_\mu + 1)\Big] \,, \tag{2}$$

where R is the Ricci scalar, λ is a Lagrange multiplier enforcing the normalization condition $n^\mu n_\mu = -1$, and where $\mathcal{K}$ represents the most general Lagrangian density that is quadratic in the derivatives of n^μ :

$$\mathcal{K} = \mathcal{K}^{\mu\nu\rho\sigma}\nabla_\mu n_\rho \nabla_\nu n_\sigma \,, \tag{3a}$$

$$\mathcal{K}^{\mu\nu\rho\sigma} = c_1 g^{\mu\nu}g^{\rho\sigma} + c_2 g^{\mu\rho}g^{\nu\sigma} + c_3 g^{\mu\sigma}g^{\nu\rho} + c_4 n^\mu n^\nu g^{\rho\sigma} \,, \tag{3b}$$

where c_1, c_2, c_3 and c_4 are dimensionless constants, left unspecified at this stage. Constraints in the Solar System computed from Parametrized Post-Newtonian parameters have been obtained in [7].

The non-canonical generalization of the previous action has been proposed in [18, 8], as a relativistic extension of MOND. It consists of replacing the æther action $\mathcal{K}$ by a free function $F(\mathcal{K})$, i.e. of considering the Lagrangian

$$\mathcal{L}_{\text{non-canonical}\,Æ} = \frac{\sqrt{-g}}{16\pi}\Big[R + F(\mathcal{K}) + \lambda(n^\mu n_\mu + 1)\Big] \,. \tag{4}$$

More generally, one could imagine introducing several arbitrary functions F_1, F_2, F_3 and F_4 corresponding to the various terms in (3). In the non-relativistic limit, specifying the behaviour of the fonction $F(\mathcal{K})$ around $\mathcal{K} = 0$ allows to recover the modified Poisson equation (1). The class of cosmologies that are possibly produced by this type of models has been extensively studied in [19].

3 From the Æther to the Khronon

Instead of directly using a timelike dynamical vector field n^μ in the action, Lorentz invariance violation can be realized by introducing a preferred foliation of spacetime. The link between these two formulations has been studied in [10]. The foliation consists of hypersurfaces of constant value of a scalar field τ, which we will call the “Khronon” field following [5]. It defines a hypersurface-orthogonal unit vector field n_μ, whose relation to the Khronon field τ is:

$$n_\mu = -N\,\partial_\mu\tau \,, \quad \text{with} \quad N = \frac{1}{\sqrt{-g^{\rho\sigma}\partial_\rho\tau\partial_\sigma\tau}} \,. \tag{5}$$

We see that the condition for the Khronon field to define a well-behaved spacetime foliation is that its gradient must remain timelike everywhere. Recall that, in general, a unit timelike æther vector does not define a foliation of spacetime; the condition for it to be hypersurface-orthogonal is $n_{[\mu}\nabla_\nu n_{\rho]} = 0$ (the so-called Frobenius theorem). Notice also that the fundamental ingredient of the theory is now the scalar field τ, while in Einstein-Æther theory it is the æther vector field, with three degrees of freedom (one being suppressed by the unit-norm constraint) instead of one. An advantage of the formulation (5) is that the normalization condition is automatically satisfied and we do not need a Lagrange multiplier in the action.

[1] We use the $(-+++)$ convention for the metric, and often set $G = c = 1$.

Given this spacetime foliation, further geometrical definitions are:

$$\gamma_\mu{}^\nu = \delta_\mu{}^\nu + n_\mu n^\nu \ , \quad K_{\mu\nu} = \gamma_\mu{}^\rho \nabla_\rho n_\nu \ , \quad a_\mu = n^\nu \nabla_\nu n_\mu \ , \tag{6}$$

where $\gamma_\mu{}^\nu$ is the projector orthogonal to n^μ, $K_{\mu\nu}$ is the hypersurface's extrinsic curvature tensor and a_μ is the spacelike four-acceleration of the congruence orthogonal to the hypersurface with velocity n_μ. We also define the projected covariant derivative operator as, for instance: $D_\mu V^\nu = \gamma_\mu{}^\rho \gamma_\sigma{}^\nu \nabla_\rho V^\sigma$. Those definitions could be done formally in the non-hypersurface-orthogonal case, but the following important relation is specific to this case:

$$a_\mu = D_\mu \ln N \tag{7}$$

and, in addition, the extrinsic curvature is symmetric: $K_{\mu\nu} = K_{\nu\mu}$.

We are now able to rewrite the four terms written in Eq. (3) as the basic ingredients of the Lagrangian density of the Khronon field, expressed in terms of extrinsic curvature and acceleration:

$$\text{Term } c_1 : \ \nabla_\mu n_\nu \nabla^\mu n^\nu = K_{\mu\nu} K^{\mu\nu} - a^2 \ , \tag{8a}$$
$$\text{Term } c_2 : \ (\nabla_\mu n^\mu)^2 = K^2 \ , \tag{8b}$$
$$\text{Term } c_3 : \ \nabla_\mu n_\nu \nabla^\nu n^\mu = K_{\mu\nu} K^{\mu\nu} \ , \tag{8c}$$
$$\text{Term } c_4 : \ n^\mu n^\nu \nabla_\mu n_\rho \nabla_\nu n^\rho = a^2 \ , \tag{8d}$$

where $a^2 = a_\mu a^\mu$ and $K = K_\mu{}^\mu$ is the trace of the extrinsic curvature. We see, as was pointed out in [10], that only three out of these four terms are actually independent in the hypersurface-orthogonal case. We can go further by investigating the fates of the extrinsic curvature and acceleration in two regimes of interest, the non-relativistic or post-Newtonian limit and the homogeneous and isotropic cosmology. In the post-Newtonian limit and in adapted coordinates, *i.e.* when the time coordinate t is identified with τ, one obtains (see below):

$$a_i = \frac{1}{c^2} \partial_i \phi + \mathcal{O}(4) \ , \quad \text{and} \quad K_{ij}, \ K = \mathcal{O}(3) \ , \tag{9}$$

with ϕ the Newtonian potential and where $\mathcal{O}(n)$ means terms of order at least $1/c^n$. On the other hand, when considering a perfectly homogeneous and isotropic (FLRW) Universe, where the foliation is identical to the cosmic time foliation, we have:

$$a_\mu = 0 \ , \quad \text{and} \quad K_{ij} K^{ij} = 3H^2, \ K^2 = 9H^2 \ , \tag{10}$$

where H is the standard Hubble parameter.

This means that the c_1 and c_4 terms are the only ones to contribute in the non-relativistic regime, and that the c_4 term vanishes in the usual cosmological background. However, notice that the c_1 term switches sign between the two regimes, whereas the c_4 term is positive in any case. In the model discussed below, we use only this a^2 term as the basic ingredient to recover MOND in the non-relativistic limit as an alternative to dark matter at the galactic scale, leaving the cosmology aside.

4 Specific example of MOND theory

4.1 Covariant formulation

In the 4D covariant point of view, the model constitutes a modification of General Relativity (GR) by the introduction of an additional scalar field, the Khronon τ. We introduce in the action a free function of the norm of the acceleration a:

$$\mathcal{L} = \frac{\sqrt{-g}}{16\pi}\big[R - 2f(a)\big] + \mathcal{L}_\mathrm{m}[g_{\mu\nu}, \Psi] \,. \tag{11}$$

This choice corresponds to the c_4 term in the Einstein-Æther action. We also assume the standard coupling of matter fields Ψ to the metric. The function $f(a)$ is to be specified later, in order to recover MOND in the weak-field limit and GR in the strong-field regime. Variation of the action with respect to the metric and to the τ field yields the field equations:

$$G^{\mu\nu} + f(a)g^{\mu\nu} + 2n^\mu n^\nu \nabla_\rho\left[\chi(a)a^\rho\right] - 2\chi(a)a^\mu a^\nu = 8\pi\, T^{\mu\nu} \,, \tag{12a}$$

$$\nabla_\mu\left[n^\mu \nabla_\nu(\chi(a)a^\nu)\right] = \frac{1}{2}n^\nu\nabla_\nu f + \chi(a)\, a^\mu a^\nu K_{\mu\nu} \,, \tag{12b}$$

with $T^{\mu\nu}$ the matter stress-energy tensor, and where we used the short-hand notation $\chi(a) \equiv f'(a)/2a$. The second equation, which we call the τ-equation, is of fourth order in the derivatives. We will see however that, in adapted coordinates, it becomes of first order only in time derivatives of geometrical quantities. If, from the first equation, which we call the modified Einstein equation, we define an equivalent stress-energy tensor $T_\tau^{\mu\nu}$ for the Khronon field, one can see that the τ-equation is in fact equivalent to $\nabla_\nu T_\tau^{\mu\nu} = 0$. Hence, because of the Bianchi identity, the matter conservation equation $\nabla_\nu T^{\mu\nu} = 0$ and the modified Einstein equation together contain the τ-equation.

4.2 3+1 formulation

We now write the 3+1 formulation of the theory in adapted coordinates, choosing $t = \tau$. With standard definitions for the lapse N, the shift N_i and the spatial metric γ_{ij}, the 3+1 parametrization of the metric reads

$$ds^2 = -(N^2 - N_i N^i)\mathrm{d}t^2 + 2N_i \mathrm{d}t\mathrm{d}x^i + \gamma_{ij}\mathrm{d}x^i\mathrm{d}x^j \,. \tag{13}$$

In these adapted coordinates, we have $n_\mu = (-N, 0)$ and $a_i = \partial_i \ln N$, with N being now a geometrical quantity. The 3+1 form of the action is then:

$$\mathcal{L} = \frac{\sqrt{\gamma}}{16\pi}N\big[\mathcal{R} + K_{ij}K^{ij} - K^2 - 2f(a)\big] + \mathcal{L}_\mathrm{m}[N, N_i, \gamma_{ij}, \Psi] \,. \tag{14}$$

The τ field is not a dynamical field anymore — it has been absorbed into the time coordinate. Its contribution to the action is purely geometric, $f(a)$ depending now only on the gradient of the lapse N. This term explicitly breaks Lorentz invariance. Varying the action with respect to N, N_i and γ_{ij}, we obtain:

$$\mathcal{R} + K^2 - K_{ij}K^{ij} - 2f + 4\chi a^2 + 4D_i(\chi a^i) = 16\pi\,\varepsilon \,, \tag{15a}$$

$$D_j\left(K^{ij} - \gamma^{ij}K\right) = -8\pi J^i \,, \tag{15b}$$

$$\begin{aligned}\mathcal{G}^{ij} + \frac{1}{N}D_t\left(K^{ij} - \gamma^{ij}K\right) &+ \frac{2}{N}D_k\left[N^{(i}(K^{j)k} - \gamma^{j)k}K)\right] \\ &+2K^{ik}K^j{}_k - KK^{ij} - \frac{1}{2}\gamma^{ij}\left(K^{kl}K_{kl} + K^2\right) \\ &-\frac{1}{N}\left(D^iD^jN - \gamma^{ij}D_kD^kN\right) - 2\chi a^i a^j + f\gamma^{ij} = 8\pi\mathcal{T}^{ij} \,,\end{aligned} \tag{15c}$$

where $\delta\mathcal{L}_m/\delta N \equiv -\sqrt{\gamma}\varepsilon$, $\delta\mathcal{L}_m/\delta N_i \equiv \sqrt{\gamma}J^i$ and $\delta\mathcal{L}_m/\delta\gamma_{ij} \equiv N\sqrt{\gamma}\mathcal{T}^{ij}/2$.

4.3 Equivalence between the formulations

The two formulations of our model seem quite different, since the τ field is a dynamical field in the 4D point of view while it becomes a mere time coordinate in the 3+1 point of view. It has been pointed out in [10] that the fact that the τ-equation is contained in the modified Einstein equation and the conservation of the matter stress-energy tensor allows one to consistently treat it as a coordinate.

We explicitly checked this equivalence between the two formulations at the level of the field equations, by verifying that the 3+1 projection (after variation) of the 4D equations was in agreement with the 3+1 ones, obtained by the variation with respect to geometrical quantities after projection. We also checked that the 3+1 projection of the τ-equation, namely

$$D_t\left[D_i(\chi a^i)+\chi a^2-\frac{f}{2}\right]+NK\Big(D_i(\chi a^i)+\chi a^2\Big)-N\chi\, a^i a^j K_{ij}=0\,, \tag{16}$$

where $D_t\equiv\partial_t-N^kD_k$, was indeed contained in the field equations (15) and the 3+1 writing of the conservation of matter stress-energy tensor. Notice that this equation (16) has now become of first order only in time derivatives of geometrical quantities.

4.4 Recovering MOND in the non-relativistic regime

For a system at rest with respect to the preferred frame, we may write, in the non-relativistic (NR) limit, restoring the c factors:

$$N=1+\frac{\phi}{c^2}+\mathcal{O}\left(4\right),\quad N_i=\mathcal{O}\left(3\right),\quad \gamma_{ij}=\delta_{ij}\left(1-\frac{2\psi}{c^2}\right)+\mathcal{O}\left(4\right). \tag{17}$$

Here ϕ and ψ are the usual Newtonian potentials, and we recall that $a_i=\partial_i\phi/c^2+\mathcal{O}(4)$. Combining the 3+1 field equations (15), we first obtain the equality of the Newtonian potentials, $\phi=\psi+\mathcal{O}(2)$, crucial for the dark matter seen by gravitational lensing [14], and we get a modified Poisson-like equation,

$$D_i\left[(1+\chi)a^i\right]+f+a^2-\frac{1}{N}D_tK-K^{ij}K_{ij}=4\pi\left(\varepsilon+\frac{2}{N}N_iJ^i+\mathcal{T}\right)\,, \tag{18}$$

which reduces in the NR limit to $\boldsymbol{\nabla}\cdot\left[(1+\chi)\,\boldsymbol{\nabla}\phi\right]=4\pi G\rho+\mathcal{O}\left(2\right)$, with ρ the ordinary rest-mass density of matter. We see that there is a one-to-one correspondence between the MOND μ function and the function f in the action, namely $\mu=1+\chi$ where $\chi(a)=f'(a)/2a$. Requirements on f to recover MOND are as follows (Λ_∞ and Λ_0 being two constants):

$$f(a)\sim\Lambda_\infty\quad\text{in the strong-field regime } a\to\infty, \tag{19a}$$

$$f(a)=\Lambda_0-a^2+\frac{2a^3}{3a_0}+\mathcal{O}\left(\frac{a^4}{a_0^2}\right)\quad\text{in the weak-field regime } a\to 0. \tag{19b}$$

Note that the usual strong-field condition would be $f'(a)/a\to 0$ (so that we recover the standard Poisson equation), but here we imposed a stronger condition when $a\to\infty$ in order to recover exactly GR with a cosmological constant Λ_∞ in the strong-field regime.

4.5 Solar System effects

We can get a rough estimate of the smallness of MOND effects in the Solar System, assuming that (19a) holds, which as we said is in fact more restrictive than the usual MOND requirement $\chi(a) \to 0$. To this end we write (with $c = 1$)

$$f(a) \simeq \Lambda_\infty + k a_0^2 \left(\frac{a_0}{a}\right)^\alpha \quad (\text{when } a \to \infty)\,, \tag{20}$$

with k a dimensionless number of order one. This constant is fixed in order of magnitude by the zero-point of the function f and the numerical coincidence $\Lambda \sim a_0^2$. Then, translating the MOND equation in spherical symmetry as $(1+\chi)g = g_\mathrm{N}$, with g_N the Newtonian acceleration, and inverting, one obtains

$$g \simeq g_\mathrm{N}\left[1 + \frac{k\alpha}{2}\left(\frac{a_0}{g_\mathrm{N}}\right)^{2+\alpha}\right]. \tag{21}$$

Defining the MOND transition radius R_0 by $a_0 \equiv GM/R_0^2$, we have that $(a_0/g_\mathrm{N})^{2+\alpha} = (r/R_0)^{4+2\alpha}$. Since numerically $R_0 \simeq 7100$ AU, we see that within a Neptune orbit ($\simeq 30$ AU), the relative effect is at most of the order of 10^{-12} for α close to 0, and is at most 10^{-15} for a typical value $\alpha \simeq 1$. Relativistic corrections in the Solar System are of the order of $(v/c)^2 \simeq 10^{-8}$, and typical constraints on the values of PPN parameters [17] correspond to deviations from GR of the order of $10^{-8} \times 10^{-4} = 10^{-12}$. Our requirement (20) for recovering GR implies that the theory passes the Solar-System tests.

5 Conclusion

We investigated a simple model for a relativistic extension of MOND based on a preferred time foliation. We discussed how it relates to the more general framework of non-canonical Einstein-Æther theories and why it selects out of it the minimal ingredients required for recovering MOND in the non-relativistic limit. We analyzed the two points of view for the model, 4D or 3D, and discussed their equivalence. We investigated the non-relativistic limit and estimated the size of Solar-System effects. Further work is needed to study the cosmology of the model, and possibly to extend it in order to account for the missing mass problem at large cosmological scales.

References

[1] J.D. Bekenstein. Relativistic gravitation theory for the MOND paradigm. *Phys. Rev. D*, 70:083509, 2004.

[2] J.D. Bekenstein and M. Milgrom. *Astrophys. J.*, 286:7, 1984.

[3] L. Blanchet and A. Le Tiec. Dipolar dark matter and dark energy. *Phys. Rev. D*, 80:023524, 2009.

[4] L. Blanchet and S. Marsat. Modified gravity approach based on a preferred time foliation. *Phys. Rev. D*, 84(4):044056, August 2011.

[5] D. Blas, O. Pujolàs, and S. Sibiryakov. Models of non-relativistic quantum gravity: the good, the bad and the healthy. *J. High Energy Phys.*, 4:18–+, April 2011.

[6] B. Famaey and S. McGaugh. Modified Newtonian Dynamics: A Review. *ArXiv e-prints*, December 2011.

[7] B. Foster and T. Jacobson. Post-Newtonian parameters and constraints on einstein-æther theory. *Phys. Rev. D*, 73:064015, 2006.

[8] A. Halle, H. S. Zhao, and B. Li. A nonuniform dark energy fluid: Perturbation equations. *Astrophys. J. Suppl.*, 177:1, 2008.

[9] P. Hořava. Quantum gravity at a Lifshitz point. *Phys. Rev. D*, 79(8):084008–+, April 2009.

[10] T. Jacobson. Extended Hořava gravity and Einstein-æther theory. *Phys. Rev. D*, 81(10):101502–+, May 2010.

[11] T. Jacobson and D. Mattingly. Gravity with a dynamical preferred frame. *Phys. Rev. D*, 64(2):024028–+, July 2001.

[12] M. Milgrom. *Astrophys. J.*, 270:365, *ibid.* 270:371, *ibid.* 270:384, 1983.

[13] M. Milgrom. Bimetric MOND gravity. *Phys. Rev. D*, 80(12):123536–+, December 2009.

[14] R. H. Sanders and S. McGaugh. Modified Newtonian Dynamics as an Alternative to Dark Matter. *Ann. Rev. Astron. Astrophys.*, 40:263, 2002.

[15] R. H. Sanders. Hiding Lorentz Invariance Violation with MOND. *ArXiv e-prints*, May 2011.

[16] R. H. Sanders. A stratified framework for scalar-tensor theories of modified dynamics. *Astrophys. J.*, 480:492, 1997.

[17] C. M. Will. Theory and experiment in gravitational physics. Cambridge University Press (1993).

[18] T. G. Zlosnik, P. G. Ferreira, and G. D. Starkman. Modifying gravity with the æther: An alternative to dark matter. *Phys. Rev. D*, 75:044017, 2007.

[19] J. Zuntz, T. G. Zlosnik, F. Bourliot, P. G. Ferreira, and G. D. Starkman. Vector field models of modified gravity and the dark sector. *Phys. Rev. D*, 81(10):104015, May 2010.

CDJ formulation from the instanton representation of Plebanski gravity

Eyo Ita III
United States Naval Academy, Annapolis, MD
Email*: ita@usna.edu*

Abstract

We show that a certain action which gives rise to the pure spin connection formulation of gravity by CDJ can be consistently derived from the action for the instanton representation of Plebanski gravity (IRPG). This is an illustrative example of when certain symmetries of the basic fields commute with the symmetries of the equations of motion.

1 Reduction of the IRPG action

Generally, when one reduces degrees of freedom of the basic variables at the level of an action I one must be careful to ensure that one is not restricting the space of solutions, in order that the reduced action I_0 still corresponds to the starting theory. Inconsistencies can arise when one makes gauge-fixing choices at the level of the action, or when one eliminates fields from an action using the equations of motion for other, different fields. There is a certain action forming an intermediate step in the derivation of the pure spin connection formulation for gravity [1] by Jacobson, Dell and Capovilla given by

$$I_0 = \int_M \big(\Psi_{ae} F^a \wedge F^e - \eta\big(\Lambda + \mathrm{tr}\Psi^{-1}\big)\big), \tag{1}$$

where $F^a = \frac{1}{2} F^a_{\mu\nu} dx^\mu \wedge dx^\nu$ is a $SO(3,C)$ curvature two form, $\Psi_{ae} \in SO(3,C) \times SO(3,C)$ a three by three matrix, and Λ is the cosmological constant. The action I_0 was obtained by elimination of certain auxiliary fields from Plebanski's action [2]. In the present paper we will show that there is another action which consistently gives rise to I_0 through the elimination of auxiliary fields. This action is referred to as the instanton representation of Plebanski gravity (IRPG), derived from Plebanski's action in [3].

The basic variables for the IRPG are a $SO(3,C)$ gauge connection A^a_μ and matrix $\Psi_{ae} \in SO(3,C) \otimes SO(3,C)$.[1] The action for the instanton representation of Plebanski gravity is given by

$$I_{Inst} = \int dt \int_\Sigma d^3x \bigg[\Psi_{ae} B^i_e \big(F^a_{0i} - \epsilon_{ijk} B^j_a N^k\big) \\ -N(\mathrm{det}B)^{1/2}\sqrt{\mathrm{det}\Psi}\big(\Lambda + \mathrm{tr}\Psi^{-1}\big)\bigg], \tag{2}$$

where $B^i_a = \frac{1}{2}\epsilon^{ijk} F^a_{jk}$ and F^a_{0i} are the spatial and temporal components of the $SO(3,C)$ field strength $F^a_{\mu\nu}$, and N and N^k are auxiliary fields (e.g. the lapse function and shift vector of metric General Relativity). Also,

[1] For index conventions, internal $SO(3,C)$ indices are labelled by symbols from the beginning of the Latin alphabet $a, b, c, \ldots$, and spatial indices i, j, k from the middle. Greek symbols $\mu, \nu, \ldots$ denote 4-dimensional spacetime indices.

we will assume $(\det\Psi)$ and $(\det B)$ are nonzero, which restricts the validity of (2) to Petrov Type I, D and O spacetimes. The equation of motion for Ψ_{ae} is given by

$$\frac{\delta I_{Inst}}{\delta\Psi_{ae}} = B^i_e\big(F^a_{0i} - \epsilon_{ijk}B^j_aN^k\big) + N(\det B)^{1/2}\sqrt{\det\Psi}(\Psi^{-1}\Psi^{-1})^{ea} = 0. \tag{3}$$

Note, defining $\epsilon^{0ijk} \equiv \epsilon^{ijk}$ and using the relation

$$B^i_{(e}F^{a)}_{0i} = \frac{1}{2}\epsilon^{ijk}F^{(e}_{jk}F^{a)}_{0i} = \frac{1}{8}F^a_{\mu\nu}F^e_{\rho\sigma}\epsilon^{\mu\nu\rho\sigma}, \tag{4}$$

that the symmetric part of the equation of motion (3) is given by

$$\frac{1}{8}F^a_{\mu\nu}F^e_{\rho\sigma}\epsilon^{\mu\nu\rho\sigma} + N(\det B)^{1/2}\sqrt{\det\Psi}(\Psi^{-1}\Psi^{-1})^{(ea)} = 0. \tag{5}$$

For the antisymmetric part we simply contract (3) with ϵ_{dae} which gives

$$\epsilon_{dea}B^i_eF^a_{0i} = \epsilon_{ijk}\epsilon_{dea}B^i_eB^j_aN^k = 2(\det B)N^k(B^{-1})^d_k. \tag{6}$$

This enables us to solve for the auxiliary field N^i as

$$N^k = \frac{1}{2}\epsilon^{kij}F^a_{0i}(B^{-1})^a_j. \tag{7}$$

It will be useful to write the Lagrangian (2) in covariant from by separating Ψ_{ae} into its symmetric and antisymmetric parts $\Psi_{ae} = \Psi_{(ae)} + \frac{1}{2}\epsilon_{aed}\psi_d$, where $\psi_d = \epsilon_{dae}\Psi_{ae}$ (hence $\Psi_{[ae]} = \frac{1}{2}\epsilon_{aed}\psi_d$). Note that the integrand of the N^k term in (2) can be written as $\epsilon_{ijk}N^iB^j_eB^k_a\Psi_{ae} = (\det B)N^i(B^{-1})^d_i\psi_d$. Hence the action (2) can be written as

$$I_{Inst} = \int_M d^4x\bigg[\frac{1}{8}\Psi_{ae}F^a_{\mu\nu}F^e_{\rho\sigma}\epsilon^{\mu\nu\rho\sigma}$$
$$+\big(\frac{1}{2}\epsilon_{dae}F^a_{0i}B^i_e + N^i(B^{-1})^d_i\big)\psi_d - N(\det B)^{1/2}\sqrt{\det\Psi}\big(\Lambda + \mathrm{tr}\Psi^{-1}\big)\bigg]. \tag{8}$$

The equation of motion for N^i implies that $\psi_d = 0$. But since ψ_d is also an independent dynamical field, then it is permissible to set $\psi_d = 0$ only after, not before, writing down its Lagrange equation of motion

$$\frac{\delta I_{Inst}}{\delta\psi_d}\bigg|_{\psi_d=0} = \frac{1}{2}\epsilon_{dae}F^a_{0i}B^i_e + N^i(B^{-1})^d_i(\det B) = 0. \tag{9}$$

Similarly, the equation of motion for N is equivalent to $\Lambda + \mathrm{tr}\Psi^{-1} = 0$. The solution to (9) is given precisely by (7). The result is that the antisymmetric part of the equation of motion for Ψ_{ae} is the same as the equation of motion for the antisymmetric part of Ψ_{ae}.

To find the equation of motion for the connection A^a_μ it will be convenient to use the following relation $\epsilon_{ijk}N^iB^j_eB^k_a\Psi_{[ae]} = \frac{1}{2}\epsilon_{ijk}N^iB^j_aB^k_e\epsilon_{aed}\psi_d$. Then the action (8) can also be written as

$$I_{Inst} = \int_M d^4x\bigg[\frac{1}{8}\Psi_{ae}F^a_{\mu\nu}F^e_{\rho\sigma}\epsilon^{\mu\nu\rho\sigma} + \frac{1}{2}\epsilon_{dae}\big(F^a_{0j}B^j_e - \epsilon_{ijk}N^iB^j_eB^k_a\big)\psi_d$$
$$-N(\det B)^{1/2}\sqrt{\det\Psi}\big(\Lambda + \mathrm{tr}\Psi^{-1}\big)\bigg]. \tag{10}$$

The equation of motion for A^a_μ can be found by integration by parts of all terms containing the connection, which yields

$$\frac{\delta I\delta A^a_\mu}{=} - \epsilon^{\mu\nu\rho\sigma}D_\nu(\Psi_{ae}F^e_{\rho\sigma}) - \frac{1}{2}\delta^\mu_i\epsilon^{jml}D_m\bigg[\epsilon_{dag}\big(F^a_{0j} - 2\epsilon_{jki}B^k_aN^i\big)\psi_d$$
$$+(B^{-1})^g_jN(\det B)^{1/2}\sqrt{\det\Psi}\big(\Lambda + \mathrm{tr}\Psi^{-1}\big)\bigg] = 0. \tag{11}$$

Note, on solution to the N and N^k equations, that the terms in large brackets in (11) vanish. Therefore on-shell, (11) reduces to

$$\frac{\delta I \delta A^a_\mu}{=} \epsilon^{\mu\rho\sigma\nu} F^e_{\rho\sigma} D_\nu \Psi_{(ae)} = 0, \tag{12}$$

where we have used the Bianchi identity $\epsilon^{\mu\nu\rho\sigma} D_\nu F^e_{\rho\sigma} = 0$. Note that we can eliminate ψ_d and N^i by evaluating the action (8) on the critical point $\psi_d = 0, N^i = \frac{1}{2}\epsilon^{ijk} F^a_{0j} (B^{-1})^a_k$, which leads to

$$\begin{aligned} I_0 &= I_{Inst}\Big|_{\psi_d=0, N^i=\frac{1}{2}\epsilon^{ijk} F^a_{0j}(B^{-1})^a_k} \\ &= \int_M d^4x \left[\frac{1}{8} \Psi_{ae} F^a_{\mu\nu} F^e_{\rho\sigma} \epsilon^{\mu\nu\rho\sigma} + \eta\big(\Lambda + \mathrm{tr}\Psi^{-1}\big) \right] \end{aligned} \tag{13}$$

where $\eta = \sqrt{\mathrm{det}B}\sqrt{\mathrm{det}\Psi}$, whence $\Psi_{ae} = \Psi_{(ae)}$ is now symmetric. Note that the Ψ_{ae} equation of motion of (13) is precisely the symmetric part of the equation of motion for Ψ_{ae} in (5), and moreover that (12) can be seen as the equation of motion for A^a_μ from (13). Additionally, the action (13) is precisely the same action as (1) which means the following things: (i) $I_0 \subset I_{Inst}$, namely that I_{Inst} is a different action from the one leading to the CDJ formalism, and contains this action as a subset (ii) the symmetries of the equations of motion commute with the symmetries of the Lagrangian I_{Inst} in this case. (iii) In a certain interpretation, N^i and ψ_d can be unified into one six-component field Φ_α. Then elimination of Φ_α from I_{Inst} through its equations of motion to get I_0 is a self-consistent procedure.

References

[1] R. Capovilla, J. Dell and T. Jacobson 'A pure spin connection formulation of gravity' Class. Quantum Grav. 8 (1991) 59-73

[2] Jerzy Plebanski 'On the separation of Einsteinian substructures' J. Math. Phys. Vol. 18, No. 2 (1977)

[3] Eyo Ita 'Instanton Representation of Plebanski Gravity. Gravitational Instantons from the Classical Formalism', The Abraham Zelmanov Journal, 2011, volume 4, pages 36-71

Extended Bargmann-Wigner Equations in Flat and Curved Space-time

Masakatsu Kenmoku

Nara Women's University, Kitauoya-nishi-machi, Nara 630-8506, Japan

Email : kenmoku@asuka.phys.nara-wu.ac.jp

Abstract

Extended Bargmann-Wigner equations are formulated for lower spin states as well as higher spin states in falt and surved space-time. The exact current conservation law is derived using the Lagrange formulation of the extended Bargmann-Wigner equations. One of interesting applications is the radiance problem of fermions and bosons in rotationg black hole space-time.

1 Introduction

There is a long standing problem for the super-radiance effect by bosonic particles in highly rotating black hole space-time[1]. Therefore highly rotating black holes can be unstable for the scattering by bosons but known to be stable for the scattering by fermions.

The relations aomng the incident, transmission and reflection probabilities for for the scattering by massless aprticles with arbitrary spins s and the frequency ω in rotation black hole space-time are summarized in the following [2]

$$| R_{\rm s}^{(\rm inc)} |^2 = \frac{(2\omega)^{4\rm s}}{| C_s |^2} | R_{\rm s}^{(\rm ref)} |^2 + \delta_{\rm s} | R_{\rm s}^{(\rm trans)} |^2 \tag{1}$$

where $C_{\rm s}$ denotes the Starobinsky constants and $\delta_{\rm s}$ the transmission coefficients for each spin as

$$\delta_{1/2},\ \delta_{3/2} \propto \text{pos. value} \quad \text{vs.} \quad \delta_0,\ \delta_1,\ \delta_2 \propto \text{can be negative value} . \tag{2}$$

These equations show that the super-radiance can occur for bosons but not for fermions.

In order to understand the origin of the difference between bosons and fermions for the super-radiance problem in rotation black hole space-time, the exact fermion-boson relation should be an effective method using the extended version of the Bargmann-Wigner equations [3].

2 Extended Bargmann-Wigner equations in curved space-time

The extended Bargmann-Wigner equations for the bi-spinor field $\Psi(x)$ in curved space is expressed as

$$(\gamma \cdot D + m)\Psi(x) + \Psi(x)(\overleftarrow{D} \cdot \gamma + m) = 0 , \tag{3}$$

where the covariant derivative is defined in local Minkowski space using spin connection $\omega^{ij}{}_{,\mu}$ and spin operator Σ_{ij} :

$$D_\mu \psi = \partial_\mu \psi + \frac{1}{4} \omega^{ij}{}_{,\mu} \Sigma_{ij} \psi . \tag{4}$$

The bi-spinor field is expanded by boson fields as

$$\Psi(x) = aS(x) + b\gamma_5 P(x) + c\gamma^\mu V_\mu(x) + d\gamma_5\gamma^\mu A_\mu(x) + \frac{e}{2}\gamma_5\Sigma^{\mu\nu}F_{\mu\nu}(x) \ , \tag{5}$$

where the covariant derivative is defined in curved space using the affine connection $\Gamma^\lambda_{\nu\mu}$:

$$\nabla_\mu A_\nu = \partial_\mu A_\nu - \Gamma^\lambda_{\nu\mu}A_\lambda \ . \tag{6}$$

The field equations for the bosonic fields are obtained from equation (3) as

$$(\nabla^\mu\partial_\mu - m^2)S(x) \ = \ 0 \ , \ V_\mu(x) = \partial_\mu S(x) \ , \ P(x) = 0 \tag{7}$$

$$(\nabla^\mu\nabla_\mu - m^2)A_\nu(x) \ = \ 0 \ , \ F_{\mu\nu}(x) = \nabla_\mu A_\nu(x) - \nabla_\nu A_\mu(x) \ . \tag{8}$$

Conserved currents are obtained and expressed in two ways as bi-spinor form and bosonic form:

$$J_\mu = \frac{i}{4}\mathrm{Tr}\ \bar{\Psi}\gamma_\mu\Psi \ , \ = -i(S^*V_\mu - S\ V^*_\mu + A^\nu F^*_{\nu\mu} - A^{\nu\ *}F_{\nu\mu}) \ . \tag{9}$$

3 Application: Radiation problem in rotating black hole space-time

As one of important applications, the radiation problem in rotating black hole space-time is considered [4, 5]. The radial equations for the spacial infinity $(r = \infty)$ and near horizon $(r = r_{\mathrm{H}})$ can be considered as free motion introducing the new coordinate

$$dr^*/dr = (r^2 + a^2)/\Delta \quad (\Delta = r^2 - 2Mr + a^2) \ , \tag{10}$$

where M and a denote the mass and angular momentum of black holes respectively. The asymptotic radial solutions for bosons are obtained as

$$\phi(r) \ \sim \ R_B^{(inc)}\exp{(-ip_\infty r^*)} + R_B^{(ref)}\exp{(ip_\infty r^*)} \quad (r \sim \infty) \tag{11}$$

$$\sim \ R_B^{(trans)}\exp{(-ip_H r^*)} \quad (r \sim r_H) \tag{12}$$

where $p_\infty = \sqrt{\omega^2 - \mu^2}$ and $p_H = \omega - \Omega_H m$ denote the momenta of scalar bosons. Corresponding radial solutions are obtained for fermions.

The current conservations relations connecting the current at infinity with that near horizon for bosons and fermions as

$$(\mid R_B^{(inc)} \mid^2 - \mid R_B^{(ref)} \mid^2)\ p_\infty \ = \ \mid R_B^{(trans)} \mid^2 \ p_H \ , \tag{13}$$

$$\mid R_F^{(inc)} \mid^2 - \mid R_F^{(ref)} \mid^2 \ = \ \mid R_F^{(trans)} \mid^2 \ . \tag{14}$$

On the other hand, the conserved current relations between bi-spinor and bosonic fields at $r = \infty$ derive the relation among them as

$$(\mid R_B^{(inc)} \mid^2 - \mid R_B^{(ref)} \mid^2)\ p_\infty = (\mid R_F^{(inc)} \mid^2 - \mid R_F^{(ref)} \mid^2)\ \mu \ . \tag{15}$$

From the equations (13)-(15), the current relation near horizon is obtained

$$\mid R_F^{(trans)} \mid^2 \ \mu = \mid R_B^{(trans)} \mid^2 p_H \quad \Rightarrow \quad 0 < p_H = \omega - \Omega_H m \tag{16}$$

The last inequality relation $0 < p_H = \omega - \Omega_H m$ shows that the super-rqadiance for the bosonic particles in rotating black hole space-time does not occur.

4 Summary

The summary of the report is as follows:

- Extended Bargmann-Wigner equations are investigated and the conserved current is derived.
- Application for radiation problem in rotating black hole space-time is studied and the super-radiance problem in rotating black hole space-time is shown not to occur.

References

[1] See for example, W. Press and S. Teukolsky, Nature **238** (1972) 211.

[2] See for example, S. Mano and E. Takasugi, Prog. Theor. Phys., **96** (1997) 213.

[3] V. Bargmann and E. P. Wigner, Proc. Nat. Acad. Sci. (U.S.A.), **34** (1948) 211.

[4] W. G. Unruh, Phys. Rev. **D 10** (1974) 3194.

[5] K. Maeda, Prog. Theor. Phys., **55** (1976) 1677.

A new theory of relativistic reference frames: the case of an accelerated observer in Minkowski space-time *

Olivier Minazzoli

Jet Propulsion Laboratory, California Institute of Technology,

4800 Oak Grove Drive, Pasadena, CA 91109-0899, USA

Email : ominazzoli@gmail.com

Abstract

We study accelerating relativistic coordinate systems in Minkowski space-time under the harmonic (isotropic) gauge. The method employed allows one to get the perturbative accelerated metric, and the two sets of coordinate transformations: from the inertial to the accelerated frame and vice versa. The method is based on analytical solutions of sets of both gauge and dynamical conditions that define the local accelerated system of reference. The method can directly be extended to the General Relativity case (and possibly to any other theory of space-time) and represents an alternative to the usual theories of reference frames (Brumberg and Kopeikin, Nuovo Cimento B Serie 103, 63 (1989) and Damour, Soffel and Xu, Phys. Rev. D 43, 3273 (1991)).

1 Introduction

The relativistic theory of the coordinate system associated to an accelerated observer has been worked out by several authors [2, 3, 4, 5, 6, 7] [1]. There, the coordinate system is constructed as described in Synge's book [2] : a tetrad is Fermi-Walker transported along the observer world-line. From each proper time τ on the world-line is issued three space-like geodesics associated to the tetrad orientation, such that the 3 affine parameters of the space-like geodesics issued at the observer's proper time τ, define the spatial coordinates at the coordinate time τ. These coordinates are dubbed *Fermi coordinates* by Synge [2].
On an other hand, cellestial reference frame theories, that are used in the context of space observation, experimentation and navigation, are based on the harmonic coordinates [9, 10]. Meaning that those coordinates are not constructed through a procedure as for the Fermi coordinates, but are first restricted by partial differential equations applied on the coordinate transformation functions (the gauge conditions) and then furthermore restricted by dynamical conditions that "pinpoint" the reference system to an observer.
The authors of [1] recently developped a new approach to get a full cellestial reference frame theory. In our work [1], we used this new approach to study the simpler case of an accelerated observer in a flat space-time. Hence we got the metric associated to a non-rotating accelerated observer in harmonic coordinates, along with the associated coordinate transformations from – and to – an inertial reference system. Here we present some features of this result along with an alternative way to get the dynamical conditions. Moreover, we will use the notation conventions of the IAU [11, 9, 3].

*This communication is partially based on the work made in [1].

[1]Note that the transformations leading the the Fermi coordinates have been worked out only very recently [12].

2 Principle

2.1 The direct transformation

Lets start from the metric in an inertial coordinate system, where it can be written such that it takes its Minkowski form. Lets define the following coordinate transformations $x^\alpha(X^\sigma)$, parametrized by three arbitrary functions (K, L, Q^i) in an perturbative expansion:

$$x^0 = X^0 + c^{-2}K(X^\alpha) + c^{-4}L(X^\alpha) + O(c^{-5}), \tag{1}$$
$$x^i = X^i - X_0^i(X^0) + c^{-2}Q^i(X^\alpha) + O(c^{-3}), \tag{2}$$

where $\{x\}$ are the inertial coordinates, while $\{X\}$ are the coordinates that will be associated to the observer. The covariant metric corresponding to the newly defined coordinates writes:

$$\begin{aligned}
G_{00} &= -1 + c^{-2}\left\{v_{X0}^2 - 2\frac{\partial K}{\partial X^0}\right\} + c^{-4}\left\{-2v_{X0}^l c\frac{\partial Q^l}{\partial X^0} - 2\frac{\partial L}{\partial X^0} - \left(\frac{\partial L}{\partial X^0}\right)^2\right\} + O(c^{-5}) \\
G_{0i} &= c^{-1}\left\{-v_{X0}^i - c\frac{\partial K}{\partial X^i}\right\} + c^{-3}\left\{c\frac{\partial Q^i}{\partial X^0} - v_{X0}^l\frac{\partial Q^i}{\partial X^i} - c\frac{\partial K}{\partial X^0}\frac{\partial K}{\partial X^i} - \frac{1}{c}\frac{\partial L}{\partial X^i}\right\} + O(c^{-4}) \\
G_{ij} &= \delta_{ij} + c^{-2}\left\{\frac{\partial Q^i}{\partial X^j} + \frac{\partial Q^j}{\partial X^i} - \frac{1}{c^2}\frac{\partial K}{\partial X^i}\frac{\partial K}{\partial X^j}\right\} + O(c^{-3})
\end{aligned} \tag{3}$$

The space-time being flat, it a fortiori satisfies the algebraic condition allowing the Strong Spatial Isotropy Condition (SSIC) to be imposed [9]. Hence, one can write the metric associated to the accelerated observer in the form used in [9] ($ds^2 = (-1+2W/c^2-2W^2/c^4)(dX^0)^2+...$), thus restricting the harmonic coordinates subset to a sub-subset satisfying the SSIC. This condition fixes a part of K and Q^i:

$$K = c\left\{-v_{X0}^l X^l\right\} + K_0(X^0), \quad Q^i = Q_0^i(X^0) + \left[\frac{1}{2}v_{X0}^i v_{X0}^l + q_1^{[il]}(X^0)\right]X^l + \sum_{l>1} Q_L(X^0)X^L, \tag{4}$$

where $v_{X0}^i \equiv c dX_0^i/dX^0$. $-Q_0^i(X^0)$ is the first perturbative order of the position of the center of the frame – not associated to any observer so far. It could be put equal to zero by a redifinition $X_0^i + Q_0^i \to X_0^i$ as in [10, 11]. However, explicitely keeping it allows to get the equation of motion at the first perturbative order when getting the transformations [1]. Q^i is furthermore constrained by using the harmonic gauge condition $\Box_G\ x^\alpha = 0$: $\sum_{l>1} Q_L^i(X^0)X^L = -\frac{1}{2}a_{X0}^i X^2 + a_{X0}^l X^l X^i$, where $a_{X0}^i \equiv c^2 d^2X_0^i/(dX^0)^2$.

2.2 The dynamical condition

In addition to the gauge conditions, dynamical conditions have to be imposed in order to pinpoint the reference frame to the observer. Here is presented a way to get those dynamical conditions that is less general than in [1], but in our opinion more easy to understand. It is shown in [8] that for an observer in free fall, the coordinates can be chosen such that the connexions are null at the observer's geodesic. In the non-geodesic case, not all the connexions are null. Indeed, the accelerated equation of motion writes in the coordinate time parametrisation:

$$\frac{d^2X^i}{(dX^0)^2} + \left(\Gamma_{\alpha\beta}^i - \Gamma_{\alpha\beta}^0\frac{dX^i}{dX^0}\right)\frac{dX^\alpha}{dX^0}\frac{dX^\beta}{dX^0} = c^{-2}\left(\frac{d\tau}{dX^0}\right)^2\left[f^i - f^0\frac{dX^i}{dX^0}\right], \tag{5}$$

where f^α is, by definition, the 4-vector acceleration, and τ is the proper time on the worldline satisfying the equation of motion. Hence, the requirement that the reference frame always remains centered on the observer ($d^2X^i/(dX^0)^2|_\Omega = 0$ and $dX^i/dX^0|_\Omega = 0$, where $|_\Omega$ stands for the limit on the worldline, leads to the condition $\Gamma_{00}^i|_\Omega = c^{-2}\left(\frac{d\tau}{dX^0}\right)^2 f^i \equiv c^{-2}b^i$. In terms of potentials, this condition reduces to $\partial_i W|_\Omega =$

$-b^i + O(c^{-3})$. The conditions on the other potentials being unchanged compared to the geodetic case, we derive the whole K, L, Q^i functions, up to terms that don't contribute to the equation of motion [1] (ie. remaining gauge freedom that can be put equal to zero for convenience).

2.3 The inverse transformation

Now, parametrizing $X^\sigma(x^\alpha)$ by three functions $\hat{K}, \hat{L}, \hat{Q}$ [2] and getting the contravariant metric associated to the transformation $X^\sigma(x^\alpha)$ instead of the covariant one in the direct case, we deduce $W(X^\sigma(x^\alpha))$ and $W^i(X^\sigma(x^\alpha))$ (ie. the potentials written in terms of $\hat{K}, \hat{L}, \hat{Q}$ instead of K, L, Q as in (3)). Moreover, the condition $\partial_{X^i} W(X^\sigma) = -b^i + O(c^{-3})$ leads to the following equivalent condition $\partial_{x^i} W(X^\sigma(x^\alpha)) = -b^i + c^{-2}\{-\frac{1}{2} v^i_{X0} v^l_{X0} a^l_{X0} + q_1^{[il]}(X^0)\} + O(c^{-3})$. Hence, by applying the same procedure as previously, but with the latter condition, one gets the functions $\hat{K}, \hat{L}, \hat{Q}$ (ie. the inverse transformation).

2.4 The link with Fermi coordinates

The transformations between the Fermi coordinates X^α_F and the SSIC harmonic ones X^α are $X^0_F = X^0 + c^{-4}\{\frac{1}{10}\dot{a}^k_{X0} X^l X^2\} + O(c^{-5})$, $X^i_F = X^i + c^{-2}\{\frac{1}{2} a^i_{X0} X^2 - a^l_{X0} X^l X^i\} + O(c^{-4})$.

Aknowledgment

This research was supported by an appointment to the NASA Postdoctoral Program at the Jet Propulsion Laboratory, California Institute of Technology, administered by Oak Ridge Associated Universities through a contract with NASA.

References

[1] Turyshev, Slava G.; Minazzoli, Olivier L.; Toth, Viktor T, *Accelerating relativistic reference frames in Minkowski space-time*, J. Math. Phys., March 2012

[2] J. L. Synge, Relativity: The General Theory (North-Holland, Amsterdam, 1960).

[3] C. W. Misner, K. S. Thorne, and J. A. Wheeler, Gravitation (Freeman, San Francisco, 1973).

[4] Ni, Wei-Tou, Zimmermann, Mark, *Inertial and gravitational effects in the proper reference frame of an accelerated, rotating observer*, Physical Review D (Particles and Fields), Volume 17, Issue 6, 15 March 1978, pp.1473-1476.

[5] Ni, Wei-Tou, *On the Proper Reference Frame and Local Coordinates of an Accelerated Observer in Special Relativity*, Chinese Journal of Physics, vol. 15, Issue 1, p.51.

[6] Li, Wann-Quan; Ni, Wei-Tou, *On an Accelerated Observer with Rotating Tetrad in Special Relativity*, Chinese Journal of Physics, vol. 16, Issue 4, p.214.

[7] Li, Wann-Quan; Ni, Wei-Tou, *Coupled inertial and gravitational effects in the proper reference frame of an accelerated rotating observer*, Journal of Mathematical Physics, Vol. 20, p. 1473 - 14804.

[8] Manasse, F. K.; Misner, C. W., *Fermi Normal Coordinates and Some Basic Concepts in Differential Geometry*, Journal of Mathematical Physics, Vol. 4, p.735-745.

[9] Damour, T.; Soffel, M.; Xu, C., *General-relativistic celestial mechanics I. Method and definition of reference systems*, Physical Review D (Particles and Fields), Volume 43, Issue 10, 15 May 1991, pp.3273-3307.

[2] as for the direct transformation $x^\sigma(X^\alpha)$ in (1-2) with K, L, Q.

[10] Brumberg, V. A.; Kopejkin, S. M., *Relativistic reference systems and motion of test bodies in the vicinity of the Earth*, Nuovo Cimento B, Vol. 103, No. 1, p. 63 - 9.

[11] Soffel, M. et al., *The IAU 2000 Resolutions for Astrometry, Celestial Mechanics, and Metrology in the Relativistic Framework: Explanatory Supplement*, The Astronomical Journal, Volume 126, Issue 6, pp. 2687-2706.

[12] Klein, David; Collas, Peter, *General transformation formulas for Fermi Walker coordinates*, Classical and Quantum Gravity, Volume 25, Issue 14, pp. 145019 (2008).

On the choice of reference for the covariant Hamiltonian boundary term

James M. Nester[1,2], *Chiang-Mei Chen*[1], *Jian-Liang Liu*[1], *Ming-Fan Wu*[1]

[1] *Department of Physics & Center for Mathematics and Theoretical Physics, National Central University, Chungli 320, Taiwan*

[2] *Graduate Institute of Astronomy, National Central University, Chungli 320, Taiwan*

Email : nester@phy.ncu.edu.tw

Abstract

The Hamiltonian for dynamic geometry gravity theories generates the dynamical evolution of a spatial region along a time-like vector field. It includes a boundary term, which determines both the value of the Hamiltonian and the boundary conditions. From the value one obtains the quasi-local quantities: energy-momentum, angular-momentum/center-of-mass. The boundary term depends not only on the dynamical variables but also on their reference values, which determine the ground state (with vanishing quasi-local values). For our preferred boundary term for Einstein's GR we propose 4D isometric matching and extremizing the energy to determine the reference metric and connection values. The quasi-local energy values for spherically symmetric metrics have been calculated.

Energy-momentum is the source of gravity. Gravitating bodies can exchange energy-momentum with gravity—locally, yet there is no well defined energy-momentum density for gravity itself (this can be understood as a consequence of the equivalence principle). Early approaches used non-covariant, inherently reference frame dependent, energy-momentum complexes: *pseudotensors*. They had two ambiguities: (1) Which reference frame? (2) Which expression? (e.g., that of Einstein, Papapetrou, Landau & Lifshitz, Bergmann & Thompson, Møller, Goldberg, or Weinberg?)

The modern idea is *quasi-local* (associated with a closed 2-surface) [1]. One approach is via the Hamiltonian (the generator of time evolution). In fact this includes all the classical pseudotensors as special cases, while taming their ambiguities, providing clear physical/geometric meaning [2, 3, 4]

For geometric gravity theories the Hamiltonian 3-form is a conserved Noether current as well as the generator of the evolution of a spatial region along a space-time displacement vector field: $\mathcal{H}(N) = N^\mu \mathcal{H}_\mu + d\mathcal{B}(N)$, with $d\mathcal{H}(N) \propto$ field eqns $\simeq 0$, where $N^\mu \mathcal{H}_\mu$, which generates the evolution equations, is proportional to field equations (initial value constraints) and thus vanishes "on shell". Hence the value is determined by the total differential (boundary) term,

$$E(N, \Sigma) := \int_\Sigma \mathcal{H}(N) = \oint_{\partial\Sigma} \mathcal{B}(N); \tag{1}$$

it is *quasi-local*. But $\mathcal{B}(N)$ can be modified without destroying the conservation property, consequently one can arrange for almost any conserved value. Fortunately the Hamiltonian role tames that freedom.

One must look to the boundary term in the *variation* of the Hamiltonian. Requiring it to vanish yields the boundary conditions. Modifying the boundary term modifies the boundary conditions. The various traditional pseudotensors are each associated with a particular boundary condition.

In order to accommodate suitable boundary conditions one must, in general, also introduce certain *reference values* which represent the ground state of the field—the "vacuum".

For GR we [2] proposed (here $\Delta\alpha := \alpha - \bar{\alpha}$ with $\bar{\alpha}$ being the reference value)

$$\mathcal{B}(N) = \frac{1}{2\kappa}(\Delta\Gamma^{\alpha}{}_{\beta} \wedge i_N \eta_{\alpha}{}^{\beta} + \bar{D}_{\beta} N^{\alpha} \Delta\eta_{\alpha}{}^{\beta}), \qquad \eta^{\alpha\beta\cdots} := *(\vartheta^{\alpha} \wedge \vartheta^{\beta} \wedge \cdots) \tag{2}$$

corresponding to fixed orthonormal coframe ϑ^{μ} ($\sim$ metric) on the boundary: $\delta\mathcal{H}(N) \sim di_N(\Delta\Gamma^{\alpha}{}_{\beta} \wedge \delta\eta_{\alpha}{}^{\beta})$. Like other choices, at spatial infinity it gives the desired values. Its special virtues: (i) at null infinity: the Bondi-Trautman energy & the Bondi energy flux, (ii) it is "covariant", (iii) it has a positive energy property, (iv) for small spheres, a positive multiple of the Bel-Robinson tensor, (v) first law of thermodynamics for black holes, (vi) in certain cases it reduces to the Brown-York expression, hence spherically it has the hoop property.

For all other fields it is appropriate to choose vanishing reference values as the ground state—the vacuum. But for geometric gravity the standard ground state is the non-vanishing Minkowski metric. A non-trivial reference is *essential*.

With standard Minkowski coordinates y^i, a reference Killing field has the form $N^k = N_0^k + \lambda_0^k{}_l y^l$, where $\lambda_0^{kl} = \lambda_0^{[kl]}$, with N_0^k and λ_0^{kl} being constants. The 2-surface integral of the boundary term then has a value which gives the quasi-local energy-momentum and angular momentum/center-of-mass:

$$\oint_S \mathcal{B}(N) = -N_0^k p_k(S) + \frac{1}{2}\lambda_0^{kl} J_{kl}(S). \tag{3}$$

The integrals $p_k(S)$, $J_{kl}(S)$ in the spatial asymptotic limit agree with accepted expressions for these quantities.

For quasi-local energy-momentum one takes the vector field to be a translational Killing field of the Minkowski reference. Then the second term in (2) makes no contribution. With vanishing reference the first term is just Freud's 1939 superpotential for the Einstein pseudotensor. Thus effectively we are now simply proposing good coordinates for the Einstein pseudotensor.

Choose, in a neighborhood of the desired spacelike boundary 2-surface S, 4 smooth functions y^i, $i = 0, 1, 2, 3$ with $dy^0 \wedge dy^1 \wedge dy^2 \wedge dy^3 \neq 0$ and then define a Minkowski reference by $\bar{g} = -(dy^0)^2 + (dy^1)^2 + (dy^2)^2 + (dy^3)^2$. This is equivalent to finding a diffeomorphism for a neighborhood of the 2-surface into Minkowski space. The reference connection has the form $\bar{\Gamma}^{\alpha}{}_{\beta} = x^{\alpha}{}_i(\bar{\Gamma}^i{}_j \Lambda^j{}_{\beta} + dy^i{}_{\beta}) = x^{\alpha}{}_i dy^i{}_{\beta}$. Then with constant N^k our quasi-local expression takes the form

$$\mathcal{B}(N) = N^k x^{\mu}{}_k (\Gamma^{\alpha}{}_{\beta} - x^{\alpha}{}_j \, dy^j{}_{\beta}) \wedge \eta_{\mu\alpha}{}^{\beta}. \tag{4}$$

We propose taking the optimal embedding as the one which gives the extreme value to the associated invariant mass $m^2 = -p_i p_j \bar{g}^{ij}$. This is reasonable, considering the expectation that quasi-local energy should be non-negative and vanishing only for Minkowski space.

York, and Wang and Yau and others have used embeddings isometrically matching the 2-surface metric. Our "new" proposal (which was suggested by Szabados in 2000) is complete 4D isometric matching on S: $g_{\mu\nu}|_S = \bar{g}_{\mu\nu}|_S = \bar{g}_{ij} y^i{}_{\mu} y^j{}_{\nu}|_S$, on the 2-surface of constant t, r this is 10 constraints on the 12 embedding functions y^i_t, y^i_r, y^i ($\Longrightarrow y^i_{\theta}, y^i_{\phi}$).

To determine the other 2 select the optimal "best matched" reference by energy extremization. Use the value of the boundary term to measure the difference between the dynamical boundary values and the reference boundary values and minimize. There are 2 different situations.

I: Given a 2-surface S take the inf of m^2. This should determine the reference up to Poincaré transformations. **II:** Given a 2-surface S and a vector field N, take the inf of $E(N, S)$. [Afterward one could extremize over the choice of N.]

We have tested this proposal on spherically symmetric metrics (both the static Reissner-Nordström–(Anti)-de Sitter and the dynamic FLRW cosmology) and found reasonable results. For the details see the reports [5, 6].

This work was supported by the National Science Council of the R.O.C. under the grants NSC-100-2119-M-008-018 and NSC 99-2112-M-008-005-MY3 and in part by the National Center of Theoretical Sciences (NCTS).

References

[1] L.B. Szabados, Living Rev. Relativity 12 (2009) 4.

[2] C.-M. Chen, J.M. Nester and R.S. Tung, Phys. Lett. A 203 (1995) 5; Phys. Rev. D 72 (2005) 104020.

[3] C.-M. Chen and J.M. Nester, Class. Quantum Grav. 16 (1999) 1279; Gravitation & Cosmol. 6 (2000) 257.

[4] J.M. Nester, Class. Quantum Grav. 21 (2004) S261; Prog. Theor. Phys. Supp. 172 (2008) 30.

[5] M.-F. Wu, C.-M. Chen, J.-L. Liu and J.M. Nester, Phys. Lett. A 374 (2010) 3599; Phys. Rev. D 84 (2011) 085047.

[6] J.-L. Liu, C.M. Chen and J.M. Nester, Class. Quantum Grav. 28 (2011) 195019.

Quantum Gravity

Dimitry Gal'tsov, Kirill Bronnikov, Marina Romanova, Vitaly Melnikov, Andrey Doroshkevich, Gennady Bisnovatyi-Kogan, Vlatcheslaw Mukhanov and Roland Triay

Wei-Tou Ni, Ganesh Khapekar, Dnyaneshwar Pawar, Sharad Kandalkar, Roland Triay, Vasudeo Patil, Sang Pyo Kim, Ki Cheong (Franky) Wong and Ilka Petermann

Black holes in loop quantum gravity

Hanno Sahlmann
Asia Pacific Center for Theoretical Physics, Pohang (Korea), and
Physics Department, Pohang University for Science and Technology, Pohang (Korea)
Email : sahlmann@apctp.org

Abstract

When describing certain types of black holes in loop quantum gravity, one finds a beautiful interplay between quantum Chern-Simons theory, which describes the surface geometry of the black hole, and the quantum geometry of the bulk space-time. One can calculate the black hole entropy and find the Bekenstein-Hawking area law for macroscopic black holes. I review these developments and also discuss some recent ideas of mine regarding a description of black holes that is fully intrinsic to loop quantum gravity.

1 Introduction

Black holes are fascinating objects predicted by general relativity. They even point beyond the classical theory, because of the singularities within, and because of the intriguing phenomenon of black hole thermodynamics [1]. Therefore they are a tempting subject of investigation in any theory of quantum gravity. Loop quantum gravity (LQG)is able to successfully describe black hole horizons in the quantum theory. Within this description, it is possible to identify degrees of freedom that carry the black hole entropy, and prove, for a large class of black holes, the Bekenstein-Hawking area law.

LQG is based on a canonical description of gravity in terms of conjugate fields A, and E on a spatial slice of a globally hyperbolic spacetime. A is an SU(2) gauge field, and E a triad of tensor densities. E encodes the spatial geometry via

$$|\det q|q^{ab} = E^a_I E^b_J \delta^{IJ} \tag{1}$$

where q_{ab} is the spatial metric. A is related to the extrinsic curvature of the spatial slice. These fields become operator valued distributions on a Hilbert space $\mathcal{H}$. To be more precise, only the holonomies of A and the fluxes (two dimensional integrals) of E become well defined operators. The holonomies are creation operators for one dimensional excitations of the spatial geometry. A basis in $\mathcal{H}$ is labeled by *spin networks*, i.e. oriented graphs on which each edge is marked by an irreducible representation of SU(2). The edges can be understood as carriers of area, since they endow surfaces they intersect with an area quantum

$$A_j = 8\pi\iota l_{\mathrm{P}}^2\sqrt{j(j+1)} \tag{2}$$

where l_{P}^2 is Planck length, ι is the Barbero-Immirzi parameter of LQG, and j is the spin label of the SU(2) representation. Such quantum states are then subject to constraint equations which can be understood as a quantum version of Einstein's equations. More information about LQG can for example be found in [2, 3, 4, 5].

The picture of a black hole horizon that arises in loop quantum gravity is roughly as follows: Spin net edges pierce the horizon H and endow it with area. The degrees of freedom on H are described by a Chern-Simons (CS) theory, which couples to the punctures by the spin network edges. The quantum states of this

CS theory supply the microstates for the black hole entropy. The development of the whole subject is quite rich, thus our description will leave out many interesting aspects and references. A very nice review is given in [6].

The first ideas were developed by Krasnov and Rovelli [7]: Spin network edges pierce the horizon and endow it with area. The number of configurations of these edges modulo diffeomorphisms for a given total area is counted to obtain the entropy. A systematic and detailed treatment is that by Ashtekar Baez, and Krasnov [8], in which was realized that the degrees of freedom on the horizon are described by a CS theory and are essential in the calculation of the entropy. [8] does contain errors in the state counting however. These errors were corrected in by Domagala and Lewandowski in [9], where the horizon Hilbert space was correctly derived, its elements characterized in a combinatorial way, and the entropy calculation stated in combinatorial terms and partially carried out. The combinatorial problem was fully solved in [10]. In [11, 12], Kaul and Majumdar assumed that a partial gauge fixing that had been used in [8] was unnecessary, and they stated and solved the ensuing combinatorial problem for the black hole entropy. They thus determined the area-entropy relation in the resulting more natural, but technically more challenging setting. In cite [13, 14], it was shown that dropping the partial gauge fixing as in [11, 12] can in fact be fully justified. This led to additional new insights [15]. In our description below, we will follow [13, 14]. There are also several exciting new developments which we will describe below.

2 Spherically symmetric isolated horizons

The LQG description of black holes does not start from solutions of the full theory. Rather, it is a quantization gravity on a manifold with boundary Δ. In the simplest case, the boundary is assumed to be null, with topology $\mathbb{R}\times S^3$. Δ is required to be an *isolated horizon*, a quasi-local substitute for an event horizon [16]. This imposes boundary conditions on the fields A and E at H, the intersection of the spatial slice with Δ,

$$*E=-\frac{a_H}{\pi(1-\iota^2)}F(A). \tag{3}$$

a_H denotes the area of the horizon H. Furthermore, the symplectic structure acquires a surface term. The latter suggests, together with some technical aspects of the kinematical Hilbert space used in LQG, to quantize the fields on the horizon separately from the bulk fields. The latter are quantized in the standard way of LQG. The only new aspect is that now edges of a spin network can end on the horizon. The such ends of spin network edges are described by quantum numbers $m_p\in\{-j_p,-j_p+1,\ldots,j_p-1,j_p\}$, where j_p is the representation label of the edge ending on the horizon, and p is a label for the endpoint ("puncture"). The quantum number represents the eigenvalue of the component of E normal to the horizon at the puncture.

The boundary term in the symplectic structure is that of a SU(2)CS theory with level $k=a_H/(2\pi\iota(1-\iota^2)\ell_{\mathrm{P}}^2)$, and punctures where spin network edges of the bulk theory end on the surface. The quantized CS connection is flat, locally, but there are degrees of freedom at the punctures. These are – roughly speaking – described by quantum numbers s_p, m'_p, where the former is a half-integer, and $m'_p\in\{-s_p,-s_p+1,\ldots,s_p-1,s_p\}$. There is a constraint on the set of m'_p's coming from the fact that H is a sphere, and hence a loop going around all the punctures is contractible, and the corresponding holonomy must hence be trivial. The Hilbert space is equivalent to a subspace of the singlet component of the tensor product $\pi_{s_1}\otimes\pi_{s_2}\otimes\ldots$ ranging over all punctures. The boundary condition (3) can be quantized to yield an operator equation. The solutions are tensor products of bulk and boundary states in which the quantum numbers (s_p,m'_p) and (j_p,m_p) are equal to each other at each puncture.

Now, if one fixes the quantum area of the black hole to be a, this bounds the number of punctures and the spins (j_p) labeling the representations. It becomes a rather complicated combinatorial problem to determine the number $N(a)$ of quantum states with area a that satisfy the quantum boundary conditions. It was solved in [11, 12], and later, independently in [17]. It turns out that

$$S(a) := \ln(N(a)) = \frac{\iota}{\iota_{\mathrm{SU}(2)}} \frac{a}{4\pi l_P^2} - \frac{3}{2} \ln \frac{a}{l_P^2} + O(a^0) \tag{4}$$

as long as $\iota \leq \sqrt{3}$. Here, $\iota_{\mathrm{SU}(2)} \approx 0.274$ is a certain numerical constant. One thus obtains the Bekenstein-Hawking area law upon setting $\iota = \iota_{\mathrm{SU}(2)}$.

The formalism can be generalized to rotating IHs [18] and static IHs with arbitrary surface geometry [19, 20]. Surprising fine structure of the area spectrum has been found [21, 22] and analyzed [23, 24, 25, 26, 27].

The latest development in this line of research is an assignment of a quasi-local energy

$$E_j = \frac{A_j}{8\pi\ell} \tag{5}$$

to a puncture with spin j [28]. ℓ is a characteristic distance of the local observers to the horizon. The formulation of the thermodynamics for the horizon system using this energy then gives the Bekenstein-Hawking relation without any tuning of the Babero-Immirzi parameter ι [29]. At the same time, similar but complementary results have been obtained from the path integral approach to LQG [30]. In particular, the Bekenstein-Hawking relation holds, irrespective of the value of the Babero-Immirzi parameter.

3 Towards an intrinsic description

The quantization of isolated horizons as briefly sketched above is a remarkable success of LQG. However, it is only an effective description, in the sense that it uses a number of elements that are not intrinsic to the formalism of LQG. Recently, I have done some work [31, 32, 33] in order to describe isolated horizons from within loop quantum gravity, that is, without introducing a boundary in the classical theory and quantizing the CS theory separately. The idea is to impose a quantum version of (3) directly in the quantum theory. However, since there is no operator corresponding to $F(A)$ in the quantum theory, one has to "exponentiate" (3), as we will describe now.

Usually, the field E is integrated over surfaces in the quantum theory, but it turns out that even the non-integrated quantum field makes sense as an operator valued distribution $\widehat{E}$. Then given a surface S without self-intersections, and a system of paths that connect all points of the surface with some base-point on the edge of the surface, one defines

$$W_S = \mathbb{I}_2 + 8\pi i c \int_S \mathrm{ad}_{h_s}(\widehat{\Sigma}(s)) + (8\pi i c)^2 \int_{S^2} K_{s,s'} \,\mathrm{ad}_{h_s}(\widehat{\Sigma}(s))\,\mathrm{ad}_{h_{s'}}(\widehat{\Sigma}(s')) + \ldots \tag{6}$$

Here, K is an integration kernel that implements a *surface ordering* and the holonomies h_s connect the point s on the surface with the base point via the path system. There are two problems with the above definition. The first is that consecutive actions of $\widehat{E}^a(p)$ give rise to delta distributions that are concentrated precisely at the boundary of integration enforced by surface ordering, and a prescription for the evaluation of these has to be adopted. This can be resolved via a standard regularization. The second problem is that the operators $\widehat{E}_I(p)$ at a fixed point p do not commute, therefore there is an ordering ambiguity inherent in the above definition. This ambiguity can be fixed [31] using the *Duflo map*. This is a quantization map Υ from the free algebra of symbols $\{E_I\}_I$ with the Poisson bracket $\{E_I, E_J\} = f_{IJ}{}^K E_K$, ($f$ being the structure constants of a semisimple Lie-algebra $\mathfrak{g}$) into the universal enveloping algebra $U(\mathfrak{g})$, extending the map $E_I \mapsto X_I$ on generators. The defining property of Υ is that it is an *algebra isomorphism* between the invariant subspaces under the action of the corresponding Lie group G. Υ is an improved version of symmetric quantization χ,

$$\Upsilon = \chi \circ j^{\frac{1}{2}}(\partial), \tag{7}$$

where $j^{\frac{1}{2}}(\partial)$ is a differential operator that can be obtained by inserting derivatives ∂^I into the following function on $\mathfrak{g}$:

$$j^{\frac{1}{2}}(x) = \det{}^{\frac{1}{2}}\left(\frac{\sinh\frac{1}{2}\operatorname{ad}x}{\frac{1}{2}\operatorname{ad}x}\right) = 1 + \frac{1}{48}\left\|x\right\|^2 + \ldots, \tag{8}$$

with $\left\|x\right\|^2 = \operatorname{Tr}(\operatorname{ad}_x^2)$ the square of the Cartan-Killing norm of G. For G=SU(2) on finds for example $\Upsilon(\left\|E\right\|^2) = \Delta_{\mathrm{SU}(2)} + \frac{1}{8}\mathbb{I}$, where $\Delta_{\mathrm{SU}(2)}$ is the Laplacian. Using Υ to order powers of E the action of the operator W_S becomes well defined. For SU(2) and spin nets $|\,|_{j'}\rangle$ intersecting S transversally once with spin j, one finds for example

$$\operatorname{Tr}_j\left(W_S\right)|\,|_{j'}\rangle = \frac{\sin\left[\pi c(2j+1)(2j'+1)\right]}{\sin\left[\pi c(2j'+1)\right]}|\,|_{j'}\rangle. \tag{9}$$

The states $|\,|_j\rangle$ are however not eigenstates of the operator valued matrices W_S themselves. Rather, they are mapped into linear combinations of new spin networks which involve edges that are part of the path system on S.

Coming back to black holes, we thus call a surface H a spherically symmetric quantum IH, if the surface ordered exponential of (3),

$$\operatorname{Tr} h_{\partial S}\Psi = \operatorname{Tr} W_S \Psi, \tag{10}$$

is valid for all surfaces S lying entirely within H. Here, the operators W_S are evaluated with $c = -\pi\iota(1-\iota^2)\ell_{\mathrm{P}}^2/2a_H$. Solutions Ψ of this equation do not exist in the standard representation of LQG, but arguably in other representations. A spin network $|\psi\rangle$ determines puncture data $\mathcal{P} = \{(p_1, j_1, m_1)\ldots(p_N, j_N, m_N)\}$ given by points p_i on H irreducible representations j_i and and magnetic quantum numbers m_i. $\mathcal{P}$ defines a functional on functions of traces of loops that encircle at most one puncture: $\mu(\prod_i \operatorname{Tr}_{k_i}(h_{\alpha_i})) := \prod_i \operatorname{Tr}_{k_i}(g_{j_i})$. This functional is positive and consistent with all the relations among these traces. It is however not yet clear whether it extends all holonomy functionals on H. The resulting horizon theory seems to reproduce many of the results that have been obtained earlier [13, 34], up to the fact that the fluxes E, pulled back to the horizon are still a-priori independent degrees of freedom describing the intrinsic geometry of H. Indeed, it seems that the remaining degrees of freedom on H are those of an ISU(2) CS theory.

References

[1] R. M. Wald, Living Rev. Rel. **4**, 6 (2001) [arXiv:gr-qc/9912119].

[2] T. Thiemann, arXiv:gr-qc/0110034.

[3] C. Rovelli, Living Rev. Rel. **11**, 5 (2008).

[4] A. Ashtekar and J. Lewandowski, Class. Quant. Grav. **21**, R53 (2004) [arXiv:gr-qc/0404018].

[5] K. Giesel and H. Sahlmann, arXiv:1203.2733 [gr-qc].

[6] J. F. Barbero G., J. Lewandowski and E. J. S. Villasenor, arXiv:1203.0174 [gr-qc].

[7] K. Krasnov and C. Rovelli, Class. Quant. Grav. **26**, 245009 (2009) [arXiv:0905.4916 [gr-qc]].

[8] A. Ashtekar, J. C. Baez and K. Krasnov, Adv. Theor. Math. Phys. **4**, 1 (2000) [arXiv:gr-qc/0005126].

[9] M. Domagala and J. Lewandowski, Class. Quant. Grav. **21**, 5233 (2004) [arXiv:gr-qc/0407051].

[10] K. A. Meissner, Class. Quant. Grav. **21**, 5245 (2004) [arXiv:gr-qc/0407052].

[11] R. K. Kaul and P. Majumdar, Phys. Lett. B **439**, 267 (1998) [arXiv:gr-qc/9801080].

[12] R. K. Kaul and P. Majumdar, Phys. Rev. Lett. **84**, 5255 (2000) [arXiv:gr-qc/0002040].

[13] J. Engle, A. Perez and K. Noui, Phys. Rev. Lett. **105**, 031302 (2010) [arXiv:0905.3168 [gr-qc]].

[14] J. Engle, K. Noui, A. Perez and D. Pranzetti, Phys. Rev. D **82**, 044050 (2010) [arXiv:1006.0634 [gr-qc]].

[15] E. Bianchi, Class. Quant. Grav. **28**, 114006 (2011) [arXiv:1011.5628 [gr-qc]].

[16] A. Ashtekar, C. Beetle, O. Dreyer, S. Fairhurst, B. Krishnan, J. Lewandowski and J. Wisniewski, Phys. Rev. Lett. **85**, 3564 (2000) [arXiv:gr-qc/0006006].

[17] I. Agullo, G. J. Fernando Barbero, E. F. Borja, J. Diaz-Polo and E. J. S. Villasenor, Phys. Rev. D **80**, 084006 (2009) [arXiv:0906.4529 [gr-qc]].

[18] A. Ashtekar, J. Engle and C. Van Den Broeck, Class. Quant. Grav. **22**, L27 (2005) [arXiv:gr-qc/0412003].

[19] C. Beetle and J. Engle, Class. Quant. Grav. **27**, 235024 (2010) [arXiv:1007.2768 [gr-qc]].

[20] A. Perez and D. Pranzetti, Entropy **13**, 744 (2011) [arXiv:1011.2961 [gr-qc]].

[21] A. Corichi, J. Diaz-Polo and E. Fernandez-Borja, Phys. Rev. Lett. **98**, 181301 (2007) [arXiv:gr-qc/0609122].

[22] A. Corichi, J. Diaz-Polo and E. Fernandez-Borja, Class. Quant. Grav. **24**, 243 (2007) [arXiv:gr-qc/0605014].

[23] J. Diaz-Polo and E. Fernandez-Borja, Class. Quant. Grav. **25**, 105007 (2008) [arXiv:0706.1979 [gr-qc]].

[24] H. Sahlmann, Phys. Rev. D **76**, 104050 (2007) [arXiv:0709.2433 [gr-qc]].

[25] I. Agullo, E. F. Borja and J. Diaz-Polo, JCAP **0907**, 016 (2009) [arXiv:0903.1667 [hep-th]].

[26] I. Agullo, J. Fernando Barbero, E. F. Borja, J. Diaz-Polo and E. J. S. Villasenor, Phys. Rev. D **82**, 084029 (2010) [arXiv:1101.3660 [gr-qc]].

[27] G. J. Fernando Barbero and E. J. S. Villasenor, Phys. Rev. D **83**, 104013 (2011) [arXiv:1101.3662 [gr-qc]].

[28] E. Frodden, A. Ghosh and A. Perez, arXiv:1110.4055 [gr-qc].

[29] A. Ghosh and A. Perez, Phys. Rev. Lett. **107**, 241301 (2011) [Erratum-ibid. **108**, 169901 (2012)] [arXiv:1107.1320 [gr-qc]].

[30] E. Bianchi, arXiv:1204.5122 [gr-qc].

[31] H. Sahlmann and T. Thiemann, J. Geom. Phys. **61**, 1104 (2011) [arXiv:1101.1690 [gr-qc]].

[32] H. Sahlmann, Phys. Rev. D **84**, 044049 (2011) [arXiv:1104.4691 [gr-qc]].

[33] H. Sahlmann and T. Thiemann, Phys. Rev. Lett. **108**, 111303 (2012) [arXiv:1109.5793 [gr-qc]].

[34] J. Engle, K. Noui, A. Perez and D. Pranzetti, JHEP **1105**, 016 (2011) [arXiv:1103.2723 [gr-qc]].

Sang-Jin Sin

Roland Triay, Pierre Darriulat, Yannick Giraud-Héraud and Cyrille Rosset

On the unitarity and renormalizability of higher derivative gravity in 3 and higher dimensions

Nobuyoshi Ohta

Department of Physics, Kinki University, Higashi-Osaka, Osaka, 677-8502, Japan

Email : ohtan@phys.kindai.ac.jp

Abstract

We study the condition on which the theory is unitary and stable in three-dimensional gravity with most general quadratic curvature, Lorentz-Chern-Simons and cosmological terms. We provide the complete classification of the unitary theories around flat Minkowski and (anti-)de Sitter spacetimes. We also argue that three-dimensional gravity that contains quadratic scalar curvature and Ricci tensor is renormalizable, but those theories with special relation between their coefficients including new massive gravity are not.

1 Introduction

We start with the discussion why it is interesting to consider higher derivative gravity. The quest of quantum theory of gravity is the long standing problem in theoretical physics. In 4D, Einstein's general relativity is nonrenormalizable. Fortunately quadratic theory is known to be renormalizable at the cost of the loss of unitarity [1]. Here we should note that the Einstein theory is only a low-energy effective theory. If one considers quantum theory, e.g. string theory, these higher-order terms alway appear, but these terms are usually regarded as small corrections. Here we consider these terms those we should quantize.

Recently very interesting developments took place in 3D gravity [2]. It has been shown that we can have unitary and possibly renormalizable gravity theory though in 3D. It is known that the Einstein theory describes no dynamical degree of freedom. However recent developments revealed that:

- Einstein + CS term gives unitary massive spin-2 particle due to higher derivative term [3],
- Einstein + $\alpha R^2 (\alpha > 0)$ gives unitary massive theory,
- $(\text{Einstein}) + \alpha R^2 + \beta R_{\mu\nu}^2$ describes unitary theory for $\alpha = -\frac{3}{8}\beta$ which is called new massive gravity [2].

Here we provide a complete classification of the general theory and examine the renormalizability.

2 Unitarity

We consider the higher derivative theory with the action

$$S = \frac{1}{\kappa^2} \int d^3x \Big\{ \sqrt{-g} \Big[\sigma R - 2\Lambda_0 + \alpha R^2 + \beta R_{\mu\nu}^2 \Big] + \mathcal{L}_{LCS} \Big\}, \tag{1}$$

where κ^2 is the three-dimensional gravitational constant, α, β, μ and $\sigma (= 0, \pm 1)$ are constants, Λ_0 is a cosmological constant, and the last term is the LCS term

$$\mathcal{L}_{LCS} = \frac{1}{2\mu} \epsilon^{\mu\nu\rho} (\Gamma^{\alpha}_{\mu\beta} \partial_\nu \Gamma^{\beta}_{\rho\alpha} + \frac{2}{3} \Gamma^{\alpha}_{\mu\gamma} \Gamma^{\gamma}_{\nu\beta} \Gamma^{\beta}_{\rho\alpha}), \tag{2}$$

where Γ is the usual Levi-Civita connection for the spacetime metric g.

To study the unitarity of the theory on the Minkowski space, we decompose the metric fluctuation $h_{\mu\nu} = g_{\mu\nu} - \eta_{\mu\nu}$ into their orthogonal parts:

$$\left\{ \begin{array}{l} h_{ij} = 2\partial_{(i}h_{j)} + \epsilon^{il}\epsilon^{jk}\phi_{jk}, \\ h_{0i} = \eta_i + \epsilon^{ij}\psi_j, \\ h_{00} = n. \end{array} \right. \quad \underset{\text{gauge fixing}}{\Rightarrow} \quad \left\{ \begin{array}{l} h_{ij} = \epsilon^{il}\epsilon^{jk}\phi_{jk}, \\ h_{0i} = \epsilon^{ij}\psi_j, \\ h_{00} = n. \end{array} \right. \tag{3}$$

Here subscripts on the indexless variables (ϕ, η, ψ) represent normalized spatial derivatives $\partial_i/\sqrt{-\partial^2}$. (Gauge invariance is used to set h_i and η of the metric to zero.) Substituting (3) into the action (1), we get

$$\begin{aligned} S &= \int d^3x \Big[\frac{\beta}{2}\tilde{\psi}\Box\tilde{\psi} + \frac{\sigma}{2}\tilde{\psi}^2 + \Big(\alpha + \frac{\beta}{2}\Big)[(\partial_k^2 n)^2 + (\Box\phi)^2] + 2\Big(\alpha + \frac{\beta}{4}\Big)(\partial_k^2 n)(\Box\phi) \\ &\quad - \frac{\sigma}{2}\phi\,\partial_k^2\, n + \frac{1}{2\mu}\tilde{\psi}(\partial_k^2 n - \Box\phi)\Big], \end{aligned} \tag{4}$$

If $\alpha + \frac{\beta}{2}$ is not zero,

$$\mathcal{L}_2 = \Big(\alpha + \frac{\beta}{2}\Big)\left[\partial_k^2 n + \frac{(\alpha + \frac{\beta}{4})\phi - \frac{\sigma}{4}\phi + \frac{1}{4\mu}\tilde{\psi}}{\alpha + \frac{\beta}{2}}\right]^2 - \frac{(\alpha + \frac{3}{8}\beta)\beta}{\alpha + \frac{\beta}{2}}(\Box\phi)^2 + \cdots. \tag{5}$$

We thus find that the theory has a dipole ghost unless $(\alpha + \frac{3}{8}\beta)\beta = 0$.

For $\alpha + \frac{3}{8}\beta = 0$, the $\tilde{\psi}$ and ϕ fields are not ghost if

$$\beta > 0, \quad \sigma \leq 0, \tag{6}$$

which is known as new massive gravity.

For $\beta = 0$, we must have $\sigma = +1$ in order to be free from ghost, and $\alpha > 0$ for stability. Then the theory is unitary, stable and possibly renormalizable though in 3D.

If $\alpha + \frac{\beta}{2}$=0, there is always ghost in the combination of $\nabla^2 n$ and ϕ. The result is summarized in Table 1 [4, 5].

Table 1: Unitary theories around Minkowski vacuum

α, β	σ	μ	number of modes
$\alpha = -\frac{3}{8}\beta, \beta > 0$	$\sigma = -1$	arbitrary	2 (1 for $\mu \to \infty$)
$\alpha = -\frac{3}{8}\beta, \beta > 0$	$\sigma = 0$	arbitrary	1
$\alpha > 0, \beta = 0$	$\sigma = +1$	$\mu = \infty$	1

We can also study the unitarity around maximally symmetric spaces (de Sitter and anti-de Sitter) using the parametrization:

$$h_{\mu\nu} = h^T_{\mu\nu} + \nabla_\mu\xi_\nu + \nabla_\nu\xi_\mu + \nabla_\mu\nabla_\nu\eta - \frac{1}{3}\bar{g}_{\mu\nu}\Box\eta + \frac{1}{3}\bar{g}_{\mu\nu}h, \tag{7}$$

$$\text{with} \;:\; \nabla^\lambda h^T_{\lambda\mu} = 0, \qquad \bar{g}^{\mu\nu}h^T_{\mu\nu} = 0, \qquad \nabla^\lambda\xi_\lambda = 0. \tag{8}$$

The quadratic action turns out to be

$$\begin{aligned}\mathcal{L}_2 &= \frac{1}{4}h^T_{\mu\nu}(\Box-2\Lambda)\Big[\{\beta(\Box-2\Lambda)+4(3\alpha+\beta)\Lambda+\sigma\}\bar{g}^{\mu\rho}\bar{g}^{\nu\sigma}+\frac{1}{\mu}\epsilon^{\mu\lambda\rho}\bar{g}^{\nu\sigma}\nabla_\lambda\Big]h^T_{\rho\sigma}\\ &\quad+\frac{1}{18}\hat{\eta}[(8\alpha+3\beta)\Box+4(3\alpha+\beta)\Lambda-\sigma]\Box\hat{\eta}\\ &\quad-\frac{1}{9}h[(8\alpha+3\beta)\Box+4(3\alpha+\beta)\Lambda-\sigma]\sqrt{\Box(\Box+3\Lambda)}\,\hat{\eta}\\ &\quad+\frac{1}{18}h[(8\alpha+3\beta)\Box+4(3\alpha+\beta)-\sigma](\Box+3\Lambda)h. \end{aligned}\tag{9}$$

By checking the residues of the propagators, one can show that the unitary and stable theories are classified as in Table 2 [5]. It is important to realize that this complete analysis is possible only by off-shell analysis. In particular, it turns out that the unitarity of the AdS irrep is not enough to ensure the unitarity of the field theory.

Table 2: Unitary theories around maximally symmetric spacetimes

α,β	Λ	σ	μ
$\alpha=-\frac{3}{8}\beta,\beta>0$	negative, $0>\Lambda>\Lambda_+$	$\sigma=-1$	arbitrary
$\alpha=-\frac{3}{8}\beta,\beta>0$	positive, $\frac{2}{\beta}>\Lambda>0$	$\sigma=-1$	arbitrary
$\alpha>0,\beta=0$	negative, $0>\Lambda>-\frac{1}{12\alpha}$	$\sigma=+1$	$\mu=\infty$
$\alpha<0,\beta=0$	negative, $\Lambda<-\frac{\sigma}{12\alpha}$, and $\Lambda\leq\frac{\sigma}{12\alpha}$	all	$\mu=\infty$
$\alpha>0,\beta=0$	positive, $\frac{1}{20\alpha}\geq\Lambda>0$	$\sigma=+1$	$\mu=\infty$

3 Renormalizability

Another important property of such higher derivative theory is whether it is renormalizable or not [6]. Though we can have topological mass term given by the gravitational Chern-Simons term, we do not consider it here for simplicity. The theory describes a massless spin-2 graviton (with positive excitation), a massive spin-2 (with negative excitation) and a massive scalar in general. We do not have to include Riemann squared because there is no independent Riemann tensor in 3D.

We define the fluctuation around the Minkowski background by $\tilde{g}^{\mu\nu}\equiv\sqrt{-g}\,g^{\mu\nu}=\eta^{\mu\nu}+\kappa h^{\mu\nu}$. We then find the quadratic term is given by

$$\begin{aligned}\mathcal{L}_2 = \frac{1}{4}h^{\mu\nu}\Big[&P^{(2)}(\beta\Box+\sigma)+P^{(0,s)}\{(8\alpha+3\beta)\Box-\sigma\}+2P^{(0,w)}\{(8\alpha+3\beta)\Box-\sigma\}\\ &+\sqrt{2}(P^{(0,sw)}+P^{(0,ws)})\{(8\alpha+3\beta)\Box-\sigma\}\Big]_{\mu\nu,\rho\sigma}\Box h^{\rho\sigma},\end{aligned}\tag{10}$$

where we have defined the projection operators as

$$
\begin{aligned}
&P^{(2)}_{\mu\nu,\rho\sigma} = \frac{1}{2}(\theta_{\mu\rho}\theta_{\nu\sigma} + \theta_{\mu\sigma}\theta_{\nu\rho} - \theta_{\mu\nu}\theta_{\rho\sigma}), \quad P^{(0,s)}_{\mu\nu,\rho\sigma} = \frac{1}{2}\theta_{\mu\nu}\theta_{\rho\sigma}, \\
&P^{(0,w)}_{\mu\nu,\rho\sigma} = \omega_{\mu\nu}\omega_{\rho\sigma}, \quad P^{(1)}_{\mu\nu,\rho\sigma} = \frac{1}{2}(\theta_{\mu\rho}\omega_{\nu\sigma} + \theta_{\mu\sigma}\omega_{\nu\rho} + \theta_{\nu\rho}\omega_{\mu\sigma} + \theta_{\nu\sigma}\omega_{\mu\rho}), \\
&P^{(0,sw)}_{\mu\nu,\rho\sigma} = \frac{1}{\sqrt{2}}\theta_{\mu\nu}\omega_{\rho\sigma}, \quad P^{(0,ws)}_{\mu\nu,\rho\sigma} = \frac{1}{\sqrt{2}}\omega_{\mu\nu}\theta_{\rho\sigma},
\end{aligned}
\tag{11}
$$

with

$$
\theta_{\mu\nu} = \eta_{\mu\nu} - \frac{\partial_\mu\partial_\nu}{\Box}, \qquad \omega_{\mu\nu} = \frac{\partial_\mu\partial_\nu}{\Box}. \tag{12}
$$

$P^{(2)}, P^{(1)}, P^{(0,s)}$ and $P^{(0,w)}$ are the projection operators onto spin 2, 1 and 0 parts, and they satisfy the completeness relation

$$
(P^{(2)} + P^{(1)} + P^{(0,s)} + P^{(0,w)})_{\mu\nu,\rho\sigma} = \frac{1}{2}(\eta_{\mu\rho}\eta_{\nu\sigma} + \eta_{\mu\sigma}\eta_{\nu\sigma}), \tag{13}
$$

on the symmetric second-rank tensors.

The gauge fixing term and Faddeev-Popov (FP) ghost terms are concisely written as

$$
\mathcal{L}_{GF+FP} = -B_\mu\partial_\nu h^{\mu\nu} - i\bar{c}_\mu\partial_\nu\mathcal{D}^{\mu\nu}{}_\rho c^\rho + \frac{a}{2}B_\mu B^\mu, \tag{14}
$$

where $\mathcal{D}^{\mu\nu}{}_\rho c^\rho \equiv \tilde{g}^{\mu\rho}\partial_\rho c^\nu + \tilde{g}^{\nu\rho}\partial_\rho c^\mu - \tilde{g}^{\mu\nu}\partial_\rho c^\rho - \partial_\rho\tilde{g}^{\mu\nu}c^\rho$, a is a gauge parameter and the indices are raised and lowered with the flat metric. Then the propagator is given by

$$
\begin{aligned}
D_{\mu\nu,\rho\sigma}(k) \;=\; &\frac{1}{(2\pi)^4}\Big[\frac{P^{(2)}}{k^2(\beta k^2 - \sigma)} + \frac{P^{(0,s)}}{k^2\{(8\alpha+3\beta)k^2+\sigma\}} \\
&-\frac{a}{2k^2}(2P^{(1)} + 2P^{(0,s)} + P^{(0,w)} - \sqrt{2}(P^{(0,sw)} + P^{(0,ws)})\Big]_{\mu\nu,\rho\sigma}.
\end{aligned}
\tag{15}
$$

The most important property is that it damps as k^{-4} for large momentum. It can be shown that the theory becomes power-counting super-renormalizable [6]. However, there are two important exceptional cases: $8\alpha + 3\beta = 0$ and $\beta = 0$. The former case corresponds to the new massive gravity. Although this theory is found to be unitary either for $8\alpha + 3\beta = 0$ or $\beta = 0$, the renormalizability fails precisely in these cases and the theory is not renormalizable. It may appear that the scalar modes decouples for $8\alpha + 3\beta = 0$ but the interaction breaks the decoupling [6].

4 Critical theories in higher dimensions

The three-dimensional topological gravity is known to describe massive spin 2, with positive excitation energy for $\sigma = -1$ (opposite to conventional sign). This means that the theory is not unitary for Einstein term with conventional sign $\sigma = +1$, which is inevitable in 4D. But BTZ black hole has positive mass for $\sigma = +1$. So there is a conflict between unitarity and positive energy. However for special CS coupling μ, the massive spin 2 becomes massless, and both can be positive for $\sigma = +1$. This is what is known as the critical theory. The theory is stable, and possibly unitary and renormalizable, with the possibility of extension to 4D.

Consider the problem in general dimensions with the action:

$$S = \frac{1}{2\kappa_D^2}\int d^D x\sqrt{-g}\left[R - 2\Lambda + \alpha R^2 + \beta R_{\mu\nu}^2 + \gamma R_{GB}^2\right]. \tag{16}$$

A straightforward calculation yields, for $D = 3$ and 4,

$$\begin{aligned}\mathcal{L}_2 \;=\;& \frac{1}{4}h_{\mu\nu}^T\Big(\Box - \frac{4}{(D-1)(D-2)}\Lambda\Big)\Big[\beta\Big(\Box - \frac{4}{(D-1)(D-2)}\Lambda\Big) \\ &+\frac{4}{D-2}\Lambda(D\alpha+\beta)+\sigma\Big]h_{\rho\sigma}^T + \frac{(D-1)(D-2)}{4D^2}\Big[\hat{\eta}\Delta\Box\hat{\eta} \\ &-2h\Delta\sqrt{\Box\Big(\Box + \frac{2D}{(D-1)(D-2)}\Lambda\Big)}\;\hat{\eta} + h\Delta\Big(\Box + \frac{2D}{(D-1)(D-2)}\Lambda\Big)h\Big],\end{aligned} \tag{17}$$

where we have defined

$$\begin{aligned}\hat{\eta} &\equiv \sqrt{\Box\Big(\Box + \frac{2D}{(D-1)(D-2)}\Lambda\Big)}\;\eta, \\ \Delta &\equiv \frac{4(D-1)\alpha + D\beta}{D-2}\Box - \frac{4(D-4)}{(D-2)^2}(D\alpha+\beta)\Lambda - \sigma.\end{aligned} \tag{18}$$

The condition for the absence of spin-0 mode is

$$4(D-1)\alpha + D\beta = 0 \quad\Leftrightarrow\quad \alpha + \frac{3}{8}\beta = 0 \text{ in 3D} \tag{19}$$

Then $\beta > 0$ was enough for the absence of ghost in 3D, because the Einstein term does not contain propagating mode in 3D. However here the situation is different in 4D. We have to require further the cancellation of the ghost mode from there. Requiring i) there is no spin-0 mode, ii) system is stable iii) there is a unique vacuum in the theory, we should have

$$\alpha = -\frac{D(D-3)}{(D-1)_2}\gamma, \quad \beta = \frac{4(D-3)}{D-2}\gamma, \quad \Lambda = -\frac{D}{8\alpha} = \frac{(D-1)_2}{8(D-3)\gamma}, \tag{20}$$

where we have defined $(D-m)_n = (D-m)(D-m-1)\cdots(D-n)$.

The system becomes Einstein plus Weyl-squared theory with a cosmological constant. However, generalizing the previous discussions of renormalizability in 3D, the theory is renormalizable without these restrictions (no hope of unitarity) but not with those.

5 Discussions

We have studied the unitarity, stability and renormalizability of 3D higher derivative gravity, and identified the conditions. We further extended the consideration to critical theory in 4D. It is quite surprising and/or disappointing that the unitarity and renormalizability are incompatible with each other.

We end this paper with possible future directions: 1. Study of quantum effects, in relation with asymptotic safety. 2. It would be interesting to find black hole solutions in critical theories. So far no such solutions has not been found in higher dimensions. 3. It may be useful to try to find BPS solutions with the recently developed critical supergravity. 4. Cosmological solutions should be interesting. 5. Quadratic action is special to 4 dimensions. Higher order terms are allowed in higher dimensions. The conditions for unitarity and so on are not known.

Acknowledgement:

I would like to thank the organizers for invitation to this wonderful workshop. This work was supported in part by the Grant-in-Aid for Scientific Research Fund of the JSPS (C) No. 20540283, No. 21 · 09225 and (A) No. 22244030.

References

[1] K. S. Stelle, Phys. Rev. D **16** (1977) 953.

[2] E. A. Bergshoeff, O. Hohm and P. K. Townsend, Phys. Rev. Lett. **102** (2009) 201301 [arXiv:0901.1766 [hep-th]].

[3] S. Deser, R. Jackiw and S. Templeton, Annals Phys. **140** (1982) 372 [Erratum-ibid. **185** (1988) 406]

[4] S. Deser, Phys. Rev. Lett. **103** (2009) 101302 [arXiv:0904.4473 [hep-th]].

[5] N. Ohta, Class. Quant. Grav. 29 (2012) 015002 [arXiv:1109.4458 [hep-th]].

[6] K. Muneyuki and N. Ohta, arXiv:1201.2058 [hep-th].

Cosmology and GR limit of Hořava-Lifshitz gravity

Shinji Mukohyama
IPMU, The University of Tokyo, Kashiwa, Chiba 277-8582, Japan
Email : shinji.mukohyama@ipmu.jp

Abstract

A power-counting renormalizable theory of gravitation recently proposed by Hořava has a number of intriguing cosmological implications. In particular, the anisotropic scaling with the dynamical critical exponent $z = 3$ solves the horizon problem and leads to scale-invariant cosmological perturbations even without inflation.

1 Introduction

One of the biggest difficulties in attempts toward the theory of quantum gravity is the fact that general relativity is non-renormalizable. This would imply loss of theoretical control and predictability at high energies. In January 2009, Hořava proposed a new theory of gravity to evade this difficulty by invoking a Lifshitz-type anisotropic scaling at high energy [1]. This theory, often called Hořava-Lifshitz gravity, is power-counting renormalizable and is expected to be renormalizable and unitary. Having a new candidate theory for quantum gravity, it is important to investigate its cosmological implications.

There are a number of interesting cosmological implications of Hořava-Lifshitz gravity. For example, higher spatial curvature terms lead to regular bounce solutions in the early universe. Higher curvature terms might also make the flatness problem milder. The anisotropic scaling provides a new mechanism for generation of primordial magnetic seed field, and also modifies the spectrum of gravitational wave background via a peculiar scaling of radiation energy density. In parity-violating version of the theory, circularly polarized gravitational waves can also be generated in the early universe. The lack of local Hamiltonian constraint leads to dark matter as an integration "constant".

In the following we first explain the anisotropic scaling as the idea behind power-counting renormalizability of the theory. We then argue that the anisotropic scaling with $z = 3$ solves the horizon problem and leads to scale-invariant cosmological perturbations, even without inflation [2]. For the construction of the theory and more detailed discussion of cosmology and general relativity limit, see the review [3] and the latest article [4].

2 Anisotropic scaling and power-counting renormalizability

2.1 Power-counting

Let us begin with heuristically explaining the usual power-counting argument in field theory. As the simplest example, let us consider a scalar field with the canonical kinetic term:

$$\frac{1}{2}\int dt d^3\vec{x}\ \dot{\phi}^2, \tag{1}$$

where an overdot represents a time derivative. The scaling dimension of the scalar field ϕ is determined by demanding that the kinetic term be invariant under the scaling

$$t \to bt, \quad \vec{x} \to bx, \quad \phi \to b^{-s}\phi, \tag{2}$$

where b is an arbitrary number and s is the scaling dimension to be determined. The invariance of the kinetic term under the scaling leads to the condition

$$1 + 3 - 2 - 2s = 0, \tag{3}$$

where 1 comes from dt, 3 from $d^3\vec{x}$, -2 from two time derivatives and $-2s$ from two ϕ's. Thus, we obtain $s = 1$. In other words, the scalar field scales like energy. With this scaling in mind, it is easy to see that an n-th order interaction term behaves as

$$\int dt d^3\vec{x}\phi^n \propto E^{-(1+3-ns)}, \tag{4}$$

where E is the energy scale of the system of interest. Here, the minus sign in the exponent comes from -1 in $E \to b^{-1}E$, 1 in the parentheses comes from dt, 3 from $d^3\vec{x}$ and $-ns$ from ϕ^n. Now, it is expected that we have a good theoretical control of ultraviolet (UV), i.e. high E, behaviors if the exponent is non-positive. Since $s = 1$, this condition leads to $n \leq 4$. This is the power-counting renormalizability condition.

We are interested in gravity. Unfortunately, Einstein gravity is not power-counting renormalizable. This is because the curvature is a highly nonlinear functional of the metric and there are graviton interaction terms with n higher than 4. The non-renormalizability is one of difficulties in attempts to quantize general relativity.

2.2 Abandoning Lorentz symmetry

As already stated, Hořava-Lifshitz gravity is power-counting renormalizable. How does it evade the above argument? The basic idea is very simple but potentially dangerous: abandoning Lorentz symmetry and invoking a different kind of scaling in the UV. The scaling invoked here, often called *anisotropic scaling* or *Lifshitz scaling*, is

$$t \to b^z t, \quad \vec{x} \to bx, \quad \phi \to b^{-s}\phi, \tag{5}$$

where z is a number called *dynamical critical exponent*.

Let us now see how the power-counting argument changes if the scaling is anisotropic as in (5). Invariance of the canonical kinetic term (1) under this scaling leads to

$$z + 3 - 2z - 2s = 0, \tag{6}$$

where z comes from dt, 3 from $d^3\vec{x}$, $-2z$ from two time derivatives and $-2s$ from two ϕ's. Then we obtain

$$s = \frac{3 - z}{2}. \tag{7}$$

This of course recovers the previous result $s = 1$ for $z = 1$. What is interesting here is that $s = 0$ if $z = 3$. This implies that, if $z = 3$, the amplitude of quantum fluctuations of ϕ does not change as the energy scale of the system changes. The n-th order interaction term behaves as

$$\int dt d^3\vec{x}\phi^n \propto E^{-(z+3-ns)/z}, \tag{8}$$

where $-1/z$ in the exponent comes from $-z$ in $E \to b^{-z}E$, z in the parentheses comes from dt, 3 from $d^3\vec{x}$ and $-ns$ from ϕ^n. For $z = 3$ (and thus $s = 0$), the exponent is negative for any n and, therefore, any nonlinear interactions are power-counting renormalizable. For $z > 3$, the theory is power-counting super-renormalizable.

¿From the above consideration, it is expected that gravity may become renormalizable if the anisotropic scaling with $z \geq 3$ is realized in the UV.

3 Scale-invariant cosmological perturbations from $z = 3$ scaling

In this section we show that the anisotropic scaling with the minimal z, i.e. $z = 3$, leads to a new mechanism for the generation of scale-invariant cosmological perturbations. Intriguingly, this mechanism works even without inflation.

3.1 Usual story with $z = 1$

Before explaining the new mechanism, let us remind ourselves of the usual story with $z = 1$.

Cosmological perturbations are analyzed by perturbative expansion around a FRW background. In the linearized level, perturbations are Fourier expanded and the evolution of each mode is characterized by the frequency ω defined by the dispersion relation

$$\omega^2 = c_s^2 \frac{k_c^2}{a^2}, \tag{9}$$

where c_s is the sound speed, k_c is the comoving wave number and a is the scale factor of the universe. For simplicity we assume that the time dependence of c_s, if any, is slow compared with the cosmological time scale H^{-1}, where $H = \dot{a}/a$ is the Hubble expansion rate. (For example, c_s is identically 1 for a canonical scalar field with any potential.)

If a mode of interest satisfies $\omega^2 \gg H^2$ then the evolution of the mode is not affected by the expansion of the universe and the mode just oscillates. When $\omega^2 \ll H^2$, on the other hand, the expansion of the universe is so rapid that the Hubble friction freezes the mode and the mode stays almost constant. Generation of cosmological perturbations from quantum fluctuations is nothing but the oscillation followed by the freeze-out. Therefore, the condition for generation of cosmological perturbations is

$$\frac{d}{dt}\left(\frac{H^2}{\omega^2}\right) > 0. \tag{10}$$

With the $z = 1$ dispersion relation (9), this condition is equivalent to $\ddot{a} > 0$ for expanding universe ($\dot{a} > 0$). Therefore, if $z = 1$ then generation of cosmological perturbations from quantum fluctuations requires accelerated expansion of the universe, i.e. inflation. For example, for power law expansion $a \propto t^p$, $p > 1$ is required.

Observational data of the cosmic microwave background strongly indicates that the primordial cosmological perturbations have an almost scale-invariant spectrum. It is easy to see that the scale-invariance also requires inflation. From the scaling (2) with $s = 1$, the amplitude of quantum fluctuations of the scalar field should be proportional to the energy scale of the system. In cosmology the energy scale is set by the Hubble expansion rate H. Thus, we expect that

$$\delta\phi \propto H. \tag{11}$$

Since cosmological perturbations with different scales are generated at different times, the scale-invariance is nothing but the constancy of the right hand side of (11). Noting that $H = \dot{a}/a$, this implies the exponential expansion of the universe $a \propto \exp(Ht)$, namely inflation.

We have seen that, for $z = 1$, both the generation of cosmological perturbations and the scale-invariance of generated perturbations require the existence of an inflationary epoch in the early universe.

3.2 The story in the UV with $z = 3$

The condition (10) for generation of cosmological perturbations is valid irrespective of the dispersion relation. In Hořava-Lifshitz gravity, to realize the anisotropic scaling (5), the dispersion relation for a physical degree of freedom in the UV should be

$$\omega^2 = M^2 \times \left(\frac{k_c^2}{M^2 a^2} \right)^z , \tag{12}$$

where M is some energy scale. By substituting this to the condition (10) we obtain $d^2(a^z)/dt^2 > 0$ for expanding universe ($\dot{a} > 0$). Since $z \geq 3$ in Hořava-Lifshitz gravity at high energy, generation of cosmological perturbations from quantum fluctuations does not require accelerated expansion of the universe, i.e. inflation. For example, power law expansion $a \propto t^p$ with $p > 1/z$ satisfies the condition.

In this way, the anisotropic scaling provides a solution to the horizon problem. Essential reason for this is that perturbations freeze-out not at the Hubble horizon but at the *sound horizon*, defined by $\omega \sim H$. The physical radius of sound horizon is thus $\sim (M^{z-1}H)^{-1/z}$. In the UV epoch ($H \gg M$), the sound horizon is far outside the Hubble horizon and can therefore accommodate scales much longer than the Hubble horizon size. In order to stretch microscopic scales to cosmological scales, we just need to have a long enough expansion history (satisfying the condition $d^2(a^z)/dt^2 > 0$) in the UV epoch. Note that M is not a cutoff scale of a low energy effective theory but is just the scale at which the theory starts exhibiting the anisotropic scaling, provided that Hořava-Lifshitz gravity is UV complete.

For general z, the formula (7) implies that the amplitude of quantum fluctuations of ϕ should be

$$\delta\phi \sim M \times \left(\frac{H}{M} \right)^{\frac{3-z}{2z}} , \tag{13}$$

where M is defined through the dispersion relation (12). This is of course consistent with the well-known result (11) for $z = 1$ and the result in ghost inflation $\delta\phi \sim (M^3 H)^{1/4}$ for $z = 2$. On the other hand, in Hořava-Lifshitz gravity with the minimal value of z ,i.e. $z = 3$, (13) is reduced to $\delta\phi \sim M$, implying that the amplitude of quantum fluctuations does not depend on the Hubble expansion rate. This means that the spectrum of cosmological perturbations in Hořava-Lifshitz gravity with $z = 3$ is automatically scale-invariant even without inflation.

3.3 A simple model

We have shown that the anisotropic scaling with $z = 3$ naturally leads to a new mechanism for generation of scale-invariant cosmological perturbations. As a simple implementation of the mechanism, let us consider a free scalar field described by the action

$$I = \frac{1}{2} \int dt d^3\vec{x} N \sqrt{g} \left[\frac{1}{N^2} (\partial_t \phi - N^i \partial_i \phi)^2 + \phi \mathcal{O} \phi \right] , \tag{14}$$

where

$$\mathcal{O} = \frac{\Delta^3}{M^4} - \frac{\kappa\Delta^2}{M^2} + c_\phi^2\Delta - m_\phi^2, \quad \Delta = g^{ij}D_iD_j \tag{15}$$

In the UV, the first term in $\mathcal{O}$ is dominant and the scalar field action exhibits the $z = 3$ scaling. In this regime it is easy to find the mode function in a flat FRW background as [2]

$$\phi_{\vec{k}_c} = \frac{e^{i\vec{k}_c\cdot\vec{x}}}{(2\pi)^3} \times 2^{-1/2}k_c^{-3/2}M\exp\left(-i\frac{k_c^3}{M^2}\int\frac{dt}{a^3}\right), \tag{16}$$

where a is the scale factor, t is the proper time, $\vec{k}_c$ is the comoving wave number and $k_c = |\vec{k}_c|$. Note that this is not just WKB approximation but actually exact and applicable to both subhorizon and superhorizon scales in any background $a(t)$, provided that the first term in $\mathcal{O}$ is dominant. The mode function approaches a constant value in the $a \to \infty$ limit if and only if the integral $\int^\infty dt/a^3$ converges. For power-law expansion $a \propto t^p$, this condition is satisfied if $p > 1/3$, and agrees with the condition for the freeze-out after oscillation discussed after (12). Provided that the integral converges, the power-spectrum is calculated as

$$\mathcal{P}_\phi = \frac{k_c^3}{2\pi^2}\left|(2\pi)^3\phi_{\vec{k}_c}\right|^2 = \left(\frac{M}{2\pi}\right)^2. \tag{17}$$

This is manifestly scale-invariant in accord with the general argument after (13). In this way, scale-invariant cosmological perturbations of the scalar field can be generated even without inflation.

After scales of interest exit the sound horizon, cosmological perturbations of the scalar field can be converted to curvature perturbations by either curvaton mechanism or modulated decay of heavy particles or/and oscillating fields. For example, it is possible to suppose that the scalar field ϕ itself plays the role of a curvaton [2]. When the Hubble expansion rate becomes as low as m_ϕ, ϕ starts rolling and eventually decays to radiation. Perturbations of ϕ are converted to those of radiation energy density and thus curvature perturbations.

In the IR, the first two terms in $\mathcal{O}$ can be neglected and the usual $z = 1$ scaling is recovered. In this epoch, unless the universe is in an inflationary phase, physical scales re-enter the horizon as usual.

References

[1] P. Horava, Phys. Rev. D **79**, 084008 (2009) [arXiv:0901.3775 [hep-th]].

[2] S. Mukohyama, JCAP **0906**, 001 (2009) [arXiv:0904.2190 [hep-th]].

[3] S. Mukohyama, Class. Quant. Grav. **27**, 223101 (2010) [arXiv:1007.5199 [hep-th]].

[4] A. E. Gumrukcuoglu, S. Mukohyama and A. Wang, Phys. Rev. D **85**, 064042 (2012) [arXiv:1109.2609 [hep-th]].

Phan Bao Ngoc, Pham Ngoc Diep, Nguyen van Khanh and Nguyen Anh Vinh

Koji Hashimoto and Nobuyoshi Ohta

Revisit to Bubbles and Walls

Bum-Hoon Lee[1] *& Wonwoo Lee*[2]
[1] *Department of Physics and BK21 Division, Sogang University, Seoul 121-742, Korea*
[2] *Center for Quantum Spacetime, Sogang University, Seoul 121-742, Korea*
Email : bhl@sogang.ac.kr

Abstract

We discuss the nucleation process of a bounce solution in this presentation. If the theory has multiple minima then the false vacuum state decays to the true vacuum state, i.e. the phase transition proceeds by the nucleation of a vacuum bubble. After the nucleation in Euclidean space, we apply the analytic continuation to Lorentzian spacetime. We discuss the collision of the nucleated vacuum bubbles in Lorentzian spacetime.

1 Introduction

If we imagine the very early universe had have the high vacuum energy including the very high density and temperature, then we want to know how the high vacuum energy can decay to the lower one accorded with recent cosmological observations [1]. The theory of phase transition at finite temperature may become one of the most useful tools to describe reducing the vacuum energy. To simplify things, once we consider a potential barrier between the symmetric and broken phases. If there is a barrier between them, the transition corresponds to the first-order phase transition. Otherwise, the transition corresponds to the second-order phase transition. If we step into the questions on the initial state or the beginning of our universe, we may stand on speculations to answer the complicated questions. We may speculate on the nothing and the something. Vilenkin proposed the beginning of the universe by a tunneling process from nothing [2], in which nothing means a state without the concept of classical spacetime [3]. The authors in Ref. [4] also proposed our universe closed and rounded off in the past, consequently there is no boundary to the past. It seems to avoid the initial singularity. Sometimes one has an attempt to venture into directly eliminating the initial singularity; for example, by a repulsive force in the context of loop quantum cosmology [5].

On the other hand, the discovery of the eternal inflationary scenario [2, 6, 7] and the string theory landscape [8, 9] caused the revival of an inflationary multiverse scenario [10], in which it would seem that the author wanted to suggest a universe without the cosmological singularity problem using an interesting feature of self-reproducting or regenerating exponentially expanding universe. The eternal inflation is related to the expanding false vacuum with a positive cosmological constant, which means that the inflation is eternal into the future. If the theory has multiple minima then the false vacuum state decays to the true vacuum state, i.e. the phase transition proceeds by the nucleation of a vacuum bubble. The string theory landscape is a theory that involves a huge number of different metastable and stable vacua [11, 12], which were caused by different choices of Calabi-Yau manifolds and generalized magnetic fluxes. The huge number of different vacua can be approximated by the potential of a scalar field. The important thing is the fact that once de Sitter vacuum can exist then the inflationary expansion is eternal into the future and has the possibility of self-reproduction.

¿From above scenarios, the study whether the tunneling process in the potential with stable and metastable vacua, or even tachyonic behavior is possible has been acquired renewed interest. In this work, we study the tunneling process under the simple double well potential as a toy model. To obtain the general solutions including the effect of the backreaction by the solution, we solve the coupled equations for the gravity and the scalar field simultaneously. Although the model is a simple toy model, it may still be useful as an example of how the tunneling process occurs in various shapes of the potential provided by the above scenarios.

In the next section, we set up the basic framework for this work. In section 3, we simple present the possible types of a vacuum bubble. In section 4, we introduce our work on the collision of vacuum bubbles. The results are discussed in section 5.

2 The setup for this work

Let us consider the following action:

$$S = \int_{\mathcal{M}} \sqrt{-g} d^4 x \left[\frac{R}{2\kappa} - \frac{1}{2} \nabla^{\alpha} \Phi \nabla_{\alpha} \Phi - U(\Phi) \right] + \oint_{\partial \mathcal{M}} \sqrt{-h} d^3 x \frac{K - K_o}{\kappa}, \tag{1}$$

where $g \equiv det g_{\mu\nu}$, $\kappa \equiv 8\pi G$, R denotes the scalar curvature of the spacetime $\mathcal{M}$, K and K_o are the traces of the extrinsic curvatures of $\partial\mathcal{M}$ in the metric $g_{\mu\nu}$ and $\eta_{\mu\nu}$, respectively, and the second term on the right-hand side is the boundary term [13]. The gravitational field equations can be obtained properly from a variational principle with this boundary term. This term is also necessary to obtain the correct action.

The potential $U(\Phi)$, which represents the energy density of a homogeneous and static scalar field, has two non-degenerate minima one corresponding to the metastable vacuum or the false vacuum and the other to the true vacuum, separated by a potential barrier:

$$U(\Phi) = \frac{\lambda}{8} (\Phi^2 - a^2)^2 + \frac{\epsilon}{2a} (\Phi + a) + U_o, \tag{2}$$

where λ, ϵ, and a are positive parameters.

In the semiclassical approximation, the background vacuum decay rate or the bubble nucleation rate per unit time per unit volume is given by

$$\Gamma / V \simeq A e^{-B}, \tag{3}$$

where the leading semiclassical exponent B coincides with the difference between Euclidean action corresponding to bubble solution and that of the background, and the subleading prefactor A was studied in Refs. [14]. We are interested in finding the coefficient B.

To evaluate B and show the existence of the solution, one has to take the analytic continuation to Euclidean space. We assume the $O(4)$ symmetry for both the geometry and the scalar field as in Ref. [15]

$$ds^2 = d\eta^2 + \rho^2(\eta) \left[d\chi^2 + \sin^2 \chi \left(d\theta^2 + \sin^2 \theta d\phi^2 \right) \right]. \tag{4}$$

In this case Φ and ρ depend only on η, and the Euclidean field equations for them can be written in the form:

$$\Phi'' + \frac{3\rho'}{\rho} \Phi' = \frac{dU}{d\Phi} \text{ and } \rho'' = -\frac{\kappa}{3} \rho (\Phi'^2 + U), \tag{5}$$

respectively and the Hamiltonian constraint is given by

$$\rho'^2 - 1 - \frac{\kappa \rho^2}{3} \left(\frac{1}{2} \Phi'^2 - U \right) = 0. \tag{6}$$

In order to yield the solution the constraint requires a delicate balance among the terms.

Now we have to consider the boundary conditions to solve Eqs. (5) and (6). There are two different methods. The first one is an initial value problem, in which we impose the initial conditions for the equations. For this to work, initial conditions are provided for the values of the fields ρ and Φ or their derivatives ρ' and Φ' at $\eta = 0$ as follows:

$$\rho|_{\eta=0} = 0, \quad \frac{d\rho}{d\eta}\Big|_{\eta=0} = 1, \quad \Phi|_{\eta=0} = \Phi_o, \quad \text{and} \quad \frac{d\Phi}{d\eta}\Big|_{\eta=0} = 0, \tag{7}$$

where the first condition means that the space including a solution is a geodesically complete space. The second condition stems from Eq. (6). The fourth condition $\Phi' = 0$ is due to the regularity condition as can be seen from the first equation in Eq. (5). However, the third condition for the initial value of Φ is not determined. One should find the initial value of Φ using the undershoot-overshoot procedure. The other method is a boundary value problem or a two boundary value problem. We impose conditions specified at $\eta = 0$ and $\eta = \eta_{max}$. For this to work, we choose the values of the field ρ and derivatives of the field Φ as follows:

$$\rho|_{\eta=0} = 0, \quad \rho|_{\eta=\eta_{max}} = 0, \quad \frac{d\Phi}{d\eta}\Big|_{\eta=0} = 0, \quad \text{and} \quad \frac{d\Phi}{d\eta}\Big|_{\eta=\eta_{max}} = 0. \tag{8}$$

η_{max} is the maximum value of η and will have a finite value. These conditions are useful for obtaining solutions with Z_2 symmetry.

In order to solve the Euclidean field Eqs. (5) and (6) numerically, we use dimensionless variables as in Ref [16].

3 Classification of vacuum bubbles

In the present proceedings, we shall be simply presenting the possible types of a vacuum bubble.

- The types of true vacuum bubbles [17, 18]: (1) flat bubble - large dS background, (2) flat bubble - half dS background, (3) flat bubble - small dS background, (4) AdS bubble - large dS background, (5) AdS bubble - flat dS background, (6) AdS bubble - small dS background, (7) dS small bubble - large dS background, (8) dS small bubble - flat dS background, (9) dS small bubble - small dS background, (10) AdS bubble - flat infinite background, (11) AdS bubble - AdS infinite background, (12) AdS bubble - flat finite background, (13) AdS bubble - AdS infinite background.

- The types of false vacuum bubbles [18]: (1) dS large bubble - dS small background, (2) dS half bubble - dS small background, (3) dS small bubble - dS small background, (4) dS large bubble - flat finite background, (5) dS half bubble - flat finite background, (6) dS small bubble - flat finite background, (7) dS large bubble - AdS finite background, (8) dS half bubble - AdS finite background, (9) dS small bubble - AdS finite background, (10) flat bubble - AdS finite background, (11) AdS bubble - AdS finite background.

4 Collision of vacuum bubbles

In the multiverse and cosmic landscape, study of the nucleation and subsequent dynamics of vacuum bubbles is illuminated again. On the other hand, after the primordial inflation ended some unnecessary massive particles can be overproduced [19]. Such massive particles should disappear, and this may be possible by introducing thermal inflation. In many phenomenological models of thermal inflation, it will be ended by the first order phase transition, not the second order phase transition [20]. Therefore, our universe may have some signs of the first order phase transition, bubble nucleation, and bubble percolation. With these motivations, we have studied vacuum bubble collisions with various potentials in the presence of gravity, assuming spherical, planar, and hyperbolic symmetry. We used numerical calculations from double-null formalism. We also tested symmetric and asymmetric bubble collisions, and saw details of causal structures. If the colliding energy is sufficient, then the vacuum can be destabilized, and it was also demonstrated [21].

5 Summary and Discussions

In this presentation, we have discussed bounce and instanton solutions with $O(4)$ symmetry in curved space. we have obtained numerical solutions as well as performed the analytic computations using the thin-wall approximation. There are 13 types of true vacuum bubbles and 11 types of false vacuum bubbles. We also discussed vacuum bubble collisions with various potentials in the presence of gravity.

Acknowledgments

This work was supported by the Korea Science and Engineering Foundation (KOSEF) grant funded by the Korea government(MEST) through the Center for Quantum Spacetime(CQUeST) of Sogang University with grant number R11 - 2005 - 021. WL was supported by the National Research Foundation of Korea Grant funded by the Korean Government (Ministry of Education, Science and Technology)[NRF-2010-355-C00017].

References

[1] A. G. Riess *et al.* [Supernova Search Team Collaboration], *Observational evidence from supernovae for an accelerating universe and a cosmological constant*, Astron. J. 116 (1998) 1009 [astro-ph/9805201]; S. Perlmutter *et al.* [Supernova Cosmology Project Collaboration], *Measurements of Omega and Lambda from 42 high redshift supernovae*, Astrophys. J. 517 (1999) 565 [astro-ph/9812133].

[2] A. Vilenkin, *The Birth of Inflationary Universes*, Phys. Rev. D 27 (1983) 2848.

[3] A. Vilenkin, *Quantum Origin Of The Universe*, Nucl. Phys. B252 (1985) 141.

[4] J. B. Hartle and S. W. Hawking, *Wave Function of the Universe*, Phys. Rev. D 28 (1983) 2960.

[5] M. Bojowald, *Absence of singularity in loop quantum cosmology*, Phys. Rev. Lett. 86 (2001) 5227 [gr-qc/0102069].

[6] A. D. Linde, *Eternally Existing Selfreproducing Chaotic Inflationary Universe*, Phys. Lett. B 175 (1986) 395.

[7] A. H. Guth, *Inflation and eternal inflation*, Phys. Rep. 333-334 (2000) 555 [astro-ph/0002156].

[8] R. Bousso and J. Polchinski, *Quantization of four form fluxes and dynamical neutralization of the cosmological constant*, J. High Energy Phys. 06 (2000) 006 [hep-th/0004134].

[9] L. Susskind, *The Anthropic landscape of string theory*, [hep-th/0302219].

[10] A. D. Linde, *Nonsingular Regenerating Inflationary Universe*, Cambridge University preprint, Print-82-0554.

[11] S. Kachru, R. Kallosh, A. Linde, and S. P. Trivedi, *De Sitter vacua in string theory*, Phys. Rev. D 68 (2003) 046005 [hep-th/0301240].

[12] S. K. Ashok and M. R. Douglas, *Counting flux vacua*, J. High Energy Phys. 01 (2004) 060.

[13] J. W. York, Jr., *Role Of Conformal Three Geometry In The Dynamics Of Gravitation*, Phys. Rev. Lett, 28 (1972) 1082; G. W. Gibbons and S. W. Hawking, *Action Integrals And Partition Functions In Quantum Gravity*, Phys. Rev. D 15 (1977) 2752.

[14] C. G. Callan, Jr. and S. R. Coleman, *The Fate Of The False Vacuum. 2. First Quantum Corrections*, Phys. Rev. D 16 (1977) 1762.

[15] S. Coleman and F. De Luccia, *Gravitational Effects On And Of Vacuum Decay*, Phys. Rev. D 21 (1980) 3305.

[16] W. Lee, B.-H. Lee, C. H. Lee, and C. Park, *The False Vacuum Bubble Nucleation Due To A Nonminimally Coupled Scalar Field*, Phys. Rev. D 74 (2006) 123520.

[17] B.-H. Lee and W. Lee, *Vacuum Bubbles In A De Sitter Background And Black Hole Pair Creation*, Classical Quantum Gravity 26 (2009) 225002.

[18] B.-H. Lee, C. H. Lee, W. Lee, and C. Oh, in preparation.

[19] D. H. Lyth and E. D. Stewart, *Thermal Inflation And The Moduli Problem*, Phys. Rev. D 53 (1996) 1784 [hep-ph/9510204].

[20] R. Easther, J. T. Giblin, E. A. Lim, W. I. Park and E. D. Stewart, *Thermal Inflation And The Gravitational Wave Background*, J. Cosmol. Astropart. Phys. 05 (2008) 013 [arXiv:0801.4197 [astro-ph]].

[21] D.-i. Hwang, B.-H. Lee, W. Lee, and D.-h. Yeom, *Bubble collision with gravitation*, [arXiv:1201.6109 [gr-qc]].

Quantum Gravity Corrections to the Cosmological Term

Takeo Inami & Yoji Koyama
Department of Physics, Chuo University, Bunkyo-ku, Tokyo 112, Japan
Email : inami@phys.chuo-u.ac.jp, koyama@phys.chuo-u.ac.jp

Abstract

The cosmological constant problem is a sort of hierarchy problem; the Λ is huge at high energy scale and quite small at low energy. We study the graviton loop corrections to the cosmological term Λ in de Sitter space as an approach to the cosmological constant problem. Since gravitons couple the Λ through $\sqrt{-g}$, the Λ can be regarded as a coupling constant. Hence the graviton tadpole diagrams correspond to the loop corrections to the Λ. We are particularly interested in the possible infrared divergences present in the loop corrections and its interpretation for the purpose of finding the screening mechanism of the Λ in the infrared region. In de Sitter space due to the presence of the interaction terms with the Λ, the infrared divergences may arise at two-loop and higher orders. We calculate the graviton two-loop contributions to the tadpole diagrams and evaluate the infrared effects.

1 Introduction

There are many attempts to solving the cosmological constant problem. We are interested in the infrared effects from the graviton loops on the cosmological term in de Sitter space. This work is in progress.

2 Λ as a coupling constant

The main idea is as follows. In Einstein-Hilbert action, graviton couples Λ through $\sqrt{-g}$, $S = \int d^4x(\cdots - h\Lambda + \cdots)$. The graviton loop correction of Λ is corresponds to the tadpole diagrams. The infrared effect may arise

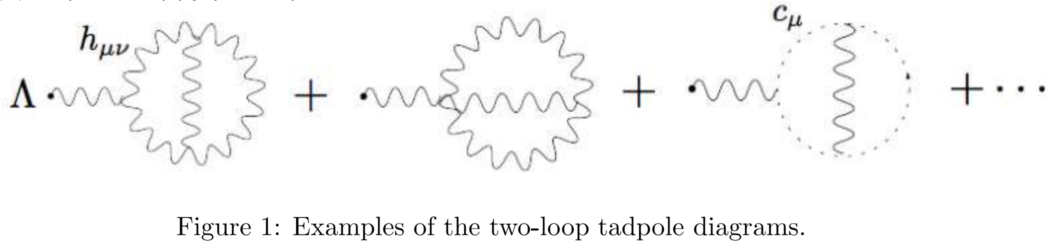

Figure 1: Examples of the two-loop tadpole diagrams.

We apply the renormalization group method to the running of Λ. In de Sitter space the coupling constants may also have the time dependence. In this case it is necessary to use the dynamical renormalization group method [1]. If the screening occurs, Λ could be effectively small at low energy scale. The explicit calculation of the two-loop tadpole diagrams was first performed by Tsamis and Woodard [2].

3 Infrared divergences

Infrared divergences may arise from the vertex integrals $\int dt \int d^3x$. In curved spaces the in-in formalism is needed to calculate the correlation functions or the expectation values of operators. In this formalism the upper limits of the time integrations are automatically introduced. Hence there is no infrared divergences from the time integrals. Instead of the infrared divergences, the time dependence is introduced.

4 Various problems

There are some problems that we should take into account [3] but the proper treatments of them and the relationship with the screening of the cosmological constant are unclear for us now.

References

[1] C. P. Burgess, L. Leblond, R. Holman and S. Shandera, JCAP **1003**, 033 (2010) [arXiv:0912.1608 [hep-th]].

[2] N. C. Tsamis and R. P. Woodard, Nucl. Phys. B **474**, 235 (1996) [arXiv:hep-ph/9602315].

[3] S. B. Giddings and M. S. Sloth, arXiv:1109.1000 [hep-th]; S. B. Giddings and M. S. Sloth, Phys. Rev. D **84**, 063528 (2011) [arXiv:1104.0002 [hep-th]]; Y. Urakawa and T. Tanaka, Prog. Theor. Phys. **122**, 779 (2009) [arXiv:0902.3209 [hep-th]]; Y. Urakawa and T. Tanaka, Prog. Theor. Phys. **125**, 1067 (2011) [arXiv:1009.2947 [hep-th]]; C. P. Burgess, R. Holman, L. Leblond and S. Shandera, JCAP **1010**, 017 (2010) [arXiv:1005.3551 [hep-th]]; M. Sasaki, Private communication.

Inhomogeneous loop quantum cosmology: approximated FRW cosmologies from the hybrid Gowdy model with matter

Daniel Martín-de Blas[1], *Mercedes Martín-Benito*[2],
Guillermo A. Mena Marugán[1]
[1]*Instituto de Estructura de la Materia, IEM-CSIC, Serrano 121, 28006 Madrid, Spain.*
[2]*MPI für Gravitational Physiscs, AEI, Am Mühlenberg 1, D-14476 Potsdam, Germany.*
Email : daniel.martin@iem.cfmac.csic.es

Abstract

We quantize the linearly polarized Gowdy T^3 model with a massless scalar field by applying a hybrid quantization that combines Loop Quantum Cosmology and Fock quantizations. This model allows us to modelize flat Friedmann-Robertson-Walker cosmologies filled with inhomogeneities, providing a perfect scenario to study the quantum back-reaction of inhomogeneities on a loop quantized homogeneous and isotropic background.

1 Introduction

Loop Quantum Cosmology (LQC) [1] applies a polymeric representation to quantize symmetry reduced systems. Cosmological singularities are resolved by employing this quantization. To extend LQC to inhomogeneous cosmological systems, a hybrid quantization has been developed using the vacuum Gowdy T^3 model [2]. This hybrid quantization combines a Fock quantization for the inhomogeneities with the LQC quantization for the homogeneous degrees of freedom.

With the aim of extending this hybrid quantization to more realistic models, we introduce in the Gowdy T^3 model a minimally coupled massless scalar field with the same symmetries as the geometry. Owing to the inclusion of matter, the model admits as subset of homogeneous and isotropic solutions those of the flat Friedmann-Robertson-Walker (FRW) model. This allows us to regard the model as a(n approximated) loop quantum FRW background with inhomogeneities propagating on it. The hybrid quantization of this model leads to the resolution of the initial singularity and the recovering of the standard Fock quantization for the inhomogeneities. We summarize here this approach, which has been detailed in Ref. [3].

2 The model and its hybrid quantization

The Gowdy T^3 model represents globally hyperbolic spacetimes with three torus spatial topology and two axial commuting Killing vector fields. After a symmetry reduction and a partial gauge fixing [2] the model can be regarded as a Bianchi I geometry with a homogeneous massless scalar field, as homogeneous background, filled with matter inhomogeneities and gravitational waves propagating along one spatial direction $\theta \in S^1$ [3]. For simplicity, we will consider the case with local rotational symmetry (LRS) where the scale factors in the two homogeneous directions evolve in identical way. Two global constraints remain to be imposed at the quantum level, the momentum constraint, $\mathcal{C}_\theta$, that generates rigid rotations in θ, and the Hamiltonian constraint, $\mathcal{C}$.

We quantize the model by means of a hybrid approach [2, 3]. For the (LRS-)Bianchi I background we adopt the *improved dynamics* of LQC [1], namely we describe the Bianchi I phase space with the coefficients of the densitized triad and the holonomies of its conjugate variable. The (LRS-)Bianchi I kinematical Hilbert space is the completion of the space spanned by the states $|\Lambda, v\rangle$ ($\Lambda \in \mathbb{R}$, $v \in \mathbb{R}^+$) in the discrete norm. The label v is proportional to the Bianchi I volume while Λ parameterizes the anisotropy in direction θ. The triad operators act diagonally on these states while the holonomy operators shift the v and Λ labels.

We quantize both matter (M) and gravitational (G) inhomogeneities using a privileged Fock quantization, obtained by demanding unitarity of the evolution and invariance of the vacuum under the gauge symmetries. These requirements select uniquely the field parameterizations and the vacuum state. As a result, we obtain two identical Fock spaces, $\mathcal{F}^f (f = M, G)$, one for each kind of inhomogeneities. An orthonormal basis is provided by the n-particle states. Finally, for the homogeneous mode of the matter field, we employ a standard Schrödinger representation.

The representation of the momentum constraint in terms of the creation and annihilation operators is straightforward. The states that satisfy the condition imposed by this constraint define a proper Fock subspace of $\mathcal{F}^M \otimes \mathcal{F}^G$.

The Hamiltonian constraint operator can be written as a sum of three terms: the Hamiltonian constraint of the flat FRW model coupled to a massless scalar, a term accounting for the anisotropies and a term accounting for the inhomogeneities (see [3] for the details). It turns out that matter and gravitational inhomogeneities contribute to the constraint in identical way. This constraint operator is constructed in such a way that it decouples the states of zero homogeneous volume ($v = 0$), and then we can remove the states analogue to the classical singularity. Moreover, it superselects the Λ and v labels, allowing us to restrict our study to a separable *superselection sector* [2]. The imposition of this constraint leads to a difference equation in v. The solutions are determined by initial data on the section of minimum v, and then we can characterize the physical Hilbert space with the Hilbert space of these initial data.

3 Conclusions

The linearly polarized Gowdy T^3 model with a minimally coupled massless scalar field is fully quantized by using a hybrid quantization that combines LQC and Fock quantizations. The initial singularity is resolved and the standard Fock quantization of the inhomogeneities is recovered.

The inclusion of the matter field does not add technical difficulties in the application of the hybrid quantization since both kind of inhomogeneities are treated in the very same way. However, the system obtained is physically more interesting than the vacuum one. In fact, the homogeneous sector of the model admits now flat FRW solutions and therefore the model provides a perfect scenario to study the quantum back-reaction of inhomogeneities on a loop-quantized flat FRW background, as well as the development of approximated methods in LQC aimed at extracting physical predictions from the theory.

Acknowledgements

This work was supported by the Spanish MICINN/MINECO Projects No. FIS2008-06078-C03-03 and No. FIS2011-30145-C03-02, and the Consolider-Ingenio Program CPAN No. CSD2007-00042. D. M-dB is supported by CSIC and the ESF under the Grant No. JAEPre-09-01796.

References

[1] A. Ashtekar and P. Singh, *Class. Quant. Grav.* **28**, 213001 (2011).

[2] L. J. Garay, M. Martín-Benito and G. A. Mena Marugán, *Phys. Rev.* D **82**, 044048 (2010).

[3] M. Martín-Benito, D. Martín-de Blas and G. A. Mena Marugán, *Phys. Rev.* D **83**, 084050 (2011).

The Casimir Force in a Schwarzschild Metric: A Proposed Experiment

Munawar Karim[1], *Ashfaque H. Bokhari*[2]
[1] *Department of Physics, St. John Fisher College, Rochester, NY 14618*
[2] *Department of Mathematics and Statistics,*
King Fahd University of Petroleum and Minerals, Dhahran, 31261, Saudi Arabia
Email : karim@sjfc.edu

Abstract

We propose an experiment to measure the Casimir force in the Schwarzschild metric on Earth;s surface. The apparatus, method of measurement and expected sensitivity is described.

1 Introduction

We propose an experiment to answer the question "do virtual quantum excitations follow geodesics?" [1]. Our apparatus is a pair of parallel plates. There is a second pair of identical plates, oriented perpendicular to the first pair. We measure the difference of the Casimir force between them. The apparatus is located on Earth's surface, aligned east-west. R^r_r and R^θ_θ elements of the Ricci tensor couple to the plates. Ricci tensor elements are calculated from the Schwarzschild metric on Earth's surface.

1.1 Description of Experiment

The Casimir force is the result of an imbalance in vacuum fluctuations [3]. A stress tensor represents the Casimir force. The tensor is renormalized and traceless [2].

$$\langle T^{\mu\nu} \rangle = \frac{\pi^2 \hbar c}{180\ d^4} \left(\frac{1}{4} \eta^{\mu\nu} - \widehat{x}^\mu \widehat{x}^\nu \right) \tag{1}$$

It is not known whether the Einstein tensor couples to a stress tensor whose source is vacuum fluctuations (equivalently if vacuum fluctuations follow geodesics). Our experiment is designed to clarify this question.

The experiment is a designed to measure the difference between the interaction of the elements R^r_r and R^θ_θ on the two Casimir plates. The apparatus is shown in the figure above.

The apparatus is rotated about the East-West axis. This serves to modulate the signal. The signal appears at twice the frequency of rotation.

1.2 Apparatus and sensitivity

The pairs of Casimir plates form two arms of an AC-bridge. Differences in the Casimir force show up as an imbalance in the null signal. With careful control of systematic uncertainities we estimate a detection sensitivity of the force difference (if it exists) of about 5 parts in 10^{10}. The presence or absence of a signal will provide the answer to the question.

Figure 1: Orthogonal pairs of Casimir plates. Polar and radial elements of the Ricci tensor couple to different plates

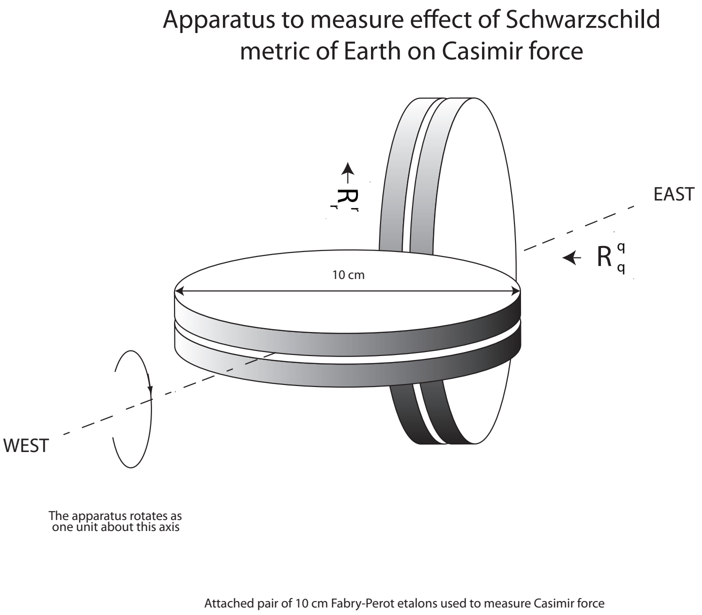

References

[1] M Karim, AH Bokhari, BJ Ahmedov, Class. Quantum Gravity vol.7, (2000)

[2] LS Brown and GJ Maclay, Phys. Rev., vol. 184 (1969)

[3] HBG Casimir, Proc. Ned. Aka. Wettenshappen, Amsterdam vol. 51, 793 (1948)

A Conflict of Quantum Predictions Related to the Equivalence Principle

Steve Wilburn[1], *Douglas Singleton*[2]
[1] *California State University, Fresno*
[2] *California State University, Fresno*
Email : SWilburn@csufresno.edu

Abstract

Observers in the space-time of a black hole and accelerating observers are both predicted to measure a particular temperature - the Hawking temperature for the fixed observer near a black hole; the Unruh temperature for the accelerated observer. We compare the temperatures measured by a static observer near a black hole with the temperature measured by an accelerating observer. For the same local acceleration these observers will measure different temperatures, thus allowing one to distinguish the two cases and giving a violation of the equivalence principle. As the static observer near the black hole approaches the horizon the two temperatures approach the same value and the equivalence principle is restored.

1 Introduction

The equivalence principle, as stated by Einstein in [1] equates the local acceleration of a stationary observer in a gravitational background to linear acceleration of an observer in flat Minkowski spacetime. From this local coordinate transformation comes all of General Relativity.

It has been shown that both of the situations described are predicted to give rise to a temperature through quantum effects [2][3]. In the case of a stationary observer in a gravitational background the temperature measured is known as the Hawking temperature, while a linearly accelerated observer in flat spacetime measures what is called the Unruh temperature.

In our published paper [4] we explored whether these two situations, when accounting for these purely quantum phenomena, remained exactly 'equivalent'.

2 Temperature Measurements

A massless scalar field, $\phi(\mathbf{x})$, is used as the test model for the predictions. The evolution of the scalar field is described by the Klein-Gordon wave equation. The field ϕ is expanded about the wave-mode solutions to the Klein-Gordon equation in a given spacetime. In general our calculations are not affected by reducing the situations to 2-Dimensions and so our calculations deal only with $\phi(x,t)$ Coupling ϕ to an Unruh-DeWitt detector allows an observation of excitations due to the presence of particles, which can be interpreted in the usual way as a temperature.

The details of all calculations are found properly in a combination of references [4][5]. The results of the calculations agree with the commonly accepted predictions for both the Hawking and Unruh temperatures.

$$k_B T_{U,M} = \frac{\hbar a}{2\pi c} \tag{1}$$
$$k_B T_{H,U} = \frac{\hbar c^3}{8\pi GM\sqrt{1-2GM/c^2R}} \tag{2}$$

2.1 Vacua

The subscripts U,M and H,U indicate that the calculation for the Unruh temperature was calculated with respect to the Minkowski vacuum and the Hawking temperature with respect to the Unruh vacuum. These are important details. These vacua were specified for good physical reasons.

In the case of a linearly accelerated observer one can define a vacuum (the ground state of the allowed wave-mode solutions for ϕ) with respect to many sets of coordinates. Choosing coordinates (x,t) to describe the position of the observer as measured by a lab frame leads to a hyperbolic trajectory. This result is commonly known as the Rindler observer. This choice leads to the predicted Unruh temperature in (1) and corresponds to an observer accelerating through an intertial vacuum. Choosing instead to calculate the response of the Unruh-DeWitt detector with respect to 'Rindler Coordinates' (η,ζ) assumes that the accelerated observer travels along with a vacuum defined through these naturally accelerated coordinates and leads to the measurement of 0 temperature. This calculation does not reflect the intended construction of the situation and so we use the first result, which is widely accepted.

The Hawking temperature is fraught with similar concerns in the choice of vacuum. Choosing simply to formulate the vacuum with respect to Schwarzschild coordinates leads to a measurement of 0 temperature. This choice also leads to a divergence of the energy-momentum tensor at the event horizon. This ramification leads us to similarly reject this formulation as being unsimilar to the situation we wished to construct. The more proper definition of the gravitational vacuum comes through the use of Kruskal coordinates which rightly place any singularities at the origin of the coordinate system, where we expect it to be. The Kruskal coordinates define a vacuum known as the Unruh vacuum, in which the Unruh-DeWitt detector is predicted to measure the accepted Hawking temperature in (2).

3 Results

The magnitude of the acceleration measured by a fixed observer at $r = R$ in the Schwarzschild space-time, relative to a local freely falling frame, is

$$a_S = \frac{GM}{R^2\sqrt{1-2GM/c^2R}} \; . \tag{3}$$

Substituted into (1) gives an expected Unruh temperature

$$k_B T_{RM} = \frac{\hbar GM}{2\pi c R^2\sqrt{1-2GM/c^2R}} \; . \tag{4}$$

Comparing this with the Hawking temperature defined in (2) it is clear that $T_{U,M} < T_{H,U}$ when $R > 2GM/c^2$. In this detailed way it is shown that the equivalence principle is violated. In the same way the equivalence principle is restored in form and value at the horizon itself, $T_{U,M} = T_{H,U}$ when $R = 2GM/c^2$.

References

[1] Einstein, A (1920). "Relativity: The Special and General Theory" New York: Henry Holt

[2] W.G. Unruh, Phys. Rev. D **14**, 870 (1976)

[3] Hawking, SW (1974). "Black hole explosions?". *Nature*, Volume 248, Issue 5443, pp. 30-31

[4] Wilburn, S & Singleton, D (2011). "Hawking radiation, Unruh radiation and the equivalence principle" *Physical Review Letters* Issue 107

[5] Birrell, N. D. & Davies, P.C.W. (1982) "Quantum Fields in Curved Space" Cambridge: Cambridge University Press

Length Scale in Horava Gravity Through Landau Phase Transition

Sudipta Das and Subir Ghosh
Physics and Applied Mathematics Unit, Indian Statistical Institute
203 B. T. Road, Kolkata 700108, India

Abstract

We study a crucial aspect of the presence of higher derivative terms in the Horava model of gravity which generates an instability in the Minkowski ground state. The higher derivative coupling coefficient introduces a length scale in the metric and the metric also becomes space-dependent. The translation invariance is spontaneously broken in the process. The phenomenon is interpreted as a form of Landau liquid-solid phase translation. The (metric) condensate acts like a source that modifies the Newtonian potential below the length scale but keeps it unchanged for sufficiently large distance.

1 Introduction and Formalism:

Horava's [1] novel proposal of a UV complete model of Gravity states that it is admissible for a fundamental theory of Gravity to be Lorentz non-invariant at ultra high energy or short distance, as long as Lorentz invariance and Einstein General Relativity (GR) is recovered at low energy. This has brought about a paradigm shift in the way of thinking of High Energy Physicists but is quite conventional for Condensed Matter Physicists where maintenance of Lorentz invariance is not an issue at all. Higher derivative covariant terms in Einstein gravity improves the UV behavior but brings in insurmountable ghost problems [2]. To overcome this in Horava Gravity (HG) only higher order *spatial* derivative terms are kept. These explicitly Lorentz breaking terms do not introduce ghosts and at the same time can cure the UV divergence problems.

On the other hand, the higher derivative nature of the Horava model opens up a completely new line of thought that is of interest to us: instability in the flat metric ground state. This can lead to a Spontaneous Symmetry Breaking (SSB) as regards to translation symmetry only. *This phenomenon is a liquid-solid type of phase transition in the space(time) itself a la Landau [3].* A short distance length scale is generated in the process of transition from a homogeneous ($\sim$ liquid like) phase ground state to an inhomogeneous ($\sim$ solid like) condensate phase ground state in spacetime. Hence our work strengthens the claim of HG as a viable model for Quantum Gravity because the physics below this scale is affected while GR is recovered for distances sufficiently above this scale. Fortunately we know explicitly how to proceed in Condensed Matter Physics [4], where the physics is naturally non-relativistic. Since we are in the Horava framework of gravity where Lorentz invariance is explicitly broken, formalisms exploited in (non-relativistic) Condensed Matter Physics is applicable in the present scenario as well. In a series of pioneering works Alexander and Mctague [4] were able to construct a solid crystalline lattice (where translation and rotation symmetries are lost), from a liquid phase (where the symmetries are intact), through SSB. In order to achieve this, the condensate VEV can not be a constant that we generally encounter in Particle Physics. Rather, the Fourier transform of non-zero VEV of condensate minimizing the free energy must have support at a *non-vanishing momentum*. Evidently, this requirement translates, in the coordinate space, to the parent lagrangian undergoing SSB, as having *higher (at least fourth) order derivative* terms that are quadratic in the field. The field in question is identified with the difference between the (inhomogeneous) density for solid and (constant) density of liquid, that acts as the order parameter. The ideas developed in [4] were applied in High Energy Physics in the context of string compactification by [5].

2 SSB of Higher Derivative Scalar Theory:

We consider a toy model,

$$S = \int d^4x \left[\frac{1}{2}\phi(-\partial_0^2 - \partial_i^2)\phi - \frac{\alpha^2}{4}\phi(\partial_i^2)^2\phi - V(\phi) \right]. \tag{1}$$

that will resemble Horava model after some restriction on the metric fluctuation. For the present we drop the potential $V(\phi)$ as we focus on minimizing the kinetic energy but higher order terms in the potential are needed to stabilize the system. (We thank Prof. S.Mukhoyama for pointing this out.)

With the flat metric $\eta_{\mu\nu} \equiv diag(-1,1,1,1)$ energy is

$$H = \int d^3x \, [\frac{1}{2}\dot{\phi}^2 - \frac{1}{2}(\partial_i\phi)^2 + \frac{\alpha^2}{4}\phi(\partial_i^2)^2\phi]. \tag{2}$$

To minimize the energy we consider a static ground state that (with Fourier decomposition $\phi(x) = \frac{1}{(2\pi)^3}\int \phi(k)e^{ik.x}dk,$) becomes in momentum space

$$H = -\frac{1}{2}k^2\phi(\vec{k})\phi(-\vec{k}) + \frac{\alpha^2}{4}(k^2)^2\phi(\vec{k})\phi(-\vec{k}). \tag{3}$$

Clearly $H[k^2 = 0] = 0$ but $H[k^2 = 1/\alpha^2] = -\frac{1}{4\alpha^2}$ showing that the minimum of kinetic energy (3) occurs at $k^2 = \frac{1}{\alpha^2}$. Here we used the notation $|\vec{k}|^2 = k^2$. The condensate value of $< \phi(x) >$, (that minimizes the energy), has a nontrivial coordinate dependence:

$$< \phi(\mid x \mid) >= \frac{1}{(2\pi)^3}\int d^3k\delta(k^2 - \frac{1}{\alpha^2})C(\alpha k)e^{ik.x} = \frac{C}{(2\pi)^2}\frac{sin(\mid x \mid /\alpha)}{|x|}, \tag{4}$$

with C a dimensionless number. In (4) the condensate $< \phi(\mid x \mid) >$ is x-dependent, so that translation invariance is lost but rotational symmetry is preserved. For large α energy H in (3) is minimum for $k^2 = 0$ and the condensate $< \phi(\mid x \mid) >$ in (4) becomes $\mid x \mid$-independent constant.

One can consider fluctuations above the condensate by shifting the field, i.e. $\phi(x) \rightarrow \phi(x) - \phi(\mid x \mid)$ leading to a translation *non*-invariant (but rotation invariant) theory. There is an underlying periodic nature of the translation symmetry broken phase. We perform the same exercise on the Horava model of Gravity in weak field approximation.

3 SSB of Higher Derivative Horava Gravity:

We consider the higher derivative terms as perturbations on the linearized Horava gravity action (which reproduces Einstein's GR theory in the low-energy (IR) limit). We intend to introduce a short distance scale ($\sim$ Planck length) in the Horava action that will break the translation invariance, without affecting the rotational symmetry. We introduce the deformation directly in the metric as a fluctuation and the condensate plays the role of a (tensorial) order parameter in the continuum-discrete spacetime phase transition. As we have extensively discussed before, this requires the introduction of higher derivative terms in the action, $R^{ij}R_{ij}$ and $(g^{ij}R_{ij})^2$. Apart from the conventional $(g^{ij}R_{ij})$-term, the above are needed to ensure that the kinetic term is minimized for a non-zero momentum.

We start with the action S

$$S = \int dtd^3x\sqrt{g}N(K_{ij}K^{ij} - \lambda K^2 + AR + BR_{ij}R^{ij} + CR^2). \tag{5}$$

Here g_{ij} is the spatial metric, A, B, C are three dimension-full parameters of the theory, $N, N_i(x,t)$ are the Lapse and Shift functions respectively, R is the spatial Ricci scalar and K_{ij} is the extrinsic curvature,

$$K_{ij} = \frac{1}{2N}(\partial_0 g_{ij} - \nabla_i N_j - \nabla_j N_i). \tag{6}$$

For $\lambda = 1$, $A = 1$ and $B = C = 0$ Horava gravity reduces to Einstein's gravity. In the weak field approximation $g_{ij} = \delta_{ij} + h_{ij} \quad , \quad N = 1 + n \quad , \quad N_i = n_i$ we find K_{ij}, R_{ij} to be

$$K_{ij} = \frac{1}{2}(\partial_0 h_{ij} - \partial_i n_j - \partial_j n_i) \ \ , \ \ K = \delta^{ij} K_{ij} = \frac{1}{2}(\partial_0 h - 2\partial_i n^i),$$

$$R_{ij} = \frac{1}{2}(\partial^k \partial_i h_{jk} + \partial^k \partial_j h_{ik} - \partial^2 h_{ij} - \partial_i \partial_j h) \ \ , \ \ R = \partial_i \partial_j h^{ij} - \partial^2 h. \tag{7}$$

Using (7) and the relation $\sqrt{g} R = \frac{1}{2} h_{ij} \left(-R^{ij} + \frac{1}{2}\delta^{ij} R\right)$ it is straightforward to write down the action in second order in h. Using the notation $h = \delta^{ij} h_{ij} \quad , \quad \partial^2 = \partial_i \partial^i = \delta^{ij}\partial_i \partial_j$. we recover the canonical Hamiltonian density (using the momentum constraints and the gauge $n_i = 0$),

$$\mathcal{H} = \pi_{ij}\pi^{ij} - \frac{1}{4} h_{ij}(\partial^2 h^{ij} - 2\partial_k \partial^i h^{jk} + 2\partial^i \partial^j h - \delta^{ij}\partial^2 h)$$

$$-\frac{B}{4}(\partial^k \partial_i h_{jk} - \partial^2 h_{ij} + \partial^k \partial_j h_{ik} - \partial_i \partial_j h)(\partial_l \partial^i h^{jl} - \partial^2 h^{ij} + \partial_l \partial^j h^{il} - \partial^i \partial^j h). \tag{8}$$

In the static limit $\pi_{ij} = 0$ and with $h_{ij} = \delta_{ij} h$ for the sake of convenience, the Hamiltonian (8) can be written in the Fourier space as $\mathcal{H}_{static}(p)$,

$$\mathcal{H}_{static}(p) = -\frac{p^2}{6} h(p) h(-p) \left(1 - \frac{17B}{5} p^2\right). \tag{9}$$

The minimum of this (9) occurs at

$$p^2 = \frac{1}{\alpha^2} = \frac{5}{34B}.$$

Now, to consider the SSB effects, let us consider fluctuations $\tilde{h}_{\mu\nu}$ above the condensate,

$$h_{ij} = \delta_{ij} f(\mid \vec{x} \mid) + \tilde{h}_{ij}(x)$$

$$h_{00} = \tilde{h}_{00} = -2\phi \quad , \quad h_{0i} = 0, \tag{10}$$

where $f(\mid \vec{x} \mid)$ is a purely spatial function. The tensorial structure of the condensate is taken to be $\delta_{ij} f$ since a constant vector will break rotational invariance. $\tilde{h}_{\mu\nu}$ is treated as the order parameter.

In a similar way as the scalar theory case (4), we have the explicit form of $f(r)$ as

$$f(r) = \nu \frac{GM sin(r/\alpha)}{r}, \tag{11}$$

where $r = |x|$ stands for the radial coordinate, coming from the energy minimization arguments (9). For later convenience we have expressed the constant as νGM where ν is a dimensionless constant and G the gravitational constant and M the mass of a point source to conform with the Newtonian limit. We conveniently choose $\nu = 1$ throughout the rest of our paper.

In terms of the metric (10), the lagrangian becomes

$$\mathcal{L} = \frac{1}{4}[\partial_0 \tilde{h}_{ij} \partial_0 \tilde{h}^{ij} - \lambda(\partial_0 \tilde{h})^2] + \frac{A}{4}\tilde{h}_{ij}(\partial^2 \tilde{h}^{ij} - 2\partial_k \partial^i \tilde{h}^{jk} + 2\partial^i \partial^j \tilde{h} - \delta^{ij}\partial^2 \tilde{h})$$

$$+An(\partial_i \partial_j \tilde{h}^{ij} - \partial^2 \tilde{h}) + C(\partial_i \partial_j h^{ij} - \partial^2 h)(\partial_k \partial_l h^{kl} - \partial^2 h)$$

$$+\frac{B}{4}(\partial^k \partial_i \tilde{h}_{jk} - \partial^2 \tilde{h}_{ij} + \partial^k \partial_j \tilde{h}_{ik} - \partial_i \partial_j \tilde{h})(\partial_l \partial^i \tilde{h}^{jl} - \partial^2 \tilde{h}^{ij} + \partial_l \partial^j \tilde{h}^{il} - \partial^i \partial^j \tilde{h})$$

$$+\frac{A}{2}\tilde{h}^{ij}(\partial_i \partial_j f - \delta_{ij}\partial^2 f) - 4C\tilde{h}^{ij}(\partial_i \partial_j \partial^2 f - \delta_{ij}(\partial^2)^2 f) - \frac{3B}{2}\tilde{h}^{ij}(\partial_i \partial_j \partial^2 f - \delta_{ij}(\partial^2)^2 f). \tag{12}$$

Following standard literature [7], we decompose $\tilde{h}_{\mu\nu}$ as:

$$\tilde{h}_{00} = -2n = -2\phi \quad , \quad \tilde{h}_{0i} = 0 \quad , \quad \tilde{h}_{ij} = 2s_{ij} - 2\psi\delta_{ij}, \tag{13}$$

where s_{ij} is traceless. Using the above decomposition (13) and considering the static limit (hence dropping all time derivatives), the equations of motion are obtained by varying the lagrangian (12) with respect to the fields n and $\tilde{h}^{ij}$:

$$\partial^2\psi = \frac{1}{2}\partial^2 f, \tag{14}$$

$$A(\partial_i\partial_j - \delta_{ij}\partial^2)(\phi-\psi) + A\partial^2 s_{ij} + \frac{A}{2}(\partial_i\partial_j - \delta_{ij}\partial^2)f + 8C\partial^2(\partial_i\partial_j - \delta_{ij}\partial^2)\psi$$

$$-4C\partial^2(\partial_i\partial_j - \delta_{ij}\partial^2)f + B(\partial^2)^2 s_{ij} - 3B\delta_{ij}(\partial^2)^2\psi - \frac{3B}{2}\partial^2(\partial_i\partial_j - \delta_{ij}\partial^2)f = 0. \tag{15}$$

Using the explicit expression of $f(r)$ (11), after some computations that is conventional in GR we find

$$\phi(r) = -\frac{GM}{r} + \frac{3BGM}{4A\alpha^2}\frac{sin(\frac{r}{\alpha})}{r}. \tag{16}$$

The modified Newtonian potential derived above in (16) is shown in the Figure. One can see that the fluctuations die out for sufficiently large distance $r >> \alpha$ but can have non-trivial effects for $r \sim \alpha$.

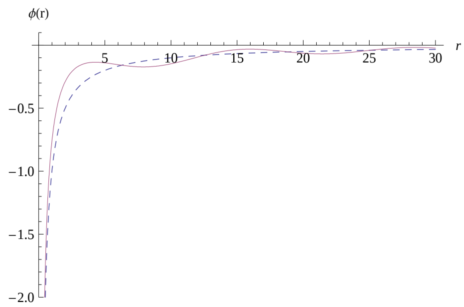

Figure 1: *Plot of the usual Newtonian potential (dashed line in the plot) and the modified Newtonian potential as described in previous paragraph (solid line in the plot) vs r with $\alpha = 2$.*

4 Conclusion:

To conclude, we have shown that higher derivative terms in the Horava model of gravity can lead to an instability and a spontaneous breaking of translation symmetry of the space takes place. Hence ground state gets modified from the conventional Minkowski vacuum metric to a space dependent form. This is an example of Landau type of liquid-solid phase transition occurring in the space itself. A length scale also appears in the resulting metric in a natural way. The Newtonian potential is recovered for distances large compared to this scale. Consequences of this novel form of spatial metric is worth pursuing. We conclude by noting that although it is true that a linearized version can not capture all the good and controversial features of the exact model, our present analysis shows that in the exact Horava theory as well one has to keep in mind the type of Landau phase transition that we have proposed here simply due to the higher derivative nature of the theory.

Acknowledgments: We thank Professor Chetan Nayek and Professor Eliezer Rabinovici for helpful correspondences.

References

[1] P. Horava, JHEP 0903, 020 (2009) [arXiv:0812.4287]; Phys. Rev. D 79 (2009) 084008 [arXiv:0901.3775]; Phys. Rev. Lett. 102, 161301 (2009) [arXiv:0902.3657]; P. Horava and C. M. Melby-Thompson, Phys. Rev. D 82 (2010) 064027 [arXiv:1007.2410].

[2] K. S. Stelle, Gen. Rel. Grav. 9 353 (1978).

[3] L. D. Landau, Phys. Z. Soviet II 26, 545 (1937).

[4] S. Alexander and J. Mctague, Phys. Rev. Lett. 41 703 (1978); S. Alexander, Symmetries and Broken Symmetries in Condensed Matter Physics, ed. N. Boccara (IDSET Paris,1981) p. 141, and references therein; Journal de Physique, Colloque C3, March 1985.

[5] E. Rabinovici, Spontaneous Breaking of Space-Time Symmetries, *Lect. Notes Phys. 737 (2008) 573-605.* [arXiv:0708.1952]; S. Elitzur, A. Forge and E. Rabinovici, Nucl. Phys. B 359 (1991) 581.

[6] R. L. Arnowitt, S. Desser and C. W. Misner, Gravitation: an Introduction to Current Research (Wiley 1962), chapter 7, pp 227-265.

[7] S. Carroll, *Spacetime and Geometry, An Introduction to General Relativity*, Addison Wesley, 2004.

New formulation of Horava-Lifshitz quantum gravity as a master constraint theory

Hoi-Lai Yu[1], *Chopin Soo*[2] *& Jinsong Yang*[2]
[1]*Institute of Physics, Academia Sinica, Nankang, Taipei 11529, Taiwan*
[2] *Department of Physics, National Cheng Kung University, Tainan 70101, Taiwan*
Email : hlyu@phys.sinica.edu.tw

Abstract

A new formulation of non-projectable Horava-Lifshitz gravity, naturally *realized as a representation of the master constraint algebra* studied by loop quantum gravity researchers, is presented. This yields a consistent canonical theory with first class constraints. It captures the essence of Horava-Lifshitz gravity in retaining only spatial diffeomorphisms (instead of full space-time covariance) as the physically relevant non-trivial gauge symmetry; at the same time the local Hamiltonian constraint needed to eliminate the extra mode is equivalently enforced by the master constraint.

1 Introduction

The conceptual breakthrough in Horava's [1] work is the realization that a key obstacle to the viability of perturbative quantum gravity as a renormalizable field theory lies in the deep conflict between unitarity and space-time general covariance: the renormalizability of general relativity can be improved and achieved through the introduction of higher derivative terms, but space-time covariance requires higher time as well as spatial derivatives of the same order, thus compromising the stability and unitarity of the theory. The loss of unitarity is signaled by the occurrence of a ghost term in the resummed effective graviton propagator. Horava elects to keep unitarity but relinquishes full space-time covariance to retain only spatial diffeomorphism symmetry at the fundamental level, and seeks to recover general relativity at low curvatures. This bold procedure leads to the crucial decoupling of temporal from spatial contributions in the graviton propagator. There is, in our view, a related development, in loop quantum gravity, which is perhaps not as well known: the application of the master constraint program [2] to non-perturbative quantization of Einstein's theory. In the effort it has been fruitful to seek representations not of the Dirac algebra, but of the master constraint algebra which has the advantages of having structure constants rather than structure functions, and of spatial diffeomorphisms forming an ideal (thus allowing for the crucial decoupling of the equivalent quantum Hamiltonian constraint from spatial diffeomorphism generators).

Our work[3] demonstrates that it is apposite, and also natural, to formulate Horava-Lifshitz theory as a representation of the master constraint algebra. Unlike the original non-projectable formulation of Horava-Lifshitz theory, our construction yields a consistent canonical theory with first class constraints. Observables of the resultant theory are also discussed. In addition our formulation realizes, in an explicit manner, the claim in Ref. [4] that time-reparamatrization symmetry of Horava-Lifshitz gravity is on-shell trivial. Some errors in the derivation of the consistency conditions [5] for general relativity with deformed supermetric are also pointed out.

2 Features of Horava-Lifshitz gravity with detailed balance

We begin by recasting the original formulation of Horava-Lifshitz gravity [1] in a compact form which highlights certain features and structures of the theory. In the canonical mould, the theory may be written as

$$S = \int \pi^{ij}\dot{q}_{ij}\, d^3x\, dt - \int (NH + N^i H_i)\, d^3x\, dt, \tag{1}$$

wherein the super-Hamiltonian is $H = \frac{\kappa^2}{2}\frac{G_{ijkl}}{\sqrt{q}}[\pi^{ij}\pi^{kl} + \frac{\delta W_{\rm T}}{\delta q_{ij}}\frac{\delta W_{\rm T}}{\delta q_{kl}}]$; and $H_i = 2q_{ij}\nabla_k \pi^{kj} = 0$ is the super-momentum constraint. The (inverse) DeWitt supermetric, with deformation parameter λ which is allowed to deviate from unity, is $G_{ijkl} = \frac{1}{2}(q_{ik}q_{jl} + q_{il}q_{jk}) - \frac{\lambda}{3\lambda-1}q_{ij}q_{kl}$. Dependent only on the 3-geometry, $W_{\rm T}$ is (up to 3rd order in spatial derivatives of the metric) the sum of a Chern-Simons action of the spatial affine connection and the spatial Einstein-Hilbert action with cosmological constant i.e. $W_{\rm T} = W_{\rm CS} + W_{\rm EH\Lambda}$, with

$$\begin{aligned} W_{\rm CS} &= \frac{1}{4w^2}\int \tilde{\epsilon}^{ikj}(\Gamma^l_{im}\partial_j\Gamma^m_{kl} + \frac{2}{3}\Gamma^l_{im}\Gamma^m_{jn}\Gamma^n_{kl})\, d^3x, \\ W_{\rm EH\Lambda} &= \frac{\mu}{2}\int \sqrt{q}(R - 2\Lambda_W)\, d^3x; \end{aligned} \tag{2}$$

and the Cotton tensor density can be expressed as $\tilde{C}^{ij} = w^2\frac{\delta W_{\rm CS}}{\delta q_{ij}}$. The Hamiltonian constraint can be succinctly rewritten as [1]

$$H = \frac{\kappa^2}{2\sqrt{q}}G_{ijkl}Q^{ij}_+ Q^{kl}_- = 0, \tag{3}$$

with $Q^{ij}_\pm := \pi^{ij} \pm i\frac{\delta W_{\rm T}}{\delta q_{ij}}$. As quantum operators, $\hat{Q}_\pm$ take on the interesting form $\hat{Q}^{ij}_\pm = e^{\pm\frac{W_{\rm T}}{\hbar}}\hat{\pi}^{ij}e^{\mp\frac{W_{\rm T}}{\hbar}}$. Note also that $Q_\pm$ are hermitian conjugates of each other if $W_{\rm T}$ is hermitian (classically real), and are separately hermitian if $W_{\rm T}$ is purely anti-hermitian (classically pure imaginary). In both cases, the classical expression for H remains real [2].

An observation on the values of the coupling constants is also apposite here: The superspace metric [7], $\delta S^2 \equiv G^{ijkl}\delta q_{ij}\delta q_{kl}$, has signature $({\rm sgn}[\frac{1}{3}-\lambda], +, +, +, +, +)$. So the corresponding Wheeler-DeWitt equation [7] comes equipped with an 'intrinsic time' [7] for $\lambda > \frac{1}{3}$. Unlike the space-time covariant Einstein-Hilbert theory, deformation of λ from unity should be allowed as it does not violate the 3-dim. diffeomorphism symmetry of the theory. Moreover, λ is expected to flow as a renormalization parameter. Intriguingly, the emergent speed of light $c = \frac{\kappa^2\mu}{4}\sqrt{\frac{\Lambda_W}{1-3\lambda}}$, the cosmological constant $\frac{3}{2}\Lambda_W$, and Newton's gravitational constant $G = \frac{\kappa^2 c^3}{32\pi}$ can all be phenomenologically positive for $\lambda > \frac{1}{3}$ only if μ is pure imaginary and κ is real. Then H and the action is real only if w^2 is pure imaginary. This set of values renders $W_{\rm T}$ to be pure imaginary, and thus $Q_\pm$ become individually hermitian.

The supermetric and $Q_\pm$ do not commute among themselves, so whether $\Psi_{Q_\pm} = Ie^{\pm\frac{W_{\rm T}}{\hbar}}$, which are annihilated by $\hat{Q}^{ij}_\pm$ (if I satisfies $\frac{\delta I}{\delta q_{ij}} = 0$), qualify as exact solutions depends on ordering ambiguities in H; but it should be noted that such states (with slowly varying I) are nevertheless semi-classical; and a pure imaginary $W_{\rm T}$ leads to real $\pi^{ij} = \mp i\frac{\delta W_{\rm T}}{\delta q_{ij}}$ solving the Hamilton-Jacobi equation with $\pm iW_{\rm T}$ as Hamilton functions [3]. The form of the Hamiltonian with $Q_\pm$ gives a new and interesting perspective, not just on

[1] After our initial discussion in Ref.[3], this particular form of the Hamiltonian constraint has also been investigated in Ref.[6].

[2] The classical Hamiltonian constraint reduces to the algebraic equation $\frac{1}{2}{\rm Tr}(Q_+Q_- + Q_-Q_+) - \frac{\lambda}{3\lambda-1}{\rm Tr}(Q_+){\rm Tr}(Q_-) = 0$, wherein the trace is taken with the indices of $Q^{ij}_\pm$ raised and lowered by the spatial metric.

[3] $W_{\rm CS}$ (hence $W_{\rm T}$) is not invariant under large gauge transformations; so $\Psi_{Q_\pm}$, like θ-angle states, will then acquire an additional phase factor. For the case of real $W_{\rm T}$, $\Psi_{Q_\pm}$ are not large gauge-invariant even up to a phase, and they should, on this basis alone, be disqualified as physical states unless I can compensate by producing an inverse factor [8].

Horava-Lifshitz gravity (which corresponds to a theory with up to 3rd order spatial derivatives of the metric in $W_{\rm T}$); but also on the whole class of related theories which can be obtained by adjusting 3-geometry terms in $W_{\rm T}$. However, it is crucial that the constraint algebra must be consistent before any such theory is viable. Both the projectable and non-projectable version of the theory face serious challenges.

3 Inconsistency of non-projectable Horava-Lifshitz gravity

Non-projectable Horava-Lifshitz gravity with space-time dependent lapse function $N(x)$ is also problematic. $\pi_N(x) = 0$ does lead to the secondary local constraint $H(x) = 0$. But the constraint algebra with the full $W_{\rm T}$ of Horava-Lifshitz gravity suffers from serious problems, whereas the Dirac algebra is obtained for covariant 4-dimensional Einstein-Hilbert action with cosmological constant. In fact for Horava-Lifshitz gravity, $\{H(x), H[N]\} = (\triangle + \omega)N(x)$, wherein $\triangle$ contains spatial derivatives acting on N and ω does not (for explicit expressions of the Poisson bracket the reader may consult Refs. [4, 9]), and smeared constraints are denoted by square brackets i.e. $H[N] := \int NHd^3x$. Furthermore $(\triangle + \omega)$ can have zero modes; and the only consistent solution is $N = 0$ [4]. Strictly speaking, $N = 0$ considered as a special case of a gauge-fixing condition $N = f$ results in $\{N(x) - f, \pi_N(y)\} = \delta(x - y)$ with non-vanishing determinant. So the condition does give a formally 'consistent' system with two second class constraints, $\pi_N = N = 0$, in addition to $\pi_{N^i} = H_i = H = 0$ which are stable under evolution *provided* $N = 0$. But this formal consistency, achieved at the cost of vanishing N, is of dubious value (since any constraint can be made stable with $N = 0$; furthermore the ADM spacetime metric is degenerate for vanishing lapse function). At the very least the situation demands a more physical explanation. On the other hand, Dirac's algorithm for the analysis of constrained canonical systems [10] should reveal the true gauge symmetries of the theory. For Horava-Lifshitz gravity, the requirement of vanishing lapse function from the algorithm seems to signal that *only* 3-dim. spatial diffeomorphism symmetry is physically relevant. Such theories cannot obey the Dirac algebra which is the hallmark of space-time covariance and the embeddability of hypersurface deformations, and from which Einstein's geometrodynamics can be uniquely recovered [11].

There can be interesting modifications to the Dirac algebra in theories without full space-time covariance. For example, in the extreme limit of $W_{\rm T} = 0$ corresponding to ultra-local gravity with $H = \frac{2\kappa'}{\sqrt{q}} G_{ijkl}\pi^{ij}\pi^{kl}$, a strongly vanishing commutator, $\{H[N], H[M]\} = 0$ (even for $\lambda \neq 1$), replaces the usual commutation relation in the Dirac algebra [11]. When a scalar curvature term is added to the previous ultralocal theory in deformations of Einstein-Hilbert theory with $\lambda \neq 1$ and $H = (\frac{2\kappa'}{\sqrt{q}} G_{ijkl}\pi^{ij}\pi^{kl} - \frac{\sqrt{q}}{2\kappa'} R)$, stability of the primary constraints $\pi_N = \pi_{N^i} = 0$ with respect to the Hamiltonian $H_{\rm primary} = \int d^3x \left(\Lambda\pi_N + \Lambda^i\pi_{N^i} + NH + N^iH_i\right)$ results in $H = H_i = 0$. Preservation of these secondary constraints under evolution leads to

$$\begin{aligned} \{H[M], H_{\rm primary}\} &= -H[\mathcal{L}_{\vec{N}}M] + H_i[(M\nabla^i N - N\nabla^i M)] \\ &- \frac{2(1-\lambda)}{3\lambda - 1}\int (M\nabla^i N - N\nabla^i M)\nabla_i \pi \, d^3x \, . \end{aligned} \tag{4}$$

For general relativity with $\lambda = 1$ the constraints are already first class at this stage. With $\lambda \neq 1$, the consequent secondary constraint $Z_i := \nabla_i \pi = 0$ leads to

$$
\begin{aligned}
&\{Z_i[\xi^i], Z_j[\chi^j]\} = Z_i \left[\frac{3}{2}(\chi^i \nabla_j \xi^j - \xi^i \nabla_j \chi^j)\right], \\
&\{H_i[N^i], Z_i[\xi^i]\} = Z_i \left[\mathcal{L}_{\vec{N}} \xi^i\right], \\
&\{Z_i[\xi^i], H[N]\} = Z_i \left[-\frac{2\kappa'}{(3\lambda - 1)\sqrt{q}} N \pi \xi^i\right] - H \left[\frac{3}{2} N \nabla_i \xi^i\right] \\
&- \frac{1}{\kappa'} \int d^3x \sqrt{q}\,(\nabla_j \xi^j) W,
\end{aligned} \tag{5}
$$

with $W := \left[-\nabla^2 + R + \frac{2\kappa'^2 \pi^2}{(3\lambda - 1)q}\right] N$. Thus $W = 0$ is required for stability of $Z_i := \nabla_i \pi = 0 \Leftrightarrow \pi = K(t)\sqrt{q}$. The constraint $H = 0$ allows us to write $R = \frac{4\kappa'^2}{q}\left(\overline{\pi}_{ij}\overline{\pi}^{ij} - \frac{1}{3(3\lambda - 1)}\pi^2\right)$, wherein $\overline{\pi}^{ij} := \pi^{ij} - \frac{1}{3} q^{ij} \pi$ is the traceless part of the momentum. Together with $\pi = K\sqrt{q}$, the condition on N then becomes

$$
W = \left[-\nabla^2 + \frac{4\kappa'^2}{q}\overline{\pi}_{ij}\overline{\pi}^{ij} + \frac{2\kappa'^2 K^2}{3(3\lambda - 1)}\right] N = 0. \tag{6}
$$

Since $-\nabla^2$ and $\frac{4\kappa'^2}{q}\overline{\pi}_{ij}\overline{\pi}^{ij}$ are both positive semi-definite operators, $W = 0$ can have non-vanishing solution [4] for N only if $\lambda < \frac{1}{3}$. For $\lambda < \frac{1}{3}$, the resultant theory (counting the 6 conjugate pairs (q_{ij}, π^{ij}), $H_i = 0$ as first class and $H = 0, \widetilde{\pi} = K\sqrt{q}$ as second class constraints) has $\frac{1}{2}[12 - 3(2) - 2(1)] = 2$ degrees of freedom, but does not contain Einstein's theory ($\lambda = 1$) as a special case. For $\lambda > \frac{1}{3}$, we are lead to the fact $N = 0$ is the only solution for $W = 0$. Thus Ref. [5] is incorrect in its conclusions. Although secondary constraints arise, a non-trivial solution exists for N for $\lambda < \frac{1}{3}$. However, for $\lambda \geq \frac{1}{3}$ (and for non-projectable Horava gravity with local Hamiltonian constraint) only $N = 0$ is allowed.

4 Horava-Lifshitz gravity as a master constraint theory

As structure *functions* are present in the commutator of two Hamiltonian constraints, the Dirac algebra is not the Lie algebra of 4-dimensional diffeomorphisms. But H_i and H constraints do generate 4-dimensional diffeomorphisms on-shell(modulo the constraints and equations of motion). In a theory which possesses at the fundamental level only 3-dimensional diffeomorphisms as gauge symmetry, we expect the constraints to generate, *on-shell, only spatial diffeomorphisms.* There is a formulation which precisely achieves this goal, and which at the same time gives rise to a condition equivalent to the local constraint $H(x) = 0$ – thus eliminating the problematic extra scalar graviton mode. For Horava-Lifshitz gravity, simultaneous requirement of a *local* H constraint and an involutive constraint algebra seems impossible without $N = 0$. Our proposal[3] is for theories with *only* spatial diffeomorphism invariance as the physical gauge symmetry, in particular Horava-Lifshitz gravity, to be formulated as representations of the master constraint algebra which has been studied by researchers in loop quantum gravity in their attempt to quantize Einstein's theory non-perturbatively [2]. The master constraint operator $\mathbf{M}$, which is tailored to be invariant under spatial diffeomorphisms (with $H(x)$ being a scalar density of weight 1), is defined as $\mathbf{M} := \int_\Sigma \frac{[H(x)]^2}{\sqrt{q(x)}} d^3x$. For any real valued $H(x)$, the integrand is positive-semi-definite; and the master constraint equation, $\mathbf{M} = 0$, is mathematically equivalent

[4] N can be expanded in terms of eigenfunctions of the Hermitian operator $-\nabla^2 + \frac{4\kappa'^2}{q}\overline{\pi}_{ij}\overline{\pi}^{ij}$. Then N is non-trivial iff $-\frac{16\kappa'^2 K^2}{3(3\lambda - 1)}$ coincides with at least one of its (positive semi-definite) eigenvalues. This can be achieved *only* for $\lambda < \frac{1}{3}$.

to $H(x) = 0$ everywhere on the Cauchy surface Σ. Thus the master constraint equation replaces the infinite number of local restrictions ($H = 0$) by a single global restriction. This equivalence has furthermore been demonstrated rigorously in the quantum context for various non-trivial models, including for quantum field theories [2]. The upshot is a simple closed constraint algebra (with structure *constants*) which is first class. The master constraint algebra is just

$$\begin{aligned}&\{H_i[N^i], H_j[N'^j]\} = H_i[\mathcal{L}_{\vec{N}} N'^i],\\ &\{H_i[N^i], \mathbf{M}\} = 0\,, \quad \{\mathbf{M}\,, \mathbf{M}\} = 0.\end{aligned} \tag{7}$$

The canonical action for Horava-Lifshitz gravity can then be consistently adopted as

$$S = \int \pi^{ij}\dot{q}_{ij}\, d^3x dt - \int \frac{N(t)}{\epsilon_o}\mathbf{M} dt - \int N^i H_i\, d^3x dt, \tag{8}$$

with H of the form in Eq.(3); ϵ_o has the physical dimension of energy density. Such theories consistently generate equations of motion which are (on-shell) equivalent to spatial diffeomorphisms since

$$\{q_{ij}, \frac{N(t)}{\epsilon_o}\mathbf{M} + H_k[N^k]\}|_{\mathbf{M}=0\Leftrightarrow H=0} \approx \{q_{ij}, H_k[N^k]\} = \mathcal{L}_{\vec{N}} q_{ij}, \tag{9}$$

(and similarly for π^{ij}). Our new formulation also realizes the claim in Ref. [4] that time-reparamatrization symmetry of Horava-Lifshitz gravity and freedom in the choice of $N(t)$ is on-shell trivial. We should remark that in general relativity with first class local constraints $H = H_i = 0$, a Dirac observable, O, must commute with both H_i and H. This is equivalent to the requirement $\{O, \{O, \mathbf{M}\}\}|_{\mathbf{M}=0} = 0$ [2]. But for the theory at hand, one can read off from the action that weak observables O should commute (weakly) with $\mathbf{M}$ and H_i; which (analogous to computations in Eq.(9)) is equivalent to $\{O, H_i\} \approx 0$. This weaker criterion (instead of also requiring vanishing $\{O, \{O, \mathbf{M}\}\}|_{\mathbf{M}=0}$) of allowing for observables of 3-geometry on the constraint surface is physically reasonable as observables of the theory should be invariant only with respect to the local gauge symmetry of spatial diffeomorphisms. In such theories, two configurations differing by four-dimensional, rather than spatial, coordinate transformations can be physically inequivalent. It is to be noted our formulation of Horava-Lifshitz gravity *also requires the lapse function to depend only on* t.

In retrospect, 'troubles' in the constraint algebra of Horava-Lifshitz gravity with *local* Hamiltonian constraint are to be expected of a canonical theory of 3-geometry which fundamentally possesses only spatial diffeomorphism invariance. A new, and natural, canonical formulation of Horava-Lifshitz gravity as a representation of the master constraint algebra can be consistently constructed. Moreover, the local Hamiltonian constraint which is needed (as in Einstein's theory) to remove the problematic scalar graviton mode, is equivalently enforced by the master constraint. Although the Legendre transformation to Lagrangian formulation can be performed, it may not be particularly useful given the lack of 4-dimensional general covariance, and will not be pursued here as the canonical Hamiltonian formulation is already *manifestly covariant* with respect to the full spatial diffeomorphism symmetry of the theory. It is also noteworthy that, rather than working directly with the quantum version of the intractible Dirac algebra, the loop quantum gravity community has instead found it fruitful to seek quantum representations of general relativity through the master constraint algebra [2]. Horava-Lifshitz gravity is in fact an explicit, and highly non-trivial representation, of a master constraint theory with spatial diffeomorphism invariance. In not satisfying the Dirac algebra with local Hamiltonian constraint, Horava-Lifshitz gravity is in fact more naturally associated with the master constraint theory than Einstein's general relativity. The expectation (albeit at the level of perturbative quantum field theory) of the absence of negative norm ghosts is also encouraging. With a positive-definite norm, the quantum theory with $\hat{\mathbf{M}} := \int \widehat{\frac{H^\dagger H}{\sqrt{q}}}\, d^3x$ does lead to $\hat{\mathbf{M}}|\Psi\rangle = 0 \Leftrightarrow \hat{H}|\Psi\rangle = 0$. This new formulation of Horava-Lifshitz theory offers the exciting perspective that the perturbative as well as non-perturbative aspects of a theory of quantum gravity may become accessible through both the methodologies of perturbative renormalizable quantum field theories and non-perturbative quantum representations of the master constraint algebra.

References

[1] P. Horava, Phys. Rev. D **79**, 084008 (2009).

[2] T. Thiemann, Class. Quantum Grav. **23**, 2211 (2006).

[3] C. Soo, J. Yang and H. L. Yu, Phys. Lett. B **701**, 275(2011); [arXiv:1007.1563].

[4] M. Henneaux, A. Kleinschmidt and G. LucenaGomez, Phys. Rev. D **81**, 064002 (2010); [arXiv:1004.3769].

[5] J. Bellorin and A. Restuccia, [arXiv:1004.0055].

[6] P. Horava and C. M. Melby-Thompson, *Phys. Rev.* D **82**, 064027 (2010).

[7] Bryce S. DeWitt, Phys. Rev. **160**, 1113 (1967).

[8] C. Soo, Class. Quantum Grav. **19**, 1051 (2002)).

[9] M. Li and Y. Pang, JHEP **0908**, 015 (2009).

[10] P. A. M. Dirac, *Lectures in Quantum Mechanics* (Yeshiva University Press, New York, 1964).

[11] S. Hojman, K. Kuchar and C. Teitelboim, Nature Phys. Sci. **245**, 97 (1973); Ann. Phys.**96**, 88 (1976).

Strings, Branes and Extra Dimensions

Visiting the Quang Trung Museum : Masakatsu Kenmoku, Vitaly Melnikov, Wei-Tou Ni and Sang Pyo Kim

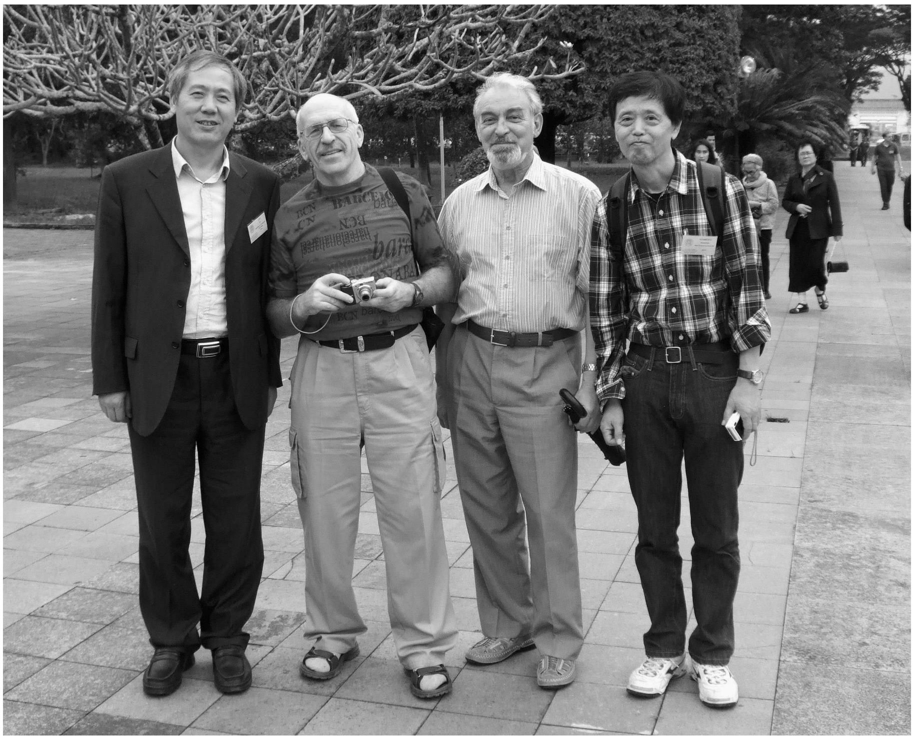

Jun Luo, Kirill Bronnikov, Vitaly Melnikov and Masakatsu Kenmoku

Universality classes of Symmetry Energy in holographic QCD

Sang-Jin Sin[1], *Yunseok Seo*[1]
[1] *Department of Physics, Hanyang University, Seoul 133-791, Korea*
Email :sjsin@hanyang.ac.kr

Abstract

We consider nuclear symmetry energy of dense matter using holographic QCD. We calculate it in a various holographic QCD models and show that the scaling index of the symmetry energy in dense medium does not change under the smooth deformation of the metric and that of the embedding shape of the probe brane. We find that the scaling power depends only on the dimensionality of the branes and space-time. Therefore the scaling index of the symmetry energy characterizes the universality classes of holographic QCD models. We tried to relate the scaling power to the non-fermi liquid behavior of the interacting nucleons.

1 Introduction

Nuclear symmetry energy is one of key words in nuclear physics as well as in astrophysics. Its density dependence is a core quantity of asymmetric nuclear matter which has important effects on heavy nuclei and is essential to understand neutron star properties. A big surprise is that such an important quantity is still poorly understood after 80 years of its definition, especially in the supra-saturation density regime. See [1, 2] for a review and a recent discussion. Given this situation, it would be very interesting if we can examine the behavior of the nuclear symmetry energy at high densities with a reliable calculational tool. Recently [3] we used a gauge/gravity duality [4, 5, 6] to calculate the nuclear symmetry energy. We treated the dense matter in confined phase using the method developed in our previous paper [7, 8]. Our result showed that the symmetry energy should be stiff in high density and its density dependence goes like $\sim \rho^{1/2}$. There, we attributed the stiffness to the repulsion due to the Pauli principle and suggested the relation of the scaling exponent to the anomalous dispersion relation.

The purpose of this talk is to report of the result examining the universality of the symmetry energy[9]: if the result changes under small variation of the gluon dynamics, it would not be very interesting since the true gravity dual of QCD is yet unknown. We will first calculate the deformation of the metric under certain class of the D brane configurations and show that the result is not much dependent on the metric deformation. The scaling behavior is rather insensitive whether we use the flat embedding or exact shape of the brane embedding, showing the universality of the result. On the other hand, we will see that the scaling exponent depends on the dimensionality of the color and flavor branes. We call such discrete dependence of the scaling dimension as the universality class of the symmetry energy.

2 Symmetry energy in holographic QCD

Let N, Z be the nucleon and proton numbers respectively, A be their sum and ρ is total baryon density. Then energy *per nucleon* in nuclear matter system can be expanded as a function of the isospin asymmetry parameter $\alpha = (N-Z)/A$,

$$E(\rho,\alpha) = E(\rho,0) + E_{\rm sym}(\rho)\alpha^2 + O(\alpha^4). \tag{1}$$

The bulk nuclear symmetry is defined as the coefficient $E_{\rm sym}(\rho)$ in the above expansion. There is no term which is odd power in α due to the exchange symmetry between protons and neutron in nuclear matter. It is a energy cost per nucleon to deviate the line $Z = N$.

To calculate nuclear symmetry energy in holographic QCD, we introduce two flavor Dq branes for up and down quarks in the metric background created by the N_c of Dp color branes. For simplicity, we assume that masses of up and down quarks are the same so that two branes have same asymptotic positions. For the confining geometry, we can introduce a baryon by the baryon vertex [15] which are a compact $D(8-p)$ branes wrapping the S^{8-p} transverse to the Dp. If there are Q of them we distribute them homogeneously along the 3 non-compact spatial direction of Dp. From each baryon vertex, N_c of the strings emanate and end at one of the probe branes. Let Q_1, Q_2 strings end on up and down branes respectively. The end points of the strings have $U(1)$ charges that will create the $U(1)$ gauge field on each brane. Such $U(1)$ charges are responsible for the quark density of each type of quarks.

The total free energy of the system can be written as

$$\mathcal{F}_{\rm total}(Q) = \mathcal{F}(Q) + \mathcal{F}^{(1)}_{Dq}(Q_1) + \mathcal{F}^{(2)}_{Dq}(Q_2), \tag{2}$$

where Q is number density of source and $\mathcal{F}(Q)$ is a quantity which depends only on total charge Q as we will discuss later. We can define total charge density and asymmetry parameter as

$$Q = Q_1 + Q_2, \qquad \tilde{\alpha} = \frac{Q_1 - Q_2}{Q}. \tag{3}$$

If we fix the asymptotic value of two probe brane to be same, the total free energy has minimum at $\tilde{\alpha} = 0$ [8]. Then we can expand total free energy in $\tilde{\alpha}$;

$$\mathcal{F}_{\rm total}(Q) = E_0 + E_1\tilde{\alpha} + E_2\tilde{\alpha}^2 + \cdots . \tag{4}$$

The first term, $E_0 = \mathcal{F}(Q) + 2\mathcal{F}_{Dq}\left(\frac{Q}{2}\right)$, can be identified with the free energy for symmetric matter. The second term in (4) is zero because (2) is symmetric in Q_1, Q_2. The symmetry energy is defined from the energy per nucleon and given by

$$S_2 = \frac{E_2(Q)}{Q} = \frac{Q}{4}\cdot \left.\frac{\partial^2 \mathcal{F}^{(1)}_{Dq}(Q_1)}{\partial Q_1^2}\right|_{Q_1=Q/2}. \tag{5}$$

To calculate symmetry energy from D-brane set up, we consider probe Dq brane spans along $(t, \vec{x}_d, \rho)$ and wraps S^n where $n = q-d-1$. The induced metric on Dq brane can be written in general form;

$$ds^2_{Dq} = -G_{tt}dt^2 + G_{xx}d\vec{x}_d^2 + G_{\rho\rho}d\rho^2 + G_{\Omega\Omega}d\Omega^2_{q-d-1}. \tag{6}$$

To introduce number density, we turn on time component of $U(1)$ gauge field on the probe brane whose action is given by

$$S_{Dq} = \mu_q \int d\sigma^{q+1} e^{-\phi}\sqrt{\det(g + 2\pi\alpha' F)}, \tag{7}$$

where μ_q is tension of Dq brane. The free energy can be identified with the action for fixed charge sector, which is the Legendre transformation of the original action with respect to the gauge field,

$$\mathcal{F}_{Dq}(\tilde{Q}) = \tau_q \int d\rho \sqrt{G_{tt}G_{\rho\rho}} \sqrt{\tilde{Q}^2 + e^{-2\phi} G_{xx}^d G_{\Omega\Omega}^n}, \tag{8}$$

where $\tau_q = \mu_q V_d \Omega_n$ and V_d is a volume of non-compact space. The dimensionless parameter $\tilde{Q}$ is related to the number density of source as $\tilde{Q} = Q/(2\pi\alpha'\tau_q)$. From (5) we symmetry energy is given by;

$$S_2 = 2\tau_q \int d\rho \frac{\tilde{Q}\sqrt{G_{tt}G_{\rho\rho}} e^{-2\phi} G_{xx}^d G_{\Omega\Omega}^n}{\left(\tilde{Q}^2 + 4e^{-2\phi} G_{xx}^d G_{\Omega\Omega}^n\right)^{3/2}}. \tag{9}$$

This result can be applied for general Dp brane background and we will apply it to confined phase as well as deconfined one.

We first discuss symmetry energy in the **confined phase**. There are several examples of the metric background corresponding to the confining phase. In the case of $D4$ brane, the geometry is obtained by (double) Wick rotating time and a compact spatial direction. In $D3$ brane case, we use the non-supersymmetric geometry with nontrivial dilaton field. In such geometries, the net force on the probe brane is repulsive.

We identify the chiral symmetry as the the symmetry rotating the probe brane in the transverse plane following [10]. In the limit of zero quark mass, this symmetry is spontaneously broken due to the repulsive nature of the net force. As a consequence, the value of chiral condensation has finite value and the baryon vertex is allowed to exist. The baryon vertices play a role of source of $U(1)$ gauge field on probe Dq brane as we discussed in previous section.

To make the system stationary, we have to impose 'force balance condition' between baryon vertex and probe brane. The symmetry energy can be understood as the energy costs when the system is deviated from symmetric matter. To achieve the deviation, we need to attach different number of charges(strings) on each brane, which in turn gives different embedding for each probe brane. The schematic figure is drawn in Figure. 1. We first solve the equation of motion for probe brane numerically with given charge and quark mass together with force balance condition. Then substituting the solution to (9), we can calculate the symmetry energy.

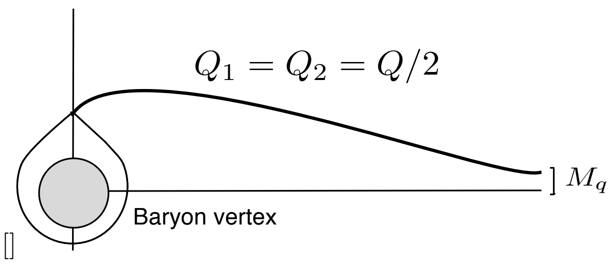

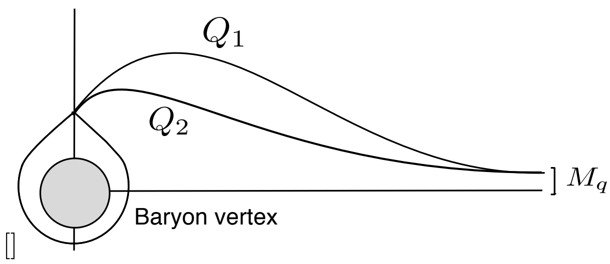

Figure 1: Schematic figure of D-brane configuration for (a) symmetric matter and (b) asymmetric matter.

For the given boundary space-time, the density dependence of symmetry energy seems to depend on the dimensionality of D-brane system we use. For the 3+1 dimensional boundary theory, the probe brane should be $D6$ for $D4$ brane background and it should be $D7$ for $D3$ background. In the case of $D6$ brane,

$S_2 \sim \varrho^{1/2}$. On the other hand $S_2 \sim \varrho^{1/3}$ for $D7$ probe in $D3$ background. These differences appear in all other probe brane cases as well.

We can also consider symmetry energy in **deconfined phase**, namely, in quark matter instead of nuclear matter. The background geometry is a black brane. To introduce finite density or chemical potential, we introduce fundamental strings which connect black hole horizon and probe brane. The end points of fundamental strings attached on probe provide sources of $U(1)$ gauge field. Since the fundamental strings can move freely along the $D3$ direction of the black brane horizon, the boundary system can be identified as the system of freely moving quarks.

In the case of $D7$ brane, for low temperature, the symmetry energy goes like $S_2 = 0.32\tilde{Q}^{1/3}$ while at high temperature, the symmetry energy grows linearly. The symmetry energy line at low temperature for $D5$ probe case goes like $S_2 = 0.5\tilde{Q}^{1/2}$ and it becomes linear at high temperature. In the case of $D3$ probe, symmetry energy has linear behavior for all temperature. We emphasize that the result is based on the actual numerical calculation without any approximation.

3 Scaling property and universality classes

In this section, we want to understand the scaling behavior of the symmetry energy which is calculated in various models and various phases. We can re-derive these power behavior of symmetry energy analytically. To do this, we consider the ideally simplified case: BPS metric background and flat embedding of probe branes. In this case, background geometry becomes geometry of black Dq brane;

$$ds_{10}^2 = Z_p^{-1/2}(-dt^2 + d\vec{x}_p^2) + Z_p^{1/2} d\vec{x}_\perp^2, \tag{10}$$

with $e^{2\phi} = Z_p^{\frac{3-p}{2}}$. We now consider the general result for the symmetry energy given in eq. (9). The term in the square root becomes 1 and

$$\begin{aligned} e^{-2\phi} G_{xx}^d \left(\frac{G_{\perp\perp}}{\xi^2}\right)^{q-d-1} &= Z_p^{\frac{p-3}{2}} \cdot Z_p^{-\frac{d}{2}} \cdot Z_p^{\frac{q-d-1}{2}} \\ &= Z_p^{\frac{1}{2}(p+q-2d-4)}. \end{aligned} \tag{11}$$

The value of $p+q-2d$ is precisely equal to the number of Neuman-Dirichlet (ND) direction of Dp/Dq system. Therefore, if we focus on the system which is supersymmetric configurations or a smooth deformation of them, the exponent becomes zero. In this case the symmetry energy (9) for flat embedding can be calculated analytically:

$$S_2 = 2\tau_q \int d\rho \frac{\tilde{Q}\rho^{2n}}{\left(\tilde{Q}^2 + 4\rho^{2n}\right)^{3/2}} = c_n \tilde{Q}^{\frac{1}{n}}, \tag{12}$$

where $c_n = 2\tau_q \frac{2^{-2-1/n}\Gamma\left(\frac{1}{2n}\right)\Gamma\left(\frac{n-1}{2n}\right)}{n^2\sqrt{\pi}}$ and $n = q-d-1$ so that the density dependence of symmetry energy is $S_2 \sim Q^{\frac{1}{q-d-1}}$. This result reproduces all the result we obtained in previous section numerically.

Notice that both the background and embedding used here are far from the real situation: real background is a deformation of such BPS solution and the embedding is non-trivial deformation from such a flat embedding. Nevertheless, the scaling exponent is the same as the actual configuration used for numerical computation of previous sections. The point is that neither smooth deformation of the metric nor the deformation of the embedding shape seem to change the scaling behavior of the symmetry energy. The exponent of symmetry energy depends only on the dimensionality of probe brane and dimension of non-compact directions. *Therefore the scaling exponents depend only on the universality classes.*

4 Discussion

We considered the asymmetry energy for both nuclear matter as well as the quark matter. The symmetry energy has a power like density dependence with characteristic exponent which is invariant under the smooth deformation of the metric as well as smooth deformation of the embedding. It only depends on the dimensionality of the D-brane system modeling the QCD dynamics. Therefore it is a index for the universality class. The physical interpretation of the scaling exponent is still open question but we give a trial interpretation in terms of the *Non-fermi liquid nature of the nuclear matter.* According to the fermi gas model of nuclei, the Energy of the nuclei is the sum of the kinetic energies of neutrons and protons which are moving non-relativistically, namely,

$$E = \frac{3}{5}(N_p\epsilon_{Fp} + N_n\epsilon_{Fn}) \tag{13}$$

$$= \frac{3}{5}\epsilon_F A + \frac{1}{3}\epsilon_F A\delta^2 + \mathcal{O}(\delta^4), \tag{14}$$

where $A = N_p + N_n$ is the mass number and ϵ_F is the fermi energy for A, $\delta = \frac{(N_p-N_n)}{(N_p+N_n)}$. One can see that the symmetry energy per nucleon is $\epsilon_F/3$. Therefore fermi gas model demonstrates the origin of the symmetry energy as the Pauli principle. What happens if we include the interaction energy of the nucleons? The answer is largely unknown. Depending on how one includes the interaction, the answers are different from one another. In some of the traditional approach, interactions are taken care of by adding a polynomial in density, which means that scaling property ($\sim \rho^\alpha$) should be destroyed by the interaction. However, this is not what we get. In our approach, scaling property remains even in the large density limit. Notice that for the most interesting case of $D4/D6$ and $D3/D7$, the scaling exponents are $1/2$ and $1/3$ respectively. Comparing this with the non-interacting gas which gives $S_2 \sim \rho^{2/3}$, one can see that the symmetry energy of $D4/D6$ implies an anomalous dispersion relations which is neither relativistic nor non-relativistic one. For the $D3/D7$ case, the scaling is the same as the relativistic particles. If we naively extrapolate the relation $S_2 \sim \epsilon_F$, $S_2 \sim \rho^{1/2}$ means the anomalous dispersion relation $\epsilon \sim k^{3/2}$. One may want to associate this as the example of transformation of a particle to un-particle [13]

One may also expect that such anomalous dispersion relation is related to the non-fermi liquid nature of the strongly interacting fermion system. In the presence of the fermi sea, one expect that elementary excitations are quasi particles with renormalized charge and mass. However, when the interactions are strong, such quasi-particles will lose applicability. Using the AdS/CFT duality and utilizing the AdS at UV and the AdS_2 at the IR, it was shown in[14] that

$$G(\omega, k) = \frac{1}{\omega - v_F k_\perp - C\omega^{2\nu}}, \tag{15}$$

where $k_\perp$ is the momentum measured from the fermi surface. If $\nu < 1/2$, the dispersion relation becomes $\omega \sim k_\perp^{1/2\nu}$. For example, if $\nu = 1/3$ we get $\omega \sim k_\perp^{3/2}$. These phenomena are all beyond the fermi liquid behavior. For D3/D7 case, the exponent indicate that the system is marginally fermi liquid case. More systematic investigation on this matter is strongly desired.

Acknowledgments

This work was supported by the NRF grant funded by the Korea government(MEST) through the Mid-career Researcher Program with grant No. 2010-0008456.

References

[1] L.W. Chen, C.M. Ko, and B.A. Li, Phys. Rev. Lett. **94**, 032701 (2005).

[2] C. Xu and B. A. Li, Phys. Rev. C **81**, 064612 (2010) [arXiv:0910.4803 [nucl-th]].

[3] Y. Kim, Y. Seo, I. J. Shin and S. -J. Sin, JHEP **1106**, 011 (2011) [arXiv:1011.0868 [hep-ph]].

[4] J. M. Maldacena, Adv. Theor. Math. Phys. **2**, 231 (1998).

[5] M. Kruczenski, D. Mateos, R. C. Myers and D. J. Winters, JHEP **0405**, 041 (2004) [arXiv:hep-th/0311270].

[6] T. Sakai and S. Sugimoto, Prog. Theor. Phys. **113**, 843 (2005)
J. Erlich, E. Katz, D. T. Son and M. A. Stephanov, Phys. Rev. Lett. **95**, 261602 (2005)
L. Da Rold and A. Pomarol, Nucl. Phys. B **721**, 79 (2005)

[7] Y. Seo and S.-J. Sin, JHEP **0804**, 010 (2008).

[8] Y. Kim, Y. Seo, and S.-J. Sin, JHEP **1003**, 074 (2010).

[9] Y. Seo and S. -J. Sin, JHEP **1202**, 039 (2012) [arXiv:1201.0459 [hep-th]].

[10] N. J. Evans, S. D. H. Hsu and M. Schwetz, Phys. Lett. B **382**, 138 (1996) [arXiv:hep-ph/9605267].

[11] S. S. Gubser, arXiv:hep-th/9902155.
A. Kehagias and K. Sfetsos, Phys. Lett. B **454** (1999) 270

[12] Y. Seo, J. P. Shock, S. -J. Sin, D. Zoakos, JHEP **1003**, 115 (2010). [arXiv:0912.4013 [hep-th]].

[13] H. Georgi, Int. J. Mod. Phys. A **25**, 573 (2010).

[14] T. Faulkner, H. Liu, J. McGreevy and D. Vegh, Phys. Rev. D **83**, 125002 (2011) [arXiv:0907.2694 [hep-th]].

[15] E. Witten, “Baryons and branes in anti de Sitter space,” JHEP **9807**, 006 (1998).

Open inflation in the string landscape

Misao Sasaki
Yukawa Institute for Theoretical Physics, Kyoto University, Kyoto 606-8502, Japan
Email: misao@yukawa.kyoto-u.ac.jp

Abstract

Open inflation is receiving renewed interest in the context of the string theory landscape. Since there are a large number of metastable de Sitter vacua in the string landscape, tunneling from one vacuum to another occurs frequently through the bubble nucleation and open inflation is naturally realized. We argue that though the universe appears to be very flat, a small deviation of Ω_0 from unity can make the effect of tensor-type perturbations on the large angle CMB anisotropy significant. Thus we are already testing the string landscape against observations.

1 Introduction

Open inflation is attracting a renewed interest in the context of the string landscape. Since there are a large number of metastable de Sitter vacua in the string landscape, tunneling transitions between metastable vacua through the bubble nucleation occur frequently, and one of those transitions from a high energy false vacuum to a lower energy vacuum might have lead to our universe. If we assume our universe has been born out of bubble nucleation, then our universe must have gone through an era of inflation after that transition. Since the geometry inside the bubble is an open universe, this gives a natural realization of open inflation.

Although the deviation of Ω_0 from unity is small by the observational bound, we argue that the effect of this small deviation on the large angle CMB anisotropies can be significant for tensor-type perturbation in open inflation scenario.

We consider the situation in which there is a large hierarchy between the energy scale of the quantum tunneling and that of the slow-roll inflation in the nucleated bubble. If the potential just after tunneling is steep enough, a rapid-roll phase appears before the slow-roll inflation. In this case the power spectrum is basically determined by the Hubble rate during the slow-roll inflation. On the other hand, if such rapid-roll phase is absent, the power spectrum keeps the memory of the high energy density there in the large angular components.

Furthermore, the amplitude of large angular components can be enhanced due to the effects of the wall fluctuation mode if the bubble wall tension is small. Therefore, although even the dominant quadrupole component is suppressed by the factor $(1-\Omega_0)^2$, one can construct some models in which the deviation of Ω_0 from unity is large enough to produce measurable effects [1].

2 Open inflation

We consider false vacuum decay in a system consisting of a minimally coupled scalar field, ϕ with Einstein gravity. The action is given by

$$S = \int \sqrt{-g}\mathrm{d}^4x \left[\frac{1}{2\kappa}R - \frac{1}{2}g^{\mu\nu}\partial_\mu\phi\partial_\nu\phi - V(\phi)\right]. \tag{1}$$

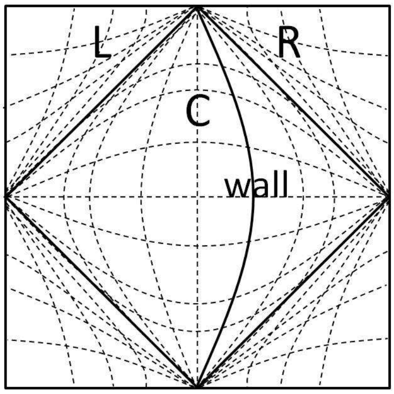

Figure 1: The Penrose diagram of a universe with bubble nucleation. The region R is an open universe inside the bubble, which corresponds to our universe.

An $O(4)$-symmetric bubble nucleation is described by the Euclidean solution (instanton). The metric is given by

$$ds^2 = a_{\rm E}^2 \left(d\eta_{\rm E}^2 + d\chi_{\rm E}^2 + \sin^2 \chi_{\rm E} d\Omega^2 \right) , \tag{2}$$

and the background scalar field is denoted by $\phi = \phi(\eta_{\rm E})$. The Euclidean equations are given by

$$\left(\frac{a'_{\rm E}}{a_{\rm E}} \right)^2 - 1 = \frac{\kappa}{3} \left(\frac{1}{2} \phi'^2 - V(\phi) a_{\rm E}^2 \right) , \tag{3}$$

$$a_{\rm E} \left(\frac{\dot{a}_{\rm E}}{a_{\rm E}} \right)^{\cdot} + 1 = -\frac{\kappa}{2} \phi'^2 , \tag{4}$$

$$\ddot{\phi} + 2 \frac{\dot{a}_{\rm E}}{a_{\rm E}} \dot{\phi} - V'(\phi) a_{\rm E}^2 = 0 , \tag{5}$$

where the prime represents differentiation with respect to $\eta_{\rm E}$.

The background geometry and the field configuration in the Lorentzian regime are obtained by the analytic continuation of the bounce solution. The coordinates in the Lorentzian regime are given by

$$\eta_{\rm E} = \eta_{\rm C} = -\eta_{\rm R} - \frac{\pi}{2} i = \eta_{\rm L} + \frac{\pi}{2} i , \tag{6}$$

$$\chi_{\rm E} = -i\chi_{\rm C} + \frac{\pi}{2} = -i\chi_{\rm R} = -i\chi_{\rm L} , \tag{7}$$

$$a_{\rm E} = a_{\rm C} = i a_{\rm R} = i a_{\rm L} . \tag{8}$$

The Penrose diagram for this open FLRW universe is presented in Fig. 1.

After tunneling, the scalar field starts to roll down the potential. If the vacuum energy of the false vacuum is high, as expected in the string theory landscape, there will be a phase during which the scalar field rolls down rapidly. This rapid roll phase will end when the energy scale becomes sufficiently low and a slow-roll phase commences which should last just about 50 to 60 e-folds, to make our universe slightly open, $1-\Omega_0 \sim 10^{-2}-10^{-3}$.

To study the field dynamics inside the bubble, it is useful to recall the identity,

$$\frac{\mathrm{d}\ln\rho_\phi}{\mathrm{d}\ln a_{\mathrm{R}}} = -3\,(1+w_\phi)\ , \tag{9}$$

where $\rho_\phi = \dot{\phi}^2/2+V$, $p_\phi = \dot{\phi}^2/2-V$ and $w_\phi \equiv p_\phi/\rho_\phi$. The asymptotic boundary conditions at the nucleation point are given by

$$a_{\mathrm{R}}(t) = t\,, \quad \dot{\phi}(t) = -\frac{V'(\phi_*)}{4}t\,. \tag{10}$$

Thus, we have

$$1+w_\phi = \mathcal{O}\left(\frac{\dot{\phi}^2}{V}\right) = \mathcal{O}\left(\epsilon_* H_*^2 t^2\right)\ . \tag{11}$$

where we have introduced

$$\epsilon \equiv \frac{1}{2\kappa}\left(\frac{V'}{V}\right)^2\ , \tag{12}$$

and $\epsilon_* = \epsilon(\phi_*)$ and $H_*^2 \equiv \kappa V(\phi_*)/3$.

As an example, the evolution of various quantities inside the bubble for a potential of the form,

$$\frac{\kappa}{3}V(\phi) = \left(H_*^2 - H_{\mathrm{R}}^2\right)\exp\left[\sqrt{2\kappa\epsilon_*}\,(\phi-\phi_*)\right] + H_{\mathrm{R}}^2\,, \tag{13}$$

where $H_* \gg H_R$, is shown in Fig. 2, where the constant term H_{R}^2 is added to realize slow-roll inflation after the rapid-roll phase. As seen from this figure, during the rapid-roll phase there is a tracking behavior for $\epsilon_* \gtrsim 1$. In particular, for $\epsilon_* = O(1)$, the scalar field energy dominates over the curvature term during the rapid-roll phase. As discussed later, this makes all the perturbations existed at the time of nucleation to be effectively frozon until the subsequent slow-roll phase. In short, the memory of the previous false vacuum remains in the spectrum of perturbations inside the bubble.

3 Tensor spectrum in the landscape

The tensor spectrum in the bubble universe may be calculated following the method developed in [2, 3]. The important point is that it reflects both the properties of the tunneling and the evolution inside the bubble. More specifically there are effects from the fluctuations of the bubble wall and the evolution during the rapid-roll phase inside the bubble.

The effect of the bubble wall fluctuations was discussed already in [4], where it was found that the infrared part of the spectrum is dominated by the wall fluctuations if the wall is sufficiently soft, that is, if the wall tension is small, $\Delta s = \kappa S_1/2H_* \ll 1$, where S_1 is the wall tension. Here let us focus on the effect of the evolution inside the bubble.

The resulting spectrum for the potential (13) is shown in Fig. 3. The solid curves are, from top to bottom, the spectrum with $\epsilon_* = 0.5,\ 0.8,\ 1,\ 10,\ 10^2$ and 10^4. Here the contribution from the wall fluctuation mode is assumed to be negligible. As seen from this figure, it is clear that the infrared part of the spectrum is enhanced substantially for $\epsilon_* = O(1)$. This means that the memory of the large vacuum fluctuations associated with the high vacuum energy right after the tunneling is preserved if $\epsilon_* = O(1)$ and can affect the observable part of the spectrum if $1-\Omega_0$ is not too small.

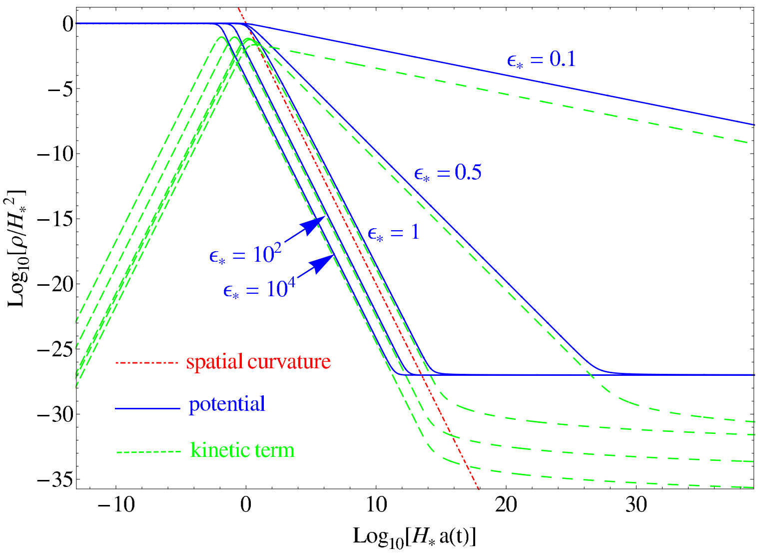

Figure 2: The evolution inside the bubble for an exponential type potential model.

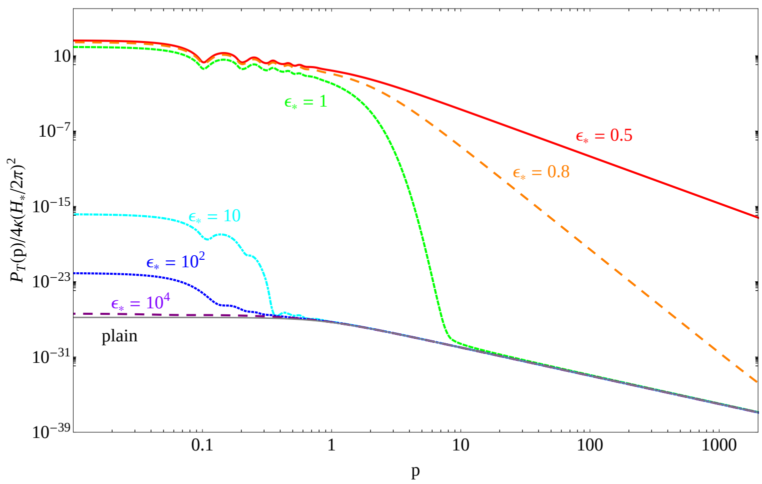

Figure 3: The tensor-type power spectrum with the exponential-type potential, Eq. 13. For comparison, we also plot the plain spectrum by the thin gray line.

4 CMB temperature anisotropy

We translate the spectrum for tensor-type perturbation obtained in the preceding subsection into CMB temperature anisotropies, following the discussion given in Ref. [4]. The large-angle CMB temperature

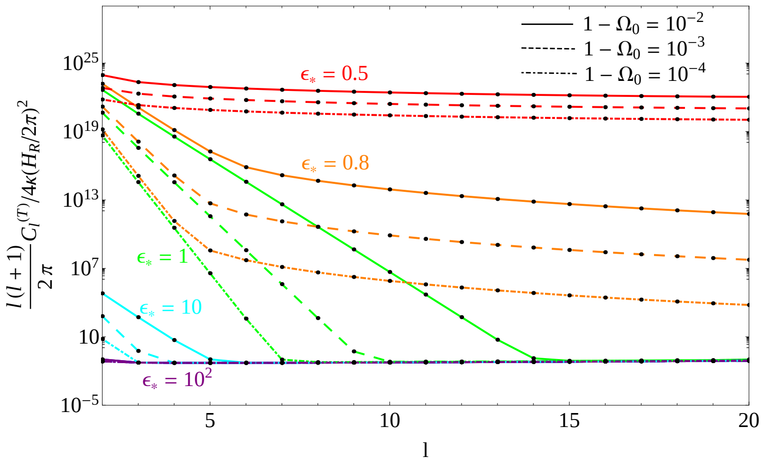

Figure 4: The CMB angular power spectrum from the tensor type perturbations for the exponential-type potential.

anisotropies due to tensor-type perturbation are simply evaluated by the Sachs-Wolfe formula

$$\frac{\Delta T}{T}(\hat{\boldsymbol{n}}) = -\frac{1}{2}\int_{\eta_{\rm LSS}}^{\eta_0} \mathrm{d}\eta \delta g'_{ij}\left(\eta, x^i(\eta)\right)\hat{n}^i\hat{n}^j\,, \tag{14}$$

where η_0 and $\eta_{\rm LSS}$, respectively, denote the conformal time at the present epoch and that at the last scattering surface, $\hat{n}^i$ is the unit vector along the observer's line-of-sight and $x^i(\eta) = (\eta_0 - \eta)\,\hat{n}^i$ represents the photon trajectory.

The CMB multipole moments for the tensor type perturbations for the exponential-type potential (13) are shown in Fig. 4. The parameters are $\epsilon_* = 0.5\,,\ 0.8\,,\ 1\,,\ 10$ and 10^2. Again for simplicity, the effect of the wall fluctuations is neglected. We see that the tensor CMB angular power spectrum for small ℓ behaves like $(1-\Omega_0)^\ell$, while it agrees with the scale invariant inflationary tensor spectrum for large ℓ. Compared with the amplitude of the tensor perturbation for the standard slow-roll inflation, there is significant enhancement for small ℓ for $\epsilon_* \lesssim 1$. Hence, we find that, unless ϵ is not extremely large, rapid rolling down affects the CMB spectrum at low ℓ significantly.

Now let us briefly mention the effect of the bubble wall fluctuations. It is known that the CMB angular spectrum can be approximately decomposed into two pieces:

$$C_\ell^{(\rm T)} = P_{\rm W}\,\tilde{C}_\ell^{(\rm W)} + C_\ell^{(\rm T,res)}\,, \tag{15}$$

where $P_{\rm W}\,\tilde{C}_\ell^{(\rm W)}$ represent contributions due to wall fluctuations:

$$P_{\rm W} = \int_0^\infty \mathrm{d}p P_{\rm T}(p)\,, \tag{16}$$

and

$$\frac{\ell(\ell+1)}{2\pi}\tilde{C}_\ell^{(\rm W)} \approx \frac{(\ell+2)!(\ell+1)!}{800\pi(\ell-1)\Gamma(\ell+3/2)}(1-\Omega_0)^\ell\,. \tag{17}$$

The residual component, $C_\ell^{(\mathrm{T,res})}$ corresponds to the continuous spectrum due to standard tensor perturbations, as the residual piece of the spectrum. Note that Fig. 4 basically corresponding to $C_\ell^{(\mathrm{T,res})}$.

We note that both modes at $p \approx 0$ and at $p \gtrsim 1$ contribute to the CMB quadrupole, but the former modes physically represent the wall fluctuation degree of freedom. As seen from Eq. (17), the effects of wall fluctuation mode mainly appear in the quadrupole of CMB temperature fluctuation. The amplitude of the wall fluctuation mode can be also evaluated analytically. We find

$$\frac{P_{\mathrm{W}}}{2\kappa H_*^2} \propto \frac{1}{\Delta s}\,. \tag{18}$$

Thus the amplitude of the wall fluctuations can be significantly enhanced when the wall tension is small.

5 Summary

In this talk, we considered an open inflation in the context of the string theory landscape. We assumed that our universe is an open universe with a moderately small $1-\Omega_0$, born as a bubble nucleated through false vacuum decay. We then discussed that the infrared part of the tensor perturbation can contain the memory of the string landscape, and hence can constrain the landscape considerabley. In fact, we argued that the current observational data already constain the string theory landscape, and near-future data may be able to make yet more strong statements on the string theory landscape. Apparently this is a very exciting topic which should be studied further.

Acknowledgments

The topic discussed here is based on the collaborative work with D. Yamauchi, A. Linde, A. Naruko and T. Tanaka. I thank them for fruitful collaborations. This work was supported by Grant-in-Aid for the global COE program, “The Next Generation of Physics, Spun from Universality and Emergence” at Kyoto University, by JSPS Grant-in-Aid for Scientific Research (B) No. 17340075, (A) No. 18204024, and by Grant-in-Aid for Creative Scientific Research No. 19GS0219.

References

[1] D. Yamauchi, A. Linde, A. Naruko, M. Sasaki and T. Tanaka, Phys. Rev. D **84**, 043513 (2011) [arXiv:1105.2674 [hep-th]].

[2] J. Garriga, X. Montes, M. Sasaki and T. Tanaka, “Canonical quantization of cosmological perturbations in the one-bubble open universe,” Nucl. Phys. B **513**, 343 (1998) [arXiv:astro-ph/9706229].

[3] J. Garriga, X. Montes, M. Sasaki and T. Tanaka, “Spectrum of cosmological perturbations in the one-bubble open universe,” Nucl. Phys. B **551**, 317 (1999) [arXiv:astro-ph/9811257].

[4] M. Sasaki, T. Tanaka and Y. Yakushige, “Wall fluctuation modes and tensor CMB anisotropy in open inflation models,” Phys. Rev. D **56**, 616 (1997) [arXiv:astro-ph/9702174].

Exact Solutions in Gravity and Cosmology with Extra Dimensions

V.N. Melnikov
Center for Gravitation and Fundamental Metrology, VNIIMS, and
Institute of Gravitation and Cosmology, PFUR,
46 Ozernaya Str. 119361, Moscow, Russia
Email : melnikov@phys.msu.ru

Abstract

New challenges to theoretical physics and the role of gravity and cosmology are discussed. Problems of gravitation as the fundamental interaction are also analyzed. Results of integrable gravitational and cosmological models with extra dimensions with scalar fields, forms and other matter sources are presented. Their role in solving basic problems of modern cosmology and black hole physics, such as the present acceleration of the Universe, nonsingular initial state, stability of fundamental constants etc. is pointed out.

1 Introduction

Gravitation as a fundamental interaction that acts at all scales, but still not well understood at a quantum level, is a missing link to the unification of all physical interactions [1, 2, 3]. Discovery of the present acceleration of the Universe, dark matter and dark energy problems are also a great challenge to modern physics, which may bring to a new revolution in it. Possible variations of fundamental physical constants (FPC) is the third major problem nowadays [4, 5, 6]. Present limits on variations of four physical interactions are the following:

$\dot{\alpha}/\alpha$ — less than 10^{-17}/y (clocks-present epoch),
$\dot{g}_w/g_w$ — less than 10^{-12}/y (Schlyakhter, Oklo),
$\dot{g}_s/g_s$ — less than 10^{-18}/y (Schlyakhter, Oklo),
$\dot{G}/G$ — less than 5 x 10^{-13}/y (Pitieva-RR, Turyshev-LLR, present epoch).

Data about the anisotropy of the fine structure constant variations from QSO spectra at z = (0.5 - 3), or (2-10 bn years ago): they have different signs of the relative variation of α leading to: $\alpha < \alpha_0$ in the Northern (Keck, Hawaii) and $\alpha > \alpha_0$, in the Southern Hemispheres (VLT, Chile), α_0 - present value of α. This anisotropy is of the dipole type (Australian dipole), its axis:

(17.3 + 0.6) h; (-61 + 9) degrees. α at any r (in bn years) of space:

$\delta\alpha/\alpha_0 = (1.10 + 0.25)$ x $10^{-6} r \cos\psi$,

ψ is the angle between the direction to QSO and the dipole one.

Results of these recent observations - confirmation of theoretical predictions on possible variations of FPC at cosmological scales.

If time and space variations of α will be confirmed, it will bring to serious changes in our conception of laws of physics and Nature as well. Some theoretical models explaining these variations of α already appeared using ideas of a domain wall and generalized theories of varying α, namely: existence of a domain wall crossing the Hubble volume in the model of a scalar field interacting with electromagnetic and fermion fields; a runaway domain wall due to the potential of the scalar field without a limit below; generalization of the BSBM-theory with varying α etc.

As all attempts to quantize general relativity in a usual manner failed and it was proved that it is not renormalizable, it became clear that the promising trend is along the lines of unification of all physical interactions which started in the 70's. About this time the experimental investigation of gravity in strong fields and gravitational waves started giving a speed up in theoretical studies of such objects with strong gravitational fields as pulsars, black holes and wormholes, QSO, SN, AGN, early Universe etc., which continues now.

In experimental activities some crucial next generation gravitational experiments verifying predictions of unified schemes will be important. Among them are: MICROSCOPE, STEP - testing the Equivalence Principle, SEE - testing the inverse square law, or new non-newtonian interactions, EP, possible variations of G with time, measurements of its absolute value with unprecedented accuracy [7]. Of course, gravitational waves problem, verification of torsional, rotational, 2nd order and strong field effects remain important also.

Other very important feature, which may be envisaged, is an increasing role of fundamental physics studies, gravitation, cosmology and astrophysics in particular, in space experiments [8]. Unique microgravity environments and modern technologies give nearly ideal place for gravitational experiments which suffer a lot on Earth from its relatively strong gravitational field and gravitational fields of nearby objects as there is no way of screening gravity.

In the development of relativistic gravitation and dynamical cosmology we may notice three distinct stages: first, investigation of models with matter sources in the form of a perfect fluid, as was originally done by Einstein and Friedmann. Second, studies of models with sources as different physical fields, starting from electromagnetic and scalar ones, both in classical and quantum cases (see our results in [4]). And third, which is really topical now, application of ideas and results of unified models for treating fundamental problems of cosmology, black hole and wormholes physics, especially in high energy regimes and for explanation of the present acceleration of the Universe, dark matter and dark energy problems. Multidimensional gravitational models play an essential role in the latter approach.

The necessity of studying multidimensional models of gravitation and cosmology [1, 2, 3] is motivated by several reasons. First, the main trend of modern physics is the unification of all physical interactions. During recent decades there has been a significant progress in unifying weak and electromagnetic interactions, some more modest achievements in GUT, supersymmetric, string and superstring theories.

Now, theories with membranes, p-branes and M-theory are being created and studied. Having no definite successful theory of unification now, it is desirable to study the common features of these theories and their applications to solving basic problems of modern gravity and cosmology.

Second, multidimensional gravitational models, as well as STT, are theoretical frameworks for describing possible temporal and range variations of FPC [4, 5, 6]. The possible discovery of α variations and its anisotropy is now at a critical investigation.

Lastly, applying multidimensional gravitational models to basic problems of modern cosmology and BH physics, we hope to find answers to such long-standing problems as singular or nonsingular initial states, creation of the Universe, creation of matter and its entropy, cosmological constant, coincidence problem, origin of inflation and specific scalar fields which may be necessary for its realization, isotropization and graceful exit problems, stability and nature of FPC [8], possible number of extra dimensions, their stable compactification, new data on present acceleration of the Universe, DM and DE etc.

Multidimensional gravitational models are certain generalizations of GR which is tested reliably for weak fields up to 0.0001 and partially in strong fields (binary pulsars), so it is quite natural to inquire about their possible observational or experimental windows. These windows are:

– possible deviations from the Newton and Coulomb laws,

– possible variations of the effective G with a time rate less than the Hubble one,
– possible existence of monopole modes in gravitational waves,
– different behavior of strong field objects, such as multidimensional black holes, wormholes and AGN,
– standard cosmological tests,
– possible non-conservation of energy in strong field objects and accelerators, if braneworld or similar ideas about gravity in the bulk turn out to be true, etc.

Since modern cosmology has already become a unique laboratory for testing standard unified models at energies far beyond the level of existing and future man-made accelerators, there is a possibility of using cosmological and astrophysical data for discriminating between future unified schemes. Data on possible FPC time variations or possible deviations from the Newton law should also contribute to the unified theory choice.

As no accepted unified model exists, in our approach [1, 2, 9] we adopted models, based on multidimensional Einstein equations with or without sources of different nature as: cosmological constant, perfect and viscous fluids, scalar and electromagnetic fields and their possible interactions, dilaton and moduli fields, fields of antisymmetric forms (related to p-branes) etc.

Our program main objective was and is to obtain integrable models and then to analyze them in cosmological, spherically and axially symmetric cases. It was done mainly within the Riemann geometry. We tried to single out models, which do not contradict available experimental or observational data, on variations of G as well.

As our model [1, 2, 3] we use n Einstein spaces of constant curvature with sources as (m+1)-component perfect fluid or different fields or form-fields, cosmological or spherically symmetric metric and manifold as a direct product of factor-spaces of arbitrary dimensions. These models are low energy limits of the unified models. Then in harmonic time gauge we show that Einstein multidimensional equations are equivalent to Lagrange equations with a non-diagonal in general minisuperspace metric and some exponential potential. After diagonalization of this metric we perform reduction to sigma-model and Toda-like systems, further to Liouville, Abel, generalized Emden-Fowler Eqs. etc. and find exact solutions. We suppose that extra spaces are constant, or dynamically compactified, or like torus, or large, but with barriers, walls etc.

So, we realized this program (from 1988) [1, 2, 3, 9] obtaining exact **cosmological solutions** with the following sources:

- Λ , Λ + minimal scalar field (singled out non-singular, dynamically compactified, inflationary, 1994);
- perfect fluid, PF + scalar field (e.g. nonsingular, inflationary solutions, 94);
- viscous fluid (e.g. nonsingular, generation of mass and entropy, quintessence and coincidence in 2-component model, 2000, 2001);
- with stochastic behavior near the singularity, billiards in Lobachevsky space, D=11 is critical, φ destroys billiards (1994);
- for all above cases Ricci-flat solutions were obtained for any n, also with curvature in one factor-space; with curvatures in 2 factor-spaces only for total N=10, 11, 1996;
- fields: scalar, dilatons, forms of arbitrary rank (1997, 1998) - inflationary, Λ generation by forms (p-branes), 1998;
- first billiards for dilaton-forms (p-branes) interaction (1999);
- quantum variants (solutions of WDW-equation [10]) for all above cases;
- dilatonic fields with potentials [11], billiard behavior for them also.

For many of these integrable models we calculated the time variation of the effective G. Comparison with the present experimental bounds allowed to choose some viable classes of solutions.

Solutions depending on r in any dimensions were obtained:

- generalized Schwarzchild, generalized Tangerlini (BH's are singled out), also with minimal scalar field (no BH's);
- generalized Reissner-Nordstrom (BH's also are singled out), the same plus φ (no BH's);
- multi-temporal;
- for dilaton-like interaction of φ and electromagnetic fields (BH's exist only for a special case);
- stability studies (stable solutions only for the BH case above);
- the same was done for dilaton-forms (p-branes) interaction,
- stability found only for one form case.

PPN parameters different from GR for most of the models were calculated.

2 Multidimensional Models

In all unified theories, 4-dimensional gravitational and cosmological models with extra fields were obtained by dimensional reduction based on the decomposition of the manifold $M = M^4 \times M_{\rm int}$, where M^4 is our 4-dimensional manifold and $M_{\rm int}$ is some internal manifold.

The earlier papers dealt with multidimensional Einstein equations and with a block-diagonal cosmological or spherically symmetric metric defined on the manifold $M = R \times M_0 \times \cdots \times M_n$ of the form $g = -dt \otimes dt + \sum_{r=0}^{n} a_r^2(t) g^r$, where (M_r, g^r) are Einstein spaces, $r = 0, \ldots, n$. In some of them a cosmological constant and simple scalar fields were also used [10].

Such models are usually reduced to pseudo-Euclidean Toda-like systems. There exists a special class of equations of state that gives rise to Euclidean Toda models [12].

Cosmological solutions are closely related to solutions with spherical symmetry. Moreover, the scheme of obtaining the latter is very similar [1, 13]. The Schwarzschild solution was generalized to the case of n internal Ricci-flat spaces and it was shown that a BH configuration takes place when the scale factors of internal spaces are constant. It was shown also that a minimally coupled scalar field is incompatible with the existence of BH's. Similar generalization of the Tangerlini solution was obtained, and an investigation of singularities was performed. These solutions were also generalized to the electro-vacuum case with and without a scalar field [14, 15]. Here, it was also proved that BH's exist only when a scalar field is switched off. Deviations from the Newton and Coulomb laws were obtained depending on mass, charge and number of dimensions. In [15] spherically symmetric solutions were obtained for a system of scalar and electromagnetic fields with a dilaton-type interaction and also deviations from the Coulomb law were calculated depending on charge, mass, number of dimensions and dilaton coupling. Multidimensional dilatonic BH's were singled out. A theorem was proved in [15] that "cuts" all non-BH configurations as being unstable under even monopole perturbations. In [16] the extremely charged dilatonic BH solution was generalized to a multi-center (Majumdar-Papapetrou) case when the cosmological constant is non-zero.

The low-energy limit of unified theories leads to multidimensional models with p-branes.

Exact solutions with "branes"

In our papers several classes of the exact solutions for the multidimensional gravitational model governed by the Lagrangian

$$\mathcal{L} = R[g] - 2\Lambda - h_{\alpha\beta} g^{MN} \partial_M \varphi^\alpha \partial_N \varphi^\beta - \sum_a \frac{1}{n_a!} \exp(2\lambda_{a\alpha}\varphi^\alpha)(F^a)^2 \tag{1}$$

were considered. Here g is metric, $F^a = dA^a$ are forms of ranks n_a and φ^α are scalar fields and Λ is a cosmological constant (the matrix $h_{\alpha\beta}$ is invertible).

In [9] certain classes of p-brane solutions to field equations, obtained by us earlier, were presented.

These solutions have a block-diagonal metrics defined on D-dimensional product manifold, i.e.

$$g = e^{2\gamma} g^0 + \sum_{i=1}^{n} e^{2\phi^i} g^i, \qquad M_0 \times M_1 \times \ldots \times M_n, \tag{2}$$

where g^0 is a metric on M_0 (our space) and g^i are fixed Ricci-flat (or Einstein) metrics on M_i (internal space, $i > 0$). The moduli γ, ϕ^i and scalar fields φ^α are functions on M_0 and fields of forms are also governed by several scalar functions on M_0. Any F^a is supposed to be a sum of monomials, corresponding to electric or magnetic p-branes (p-dimensional analogues of membranes), i.e. the so-called composite p-brane ansatz is considered [17, 18, 19].

$p = 0$ corresponds to a particle, $p = 1$ to a string, $p = 2$ to a membrane etc. The p-brane world-volume (world-line for $p = 0$, world-surface for $p = 1$ etc.) is isomorphic to some product of internal manifolds: $M_I = M_{i_1} \times \ldots \times M_{i_k}$ where $1 \le i_1 < \ldots < i_k \le n$ and has dimension $p + 1 = d_{i_1} + \ldots + d_{i_k} = d(I)$, where $I = \{i_1, \ldots, i_k\}$ is a multi-index describing the location of p-brane and $d_i = \dim M_i$. Any p-brane is described by the triplet (p-brane index) $s = (a, v, I)$, where a is the color index labeling the form F^a, $v = e(lectric), m(agnetic)$. For the electric and magnetic branes corresponding to form F^a the world-volume dimensions are $d(I) = n_a - 1$ and $d(I) = D - n_a - 1$, respectively. The sum of this dimensions is $D - 2$. For $D = 11$ supergravity we get $d(I) = 3$ and $d(I) = 6$, corresponding to electric $M2$-brane and magnetic $M5$-brane.

Some our recent results on theoretical models with variations of G, FPC, billiards, solutions with branes and black branes and planned transitions to new definitions of SI units see in [20, 21], [22], [23] and [24] correspondingly. More details may be found in [25].

Acknowledgments

The work was supported in part by the RFBR grant 11-02-91155-GFEN-a and by the FTsP "NNPKIR" for 2009-2013.

References

[1] V.N. Melnikov, Multidimensional Classical and Quantum Cosmology and Gravitation. Exact Solutions and Variations of Constants. CBPF-NF-051/93, Rio de Janeiro, 1993.
V.N. Melnikov, in Cosmology and Gravitation, ed. M. Novello, Editions Frontieres, Singapore, 1994, p. 147.

[2] V.N. Melnikov, Multidimensional Cosmology and Gravitation, CBPF-MO-002/95, Rio de Janeiro, 1995.
V.N. Melnikov, in Cosmology and Gravitation. II, ed. M. Novello, Editions Frontieres, Singapore, 1996, p. 465.

[3] V.N.Melnikov, Exact Solutions in Multidimensional Gravity and Cosmology III. CBPF-MO-03/02, Rio de Janeiro, 2002.

[4] K.P. Staniukovich and V.N. Melnikov, Hydrodynamics, Fields and Constants in the Theory of Gravitation, Energoatomizdat, Moscow, 1983. (in Russian). English translation of first 5 sections in
V.N. Melnikov, Fields and Constraints in the Theory of Gravitation, CBPF MO-02/02, Rio de Janeiro, 2002.

[5] V. de Sabbata, V.N. Melnikov and P.I. Pronin, Theoretical Approach to Treatment of Non-Newtonian Interactions, *Prog. Theor. Phys.*, 88(1992)623.

[6] V.N. Melnikov, in Gravitational Measurements, Fundamental Metrology and Constants, eds. V. de Sabbata and V.N. Melnikov, Kluwer Academic Publ., Dordtrecht, 1988, p. 283.

[7] A.J.Sanders, V.N.Melnikov et al., Project SEE (Satellite Energy Exchange): an International Effort to Develop a Space-based Mission for Precise Measurements of Gravitation, *Class.Quant.Grav.*, 17 (2000) 2331.

[8] V.N.Melnikov, Gravity as a Key Problem of the Millennium, in Proc.2000 NASA/JPL Conference on Fundamental Physics in Microgravity, NASA Document D-21522, 2001, p.4.

[9] V.D. Ivashchuk and V.N. Melnikov, Exact solutions in multidimensional gravity with antisymmetric forms, topical review, *Class. Quantum Grav.*, 18 (2001) R82.

[10] U. Bleyer, V.D. Ivashchuk, V.N. Melnikov and A.I. Zhuk, Multidimensional Classical and Quantum Wormholes in Models with Cosmological Constant, *Nucl. Phys.* B, 429 (1994) 117.

[11] V.D. Ivashchuk, V.N. Melnikov and A.B. Selivanov, Cosmological solutions in multidimensional model with multiple exponential potential, *JHEP*, 0309 (2003) 059.

[12] V.R. Gavrilov, V.D. Ivashchuk and V.N. Melnikov, Integrable Pseudo-Euclidean Toda-like Systems in Multidimensional Cosmology with Multicomponent Perfect Fluid, *J. Math. Phys.*, 36 (1995) 5829.

[13] V.D. Ivashchuk and V.N. Melnikov, Multidimensional cosmology with m-component perfect fluid, *Int. J. Mod. Phys. D*, 3 (1994), 795.

[14] V.D. Ivashchuk and V.N. Melnikov, Multidimensional generalization of Tangerlini solution, *Class. Quantum Grav.*, 11 (1994) 1793.

[15] K.A. Bronnikov and V.N. Melnikov, *Annals of Physics (N.Y.)* Black Holes in Multidimensional Dilaton Gravity: Existence and Stability, 239 (1995) 40.

[16] V.D. Ivashchuk and V.N. Melnikov, Extremal dilatonic black holes in string-like model with cosmological term, *Phys. Lett. B*, 384 (1996) 58 .

[17] V.D. Ivashchuk and V.N. Melnikov, Multidimensional classical and quantum cosmology with intersecting p-branes, *J. Math. Phys.*, 39 (1998) 2866.

[18] V.D. Ivashchuk and V.N. Melnikov, Intersecting p-Brane Solutions in Multidimensional Gravity and M-Theory,*Grav. Cosmol.*, 2 (1996) 297.

[19] V.D. Ivashchuk and V.N. Melnikov, Generalized Intersecting P-brane Solutions from Sigma-model Approach, *Phys. Lett. B*, 403 (1997) 23.

[20] V.N. Melnikov, FPC and Theoretical Models for Time Variation of G, *Progr.Theor.Phys.*, Suppl., N 172 (2008) 182.

[21] V.N. Melnikov, Models of G Time Variations in Diverse Dimensions, *Frontiers of Physics*, 4 (2009) 75.

[22] V.D. Ivashchuk and V.N. Melnikov, On the billiard approach in multidimensional cosmological models, *Grav. Cosmol.*, 15 (2009) 49.

[23] V. D. Ivashchuk and V. N. Melnikov, Black brane solutions related to non-singular Kac-Moody algebras, *Grav. Cosmol.*, 17 (2011) 7.

[24] V.N. Melnikov, Multidimensional Cosmology, Constants and Transition to New SI Units, *Int. J. Mod. Phys. A*, 26 (2011) 3788.

[25] See other papers for V.N. Melnikov in e-archive, gr-qc and hep-th.

Traditional Cham sword dance

Cultural Exhibition : Roland Triay (vainly trying to shake the hand of an artist)

On M2 and M5 Branes

Kimyeong Lee
Korea Institute for Advanced Study

Abstract

In this talk, I review briefly my works on M2 and M5 branes. Especially I focus on our recent work on the relation between the 1/4 BPS junctions in the Coulomb phase of the 6-dim (2,0) superconformal field theories related to M5 branes and the mysterious N-cubic degrees of freedom on N M5 branes are elaborated [1, 2]. The detail references can be found in these works.

1 Introduction

Almost all phenomena in Nature are mediated by four fundamental forces which are strong, weak, electromagnetic and gravitational. The Standard Model which is the quantum field theoretic description of strong, weak and electromagnetic forces has been established about 40 years ago. The general relativity which is the classical theory for the gravitational force can also be quantized as a quantum field theory. However this version of quantum gravity is incomplete in ultra-violet region of energy and needs a modification in short-distance. The only successful version is the superstring theories which have been discovered and studied as the consistent quantum gravity theory since the late 70's.

The five consistent superstring theories in 10-dim have been known in early 80's [3] and are now known to be unified to 11-dim M-theory [4]. In the flat 11-dim background, M-theory has only one parameter, 11dim Planck length ℓ_P, which provides the mass or length scale to the problem. The low energy dynamics is governed by the 11-dim supergravity whose fields are the metric tensor g_{MN}, the gaugino field ψ_M and the anti-symmetric tensor field C_{MNP}. Besides the massless gravity multiplet associated with these fields, there are membrane-like objects which are sources for the 3-form tensor field C_{MNP}. The electric source is 2-dim 1/2 BPS M2 branes and the magnetic source is 5-dim 1/2 BPS M5 branes.

In addition M-theory is purely quantum and so $\hbar = 1$. The electric and magnetic charge of M2 and M5 branes are fixed without any adjustable parameters. The ultimate understanding of the string/M-theory needs the understanding of the physics of M2 and M5 branes also.

2 Physics on M2 Branes

The M theory can be obtained from the strong coupling limit of the type IIa string theory in 10-dim. In the strong coupling limit, an additional spatial direction appears. D0 branes in this string theory are Kaluza-Klein modes and the string coupling constant g_s and type IIa string length scale ℓ_s are related to the compactification radius R and the Planck scale ℓ_P of the 11-dim M-theory as

$$g_s \sim \sqrt{\frac{R^2}{\ell_p^2}}, \quad \ell_s \sim \sqrt{\frac{\ell_p^3}{R}}. \tag{1}$$

The D2 brane in type IIa string theory becomes the M2 brane in the strong coupling limit. The theory on N D2 branes is the 3-dim maximally supersymmetric Yang-Mills theory with the dimensionful coupling constant, $g^2_{3dYM} \sim g_s/\ell_s \sim \sqrt{R^3/\ell_p}$. This theory is super-renormalizable and free in short-distance. Its infra-red physics is very strongly interacting and superconformal. Thus it is hard to make reasonable calculations on M2 branes.

Recent progress has been pioneered by Begger, Lambert and Gustavsson and developed further by many theorists. Especially by Aharony, Bergman, Jafferis and Maldacena [5] have discovered that $U(N)\times U(N)$ Chern-Simons theories of opposite quantized Chern-Simons levels $(k,-k)$ with hyper and twisted hyper-multiplets in the bi-fundamental representation is the right theory describing N M2-branes on C^4/Z_k orbifold. This ABJM theory is superconformal with 12 super symmetries and is dual to M-theory in $AdS_4\times S^7/Z_k$.

Our group has written the ABJM theory beforehand as a part of the general class of $\mathcal{N}=4$ theories and has related that to the physics on M2 branes. Furthermore, we have contributed in many works in the development of ABJM theory [6, 7]

3 On M5 Branes

On the other hand the low energy physics on the N parallel M5 branes are known to be the 6-dim supersymmetric (2,0) theory of A_{N-1} type. For the single M5 brane, the 6-dim supersymmetric (2,0) theory is the field theory on a two-form tensor field $B_{\mu\nu}$, 5 scalar fields $\phi_I(I=1,2,\cdots 5)$ and the fermionic field λ. The 3-form field strength $H=dB$ is selfdual $H=*H$ and so there remain only 3 degrees of freedom among the 6 d.o.f in the 2-form field. The spinor field is 6-dim chiral and fundamental under the $Sp(2)=SO(5)$ R-symmetry. The scalar is a 5-dim vector of $SO(5)_R$. The external source for the 2-form field is selfdual string. As the field strength is selfdual, the electric and magnetic strength are identical and so $\hbar=1$. This means that the (2,0) theories are purely quantum without any adjustable coupling constant.

In the Coulomb phase of the theory, say the A_1 theory on two M5 branes, there can be 1/2 BPS selfdual strings whose tension is given by the vacuum expectation value of the scalar field. This selfdual string would be a straight M2 brane stripe connecting two M5 branes. This string would carry both electric and magnetic charges for unbroken abelian 2-form tensor. In the limit where the symmetry is restored, these 1/2 BPS selfdual strings become tensionless. The physics at this symmetric phase is the intrinsically nonabelian theory of A_{N-1} type with tensionless strings. As there is no simple nonabelian generalization of the two-form tensor field, it is very hard to write down this nonabelian (2,0) theory.

When one includes the 5-dim orientifold OM5 to N M5 branes, one can show that there exists the (2,0) theory of the D_N type. One can compactify type IIb theory on K3 surface and explore the physics near the ADE type of singularities. One can take the decoupling limit of the gravity, ending up with 6-dim (2,0) theories of ADE type [8]. These are three-types of the (2,0) superconformal theories in 6-dim.

While one can break the gauge symmetry spontaneously by taking the nonzero expectation value of five scalar fields, the physics at the symmetric phase is strongly interacting without any adjustable coupling constant and mass scale. In short it is a superconformal field theory which is an extension of the Poincare supersymmetry. The superconformal symmetry is $OSp(2,6|2)$ with bosonic part is made of the 6-dim conformal group $SO(2,6)$ and $Sp(2)$ R-symmetry.

While there exists no definite field theoretic formalism, there are several other tools to explore the physics of M5 branes. One is to heat up M5 branes and explore its property via AdS-CFT correspondence to black hole solutions in $AdS_7\times S^4$. One striking result is that the entropy density on finite temperature N M5 brane grows fast as N^3 [9, 10]. This contrasts the N^2 growth in the entropy density on finite temperature N D3 branes, which is basically the dimension of the adjoint representation which is the representations of the fields in the 4-dim $\mathcal{N}=4$ supersymmetric Yang-Mills theory on N D3 branes. Clearly there are more degrees of freedom on N M5 branes whose characteristics are not obvious to us.

Another support for the N-cubic growth of the degrees of freedom comes from the anomaly analysis [11]. As the 3-form field strength and the fermions are chiral under the 6-dim Lorentz transformation, there is a gravitational anomaly which is characterized by the 8-form characteristic class. The anomaly is characterized by the parameter c_G which is the product of the dimension d_G of the group and its dual Coxeter number h_G. It turns out c_G is divisible by six for ADE type. The following table is the rank, dimension, dual Coxeter number and the anomaly coefficient for ADE groups.

Obviously the anomaly coefficient grows like N^3 for A_N and D_N type of theories. Natural speculation for the N^3 degrees of freedom is to draw the pants diagram which connects 3 M5 branes. Our counting could be

Table 1: Anomaly Coefficient c_G in terms of the rank r_G

and dimension d_G and the dual co-Coxeter number h_G

Group	r_G	d_G	h_G	$\frac{1}{3}c_G$
A_{N-1}	$N-1$	N^2-1	N	$\frac{1}{3}N(N^2-1)$
D_N	N	$N(2N-1)$	$2(N-1)$	$\frac{2}{3}N(N-1)(2N-1)$
E_6	6	78	12	312
E_7	7	133	18	798
E_8	8	248	30	2480

regarded more sophisticated version of this picture.

While it is not clear how such N^3 degrees of freedom appear in the symmetric phase, one could ask whether such large degrees of freedom are present even in the Coulomb phase. There are naturally 1/2 BPS selfdual strings whose tension is determined by the scalar field expectation value which can be translated to the distance between M5 branes. Those selfdual strings are characterized by two M5 branes which are connected by these M2 branes and so there would be $N(N-1)/2$ kinds for N M5 branes. It turns out that selfdual strings are its own anti string upon the spatial rotation. This allows selfdual strings to annihilate itself by making a simple loop and shrinking to zero size, emitting massless tensor multiplets.

To explore additional digress of freedom appearing in the Coulomb phase of the 6-dim theories, let us first compactify them to a small circle and consider the 5-dim maximally supersymmetric Yang-Mills theories which appear as the low energy dynamics ignoring the Kaluza-Klein modes.

3.1 5d Super Yang-Mills theories

One way to approach M-theory is to take the strong coupling limit of type IIa string theory. Type IIa string theory arise from the compactification of M-theory on a small circle. D0 branes in type IIa theory are Kaluza-Klein modes of this compactification. M5 branes wrapping the circle would be come D4 branes. The low energy physics on the parallel D4 branes are well-known 5-dim maximally supersymmetric Yang-Mills theory. Naturally the compactification of the 6-dim (2,0) theories on a circle leads to the 5-dim supersymmetric Yang-Mills theory as the low energy dynamics.

While one naively expects the 6-dim (2,0) theory on a circle would be equivalent to the whole dynamics of the zero mode part, that is, 5-dim supersymmetric Yang-Mills theory and the towers of Kaluza-Klein modes. The KK modes can be naturally identified with modes which carry linear momentum along the compact circle. However as Seiberg [12] noted sometime ago instanton solitons in 5-dim Yang-Mills theory also carry the same KK momentum. There are two kinds of objects to carry the same quantum number, instantons and towers of KK modes in the compactified (2,0) theory. As the 6d (2,0) theory is purely quantum, there may be some mysterious gauge symmetry which identifies these two modes. Such a principle is not yet available.

As instanton solitons in the 5-dim Yang-Mills theory carry all Kaluza-Klein momentum, one may ignore the original KK modes as double counting and may declare that the 5-dim maximally supersymmetric Yang-Mills theory is complete by its own [13]. There may be three possible hypothesis. (1) 5-dim $\mathcal{N}=2$ SYM theory is not complete by its own and needs additional the additional UV terms. (2) 5-dim $\mathcal{N}=2$ SYM theory is complete by its own but not perturbatively finite. (3) 5-dim $\mathcal{N}=2$ SYM theory is complete by its own and also perturbatively finite. There are also nonperturbative objects in the 5-dim SYM theory such as instantons and tensionless magnetic strings.

One could ask whether N-cubic degrees of freedom have disappeared completely after compactification or lingers around in certain form. As one has the Lagrangian for the 5-dim Yang-Mills theory at least, one could ask where there is an enhancement of degrees of freedom. The fields in the 5-dim YM belong to the adjoint representation and so the naive counting says that there are N^2 degrees of freedom.

One could explore what kinds of objects are in the 5-dim Yang-Mills theory. In the symmetric phase, one has N^2-1 massless vector multiplet for $SU(N)$ gauge theory for the gauge fields in the weak coupling limit. These would be dual to the 1/2 BPS massless tensor multiplet in 5-dim. It is not known how to write down 5-dim 2-form $B_{\mu\nu}$ tensor field and its field strength $H=dB$ in the nonabelian case. However for the abelian limit or weak coupling limit, there is 5-dim Poincare duality $(F=dA)=*(H=dB)$. Also there are 1/2 BPS instanton solitons which satisfy the selfdual or anti-selfdual equations $F_{ij}=\pm\tilde{F}_{ij}$ in 4 spatial dimension. A single instanton have $4h_G$ zero modes for the gauge group G. This is one place where the dual Coxeter number h_G makes appearance. There are tensionless nonabelian magnetic monopole strings which would be source for the 2-form nonabelian tensor B. It is not clear whether additional d.o.f. among these objects besides the naive counting. There is a chance in the dyonic instantons which we will mention later.

In the Coulomb phase where the gauge symmetry, say $SU(N)$ on N D4 branes, is completely broken to abelian subgroup, the BPS objects are richer. With the roots of $SU(N)$ to be $e_i-e_j,(i,j=1,2\cdots N)$. There are 1/2 BPS massless vector multiplet for $N-1$ $U(1)$ subgroups for the Cartan subgroup of $SU(N)$. There are also 1/2 BPS massive vector multiplets for $\pm(e_i-e_j)$ W and anti W bosons for the fundamental strings connecting i-th D4 brane and j-th D4 brane. Then there are also 1/2 BPS monopole strings for D2 brane connecting i-th D4 brane and j-th D4 brane. The 1/2 BPS instantons which are $D0$ branes would be attached to D4 branes if one turns on the noncommutative parameter on D4 branes. These instantons would be a collection of abelian instantons. Non of these 1/2 BPS objects could account for the N-cubic degrees of freedom.

Let us now explore the 1/4 BPS objects. These are usually combinations of 1/2 BPS objects. There are 1/4 BPS dyonic instantons whose supersymmetric index has been studied recently. There are also magnetic monopole string with linear momentum on it. or magnetic monopole string with uniform electric charge or instanton densities, and so on. However it turns out also a new-kinds of 1/4 BPS objects which is not a simple combination.

The minimal 1/16 BPS equation in 5-dim maximally supersymmetric Yang-Mills theory has been written sometime ago by Kapustin and Witten and also independently by Ho-Ung Yee and myself [14, 15]. One starts from the locking the spatial $SO(4)$ rotation in the 5-dim with the $SO(4)$ of the $SO(5)$ R-symmetry group. One can add also electric charge.

$$F_{ab}=\epsilon_{abcd}D_c\phi_d-i[\phi_a,\phi_b],\ D_a\phi_a=0, \tag{2}$$

$$A_0=\phi_5,\ D_a^2-[\phi_a,[\phi_a,\phi_5]]=0. \tag{3}$$

where $a=1,2,3,4$ and the last equation arises from the Gauss law. One could obtain the 5-dim SYM theory from the dimensional reduction of the 10-dim SYM theory with identification $\phi_I=A_{4+I}, I=1,2,3,4,5$.

When one turns on only one scalar field ϕ_4 and everything depends on the first three spatial coordinate $x^{1,2,3}$, the above equation becomes the standard BPS equation for the 1/2 BPS magnetic monopole

$$F_{ab}=\epsilon_{abc4}D_c\phi_4 \tag{4}$$

in 3-dim. In our 5-dim theory, the monopole becomes monopole string lying along x^4 axis. The asymptotic behavior of the scalar field ϕ_4 tells the symmetry breaking pattern and also determines the monopole string tension. As only one scalar field is turned on, D4 branes lie along a line along say x^8 direction determined by $A_8=\phi_4$. As two separated D4 branes lie on a line, one can connect them by D2 brane and obtain the 1/2 BPS monopole strings. These $N(N-1)/2$ monopole strings can be obtained from the above solution by the spatial and SO(5) R-symmetric transformations.

Before continue to complicated objects, one notices that there are 1/4 BPS objects which are composite of monopole strings and waves on the monopole strings, whose supersymmetric conditions are

$$\Gamma^{1238}\epsilon=\epsilon,\ \Gamma^{04}\epsilon=\pm\epsilon \tag{5}$$

There are two kinds of them, left and right movers on the monopole strings.

When there are three D3 branes, one can put them on the plane, say $7-8$ plane. The related 1/4 BPS supersymmetric condition becomes

$$\Gamma^{1238}\epsilon = \epsilon,\ \Gamma^{1247}\epsilon = \pm\epsilon \tag{6}$$

with only $\phi_{3,4}$ turned on. The resulting BPS equation become

$$\begin{gathered} F_{12} = D_3\phi_4 - D_4\phi_3,\ F_{23} = D_1\phi_4,\ F_{31} = D_2\phi_4, \\ F_{41} = D_2\phi_3,\ F_{24} = D_1\phi_3,\ F_{43} = -i[\phi_4, \phi_3], D_3\phi_3 + D_4\phi_4 = 0 \end{gathered} \tag{7}$$

This equation describes the junctions and anti-junctions of monopole strings connecting three D4 branes.

One can start from D2 brane connecting on two i-th and j-th D4 branes on 78 plane which appears as the monopole string on 34-plane. If one rotates D2 branes in 78 plane and 34 plane with the same angle, there would be a preserved supersymmetry. The preserved susy parameter satisfies

$$\Gamma^{1238}\epsilon = \epsilon,\ e^{\theta(\Gamma^{34}+\Gamma^{78})}\epsilon = \epsilon \tag{8}$$

One can see the second condition is independent of the angle θ if $\Gamma^{3478}\epsilon = \epsilon$. Once three strings are intersecting with the angle are given in the Fig.1

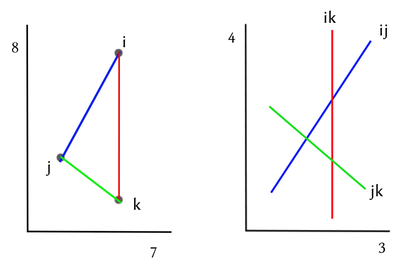

Figure 1: intersecting BPS monopole strings

When three monopole strings intersect at the same point, one can cut off half of the strings such that they make a junction as shown in Fig.2. Each segments of half strings are supersymmetric to each other and one can show easily that the string tension is balanced at the junction.

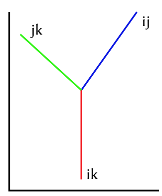

Figure 2: BPS monopole string junction

There are really junctions and anti-junctions whose orientations are reversed. To see the supersymmetry, one can see the junctions and anti-junctions satisfy the BPS condition:

$$\Gamma^{1238}\epsilon = \epsilon,\ \Gamma^{3478}\epsilon = \pm\epsilon. \tag{9}$$

The three intersecting BPS strings are made of two BPS junctions, not junctions and anti-junctions. On the other hand, one could say the 1/2 BPS monopole strings are made of annihilation of two legs of junctions and anti-junctions.

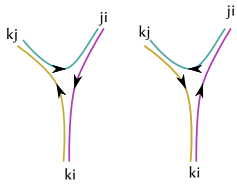

Figure 3: BPS monopole string junctions and anti-junctions

Such are 1/4 BPS monopole string junctions. One can see less supersymmetric junctions, which are non-planar and higher dimensional, are made of 1/4 BPS junctions and could be regarded as a composite objects.

One could find similar 1/4 BPS junctions in the Coulomb phase for the 5-dim SYM theory for different gauge group. One starts with the scalar field expectation value $\phi_a, a = 1, 2, 3, 4$. For each root α_i of the gauge group, there exist 1/2 BPS monopole strings of tension $|\alpha_i \cdot \phi_a|/g_{5d}^2$. For three distinct monopole strings for three roots $\alpha_i, i = 1, 2, 3$, one can find the monopole string junction when the sum of the three roots vanish.

3.2 Lifting to 6-dim

We have various 1/2 BPS objects and 1/4 BPS objects in the Coulomb phase of the 5-dim maximally supersymmetric theory. One can easily lift them to the 6-dim (2,0) theory. The massless waves and instantons become the 1/2 BPS massless waves in the abelian sub-sectors of the 6-dim theory. There would the number of the abelian sectors would be the rank of the gauge group r_G which is the dimension of the Cartan subalgebra. The monopole strings and W-bosons for each root α become the selfdual strings for each root α. Again the spatial rotation changes the orientation of the selfdual strings and so each selfdual string becomes its anti-string.

Table 2: the 1/2 BPS object in the 6-dim Coulomb phase

1/2 BPS objects	counting
massless tensor multiplets	r_G
selfdual strings	$\frac{1}{2}(d_G - r_G) = \frac{1}{2}h_G r_G$

The 1/4 BPS objects made of monopole strings with the left and right wave and the 1/4 BPS dyonic instantons get mapped to 1/4 BPS objects made of selfdual strings with left and right moving waves. The number of them would be the number of roots which is

$$A_G = d_G - r_G = r_G h_G \tag{10}$$

where h_G is the Coxeter number. For the simple-laced Lie group, the dual Coxeter and Coxeter numbers are identical.

The 1/4 monopole string junctions get uplifted to the 1/4 selfdual string junctions in 6-dim. Again the sum of the roots associated to three selfdual strings should vanish. For each such combinations α, β, γ such that α, β, γ, there are also $-\alpha, -\beta, -\gamma$. These two combinations would correspond to junctions and anti-junctions, respectively.

Let us count the possible number of 1/4 BPS junctions and anti-junctions. For A_{N-1} type, the roots are $\pm(e_i - e_j)$ with $1 \leq i < j \leq N$. The three roots whose sum vanish would be $e_i - e_j, e_j - e_k, e_k - e_i$. One can choose three distinct indices i, j, k out of N indices whose possibilities have the $N(N-1)(N-2)/6$ possible combinations. As there are junctions and anti-junctions, the number of the possible combinations would be twice larger, that is,

$$B_{A_{N-1}} = \frac{1}{3}N(N-1)(N-2) \tag{11}$$

The total 1/4 BPS charges are then

$$C_{A_{N-1}} = A_{A_{N-1}} + B_{A_{N-1}} = \frac{1}{3}N(N-1)(N+1) = \frac{1}{3}c_{A_{N-1}} \tag{12}$$

This matches to exactly one-third of the anomaly coefficient $c_{A_{N-1}}/3$ in the Table I.

Similar counting of 1/4 BPS junctions can be done for D and E type theories. For D_N theory with roots $\pm(e_i \pm e_j), 1 \leq i < j \leq N$, there are $B_{D_N} = 4N(N-1)(N-2)/3$ possible combinations of roots whose sum vanishes. The total number of 1/4 BPS objects in the D_N type theory is

$$C_{D_N} = A_{D_N} + B_{D_N} = \frac{2}{3}N(N-1)(2N-1) = \frac{1}{3}c_{D_N} \tag{13}$$

This is again one-third of the anomaly coefficient in the Table I.

For the $E_{6,7,8}$ theories, one consider find the roots for the group and find decompose them to those for the maximal A or D type subgroup plus additional roots. New types of junctions besides those arising from the maximal A or D type subgroup are shown in the Figure... Once one takes into account all these additional contributions, the number of 1/4 BPS objects for E type theories also turn out magically to be one-third anomaly coefficient as shown in our key paper

4 Mathematical Analysis

The anomaly coefficient c_G is the product of the dual Coxeter number h_G and the dimension d_G. In the simple-laced group, the dual Coxeter number is identical to the Coxeter number which is the number of roots, $d_G - r_G$ divided by the rank r_G, which implies that $d_G = (h_G+1)r_G$. This implies the trivial mathematical identity

$$\frac{1}{3}c_G = \frac{1}{3}h_G(h_G+1)r_G = h_G r_G + \frac{1}{3}r_G h_G(h_G-2) \tag{14}$$

The first of the last part is the number of roots which is the kinds of 1/4 BPS objects for waves on selfdual strings. The last of the last part is the number of 1/4 BPS junctions and anti-junctions which match with the embedding of $SU(3)$ roots to the root system of A, D, E type of theories.

Another interesting aspect arises from the AGT relation between 4d $N=2$ theory and 2d Toda models [16]. The central charge of Toda model is related that of the anomaly of the 6d (2,0) theories. Especially that the anomaly coefficient c_G appears in the the Toda model [17] as

$$c_G = 12\rho^2 \tag{15}$$

where the Weyl vector $\rho = 1/2\sum_{\alpha>0}\alpha$ is the sum of the positive roots. This is written in the convention $\alpha^2 = 2$ for the longest root. For the simple-raced group, the above relation implies

$$\frac{1}{3}c_G = \sum_{\alpha>0}\alpha^2 + 2\sum_{\alpha\neq\beta,\alpha>0,\beta>0}\alpha\cdot\beta \tag{16}$$

For simply-raced group G, two positive roots α, β is either $\alpha\cdot\beta = \pm 1$, or0. For the set of three positive roots with mutually nonvanishing inner products form the positive roots of $SU(3)$ root system. Thus the first part of RHS is again the number of roots and the second part is the kinds of the imbedded $SU(3)$ root system.

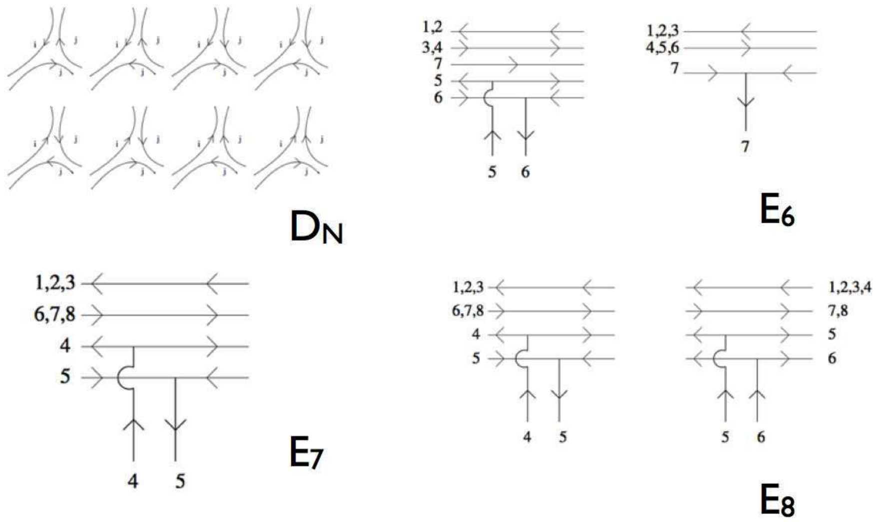

Figure 4: BPS monopole string junctions and anti-junctions

5 Finite Temperature

Let us consider the heating up the local region of the system with some finite temperature. For free string theory, the temperature cannot reach the Hagedorn temperature $T_h \sim \sqrt{T_{tenson}}$ is given by the string tension $T_{tension}$. In the 6d (2,0) theories in the Coulomb phase, selfdual strings are interacting strongly and the free string description is not adequate. One novelty is that three selfdual strings can terminate at one junction. One could imagine that the high temperature is dominated by the 55-dim spatial webs or nets of strings with junctions and anti-junctions at each joint. The entropy density could be characterized by the number of species of these junctions. Some consistent calculation is necessary to confirm this idea.

6 Degenerate Limit and Symmetric Phase

When three M5 branes, say i, j, k th, lie on a straight line in the order of i, j, k, the 1/4 BPS junctions connecting three M5 branes collapse to 1/2 BPS object whose nature is obscure. Of course there are three 1/2 BPS self-dual strings connecting two of three M5 branes. But the junction feature suggests that there may be more 1/2 BPS states. One can make a wave along this selfdual strings and see whether there are six kinds of 1/4 BPS states, three for the selection of selfdual strings and two for left and right moving waves. The answer turns out to be no. The index counting of the dyonic instantons has show that there is indeed additional 1/4 BPS objects which seems to correspond to the wave carried by the degenerate junctions [2]. Clearly this shows also there are more degrees of freedom related to the degenerated junction.

In the symmetric phase, the selfdual strings become tensionless and would be source for the 'nonabelian' two-form tensor fields. The junctions would become tensionless. In the symmetric phase the information about the relative position of M5 branes is lost and the angle between tensionless strings in the junction would be arbitrary. The dynamics of tensionless strings and tensionless junctions are not clear at this moment.

7 Conclusion

In the last 5 years there has been a considerable progress in our understanding of M2 brane physics. However, there are still much progress to make in the physics of M5 branes. In this talk I presented our works related to M2 and M5 branes. Especially we argue that in the Coulomb phase the N-cubic degrees of freedom may be captured by the 1/4 BPS objects including junctions and anti-junction. Due to the lack of time, I have not covered our other work on M5 branes which is based on the counting the index of dyonic instantons

Acknowledgement

I would like to thank first the organizers Sangpyo Kim and Roland Triay of the conference at Quy-Nhon Vietnam for their encouragement and superb organization. The works presented here I am indebted to collaborators, Ho-Ung Yee, Stefano Bolognesi, Eunkyung Koh, Seok Kim, Seongjay Lee, Kazuo Hosomichi, Sangmin work presented here This work is supported in part by the Korean National Research Foundation via NRF-2005-0049409 through CQUeST, NRF-2009-0084601 and NRF-2006-0093850.

References

[1] S. Bolognesi, K. Lee, *1/4 BPS String Junctions and N3 Problem in 6-dim (2,0) Superconformal Theories*, Phys.Rev. D84 (2011) 126018, [arXiv:1105.5073]

[2] H. Kim, S. Kim, E. Koh, K. Lee, S. Lee *On instantons as Kaluza-Klein modes of M5-branes*, JHEP 1112 (2011) 031, [arXiv:1110.2175]

[3] M. B. Green, J. H. Schwarz, *Anomaly Cancellation in Supersymmetric D=10 Gauge Theory and Superstring Theory*, Phys. Lett. B149 (1984) 117

[4] E. Witten, *String theory dynamics in various dimensions*, [hep-th/9503124] Nucl.Phys. B443 (1995) 85-126

[5] O. Aharony, O. Bergman, D. L. Jafferis, J. Maldacena, *N=6 superconformal Chern-Simons-matter theories, M2-branes and their gravity duals*, JHEP 0810 (2008) 091 [arXiv:0806.1218]

[6] K. Hosomichi, K. Lee, S. Lee, S. Lee, J. Park, *N=4 Superconformal Chern-Simons Theories with Hyper and Twisted Hyper Multiplets* JHEP 0807 (2008) 091 [arXiv:0805.3662]

[7] K. Hosomichi, K. Lee, S. Lee, S. Lee, J. Park, *N=5,6 Superconformal Chern-Simons Theories and M2-branes on Orbifolds*, JHEP 0809 (2008) 002 [arXiv:0806.4977]

[8] E. Witten, *Some comments on string dynamics*, (1995) [arXiv:hep-th/9507121].

[9] I. R. Klebanov, A. A. Tseytlin *Entropy of near extremal black p-branes* Nucl.Phys. B475 (1996) 164-178, [arXiv:hep-th/9604089]

[10] M. Henningson and K. Skenderis, *The Holographic Weyl anomaly*, JHEP 9807, 023 (1998) [arXiv:hep-th/9806087].

[11] J. A. Harvey, R. Minasian and G. W. Moore, *NonAbelian tensor multiplet anomalies*, JHEP 9809, 004 (1998) [arXiv:hep-th/9808060]; P. Yi, *Anomaly of (2,0) theories*, Phys. Rev. D 64, 106006 (2001) [arXiv:hep-th/0106165]; K. A. Intriligator, *Anomaly matching and a Hopf-Wess-Zumino term in 6d, N=(2,0) field theories*, Nucl. Phys. B 581, 257 (2000) [arXiv:hep-th/0001205].

[12] N. Seiberg, *Five-dimensional SUSY field theories, nontrivial fixed points and string dynamics*, Phys. Lett. B 388, 753 (1996) [arXiv:hep-th/9608111].

[13] Michael R. Douglas, *On D=5 super Yang-Mills theory and (2,0) theory*, JHEP 1102, 011 (2011) [arXiv:1012.2880 [hep-th]]; N. Lambert, C. Papageorgakis and M. Schmidt-Sommerfeld, *M5-Branes, D4-Branes and Quantum 5D super-Yang-Mills*, JHEP 1101, 083 (2011) [arXiv:1012.2882 [hep-th]].

[14] A. Kapustin, E. Witten, *Electric-Magnetic Duality And The Geometric Langlands Program*, arXive:0604151[hep-th]

[15] K. Lee and H. Yee, *BPS String Webs in the 6-dim (2,0) Theories*, JHEP 0703 (2007) 057, a0rXiv:606150[hep-th]

[16] L. F. Alday, D. Gaiotto, and Y. Tachikawa, *Liouville Correlation Functions from Four-Dimensional Gauge Theories*, Lett. Math. Phys. 91 (2010) 167"197, [arXiv:hep-th/0906.3219]

[17] L. F. Alday, F. Benini, Y. Tachikawa *Liouville/Toda central charges from M5-branes* Phys.Rev.Lett. 105 (2010) 141601, [arXiv:0909.4776]

Transplanckian radiation in theories with extra dimensions

D.V. Gal'tsov

Department of Theoretical Physics, Moscow State University, 119899, Moscow, Russia

Email : galtsov@phys.msu.ru

Abstract

We discuss whether particles undergoing transplanckian collisions in TeV-scale gravity can deplete most of their energy on bremsstrahlung for impact parameters much larger than the gravitational radius of the presumably created black hole.

1 Introduction

The models of TeV-scale Quantum Gravity (TQG) proposed as an attempt to solve the hierarchy problem open the possibility to study physics beyond the Planck's scale. A conceptually and technically simplest TQG model suggested by Arkani-Hamed, Dimopoulos and Dvali (ADD) [1] and further elaborated in [2] assumes that the standard model particles reside in the four-dimensional sector of space-time $\mathcal{M}_4$, while gravity propagates in the D-dimensional bulk with the $d = D - 4$ flat dimensions compactified on a torus $\mathcal{T}^d$. D-dimensional gravity is strong, the corresponding Planck mass M_* being of the order of TeV. The Planck length l_* and the gravitational radius r_s associated with the center-of mass energy $\sqrt{s}$ in the ADD model are

$$l_* = \left(\frac{\hbar G_D}{c^3}\right)^{\frac{1}{d+2}} \sim \frac{\hbar}{M_* c}, \quad r_s = \left(\frac{G_D \sqrt{s}}{c^4}\right)^{\frac{1}{d+1}}. \tag{1}$$

In the transplanckian (TP) particle collisions gravity not only becomes the dominant force, but it partly restores its classical character [3]. Since the gravitational radius r_s corresponding to the energy in the center of mass frame grows with s, while the de Broglie length of the particles $\lambda_B = \hbar c/\sqrt{s}$ decreases, therefore for $\sqrt{s} > M_*$ the classicality condition is satisfied

$$\lambda_B \ll l_* \ll r_S. \tag{2}$$

In the ADD model with $d \neq 1$ the classical TP region is also restricted from above [3] by the impact parameter

$$b_c \equiv \frac{1}{\sqrt{\pi}} \left(\frac{\varkappa_D^2 \Gamma(d/2)\, s}{16\pi}\right)^{1/d}. \tag{3}$$

We have therefore the following three TP sectors: [4]

1) $b > b_c$. This is the quantum sector where the scattering is dominated by the one-graviton exchange.

2) $r_s < b < b_c$. This is the eikonal sector, where the scattering amplitude is dominated by the sum of ladder and cross-ladder diagrams whose summation gives the eikonal amplitude [5]. The stationary phase approximation of the latter coincides with the classical amplitude [6]. It is also known that the semiclassical calculation of TP elastic scattering cross section in four-dimensional space-time [7] agrees with the string theory result [8]. Gravitational radiation in this region is expected to be well-described by the classical theory.

3) $b < r_s$. This is the region of strong gravity, where the main process is the formation of the black hole [9]. This was checked within an approach based on the picture of colliding waves representing ultrarelativistic particles

[10]. However this approximation is susceptible to radiation reaction [11], which is still not well understood. Various more sophisticated approaches to test the conjecture of black hole creation at colliders were suggested (see a recent review [12]), which gave additional arguments of its validity. Numerical work performed in this direction is reviewed in [13]).

Here we discuss whether gravitational radiation in TP collisions can be large enough in the region 2). If so, this could substantially modify the predicted cross-section of the formation of a black hole. Note, that for a *head-on* collision of black holes the upper bound was given by Eardley and Giddings [10] generalizing Penrose limit:

$$\epsilon \leq 1 - \frac{1}{2}\left(\frac{(D-2)\Omega_{D-2}}{2\Omega_{D-3}}\right)^{\frac{1}{D-2}}, \tag{4}$$

which gives the bound about $41,9\%$ for $D = 11$. A recent calculation [14] using the approach of D'Eath and Payne [15] gave in the first perturbative order the result slightly below this bound (the second order and numerical calculations give smaller values). However, it is known that radiation from particles plunging into the black hole *grow with the impact parameter*. Moreover, the above calculations are based on the picture of colliding waves, which itself is appropriate only if radiation losses are small, while the above values can not be considered small.

2 Eikonal and bremsstrahlung

The eikonalized elastic scattering amplitude can be presented as the integral

$$\mathcal{M}_{\text{eik}}(s,t) = 2is\int \epsilon^{i\mathbf{q}\cdot\mathbf{b}}\left(1-\epsilon^{i\chi(s,b)}\right)d^2b, \tag{5}$$

where the two-dimensional vectors $\mathbf{q}$, $\mathbf{b}$ lie in the transverse plane, with $\mathbf{b}$ playing the role of the impact parameter vector. The transverse component $\mathbf{q}$ of the momentum transfer in this approximation satisfies $\mathbf{q}^2 \approx -q^\mu q_\mu$, so that $t \simeq -\mathbf{q}^2$. This expression in the usual four-dimensional theory corresponds to summation of the ladder and crossed-ladder diagrams. The eikonal phase $\chi(s,b)$ can be obtained expanding the exponential and equating the leading term to the Born amplitude

$$\chi(s,b) = \frac{1}{2s}\int \epsilon^{-i\mathbf{q}\cdot\mathbf{b}}\mathcal{M}_{\text{Born}}(s,t)\,\frac{d^2q}{(2\pi)^2}. \tag{6}$$

The computation gives

$$\chi(s,b) = \left(\frac{b_c}{b}\right)^d, \tag{7}$$

where b_c is given by (3). Substituting this into (5) and calculating the integral in the stationary phase approximation around the point

$$b_s = \left(\frac{db_c^d}{q}\right)^{1/(d+1)}, \tag{8}$$

one recovers the purely classical result:

$$\mathcal{M}_{\text{cl}}(s,t) = \frac{4\sqrt{\pi}s\epsilon^{i(qb_s-\pi/2)}}{q\sqrt{d+1}}\left(\frac{2\sqrt{\pi}s\Gamma(d/2+1)}{M_*^{d+2}q}\right)^{\frac{1}{d+1}}, \tag{9}$$

which was obtained classically for the small angle scattering of ultrarelativistic point particles [6]

$$\text{Im}\chi \sim \left(\frac{b_r}{b}\right)^{3d+2}, \tag{10}$$

where one more length parameter b_r is introduced, satisfying the relation

$$\frac{b_r}{r_s} = \left(\frac{b_c}{r_s}\right)^{\frac{d}{3d+2}}. \tag{11}$$

In the situation when the eikonal sector of TP scattering is wide enough, $r_s \ll b_c$, one has $b_r \gg r_s$ and the impact parameter b_r can lie in the interval

$$r_s \ll b \ll b_r, \tag{12}$$

in which case $\mathrm{Im}\chi$ is not small. If the imaginary part of the eikonal is interpreted as the number of emitted gravitons whose frequency is much higher than $\omega_b = 1/b$, this would lead to the conclusion that the colliding particles can deplete all the energy for impact parameters much larger than r_s. Meanwhile, extraction of the eikonal imaginary part from the H-diagram probably is only consistent in the deep infrared region. Assuming that the spectrum is dominated by the frequencies $\omega < \omega_b$, and the number of soft gravitons is $N = \mathrm{Im}\chi$, one finds the following estimate for the radiation efficiency [3]

$$\epsilon = \frac{\Delta E}{E} \sim \left(\frac{r_s}{b}\right)^{\frac{d}{3d+3}}, \tag{13}$$

which is not catastrophical for $b > r_s$. However, classical considerations [18] indicate that the dominant region of the bremsstrahlung spectrum is $\omega \gg \omega_b$. Thus, one needs other methods to answer the question whether ϵ may become of the order of unity for $b > r_s$. An interesting approach to TP bremsstrahlung problem using the eikonal approximation in the spirit of 't Hooft was suggested by Lodone and Rychkov [17] , but so far it was applied only to gluons.

3 TP bremsstrahlung at $b \gg r_s$

In a series of papers [11, 18, 19] we calculated ultrarelativistic bremsstrahlung in $\mathcal{M}_4 \times \mathcal{T}^d$ using classical perturbation theory in momentum space, which was suggested long ago in the context of four-dimensional General Relativity [20]. Starting with the action

$$\lambda 1 S = -\sum \int m\sqrt{g_{MN}\dot{x}^M \dot{x}^N} ds + S_\phi(\phi, g) + S_{\mathrm{int}}\left[x(s), \phi, g\right] + S_g(g), \tag{14}$$

for two point particles, mutually interacting with the set of non-gravitational fields ϕ and the gravity described by bulk metric g_{MN}. The metric is presented as $g_{MN} = \eta_{MN} + \kappa_D h_{MN}$, and $x(s)$, ϕ and h_{MN} are further expanded in terms of the particle-field couplings f and the gravitational coupling κ_D. In the zero order approximation particles move freely in the opposite directions at an impact parameter b. Then we iterate the system of the particle equations of motion and the field equations up to the second order, in which radiation is manifest. This procedure presumably converges in the ultrarelativistic case when the scattering angle θ' is small, though to get more precise limits of applicability on has to go to the next iteration order, which is quite non-trivial.

One is interested in computing the total radiation efficiency ϵ and the spectral distribution under different assumptions about nature of the field dominating the interaction between the particles (mediator field), and nature of the radiation field. The set of ϕ generically contains the brane φ and the bulk Φ fields either of which can be mediator and/or radiated field. Gravity interacts with particles and with both fields φ, Φ, introducing non-linearity into the problem. Coupling constants of the particles with φ (f_0) and Φ (f_d) have different dimensions and are related though the volume of the torus V_d as $f_d^2 = f_0^2 V_d$. The corresponding classical length parameters r_d are introduced via the relation $f_d^2/r_d^{d+1} = m$, so $r_d^{d+1} = r_0^2 V_d$. The bulk fields Φ, h_{MN} depending on $x^M = (x^\mu,\ y^i)$ are expanded in the Kaluza-Klein modes $\Phi_n(x)$, $h^n_{MN}(x)$, $n \in Z^d$ which have the masses $\mu_n^2 = (2\pi\mathbf{n}^2/L^2)$.

The radiation efficiency and its spectrum depend on the nature of ϕ and on whether gravity is the dominant mediator. If not, one deals with the flat space problem in which both mediating and emitted fields are linear. This is the case of the Maxwell-Lorentz theory, which was exhaustively explored both in classical and quantum electrodynamics. The only novel here feature is presence of extra dimensions. Note that if one deals only with bulk fields, the ADD problem in $\mathcal{M}_4 \times \mathcal{T}^d$ reduces to that in D-dimensional Minkowski space provided the large number of KK modes in involved.

The frequency of radiation depends on the emission angle with respect to the direction of the collision $\omega_{\rm cr}(\theta) \simeq b^{-1}(\theta^2+\gamma^{-2})^{-1}$, where γ is the Lorentz factor in the rest frame of one of the particles. So most of the radiation is beamed inside the cone $\theta < 1/\gamma$ in any dimension D. The maximal frequency of radiation is

$$\omega_{\rm max} \simeq \omega_{\rm cr}(\theta=0) \sim \frac{2\gamma^2}{b}, \tag{15}$$

whose vicinity gives the dominant contribution. The total bremsstrahlung efficiency for different combinations of exchange modes and radiated modes reads [18] (omitting numerical coefficients):

1. brane modes exchanged and radiated: $\epsilon_{\phi\phi} \sim \gamma\, r_0^3/b^3$;
2. bulk modes exchanged brane modes radiated: $\epsilon_{\Phi\phi} \sim \gamma\,\frac{r_0}{b}\,(\frac{r_d}{b})^{2(1+d)}$;
3. brane modes exchanged, bulk modes radiated: $\epsilon_{\phi\Phi} \simeq \left(\frac{r_0}{b}\right)^2 \left(\gamma\,\frac{r_d}{b}\right)^{1+d}$;
4. bulk modes exchanged and radiated: $\epsilon_{\Phi\Phi} \simeq (\gamma\, r_d^3/b^3)^{1+d}$.

These formulas can be interpreted in terms of the effective numbers of massive KK states contributing as exchange modes $N_{\rm ex} \sim V_d/b^d$ and radiated modes $N_{\rm rad} \sim V_d\gamma^d/b^d$, where the $\gamma-$enhancement factor in $N_{\rm rad}$ accounts for modes with masses up to $\omega_{\rm max}$ emitted inside the cone $\theta_n < 1/\gamma$. in the bulk. Extra dimensions contribute to radiation efficiency with the factor $N_{\rm ex}^2$ for KK exchange modes and with the factor $N_{\rm rad}$ for radiation modes, so, e.g., $\epsilon_{\Phi\Phi} \sim \epsilon_{\phi\phi} N_{\rm ex}^2 N_{\rm rad}$. This explains the origin of an extra factor γ^d in $\epsilon_{\Phi\Phi}$. Therefore, classically, the bremsstrahlung efficiency grows with γ, and the γ-factor is d-dependent.

However, one has the quantum restriction on the frequency $\hbar\omega < m\gamma$, which for the maximal frequency $\omega = \omega_{\rm max} = 2\gamma^2/b$ gives $b_{\rm min} = \lambda_c\gamma$, where $\lambda_c = 1/m$ is the Compton length. The boundary value of the radiation efficiency $\epsilon_{\Phi\Phi} \simeq (r_d^3/(\lambda_c^3\gamma^2))^{1+d}$ thus decreases with energy.

The situation becomes more complicated if gravity is the dominant mediator [19]. The main new feature is non-linearity of the problem due to $\phi\phi h$ vertex and the three-graviton coupling, which leads to non-locality of the source in the D'Alembert equation for radiation modes:

$$\Box\Phi_n^{\rm rad} = j_n \equiv \rho_n + \sigma_n. \tag{16}$$

Here ρ_n has support on the particles world-lines, while σ_n is given in terms of lower order field perturbations; it is extended in space (including extra dimensions). It turns out that ρ_n and σ_n compete with each other and the result depends on the number of extra dimensions. In the case $d=0$, as it was shown long ago [20], these contributions mutually cancel in the frequency range

$$\omega'_{\rm max} < \omega < \omega_{\rm max}, \qquad \omega'_{\rm max} = \gamma/b = \omega_{\rm max}/2\gamma, \tag{17}$$

so the frequency is bounded by $\omega'_{\rm max} = \gamma/b$. In this case the quantum boundary $\omega'_{\rm max} < m\gamma$ is energy-independent. The efficiency of the gravitational bremsstrahlung in the gravity mediated collision in $D=4$ [20] is

$$\epsilon_{hh} \sim \gamma_{\rm cm}\, r_s^3/b^3, \tag{18}$$

where r_s is given by (1) with $d=0$. The energy-dependent restriction on b arises from the condition of smallness of the gravitational potential energy of the fast particle in the rest frame of the other, with respect to the particle energy, equivalent to $b \gg r_s\gamma_{\rm cm}$. Thus, on the boundary ϵ_{hh} remains small.

For $d \neq 0$ cancelation of local and non-local contributions also takes place but less complete, so the spectral-angular distribution still contains higher frequencies (17). The total efficiency in $D=5$ scales as $\epsilon_{hh} \sim \gamma_{\rm cm}\,\ln\gamma_{\rm cm}\cdot r_s^6/b^6$, while for $d \geq 2$ one obtains

$$\epsilon_{hh} \sim (r_s/b)^{3(d+1)}\,\gamma_{\rm cm}^{2d-1}. \tag{19}$$

Smallness of the scattering angle with respect to γ^{-1} (this restriction generalizes the one relevant for small angle bremsstrahlung calculation on the fixed background, in our two-body approach it may be overrestricting) implies

$b > r_s \gamma_{\rm cm}^{1/d+1}$, so classically we get on the boundary $\epsilon_{hh} \sim \gamma_{\rm cm}^{2(d-2)}$. This means that for $d \geq 3$ the energy is depleted for $b \gg r_s$. This result is still susceptible to quantum bounds, since for $d \neq 0$ the quantum frequency restriction on b is stronger than classical. This question is currently is under investigation [21]. If confirmed, the above estimate means that classical radiation damping may be regarded as another classicalization mechanism additional to creation of the black hole.

Acknowledgments

The author thanks the Organizing Committee of ICGA-10 for an excellent conference. He is grateful to G.Kofinas, P.Spirin and Th.Tomaras for useful comments and fruitful collaboration. The work was supported by the RFBR grant 11-02-01371-a.

References

[1] N. Arkani-Hamed, S. Dimopoulos and G. R. Dvali, Phys. Lett. B **429**, 263 (1998) ; Phys. Rev. D **59**, 086004 (1999) .

[2] G. F. Giudice, R. Rattazzi and J. D. Wells, Nucl. Phys. B **544**, 3 (1999) ; T. Han, J. D. Lykken and R. J. Zhang, Phys. Rev. D **59**, 105006 (1999)

[3] G. F. Giudice, R. Rattazzi and J. D. Wells, Nucl. Phys. B **630**, 293 (2002).

[4] S. B. Giddings and M. Srednicki, Phys. Rev. D **77**, 085025 (2008) .

[5] D. N. Kabat and M. Ortiz, Nucl. Phys. B **388**, 570 (1992) ; D. Amati, M. Ciafaloni and G. Veneziano, Nucl. Phys. B **403**, 707 (1993).

[6] D. V. Gal'tsov, G. Kofinas, P. Spirin and T. N. Tomaras, JHEP **0905**, 074 (2009) .

[7] G. 't Hooft, Phys. Lett. B **198**, 61 (1987).

[8] D. Amati, M. Ciafaloni and G. Veneziano, Phys. Lett. B197 (1987) 81; Int. J. Mod. Phys. A 3 (1988) 1615.

[9] P. C. Argyres, S. Dimopoulos and J. March-Russell, Phys. Lett. B **441**, 96 (1998) ; T. Banks and W. Fischler, arXiv:hep-th/9906038; S. B. Giddings and S. Thomas, Phys. Rev. D **65**, 056010 (2002) .

[10] D. M. Eardley and S. B. Giddings, Phys. Rev. D 66, 044011 (2002) .

[11] D. V. Gal'tsov, G. Kofinas, P. Spirin and T. N. Tomaras, Phys. Lett. B **683**, 331 (2010) .

[12] S. C. Park, arXiv:1203.4683 [hep-ph].

[13] V. Cardoso, L. Gualtieri, C. Herdeiro, U. Sperhake, P. M. Chesler, L. Lehner, S. C. Park and H. S. Reall *et al.*, arXiv:1201.5118 [hep-th].

[14] C. Herdeiro, M. O. P. Sampaio and C. Rebelo, JHEP **1107**, 121 (2011) ; F. S. Coelho, C. Herdeiro and M. O. P. Sampaio, arXiv:1203.5355 [hep-th].

[15] P. D. D'Eath and P. N. Payne, Phys. Rev. D **46**, 658 (1992).

[16] D. Amati, M. Ciafaloni and G. Veneziano, Nucl. Phys. B 347, 550 (1990).

[17] P. Lodone and V. S. Rychkov, JHEP **0912**, 036 (2009) .

[18] D. V. Galtsov, G. Kofinas, P. Spirin and T. N. Tomaras, JHEP **1005** (2010) 055 .

[19] Y. Constantinou, D. Gal'tsov, P. Spirin and T. N. Tomaras, JHEP **1111** (2011) 118 .

[20] D.V. Gal'tsov, Yu.V. Grats, In *"Modern problems of Theoretical Physics",* Moscow, Moscow State Univ. Publ., 1976, 258-273 (in Russian); D. V. Gal'tsov , Yu. V. Grats and A. A. Matyukhin, Sov. Phys. J. **23**, 389 (1980); Lorentz-covariant perturbation theory for relativistic gravitational bremsstrahlung [arXiv:1012.3060 [hep-th]].

[21] D. V. Galtsov, G. Kofinas, P. Spirin and T. N. Tomaras, in preparation.

Three limits to the physical world

Pierre Darriulat

Hanoi University of Sciences and VATLY/INST,

179 Hoang Quoc Viet, Cau Giay, Hanoi, Vietnam

Email : darriulat@mail.vaec.gov.vn

Abstract

We present a simple diagram that illustrates limits imposed to the physical world by quantum physics, gravity and dark energy.

We present below a simple diagram (Figure 1) that summarizes much of our present knowledge of the physical world. Its substance is very elementary common knowledge, most of which does not require quoting references. Its interest is in the form, not in the substance. As we are dealing with typically hundred orders of magnitude, we shall be satisfied with a precision of one order of magnitude.

In a preceding article [1] an early version had been proposed, using size (l) and mass (m) as axes. The present version uses instead two new variables, $\xi = l/m$ and $\eta = \sqrt{(lm)}$. As the diagram uses a *log-log* scale, this corresponds essentially to a 45° rotation of the axes. Units such that $\hbar = c = G = 1$ are used throughout ($\hbar$ is the Planck constant, c the velocity of light in vacuum and G Newton's gravity constant). Note that $m = \eta/\sqrt{\xi}$ and $l = \eta\sqrt{\xi}$, density being $\rho = (\xi\eta)^{-2}$.

The ξ axis is called "Heisenberg limit" in reference to Heisenberg uncertainty relations. Taking the proton as an example ($\xi \sim 10^{39}$), the quark momenta give the scale of the proton mass, m, and must exceed the reciprocal of the extension l of their wave packets which gives the scale of the proton size. Hence lm must exceed unity, and $\eta \sim 1$ corresponds indeed to the Heisenberg limit. The inclusion of elementary fields and pointlike objects in the diagram would imply accepting some convention, such as interpreting l as the Compton wavelength.

The η axis corresponds instead to the "Schwarzschild limit" in reference to the black hole singularity in the Schwarzschild metric, $m \sim l$ or $\xi \sim 1$ (precisely, the Schwarzschild radius of an object of mass m is $2m$). Known black holes are indeed found on this axis, stellar black holes (such as Cyg X, $\eta \sim 10^{39}$) as well as galactic black holes (such as Sgr A*, $\eta \sim 10^{45}$ and Cyg A, $\eta \sim 10^{49}$). The Universe ($\eta \sim 10^{60}$) is also located on this axis because it is flat and its expansion velocity, which is therefore equal to the escape velocity, reaches light velocity on its horizon. It does not mean that the Universe is a black hole: to be a black hole, an object having $\xi \sim 1$ must be isolated in space for Schwarzschild metric to apply.

At the origin, the intersection between the two above axes corresponds to the Planck scale ($\xi = \eta = 1$) where quantum physics and gravity are known to be incompatible in their present versions and where most of the current theoretical activity is taking place with extra dimensions, supersymmetry and strings.

As the diagram is in *log-log* scale, lines of equal densities are straight lines making angles of 45^o with the axes ($\xi\eta = 1/\rho^2$). Examples are nuclear matter density associated with neutron stars, $\rho_{NS} \sim 10^{-78}$; degenerated Fermi electron gas density associated with white dwarfs, $\rho_{WD} \sim 10^{-87}$; and atomic matter density, $\rho_A \sim 10^{-93}$, associated with condensed matter and with stars such as our Sun ($m \sim 10^{38}$, $l \sim 10^{44}$, $\xi \sim 10^6$ and $\eta \sim 10^{41}$). Indeed, writing m_p and m_e for the proton and electron masses, p_F for the Fermi momentum and α for the fine structure constant, it is straightforward to see that $\rho_{NS} \sim {m_p}^4$, $\rho_{WD} \sim m_p {m_e}^3$ (imposing $p_F \sim m_e/2$ to avoid excessive smearing of the surface of the Fermi sphere and noting that $\rho_{WD} \sim 8 m_p {p_F}^3$) and $\rho_A \sim m_p {m_e}^3 \alpha^3$ (using Bohr radius, $\alpha^{-1} {m_e}^{-1}$, as atomic scale). Hence $\rho_A \div \rho_{WD} \div \rho_{NS} = \alpha^3 \div 1 \div (m_p/m_e)^3 = 1 \div 10^6 \div 10^{15}$.

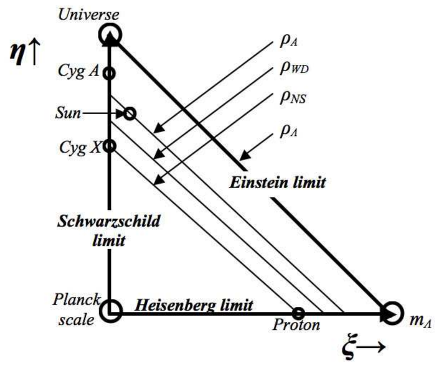

Figure 1: The ξ-η diagram (see text) in *log-log* scale with $\xi = \eta = 1$ at the origin (Planck scale) and $\xi\eta = 1/\sqrt{\rho_\Lambda} \sim 10^{60}$ on the Einstein limit.

Also shown on the diagram is the present density of the Universe, equal to the critical density in the Friedman-Lematre-Robertson-Walker metric, $\rho_{FLRW} \sim 10^{-120}$. The corresponding line is labeled “Einstein limit” in reference to Einstein’s cosmological constant: the Universe is known to be currently dark energy dominated, dark energy being well described by a cosmological constant Λ contributing a term $\rho_\Lambda = \Lambda/8\pi G$ to the energy density of the Universe ($\rho_\Lambda \sim \rho_{FLRW}$).

The third summit of the triangle made by the Heisenberg, Schwarzschild and Einstein limits corresponds to an object having $\xi \sim 10^{60}$ and $\eta \sim 1$, namely a mass m_Λ such that $\rho_\Lambda \sim {m_\Lambda}^4$, i.e. $m_\Lambda \sim 10^{-30}$ or 10 meV, in the range currently accepted for the lightest known fermions, neutrinos. It implies that dark energy − or the cosmological constant − sets a lower limit to the mass of composite quantum objects in the range of neutrino masses [2]. Indeed, lines of constant masses are straight lines $\eta = m\sqrt{\xi}$ with m ranging from the neutrino mass, $\sim 10^{-30}$, to the mass of the Universe, $\sim 10^{60}$, with the unit Planck mass ($\sim 10^{19}$ GeV) in-between. Similarly, lines of constant sizes are straight lines $\eta = l/\sqrt{\xi}$ with l ranging from the unit Planck scale ($\sim 10^{-33}$ cm) to the size of the Universe, $\sim 10^{60}$, with the scale of the “neutrino” wave packet ($\sim 10^{30}$) in the middle.

References

[1] P. Darriulat, Comm. Phys. Vietnam 18/4 (2008) 193.

[2] P.S. Wesson, Mod. Phys. Lett. A19 (2004) 1995;
C.G. Boehmer and T. Harko, Found. of Phys. 38/3 (2008) 2 and references therein.

String theory and space-time singularities

Martin O'Loughlin

University of Nova Gorica, Vipava 13, Slovenia

Email : martin.oloughlin@ung.si

Abstract

We concentrate on the particular case of a singular space-time as seen by an observer moving at the speed of light and we show that the resulting metric has a very simple universal structure provided that the original space-time had a stress-energy source that satisfies the dominant energy condition. We then demonstrate that string theory in such singular homogeneous plane wave backgrounds is exactly solvable and the essential details can be described by matrix quantum mechanics with a time-dependent potential. We discuss the possible regularisation of this singular matrix quantum mechanics.

1 Introduction

We will concentrate specifically on null singularities. We do this for a variety of reasons: space-like singularities are more difficult to treat analytically; null singularities arise as the limit of space-like ones[1]; string theory is exact in null space-times[2, 3, 4]; null singularities have a dual description via discrete light cone quantization (DLCQ)[5, 6]. We will discuss these null singularities in the context of string theory. Even though we do not have a full perturbative background independent string theory quantisation, there are non-perturbative quantisations of certain sectors of string theory and we will in fact concentrate here on the one that one obtains by taking the DLCQ limit. In this context we can actually study a limit of the space-time near a space-like singularity with strong string coupling, where gravitation and space-time enter a non-geometrical phase described by a weakly coupled Yang-Mills theory.

2 Strings to Yang-Mills

Taking a Penrose limit of space-like singularities gives rise to singular homogeneous plane wave (SHPW) space-times particularly adapted to discrete light-cone quantisation. SHPWs arise as Penrose limits of many common space-like singularities, for instance that of a FRW big bang or the singularity inside a Schwarzschild black hole. The limit retains some essential features of the space-time curvature, while rendering the background considerably simpler. In fact it was proven in [1] that *Penrose Limits of spherically symmetric space-like or time-like singularities of power-law type satisfying (but not saturating) the Dominant Energy Condition (DEC) are singular homogeneous plane waves with profile*

$$-R_{a+b+}|_{\gamma(z^+)} = A_{ab}(z^+) = -\omega_a^2 \delta_{ab} {z^+}^{-2} \tag{1}$$

The resulting SHPW metric is

$$ds^2 = -2dz^+dz^- + A_{ab}z^a z^b \frac{(dz^+)^2}{(z^+)^2} + \mathrm{d}\vec{z}^2 \tag{2}$$

The DLCQ limit with respect to this metric gives rise to a DBI lagrangian which when expanded in fluctuations leads to a quantum mechanical model with a time-dependent mass[6]. Applied to the above metric and expanding the resulting DBI action around a classical D-string trajectory, one finds

$$S = \frac{1}{2}\int d^2\sigma(-\eta^{\alpha\beta}\partial_\alpha z^a \partial_\beta z_b + \frac{A_{ab}}{t^2} z^a z^b + \frac{1}{2} g_{YM}^2 [z^a, z^b]^2). \tag{3}$$

An analysis of this lagrangian [7] has demonstrated that near the singularity (assumed to correspond to a strongly coupled string theory), the typical $[z^a, z^b]^2$ interaction is not important compared to the time-dependent mass-term arising from A/t^2.

Restricting to 1-dimension and decomposing into Fourier modes in the spatial σ direction we can reduce the near singularity physics of this system to that of an infinite number of uncoupled quantum mechanical systems with lagrangians

$$S_{bc} = \frac{1}{2}\int \mathrm{d}t \left(\dot{z}^2 - \omega_n(t)^2 z^2\right) \tag{4}$$

where

$$\omega_n(t)^2 = \frac{a(1-a)}{t^2} + kn^2. \tag{5}$$

3 Regularisation

This theory remains singular [8] at $t = 0$ and so we will attempt to regularise with the requirement that the regularisation introduces only one new scale into the potential. We will test regularity by looking for a non-singular $\epsilon \to 0$ limit of the Gelfand-Yaglom function [8, 9]. From the GY function one can then deduce the complete quantum mechanical behaviour.

One can find good regularisations which give the result (for $t_i < 0$ and $t > 0$),

$$\lim_{\epsilon\to 0} F_{t_i}(t) = \frac{1}{1-2a}(q|t|^a|t_i|^{1-a} + q^{-1}|t_i|^a|t|^{1-a}) \ , \tag{6}$$

with $q = \pm 1$.

An example of such a regularisation is;

$$\omega_\epsilon(t)^2 = \frac{a(1-a)(t^2-\beta\epsilon^2)}{(t^2+\epsilon^2)^2} \tag{7}$$

The result of this regularisation is apparently a non-singular propagation through the singularity (from $t_i < 0$ to $t > 0$), however the precise behaviour at the singularity is not addressed, and furthermore it is difficult to address as the result depends on the order of limits: $t \to 0$ or $\epsilon \to 0$. The full non-perturbative string theory can be recovered from this theory by taking the limit as $N \to \infty$ but this limit is also complicated as a result of orders of limits and infinite-dimensional matrices. The regularisation that we propose implies that something interesting may be happening at $t \to 0$ and $z \to \infty$, a point which appears to be outside the range of coordinates of the SHPW, however this is at the same time just a finite point in the original singular space-time before the Penrose limit. To further study this system one should thus carry out an expansion of neglected sub-leading terms around the null geodesic of the Penrose Limit using a Fermi-Penrose expansion.

Acknowledgements: I would like to thank Matthias Blau and Lorenzo Seri, together with whom this work was carried out.

References

[1] M.Blau, M.Borunda, M.O'Loughlin, G. Papadopoulos, *Penrose limits and space-time singularities* Class.Quant.Grav. **21**(2004)),L43.

[2] M. Blau and M. O'Loughlin, *Homogeneous plane waves* Nucl.Phys.B **654** (2003), 135.

[3] G. Papadopoulos, J. Russo, A. Tseytlin, *Solvable model of strings in a time dependent plane wave background* Class.Quant.Grav. **20** (2003), 969.

[4] M. Blau, M.O'Loughlin, G. Papadopoulos, A. Tseytlin, *Solvable Models of Strings in Plane waves* Nucl.Phys.B **673** (2003), 57.

[5] B.Craps, S. Sethi and E. Verlinde, *A matrix big bang* JHEP **0510** (2005), 005.

[6] M.Blau and M.O'Loughlin, *DLCQ and plane-wave matrix big bang models* JHEP **0809** (2008), 097.

[7] M.O'Loughlin and L. Seri, *The non-abelian gauge theory of matrix big bangs* JHEP **1007** (2010), 036.

[8] M.Blau, M.O'Loughlin, L.Seri, *Aspects of Plane Wave (Matrix) String Dynamics*, e-Print: arXiv:1112.3182 [hep-th].

[9] B.Craps, F. De Roo and O. Evnin, *Quantum evolution across singularities: The case of geometrical resolutions* JHEP **0804** (2008), 036.

Inflating wormhole in braneworld model

K. C. Wong, T. C. Harko, K. S. Cheng

The University of Hong Kong, Pokfulam, Hong Kong

Email : fankywong@gmail.com

Abstract

A fundamental ingredient of traversable wormholes is the violation of the null energy condition (NEC). However, in the braneworld models, there is extra dimension effects which could render a wormhole to satisfy the NEC. We investigate the solution of evolving wormhole in the brane world scenario, in which the wormhole is supported by the nonlocal brane world effects. We applied the solution to study inflating wormhole. The resulting evolution shows that while the physical and geometrical parameters of a zero redshift wormhole decay naturally, a wormhole satisfying general initial conditions could turn into a black hole, and exist forever.

1 Introduction

Wormhole is a connected spacetime in general relativity [1]. The metric of a spherical symmetric static wormhole is:

$$ds^2 = -e^{2\Phi(r)}dt^2 + (1 - \frac{b(r)}{r})^{-1}dr^2 + r^2\left(d\theta^2 + \sin^2\theta d\phi^2\right) \tag{1}$$

It is asymptotic to a flat spacetime and poses the flaring out condition $b - b'r > 0$ at or near the throat defined by $r_0 = b(r_0)$. The existence of wormhole in general relativity would imply a violation of NEC at the throat, i.e.

$$\lim_{r\to r_0} T_{\mu\nu}W^\mu W^\nu < 0 \tag{2}$$

where W^μ is a null vector. Moreover, it is only possible for a quantum mechanical processes to violation the NEC. In Randall-Sundrum 1-brane model, wormhole does not necessarily violate the energy condition because of the correction to the gravity. It is easier to see this in the projected 4D Einstein equation. The equation without cosmological constant and quadratic energy momentum can be given by [2]:

$$R_{\mu\nu} + \frac{1}{2}g_{\mu\nu}R = \frac{k_5^4\lambda}{6}T_{\mu\nu} - E_{\mu\nu} \tag{3}$$

The energy condition of the brane matter will become [3]:

$$\frac{k_5^4\lambda}{6}\lim_{r\to r_0} T_{\mu\nu}W^\mu W^\nu < \lim_{r\to r_0} E_{\mu\nu}W^\mu W^\nu \tag{4}$$

Therefore extra-dimensional effect allow the wormhole fulfilling NEC. Wormholes in braneworld scenario have also been considered in [4].

2 Braneworld evolving wormhole

We look for possible 5D metric such that a wormhole solution on the 4D brane will be realized. We are also interested in the case that the wormhole is asymptotic to an evolving Universe instead of static one:

$$ds^2 = -e^{2\Phi(r)}dt^2 + a^2(t)[(1 - \frac{b(r)}{r})^{-1}dr^2 + r^2 d\Omega] \tag{5}$$

A possible way to realize the wormhole in braneworld model is to allow the brane to bend locally relative to the background. i.e. $y = Y(r)$. The bulk metric around the wormhole will be:

$$^{(5)}ds^2 = -M(t,r,y)^2dt^2 + N(t,r,y)^2dr^2 + P(t,r,y)^2d\Omega + Q(t,r,y)^2dy^2 \tag{6}$$

A brane wormhole that evolving with the Universe can be constructed by assuming the suitable conditions on the embedded metric. Since wormholes are asymptotic to the background, the evolution of Universe would infer a natural evolution of the wormhole metric, in particular the evolution at the throat. For example, the dynamics of a scalar field ϕ with potential $V(\phi)$ could be written as:

$$M_{,t}(r,t,Y(r)) = \frac{V'(\phi)}{\dot{\phi}}(M(r,t,Y(r)) - 1)M(r,t,Y(r)) \tag{7}$$

We assume the scalar field evolve as the slow roll inflation solution and followed by a oscillating phase [5].

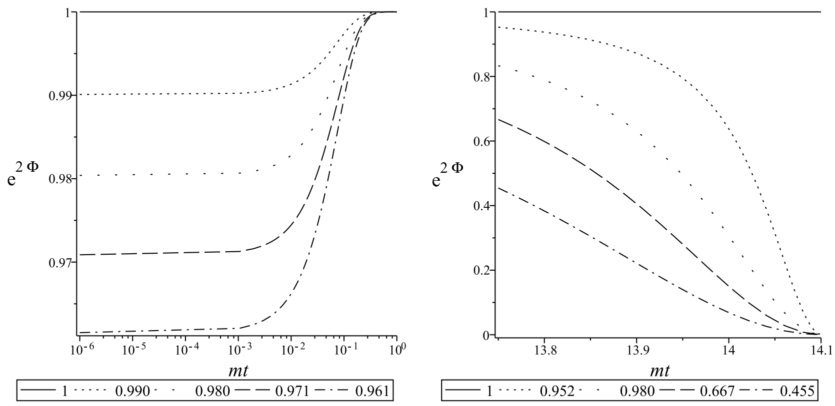

Figure 1: The evolution of wormhole's redshift function with different initial condition during inflation (left) and oscillation phase (right)

We found that wormhole with general initial condition would collapse into black hole at the first oscillation of scalar field. Therefore in the braneworld model, any macroscopic wormhole that we may observe nowadays originated after the inflation. The collapse of wormholes may also provide corrections to the formation of primordial black hole.

References

[1] M. Morris, K. Throne, Am. J. Phys. 56, 5 (1998)

[2] T. Shiromizu, K. Maeda, M. Sasaki, Phys. Rev. D 62 024012 (2000)

[3] F. S. N. Lobo, Phys. Rev. D 75 064027 (2007)

[4] K. A. Bronnikov, Sung-Won Kim, Phys. Rev. D 67 064027 (2003)

[5] S. Mizuno, K.-I. Maeda, K. Yamamoto, Phys. Rev. D 67 023516 (2003)

ADS Black Hole Solutions in Dilatonic Einstein-Gauss-Bonnet Gravity

Sasagawa Yukinori[1], *Kei-ichi Maeda*[2] *& Nobuyoshi Ohta* [3]

[1,2] *Department of Physics, Waseda University, Shinjuku, Tokyo 169-8555, Japan*

[3] *Department of Physics, Kinki University, Higashi-Osaka, Osaka 577-8502, Japan*

Email : *yukinori@gravity.phys.waseda.ac.jp*

Abstract

We find that anti-de Sitter (AdS) spacetime with a non-trivial linear dilaton field is an exact solution in the effective action of string theory, which is described by gravity with the Gauss-Bonnet (GB) curvature terms coupled to a dilaton field in the string frame. The AdS radius is determined by the spacetime dimensions and the coupling constants of curvature corrections. We also construct the asymptotically AdS black hole solutions with a linear dilaton field numerically .

1 Dilatonic Einstein-Gauss-Bonnet gravity

In the context of the string theory, the Einstein-Gauss-Bonnet(EGB) gravity has been argued to be an effective field theory with quantum corrections in [1]. Since a dilaton field plays important role in string theory, Dilatonic Einstein-Gauss-Bonnet (DEGB) gravity is studied in the context of string theory[2].

We consider DEGB gravity in string frame as an effective action of the heterotic string theory, which is given by

$$S = \frac{1}{2\kappa_D^2}\int d^Dx\sqrt{-g}\; e^{-2\phi}\Big(R + 4(\nabla\phi)^2 + \alpha_2 R_{GB}^2\Big),$$

where κ_D^2 is the D-dimensional gravitational constant, ϕ is a dilaton field, $R_{GB}^2 := R^2 - 4R_{\mu\nu}R^{\mu\nu} + R_{\mu\nu\rho\sigma}R^{\mu\nu\rho\sigma}$ is the Gauss-Bonnet curvature term, and $\alpha_2 = \alpha'/8$ is its coupling constant with α' being the Regge slope. To find a black hole solution, we assume a symmetric (depending only on r) and static spacetime, whose metric form is given by

$$ds^2 = -f(r)e^{-2\delta(r)}dt^2 + f(r)^{-1}dr^2 + r^2\gamma_{ij}^{(k)}dx^i dx^j, \tag{1}$$

where $\gamma_{ij}^{(k)}$ is the metric of $(D-2)$-dimensional maximally symmetric hypersurface with a constant curvature of the sign $k = 0, \pm1$. Hereafter we use a normalized coupling constant $\tilde{\alpha}_2 = (D-2)(D-3)\alpha_2$.

1.1 AdS spacetime

First we look for an AdS spacetime for $k = 0$. We assume the metric and dilaton field as $f = \frac{r^2}{\ell^2}$, $\delta = 0$, $\phi = \frac{p}{2}\ln\big(\frac{r^2}{\ell^2}\big)$. We find the equations for p,

$$16p^3 - 8(2D-3)p^2 + 4(D-1)(D-2)p + D(D-1) = 0\,. \tag{2}$$

The AdS radius is given by its solution p as $\ell = \sqrt{2(1+2p)}\,\tilde{\alpha}_2^{1/2}$. We find one real solution for Eq.(2), which gives an AdS space for $\alpha_2 > 0$. The specific value of p is -0.31446055, -0.30148794, and -0.27549727 for $D = 4, 5$, and 10.

This type of exact AdS solution is also found in the generalized Lovelock gravity theory, which is given in [3].

1.2 Asymptotically AdS black hole solutions

Next we look for an asymptotically AdS black hole solution. Since we expect a regular black hole, there arises a regularity condition which restrict a possible range of the horizon radius normalized by the coupling constant.

We examine to solve the field equations numerically from the horizon and obtain the asymptotically AdS black hole solution only in the case of $k = -1$. No regular asymptotically AdS black hole solution is found in four dimensions. In five dimensions, there is no lower bound but exists the upper bound, i.e., $0 < r_H \leq 0.707087\,\tilde{a}_2^{1/2}$. Note that there is no regular solution without a horizon ($r_H = 0$). In dimensions higher than five, we find both lower and upper bounds. For example, in ten dimensions, we find $0.782926\,\tilde{a}_2^{1/2} \leq r_H \leq 1.154671\,\tilde{a}_2^{1/2}$. The maximum bound on the horizon radius is given by $r_H = \sqrt{2(D-4)/(D-1)}\,\tilde{a}_2^{1/2}$.

2 Summary and Conclusion

In the DEGB gravity, we have obtained the exact AdS spacetimes with a planar symmetry and constructed the asymptotically AdS black holes numerically. These solutions are the dilatonic generalization of AdS spacetime and the AdS branch of black hole solutions in the EGB gravity. A dilaton field, which diverges logarithmically at infinity, plays the role of a negative cosmological constant.

The allowed horizon radii for asymptotically AdS black holes seem to be inherited from those of the corresponding solutions in the AdS branch in the EGB gravity. The detailed analysis on this system is given in [3]

References

[1] B. Zwiebach, Phys. Lett. B **156**, 315 (1985); B. Zumino, Phys. Rep. **137**, 109 (1986).

[2] K. Maeda, N. Ohta, and Y. Sasagawa Phys. Rev. D **80**, 104032 (2009) .

[3] K. Maeda, N. Ohta, and Y. Sasagawa Phys. Rev. D **83**, 044051 (2011) .

Karen Grahn-Goulianos, Antoni Szczurek, Tsvi Piran and Dmitry Gal'tsov

Proof that the atmosphere was great

Participants

Andrew **Beckwith**	Chongquing University, China
Chris **Belczynski**	Warsaw University, Poland
Gennady **Bisnovatyi-Kogan**	Space Research Institute, Russian Federation
Luc **Blanchet**	Institut d'Astrophysique de Paris, France
Kirill **Bronnikov**	Russian Reseach Inst. for Metrological Service , Russian Federation
Chia **Chu Chen**	National Cheng Kung University, Physics Department, Taiwan
Hai **Yang Cheng**	Academia Sinica, Taiwan
Pierre **Darriulat**	VATLY/INST, Vietnam
Dong **Hieu Dau**	College of Natural Science, CanTho University, Vietnam
Luis **Del Peral**	Universidad de Alcal, Spain
Nathalie **Deruelle**	CNRS, Laboratoire APC, Universite Paris 7, France
Andrey **Doroshkevich**	Astro Space Center of the Lebedev Physical Institute, Russian Federation
Sushil **Kumar Dubey**	Govt Model Science College of Jabalpur, India
Andrei **Frolov**	Simon Fraser University, Canada
Jonathan **Gair**	Institute of Astronomy, University of Cambridge, Great Britain
Dimitry **Gal'tsov**	Moscow State University, Russian Federation
Debashis **Gangopadhyay**	S.N.Bose National Centre For Basic Sciences, India
Subir **Ghosh**	Indian Statistical Institute, India
Yannick **Giraud-Héraud**	APC - Université Paris Diderot, France
Dmitry **Gorbunov**	INR Russian Academy of Sciences, Russian Federation
Mark **Halpern**	Dept. of Physics and Astronomy, Univ. of Br. Columbia, Canada
Sean **Hayward**	Center for Astrophysics, Shanghai Normal University, China
Duy **Hoang-Ngoc**	International University - Vietnam National University - HCMC, Vietnam
Zhon Kun **Hu**	School of Physics, Huazhong Univ. of Science and Technology, China
Takeo **Inami**	Faculty of Science, Chuo University, Japan
Eyo **Ita**	United States Naval Academy, U.S.A.
Sharad **Kandalkar**	Government Institute of Science and Humanities, Amravati, India
Munawar **Karim**	St. John Fisher College, U.S.A.
Masakatsu **Kenmoku**	Nara Women's University, Japan
Pramod **Khade**	Vidyabharati Mahavidyalaya, India
Ganesh **Khapekar**	Jagadamb Mahavidyalaya, India
Sang Pyo **Kim**	Kunsan National University, South Korea
Sumg-Won **Kim**	Ewha Womans University, South Korea
Yoji **Koyama**	Chuo University, Japan
Andrzej **Krolak**	Inst. of Mathematics, Polish Academy of Sciences, Poland
Bum-Hoon **Lee**	Sogang University, Department of Physics, South Korea
Kimyeong **Lee**	Korea Institute for Advanced Study, South Korea
Qing **Li**	Huazhong University of Science & Technology, China
Richard **Lovelace**	Cornell University, U.S.A.
Jun **Luo**	Huazhong University of Science and Technology, China
Richard **MacKenzie**	Département de physique, Université de Montréal, Canada
Kei-ichi **Maeda**	Waseda University, Japan
Manzoor **Malik**	University of Kashmir, India
Ilya **Mandel**	School of Physics and Astronomy, University of Birmingham, Great Britain

Daniel **Martin de Blas**	Instituto de Estructura de la Materia, IEM-CSIC, Spain
Olivier **Martineau-Huynh**	IHEP & IN2P3, China
John **Matthews**	University of Utah, U.S.A.
Vitaly **Melnikov**	Center for Gravitation and Fundamental Metrology, Russian Federation
Vadim **Milyukov**	Moscow State University, Russian Federation
Olivier **Minazzoli**	NASA-Jet Propulsion Laboratory, U.S.A.
Shinji **Miyoki**	Institute for Cosmic Ray Research, Tokyo University, Japan
Masaaki **Morita**	Okinawa National College of Technology, Japan
Vlatcheslaw **Mukhanov**	Arnold Sommerfeld Center for Theoretical Physics, Germany
Shinji **Mukohyama**	IPMU, University of Tokyo, Japan
James **Nester**	Department of Physics, National Central University, Taiwan
Hieu Van **Nguyen**	Vietnam Academy of Sciences and Technology, Vietnam
Khan Van **Nguyen**	Dpt. of Physics, Hanoi National Univ. of Education, Vietnam
Lan Quynh **Nguyen**	Dpt. of Physics, Hanoi National University of Education, Vietnam
Vin **Nguyen**	Hanoi National University of Education, Vietnam
Minh Phuong **Nguyen Thi**	Dpt. of Physics, Quy Nhon University, Vietnam
Wei-Tou **Ni**	SUCA, Shanghai Normal Univ. Taiwan & National Tsing Hua Univ., Taiwan
Eric **Nuss**	LUPM Université Montpellier 2, France
Martin **O'Loughlin**	University of Nova Gorica, Slovenia, Slovenia
Nobuyoshi **Ohta**	Kinki University, Japan
Manu **Paranjape**	Dpt. de physique, Université de Montréal, Canada
Masudeo **Patil**	Arts, Science And Commerce College, India
Dnyaneshwar **Pawar**	Dpt. of Mathematics, Govt. Vidarbha Inst. of Science & Humanities, India
Lka **Petermann**	University of Malaya, Department of Physics, Malaysia
Ngoc Diep **Pham**	Institute for Nuclear Science and Technology, Vietnam
Nhung Tuyet **Pham**	Institute for Nuclear Science and Technology, Vietnam
Lien Hong **Phan**	Le Qui Don University - Military Academy of Technology, Vietnam
Ngoc-Bao **Phan**	Dpt. of Physics, Internat. Univ.-Vietnam Nat. Univ. HCMC, Vietnam
Tsvi **Piran**	Racah Institute for physics, The Hebrew University of Jerusalem, Israel
Maria Dolores **Rodriguez Frias**	Space and Astroparticle Group. University of Alcala, Spain
Dorota **Rosinska**	Institute of Astronomy, University of Zielona Gora, Poland
Cyrille **Rosset**	APC/CNRS, France
Gerald **Rude**	California State University Fresno, U.S.A.
Hanno **Sahlmann**	APCTP, POSTECH Univ., South Korea
Yukinori **Sasagawa**	Waseda University, Japan
Misao **Sasaki**	Yukawa Institute for Theoretical Physics, Kyoto University, Japan
Toyokazu **Sekiguchi**	Nagoya University, Japan
Chenggang **Shao**	Dpt. of Physics, Huazhong Univ. of Science & Technology, Wuhan, China
Sang-Jin **Sin**	Hanyang University, South Korea
Vera Georgievna **Sinitsyna**	P.N. Lebedev Physical Institute RAS, Russian Federation
Vera Yurievna **Sinitsyna**	P.N. Lebedev Physical Institute RAS, Russian Federation
Dam Thanh **Son**	Inst. for Nuclear Theory, University of Washington, U.S.A.
Chopin **Soo**	National Cheng Kung University, Taiwan
Naoshi **Sugiyama**	Department of Physics, Faculty of Science, Nagoya University, Japan
Subhash **Tade**	Dep. of Math. Jawaharlal Nehru College, India
Angelo **Tartaglia**	Politecnico di Torino, DIFIS and INFN, Italy

Trinh Xuan **Thuan**	University of Virginia, U.S.A.
André **Tilquin**	Centre de Physique des Particules de Marseille, France
Ha Quoc **Tran**	Ho Chi Minh City University of Pedagogy, Vietnam
Van Thanh **Tran**	Les Rencontres du Vietnam
Van-Ly **Tran**	Laboratoire MAPMO, Universite d'Orleans, France
Khanh Quoc **Tran**	Moscow Aviation Institute - National Technological University, Vietnam
Roland **Triay**	Aix Marseille University - Centre de Physique Théorique CNRS, France
Oleg **Tsupko**	Space Research Inst. of Russian Academy of Sciences, Russian Federation
Phan **Van Dong**	Hanoi University of Education, Vietnam
Véronique **Van Elewyck**	Laboratoire APC, France
Murli Manohar **Verma**	Department of Physics, Lucknow University, India
Alex **Vilenkin**	Dpt. of Physics and Astronomy. Tufts University, U.S.A.
On Van **Vo**	University of Thu Dau Mot, Vietnam
Thuan **Vo Van**	Inst. for Nuclear Science and Technology, Vietnam
Qing Lan **Wang**	Dpt. of Physics, Huazhong University of Science and Technology, China
Steve **Wilburn**	California State University, Fresno, U.S.A.
David **Wilkowski**	Nanyang Technological University, Singapore
Ki Cheong **Wong**	The University of Hong Kong, Hong Kong
Masahide **Yamaguchi**	Tokyo Institute of Technology, Japan
Hoi-Lai **Yu**	Inst. of Physics, Academia Sinica, Taiwan
Tzu Chiang **Yuan**	Inst. of Physics, Academia Sinica, Taiwan
Bifu **Zhan**	Huazhong university of science and technology, China

Group photo with the photographer, Mr. Cû